A comparative organic geochemical and stable isotope study of the Cenomanian-Turonian organic-rich sediments from Tunisia, Germany and the UK.

by

Paul Barrett

A thesis submitted to the University of Newcastle upon Tyne in partial fulfillment of the requirements for the degree of Doctor of Philosophy in the Faculty of Science

Fossil Fuels and Environmental Geochemistry (Postgraduate Institute): NRG, University of Newcastle upon Tyne, UK

September 1998.

DECLARATION

I hereby certify that the work described in this thesis is my own, except where otherwise acknowledged, and has not been submitted for a degree at this, or any other University.

Paul Barrett.

Acknowledgments

Throughout my years as a student I have gleaned knowledge and wisdom from a variety of sources, and it is only right that I thank them now. For the task of correcting spelling, improving punctuation and expert supervision during my Ph.D. I would like to thank Richard Tyson, Paul Farrimond and Martin Jones. For all their technical support and contributions I would like to thank Ian Harrison, Paul Donnahoe, Kim Noke, Rob Hunter, Bryn Jones Stuart Petch, Clive Hetherington and Mick Jones. Many thanks to Moshen Layeb, Mongi Hammami and Mohamed Hermassi for their help in Tunisia during my field work and sample collection, and also to Heinz Hilbrecht for allowing me to use his sample set from Germany. Also thanks to British Gas and NERC who jointly sponsored this work

I am very grateful to my Mum, Dad and Troy for their belief and praise and providing a home to return to for well needed breaks. Most of all I would like to thank Helen Innes for her inspiration, laughter and ability to discuss important issues at a similar intellectual level to myself.

Abstract

A comparative multidisciplinary study has been undertaken of organic-rich Cenomanian-Turonian (C-T) sediments from Tunisia, Germany and the UK. Three hundred samples were taken from a total of 7 field localities and have been analysed using bulk and stable carbon isotope geochemistry (all samples), palynofacies (most samples) and molecular biomarker and pyrolysis geochemistry (selected samples). Most of the sections are thermally immature. All but one of the sections could be correlated using the organic carbon $\delta^{13}C$ curve, which shows a strong (<3‰) excursion at the C-T boundary, followed by a gradual return to background values (ca. –25.5‰). Relative to this excursion, there is a slight apparent difference in the stratigraphic development of the organic-rich sediments at different locations.

Of the sediments studied, the Balhoul Formation of Tunisia shows the highest concentration and best preservation of organic matter (0.2-8.0% TOC, 50-850 hydrogen index); together with darker colours and more frequent lamination, this suggests a more poorly oxygenated regime than in NW Europe (0.2-4.0% TOC, 6-140 HI), probably related to an upwelling intensified oxygen minimum zone (OMZ) on the south Tethyan margin. Data from the two northernmost (offshore) Tunisian sections indicate poorer preservation, which by modern analogy is attributed to deeperwater deposition below the suboxic core of the OMZ. Methylhopanes and bisnorhopane are abundant in the richest (OMZ core) facies.

Principal Component Analysis of kerogen pyrolysates from Py-GC and Py-MS analyses are dominated by the relative variations of aliphatic and aromatic compounds between the sections which largely reflect differences in the preservation of the predominantly marine organic matter (30-98% AOM).

CONTENTS

CHAPTER 1

1. Introduction

It has been proposed by Irving *et al.* (1974) and Tissot *et al.* (1979) that the majority of the worlds oil reserves were sourced by Jurassic and Cretaceous rocks. One of the main phases of source rock deposition world-wide was at the Cenomanian-Turonian boundary (Late Cretaceous; 91mya; Harland *et al.*, 1982). Even though much research has been done on this event the causes of organic matter deposition at this boundary are still hotly debated.

1.1 Oceanic Anoxic Events (OAE's)

During the Deep Sea Drilling Project (DSDP) Legs 32 (Moberly & Larson, 1975) and 33 (Schlanger & Jackson, 1976) carbonaceous sediments of Cretaceous age were discovered in the south, central and western Pacific. These findings greatly extended the range of known organic-rich Cretaceous deposits. Further drilling in the North and South Atlantic, during Legs 105, 135, 137, 367, 398, 551, and 603 (Herbin & Deroo, 1979; Tissot *et al.*, 1979; Herbin & Deroo, 1982) also revealed Cretaceous organic-rich sediments. These sediments, loosely termed "black shales" at the time, were frequently much more organic-rich (TOC values in the range 1% to 20%) than the associated pelagic facies, stratigraphically restricted, and clearly the result of a major change in depositional conditions which allowed the accumulation and burial of large amounts of organic matter.

Saunders *et al.* (1973) noted the presence of similar Cretaceous strata found onshore around the Caribbean. Work done by Schlanger and Jenkyns (1976) on these Cretaceous black shales led them to distinguish two distinct and separate time zones characterised by widespread deposition of organic-rich sediments, from Late Barremian through to Albian, and the Late Cenomanian through to Early Turonian. Such sediments are also found in Tethyan realm of the Mediterranean and Alpine regions (Arthur & Premoli Silva, 1982). Outcrops of Cenomanian-Turonian organic-rich sediments from Italy have already been described by van Graas *et al.* (1983) and Farrimond *et al.* (1988).

Deposition of the Cretaceous black shales coincides with times of relative sea level rise and transgression (Schlanger & Jenkyns, 1976; Haq *et al.*, 1987) which created large areas of shallow shelf seas. Schlanger and Jenkyns (1976) noted that Cretaceous black shales were deposited in a wide range of settings, including extensive shelf seas, small basins, continental margins and submarine plateaus. Their

model proposed that the newly expanded shallow shelf seas allowed for greater productivity, which itself would have led to an increased oxygen demand upon decay of the organic matter, which led to the formation of oxygen minimum zones (OMZ's). Most modern OMZ's are characterised by only a reduction of 25 to 50% of the surface oxygen concentration (Tyson & Pearson, 1991). However, other factors such as upwelling, higher productivity and warmer oceanic temperatures may increase this oxygen deficiency and result in the development of expanded oxygen minimum zones; wherever these zones make contact with the sediment /water interface organic-rich sediments are typically deposited. Events within which such conditions prevailed were termed Oceanic Anoxic Events (OAE's) by Schlanger and Jenkyns (1976), although they stated that the entire world's oceans were not stagnant, and that the OMZ was not global, but just widespread. The term OAE has been since used by several authors and is generally accepted in the literature despite its poor description.

Jenkyns (1980) identified three distinct OAE's in the Cretaceous:

1. Barremian to Albian (OAE I)
2. Cenomanian to Turonian (OAE II)
3. Coniacian to Santonian (OAE III)

It became apparent from the work done by Scholle and Arthur (1980) that distinct isotopic heavy $\delta^{13}C$ events correlated with the OAE's proposed by Schlanger and Jenkyns (1976). Based on this work Arthur *et al.* (1990) took the OAE classification further:

1. OAE Ia (Barremian-Aptian)
2. OAE Ib (L. Albian-M. Albian)
3. OAE Ic (U. Albian)
4. OAE II (Cenomanian-Turonian)
5. OAE III (Coniacian-Santonian; not in Europe cf. Tyson & Funnell, 1987)

The increase in atmospheric CO_2 during the Cretaceous (Berner, 1994) suggests a "Greenhouse" climate. In addition to the connection with transgressions, Jenkyns (1980) suggested that the spread of oxygen depleted water would have been encouraged by warmer global land and sea temperatures due to the equable climate of the Cretaceous. Higher water temperatures would lower the solubility of oxygen in the oceans (Fischer & Arthur 1977; Berger, 1979), and polar ice cap shrinkage or absence, would have caused sluggish thermohaline bottom water circulation. It has been suggested by Hakansson *et al.* (1974) and Funnell (1978) that there were no

limits on the nutrients supplied by these oceans, partly due to the supply from the opening South Atlantic through the seaway from Nigeria to Tunisia, thus allowing for increased productivity, a process which in itself creates a much larger demand for dissolved oxygen. It can be concluded that the Cretaceous seas produced sufficient organic matter that, in conjunction with aerobic and anaerobic bacterial action, rendered them oxygen deficient, to the point of being dysoxic to anoxic (cf. Tyson & Pearson, 1991).

1.2 The Cenomanian-Turonian (C-T)

Probably the most credible (in terms of being very short, less than 1 million years, and sharply defined) and best developed OAE, is the Cenomanian-Turonian Boundary Event (CTBE). The Cenomanian-Turonian OAE has an unequalled world distribution, and has been recognised in a number of oceanic sites from the Northern, Central and Southern Atlantic and the Pacific and Indian oceans. Onshore, the CTBE has been observed in Europe, North, Central and South America, and Africa (Herbin *et al.*, 1986; Schlanger *et al.*, 1987; Arthur *et al.*, 1988).

Several authors have worked on dating the Cenomanian-Turonian boundary using zone fossils (see Kauffman, 1977; Ernst *et al.*, 1979; and the Groupe de Travail Européе des Foraminifères (GTEFP), 1979). The GTEFP (1979) place the CTBE at 90myBP, in the foraminifera *Whiteinella archeocretacea* zone, bounded at its base by the late Cenomanian *Rotalipora cushmani* zone and followed by the *Praeglobotruncana helvetica* zone, which marks the basal Turonian beds. In Europe the *Actinocamax plenus* beds mark the latest Cenomanian time, followed by the *Neocardioceras juddii* zone just before the boundary and the *Mytiloides mytiloides* and *Inoceramus labiatus* zones, just after (Ernst *et al.*, 1979). Kennedy *et al.* (1981) place the Cenomanian-Turonian boundary after the *Neocardioceras juddii* zone, in the United Kingdom, and before the *Inoceramus labiatus* and *Watinoceras coloradoas* zones. A summary of zonal fossils around the Cenomanian-Turonian Boundary is given in Figure 1.1. Harland *et al.* (1982) place the boundary at 91Ma, and suggest that the event took place between 91.5 and 90.5Ma, which is the time scale that will be used within the context of this work. The period of deposition of the Cenomanian-Turonian sediments is thought to be less than 1my (Jenkyns, 1985; Arthur *et al.*, 1987; Schlanger *et al.*, 1987) making it a very sharp and distinct. The term "Cenomanian-Turonian Boundary Event" (CTBE) was first coined by de Graciansky & Deroo (1984) and Herbin *et al.* (1986) used the term to reflect the geologically short nature of the boundary.

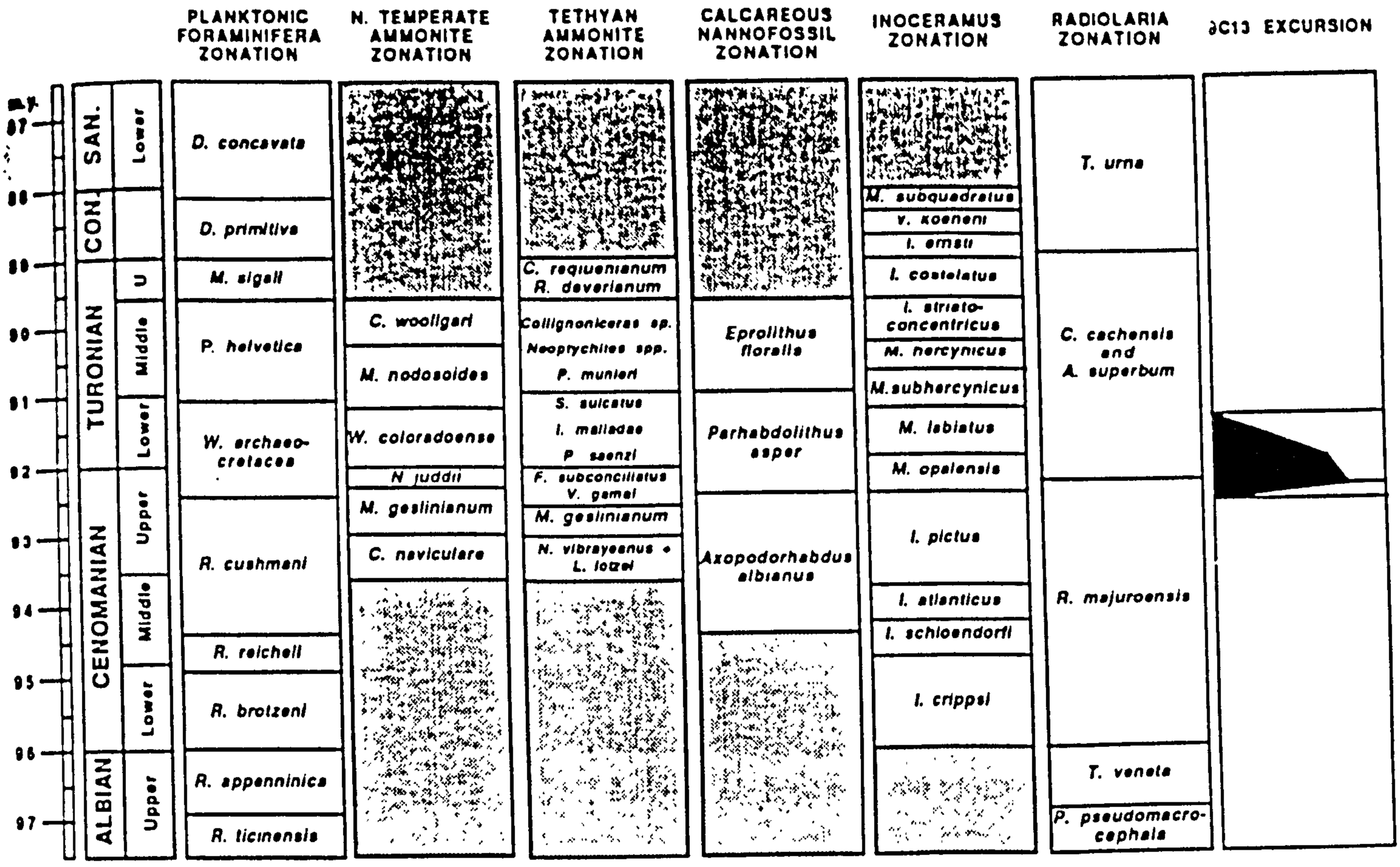

Figure 1.1 Chronostratigraphic framework and correlation of zonal schemes for the different faunal groups used for biostratigraphic correlation (after Kuhnt *et al.*, 1990).

The Cenomanian-Turonian is recorded as a time of large scale mass extinctions (Kauffman & Hart, 1996). The extinction event is characterised by widespread loss of typical Cenomanian ammonites, gastropods and bivalves, and a change from *Inoceramus*-dominated to *Mytiloides*-dominated inoceramid bivalve assemblages (Barnes *et al.*, 1996).

Deposition of Cenomanian-Turonian organic-rich sediments occurred in many differing palaeobathymetric settings including deep ocean basins, shallow shelf seas, continental shelf and plateaus. This would suggest that widespread OMZ's are associated with possible suboxic to anoxic bottom waters in basins, to allow for preservation of marine organic matter in such diverse environments. The Cenomanian-Turonian strata deposited in these environments are often thin; for example the Black Band of the UK (<0.5m ; Hart & Bigg, 1981; Barrett, 1994) and the Bonarelli Band of Italy (<1m; van Graas *et al.*, 1983), but they can also reach

greater thickness onshore and offshore, for example the Bahloul Formation of Tunisia (>40m; Herbin *et al.*, 1986) and locally in Germany (e.g. Misberg and Wunstorf >25m, Hilbrecht, 1986).

At the Cenomanian-Turonian boundary "greenhouse" conditions appear to have existed, and atmospheric CO_2 was at 2-3 times present levels (Berner, 1994). The sea level at the Cenomanian-Turonian boundary is believed to have reached a maximum of 255m higher than present day levels (Haq *et al.*, 1987); however, it is proposed by several authors (Ernst *et al.*, 1983; Hancock 1993) that there may have been a pause in the transgression near the boundary before a resumption in sea level rise. Based on figures cited in Menard and Smith (1966), Schlanger and Jenkyns (1976) and Arthur *et al.* (1987), Tyson (1995) calculated that the shelf area (<200m deep) was twice as large in the Cenomanian-Turonian compared to present day. He also suggests a 32-fold increase in areal extent of dysoxic-anoxic conditions compared to modern shelves, if 50% of the ancient shelf was oxygen deficient.

The kerogen Type of CTBE sediments is significantly different in the deep seas (where TOC and HI are higher on a regional basis) compared to earlier Cretaceous OAE's, as organic-rich layers tend to be dominated by marine organic matter, as opposed to organic-rich layers with higher terrestrial input (cf. Summerhayes, 1981; Arthur *et al.*, 1987). These studies revealed that sediments from other anoxic events such as the Aptian-Albian, on a whole contained abundant terrestrially derived plant material.

Tucholke and Voight (1979) and Summerhayes (1981 and 1987) suggest that changes in deep oceanic circulation caused by the separation of Africa from South America, during the late Cenomanian, may have caused a massive injection of nutrients into surface waters from deep Atlantic nutrient-rich waters. This injection of nutrients may have had a global effect, increasing primary productivity at the Cenomanian-Turonian boundary, until the newly available nutrients were diminished. Increased primary productivity would have increased oceanic oxygen demand, and have led to the expansion and intensification of OMZ's.

1.3 The Cenomanian-Turonian isotopic excursion

In addition to the deposition of organic-rich sediments the CTBE is recognised by an approximately 1 to 4‰ positive excursion in isotopic carbon signal in both

carbonate and organic matter carbon (Scholle & Arthur, 1980; Pratt & Threlkeld, 1984). The positive shift indicates that the preserved carbon is isotopically heavier.

The two isotopes of carbon in the geosphere are ^{12}C and ^{13}C, with carbon-12 by far the most abundant (ca. 99%). Marine organic matter is relatively rich in ^{12}C compared to ^{13}C. A large scale increase in organic matter productivity and preservation as proposed for the Cenomanian-Turonian should result in increased burial and removal of ^{12}C from the oceanic isotope pool. Logic suggests that the dissolved inorganic carbon in sea water would thus have become progressively more ^{13}C rich and any further organic matter or carbonate formed from this sea water should be relatively richer in the heavier ^{13}C isotope, producing a positive isotope excursion.

The positive excursion is found in both the carbonates and organic matter, as they are both synthesised from the dissolved ^{13}C-rich sea-water. Even where black shales are not found the CTBE can be correlated using the isotope excursion found in the carbonate record (Fig. 1.2).

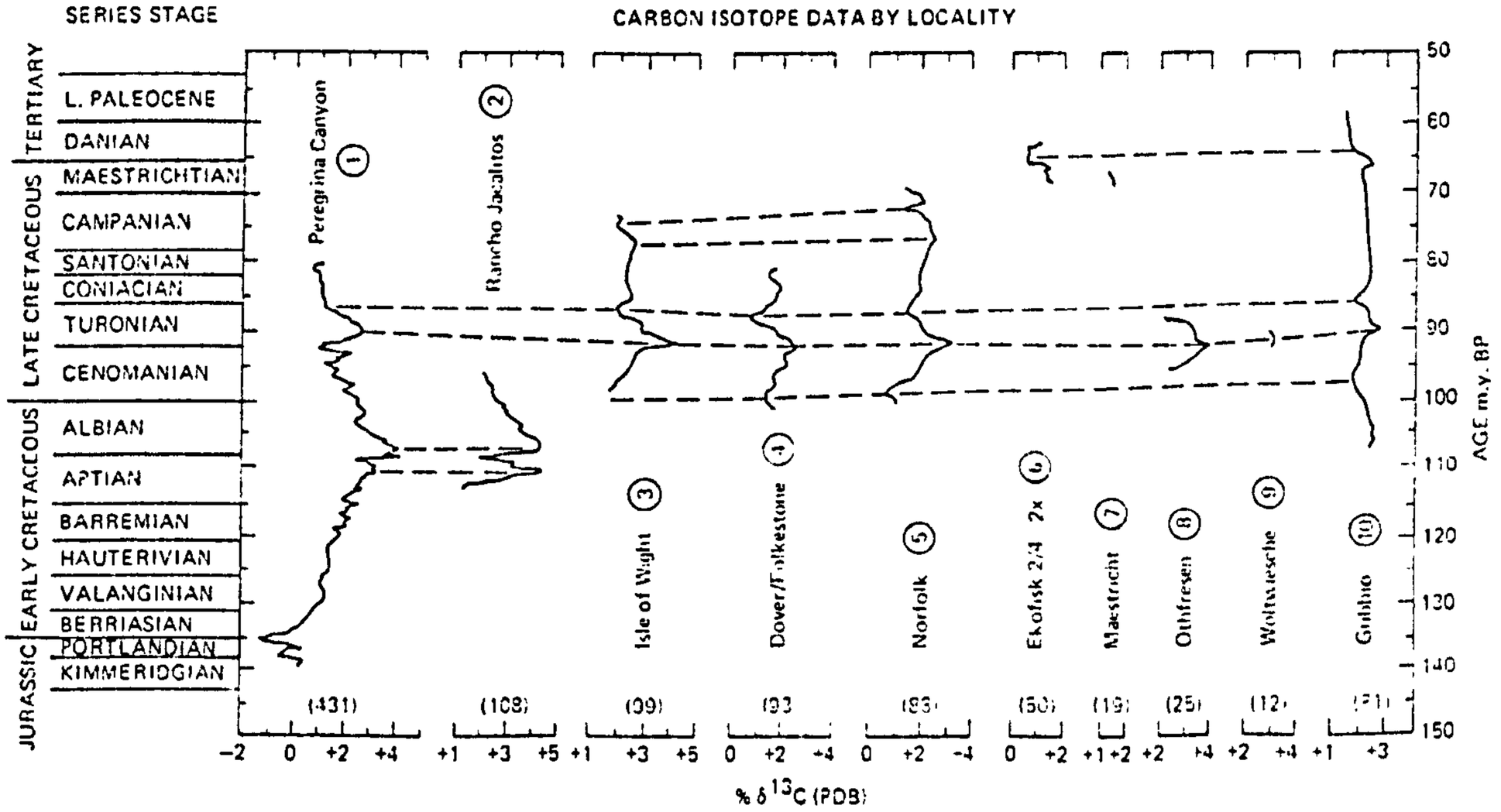

Figure 1.2 Global correlation of Cenomanian-Turonian carbonate isotope excursion (from Scholle & Arthur, 1980).

Work done by Scholle and Arthur (1980) identified the isotope excursion in North America, the United Kingdom and Eastern Europe; at these localities the values of the $\delta^{13}C$ excursion for carbonate material range from 0‰ to +1‰ (PDB) for the background limestones, up to +3‰ to +5 ‰ (PDB) at the excursion. Gale *et al.* (1993) have shown that biostratigraphic events (i.e. first appearances and

disappearances, e.g. *R. cushmani* and *N. Juddii*) and isotope excursions are synchronous at both Eastbourne (Sussex) and Pueblo (Colorado, USA). The carbonate isotope shift is from +3‰ to +5‰ (PDB) in the UK, and the kerogen isotope excursion is –28‰ to –24‰ (PDB) in the USA. A $\delta^{13}C$ organic matter event observed by Thurow *et al.* (1988) and Kuhnt *et al.* (1990) at the Cenomanian-Turonian boundary offshore Morocco records a kerogen isotope excursion from –27.8‰ to –24.3‰ (PDB). Other workers who have recorded the isotopic excursion at the CTBE include Pomerol (1983), Schlanger *et al.* (1987), Pratt *et al.* (1991), and Hilbrecht *et al.* (1996) whose work will be discussed in more detail later (Section 4.4.2).

Hasegawa (1997) records the variation in $\delta^{13}C$ of terrestrial organic matter from two sections in Japan (Table 1.1). He suggests that global isotope fluctuations were a primary factor controlling the isotope ratio of terrestrial organic matter and marine carbonates from the latest Cenomanian to the latest Turonian. Three isotopic events are recognised and correlated by Hasegawa (1997) between the Japanese sections and East Kent, UK and Gubbio, Italy (Jenkyns *et al.*, 1994).

Location	Reference	$\delta^{13}C$ org min	$\delta^{13}C$ org max	Shift (ppm)
Pueblo, Colorado	Pratt et al., 1985	-28	-24	4
Bou Grine, Tunisia	Bechtel et al., 1997	-27.7	-24.6	3
Borehole LM1, Tunisia	Bechtel et al., 1997	-27.4	-24.2	3
Oyubari, Japan	Hasegawa, 1997	-24.6	-22.3	2
Tappu, Japan	Hasegawa, 1997	-22.7	-22.4	0.3
Offshore, Morocco	Thurow et al., 1988	-27.8	-24.3	3.5

Table 1.1 Organic matter isotope curves recorded in the liturature.

The majority of isotope work has been carried out on carbonate material at the Cenomanian-Turonian boundary. The work in this study analyses the $\delta^{13}C$ of the organic matter fraction (kerogen). Other workers who have identified the kerogen $\delta^{13}C$ excursion are given in Table 1.1.

1.4 North European epeiric seas of the Boreal realm

The Cenomanian period of major marine transgression greatly affected Europe. Large areas were subjected to marine sedimentation for the first time (Fig. 1.3). The siliciclastic sedimentation of the Aptian, Albian and early Cenomanian was replaced by chalk and limestone facies, which became widespread in England and

Northern Germany, due to the diminishing terrestrial siliciclastic source areas (Tyson & Funnell, 1987). Palaeogeographic maps from Baudin (1995; Fig. 1.4) show that the majority of the UK was covered by a chalky platform and that the Lower Saxony region, Germany, was also a chalky platform environment just north of a terrigenous shelf.

An interesting phase of black shale deposition began in the European Boreal realm during the late Cenomanian to early Turonian. In the north European area this is recorded by from deposition of the Black Band, Humberside (Jenkyns, 1980), the Plenus Formation (North Sea; Burnhill & Ramsay, 1981) and the Black Shale Facies in the Lower Saxony Basin (Ernst *et al.*, 1983). There is considerable variation in the thickness of these black shales in the Boreal realm from a few centimetres of laminated black shales in the UK (Hart & Bigg, 1981; Barrett, 1994) to 30m of cyclic shale and limestones units in Germany (Hilbrecht & Dahmer, 1994). It is clear from the occurrence of these laminated black shales that large areas of the Boreal realm were prone to oxygen deficiency during this time interval. However, the benthic fauna of the CTBE at Wünstorf (Germany) suggests that oxygen concentrations at the sediment/water interface were not anoxic, and similar benthic fauna exist today which are characteristic of well developed oxygen minimum zones (Arthur *et al.*, 1987). There is also no organic geochemical evidence in the northern epeiric seas to argue for the encroachment of an OMZ from the continental margin (e.g. Jenkyns, 1985). Arthur *et al.* (1987) note the shorter duration of organic-rich deposition at the transgressional peak in these shelf areas.

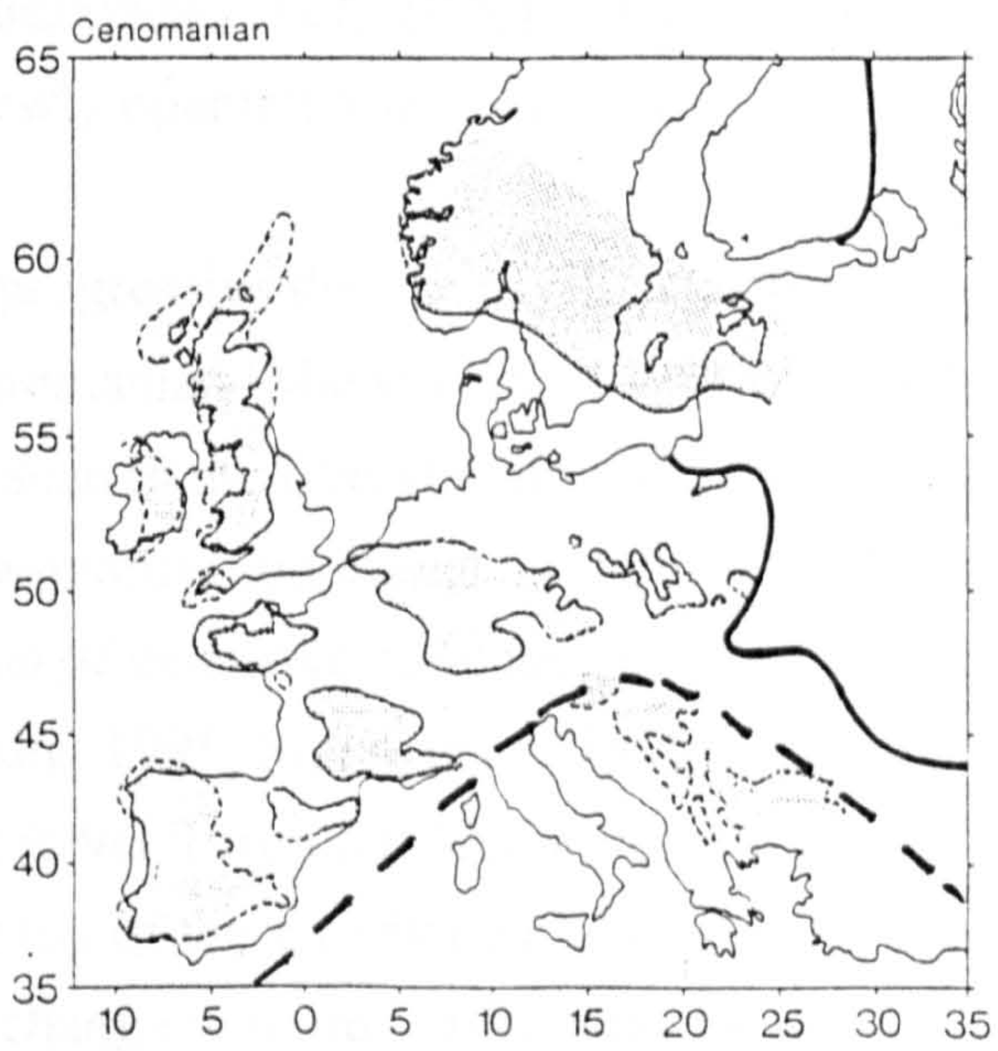

Figure 1.3 Late Cenomanian shorelines (from Tyson & Funnell, 1987) compiled from the literature and plotted on a modern day geographic map. Fine stipple indicates land

area, shorelines are indicated by a continuous line where known, and a pecked line where the stratigraphical attribution is more generalised. Axis numbers refer to modern day latitude and longitude. Lines south of the Alpine front are unreliable, as noted in Tyson and Funnell (1987).

The UK (Buckton Cliff) and German (Misberg) sections studied for this thesis were located at a similar palaeolatitude, 40°N (Fig 1.4; Baudin, 1995).

1.5 The Tethyan Realm

During the Jurassic the land mass known as Pangaea began to break up and formed the two super continents Gondwanaland and Laurasia, separated by the Tethys Ocean. During the Cenomanian the closure of the Neotethys began (Baudin, 1995) and the opening of the North and South Atlantic started. The Tethys probably had a sluggish circulation, due to the narrowing of the North Apulian seaway and its separation from the North Atlantic domain; this favoured the development of anoxic conditions (Philip *et al.*, 1993; Ricou, 1995). Only when the North and South Atlantic fully opened up did deep north-south oxygen-rich currents develop, similar to the ones observed today. These currents replenished oxygen-poor areas of the Tethys (Herbin *et al.*, 1986) and may be one explanation for the disappearance of anoxic conditions and the end of black shale deposition (Tyson & Funnell, 1987). An important palaeogeographic event during the Cenomanian was the marine connection of the Tethys with the opening south Atlantic via the Trans-Saharan seaway; this connected Tunisia to Nigeria and the Benue Trough and the Gulf of Guinea (Reyment & Dingle, 1987; Robaszynski *et al.*, 1990). This connection may have supplied nutrients from the newly opening South Atlantic.

There was a progressive decline in siliciclastic sedimentation in the Tethyan realm during the Cenomanian (Masse *et al.*, 1995), possibly linked with the decline in land masses, as was seen in the Boreal realm. On the northern margins of the African continent the shallow-marine conditions, brought about by the transgressive period, allowed the formation of extensive carbonate platforms which covered the northern shelf of Africa (Baudin, 1995; Masse *et al.*, 1995). The maximum subsidence and transgression during lower Turonian (*Mammites nodosoides* zone) may have lead to the temporary drowning of these carbonate platforms (Philip & Airund-Crumière, 1991) resulting in a change to more argillaceous facies.

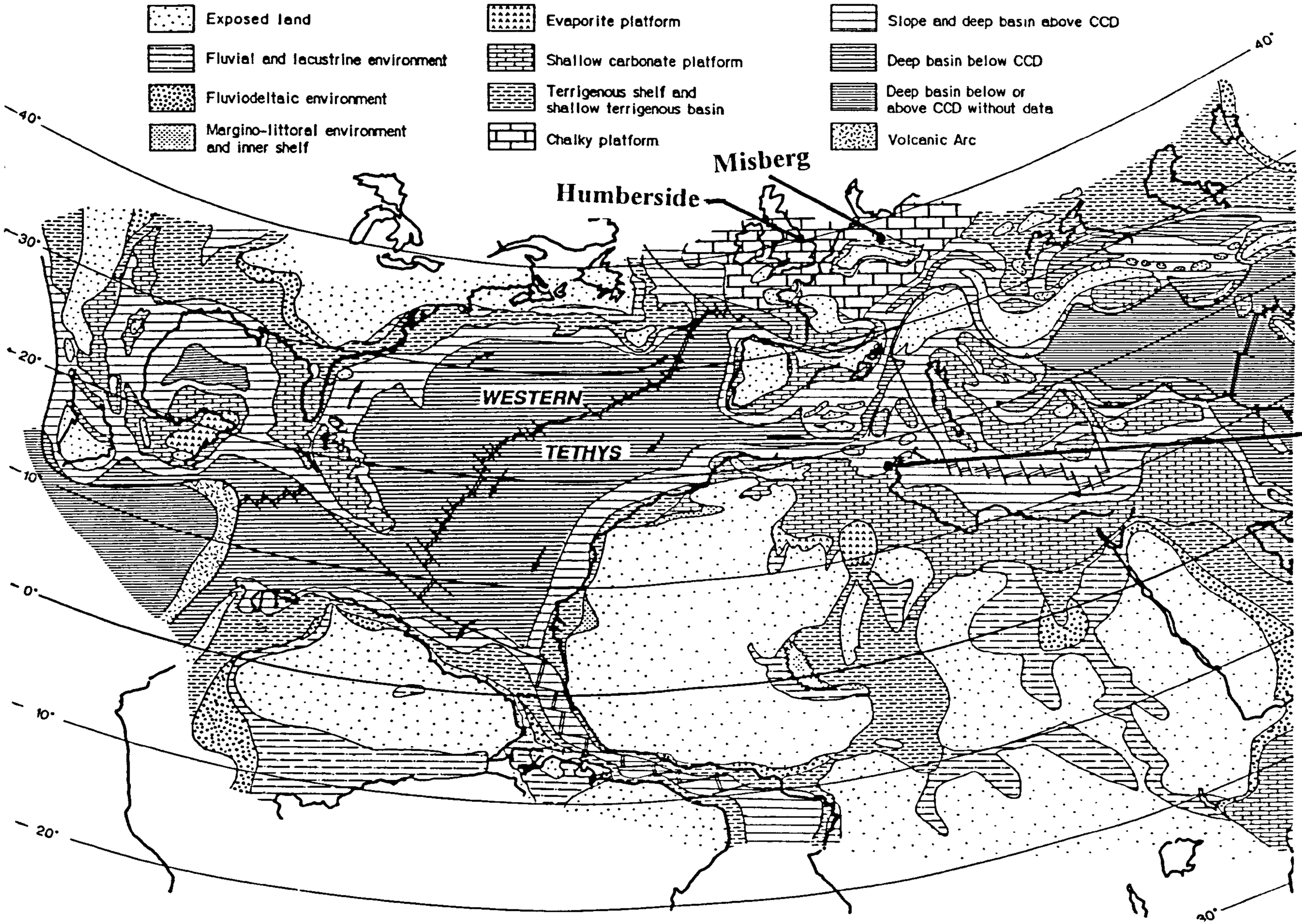

Figure 1.4 Cenomanian palaeogeography and palaeoenvironments of the Cenomanian (from Baudin, 1995). Palaeolatitudes are given at the left side of the diagram. The sections from the Boreal realm lie at approximately 40°N and the sections from the Tethyan realm lie at approximately 18°N.

The Tunisian sections studied were deposited in a slope and deep basin environment (above the carbonate compensation depth) on the northern margin of the shallow carbonate platforms that cover north-eastern Africa at this time (Baudin, 1995). Masse *et al.* (1995) describe the area of deposition for the Tunisian sections as a hemipelagic basin, just north of a carbonate platform. General facies trends can be observed in Tunisia: the Bahloul Formation changes southward from open marine to a neritic limy shelf facies (Burollet *et al.*, 1978). The Tunisian sections studied were located at a palaeolatitude of approximately 18°N during Cenomanian times (Fig 1.4; Baudin, 1995).

1.6 Aims of research

Robaszynski & Gale (1993) called for a multidisciplinary study on typical CTBE sections from the Western Interior, Northern Africa and Europe, two of which are covered by this thesis. Kuhnt *et al.* (1990) also call for better knowledge of the spatial distribution of Cenomanian-Turonian source rocks, to help determine the potential causes of their formation. They highlight the need for a multidisciplinary approach to be incorporated with more biostratigraphic data, to help understand the Cenomanian-Turonian boundary event. It is hoped that in the foreseeable future a situation will develop where there are enough data from different localities in various parts of the world, that they could be used during a session of the International Subcomission on Cretaceous Stratigraphy to decide on a globally acceptable position of the Cenomanian-Turonian boundary.

This study differs from others in that it addresses, in detail, several black shale sections from Tunisia, then compares them with a similar Cenomanian-Turonian section from Germany. Whereas many previous studies have examined smaller numbers of samples from a wide geographical area, and with only a few analytical techniques, this study offers a high resolution multidisciplinary approach to understanding the Cenomanian-Turonian event in Tunisia. The comparison with a German section is significant in that the number and spacing of alternating dark, laminated and light coloured bioturbated beds is similar at Oued Bahloul to those of Misberg, Germany (Schlanger *et al.*, 1987; Arthur *et al.*, 1987); both sections were also deposited over a similar period around 600, 000 years (Arthur *et al.*, 1987).

As the Bahloul Formation, Tunisia, is stratigraphically restricted, and deposited within a shelf, basin slope and carbonate platform environment, it provides an unequalled opportunity to study lateral palaeobathymetric variations within a

potential source rock. The geographical extent of the Bahloul may represent the impingement of an OMZ on the Southern Tethyan margin; this will be tested by examining a number of outcrops from the platform to the deeper water palaeoenvironments. These sections will include samples from the platform/basin (e.g. Oued Bahloul) and the deeper basin area (e.g. Ech Cheid). Local geochemical characteristics will be compared to the global pattern to determine the relation between local anomalies and the global $\delta^{13}C$ excursion. The geochemical characteristics, such as organic carbon maximum, hydrogen index and biomarker distribution of the shales, will be compared to the position of the local $\delta^{13}C$ excursion.

The majority of studies on the Tunisian Bahloul (e.g. Robaszynski *et al.*, 1993b; Maamouri *et al.*, 1994; and Abdallah & Meister, 1997) deal mainly with biostratigraphy, palaeoenvironments, and sequence stratigraphy. Some carbonate isotope work to confirm the existence of the excursion has been carried out by Accaire *et al.* (1996), but none that relates the bulk or molecular geochemistry to the isotope curve. Only recently has an organic carbon $\delta^{13}C$ isotope curve been determined for the Bahloul (Bechtel *et al.*, 1997). This study will present 5 new organic carbon $\delta^{13}C$ isotope profiles for the Bahloul Formation, and demonstrate how they compare to other isotope profiles from Tunisia, and considers their relationship with bulk and molecular geochemistry.

This study has also presented an excellent opportunity to study the effects of the differing palaeoenvironmental and palaeogeographical settings on the composition of kerogen pyrolysates of Cenomanian-Turonian samples. The use of Pyrolysis (Pyrolysis-gas chromatography and Pyrolysis-mass spectroscopy) techniques in the evaluation of palaeoenvironments has not been previously attempted. A high resolution study of a source rock in several palaeoenvironments is useful for testing these pyrolysis techniques. A selection of Cenomanian-Turonian samples from the differing study areas has been analysed to assess the variations in pyrolysate composition. This data has been examined using Principal Component Analysis to help identify trends in the data. Comparisons of the trends were then made with the optical, bulk and molecular geochemistry to assess the influence of palaeoenvironment on pyrolysate composition. To facilitate this approach some comparisons were then made with well characterised source rock kerogens of other palaeoenvironments and geological ages (e.g. Kimmeridge Clay, Jet Rock, Green River Oil Shale).

CHAPTER 2

2. Analytical techniques

2.1 Sample Collection and Preparation

Fresh samples from the Tunisian and UK sections were collected using a hammer and chisel and after removing the top weathered material they were wrapped in aluminium foil to avoid contamination. A record and section log were kept during sample collection. If necessary, selected samples from the complete vertical section were sub-sampled according to any lithological variations, such as sample colour and sedimentary structure. The samples were then cleaned and picked to remove extraneous material and air dried over an oven (ca. 35°C). The samples were described lithologically and their colour determined using a Geological Society of America Rock Color Chart.

The cleaned and dried samples were first coarsely crushed, using a pestle and mortar; approximately 5 grams of 1-2mm diameter fragments were kept for optical analysis and the remainder was crushed to powder in a Tema mill for geochemical analysis.

2.2 Bulk Geochemistry

2.2.1 Total Organic Carbon (TOC), Total Carbon and Total Sulphur

A known weight of powdered sample (typically 100-200mg), was weighed into a porous thimble, and treated with warm (approx. 50°C) excess 18% hydrochloric acid to remove carbonates and then washed with distilled water four times to remove the acid. The thimbles with the decarbonated sample were dried in an oven (approx. 110°C) overnight, then reweighed to obtain the carbonate content by difference. Blank thimbles were run to test that no other weight loss occurred. The samples were analysed in duplicate in a LECO carbon sulphur analyser CS 244 coupled with an HF 100 induction furnace. The values given, total organic carbon and total sulphur, were compared to a reference standard analysed every ten samples to test the calibration.

Non-decarbonated samples were also analysed on the LECO CS 244, to give the total carbon in the samples. Carbonate carbon in the samples was derived by subtracting TOC from the total carbon. The percentage calcium carbonate in the samples is derived by multiplying the carbonate carbon value by 8.33. Both methods

produced comparitive values and the former method was used for analysis throughout this thesis.

2.2.2 Rock-Eval Pyrolysis

A LECO THA-200 was used to provide screening pyrolysis data using the principles described by Espitalié *et al.* (1985a). An aliquot of crushed sample (ca. 100mg) was weighed in to a crucible and then placed in a furnace by an autosampler and heated in a stream of helium gas. The furnace heating programme comprises three phases: in the first phase, the sample was held at 100°C for 1 min while the volatile (gaseous) hydrocarbons were driven off. These were quantified by a flame ionisation detector (FID) and assigned as peak 1 (S0 mg/g sediment). During the second phase the temperature was ramped at 25°C/min to 300°C where it was held for 2 minutes while the semi-volatile free hydrocarbons were driven off to produce peak 2 (S1 mg/g sediment). The temperature was then ramped again at 25°C/min to a final temperature of 550°C, where it was held for 1.5 min. During this third phase the non-volatile organic matter (kerogen) was pyrolysed to generate hydrocarbons which were recorded as peak 3 (S2 mg/g sediment). The temperature at which maximum generation of hydrocarbons occurs during phase 3 was recorded as Tmax (°C). Samples were analysed in triplicate and the average value was taken. The relative difference between the two runs was generally well within 10%.

The TOC and pyrolysis data can be used to derive two other parameters (Espitalié *et al.*, 1985):

1) Hydrogen Index (HI): a measure of the remaining hydrocarbon potential of the kerogen:

$$HI = 100 \times (S2 / TOC)$$

2) Production Index (PI): the ratio of the amount of migrated and already generated hydrocarbons by the kerogen (S1) to the total hydrocarbon yield:

$$PI = S1 / (S1 + S2)$$

2.3 Molecular Organic Geochemistry

2.3.1 Soxtherm Extraction

An aliquot of the crushed rock (typically 30g) was weighed in to a pre-extracted cellulose thimble and then placed in a glass beaker containing an azeotropic

mixture of dichloromethane:methanol (93:7). Activated copper turnings, used to remove elemental sulphur, and anti-bumping granules, to control boiling, were also added to the beaker. The thimbles were placed on a Gerhardt Soxtherm, and extracted for 6 hours (4 hours in boiling solvent and 2 hours above solvent to rinse). The extract was then concentrated using a Buchi rotary evaporator and then half the extract was transferred to a preweighed vial, and the other extract to an unweighed vial. The extract in the weighed vial for each sample was evaporated to dryness using a stream of nitrogen to obtain the amount of total extractable organic matter (EOM) in the sample.

2.3.2 Fractionation: Thin Layer Chromatography

Glass plates (20cm × 20cm) were coated (0.5mm thickness) with Merck Kiesegel 60G. After air drying the plates were then reactivated in an oven (ca. 110°C) for several hours. Before use the plates were pre-eluted with ethyl acetate and then reactivated (ca. 110°C) for several hours. An aliquot (ca. 20mg) of EOM was added to the plate using a plate loader. A standard, consisting of C_{28} *n*-alkane, anthracene and dodecylbenzene in dichloromethane, was also applied to the side of the plate for identification of the bands. The plate was eluted with petroleum ether (b.p. 40-60°C), and when the solvent front was 1-2cm from the top of the plate the plate was removed and the solvent left to evaporate. The bands were visualised by spraying the plate with a methanolic solution of Rhodamine 6G dye Adsorptive Indicator, and viewing under Ultra Violet light. The aliphatic and aromatic bands identified in this way were then scraped from the plate into short glass elution tubes plugged with extracted cotton wool and the hydrocarbon fraction was eluted off into a round bottom flask with 70 ml dichloromethane. The fractions were concentrated on a Buchi rotary evaporator and transferred to vials.

2.3.3 Gas Chromatography (GC)

The separated aliphatic hydrocarbon fractions were analysed on a Carlo Erba 5160 gas chromatograph fitted with an on-column injector, flame ionisation detector and using a fused silica capillary column (30m × 0.25mm i.d.) coated with 0.25μm thick cross-linked methyl siloxane (HP-1). After sample injection the gas chromatograph oven was held at 50°C for 2 minutes then ramped to 300°C at a rate of 4°C/minute where it was held for 20 minutes. Helium was used as the carrier gas (flow approximately 1ml/min, inlet pressure 50kPa). Data acquisition was controlled using a VG Multichrom chromatography data system. The acquired data were stored

on DAT tape for later data processing, integration and printing. Further data processing was carried out using XChrom for Windows NT 4.0 version 2.04k, (Lab Systems plc.).

2.3.4 Gas Chromatography-Mass Spectroscopy (GC-MS)

The aliphatic hydrocarbon fractions were also analysed using a Hewlett-Packard 5890II gas chromatograph linked to a Hewlett-Packard 5972MSD (electron voltage 70eV, filament current 220μA, source temperature 160°C, multiplier voltage 1600V, interface temperature 300°C). Samples were injected using an HP7673 autosampler via a split/splitless injector (held at 280°C) and the split was opened after 1 minute. Separation was performed on a fused silica HP-1 capillary column (50m× 0.32mm id×0.25μm film thickness). The gas chromatograph was temperature programmed from 40-300°C at 4°C/min and held at final temperature for 20 minutes, with helium as the carrier gas (flow approximately 1ml/min, pressure 50kPa, split 10mls/min.). Data acquisition was controlled by a HP Vectra 486 PC chemstation computer, in either full scan mode (50-550amu/sec) or in selected ion mode (30ions, 0.7cps, 35ms dwell). The acquired data was stored on DAT tape for later data processing, integration and printing. Data processing was carried out on Hewlett-Packard Standalone Data Analysis, G1034C software version C.01.05.

2.3.5 Pyrolysis Gas Chromatography (Py-GC)

Kerogen isolates recovered from acid rock digestion (see section 2.4.1.1) were dried using a Buchner vacuum filter (Whatman ® 47mm circular GF/C glass microfibre), to remove the bulk of the water and then air dried over an oven to remove any remaining moisture content. The kerogens were then crushed and homogenised in a pestle and mortar. Approximately 5mg of each kerogen sample was loaded into individual 1.6mm (o.d.) diameter glass capillary tubes which were then loosely plugged at both ends with pre-extracted glass wool. A known volume of a poly-tertiary-butyl-styrene (PTBS) standard solution (1mg/ml dichloromethane) was added to the tube using a microlitre syringe; this was to allow for compound quantification when the results were interpreted. The tube was then loaded into the platinum coil of a CDS120 pyroprobe, and pyrolysed at 810°C for 20 seconds in a stream of helium. The pyroprobe was coupled to a Carlo Erba 5380 gas chromatograph and the pyrolysate was carried onto a fused silica capillary column (30m × 0.25mm i.d.) coated with a 5% phenyl methyl silicone (HP-5). The gas chromatograph was initially cryogenically cooled using CO_2 and was temperature programmed from 0-300°C at 4°

C/min where it was held for 20mins. Helium was used as the carrier gas (flow 1ml/min, pressure 50kPa, split 10mls/min.). Data from the FID were acquired using a VG Multichrom laboratory data system for the UK sections and the Windows based data system XChrom was used for some of the German and Tunisian sampless. The acquired data were stored on DAT tape for later data processing, integration and printing. Further data processing was carried out using XChrom for Windows NT 4.0 version 2.04k, (Lab Systems plc).

2.3.6 Pyrolysis Gas Chromatography-Mass Spectrometry (Py-GC-MS)

The samples were prepared in the same way as for Py-GC (Section 2.3.5), and used identical pyrolysis conditions (CDS coil pyroprobe, pyrolysis at 800°C for 20 seconds in a stream of helium). The pyroprobe was coupled to a Hewlett-Packard 5890 gas chromatograph via a split/splitless injector and the pyrolysate was separated on a fused silica capillary column (30m × 0.25mm i.d.) coated with a 5% phenyl methyl silicone (HP-5). Initially the gas chromatograph was cryogenically cooled to 0 °C using CO_2 and then temperature programmed from 0-300°C at 4°C/min and held at final temperature for 20 mins. Helium was used as the carrier gas (flow 1ml/min, pressure of 50kPa, split at 10mls/min), and the injector split valve was opened 1min after the sample was pyrolysed. The gas chromatograph was coupled with a Hewlett-Packard 5970MSD (electron voltage 70eV, filament current 220μA, source temperature 200°C, multiplier voltage 2500V, interface temperature 300°C). Acquisition was controlled by a HP 9000/216 chemstation computer either in full scan (50-550 amu/sec) or in selected ion mode (20 ions 0.7cps 35ms dwell) for greater sensitivity. The acquired data was stored on DAT tape for later data processing, integration and printing.

2.3.7 Pyrolysis Mass Spectrometry (Py-MS)

Kerogen isolates recovered from acid rock digestion (section 2.4.1.1), were homogenised using a pestle and mortar, and a known weight of sample (typically 0.3 to 1mg) was added to a 770°C curie point PyMS foil (Horizon Instruments Ltd.). A known amount (5μl) of PTBS standard solution (1mg/ml) was then added to the kerogen, and the foil was crimped to hold the sample. The foil was placed 1cm inside a small glass tube using tweezers and was then plugged with Quartz (silica) wool. A Viton rubber O-ring was placed 4-5mm onto the end of the glass tube to allow a seal to form in the pyrolysis chamber. The samples were analysed on a Horizon Instruments Ltd. RAPyD-400 (electron voltage 86eV, source temperature 200°C,

multiplier voltage 1840V, mass range m/z 51-200) by Mr Clive Hetherington, previously of the Biomedical Mass Spectroscopy Unit, in the Dental School, Framlington Place, Newcastle University. Data were acquired by RAPYD, a DOS based software package (Horizon Instruments Ltd.) and was then converted into Windows Excel format for further processing.

2.4 Optical Methods

2.4.1 Vitrinite Reflectance

An aliquot (ca. 0.5g) of the 1-2mm crushed sample (section 2.1) was placed in a small plastic cup and covered with liquid polystyrene resin (BUEHLER, Metset resin, Type SW, with Metset hardener). When the resin had sufficiently hardened the blocks were initially ground, to expose rock fragments on a diamond lap, using water as a lubricant. This was followed by fine grinding on carborundum papers, using propan-2-ol as a lubricant. The blocks were finally polished using three grades of alumina powders (Gallenkamp Griffen, 3/50, 5/20 and gamma grade alumina), also using propan-2-ol, until a suitable reflecting surface was achieved. Using a Carl Zeiss reflectance microscope the reflectance of the vitrinite was measured against known reflectance standards, and recorded on a pen chart. The vitrinite reflectance work was carried out by Dr. J. M. Jones.

2.4.2 Kerogen Isolation

Because the presence of a rock matrix can have an effect on the composition of the kerogen pyrolysate (Espitalié & Bordenave, 1993), the pyrolysis was carried out on isolated kerogens. Three acid digestion methods were tested to determine their effects on the pyrolysate composition, the results of which are given in Section 7.2.2.

Method 1

The first kerogen isolation technique (also used for palynological work) involved 1-2 mm size rock fragments being treated in Teflon beakers with excess 8% hydrochloric acid (HCl) for 12 hours to remove carbonates. The excess acid was decanted off, then the sample was diluted with distilled water and decanted again; this dilution and decanting was repeated twice. The sample was then treated with 40% cold hydrofluoric acid (HF) for 24 hours, to dissolve the silicates. The HF was then diluted and decanted off, and dilution and decanting was repeated as above. The

sample was further washed with excess 8% HCl for 12 hours, to remove fluorides, followed by decantation and dilution as above. The kerogen was washed with distilled water and sieved with a 10 μm nylon mesh, to remove fine debris. The kerogen was then stored in distilled water for use in palynofacies observations.

Kerogens used for pyrolysis work were dried in air over an oven (ca. 50°C) to remove any water, then homogenised. Finally, the kerogens were extracted in a Gerhardt Soxtherm with a 93:7 mix of dichloromethane:methanol for four hours to remove any free hydrocarbons.

Method 2

The second technique used sediment crushed to powder in a Tema mill, which was extracted on a Gerhardt Soxtherm (method as above) and then the kerogen was isolated by the same palynological technique described in Method 1. The resulting kerogen did not need to be homogenised, but was re-extracted in solvent in the same way as before.

Method 3

The third kerogen isolation method follows that of Jones (1980), using crushed and extracted sediment. In a Teflon beaker, excess 8% HCl was added to the sample and then stirred cold on a stirrer/heater for 24 hours, then hot (ca. 50°C) for 8 hours. The fluid was decanted off and the sample was diluted with distilled water and then centrifuged and decanted again, HF was then added to the sample to the sample and stirred hot (ca. 50°C) for 24 hours. The solution was then neutralised (to stop the action of the HF) with excess saturated boric acid and stirred for 30 mins. This solution was decanted and then washed and centrifuged twice with distilled water and decanted again. Following this, 2% HCl was added and stirred hot (ca. 50°C) for two hours, followed by decanting and washing with hot distilled water and then centrifuging and decanting again. A solution of saturated ammonium carbonate (to neutralise the HCl) was added, followed by an equal volume of hot distilled water; this was then centrifuged and decanted. An equal volume 8% HCl was then added, followed by centrifugation and decanting, and this procedure was repeated three times. The remaining kerogen was washed and centrifuged three times in hot distilled water. The kerogen was centrifuged for 20 minutes, any remaining fluid decanted and the kerogen air dried over an oven (ca. 35°C). Finally the kerogen was re-extracted in solvent in the same way as the above methods.

2.4.3 Kerogen Analysis

Microscopical analysis of kerogen used the isolated material from Method 1 (Section 2.4.2). A small amount (ca. 5 drops) of the kerogen dispersed in distilled water is dropped from a pipette onto a coverslip and left to dry overnight at room temperature; the cover slip was then mounted to a slide using Elvacite™ (Du Pont) as the recommended mounting medium (cf. Barrs & Williams 1973, p.20). The slides were examined on an Olympus BH-2 microscope. Approximately 300 kerogen particles were counted per slide. The count was recorded into groups of phytoclast type (e.g. brown or black woody material), palynomorph type (e.g. spores, pollen, and dinoflagellate cysts etc.) and Amorphous Organic Matter (AOM). The data were then recalculated into three major categories:- amorphous organic matter (AOM), palynomorphs, and phytoclasts (terrestrial or other macrophyte debris). A further count (100 particles) made on the palynomorph fraction only was carried out on some of the samples; the dinoflagellate cysts were split into 3 subgroups bases on their morphology: chorate (those with spines), proximate (those without spines), and cavate (double walled cysts). Pollen were divided into bisaccate and others. Acritarchs and prasinophytes were also counted.

The degree of preservation of the kerogen was measured using transmitted white light and incident blue light fluorescence under a ×20 air objective. Differences in preservation were identified using the fluorescence preservation scale previously developed by Tyson (1995; Tuweni & Tyson, 1994). Palynomorph fluorescence (intensity and colour) were also identified using incident blue light fluorescence and a ×20 air objective.

2.4.4 Kerogen Oxidation

A sub-set of kerogens, which on microscopical examination, were found to be AOM-dominated (>90% AOM), were oxidised (based on the method in Traverse, 1988) to remove the AOM so that further study of the palynomorphs could be facilitated. An aliquot of kerogen was placed in a plastic beaker and a 2% solution of potassium hydroxide was added (ca. 30mls) and the beaker then placed in an ultrasonic bath for 30 seconds. The solution was sieved through a 10 μm nylon mesh to remove the potassium hydroxide; this solution turns brown when removing the dissolved organic matter. The remaining particulate organic matter was rinsed with distilled water to remove the potassium hydroxide, and stored for later use. The kerogen was then mounted the same way as in section 2.4.2.

2.5 Inorganic Geochemistry

2.5.1 X-ray Diffraction (XRD)

The XRD was used only on the Buckton Cliff samples in order to correspond to some earlier MSc work and also to help quantify a carbonate determination method developed by Bryn Jones, Department of Fossil Fuels and Environmental Geochemistry, Drummond Building, University of Newcastle, NE1 7RU. Approximately 1 gram of crushed sample was loaded into an aluminium back-filled cavity mount. The samples were run on a Philips PW1710 X-ray Diffractor using SIE 122D software within a Windows environment. Samples were scanned from 3° to 80° at a scan speed of 0.02°/S. Acquisition and processing of the data were performed using XRD Traces software run within a Windows environment. Mineral peaks were identified using published data (Bayliss *et al.*, 1980).

2.5.2 Isotope Geochemistry

Approximately 1 gram of powdered sediment was washed with hot (ca. 50°C) 8% hydrochloric acid in Milli-Q^{50} ultra pure water Millipore, for 24 hours to remove all the carbonate. The solution was then filtered, using a Buchner flask, through a Whatman® 47mm circular GF/C Glass Microfibre Filter (preheated to 420°C to remove any traces of organic matter); the sediment was rinsed repeatedly with Milli-Q^{50} ultra pure water. The remaining sediment was air dried over an oven (ca. 35°C), and the dried sediments then homogenised in a pestle and mortar. The decarbonated sediments were weighed into tin capsules which were then. Samples weights were chosen so that the weight of carbon in each sample was approximately equal to the weight of carbon in the laboratory standard. The $\delta^{13}C$ composition of the standard, relative to PDB, was known. The samples were analysed on a Europa Scientific ANCA instrument. A reference standard (flour, 40% carbon, -24.3‰ PDB standard) was analysed once every four samples for calibration and at the end of the autosampler run. The samples were pyrolysed at 1500°C and the pyrolysate was transferred to a mass spectrometer where the relative amounts of the carbon isotopes were measured according to their fragment pattern. The samples were analysed by Mr Clive Hetherington previously of the Biomedical Mass Spectroscopy Unit, Newcastle University.

2.6 Statistical Analysis

2.6.1 Principal Component Analysis (PCA)

Principal Component Analysis was carried out on peak area data from Py-GC, GC-MS and Py-MS. There data were analysed using the Factor Analysis tool in SPSS for Windows; the results were then converted to principal component analysis data in an Excel spreadsheet. These results were compared with another principal component analysis statistical programme (written by P. Yendle, University of Bristol) and the results were found to be the same. Data were normalised to 100% for each sample, to avoid concentration differences between samples, autoscaled and centred within the program prior to statistical analysis (see Davies,1986, for a full description of PCA).

2.6.2 Constrained Cluster Analysis

Constrained Cluster Analysis was carried out using the DOS based MVSP software package, version 2.1. This package clusters together samples for a section based on the relative similarity of stratigraphically adjacent samples. Unlike normal hierarchical clustering, constrained clustering keeps the data in stratigraphical order when producing the dendrogram. Consequently the dendrogram can be objectively used to subdivide the sections into units based on quantitative data. Bulk geochemical data for each section were normalised, due to differing numerical magnitudes of the data, then run in MVSP using "Squared Euclidean Distance" as the similarity measure and "Unweighted Pair Group" as the clustering Method (see Kovach 1989, 1993; Kovach & Batten 1994, for a full description of Constrained Clustering Analysis).

2.6.3 SPSS for Windows

SPSS is a Windows based statistical package and was used during this work to plot data, calculate regression statistics, and descriptive statistics for the units identified from Constrained Cluster Analysis (Section 2.6.2).

CHAPTER 3

3. The Black Band, Humberside, UK.

3.1 Stratigraphy

The Black Band is a distinct dark-coloured, carbonate-rich shale of approximately 4-10cm thickness, which occurs within the lowermost marl band of the Lower Turonian Welton Chalk Formation, and is thought to be the equivalent of the Plenus Marl Member found in South East England and the Plenus Marl Formation of the North Sea (Deegan & Scull, 1977).

The earliest account of the lowermost part of the Welton Formation was given by Judd (1867) who reported a "Fuller's Earth" at this horizon. Rowe (1904) discussed a locally known "Black Band" at Speeton (TA1900 7447) which was regarded as the Yorkshire equivalent of the Plenus Marls. Then Jefferies (1963) divided this unit into eight beds based on lithology and fossil content from the section at Mersham Lime Works, Surrey. However, Jefferies could not trace his standard Plenus Marls succession further north. He did, however, show that the "sub-Plenus" erosion surface was lateral to the erosion surface that underlies the Welton Chalk Formation in the northern regions. Evidence from foraminifera (Hart & Bigg 1981) and carbon isotopes (Schlanger *et al.*, 1987) has led to the interpretation that the shales of the Black Band are stratigraphically higher than the Plenus Marls. Jeans *et al.* (1991) and Pomerol and Mortimore (1993) gave an alternative interpretation that the Black Band corresponds to part of the upper Plenus Marls. In southern England the "black shales" are not observed in the outcrops reported by Jeans *et al.* (1991) where they are replaced by organic-poor marls.

A full lithostratigraphical review of the Black Band and the Plenus Marls is given in Dodsworth (1996). The Black Band is thought to be one of the many stratigraphic units deposited globally during the Cenomanian Turonian Boundary Event (CTBE), 90.5-91.5 m.y.a. Jefferies (1963) suggests that the Black Band is probably of lowest Turonian age as it incorporates the *Actinocamax plenus* subzone. However, work by Dodsworth (1996) constrains the Black Band to the latest Cenomanian based on dinoflagellate work. This chapter covers work done on the Black Band mostly from the Buckton Cliff locality, but also includes some new isotope geochemistry on the South Ferriby samples (cf. Barrett, 1994).

3.2 Locality

The Black Band outcrops in Yorkshire, Humberside and Lincolnshire (Fig. 3.1) with well known localities including Swallow Vale (174 043), Irby Dale (1923 0518) and South Ferriby (9930 2030). The outcrop at South Ferriby is part of a large quarry operated by Rugby Cement and exposes the lower 11m of the Welton Chalk Formation with the Flixton Member including the Black Band at its base. This succession is the type locality of the Black Band where it is approximately 8cm thick and includes a central 2cm laminated "black shale"; most previous studies have been on samples from this locality (Schlanger *et al.*, 1987; Farrimond *et al.*, 1990; Barrett, 1994).

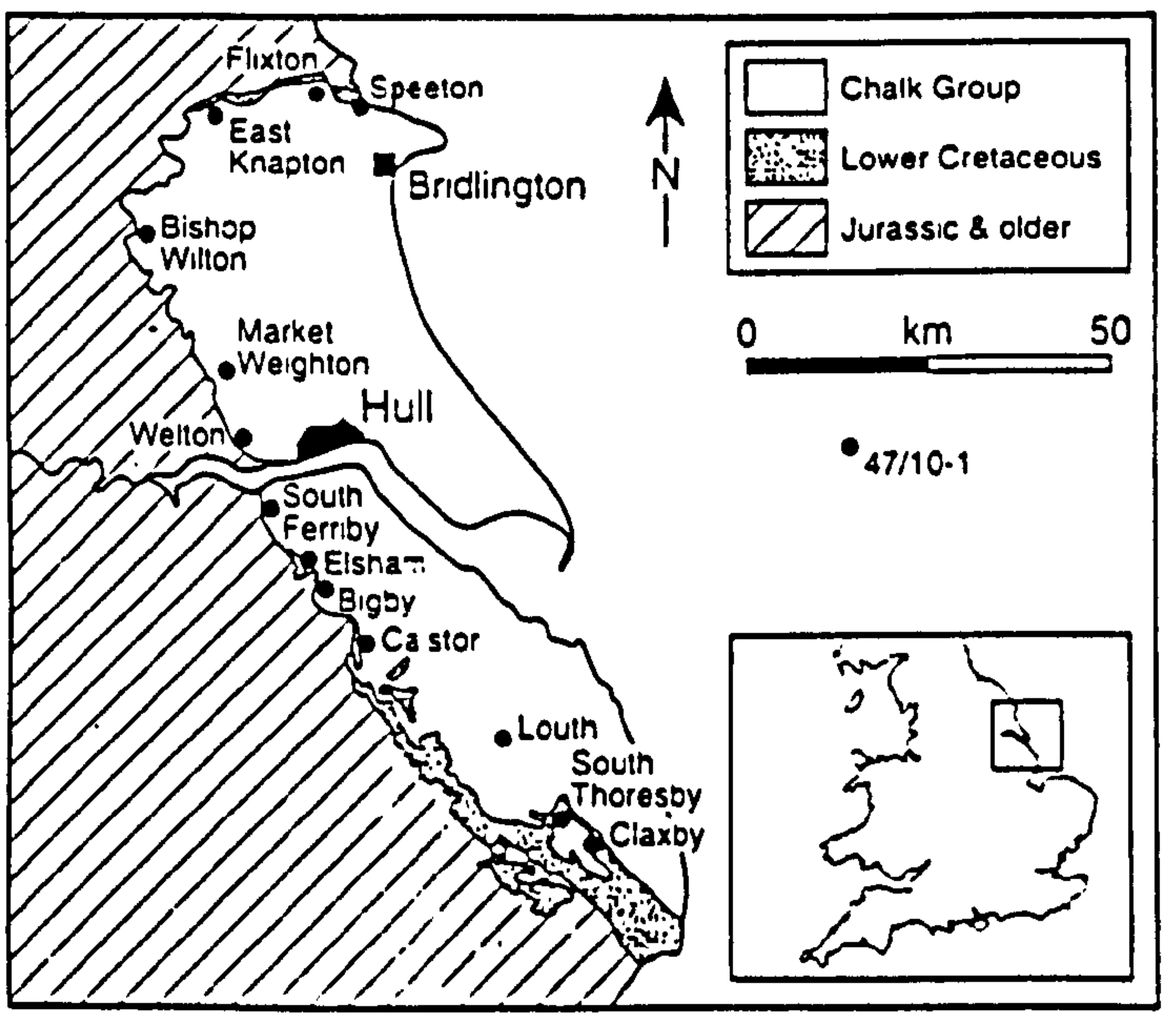

Figure 3.1 Locality map for the Buckton Cliff and South Ferriby sections (from Dodsworth, 1996). The Buckton Cliff section is located near Speeton.

The Black Band also outcrops on the coast at Buckton Cliff near Speeton, 34 miles north of South Ferriby. It occurs at beach level in a huge slipped block and can only be reached with difficulty. Here the band is only 7.5cm thick and comprises 3cm of "black shales" overlain by 4cm of clays, enveloped by bioturbated, glauconitic, hardground chalks below and hard bioturbated chalks above. The band shows lateral changes in thickness over several metres of exposure, and in some parts it is almost totally squeezed out; this is probably due to tectonic activity or possibly associated with the cliff failure.

3.1.3 Previous Work

The huge contrast between the black laminated shale and the heavily bioturbated pale clays above and below the Black Band, and the high smectite content of the clays originally led the Black Band to be interpreted as a layer of volcanic ash (Hallam & Sellwood, 1968).

Previous work on the Black Band has mostly concentrated on single samples from the darkest central part of the band at South Ferriby. Palaeontological studies by Hart and Bigg (1981) constrain the Black Band to the *Whitienella archeocretacea* zone; they also observed that ostracoda were rare but dinoflagellate cysts very common, although of low diversity. Hart and Bigg (1981) also found that sporomorphs are rare and strongly dominated by bisaccate pollen. The rarity of pollen and spores indicates that there was little terrestrial organic matter being transported into the area of deposition. The presence of a rich calcareous nannoflora in the Black Band was thought to indicate nutrient-rich surface water in the area of deposition. Hart and Bigg (1981) noted the absence of planktonic foraminifera within the Black Band and their replacement by a low diversity benthic fauna.

Marshall and Batten (1988) identified the dominant dinocysts in the central Black Band as *Cyclonephelium compactum, C. membraniphorum, C. distinctum* and *Spiniferites spp*. A paler sample from nearer the top of the band had a more diverse assemblage with the proportion of *Cyclonephelium* reduced and *Spiniferites* increased.

Work done on the Cenomanian-Turonian anoxic event in Europe by Farrimond *et al.* (1990b) included only two samples from the Black Band: one sample each from the Buckton Cliff and South Ferriby locations. The samples they analysed were a laminated, central dark grey shale from South Ferriby with a TOC of 2.4%, a sulphur content of 0.1% and a calcium carbonate content of 56%, and a laminated, black shale from Buckton Cliff with 13% TOC, 0.4% sulphur and a calcium carbonate content of 24%. Bulk geochemical and biomarker data suggested both samples were of low maturity. From gas chromatography and gas chromatography-mass spectrometry they identified the organic matter input as marine algae, particularly dinoflagellates (identified from abundant 4-methylsteranes); a low terrestrial input was also determined, and some bacterial input evident from various methanogens.

Controversy about the organic matter input of the Black Band was introduced by Jeans *et al.* (1991), who described the amorphous matter of the Black Band as not

purely algal/bacterial (cf. Farrimond *et al.*, 1990b) but also finely divided ligno-cellulosic amorphous material of terrigenous derivation based on a combination of Rock-Eval and UV-excitation/fluorescence microscopy. This was not identified from conventional organic geochemical (biomarker) analysis of the EOM (Farrimond *et al.*, 1990b). Jeans *et al.* (1991) suggested deposition in a shallow sea, with input of plant material transported under strong oxidative conditions followed by deposition in a dysoxic environment, that preserved a small but variable amount of algal and bacterial matter. Their study was partly based on a single sample from the centre of the band at South Ferriby, with a calcium carbonate content of 58%, a TOC of 3.04%, and a hydrogen index of 43, which would normally imply a very oxic depositional environment.

Barrett (1994) and Barrett *et al.* (1995) reported results on a suite of 20 samples from the Black Band at South Ferriby, attributing its origin to increased organic carbon preservation and possibly productivity. Two peaks in TOC (Fig. 3.2) were identified, the lower one with a TOC of 1.6% and the upper one with a TOC of 4.0%, separated by a pale coloured bed with 0.5% TOC. The hydrogen indices of the section were low (<142 mgHC/gTOC; Fig 3.2); however, the kerogen isolate hydrogen index value was 367 mgHC/gTOC, suggesting a significant matrix adsorption effect even at TOC values of 4%. The hydrogen indices and S2 v. TOC data suggested a Type II/III to Type III kerogen for the section. Carbonate values were generally quite high (52 to 76%; Fig 3.2) and the TOC values are not affected by carbonate dilution. There was some apparent variation in maturity through the section based on biomarker and bulk geochemical data, the organic-lean beds generally yielding higher maturities. Amorphous organic matter input varies through the section with increased algal steroid input where the TOC is found to be highest; the proportion of terrestrial material is relatively constant but typically minor through the sequence, dinoflagellates dominate the palynomorph fraction, which varies in relation to AOM. Gas chromatography also indicates algal and terrestrial inputs and also possible alkenone (coccolith input) not surprising in a carbonate-dominated regime. The presence of methanogenic bacterial activity is suggested from the observation of lycopane co-eluting with nC_{35}. Conditions were dysoxic to anoxic for only a short interval (in the black shale core, where bioturbation is absent and laminations are seen) and O_2 concentrations were approximately ≥0.2 ml/L for most of the unit (based on the presence of bioturbation).

Schlanger *et al.* (1987) report $\delta^{13}C$ carbonate data for the Black Band at South Ferriby; the greatest excursion (4.1‰) occurs just before the organic carbon maxima

observed by Barrett (1994). The $\delta^{13}C$ "spike" is restricted to the *Whitienella archeocretacea* zone which marks the Cenomanian-Turonian boundary between the *Rotalipora cushmani* and *Praeglobotruncana helvetica* zones.

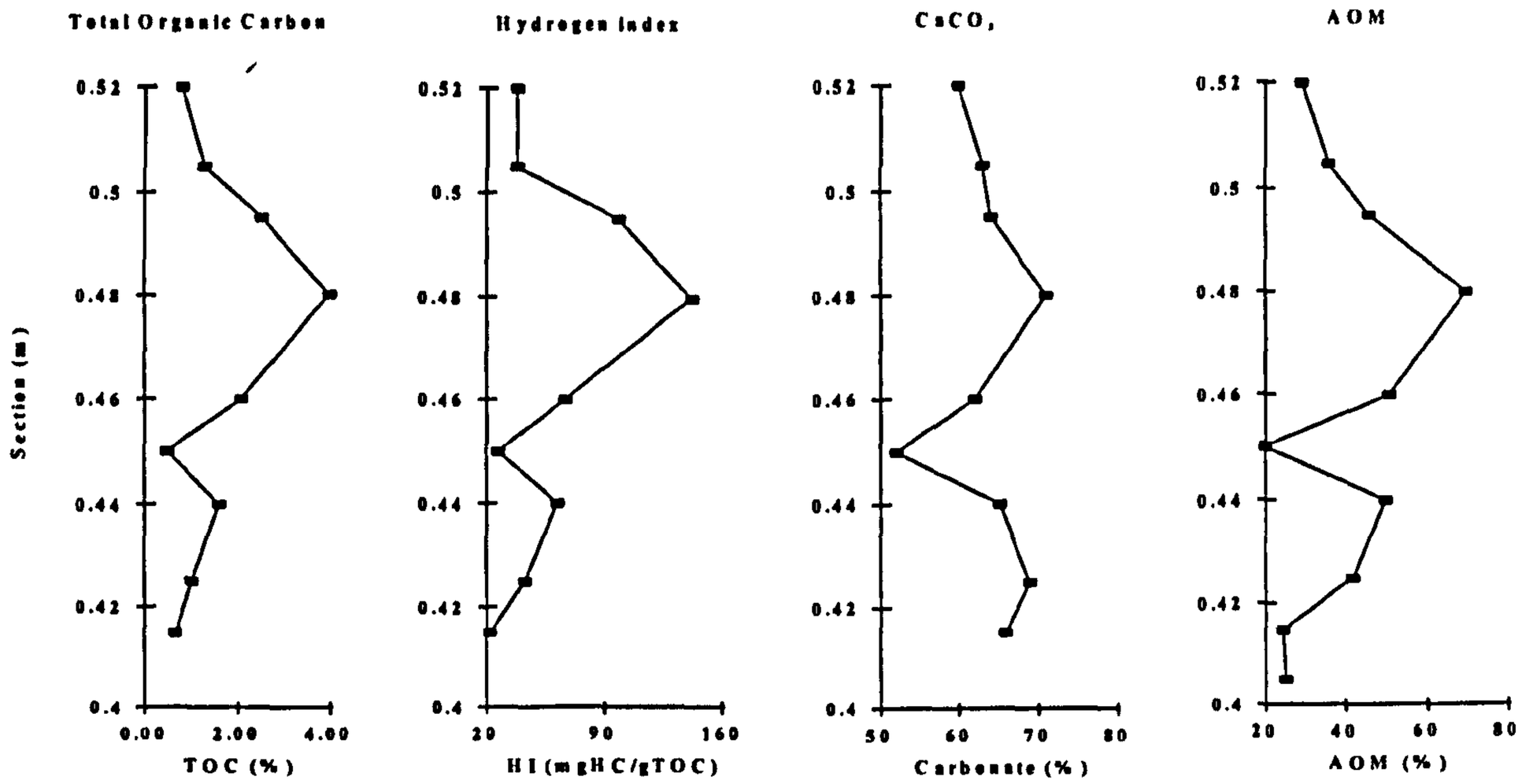

Figure 3.2 Stratigraphical plots of bulk geochemical parameters from the South Ferriby section (Barrett, 1994).

Based on faunal assemblages the Welton Chalk Formation and the marl (including the Black Band) are thought to have been deposited as pelagic shelf sediments in a relatively shallow epicontinental sea, no more than a few hundred metres deep (Jenkyns, 1985).

3.1.4 The Samples

Five samples were collected from the Buckton Cliff locality for bulk geochemistry, isotope geochemistry, molecular geochemistry and microscopy analyses; the results are presented here. The samples previously collected from South Ferriby (Barrett, 1994) were further studied to determine the isotopic signature of their kerogen. Lithological descriptions are given in Appendix 1, Table VIII.

3.2 Results

3.2.1 Bulk geochemistry

Bulk geochemistry results for Buckton Cliff are given in Appendix 1, Table VIII. The TOC values range from 0.5% in the clays to 2.4% in the "black shale"; whole rock hydrogen indices (mgHC/gTOC) are very low 20-99, and carbonate contents range from 12% to 70% (Fig. 3.3). There is a positive correlation of TOC

with hydrogen index, S2 and carbonate content values (Fig. 3.4). Rock-Eval pyrolysis and TOC analysis of a kerogen isolate of sample BC4, produced hydrogen index of 330 mgHC/gTOC, compared with the 99 mgHC/gTOC from whole rock pyrolysis. This indicates that a substantial amount of hydrocarbons (>70%) are retained during pyrolysis of these samples in the presence of the mineral matrix.

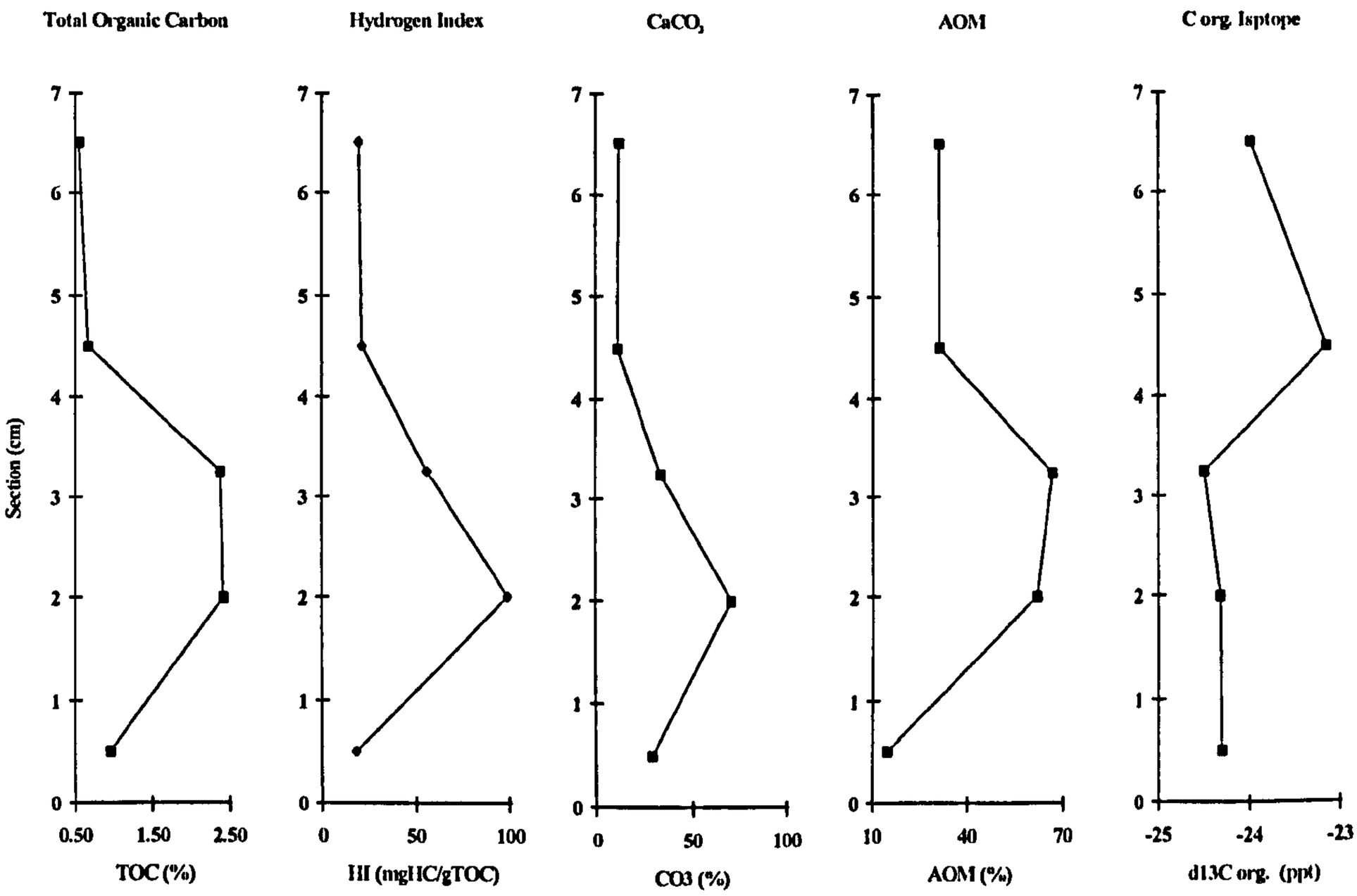

Figure 3.3 Stratigraphical plots of mean bulk and isotope geochemistry data for the Buckton Cliff section (data given in Appendix 2, Table I and Appendix 3, Table II).

3.2.2 Isotope geochemistry

The positive $\delta^{13}C$ isotopic excursion that is associated with the Cenomanian-Turonian Boundary Event (e.g. Schlanger *et al.*, 1987) is clearly observed in the Buckton Cliff section (Fig 3.3; Appendix 2, Table I) where the kerogen $\delta^{13}C$ shows an excursion from -24.5 to -23.1‰ (PDB), a positive shift of 1.5‰; however, no data were obtained for the limestones above and below the Black Band, whose kerogen may yield more negative isotope values. The organic matter $\delta^{13}C$ values for the central black shales of the South Ferriby section (Fig. 3.5) range from -26‰ to -22.7‰; however, these samples do not include the underlying and overlying chalk lithologies which may contain the onset and termination of the excursion.

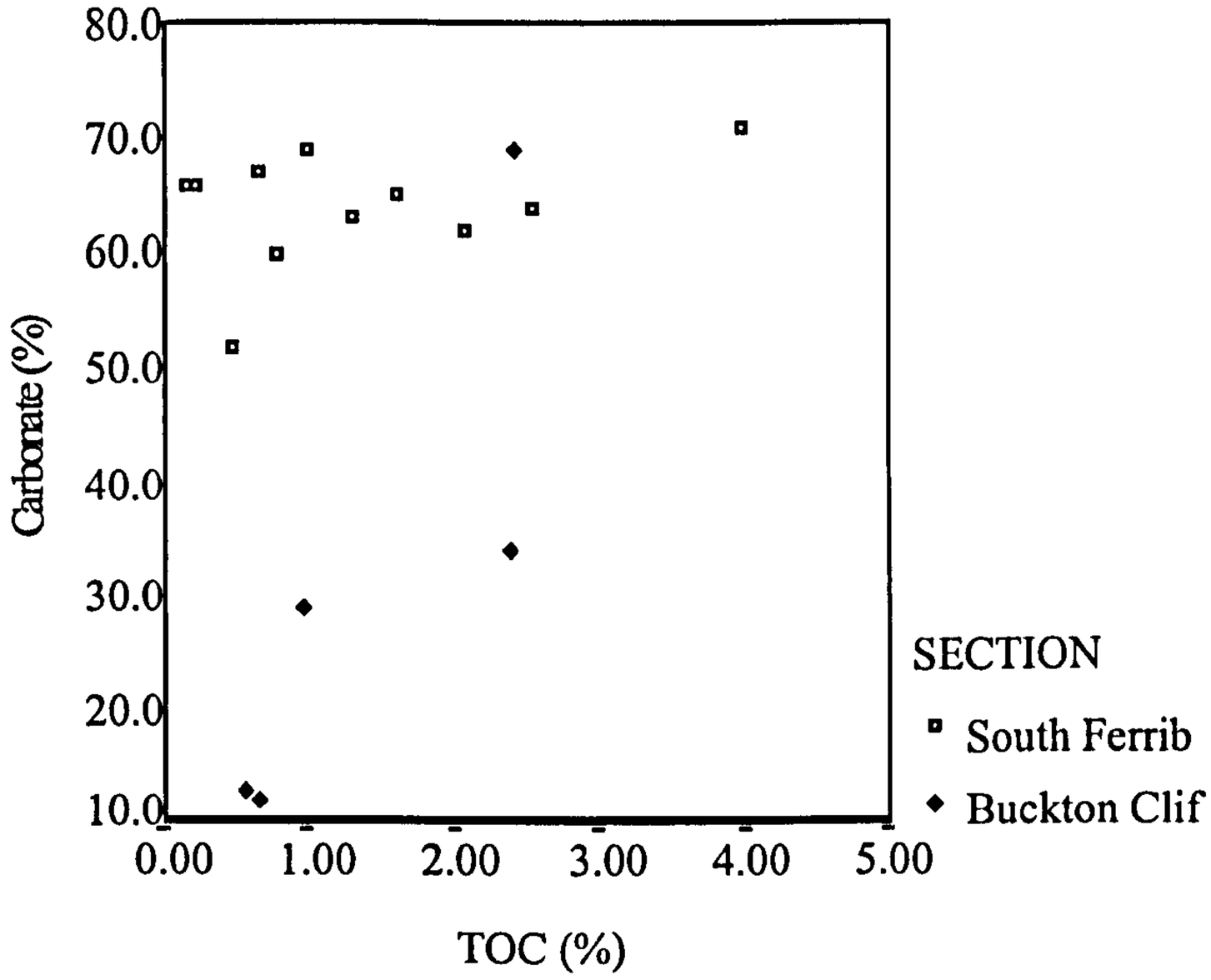

Figure 3.4 Cross plot of TOC versus carbonate data for the UK sections. The Buckton Cliff section shows some apparent correlation $r^2 = 0.69$ where as the South Ferriby section shows a poor correlation $r^2 = 0.14$.

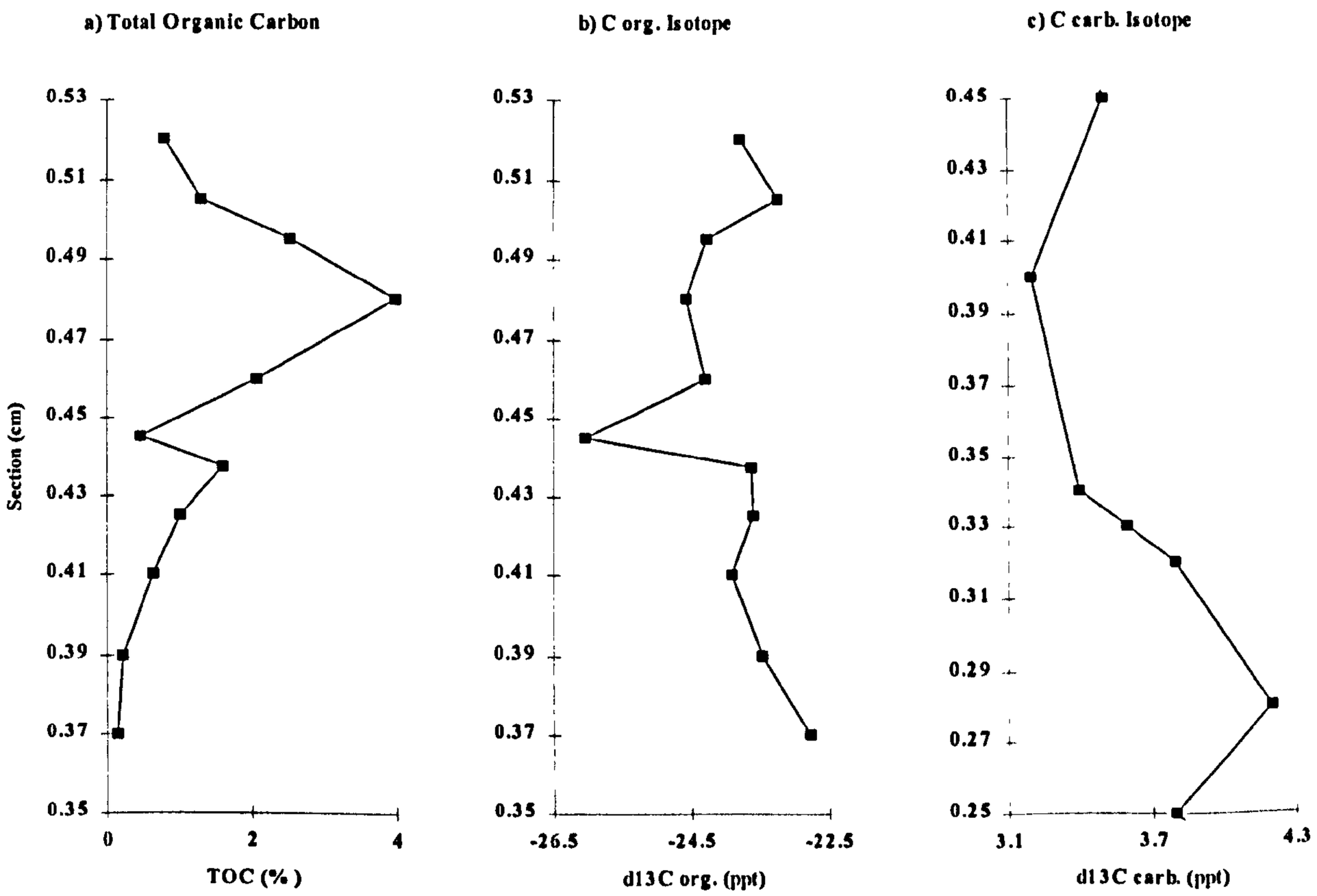

Figure 3.5 Comparison plot of TOC and isotope data for the South Ferriby section. a) Total Organic Carbon; b) kerogen carbon isotope values, (the pattern for the sample at 0.445cm suggests a dramatic change in conditions); c) carbonate isotope values (from Schlanger *et al.*, 1987; section depth are measured differently but represent the same beds). NB: organic matter and carbonate curves follow a similar trend for this part of the section.

3.2.3 Microscopy

Palynofacies observations (Appendix 3, Table II and III) show that marine-derived amorphous organic matter (AOM), with a dull to bright yellow/orange fluorescence, is generally dominant (≤66%) in the black shales, but is less abundant and less fluorescent in the organic lean samples. The relative abundance of AOM is positively correlated with TOC, S2 (Fig. 3.6) and hydrogen index. Dinoflagellate cysts dominate the palynomorph fraction (66-93%; Appendix 3, Table III), the majority of which are proximochorate cysts (>62% of the total cysts); lower dinocyst abundances occur in the organic-rich samples (BC3 and BC4), where the relative abundance of acritarchs is higher (<19%). There is a higher terrestrial content in the "outer" samples (BC1, 2 and 5), with phytoclasts representing >48% of the kerogen particles.

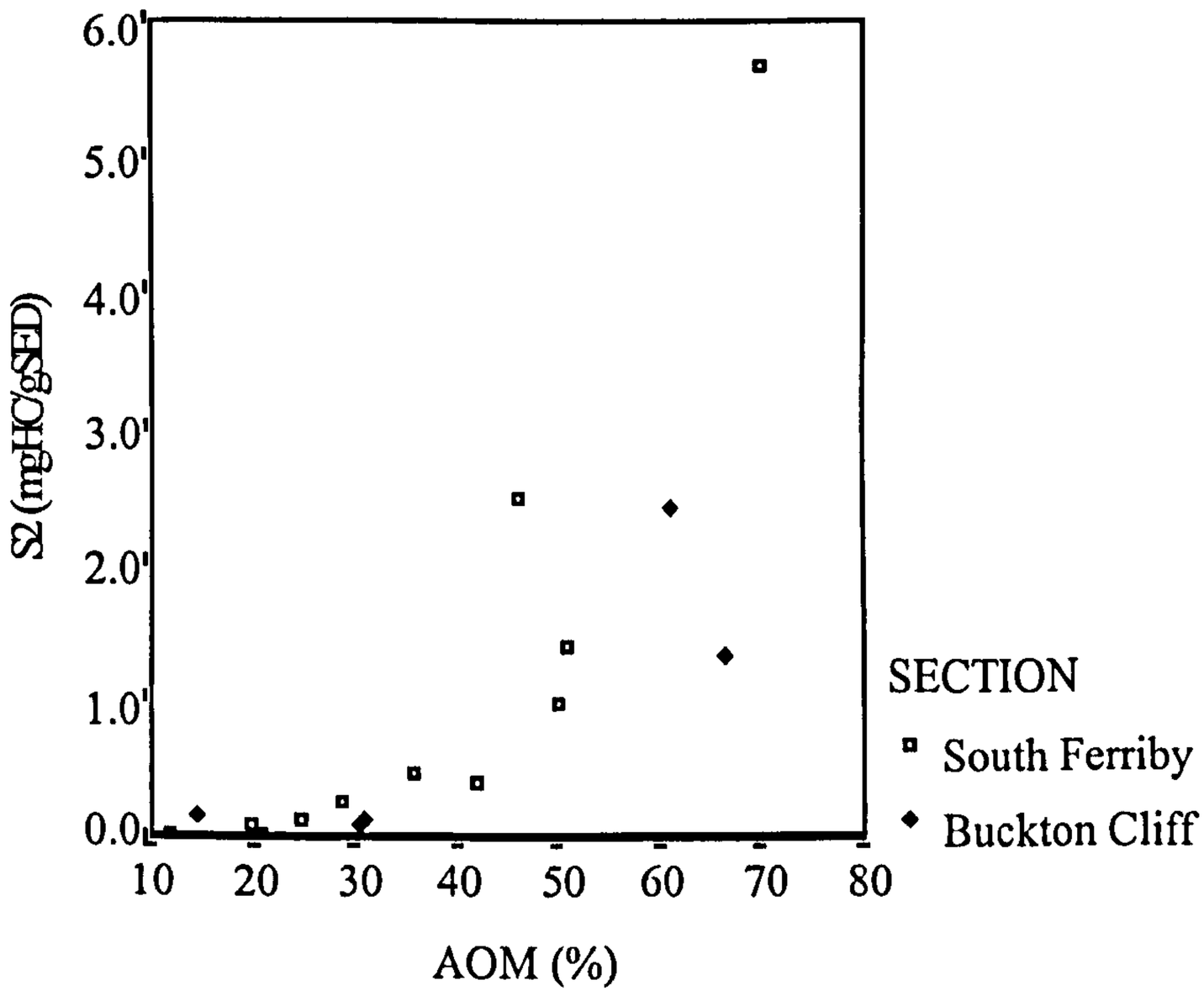

Figure 3.6 Cross plot of S2 versus AOM data for the UK sections. The data shows a good linear correlation: Buckton Cliff, $r^2 = 0.71$; South Ferriby, $r^2 = 0.70$; combined, $r^2 = 0.60$; but they show a better quadratic correlation: Buckton Cliff , $r^2 = 0.73$; South Ferriby, $r^2 = 0.90$; combined, $r^2 = 0.70$.

The vitrinite reflectance for the South Ferriby (SF) and Buckton Cliff (BC) sections (Appendix 3, Table I) determined by Dr Mick Jones were 0.28% Ro and 0.37% Ro (samples SF and BC respectively). However, the confidence level assigned to the determination of this data was low due to the rarity of the vitrinite in the samples.

3.2.4 Molecular geochemistry

The Extractable Organic Matter (EOM) content of the Buckton Cliff samples (Appendix 4, Table I) correlates well with TOC and hydrogen indices. Observations from gas chromatograms (Fig. 3.7) of the aliphatic fraction and molecular geochemistry data from the Buckton Cliff samples are recorded in Appendix 4, Table I. The *n*-alkane distribution ranges from nC_{14} to nC_{35} in sample BC4; however, due to a large unresolved complex mixture (UCM) in all samples, it is difficult to say whether this is typical for the section. The large UCM indicates that either branched and cyclic alkanes and biomarkers (e.g. hopanoids, steroids etc.) are showing through in great abundance masking the *n*-alkane distribution, or that weathering has had a great effect (e.g. Alexander, 1983; Volkman, 1986), preferentially removing some of the *n*-alkanes. The isoprenoids pristane and phytane are generally dominant over the *n*-alkanes, and the Pr/Ph ratios for each sample are all greater than 1.0.

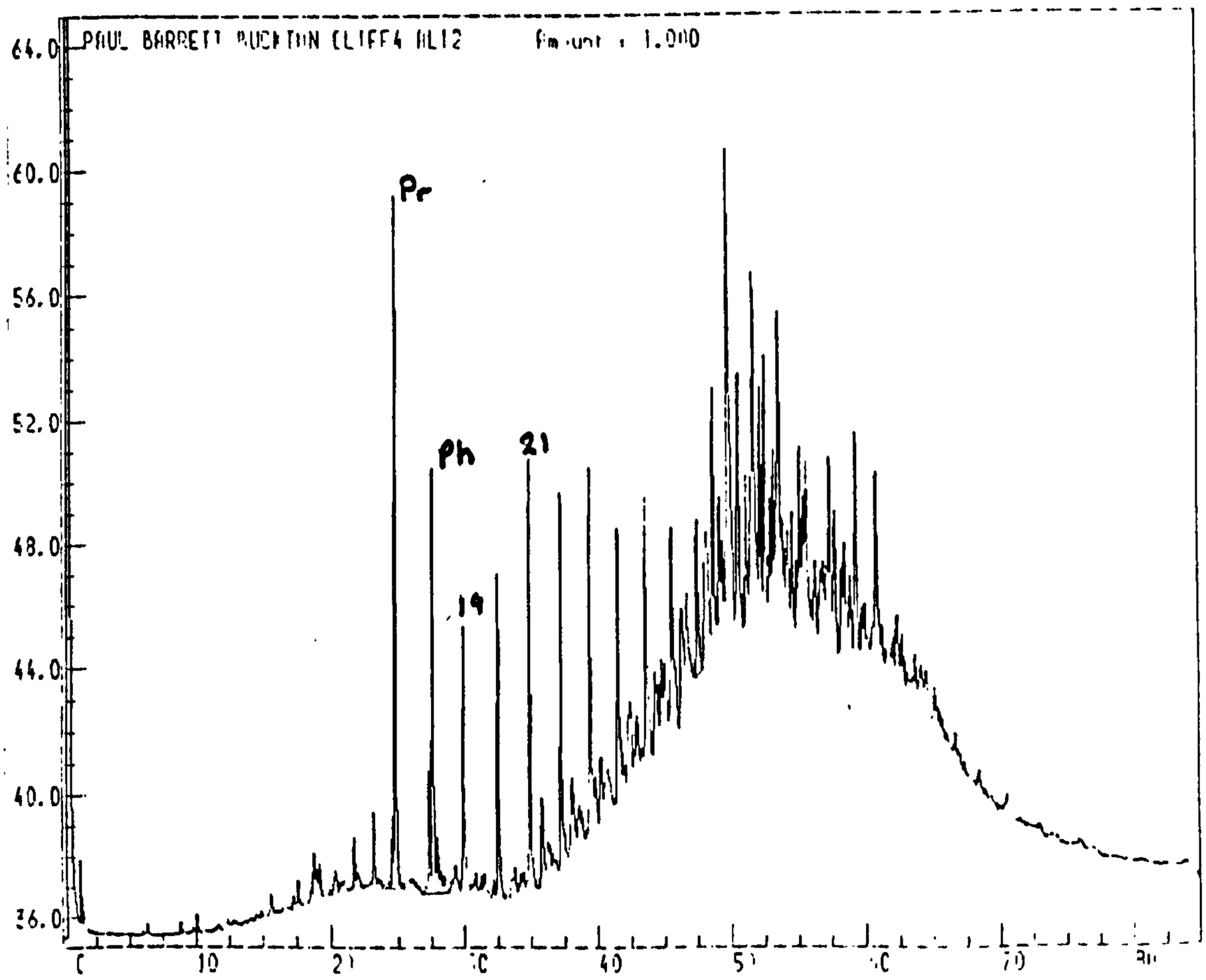

Figure 3.7 Gas chromatogram for the Buckton Cliff section (sample BC4); nC, normal alkane with carbon number; Pr, Pristane; Ph, Phytane.

Biomarker parameters calculated from GCMS traces are given in Appendix 4, Table VII. The aliphatic extracts contain abundant 17β(H), 21β(H)-hopanes hop-17(21)-enes and hop-13(18)-enes, and the side chain isomerisation in the hopanes and steranes is very low

3.2.5 X-ray Diffraction (XRD)

Samples run on XRD showed very little mineralogical variation through the section. Large quantities of calcite, some quartz, clays (montmorillonite) and trace amounts of pyrite, were identified from the XRD traces. Using the relative intensities of peaks, and comparing these to the intensities of the peaks from a known standard, percentages of carbonate material were calculated to test a method developed by Dr. Bryn Jones, Fossil Fuels and Environmental Geochemistry, University of Newcastle. These results are given in Table 3.1, along with carbonate results acquired from the Leco Carbon Analyser. The results for the different methods correlate well (r^2 = 0.97).

Sample	Section depth (cm)	TOC (%)	LECO Carbon Analyser			XRD Data Carbonate (%)
			Tot. C (%)	Inorg. C (%)	$CaCO_3$ (%)	
BC1	6.50	0.56	2.14	1.58	13	18
BC2	4.50	0.67	2.1	1.43	12	17
BC3	3.25	2.39	6.5	4.11	34	43
BC4	2.00	2.42	10.7	8.28	69	65
BC5	0.50	0.96	4.44	3.48	29	35

Table 3.1 Carbonate data determined by different techniques for the Buckton Cliff section. Key: Tot. C, total carbon; Inorg. C, inorganic carbon (total carbon - TOC) The determination of carbonate values from LECO is based on a conversion factor of 8.33 for the inorganic carbon (on the assumption that all inorganic carbon is $CaCO_3$).

3.3.Discussion

3.3.1 Bulk geochemistry characteristics

A plot of TOC v. $CaCO_3$ for the Buckton Cliff data (Fig. 3.4) shows a positive correlation (linear r^2 = 0.69); where TOC is high, $CaCO_3$ is also high, indicating that enhanced TOC is not controlled by reduced $CaCO_3$ content. Comparison with the South Ferriby data shows that carbonate contents are lower at the Buckton Cliff section. A TOC v. AOM plot (Fig. 3.8) for the Buckton Cliff data shows that they plot within the South Ferriby data cloud. There is a good covariance of the parameters (linear regression r^2 = 0.80) suggesting that increased TOC is controlled by

increased preservation of organic matter. The plot of AOM v. S2 ($r^2 = 0.71$; Fig. 3.6) also suggests that petroleum potential of the kerogen is controlled by the amounts of preserved AOM.

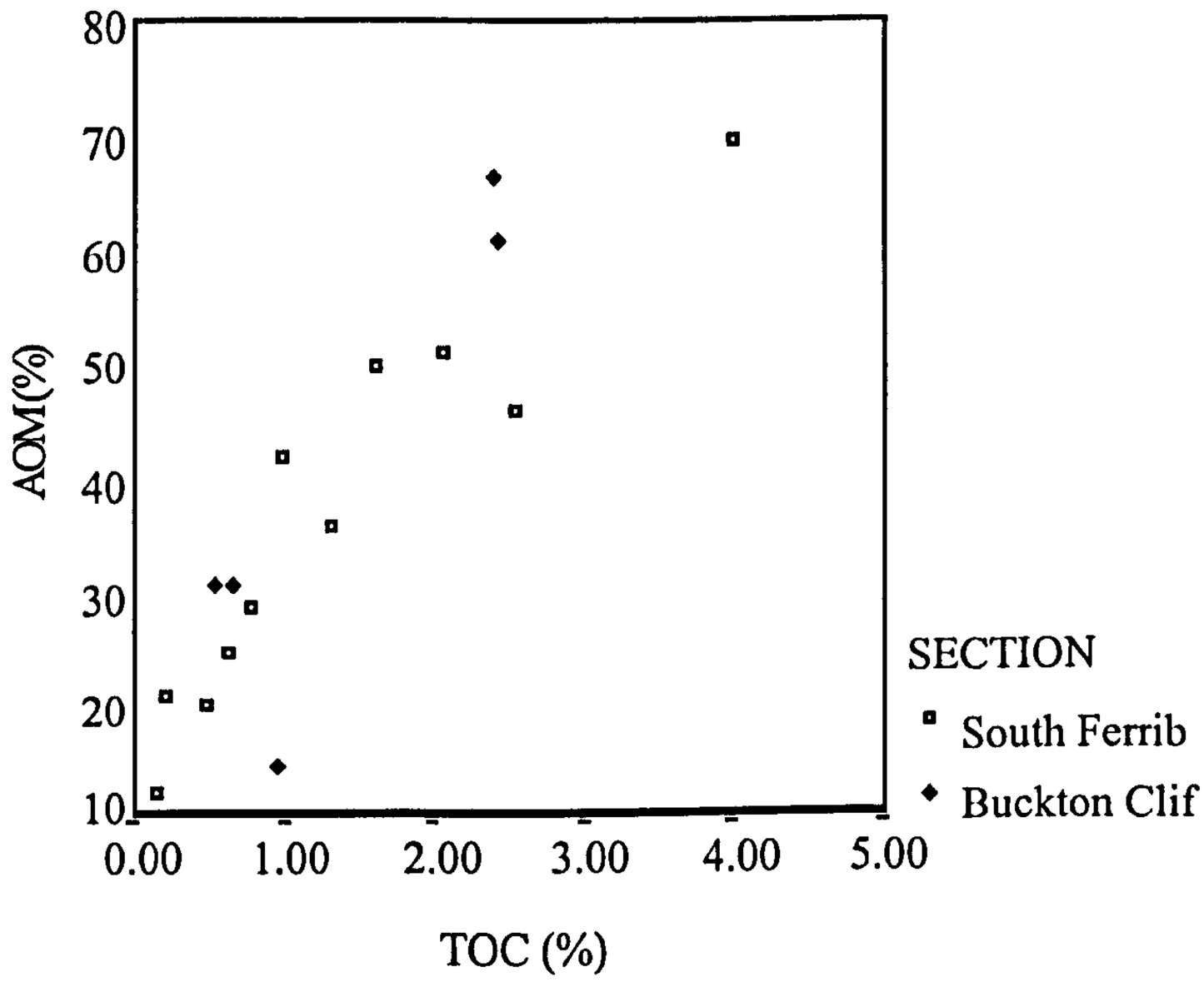

Figure 3.8 Cross plot of TOC versus AOM for the UK sections. The data shows a good correlation between these parameters: Buckton Cliff $r^2 = 0.8$; South Ferriby, $r^2 = 0.88$; combined, $r^2 = 0.81$.

The TOC results from this study do not compare well with the data published for this locality by Farrimond *et al.* (1990). They reported a TOC of 13% from a single sample, whereas this work indicates that the highest TOC is 2.4% (sample BC4). The reason for this is unclear as the section is very thin and only accessible at one place at Buckton Cliff; it may indicate a large amount of lateral variation in the Black Band over a distance of a few metres. This may have been caused by squeezing and compression of the softer lithologies by the harder chalks, or perhaps due to carbonate dissolution. Other data suggest that the value of 13% is very high and unrepresentative of the Black Band. However, as BC4 is laminated and has the highest TOC it will be treated as the most similar sample to the Farrimond *et al.* (1990) study.

3.3.2 Isotope geochemistry

The positive 1.5‰ (PDB) Buckton Cliff kerogen isotope shift is similar to the degree of shift in the carbonate isotopes observed at South Ferriby (Schlanger *et al.*, 1987). The excursion peaks in sample BC2 just above the organic carbon maximum

for Buckton Cliff in samples BC3 and BC4. Kerogen $\delta^{13}C$ values for Buckton Cliff appear to show no correlation with hydrogen index (linear regression $r^2 = 0.22$), and only a slight correlation with TOC (linear regression $r^2 = 0.44$; Fig. 3.9); however, there are too few data points for a convincing interpretation of this data.

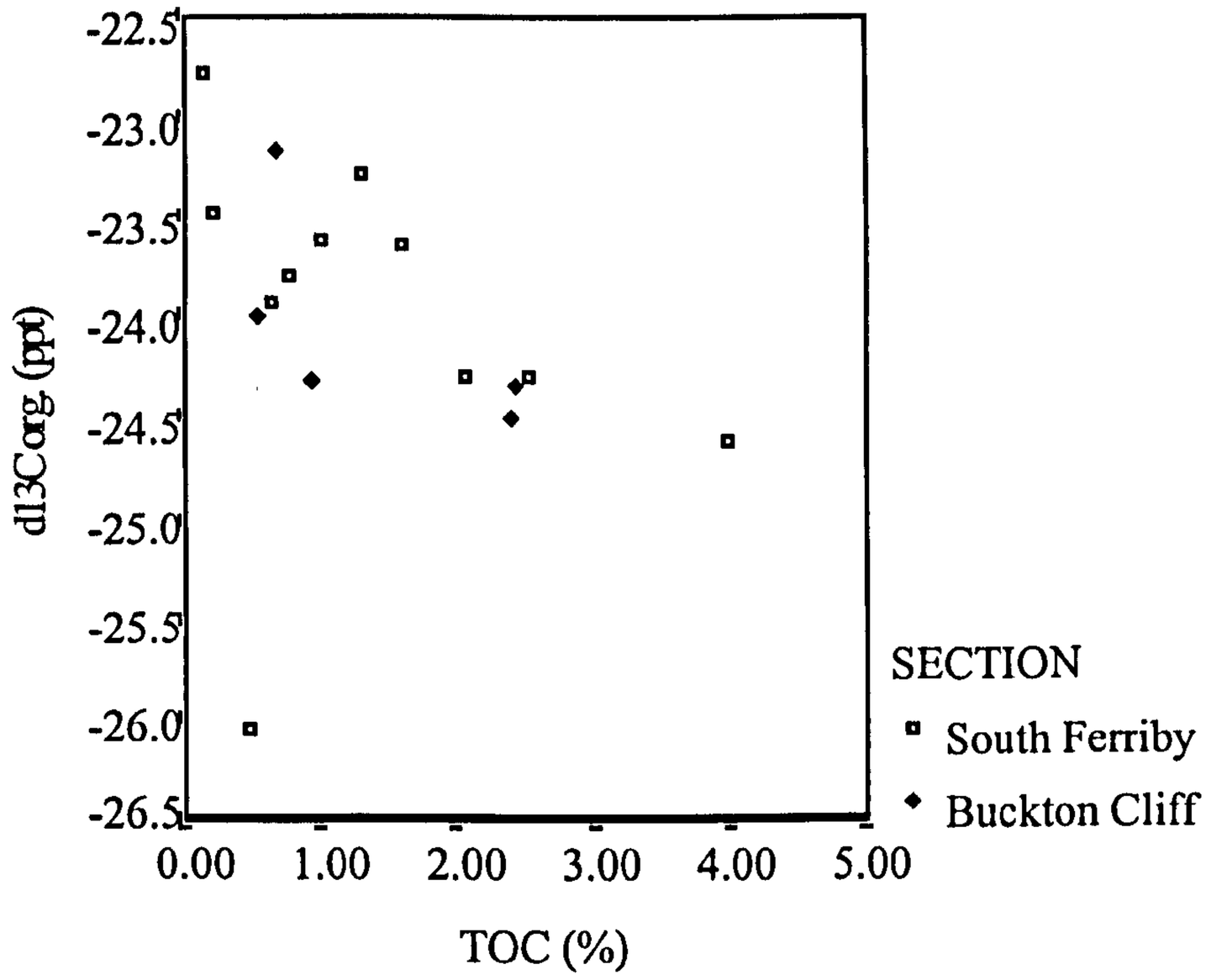

Figure 3.9 Cross plot of TOC versus $\delta^{13}C$ kerogen isotope data for the UK sections.

There is a weak correlation between the parameters for the Buckton Cliff section, $r^2 = 0.44$; and a poor correlation for the South Ferriby section, $r^2 = 0.07$. However if the anomalous point (sample SF6c, 0.445cm) is removed the correlation is better, $r^2 = 0.65$.

In contrast, the carbonate carbon isotope excursion at South Ferriby is found just before the onset of the organic-rich interval (cf. Schlanger *et al.*, 1987; Barrett, 1994). The shape of the kerogen curve for South Ferriby (Figure 3.5) follows a similar trend to the carbonate curve reported by Schlanger *et al.* (1987). If sample SF6c is removed before a regression line is fitted, a correlation appears between $\delta^{13}C$ and hydrogen index (linear regression $r^2 = 0.64$), and TOC (linear regression $r^2 = 0.65$). Sample SF6c has a very low TOC content and hydrogen index value, and high phytoclast percentage compared to the samples directly above and below it, which probably accounts for the extreme negative $\delta^{13}C$ value.

3.3.3 Organic matter maturity

The production indices (range 0.02 to 0.2) and Tmax values (range 424 to 483°C; mean 440°C; Appendix 2, Table I) which can be kerogen type dependent,

indicate that these samples are immature (Espitalié *et al.*, 1977; Orr, 1983). However, there must be some consideration of error using the THA 200, especially for organic lean samples, as blank vials give a low positive S1 value when run, possibly affecting the production index value.

The Pr/nC_{17} and Ph/nC_{18} ratios from gas chromatography (all >1; Appendix 3, Table I) also indicate a low level of maturity (Leythaeuser & Schwarzkopf, 1986). However, the values reported by Farrimond *et al.* (1990) for their sample, are much lower (both ratios =1) than the values calculated from BC4, although the Pr/Ph ratio from this study is very similar to that reported by them. This may reflect that some degree of weathering (e.g. water washing) or bacterial biodegradation has preferentially removed some of the *n*-alkanes but not affected the isoprenoids in sample BC4 (cf. Volkman, 1986).

The presence of 17β(H), 21β(H) hopanes (e.g. Ourisson *et al.*, 1987), hop-17(21)-enes and hop-13(18)-enes indicates that these samples are immature, as hopenes tend to be lost at very early stages of maturation (e.g. Ourisson *et al.*, 1979; Killops & Killops, 1993, p183), although the hop-13(18)-enes have been found at greater depths, but still well before the oil window (Farrimond *et al.*, 1986). However, there is a significant variation in the calculated biomarker maturity parameters (cf. Mackenzie *et al.*, 1980) through the section (Appendix 4, Table VII). The "outer" organic-lean samples show apparent higher maturity compared with the central organic-rich samples (BC3 and BC4). These differences are unlikely to be controlled by differing thermal histories, but more likely by differing organic matter input, such as a higher relative content of recycled oxidised organic debris which may form a low level background signal throughout the section (Farrimond *et al.*, 1988).

3.3.4 Organic matter sources

Whole rock hydrogen indices indicate a Type III/IV kerogen for the Buckton Cliff section; however, the kerogen hydrogen index for BC4 suggests a Type II/III kerogen, implying that adsorptive matrix effects of clays are affecting the S2 peak during pyrolysis (Katz, 1983; Espitalié *et al.*, 1985a). A plot of whole rock TOC v. S2 values (after Langford and Blanc-Valleron, 1990) indicates that the Buckton Cliff samples are in fact Type III kerogens, and plot on an identical slope to the South Ferriby samples (Fig. 3.10). The slope of the S2 v. TOC regression line (Y= 1.02x - 0.584) gives a true average hydrogen index (Langford & Blanc-Valleron, 1990) of 102 mgHC/gTOC, for the Buckton Cliff section, and the whole rock HI is 99. However,

Rock-Eval pyrolysis of the kerogen of BC4 gives a higher value still (330 mgHC/gTOC). This value indicates that matrix material for sample BC4 is adsorbing high quantities of generated hydrocarbons on pyrolysis (70% of hydrocarbons retained) this is similar to observations from adsorptive effects on the South Ferriby sample SF6a (60% of hydrocarbons retained; Barrett, 1994). These observations are made on a comparison of released S2 per gram available carbon, between whole rock and kerogen samples.

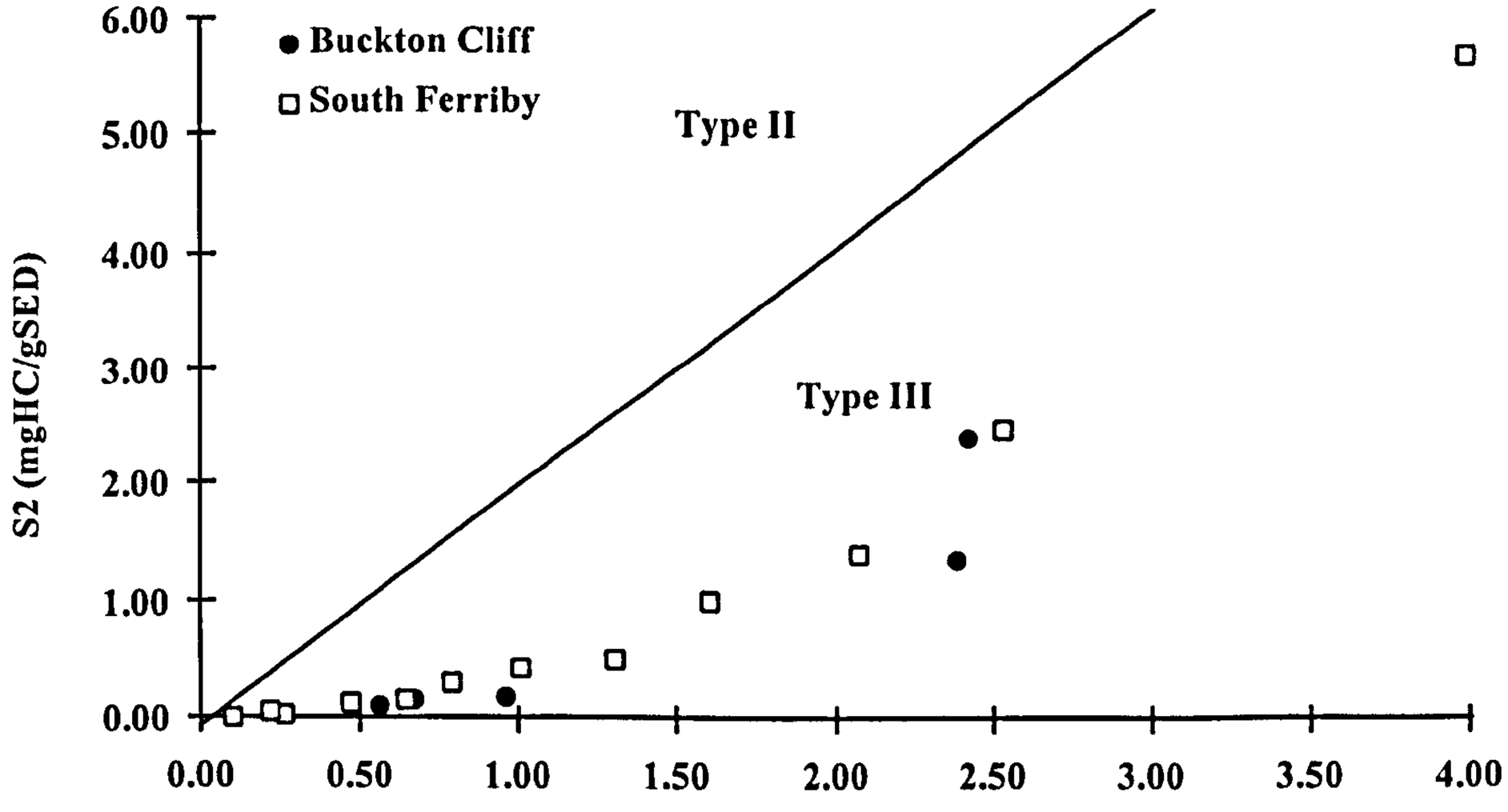

Figure 3.10 Cross plot of TOC versus S2 for the UK sections (based on Langford & Blanc-Valleron, 1990). The data for both sections follow a similar trend, and suggest that the kerogen is predominantly Type III.

The TOC v. S2 plot (Fig. 3.10) for the Buckton Cliff data shows that they plot with a strong similarity to the South Ferriby data. A good relationship with linear regression ($r^2 = 0.86$) was observed between the parameters; however, a quadratic regression fits the data slightly better ($r^2 = 0.88$). This was also seen for the South Ferriby samples (Barrett, 1994). Regression analysis for the combined data sets shows a good correlation (linear $r^2 = 0.87$; quadratic $r^2 = 0.96$). Why this occurs is unclear but may be accounted for by increased hydrocarbon adsorption by the matrix clays in more organic-lean samples. Alternatively, the data may fit onto two individual linear regression lines one for organic-rich samples and one for organic-poor samples. This may indicate a major difference in the organic matter source of the organic lean samples in comparison to the organic rich samples.

The sterane 27/29aaaR ratio, which may reflect the type of organic matter that has sourced the steranes (Huang & Meinschein, 1979) gives a range of values from

0.7 to 1.1 (Appendix 4, Table VII). The ratio for sample BC4 (1.09) is identical to that given by Farrimond *et al.* (1990). However, the interpretation that nC$_{27}$ steroids are marine sourced and that nC$_{29}$ steroids are terrestrially sourced is too simplistic, as certain marine algae can be dominated by nC$_{29}$ steroids (Volkman, 1986).

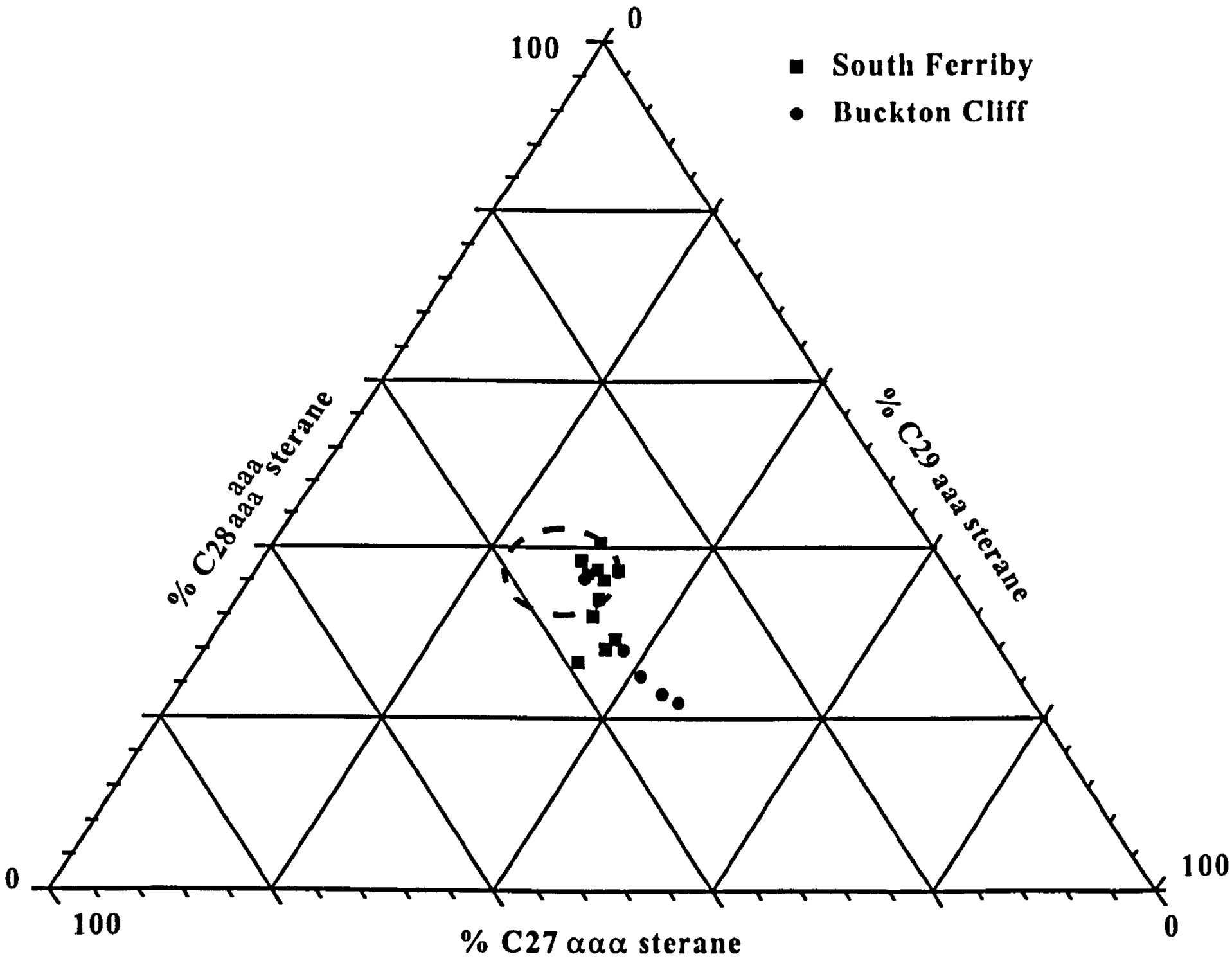

Figure 3.11 Ternary C$_{27}$-C$_{28}$-C$_{29}$ αααR sterane plot (after Huang & Meinschein, 1979) for the UK sections, based on relative amounts (%) data from Appendix 4, Table VII. Dashed area represents Farrimond *et al.*, 1990b data.

A ternary plot of 27:28:29 αααR steranes (Fig. 3.11) shows that sample BC4 plots in a similar place to the sample analysed by Farrimond *et al.* (1990) who noted that the C28 components were the most abundant steranes; the other Buckton Cliff samples plot closer towards the C$_{29}$ pole as they have relatively lower C$_{28}$ abundances. Figure 3.11 shows that the South Ferriby samples (Barrett, 1994) plot in a similar area to the BC4 sample; the strong C$_{28}$ input may reflect different algal inputs in the BC4 sample compared to the other Buckton Cliff samples (cf. Volkman, 1986). The C$_{28}$ sterane has also been attributed to the presence of diatoms and/or dinoflagellates (Peters & Moldowan, 1993). Diatoms have not been recorded in Cenomanian-Turonian samples (R. Tyson, 1998, pers comm.) and the abundance of the C$_{28}$ sterane may relate to the abundance of dinoflagellates cysts in this sample.

The approximate abundances of hopanoids and steroids (Appendix 4, Table VII), taken from peak area data, suggest that hopanoids are twice as abundant as steroids for the Buckton Cliff section; this relationship was also noted in the sample studied by Farrimond *et al.* (1990).

The presence of methylhopanes in the outer samples (BC1, 2 and 5) is interesting as these compounds are relatively infrequent in geological samples; although they are not commonly looked for. The 2α-methylhopanes are often abundant in carbonate-rich facies although they are not used diagnostically (Price *et al.*, 1987). Precursor methylhopanoids have been identified in various bacteria (Zundel & Rohmer, 1985), and their presence in the samples may be an indicator of specific bacterial input, as yet unspecified.

The dominance of dinoflagellate cysts in the palynomorph fraction (Appendix 3, Table III) is not surprising considering that they are the predominant form of fossilising phytoplankton in most marine situations, and can form a very high percentage of the fossilised organic-walled microplankton. The presence of 4-methylsteranes in the Buckton Cliff samples, identified from GCMS, suggests the presence of dinoflagellate cysts (cf. Wolff *et al.*, 1986) which is confirmed optically. There is no direct correlation between the % dinoflagellate cyst and relative % 4-methylsteranes observed at this section. The percentage of methylated steranes decreases up through the section, possibly indicating an increase in algal sourced steroids relative to dinoflagellate cysts sourced steranes. Bird *et al.* (1973) have observed the presence of 4-methylsterols in some bacteria and in cyanobacteria algae, so it may be possible for some of the 4-methyl sterane content to have a similar origin to the hopanoids although there is no further evidence to confirm this.

The significance of the relative changes in acritarch abundances in samples BC3 and 4 is unclear; they are usually abundant in brackish, hypersaline environments where dinoflagellates are inhibited (Downie *et al.*, 1971), but have also been noted in abundance in Callovian black shales from the central Atlantic (Tyson, 1984).

3.3.5 Environment of deposition.

The Buckton Cliff section shows evidence of bioturbation in sample BC5 and BC1, indicating the presence of burrowing life forms, in this case *Chondrites*. However, there is a lack of bioturbation and the presence of laminations in sample BC4, suggesting temporary dysoxic to anoxic conditions may have been achieved

from a reduction in bottom water O_2 levels below that which can sustain active burrowing organisms (i.e. <0.2ml/l; Tyson & Pearson, 1991).

Tyson (1995, p.147) suggests that a hydrogen index versus TOC plot can be used to determine whether optimum preservation has been achieved. Under these conditions the hydrogen index will level off and remain more or less constant even though the TOC may vary due to changes in sediment dilution. However, the hydrogen index may still be affected by changes in plankton type and terrestrial organic matter supply. Whole rock hydrogen indices for the Buckton Cliff section show a positive correlation with TOC (linear regression $r^2 = 0.79$) and the parameters have a similar relationship to the South Ferriby section (Fig. 3.12); however, they do not appear to level off with increasing TOC which would suggest that optimum preservation conditions for this type of organic matter were not achieved at this locality. This is also noted by the low hydrogen index for the kerogen Type suggested by optical work; optimum preservation of marine Type II kerogen ought to be at 500 to 600 mgHC/gTOC but the values for the UK sections are clearly well below this, even for the kerogen isolates.

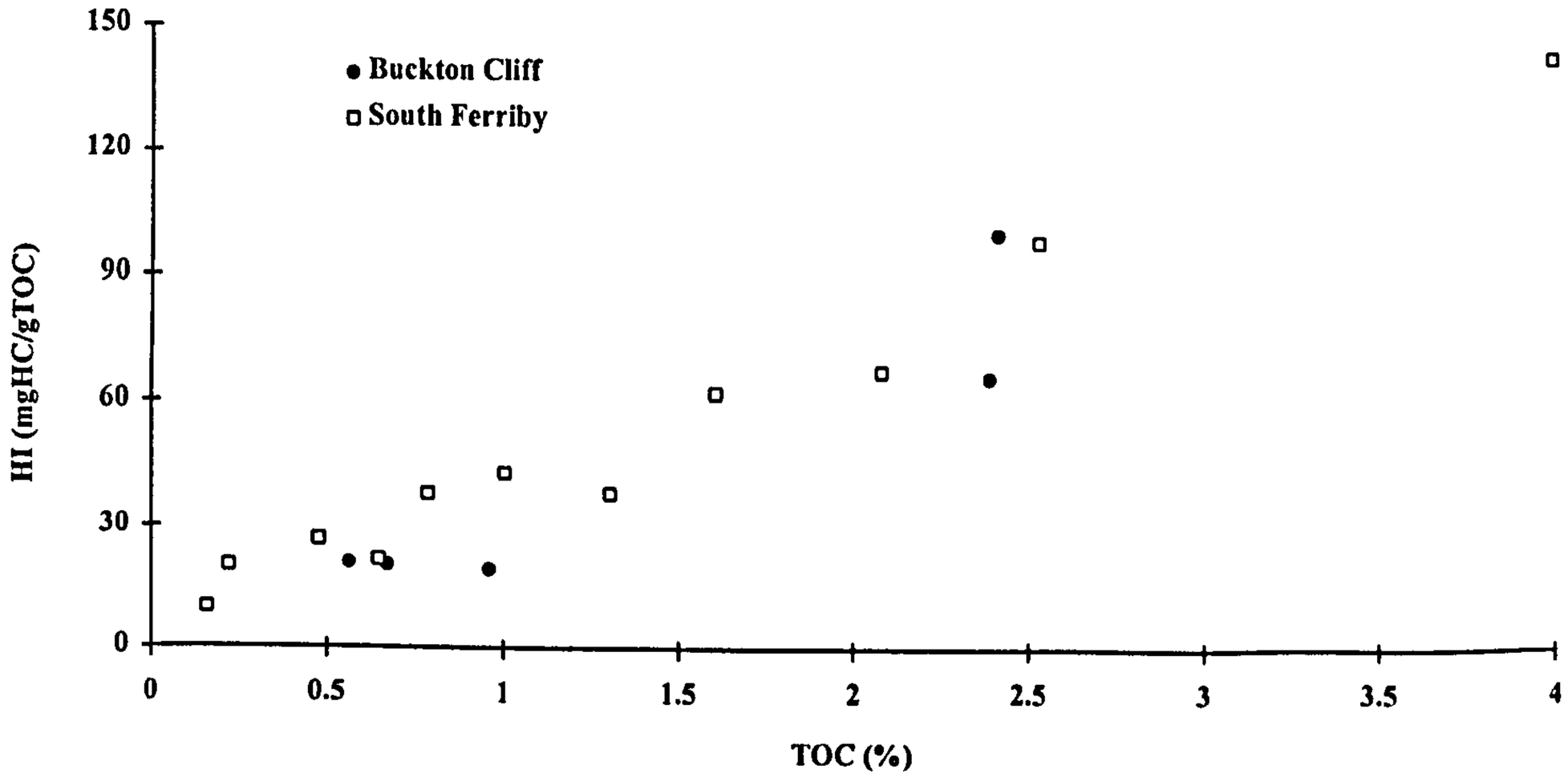

Figure 3.12 Cross plot of TOC versus hydrogen Index for the UK sections. Note that the hydrogen index does not appear to level off with increasing TOC, suggesting that optimum preservation was not achieved.

Variable preservation of the organic matter can also be assessed by variations in the appearance of the palynomorphs and the use of the relative fluorescence scale cf. Tyson (1995). The fluorescence scale values show good correlation with the hydrogen index and TOC, suggesting that it is the preservation of the organic matter that controls both of these parameters.

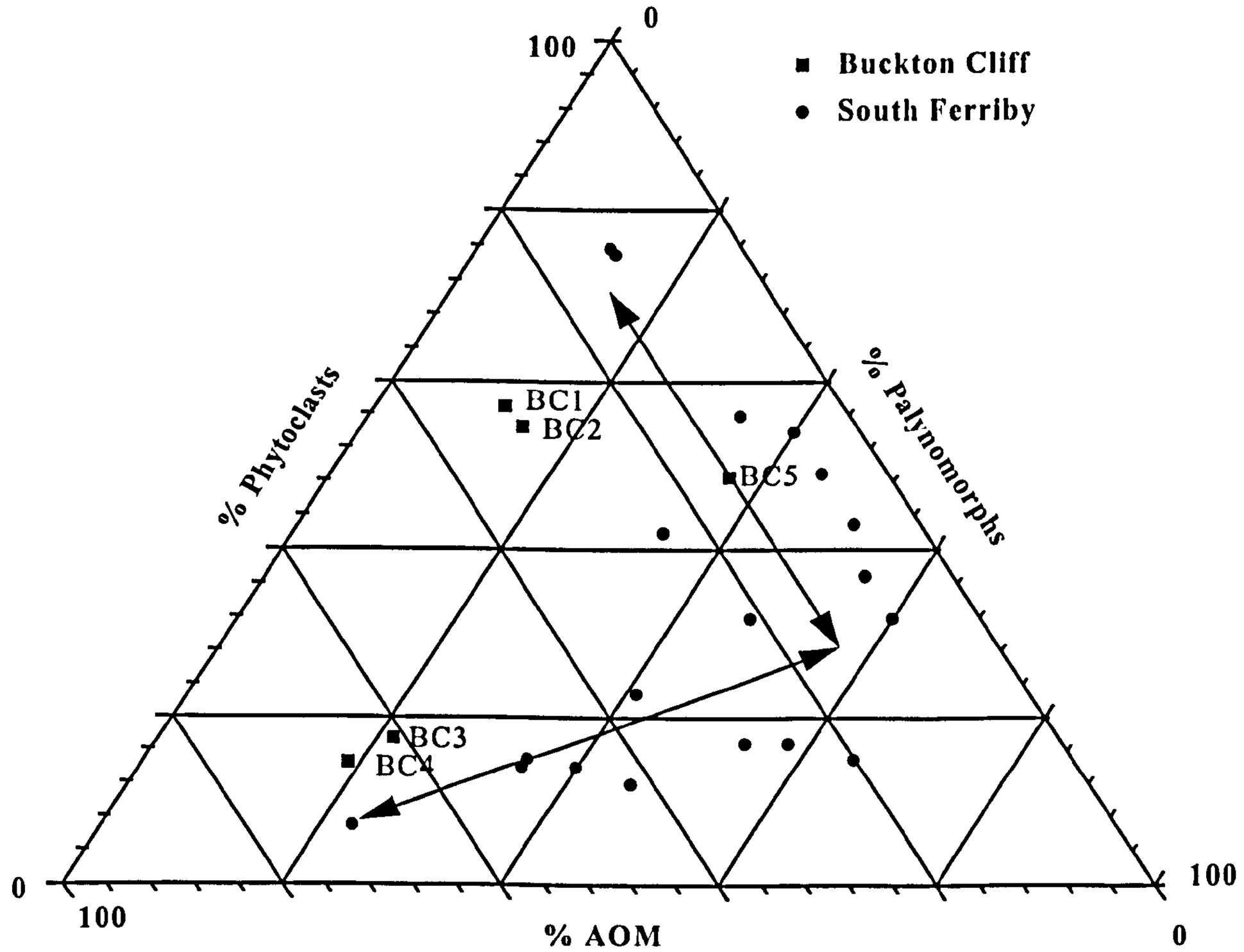

Figure 3.13 Ternary 'AOM'-Phytoclast-palynomorph kerogen plot (after Tyson, 1995) for the UK sections, based on relative numeric frequency (%RNF) data from Appendix 3, Table II and Barrett (1994). The arrow represent the change in facies type.

A ternary diagram representing relative abundance of the AOM, Phytoclasts and Palynomorphs (Fig. 3.13), indicates changes in depositional environment between the Buckton Cliff samples. The Buckton Cliff samples follow a similar trend to the South Ferriby samples (Barrett, 1994), extending in a line from the AOM pole across to the mid point on the opposite axis, a trend which is typical for many Mesozoic marine sediments (Tyson, 1993) The trend is from a chalk-marl dominated (possibly oligotrophic), oxic shelf at the base of the sequence, through to a dysoxic-anoxic (eutrophic?) shelf for the central organic-rich samples, then back to a chalk-marl dominated oxic shelf for upper samples. Higher productivity is perhaps suggested by the low diversity of dinocysts assemblages in the organic-rich facies.

The two AOM-rich samples (BC3 and 4) have variable hydrogen indices, which may reflect variable preservational conditions during deposition. The environment may have been reducing enough to preserve the physical structure of the AOM, but it was evidently oxic enough to chemically degrade the AOM. This is

clearly seen between samples BC3 and BC4 which have similar TOC and %AOM values but quite different hydrogen indices.

The relative changes in black and brown phytoclasts (Appendix 3, Table II) can provide more information than the total percentage of phytoclasts alone. Black phytoclasts dominate over the brown in the lower part of the section, suggesting that the phytoclast supply here is dominated by oxidised material. A high proportion of black wood in the phytoclast fraction is characteristic of distal settings (one removed from a fresh supply of unoxidised and untransported phytoclasts) or a proximal setting with an arid onshore climate (Summerhayes, 1987; Tyson, 1995). The black to brown phytoclast ratios (range 0.4 to 2.0) are highest in samples BC3 and BC4 , suggesting a more distal area of deposition for these two samples; the rationale is that brown wood becomes oxidised, leading to an increase in black wood, with increasing distance or duration of transport (Tyson, 1995). This agrees with the distal setting of these samples as suggested by the ternary APP diagram (Fig 3.13).

A simplistic interpretation of the Pristane/Phytane ratio for this section (Appendix 4, Table I) suggests that these samples were deposited in an oxic setting (Didyk *et al.*, 1978). However, the palynofacies data indicates that at least at some point the environment was dysoxic-anoxic (cf. Tyson, 1995). It is possible that an alternative source of isoprenoids (Ten Haven *et al.*, 1987), such as tocopherols (Goosens *et al.*, 1984) are influencing the ratio. The C_{35} hopane predominance (Bishop and Farrimond, 1995) can also be used as an anoxicity parameter, but due to poor elution it was not possible to integrate the areas of the C_{33}+ hopanes.

3.4. Principal Component Analysis of biomarker data (PCA)

Principal Component Analysis is a statistical method that can be used on large data sets, allowing trends to be identified within the data. Individual biomarkers have limitations in identifying trends in preservation, environmental conditions and organic matter input, due to the multiple sources of commonly used compounds, complex diagenetic reactions and variations in compounds preservation efficiencies. However, as a group they lend themselves readily to the multivariate PCA analysis.

The multidimensionality of the data is reduced in Principal Component Analysis, and expressed in a few linear combinations of the original variables whilst maintaining the bulk of significant data variability; this facilitates the graphic presentation of the data (Meglan, 1992). In this case the variables used are biomarker

peak areas, taken from gas chromatography-mass spectrometry (Section 2.3.4). The 38 variables used (Appendix 5, Table I) taken from Buckton Cliff and South Ferriby data were chosen from a wide range of identified peaks: C_{29} hopanes (m/z 177), tricyclic terpenoids and hopanes (m/z 191), methylated hopanes (m/z 205), hop-17(21)-enes (m/z 367), steranes (m/z 217 & 218), 4-methylsteranes (m/z 231), diasterenes (m/z 257) and 4-methyldiasterenes (m/z 271). These compounds were selected as they could be easily identified and integrated between samples and locations and suffered no coelution problems.

The data are firstly normalised, within Excel for Windows, where variables in each sample are summed to a constant total and autoscaled around the mean to give greater spread to the data; this allows for differences in sample concentration. This data are then copied from Excel to SPSS for Windows. Eigen vectors (of the correlation matrix) are then extracted from the data using the Factor Analysis routine; these correspond to the variables which explain the largest proportion of the variance within the data. The degree to which each variable contribute to the PC is shown on the "loadings plots". The variables which strongly influence PC1 will have either a large positive or negative loading on the axis, whereas those which plot close to zero have little influence. The scores show how the samples are influenced by the loadings (see Davies, 1986, for a full description of PCA).

The relationship between variables (biomarkers) are obtained from the loadings plots, which are converted from the Factor outputs of SPSS using the square root of the Eigen values. Information about how the samples relate to each other is obtained from the scores plot; in SPSS these are calculated from the normalised peak data and the loadings data.

3.4.1 PCA variations down section

Biomarker data from the Buckton Cliff section were analysed in conjunction with the South Ferriby data (Barrett, 1994) to give greater statistical meaning as five samples are too few for PCA. The first three Principal Components account for over 85% of the total variance in the scaled data set of 38 variables (Appendix 5, Table I); their controlling factors can be identified from the loadings plots. The first principal component (PC1) records the majority of the variance (51%) in the scaled data set; the loadings plots are controlled by compounds typical of mature sediments (e.g. αβ hopanes and αααS steranes) versus compounds typical of immature sediments (e.g. β β hopanes, and hop-17(21)-enes and αααR steranes). This PC is controlled by the

maturity differences between and within the sections. The scores data show a good correlation ($r^2 = 0.84$) with a sterane maturity parameter (20S/20S+R). The PC1 v. PC2 scores plots for both sections (Fig. 3.14), indicate that the South Ferriby section is more mature than the Buckton Cliff section, and that there are also variations in relative maturity within the sections themselves which show that the organic-lean sample have a higher apparent maturity. This was noted earlier in the section and the maturity order identified from PCA correlates with the observations from bulk and molecular geochemistry data (Section 3.3.3).

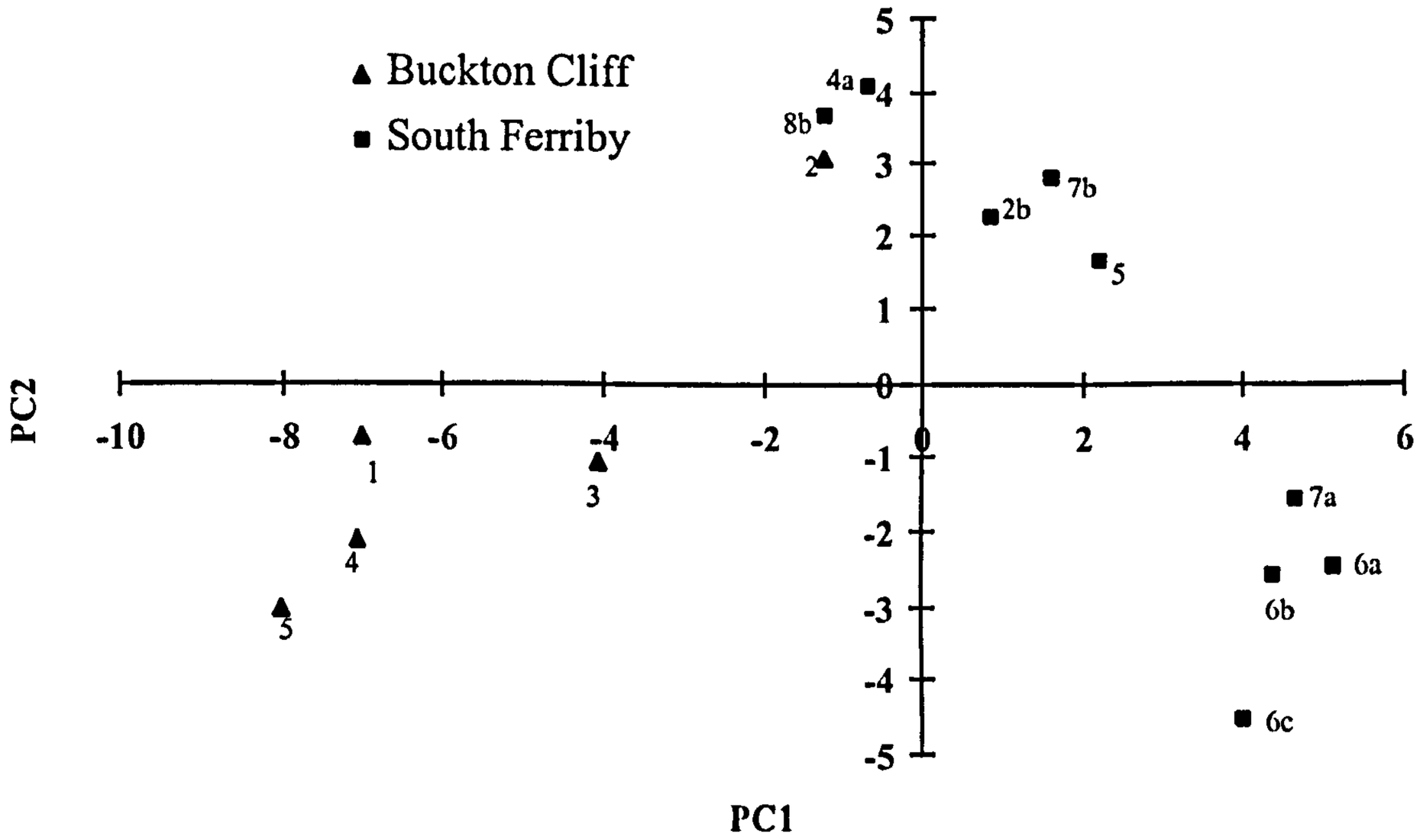

Figure 3.14 Cross plot of PC1 v. PC2 scores data for the South Ferriby and Buckton Cliff data.

The second principal component (PC2) represents 24% of the variance; the positive loadings axis is dominated by the ββ hopanes, C_{29} βα hopane, Tm, and the α ααR steranes; the negative axis is dominated by the hop-13(18)-enes, diasterenes and methyldiasterenes. The scores data show no correlation with bulk geochemistry data (TOC, S, HI, PI, Tmax or CO_3) or with any biomarker maturity parameters. It is unclear what controls this Principal Component, although the PC2 scores data for the sections do show some correlation with the PC1 scores data (South Ferriby, $r^2 = 0.80$ and Buckton Cliff, $r^2 = 0.83$).

The loadings plot for PC3 (11%) shows that the C_{28} steranes dominate the positive axis. The scores data show some correlation ($r^2 = 0.51$) with hydrogen index, the correlation being better for the individual sections (South Ferriby, $r^2 = 0.76$;

Buckton Cliff, $r^2 = 0.83$). This suggests that this Principal Component is controlled by the input of algal amorphous material. The scores data show that relative algal input is highest in samples BC2 and SF6a; these samples also had the highest TOC values.

3.5. Conclusions

The Black Band contains a variably preserved, immature, predominantly marine derived amorphous Type II/III kerogen as defined by a combination of optical and biomarker analyses. The maturity differences between the two sections varies, as noted from bulk, molecular geochemical and PCA, and is unlikely to be an effect of differing thermal histories. The aliphatic hydrocarbons of the organic-lean samples show higher apparent maturity; this may reflect input from reworked, oxidised material to the sediments, or differing diagenetic reaction in organic lean samples.

Observation from optical analyses show that terrestrial derived plant matter forms a variable contribution and is generally relatively higher in the organic-lean samples. However, marine derived AOM is still the dominant organic matter type which is consistent with observations from other workers studying the Cenomanian-Turonian boundary.

The Unresolved Complex Material observed in the gas chromatograms of the Buckton Cliff suggest that the aliphatic hydrocarbon fraction has undergone specific biodegradation, probably by water washing of the outcrop samples which has resulted in the partial removal of the *n*-alkanes from this section.

The enhanced TOC levels through the Buckton Cliff section are probably due to a combination of increased primary productivity (observed from the approximate 20-fold increase in TOC relative to the organic-lean chalks that were deposited before and after the CTBE) and enhanced preservation due to temporary suboxic-anoxic conditions which is evident from the lack of bioturbation and increased kerogen fluorescence observed in the central samples at this locality. However, the relationship between TOC and HI suggests that optimum preservation was not achieved at this locality.

CHAPTER 4

4. The "Black Shale" Facies, Germany.

4.1 Structural setting

The Lower Saxony Basin is located in north west Germany (Fig. 4.1). Its structure is that of a highly differentiated graben filled with sedimentary rocks from marine, lacustrine and hypersaline environments of Late Jurassic to Mid Cretaceous age. During the Aptian the subsidence of the fault-controlled grabens diminished and a broad basin developed. Albian, Cenomanian and Turonian sediments filled the basin, and were generally thicker than the sediments on the adjacent shelf. In the Coniacian, the basin was inverted and intruded by large lacoliths, which caused increased organic metamorphism in the overlying sedimentary rocks (Kocker *et al.*, 1994).

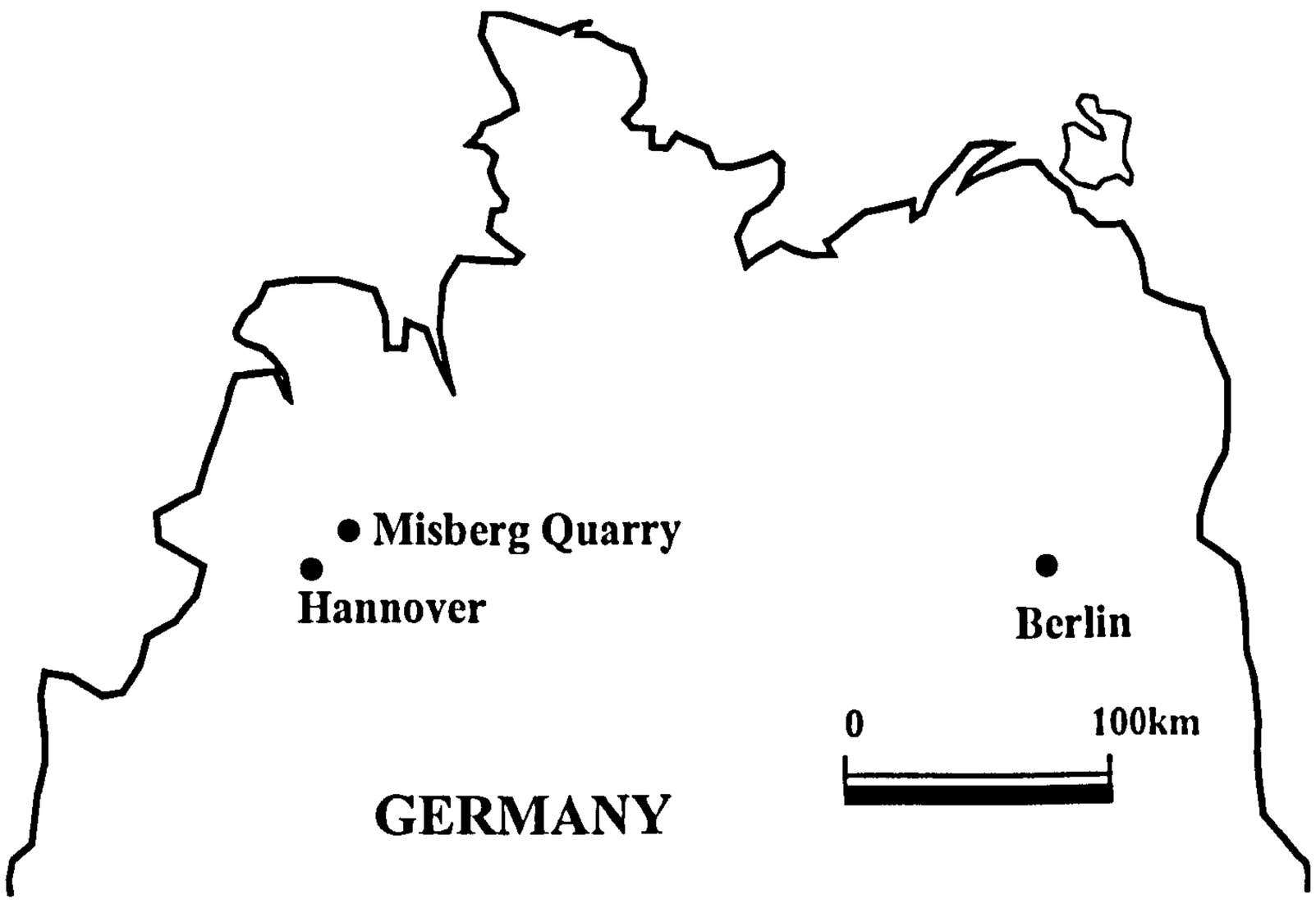

Figure 4.1 Map of Germany showing the location of the Misberg Quarry, 20km north-east of Hannover.

4.2 Stratigraphy

The Cenomanian-Turonian of the Lower Saxony Basin includes two lithofacies discriminated according to their colour (Ernst, 1975). These are the reddish brown marls and white limestones of the Rotpläner facies, and the thicker "black shale" facies comprising greenish marly limestones and black shales (Fig. 4.2). In north west German successions the base of the Cenomanian-Turonian sees a dramatic change from a pure white poorly fossiliferous limestone, the "arme rhotomagense schichten" of the *Calyoceras navicular* zone, to marly limestones of the

"black shale" facies, in the Plänerkalgruppe (Ernst *et al.*, 1979). This facies change was defined at an omission surface by Hilbrecht (1986). Bioturbation is abundant at and below this surface. Below the facies change the clays are mainly kaolinite, while above this boundary they consist of 60-70% of montmorillonite (Heim, 1957).

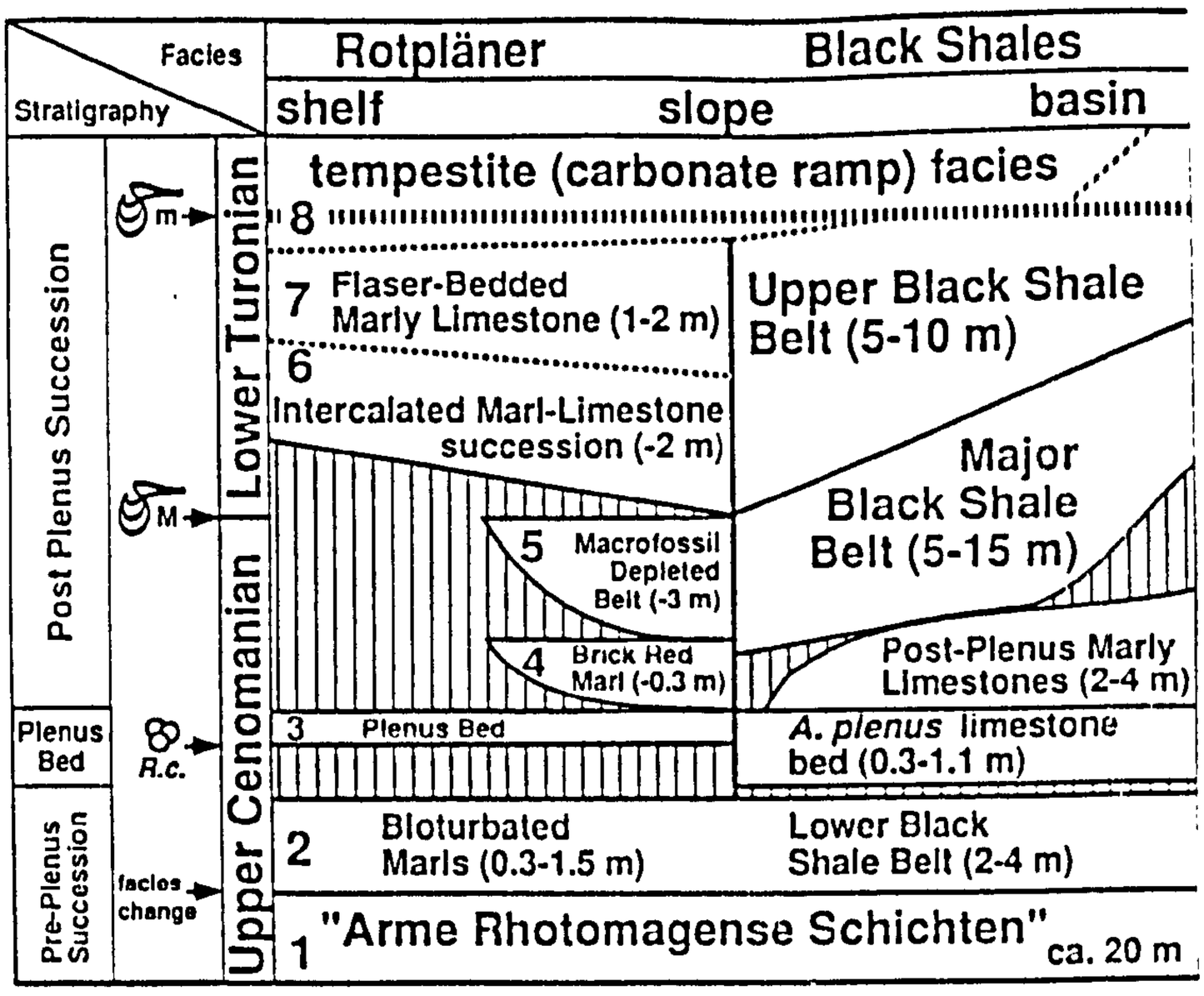

Figure 4.2 Litho- and biostratigraphic relationships between late Cenomanian and early Turonian facies units of northwestern Germany (after Hilbrecht & Dahmer 1994). Rc = *R. Cushmani*; M = *Maginotruncana*; m = *M. mytiloides* event

For many years the age of the "black shale" facies was believed to have been Early Turonian, with the Cenomanian-Turonian boundary at the base of the section; however, Ernst *et al.* (1983) and Ernst *et al.* (1984), place this boundary at a higher horizon based on invertebrate fossil evidence.

The Cenomanian-Turonian succession of the Lower Saxony Basin includes several "events" (Fig. 4.3). The first is the *Chondrites* event characterised by abundant *Chondrites* burrows. This occurs in the lowermost two metres of the basal marls, and is associated with the extinction of the foraminifera *Rotalipora cushmani* and *Rotalipora greenhornesis*. Overlying the *Chondrites* event is the omission surface which precedes a limestone unit known as the *plenus* Bank (Hilbrecht, 1986) this is an excellent marker horizon throughout north west Germany. The first acme of the inoceramid *Mytiloides mytiloides* provides an excellent marker horizon for the top of the Cenomanian-Turonian boundary successions in north west Germany (Hilbrecht,

1986), and the event is also thought to mark the base of the Turonian in Central Europe (Ernst *et al.*, 1984).

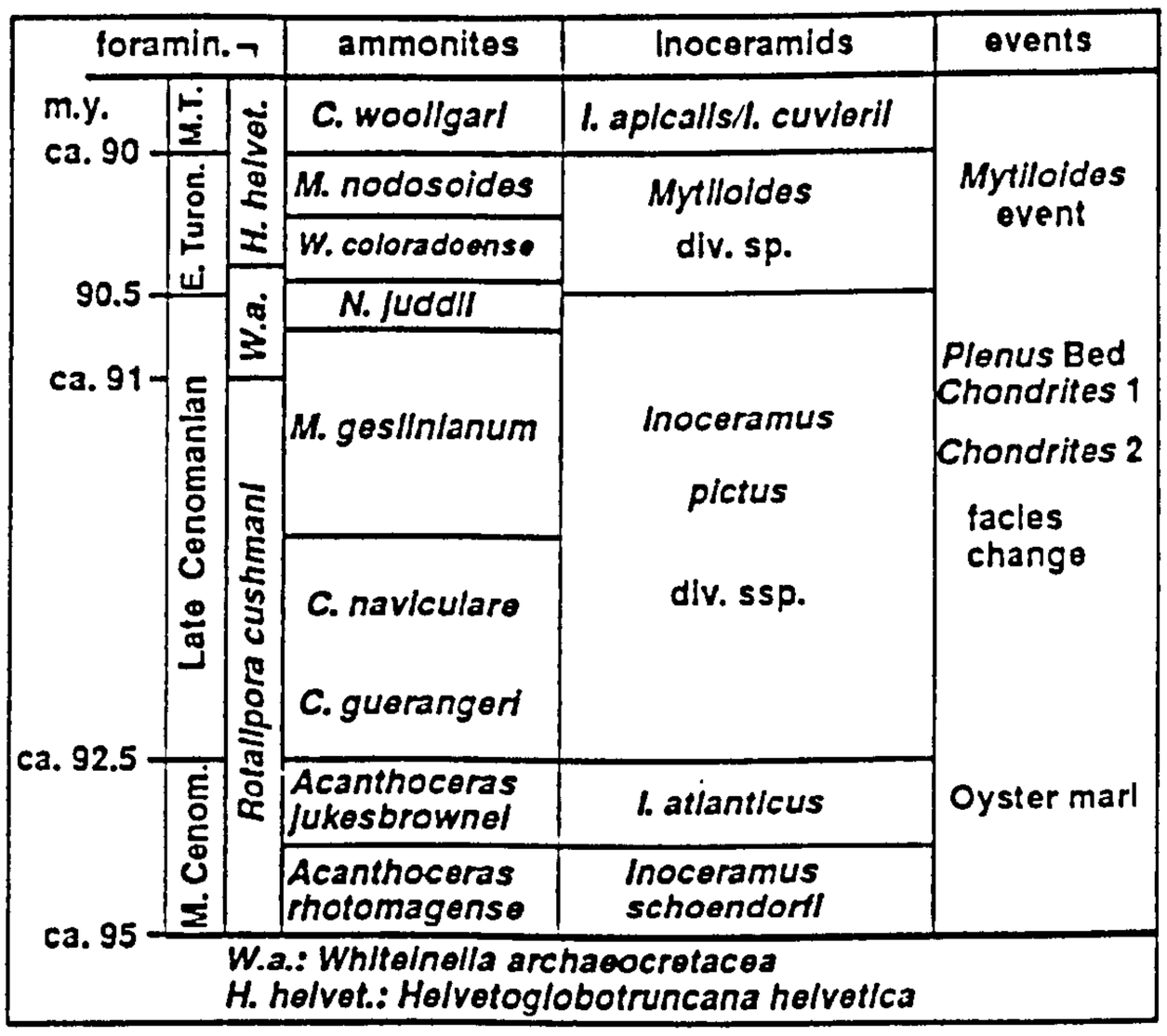

Figure 4.3 Stratigraphy of the middle Cenomanian to lower Turonian (after Hilbrecht & Dahmer, 1994)

4.2.1 Correlation with the Black Band and Plenus Formation of the UK

Hilbrecht (1986) has distinguished several characteristics for correlating between the "black shale" facies, the Black Band and the Plenus Marl Formation (Fig. 4.4). The first is the facies change, marked by an erosion surface, from organic-poor chalks and marls to organic-rich marls and shales in association with the change in clay mineralogy from kaolinite to montmorillonite. The extinction of *Rotalipora* at the erosion surface, followed by the occurrence of *A. plenus*, associated with a drop in planktonic foraminifera diversity, is also common to all locations. The entry of the inoceramid genus *Mytiloides*, in the upper *archaeocretacea* zone, and the interval of high foraminiferal diversity marked by the occurrence of *P. helvetica* and *Marginotruncana* characterise an "ecoevent" in Germany, but is less developed in England. Marshall and Batten (1988) observed a so called "*Neocardioceras* event", 11m above the facies change to the black shales at the Misberg Quarry, reflecting the first appearance of *N. juddii* and *Sciponoceras*; this is also observed in the England and the USA, and is taken to indicate the youngest ammonite zone of the Cenomanian.

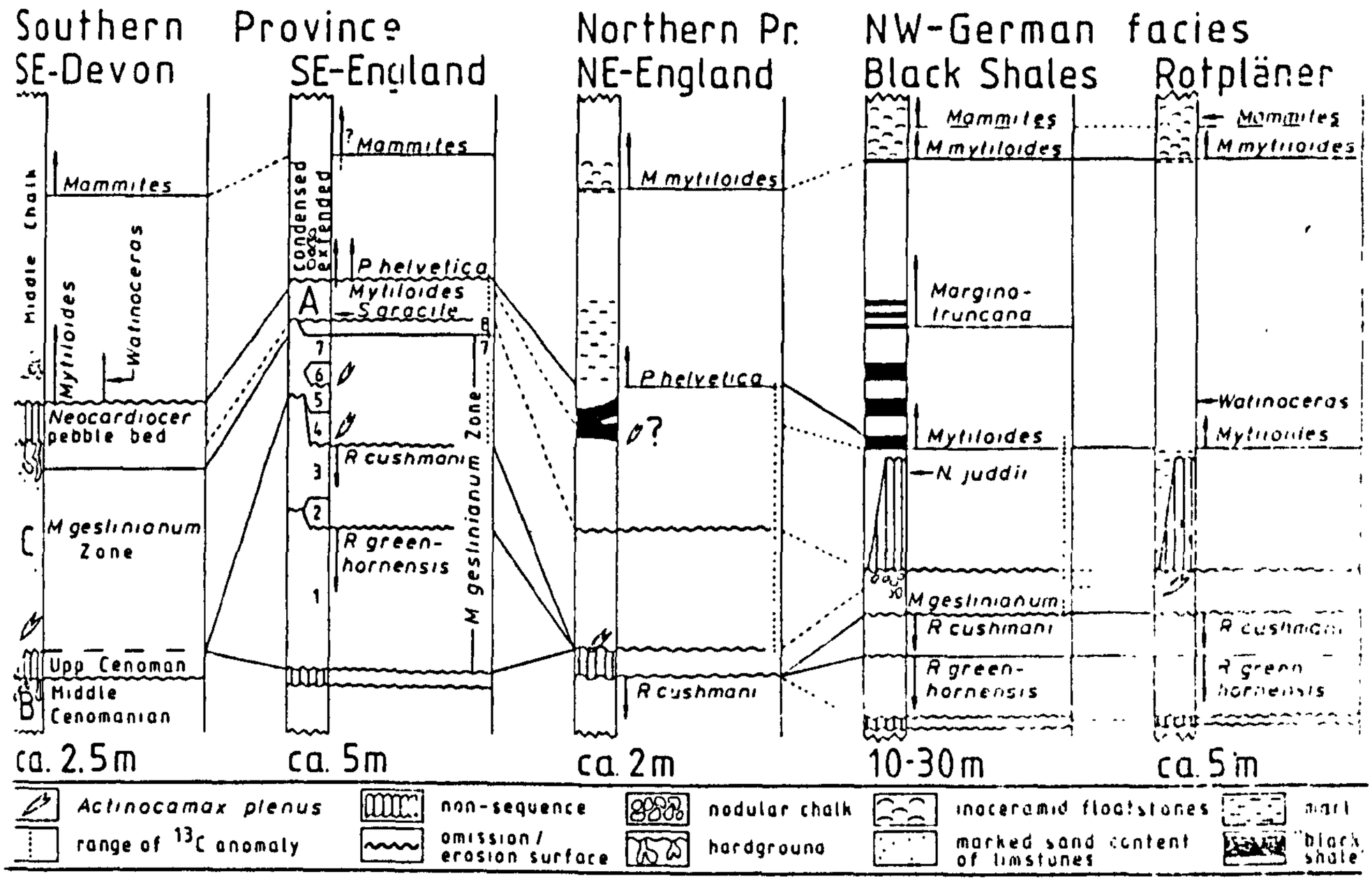

Figure 4.4 The correlation of English and German sequences of the upper Cenomanian and lower Turonian (after Hilbrecht, 1986).

4.3 The Misberg locality

The "black shale" facies is exposed in several places in Germany (Fig. 4.1). However, due to the high heat flow in some parts of the basin (cf. Kocker, 1994), only a few sections have suitably low maturity for an organic geochemical study. One of these sections is the Wunstorf Quarry, Hannover. However, this section is now heavily weathered and covered with large amounts of plant material and was not suitable for study. Another section with a suitable Cenomanian-Turonian exposure is the HPCF II quarry at Hannover-Misberg (Fig. 4.1); this quarry is abandoned and access is no longer possible, although the locality has been previously sampled by Heinz Hilbrecht (Geologisches Institut, ETH), from whom the samples were obtained.

4.4 Previous work on Misberg.

Ernst *et al.* (1979) used the Wunstorf and Salzgitter anticline sections to characterise two realms of deposition, the basin and the swell, in the north German Cretaceous shelf sea. In this paper they reviewed the stratigraphy of the Cretaceous

chalks in the Hannover-Braunschweig region of north Germany; it was here that they first described the Black Shale Facies. Hilbrecht (1986) studied the stratigraphy of the isotope excursion in this area and using biostratigraphy and isotope excursion he correlated the Eibruun marls of the north Tethys with the Black Shale Facies and the Black Band.

Marshall and Batten (1988) suggested a correlation of dinocyst assemblages with the lithology of the Cenomanian-Turonian succession at Wunstorf and Misberg Quarry. The first assemblage dominated by *Spiniferites* was characteristic of the marls, and the second assemblage dominated by both *Cyclonephelium* and *Eurydinium*, which was characteristic of the dark organic-rich horizons rich in AOM. The *Cyclonephelium/Eurydinium* assemblage was also noticed in the organic-rich Plenus Marl Formation (of Deegan & Scull, 1977) the offshore equivalent of the Black Band, UK. Marshall and Batten (1988) suggested that the assemblages were controlled by depositional conditions that favour preservation of organic matter. They concluded that the *Spiniferites* assemblage characterised an open marine environment, in agreement with the earlier work of Downie *et al.* (1971) on younger sediments. Marshall and Batten (1988) further state that the *Spiniferites* assemblage occurred in a well oxygenated open marine environment at a time when the low water oxygen concentration was restricted to the outer shelf, and that the change to the *Cyclonephelium/Eurydinium* assemblage reflects a more highly stressed environment with extension of anoxic conditions; brought about by either the formation of isolated basins with reduced circulation or impingement of an oxygen minimum.

Schlanger *et al.* (1987) record TOC values for the Wunstorf locality of 0.2% in the light grey marls and limestones rising to 1.2% to 2.8% in the black laminated shales; they also recorded a $\delta^{13}C$ carbonate isotope excursion of 2.7‰ to 4.3‰. Arthur *et al.* (1987) propose a duration of 600kyrs for deposition of the section, similar to deposition for the Bahloul Formation, Tunisia.

Hilbrecht *et al.* (1992) used carbon isotope data and biogeographic affinity of planktonic foraminifera to model and predict an upwelling zone in northern Europe during the Cenomanian-Turonian. They predicted that the increase in nutrients supplied by upwelling may have promoted productivity. They described a relationship between the foraminifera species *Helvetoglobtruncana helvetica* and *Marginotruncana* and the area of increased productivity.

Hilbrecht and Dahmer (1994) note an increase in carbonate content at the top of the Cenomanian-Turonian succession during the *M. mytiloides* event. This is controlled by increased deposition of inoceramid debris. They state that the *M. mytiloides* event in the "black shale" facies marks the end of black shale deposition.

4.4.1 Biostratigraphy

The available biozonations of the Lower Saxony basin are based on the ammonites, inoceramids and the foraminifera (Fig. 4.3; Hilbrecht, 1986). The extinction of the foraminifera *Rotalipora cushmani* and *Rotalipora greenhornesis* does not occur until after the "Arme rhotomagense Schichten" beds, just after the basal *plenus* Bank limestone of the Black Shale Facies. This is followed by the *Actinocamax plenus* belemnite zone, then the *Mytiloides* event which marks the top of the north west German Cenomanian-Turonian succession. The ammonites of the region have been studied in detail by Ernst *et al.* (1983).

4.4.2 Carbonate carbon isotope excursion

The global Cenomanian-Turonian $\delta^{13}C$ anomaly (e.g. Schlanger *et al.*, 1987) is observed in Germany, and has been reported by several authors (cf. Scholle & Arthur, 1980; Schlanger *et al.*, 1987; Hilbrecht & Hoefs, 1986). Hilbrecht and Hoefs (1986) characterised two distinct curve types for German sections: the first is a well defined "spike" preceded and followed by constant $\delta^{13}C$ values, (e.g. N.E. England and Eibrunn Marls, Germany). The second curve type exhibits a continuous rise in $\delta^{13}C$ values with a sudden increase above the *Rotalipora* extinction followed by a gradual continuous decrease (e.g. Lower Saxony). Some of the sections studied in Germany include Lengerich, where $\delta^{13}C$ values of +2‰ to +5‰ are observed (by Hilbrecht *et al.*, 1986 and 1996); Radbod 6 borehole, $\delta^{13}C$ +2‰ to +4‰; Mühlberg $\delta^{13}C$ +1.5‰ to +3‰; Wunstorf $\delta^{13}C$ +3.25‰ to +4.55‰; and Sohlde $\delta^{13}C$ +3.0‰ to +4.75‰.

The maximum $\delta^{13}C$ values are always observed in the *plenus* Bank limestone horizon, after the *Rotalipora* extinction; this is also observed in England (Hilbrecht *et al.*, 1992). Carbonate isotope $\delta^{13}C$ values from whole rock samples of the *plenus* Bank horizon at Misberg Quarry show a positive excursion from a background value of +3.3‰ rising to +4.5‰ at its maximum, then dropping back to +3.0‰, (Hilbrecht & Hoefs, 1986).

4.5 Samples

A suite of 28 samples from a 35m cyclic exposure of the Cenomanian-Turonian Boundary at Misberg Quarry was sampled by Heinz Hilbrecht (Geologisches Institut, ETH Zentrum, Sonneggstr. 5, CH-8092, Zürich. Switzerland). The samples were re-numbered for this study (Appendix 1, Table I shows their relation to Hilbrecht & Dahmer, 1994). One sample from the central organic-rich section was not available; this sample corresponds to bed 131/I in Hilbrecht and Dahmer (1994) and represents an organic-rich bed with laminations, common pyrite and fish remains. All the samples were analysed using a combination of bulk geochemistry techniques. Based on these data, 12 samples were selected which showed a wide variation in bulk geochemical characteristics, reflecting the changes through the section. These samples were then analysed using molecular geochemistry and microscopy; carbonate carbon isotope data are given in Hilbrecht and Hoefs (1986).

4.6 Results

4.6.1 Bulk geochemistry and lithological data

Lithological data for the Misberg section are given in Appendix 1, Table II. Bulk geochemistry data for the Misberg Quarry section can be found in Appendix 2, Table II and Figure 4.5. The TOC values range from 0.02 to 1.81% with four maxima above 1%. The onset and termination of the organic-rich facies occurs abruptly corresponding to samples MQ21 and MQ12 respectively. Hydrogen indices are low (56 to124 mgHC/gTOC), and total sulphur values (0.02 to 1.05%) are high for some samples relative to normal marine sediments. The TOC correlates well with S2 (r^2 = 0.86), hydrogen index (r^2 = 0.94) and Sulphur (r^2 = 0.91). Carbonate values (39-82%) appear to increase up the section, and do not exert a great control on the fluctuations in TOC (r^2 = 0.10). Samples MQ14 and MQ18 give much higher kerogen hydrogen indices (212 and 197 mgHC/gTOC respectively) compared with their whole rock equivalents (100 and 62 mgHC/gTOC respectively), suggesting a substantial amount of hydrocarbon retention by the mineral matrix during pyrolysis of the samples.

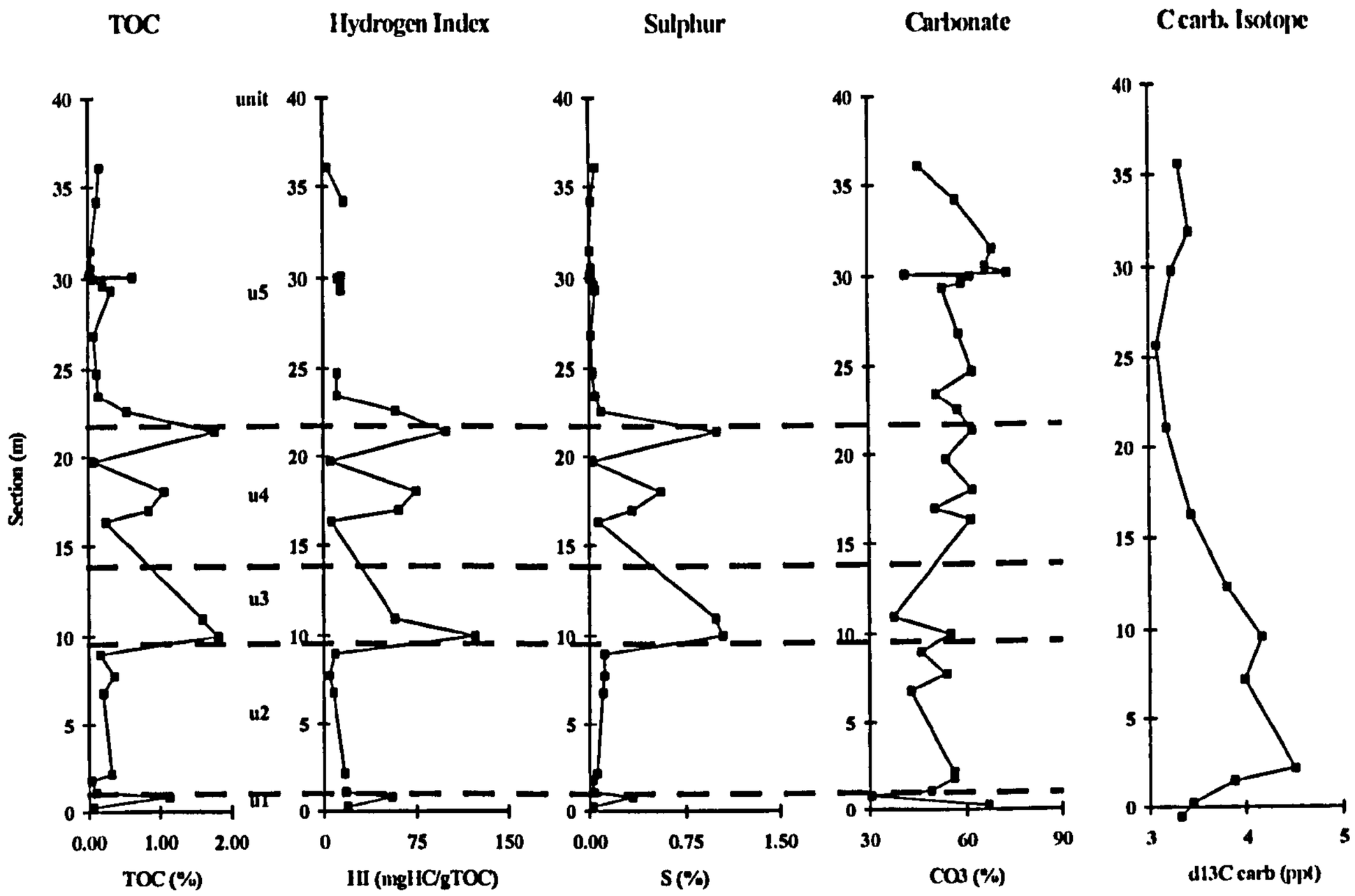

Figure 4.5 Stratigraphic plot of mean bulk geochemical data for the Misberg section (data given in Appendix 2, Table II); Carbonate carbon isotope data from Hilbrecht & Hoeffs (1986).

4.6.2 Microscopy

The vitrinite reflectance of two samples, determined by Dr J. M. Jones, (Department of Fossil Fuels and Environmental Geochemistry, University of Newcastle), were 0.27% R_o and 0.34% R_o (samples MQ10 and MQ20 respectively; Appendix 3, Table I). The confidence level assigned to the determination of this data was low, due to the rarity of vitrinite in the samples.

Palynofacies observations (Appendix 3, Table IV and V) show that weakly fluorescent marine-derived amorphous matter (AOM) is generally dominant (≤70%) in the organic-rich samples, but is less abundant and less fluorescent in the organic lean samples. With the exception of one anomalous sample (MQ20 at 10m, which does not show anomalous lithology or rock colour) the relative abundance of AOM is positively correlated with TOC ($r^2 = 0.56$), S2 ($r^2 = 0.61$) and hydrogen index ($r^2 = 0.88$). The palynomorph fraction (Appendix 3, Table V), is dominated (56 to 93%) by dinoflagellate cysts, the majority of which are of the proximochorate type (42 to 84% of the total cysts); lower relative dinocyst abundance occurs in the organic-rich samples (MQ14, 16 and 18), where the relative abundance of acritarchs is higher

(<15%). There is a higher terrestrial content in the lowermost and uppermost samples, with phytoclasts representing ≤30% of the kerogen particles.

4.6.3 Molecular geochemistry

Molecular geochemical observations from gas chromatograms of the aliphatic fraction are presented in Appendix 4, Table II. The Extractable Organic Matter (EOM; mgHC/gSED) content of the Misberg Quarry samples correlates well with TOC ($r^2 = 0.82$; Fig. 4.6) and hydrogen index ($r^2 = 0.85$; Fig. 4.7). The gas chromatograms (Fig. 4.8 a & b) all have similar *n*-alkane distributions; after an *n*-alkane maximum at nC_{17}, there is a rapid tail off after nC_{20}, with a very low abundance between nC_{20} to nC_{33}. The *n*-alkanes are more abundant than the isoprenoids pristane and phytane, and all samples show a Pr/Ph ratio of greater than 1.0.

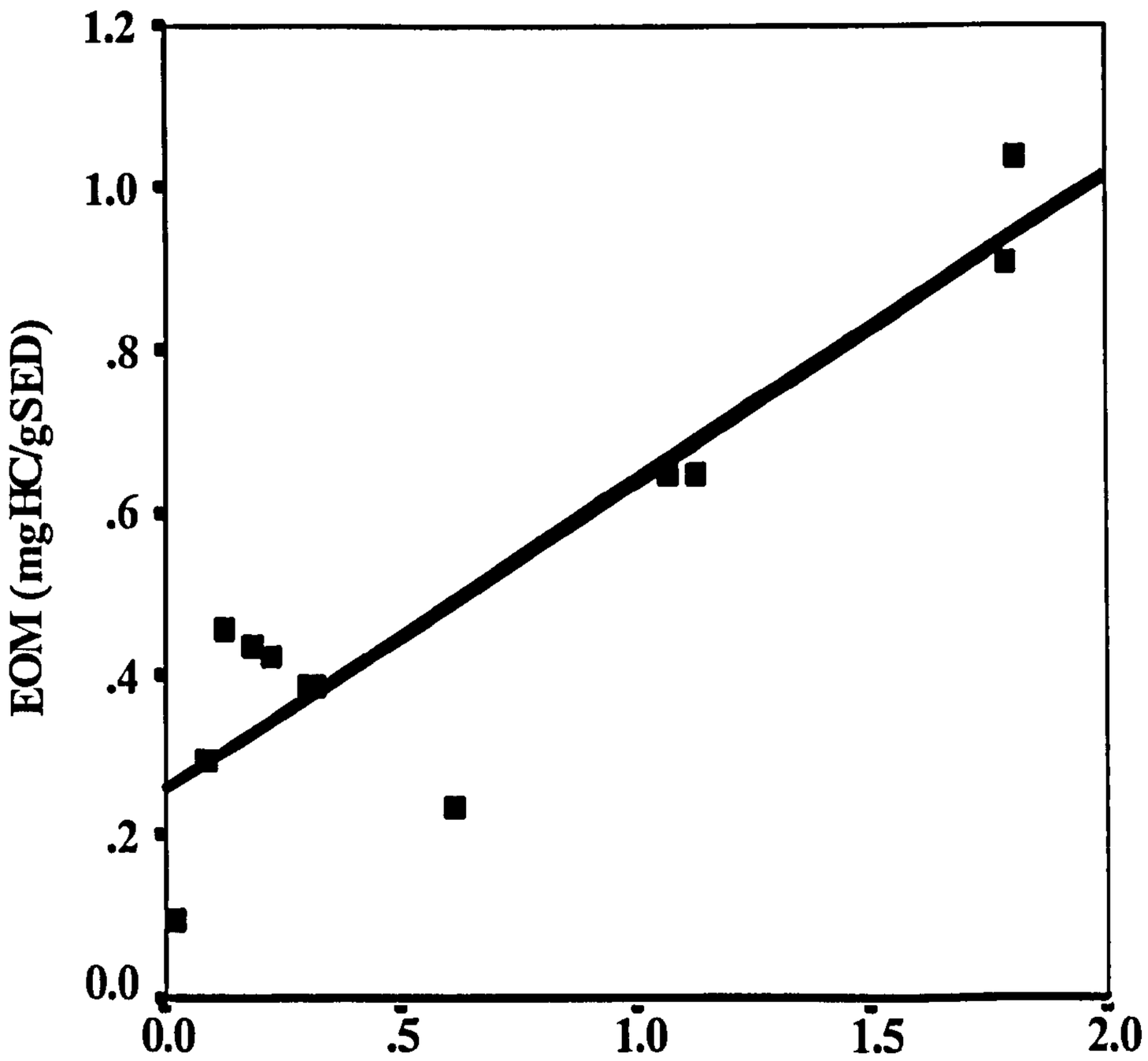

Figure 4.6 Cross plot of Extractable Organic Matter versus Total Organic Carbon for the Misberg section. The data shows a good correlation ($r^2 = 0.82$).

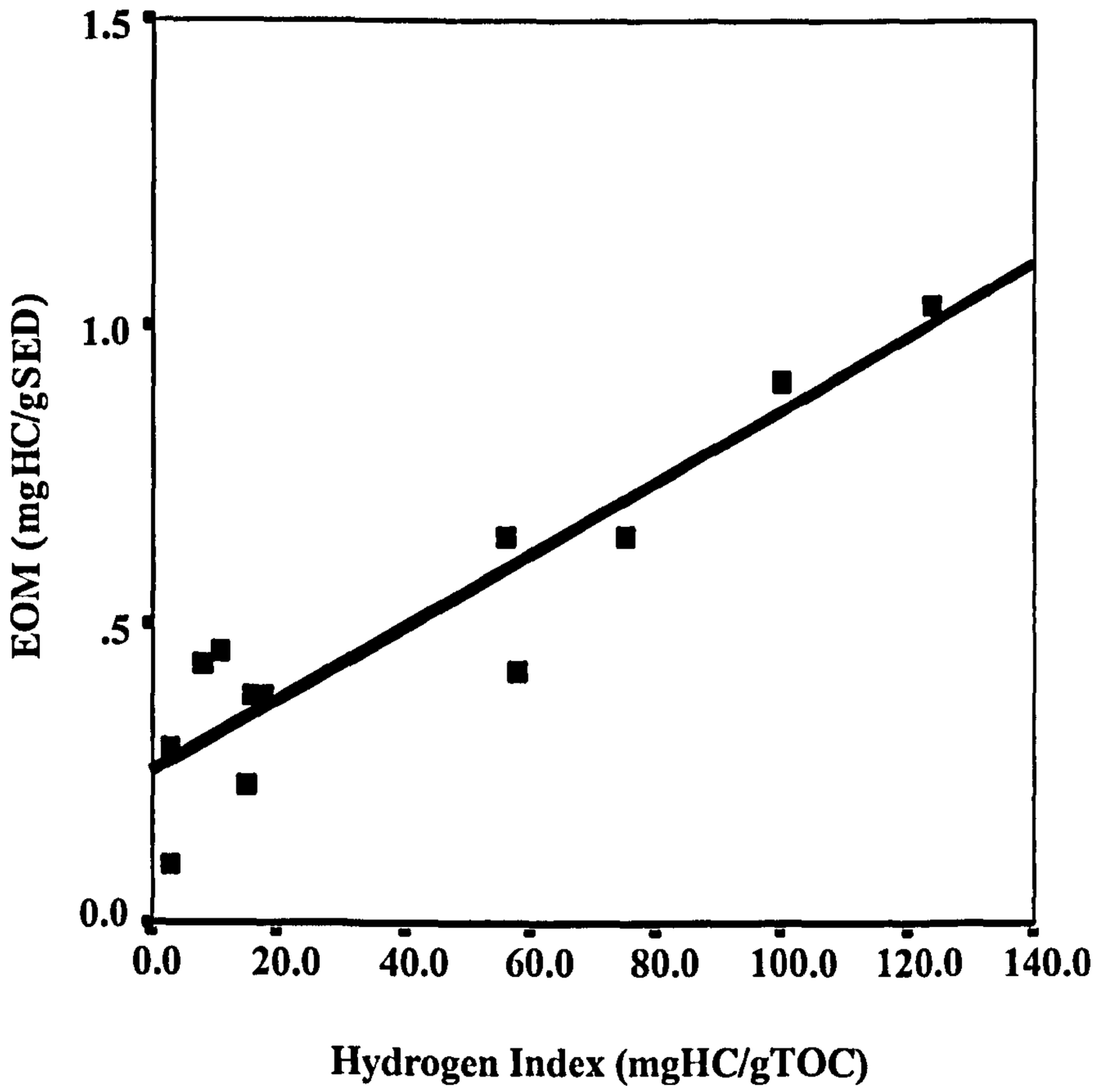

Figure 4.7 Cross plot of Extractable Organic Matter versus Hydrogen Index for the Misberg section. The data shows a good correlation ($r^2 = 0.85$).

Biomarker ratios for the aliphatic fraction (cf. Mackenzie, 1984) calculated from gas chromatography-mass spectroscopy peak area data are given in Appendix 4, Table VIII, and show wide apparent variations in maturity between the samples. Side chain isomerisation is high, and 17β (H), 21β (H) hopanes and hop-17(21)-enes are absent in these traces. Maturity parameters for the aromatic fraction (cf. Radke, 1987) run on gas chromatography-mass spectroscopy (Appendix 4, Table XII) also show a range of values.

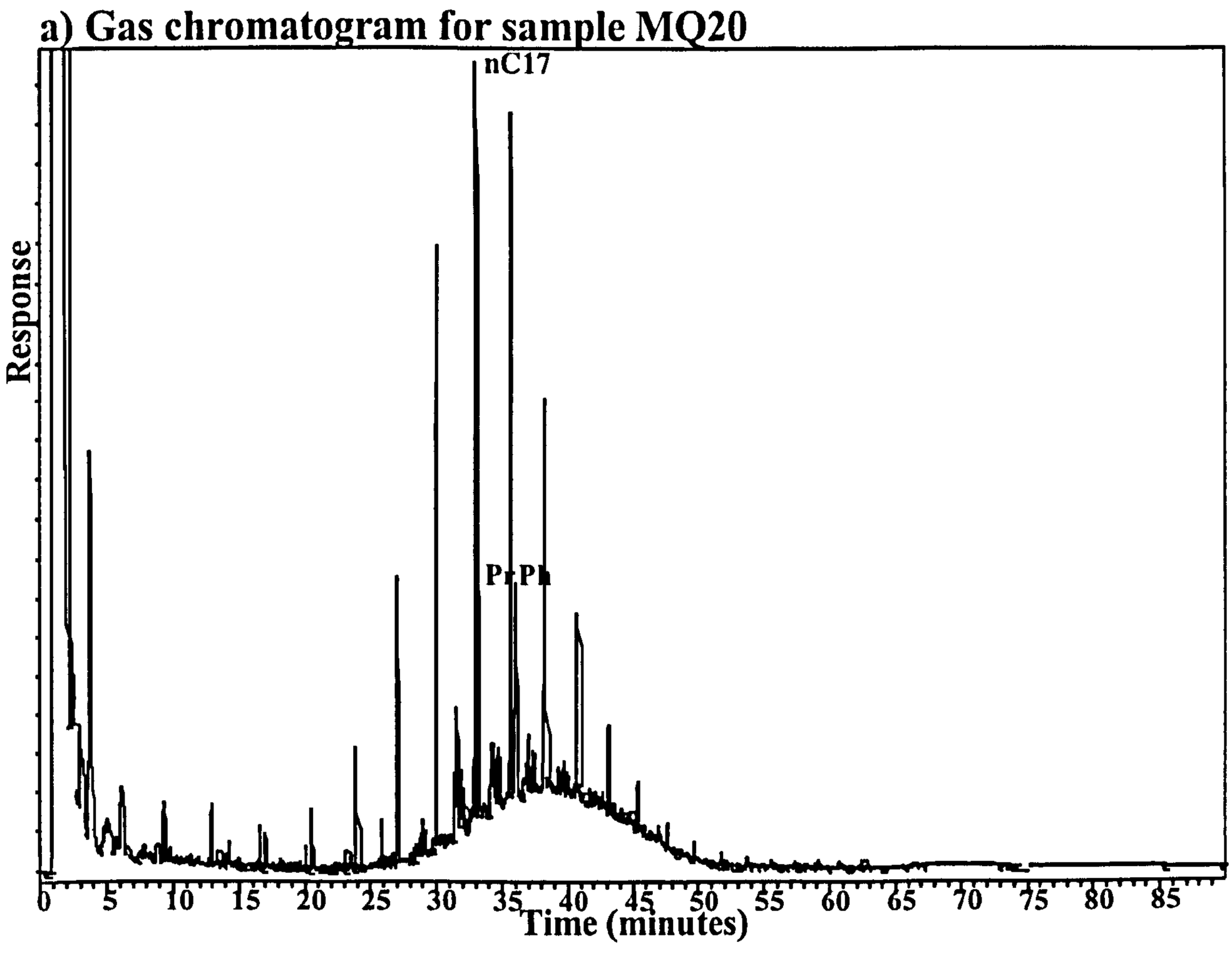

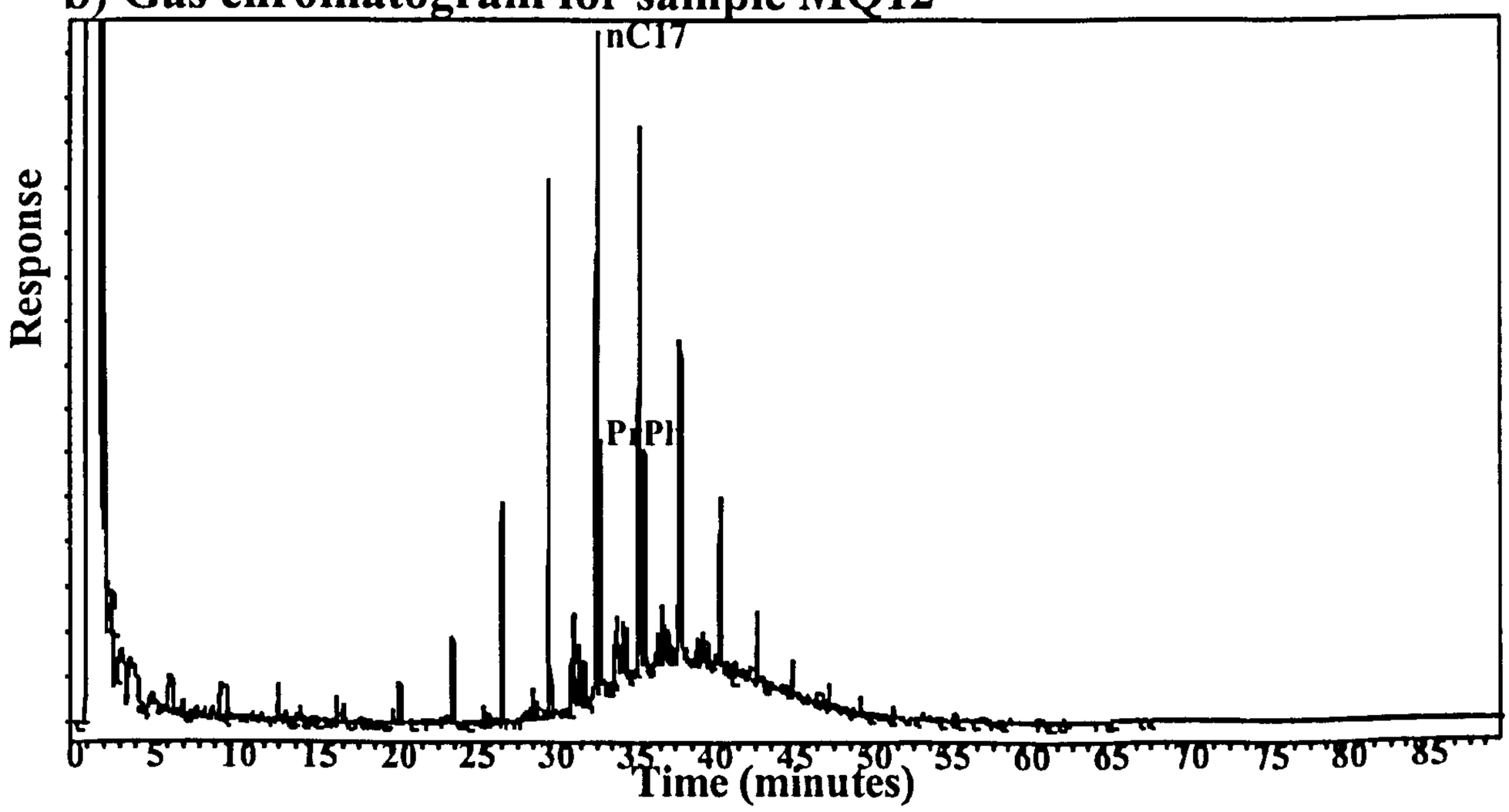

Figure 4.8 Gas chromatograms for the Misberg Quarry section; nC, normal alkane with carbon number; Pr, Pristane; Ph, Phytane; a) sample MQ20, 10.0m; b) sample MQ12, 23.5m.

4.6.4 Constrained clustering

Constrained clustering analysis carried out on the Misberg Quarry locality redefined the section into five units based upon bulk geochemistry data. This subdivision of the section allows the calculation of descriptive statistics for each of the units; the TOC, hydrogen index and CO_3 data for these units are shown in Figure 4.9.

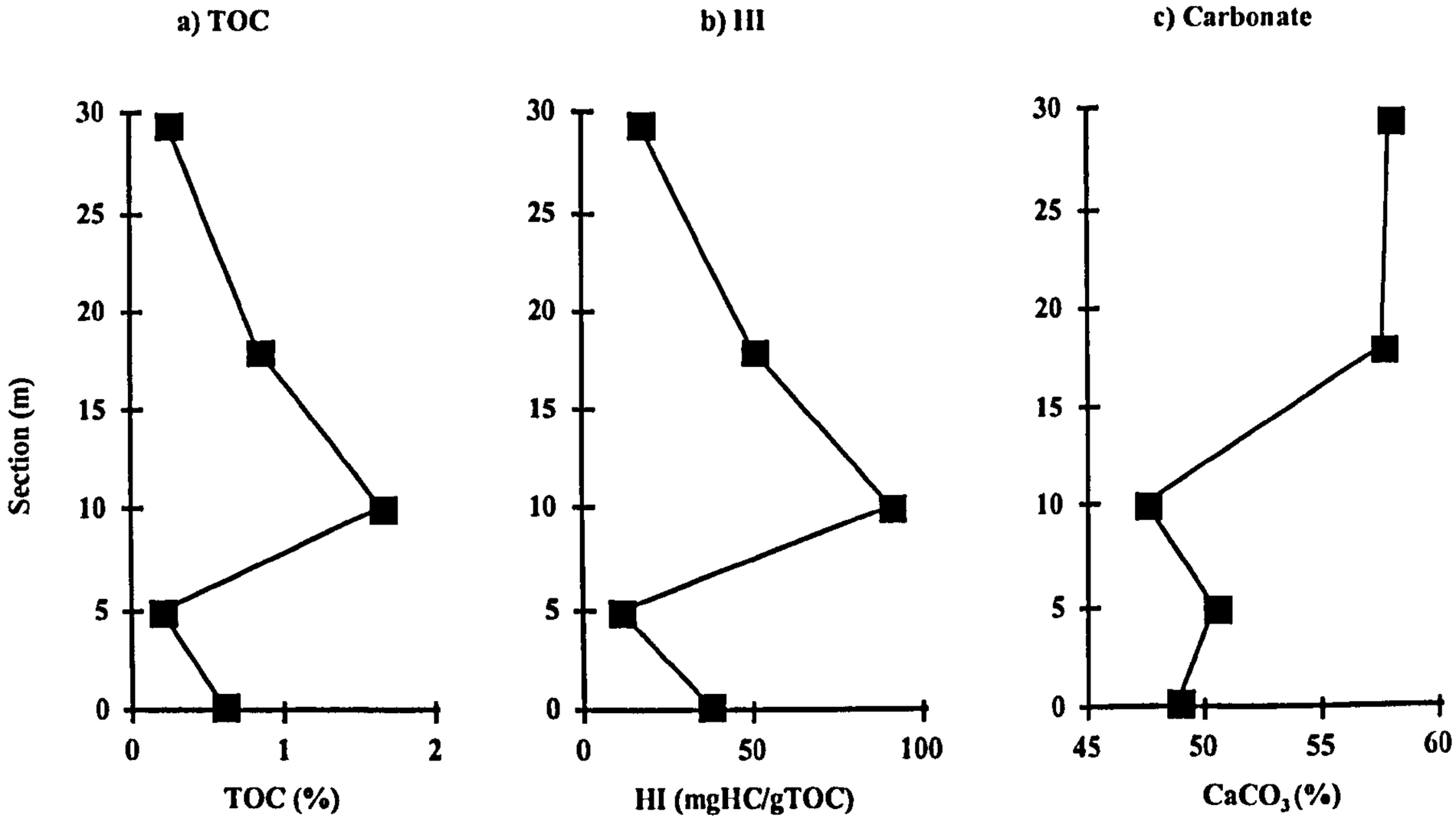

Figure 4.9 Mean bulk geochemical data from constrained clustering unit data of the Misberg Quarry section.

4.7 Discussion

4.7.1 Bulk geochemical and lithological characteristics

Comparisons of bulk geochemical and lithological data show that mean TOC, sulphur and hydrogen index values are higher in samples with a darker rock colour (Fig. 4.10). This suggests that rock colour is controlled by a combination of pyrite, organic matter content and organic matter type for this section.

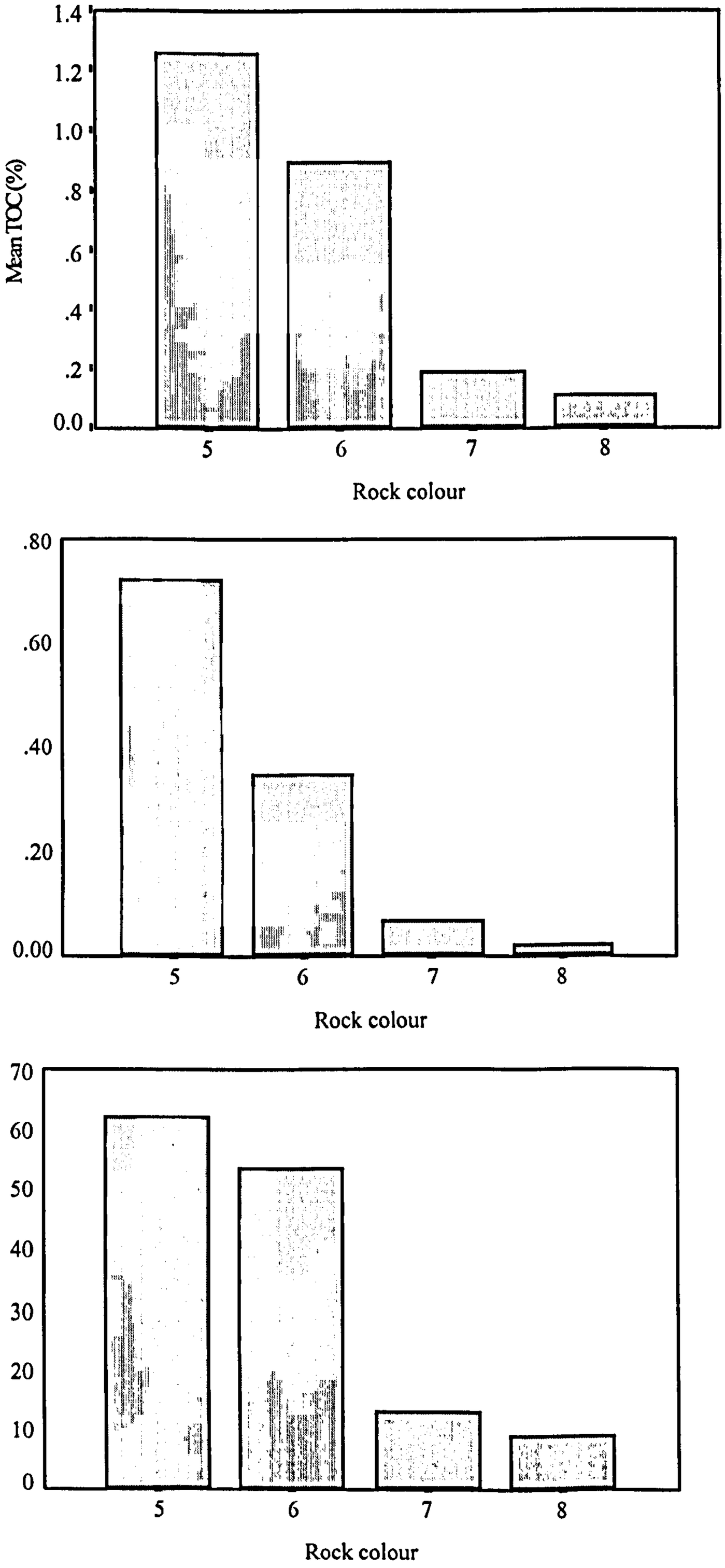

Figure 4.10 Bar charts showing average TOC, sulphur and hydrogen index for different lithological rock colours for the Misberg section. The lower numbers refer

to darker lithologies (Appendix 1) based on the American Rock Color Chart (Section 2.1).

Stratigraphic plots of mean TOC and hydrogen index values, calculated from the units (section 4.6.4), are lowest in the *A. plenus* bed and highest during the *N. juddii* event. A plot of TOC v. $CaCO_3$ (Fig. 4.11) shows no correlation (linear $r^2 = 0.01$) suggesting that carbonate dilution does not control TOC. Figure 4.5 shows the stratigraphical variation of $CaCO_3$ for Misberg Quarry. A general increase in whole rock carbonate content is observed towards the top of the section, this appears to agree with the observations made by Hilbrecht and Dahmer (1994) regarding the increase in deposition of inoceramid debris. The plot of mean carbonate data for the units defined by constrained clustering (Fig. 4.9) also indicate the general increase in carbonate contents, which reach their highest values at the start of the *M. mytiloides* event.

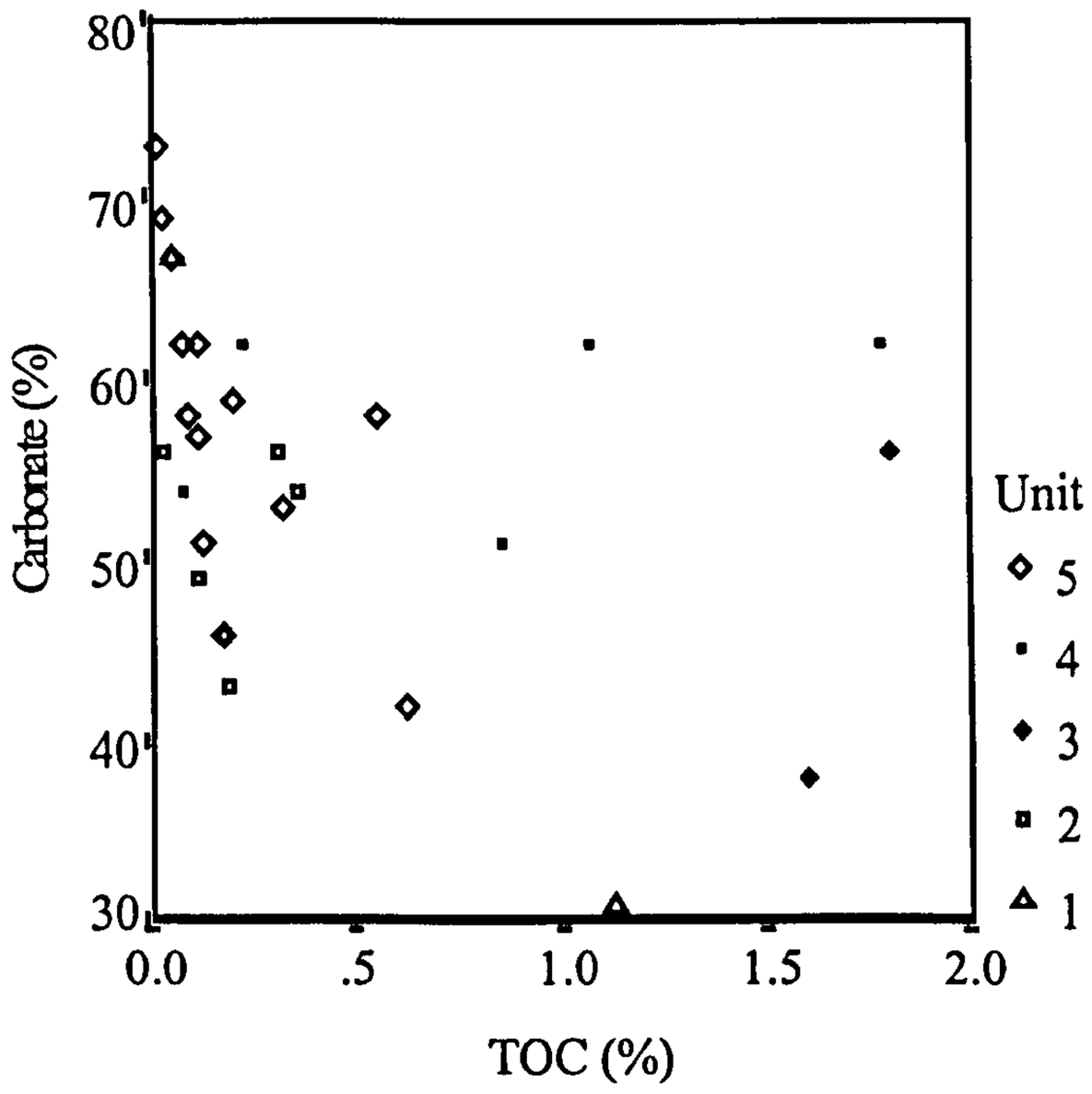

Figure 4.11 Cross plot of TOC versus wt% carbonate data for the Misberg Section. Note the poor correlation between the total data set ($r^2 = 0.10$). Unit 5 shows better correlation for these parameters ($r^2 = 0.41$).

A plot of TOC v. AOM shows a poor correlation ($r^2 = 0.20$). However, if the anomalous organic-rich, (but low AOM) sample MQ20 is removed the regression fit is much better ($r^2 = 0.56$; Fig. 4.12). This is also observed in the plot of S2 v. AOM ($r^2 = 0.11$; compared to $r^2 = 0.61$; Fig. 4.13). A good correlation of these parameters would suggest that enhanced TOC and petroleum potential are controlled by the amounts of preserved AOM. However, it is unclear why sample MQ20 does not fit the rest of the data, as it has no distinguishing lithological characteristics.

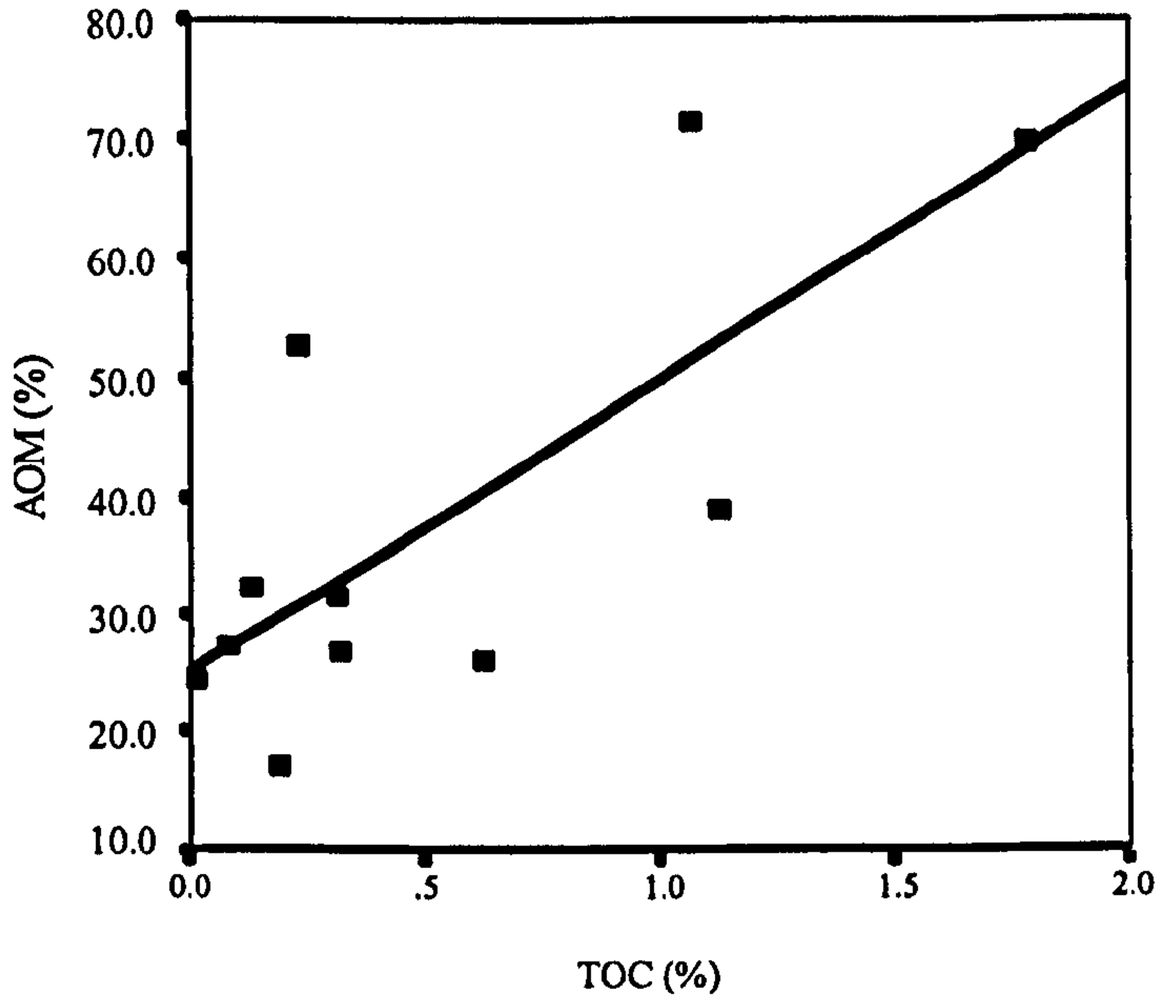

Figure 4.12 Cross plot of TOC versus Amorphous Organic Matter for the Misberg Section. The data shows some relationship ($r^2 = 0.56$).

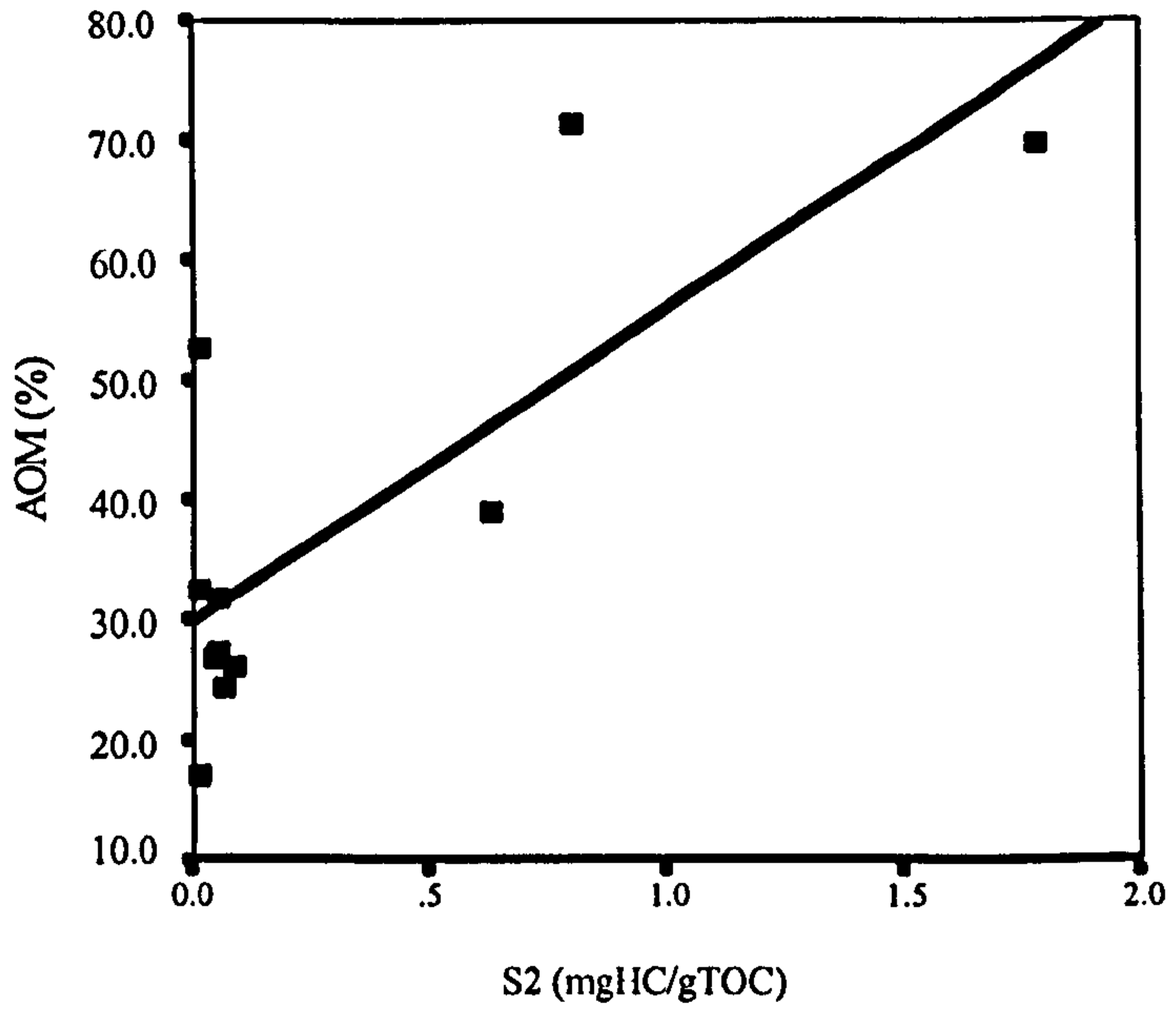

Figure 4.13 Cross plot of Rock-Eval S2 versus Amorphous Organic Matter for the Misberg Section. The data shows some relationship ($r^2 = 0.61$).

4.7.2 Isotope geochemistry

The carbonate carbon $\delta^{13}C$ isotope excursion (Hilbrecht & Hoefs , 1986) coincides with the onset of the anoxic event, and the first TOC maximum. It continues into the beginning of the "central" organic-rich black shales. Plots of TOC v. $\delta^{13}C$ and hydrogen index v. $\delta^{13}C$ (not shown) show no apparent relationship (both $r^2 = 0.03$), suggesting that the carbonate isotope excursion is not controlled by the type or amount of organic matter input; nor is there any relationship with carbonate content.

4.7.3 Organic matter maturity

The production indices (range 0.1-0.23; mean 0.12) and Tmax (range 429-436°C; mean 432°C) data from the organic-rich samples indicate that these samples are at the immature stage of hydrocarbon generation (cf. Espitalié *et al.*, 1977; Orr, 1983), which is similar to the maturity recorded at Buckton Cliff and South Ferriby.

The tailing off of *n*-alkanes observed in the gas chromatograms could be due to a relatively greater input of short chain *n*-alkanes from algal organic matter. However, weathering effects cannot be ruled out. The Pr/nC_{17} and Ph/nC_{18} ratios are all less than 1.0 (range 0.2 to 0.6; Appendix 4, Table II), indicating a slightly higher maturity (cf. Leythaeuser & Schwarzkopf, 1986) compared to the Buckton Cliff and South Ferriby samples.

The absence of 17β (H), 21β (H) hopanes (e.g. Ourisson *et al.*, 1987), and hop-17(21)-enes, suggests that these sample are slightly more mature that those from Buckton Cliff. However, hop-13(18)enes, which are normally absent in mature sediments, were observed in some traces; these hopenes have been found at greater depths than other hopenes (Farrimond *et al.*, 1986). Stratigraphic plots of the hopane and sterane maturity parameters (Fig. 4.14 and 4.15) both show high conversion of the R isomers to the S isomers (cf. Mackenzie, 1984), which suggests that the maturity of these samples is early mature, approaching the oil window. The maturity values determined for the homohopanes, in samples MQ14, 16 and 27 are slightly lower than the majority of the values for the other samples; however, as these values occur in the organic-rich (>1.0% TOC) samples they are most likely to reflect the true biomarker maturity values. The gas chromatography-mass spectroscopy traces for these samples suggested some degree of co-elution with other compounds, which has affected the ratio. Values from aromatic ratios (cf. Radke, 1987) such as the Methylphenanthrene Index (MPI-1), and the percentage triaromatic steroids to monoaromatic steroids, give similar maturity values to their aliphatic counterparts. When compared on maturity scales (e.g. Killops & Killops, 1993, p.204) the biomarker ratios indicate that the values obtained from vitrinite reflectance work are too low (Section 4.6.2).

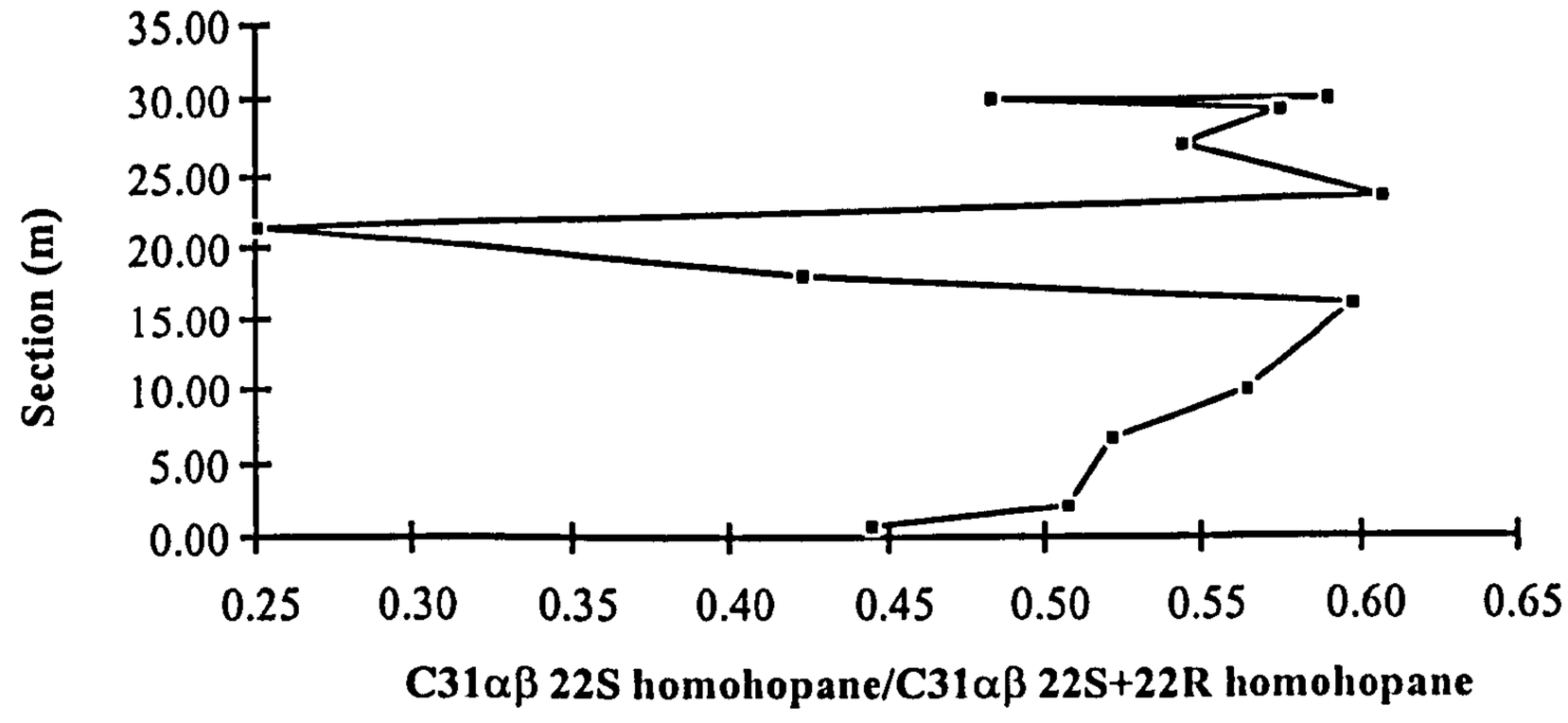

Figure 4.14 Stratigraphic plot of the homohopane maturity parameter for the Misberg section.

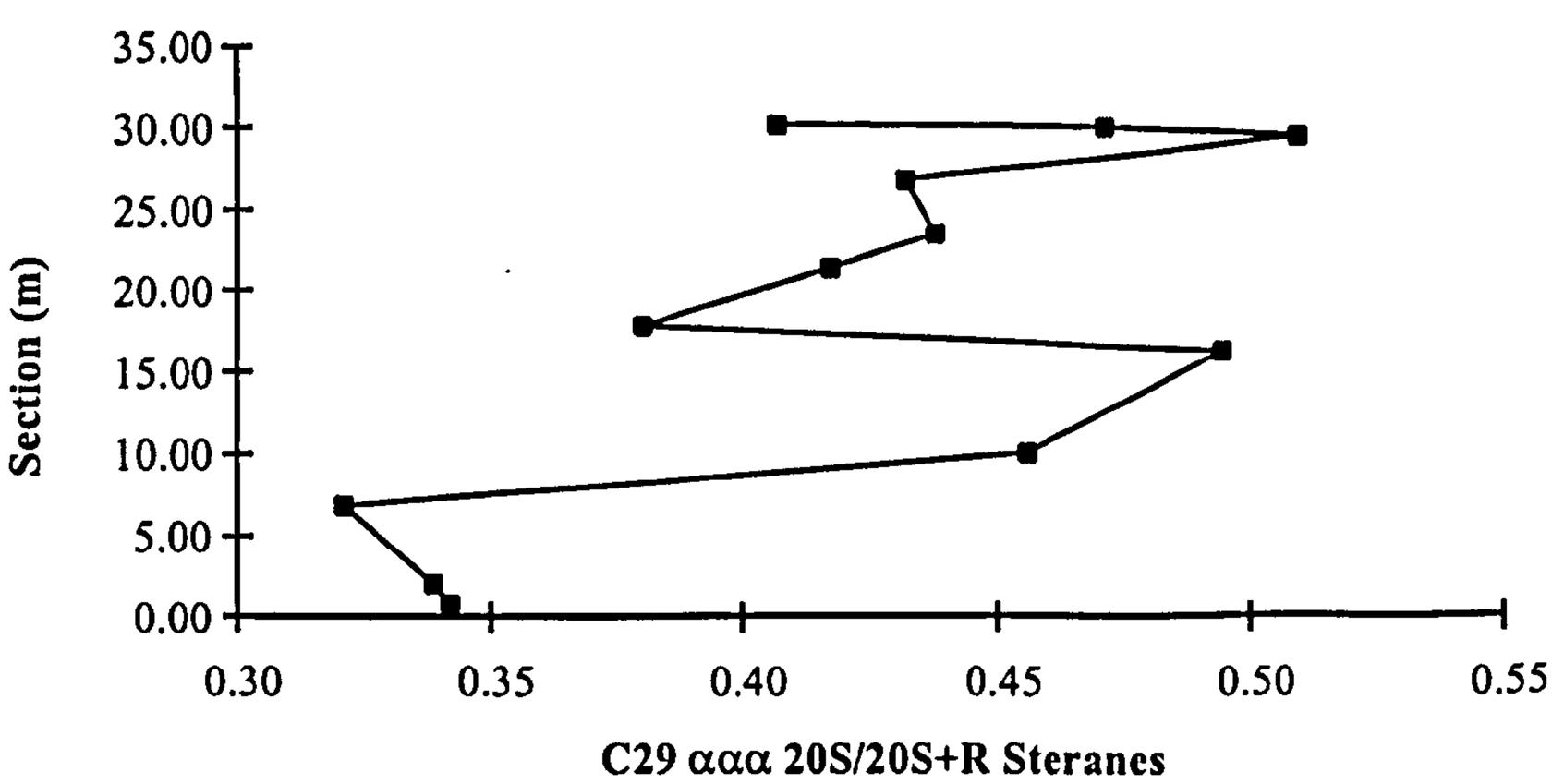

Figure 4.15 Stratigraphic plot of the homohopane maturity parameter for the Misberg section.

The apparent maturity differences observed through the section are unlikely to be a result of heating, as the interval is so narrow. These differences are more likely to be a result of differing organic facies. The Misberg samples that are rich in phytoclast material appear slightly more mature than those with less terrigenous derived material. This was also observed at Buckton Cliff (section 3.3.3), although to a higher degree. This could be due to preservational differences between the organic matter type, or a higher amount of reworked material in the samples with higher

terrestrial content. Effects of mineral interactions (Mayer, 1994; Keil *et al.*, 1994) can not be ruled out.

4.7.4 Organic matter sources

From optical examination the kerogen assemblage is dominated by marine AOM suggesting that the majority of the organic material in these samples is of algal or bacterial origin. There is also significant amount of terrestrially derived material in the form of phytoclasts.

The dominance of dinoflagellate cysts in the palynomorph fraction (Appendix 3, Table V), also seen at the Buckton Cliff locality (section 3.3.4), is not surprising considering that they are the predominant form of fossilising phytoplankton in most Mesozoic marine sediments, and can form a very high percentage of the fossilised organic-walled microplankton. The presence of 4-methyl steranes in the Misberg samples, identified from GCMS, is also consistent with the presence of dinoflagellates (cf. Wolf *et al.*, 1986). The proximochorate cyst form the dinoflagellate cysts assemblage in the Misberg samples dominates (relative numeric frequency 42% to 84%), and has highest relative abundances in the central organic-rich samples. The chorate and cavate cyst forms are relatively dominant in the organic-poor samples. This agrees with the work done by Marshall and Batten (1988). They noted that *Spiniferites* (a chorate cyst form) was dominant in the organic-poor lithologies and that *Cyclonephelium* (a proximochorate cyst form) was dominant in the organic-rich lithologies. The implications of this observation will be discussed in relation to the environment of deposition (Section 4.7.5).

Whole rock Hydrogen Indices indicate a Type IV kerogen for most samples, but a Type II/III kerogen in samples with higher TOC's (>1%). A plot of TOC v. S2 (Fig. 4.16; Langford & Blanc-Valleron, 1990) indicates a kerogen Type III/IV, and regression analysis carried out on this data shows that linear regression ($r^2 = 0.87$) fits the data well. However, as observed in the Buckton Cliff section, a quadratic regression ($r^2 = 0.93$) gives a better fit, probably due to the greater matrix effect that appears to affect all samples with TOC <0.5%. This challenges the belief that the TOC v. S2 relationship is linear (cf. Langford & Blanc-Valleron, 1990). It may be more accurate to say that a series of straight lines fits the data better, at least for some of the TOC ranges. The average hydrogen index calculated from the slope of the regression line ($y = 0.943x - 0.139$), gives a hydrogen index of 94 mgHC/gTOC (cf. Langford & Blanc-Valleron, 1990). Kerogen hydrogen index values are

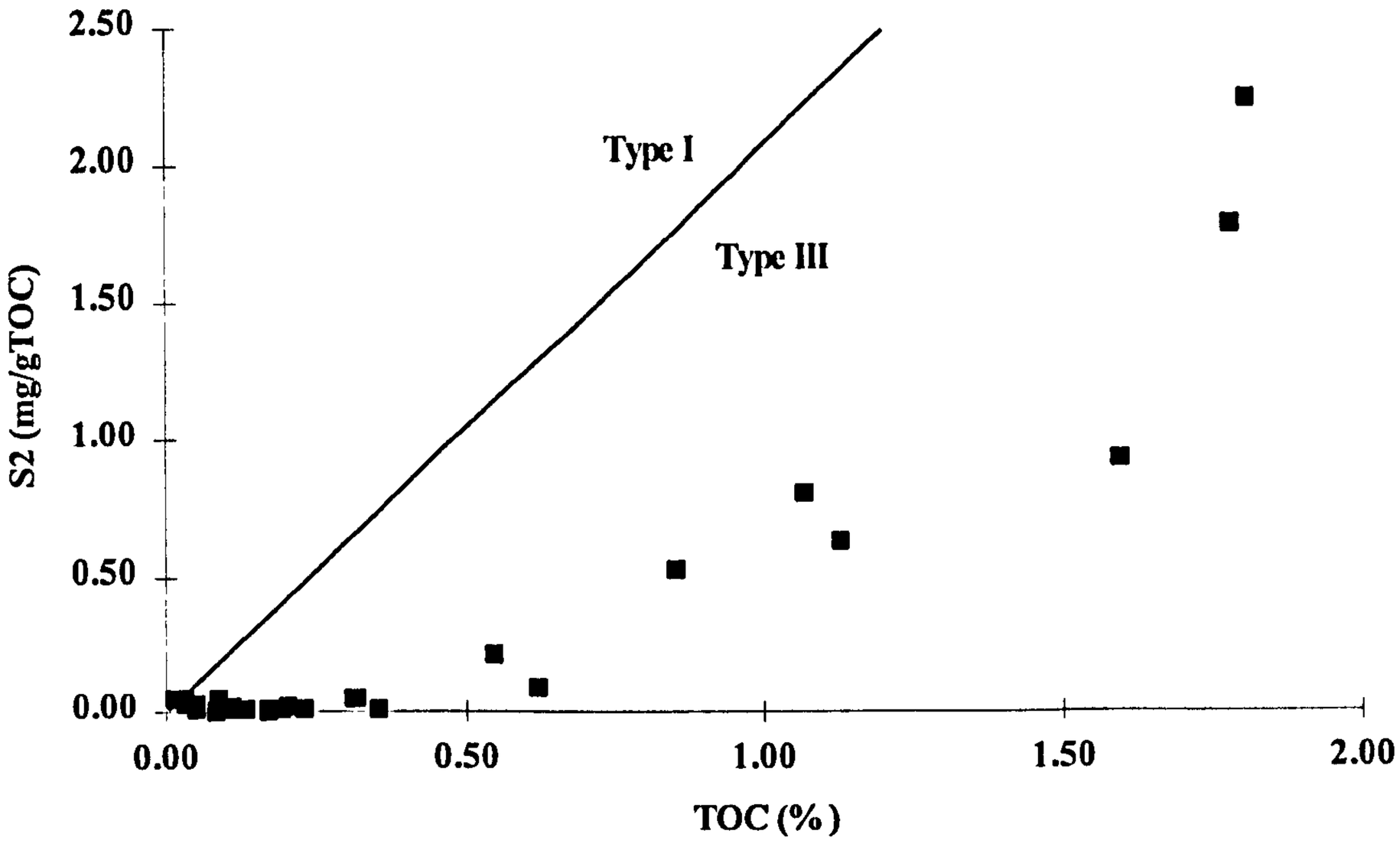

Figure 4.16 Cross plot of TOC versus S2 data for Misberg (based on Langford & Blanc-Valleron, 1990). The data plot in the Type III kerogen zone, although samples with TOC values <0.5% indicate an inert kerogen, possibly Type IV.

significantly higher (197 and 212 mgHC/gTOC, for sample MQ18 and MQ14 respectively) indicating a Type III kerogen. This suggests that adsorption by the matrix clays results in around 50% of the hydrocarbons not being released from the organic-rich samples and >90% not released from the organic-poor samples. These observations are made on a comparison of released S2 per gram TOC, between whole rock and kerogen samples.

Rock-Eval pyrogram profiles show a bimodal S2 peak (Fig. 4.17), especially in the organic-poor samples, this may indicate two different types of organic matter present in the kerogen, possibly fresh and reworked. This bimodal S2 should not affect the hydrogen index calculation, and the low values for hydrogen index in association with this form of S2 peak may be partly due to mixing of kerogen types. The Tmax will be higher for samples which show this bimodal profile, especially if maximum generation occurs in the second part of the S2 peak.

The sterane 27/29ααααR ratio which may reflect the type of organic matter that has sourced the steranes (Huang & Meinschein, 1979) gives a range of values from 0.5 to 1.3. Typically, the central organic-rich samples have relatively higher amounts of the C_{27} homologue suggesting a higher marine contribution to these sediments.

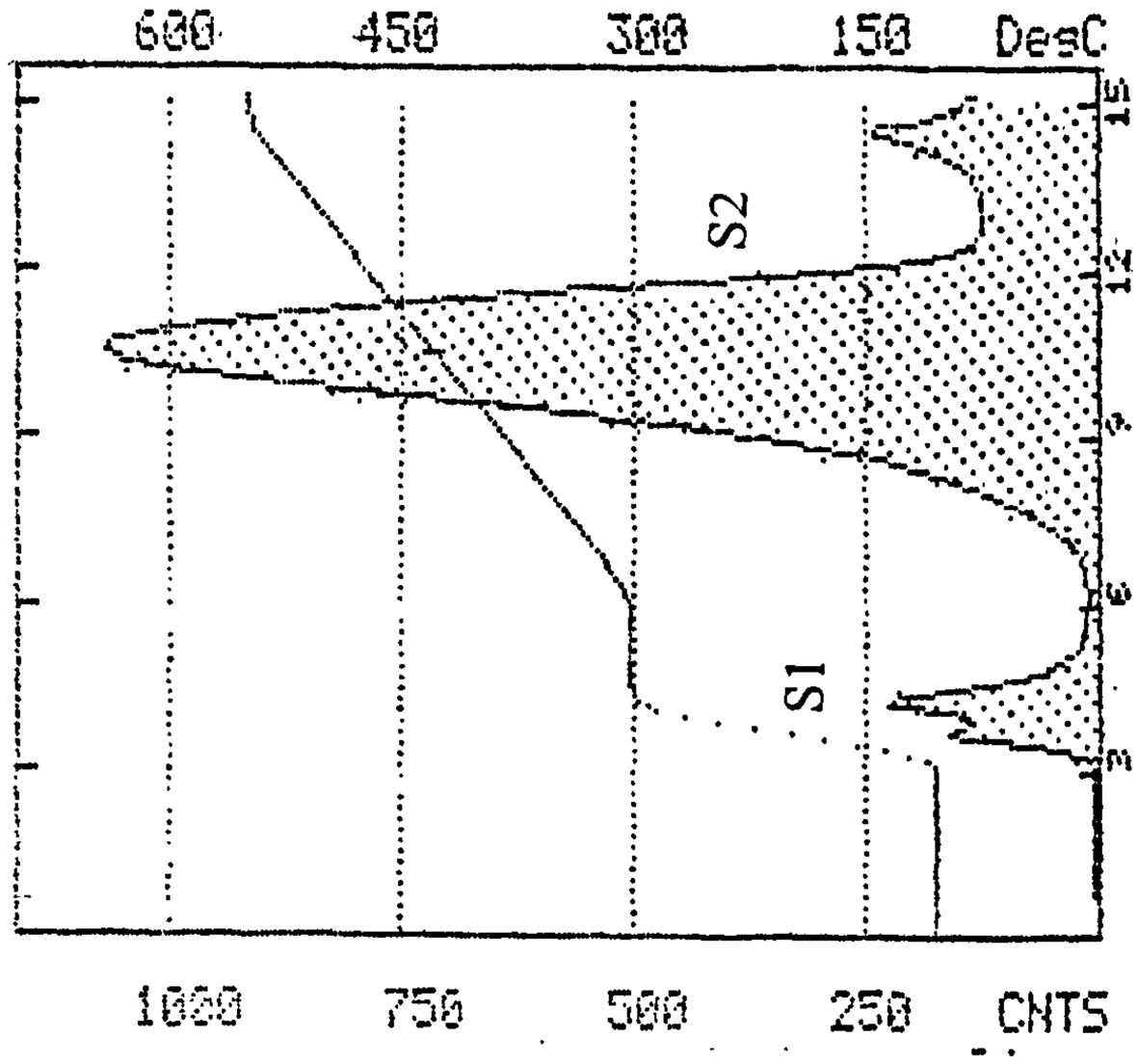

b) Rock-Eval pyrogram for MQ14

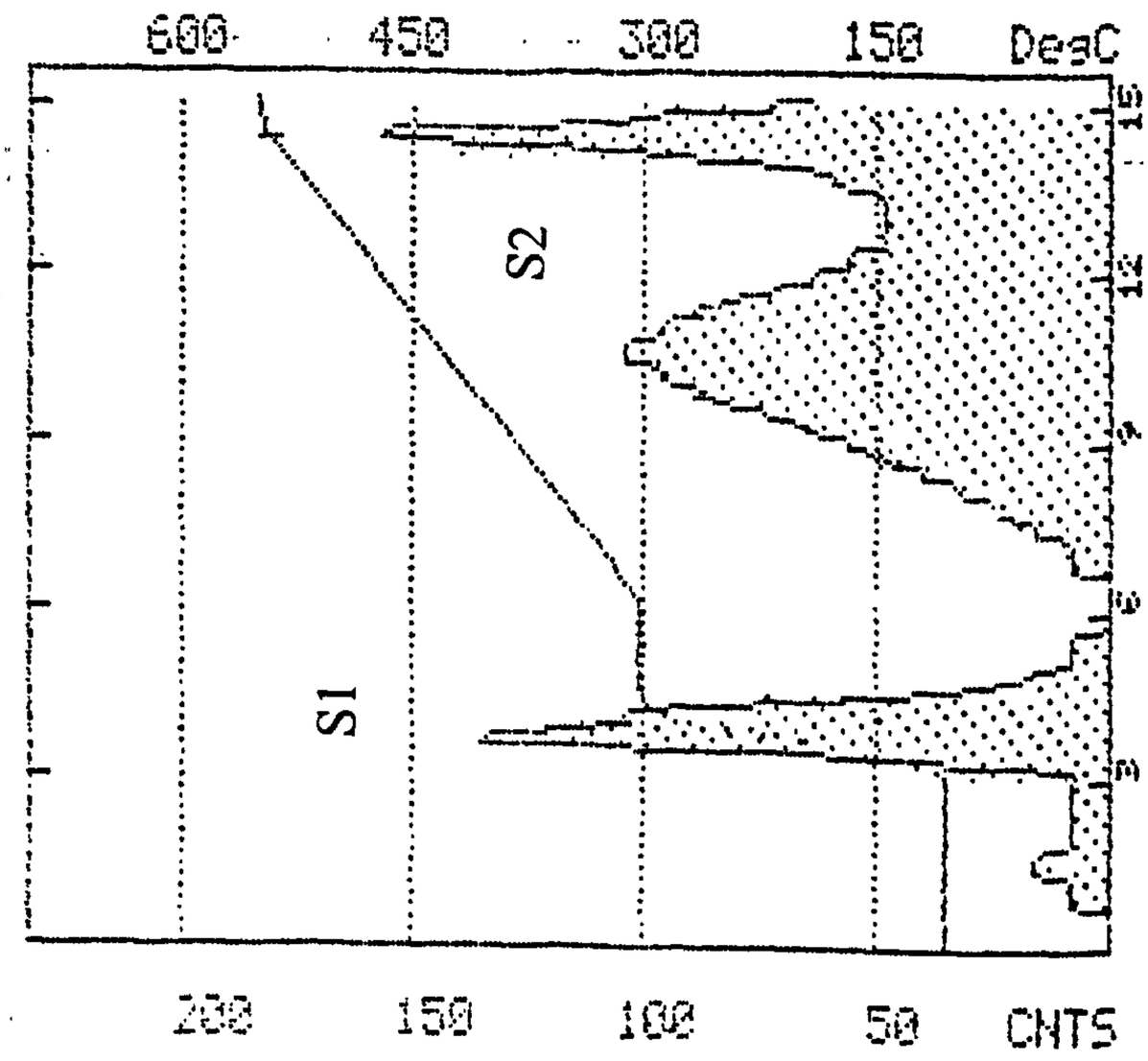

a) Rock-Eval pyrogram for MQ5

Figure 4.17 Two Rock-Eval pyrograms from the Misberg Section, showing the effect of a bimodal S2 peak on the Tmax value. The bimodal S2 peak suggests the presence of fresh and reworked organic matter.

As noted in Section 3.3.4, the interpretation that C_{27} steroids are marine sourced and that C_{29} steroids are terrestrially sourced is too simplistic, as certain marine algae can be dominated by C_{29} steroids (Volkman, 1986). A plot of this sterane ratio against AOM/Phytoclast ratio shows a poor correlation ($r^2 = 0.36$, not shown), but plotted directly against AOM, it is slightly better ($r^2 = 0.44$, not shown). This suggests that some of the C_{27} αααR sterane input is from an AOM source; a negative correlation ($r^2 = 0.40$; not shown) is observed between AOM and C_{29} αααR sterane which helps to confirm this.

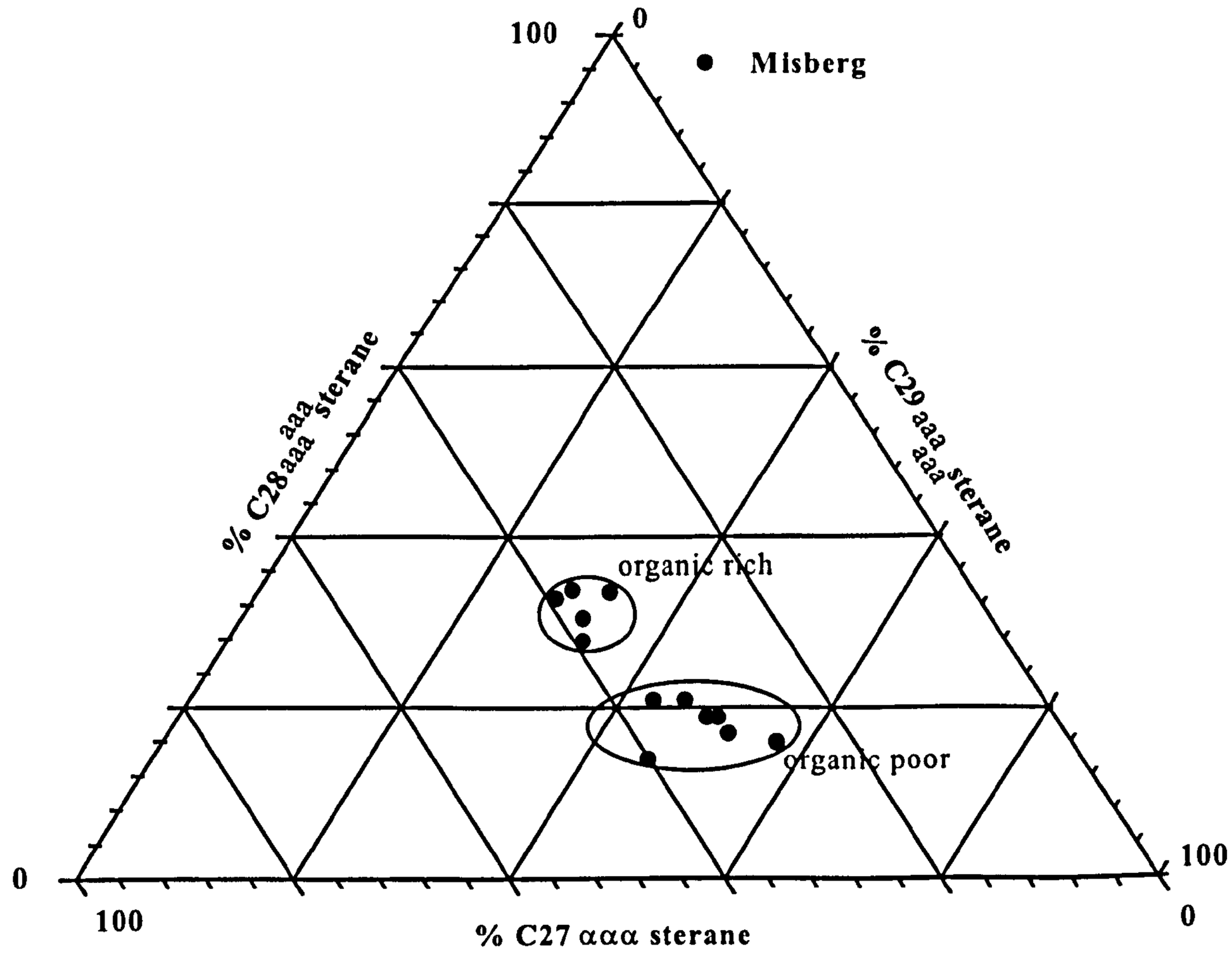

Figure 4.18 Ternary C_{27}-C_{28}-C_{29} αααR sterane plot (after Huang & Meinschein, 1979) for the Misberg section, based on relative amounts (%) data from Appendix 4, Table VIII.

A ternary plot of 27:28:29αααR steranes (Fig. 4.18), shows that samples from this locality plot in two clusters: the organic-poor samples plot closer to the C_{29} pole, where as the organic-rich samples plot with higher C_{27} and C_{28}. The organic-rich samples from Misberg plot in the same area as the organic-rich sample BC4 from Buckton Cliff, and the organic-poor Misberg samples plot in a similar area to the rest of the Buckton Cliff section. As the plotting order may reflect differing algal input, this may suggest that the main controls on algal steroidal input were similar for organic-rich and poor sediments at these two localities. It also suggests that algal

input and perhaps productivity changed during the deposition of the organic-rich samples.

Bacterial contributors to these sediment are noted in the high abundance of hopanoids in these samples (Ourisson *et al.*, 1979). The approximate abundance of hopanoids and steroids (Appendix 4, Table VIII), taken from peak area data, suggest that hopanoids are relatively more abundant than steroids for the Misberg section (although response factors are not considered). This relationship was also noted in samples from Buckton Cliff. The C_{30} αβ 2α methylhopanes show a 4-fold increase in sample MQ12 relative to the C_{30} αβ hopane (Appendix 4, Table VIII). This may be an indication of a specific bacterial input, such as cyanobacteria or methylotrophs for this sample (Zundel & Rohmer, 1985). Methanogenic bacteria are generally recorded from the presence of lycopane in the GC traces, but this could not be determined in these samples.

4.7.5 Environment of deposition

Some *Chondrites* bioturbation was observed in samples MQ26 and MQ25, at the base of the section suggesting that bottom water O_2 levels were greater than 0.2ml/L during their deposition. This corresponds to the *Chondrites* event observed by Hilbrecht (1986). Laminations are present in some of the black shales (e.g. MQ19 and MQ16) indicating that oxygen levels dropped below those that support active burrowing marine life with possible periods of temporary dysoxia-anoxia. However, there is no stabilisation of hydrogen index with increasing TOC (Fig. 4.19; $r^2 = 0.85$), suggesting that optimum preservation is not achieved at this locality The typical hydrogen index at optimum preservation for a marine Type II kerogen is 500 to 600, whereas maximum hydrogen index at this section is much lower - even the value for the kerogen isolate is only 200 mgHC/gTOC.

The relative increase in TOC levels from background values to those in the organic-rich samples is at least 18-fold. The normal increase accounted for by preservation in anoxic conditions is generally no more than 6-fold (Tyson, 1995). This suggests that either an increase in productivity and organic matter flux or a reduction in sedimentation rate also has occurred during the deposition of these samples. Hilbrecht *et al.* (1992) have predicted an upwelling zone in the Lower Saxony area, and the Misberg locality appears to lie on the southern edge of this zone.

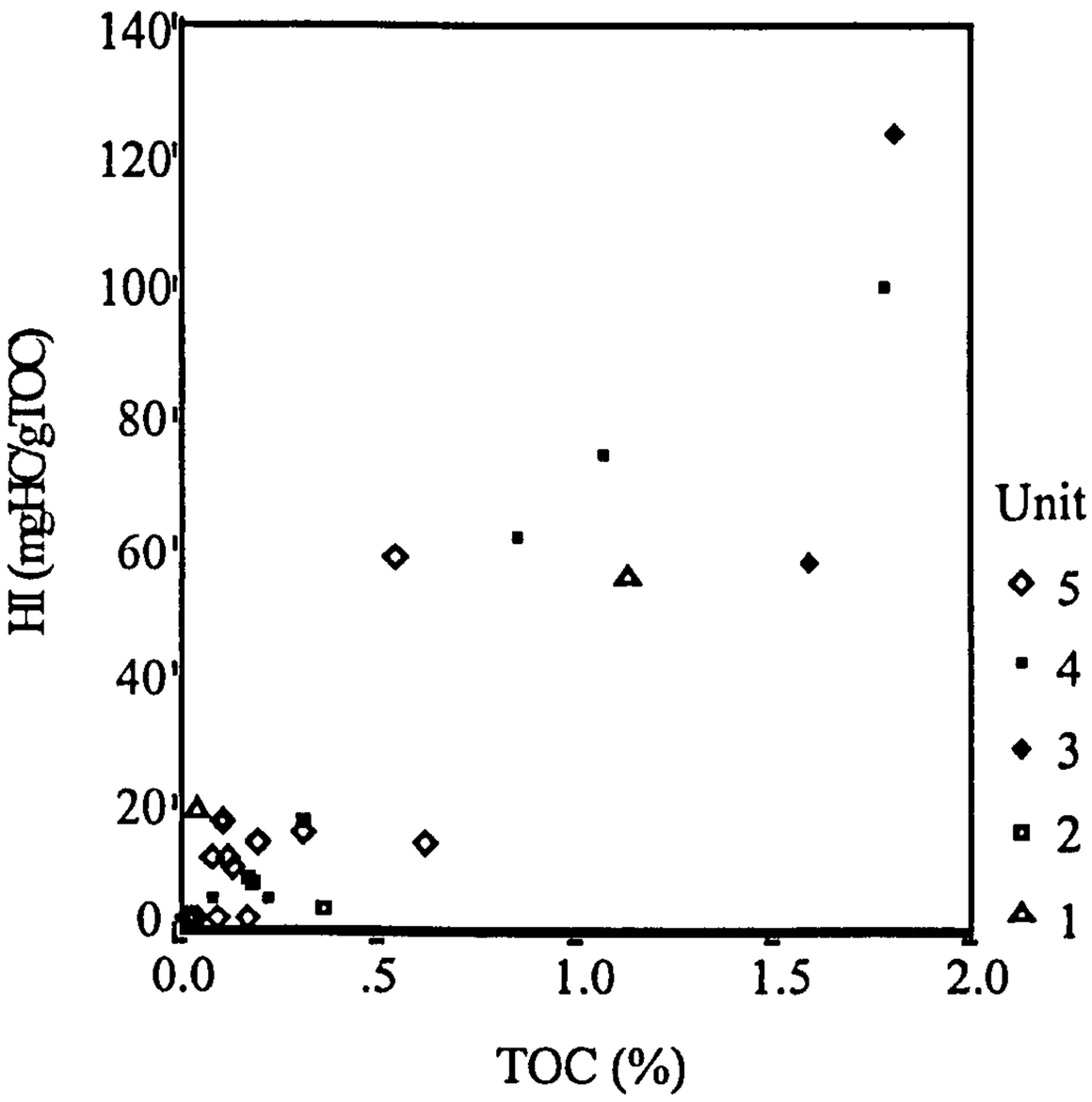

Figure 4.19 Cross plot of TOC versus hydrogen index for the Misberg section. The units from constrained clustering are identified. The data shows a good correlation (r^2 = 0.85). The hydrogen index data shows no sign of levelling off with increasing TOC, suggesting that optimum preservation conditions were not achieved.

The kerogen does not fluoresce strongly and has a reflected fluorescence preservation scale value of 3 (Tyson, 1995) which indicates that the majority of samples were deposited under poor preservational conditions. However, there is increased kerogen quality and fluorescence (preservation scale values ≤5), in the laminated, organic-rich sample MQ16, suggesting better preservation due to temporary dysoxia-anoxia. The weak fluorescence observed through most of the section implies generally more oxic conditions with only temporary periodic dysoxia-anoxia during deposition at this locality.

Figure 4.20 shows the relationship between TOC and S (wt.% value; r^2 = 0.91) for the Misberg samples. The data points fall within the "data cloud" for normal marine (oxic) sediments (Leventhal, 1983). Davies *et al.* (1988) described a relationship between hydrogen index and total sulphur contents. They observed a correlation between the parameters in samples with hydrogen indices below 150-200 mgHC/gTOC; at higher hydrogen index values there was a weaker correlation. This was interpreted as the low hydrogen index reflecting the initial metabolisable material available to the sulphate reducing bacteria, and therefore pyrite formation limited by metabolisable carbon supply. The data here show a strong correlation (r^2 = 0.79; Fig. 4.21) between these parameters, with no apparent levelling off of the data set. This

suggests that the environment in which these samples were deposited was not iron limited but was carbon limited (Davies *et al.*, 1988).

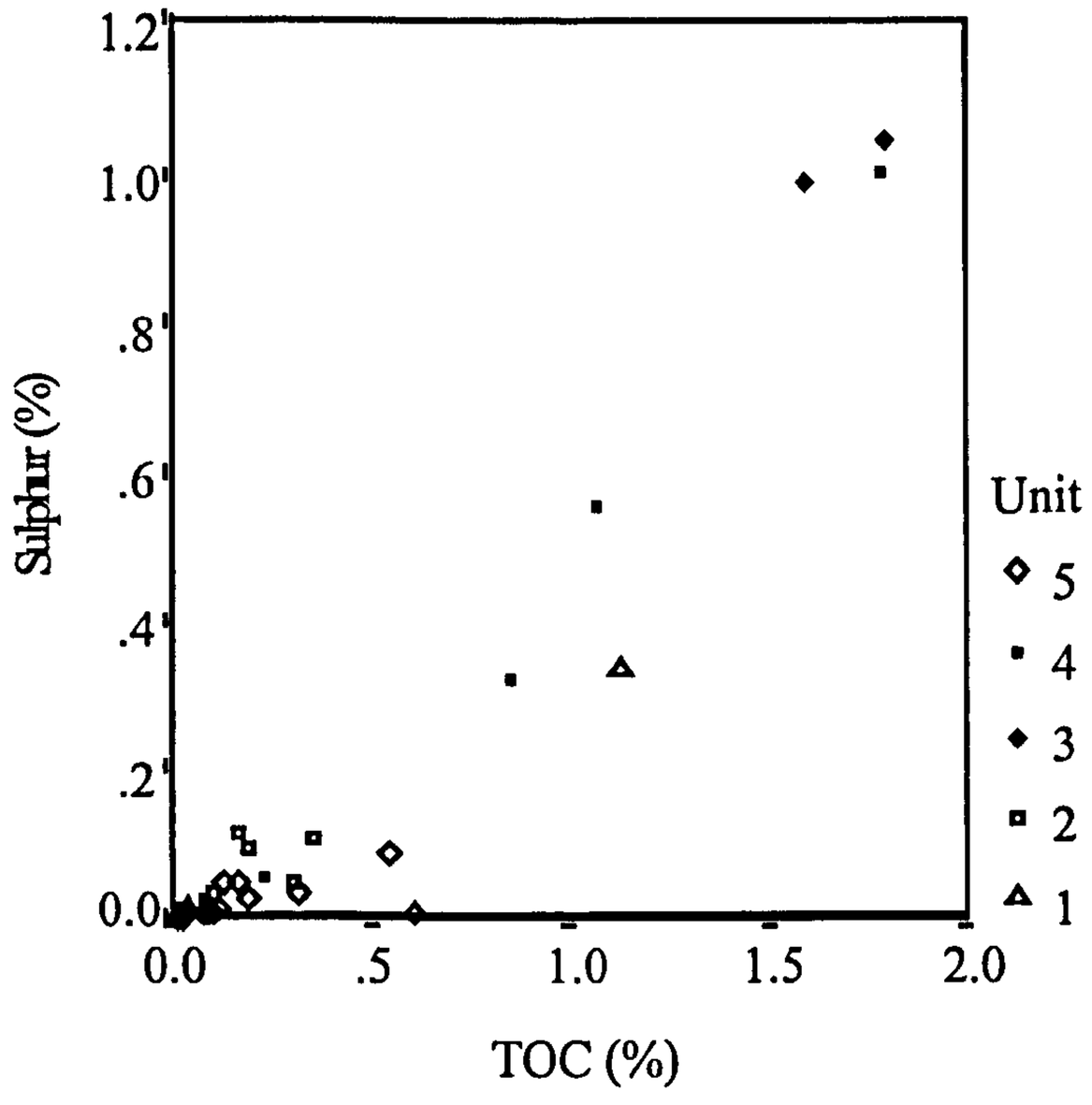

Figure 4.20 Cross plot of TOC versus Sulphur data for the Misberg section. The data shows a good correlation between the parameters ($r^2 = 0.91$). The units from constrained clustering are shown.

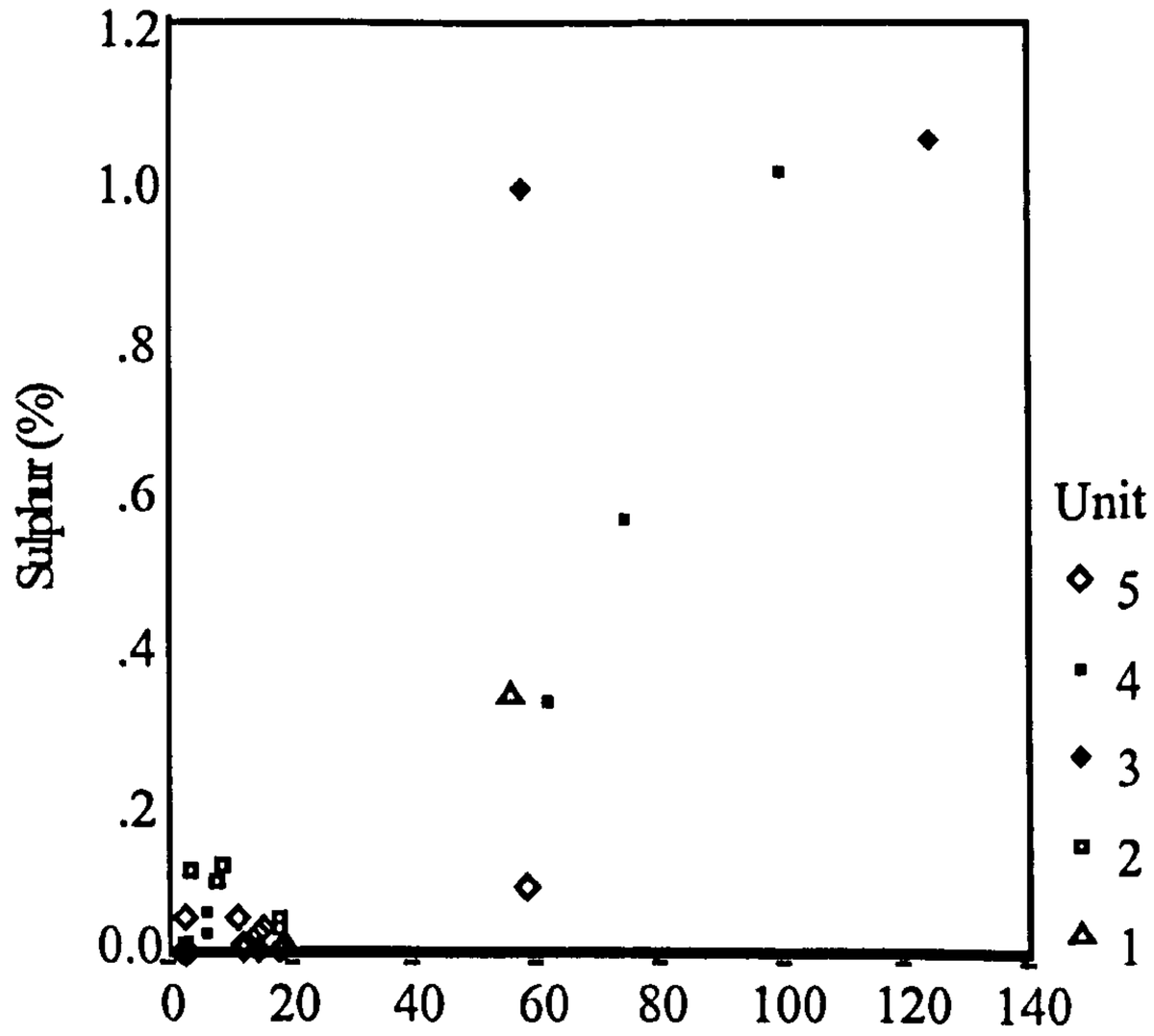

Figure 4.21 Cross plot of hydrogen index versus total sulphur (wt. %) data for the Misberg section (after Davis *et al.*, 1988, p. 883). The data shows a good correlation between the parameters ($r^2 = 0.79$).

A stratigraphical plot (Fig. 4.22) of the mean black phytoclast particle size, measured on approximately 20 square particles per sample tends to indicate that the organic-rich (highest TOC and HI) interval (MQ20 to MQ10) was deposited under the lowest energy conditions. This is based on the rationale that phytoclast particle size diminishes with increased distance of transport in an offshore direction (Batten, 1974; Habib,1982; Tyson, 1993). The relationship between mean phytoclast size and relative chorate dinoflagellate abundances (Fig. 4.23) suggests that chorate cysts are relatively more abundant in higher energy phases with a stronger circulation.

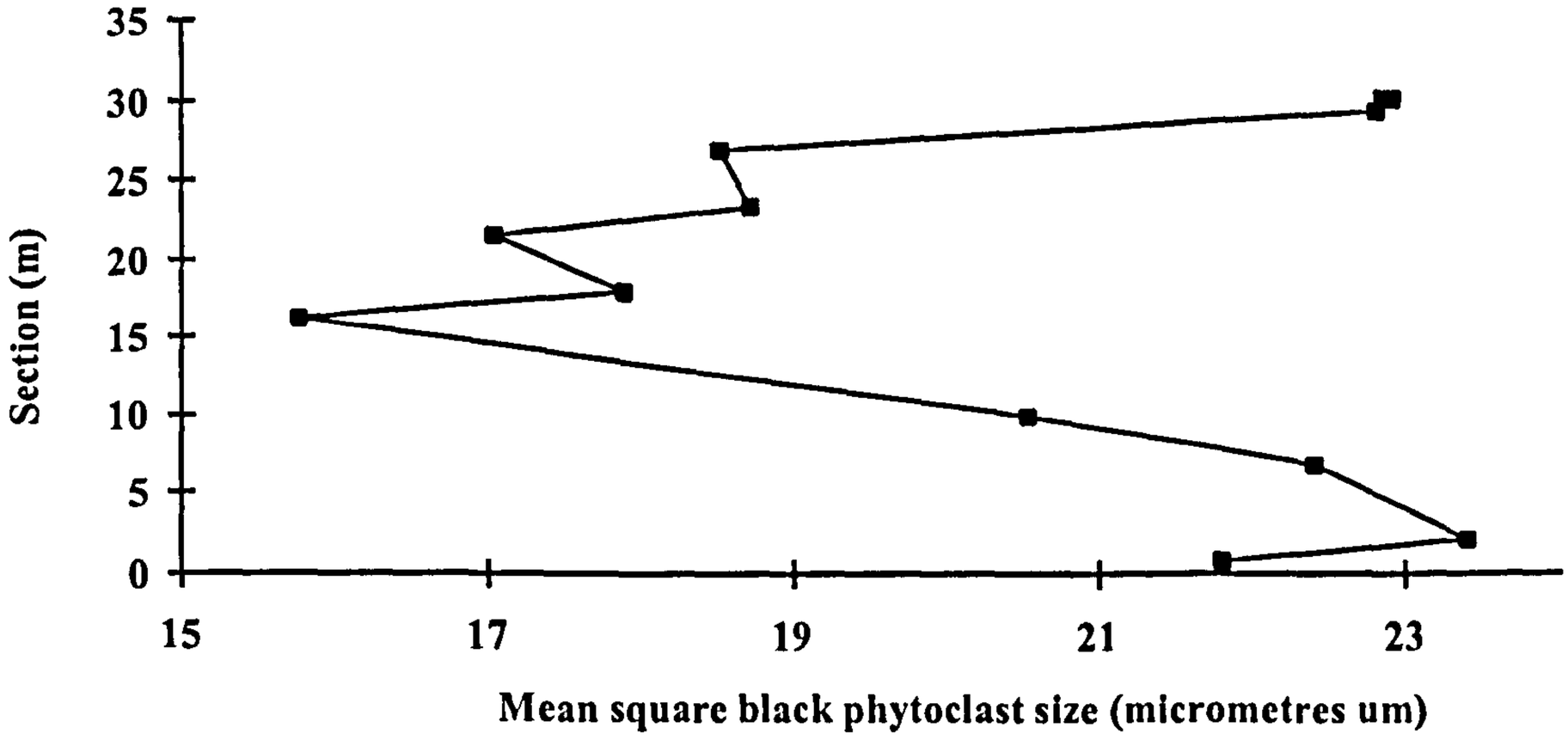

Figure 4.22 Stratigraphic plot of mean size changes in square black opaque woody material for the Misberg section. The plot suggest that the environment was more distal with lower energy between 10 to 25m.

Vozzhennikova (1965) first suggested that chorate dinoflagellate cyst forms were dominant in offshore facies. Further studies (Anderson *et al.*, 1985; Sarjeant *et al.*, 1987) indicated that the presence of processes does lead to a decrease in settling rate, but that the effect is less important than cyst size. However, the stratigraphic variation in chorate cysts (Fig. 4.23) for Misberg Quarry, shows a relative decrease in the central organic-rich samples thought to be the most distal according to phytoclast size, where the proximochorate cyst form is dominant. It has already been mentioned that *Cyclonephelium* (a proximochorate cyst form) is dominant in the organic-rich lithologies. This is because *Cyclonephelium* is a bloom-forming genus which typically results in high density low diversity assemblage in eutrophic settings, and its dominance is thus mainly a function of ecology rather than hydrodynamics. *Cyclonephelium* was probably suited to the particular environment during deposition of the organic-rich lithologies and thus either inhibited the growth of other species or simply diluted them.

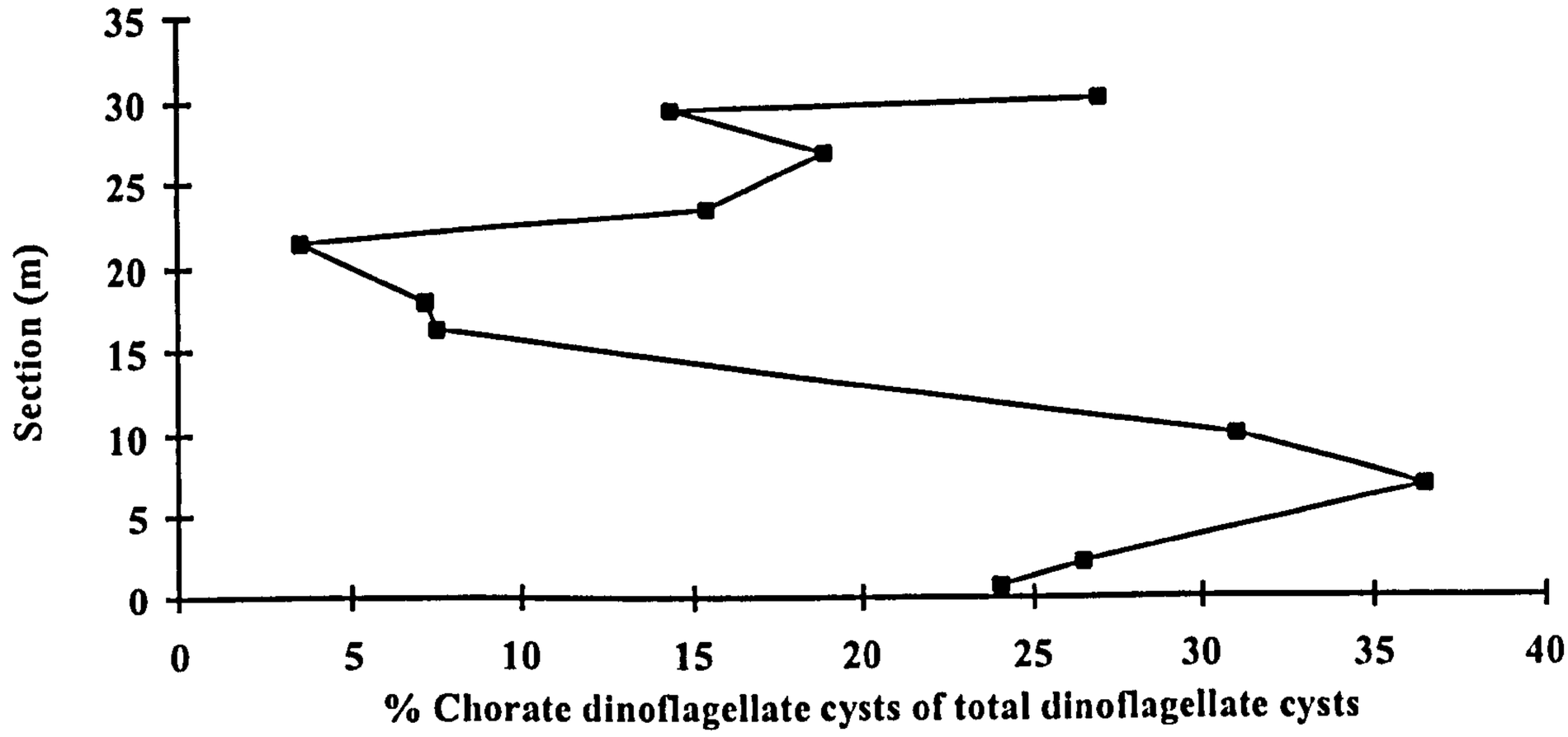

Figure 4.23 Stratigraphic plot of percentage chorate dinoflagellate cysts of total dinoflagellate cysts. The similarity with mean phytoclast size suggests that chorate dinoflagellate cysts have a higher relative abundance in higher energy phases with stronger circulation.

A ternary plot of relative percentages AOM, Palynomorphs and Phytoclasts (Fig. 4.24) indicates changes in the depositional environment (Tyson, 1995). The data follow a line from the AOM pole through to the middle of the opposite axis, which is typical of many Mesozoic marine sediments. This trend was also observed in the UK samples. The data indicate that the majority of the samples, especially the organic-poor samples, were deposited in a mud-dominated oxic shelf, with low to moderate, usually degraded AOM and abundant palynomorphs. By contrast the central organic-rich samples were deposited in a distal dysoxic-anoxic to distal dysoxic-oxic shelf environment (Tyson, 1995).

The Pristane/Phytane ratios (Appendix 4, Table II) for the section (all >1.0) indicate some degree of oxicity in the environment of deposition (Didyk *et al.*, 1978); however the palynofacies data indicate that the environment was episodically dysoxic-anoxic (cf. Tyson, 1995). An alternative source of isoprenoids, such as tocopherols (Goosens *et al.*, 1984) may be influencing the Pr/Ph ratio.

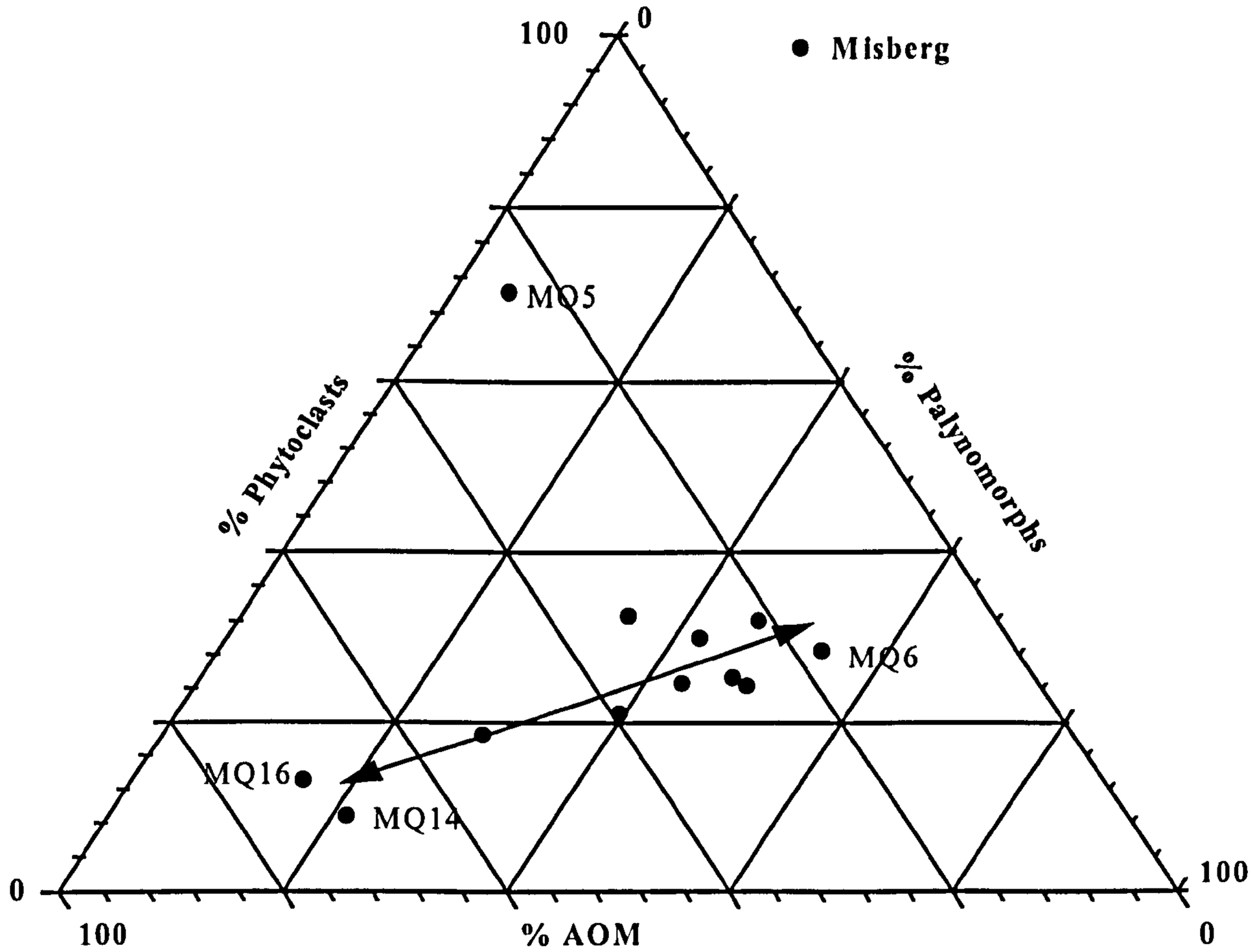

Figure 4.24 Ternary 'AOM'-phytoclast-palynomorph kerogen plot (after Tyson, 1995) for the Misberg section, based on relative numeric frequency (%RNF) data (Appendix 3, Table IV). Arrow indicates cahnge in facies between samples.

4.8 Principal Component Analysis of biomarker data

A number of biomarkers were identified from the GCMS traces and peak areas obtained for them. A total of 64 compounds (Appendix 2, Table II) were used for each sample analysed from the Misberg Quarry section, including C_{29} hopanes (m/z 177), tricyclic terpanoids and hopanes (m/z 191), methylated hopanes (m/z 205), steranes (m/z 217 & 218), 4-methylsteranes (m/z 231), diasterenes (m/z 257) and a hop-13(18)-ene (m/z 204). These compounds were selected as they could be easily identified and integrated between samples and suffered no coelution problems. These samples were analysed using Principal Component Analysis in the same way as described in Section 3.4.

4.8.1 PCA variations down section

The first three Principal Components account for over 49% of the total variance and the first Principal component (PC1) records 25% of the total variance in

the data set; the loadings plot for this Principal Component is controlled by the tricyclic terpenoids on the positive axis and the majority of the hopanoids and steroids on the negative axis. A stratigraphic plot of the PC1 scores (Fig. 4.25) shows a good correlation ($r^2 = 0.82$) with a stratigraphic plot of the tricyclic terpenoids versus all other compounds. The source of tricyclic terpenoids is not fully understood, although their widespread distribution in geological samples may suggest a bacterial origin. However, it is unclear as to whether they are natural products (e.g. Kruge *et al.*, 1990), or a degradation product of hopanoid compounds (Shi Jiyang *et al.*, 1988). This Principal Component also shows some correlation ($r^2 = 0.61$) with Pristane/Phytane; the tricyclic terpanes are relatively more abundant in samples with lower Pr/Ph, suggesting that tricyclic terpanoids may be favoured in relatively anoxic environments, or samples with elevated input of the pristane precursor e.g. such as tocopherols (Goosens *et al.*, 1984) or from algal input (Didyk *et al.*, 1978)

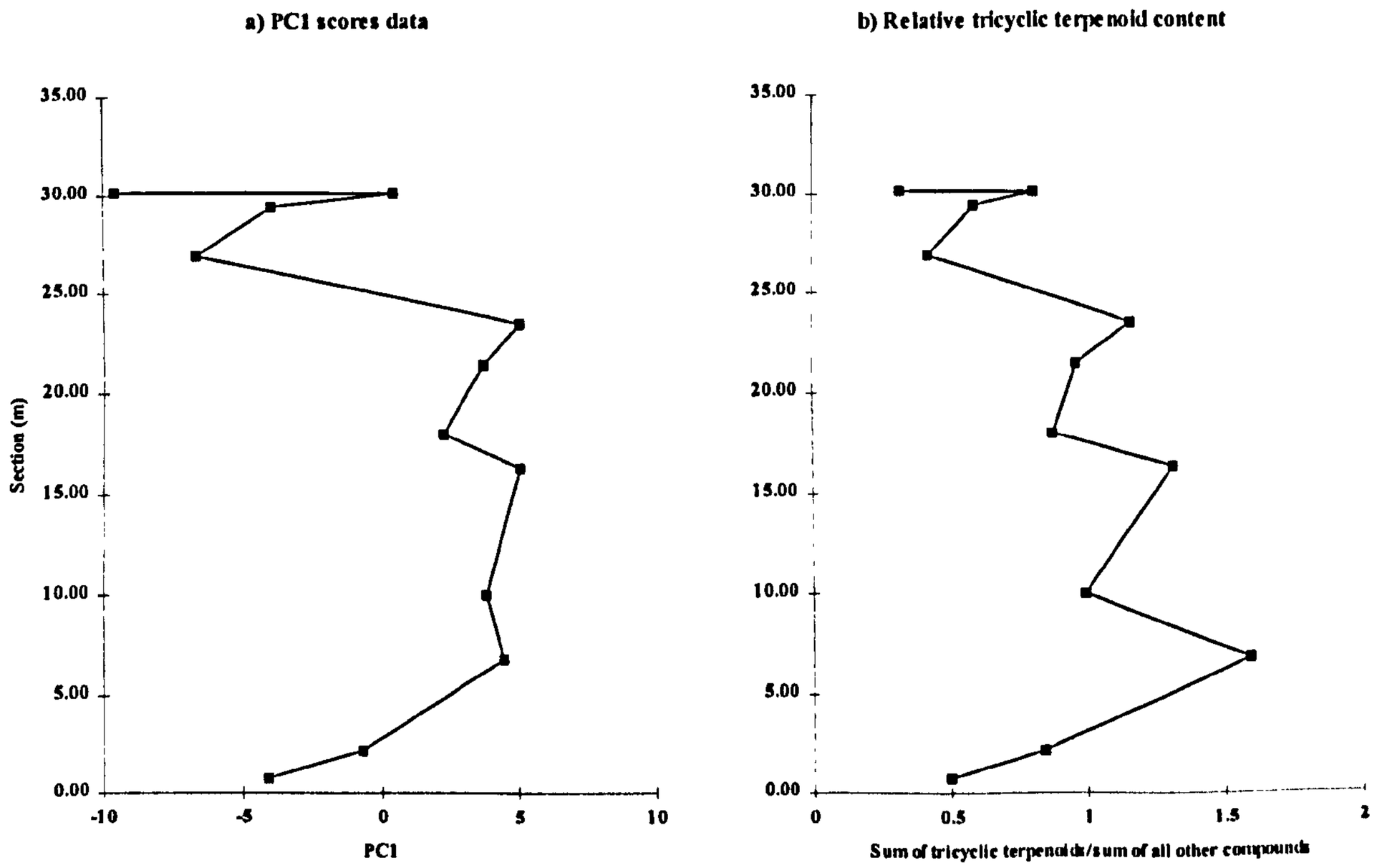

Figure 4.25 Comparison of PC1 and tricyclic terpenoid data. a) stratigraphic plot of PC1 scores data; b) stratigraphic plot of relative tricyclic terpenoids abundance.

The second Principal Component (PC2) accounts for 16% of the variance and the loadings data suggest that this PC is controlled by diasterenes and steranes. The significance of this is unclear, but it may relate to variances in the source of the algal material. There is some correlation ($r^2 = 0.48$) of the scores with carbonate contents, and also some correlation of percentage diasterenes of total sterane. This may suggest that diasterene content is higher with higher carbonate contents, which is not normally the case, as diasterenes are thought to be rearranged products of steranes catalysed by acidic clay minerals normally in the absence of carbonates (e.g. Killops & Killops,

1993, p.176) The scores data for this Principal Component show no correlation with other bulk or molecular geochemical data.

The third Principal Component (PC3) records only 8% of the total variance. It is difficult to determine from the loadings data what controls this Principal Component. The positive side of the axis is dominated by R isomer configuration compounds, the hop-13(18)-ene, and other compounds associated with immature sediments; whereas the negative side of the axis is dominated by S isomer configuration compounds. A stratigraphic plot of PC3 shows a similar profile to the C29 αααS/αααS+αααR sterane maturity ratio plot (Fig. 4.26). A plot of these two parameters suggests that samples MQ9 and MQ23, may be anomalous values, when removed the data shows a good correlation ($r^2 = 0.85$), this suggests that PC3 describes variations in apparent maturity through the section, controlled by organic matter input, or mineral/organic matter interactions.

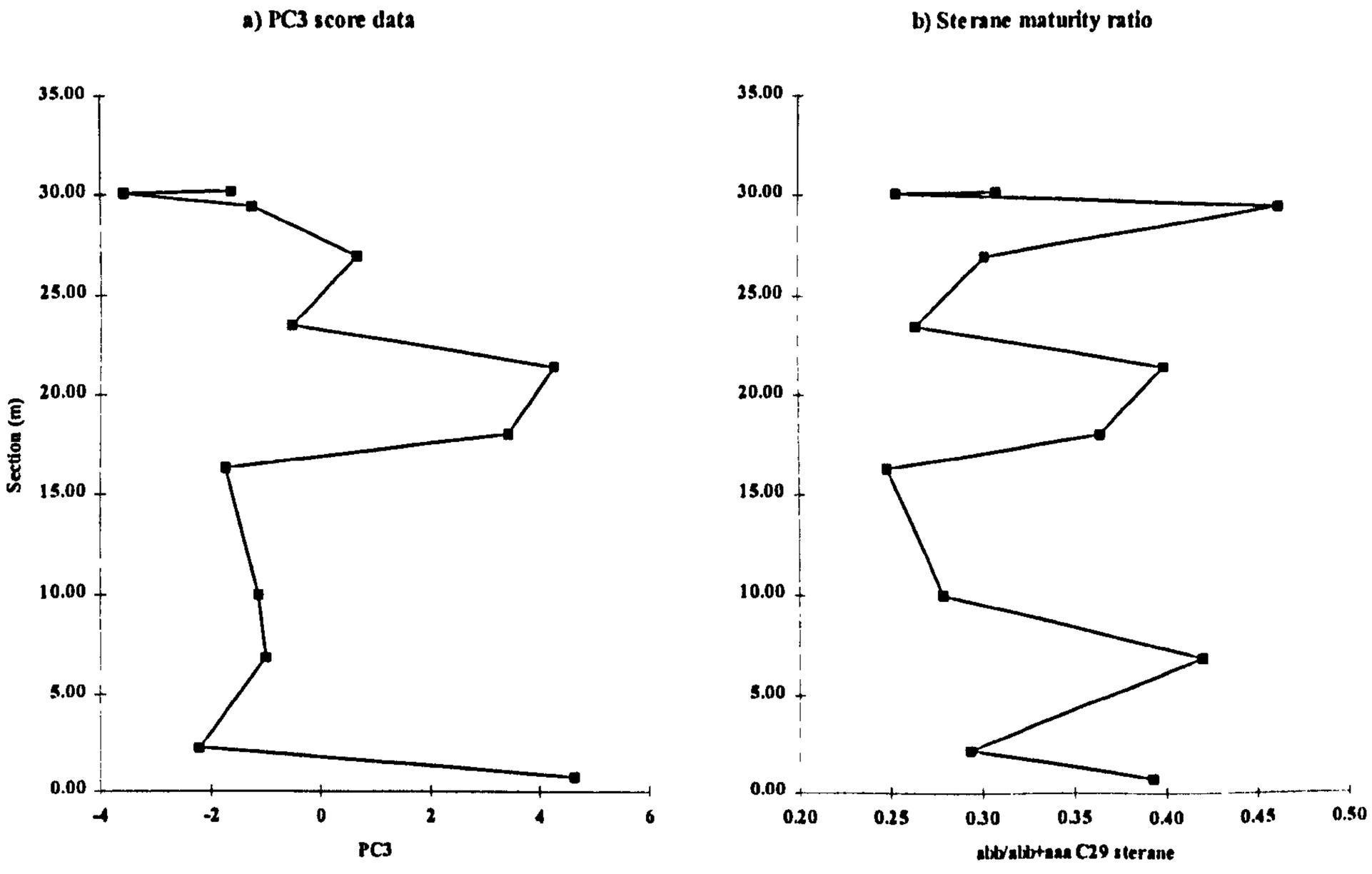

Figure 4.26 Comparison of PC3 and sterane maturity data. a) Stratigraphic plot of PC3 scores data; b) Stratigraphic plot of sterane maturity parameter.

4.9 Conclusions

The Cenomanian-Turonian Black Shale Facies of Misberg Quarry is composed predominantly of marine AOM and palynomorphs with variable fluorescence. Assessment of the preservation of the kerogen suggests that only temporary dysoxia-anoxia existed for short periods of time through the sequence, and optimum preservation conditions were not established for long periods of time.

The variations in dinoflagellate cysts assemblages compare well to those observed by Marshall and Batten, (1988) in that chorate cyst forms (especially *Spiniferites*) are dominant in the organic-poor facies, and proximochorate cyst forms (especially *Cyclonephelium*) are dominant in the organic-rich facies. This may be partly controlled by the energy of the environment, as determined from mean phytoclast particle size.

Principal Component Analysis of the biomarker data indicates that 25% of the variability in the data set is controlled by the relative abundance of tricyclic terpenoids. The correlation with Pr/Ph suggests a relationship with redox. The exact nature of their occurrence is unclear and further investigation would be necessary to fully understand this.

The relationship between TOC and S2 appears non-linear, especially between values below and above 0.5% TOC. This may indicate a more complex relationship between TOC, S2 and matrix material than that suggested by Langford and Blanc-Valleron (1990). Clearly, either the preservation and hydrocarbon potential of the organic matter changes as the TOC increases, or appears to do so because of matrix effects.

The enhanced TOC through the section is probably due to a combination of increased preservation due to suboxic to anoxic conditions and increased primary productivity (Hilbrecht *et al.*, 1992) in this area.

The TOC enrichment occurs within the carbonate $\delta^{13}C$ isotopic excursion. The organic-rich lithologies and isotope excursion start within the end of the *R. cushmani* zone, but reach a maximum in the *W. archaeocretacea* zone.

CHAPTER 5

5. The Bahloul Formation of Tunisia: Results.

5.1 Introduction

The Bahloul Formation represents the Cenomanian-Turonian Boundary Event in Tunisia, and corresponds to the major source rock in the area (Bishop, 1988). The sediments of the Bahloul Formation were deposited on the southern margin of the Tethys Ocean (Section 1.4). During the Mesozoic and the Cenezoic the vast stable platform of eastern Tunisia and the Pelagian sea progressively subsided (Burollet *et al.*, 1978). Due to the sea level rise and transgression, the Tunisian shelf was linked by a seaway to the Gulf of Guinea by way of Nigeria (Schlanger *et al.*, 1987).

The area sampled lies in the Central Tunisian Atlas of central north Tunisia (Fig. 5.1). The Tunisian Atlas is a structural unit bordered by the Tellian Alpine thrust to the north and the Kasserine structural high (located on the northern edge of the Saharan Platform) to the south. Palaeogeographically, the area lies between carbonate platforms to the south (south of Kasserine) and a basin to the north in the El-Kef region (Fig. 1.3; Philip *et al.*, 1989).

5.2 Stratigraphy

The Bahloul Formation is bound by the Dellal Member of the Albian-Cenomanian Fahdene Formation below, and the Annaba Member of the Aleg Formation of Turonian age above (Fig. 5.2). There was no apparent break in sedimentation between the Cenomanian and Turonian in eastern, central and northern Tunisia, and the boundary is placed within the Bahloul Formation (Burollet, 1956), although is not accurately located (cf. Fig 5.3).

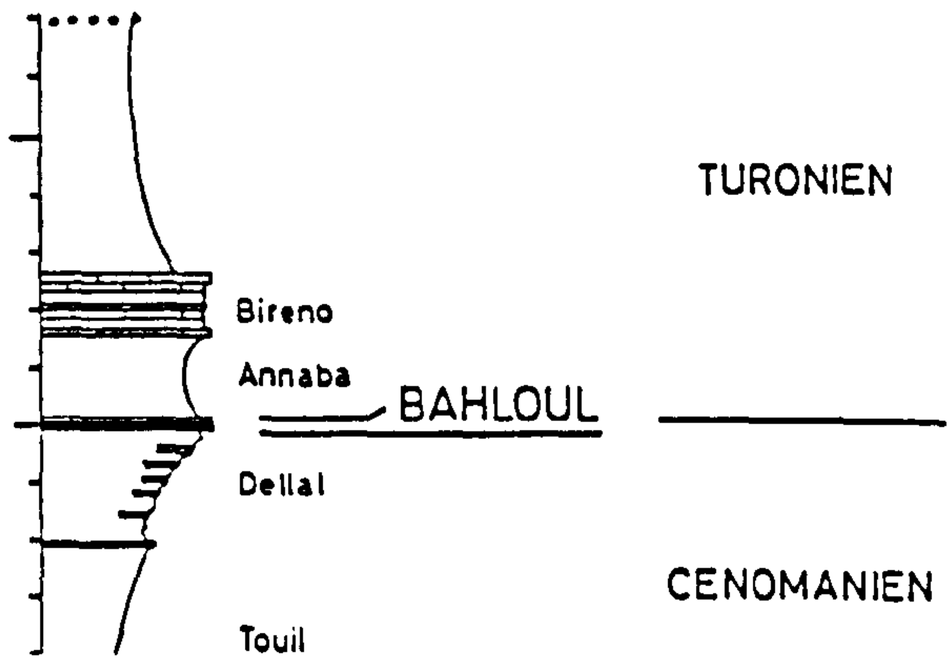

Figure 5.2 Cenomanian-Turonian stratigraphy in central north Tunisia, from Robaszynski *et al.* (1993a)

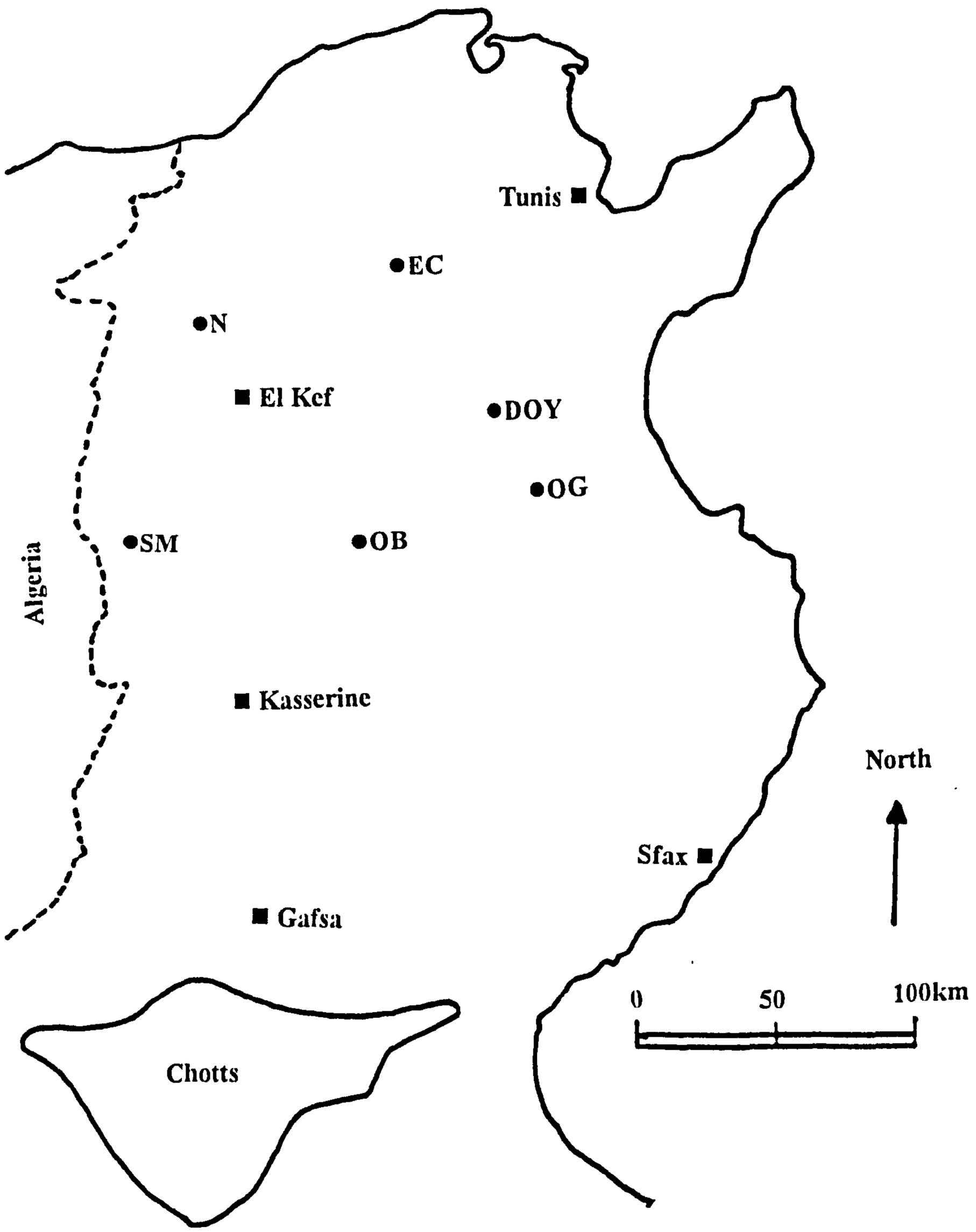

Figure 5.1 Map of Tunisia showing major cities and outcrop locations. Key: OB, Oued Bahloul; EC, Ech Cheid; DOY, Dir Oulad Yahia, OG, Oued El Gsab; N, Nebour; SM, Oued Smara; Chotts, salt flats.

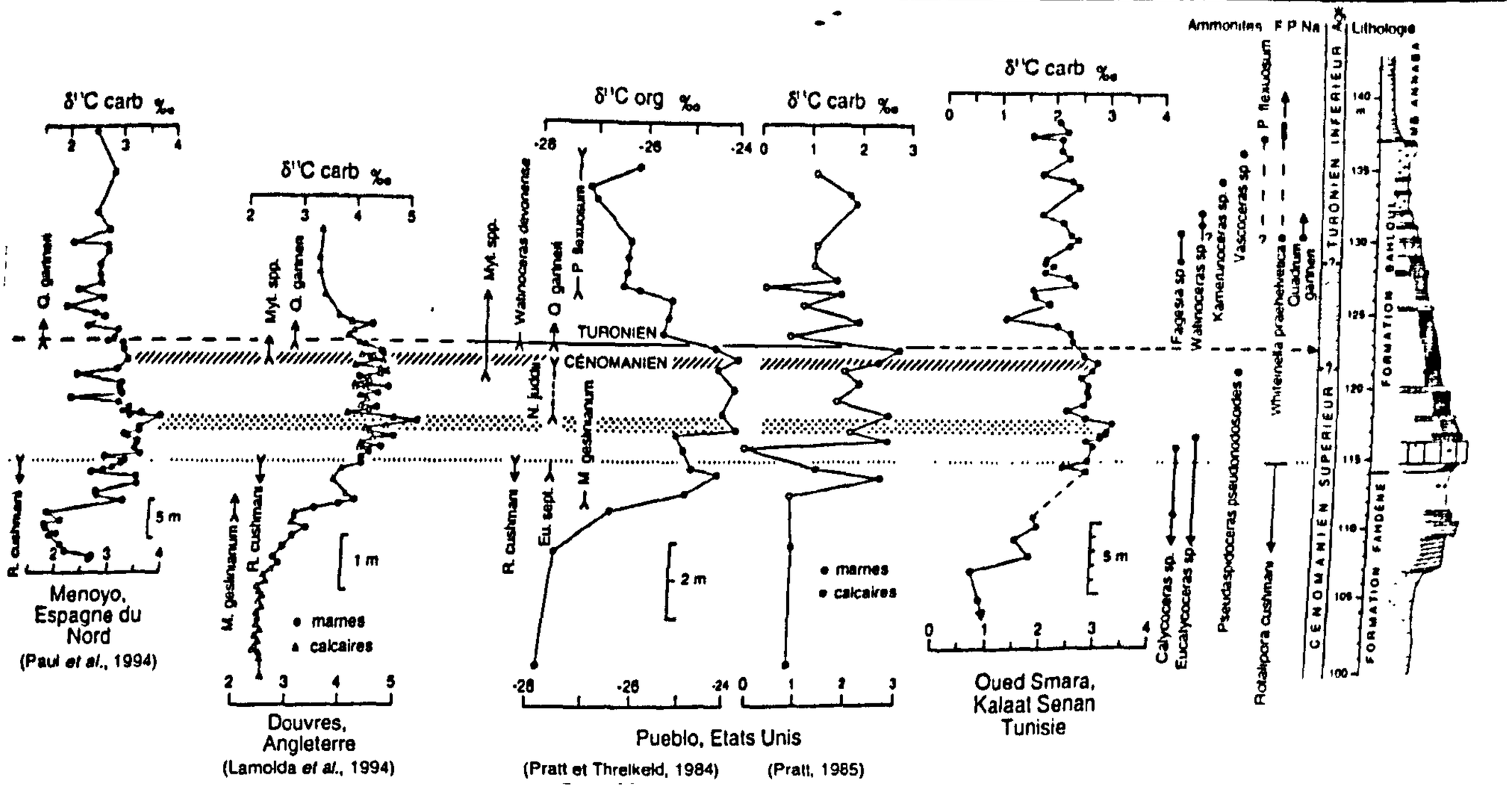

Figure 5.3 Correlation of isotope data between the Tethyan, Boreal and Atlantic realms, from Accaire *et al.* (1996).

The Bahloul Formation was first recognised by Burollet *et al.* (1954) who proposed the litholostratigraphic nomenclature for the Upper Cretaceous of central Tunisia. This nomenclature was again used by Burollet (1956) and further detail was added by Fournié (1978). In central and north central Tunisia the Bahloul Formation is characterised by dark grey to black shales and bioturbated shales (Schlanger *et al*,. 1987). However, to the south of central Tunisia the Bahloul Formation consists mainly of massive bioturbated limestones. In the southern part of central Tunisia, the Bahloul Formation is subdivided into three lithological units by Abdallah (1995): a basal limestone unit, underlain by 5-10m of massive limestones rich in ammonites; organic-poor bioturbated limestones; and a relatively organic-rich unit. Maamouri *et al.* (1994) classifies the Bahloul Formation into four units and also recognises that these units overlay a massive limestone.

5.3 Previous work

Herbin *et al.* (1986) studied seven samples from a Cenomanian-Turonian section in the Oued Bahloul area, south-east of Maktar. They recorded high TOC values of 1.1 to 4.7% and hydrogen indices in the range 260 to 670. Their samples had a moderate maturity and an average Tmax of 431°C, which they attributed to low post-Turonian accumulation rates.

Schlanger *et al.* (1987) also sampled and described the Oued Bahloul outcrop in Tunisia; they noted the alternation of fissile, perfectly laminated dark-grey to black shales with light coloured bioturbated shales. They recorded the presence of fish scales and pyrite nodules and noted that ammonite impressions are common, especially towards the top of the sequence. They observed similarities in the spacing and alternation of the dark and lighter coloured beds between the Oued Bahloul and Wünstorf sections.

The first molecular geochemical work carried out on the Bahloul Formation was by Montacer *et al.* (1988). They studied 46 samples from 7 boreholes in the Bou Grine area, northern Tunisia (Fig. 5.1), which is associated with lead-zinc mineralization. At these locations they recorded TOC values of 4 to 5%, hydrogen indices of 600 and a low maturity (Tmax 423°C). The Pr/Ph ratios of ca. 2 were interpreted as a result of migrating hydrocarbons with a higher Pr/Ph ratio than the *in situ* Bahloul Formation. The gas chromatography traces of the aliphatic fraction were unimodal with *n*-alkane maximum at nC_{17} to nC_{19}. Their gas chromatography-mass spectrometry data show large amounts of steroids and hopanes in the aliphatic fraction.

Bishop (1988) observed a TOC of almost 8% at the Oued Bahloul type locality, but the average value was 3.9%. From well cuttings in the Sfax region on the east coast of Tunisia (Fig 5.1) he recorded TOC values in the range 0.8 to 6.4%. He also mapped the area covered by the organic-rich (Bahloul) facies in Tunisia (Fig. 5.4).

Further work on samples from the Bou Grine area was conducted by Pervaz and Püttmann (1995). They studied 28 samples from a borehole in this area. The clays throughout the section are enriched in kaolinite. Bulk geochemical analysis of these samples gave TOC values in the range of 2 to 14%, and carbonate values that generally increased towards the top of the section; they observed that changes in TOC were not controlled by carbonate dilution. Reflected light microscopy gave vitrinite reflectance values of ca. 0.5%R_o. From gas chromatography-mass spectrometry of the aliphatic fraction they noted that the homohopane ratio had reached its equilibrium (0.6), and that the sterane (20S/20S+20R) value was ca. 0.36 (but 0.24 in one sample from the base of the section).

Maamouri *et al.* (1994) studied 8 sections, including the Oued Bahloul locality, from Tunisia. The biostratigraphy they observed at Oued Bahloul is given in

Figure 5.5. From the microfauna and microfacies they confirmed that the deposition of the Bahloul Formation began in the Cenomanian and ended in the Early to Mid-Turonian. The richness and pelagic nature of the fauna led them to interpret the Bahloul as a continental slope facies deposited during a transgressive episode.

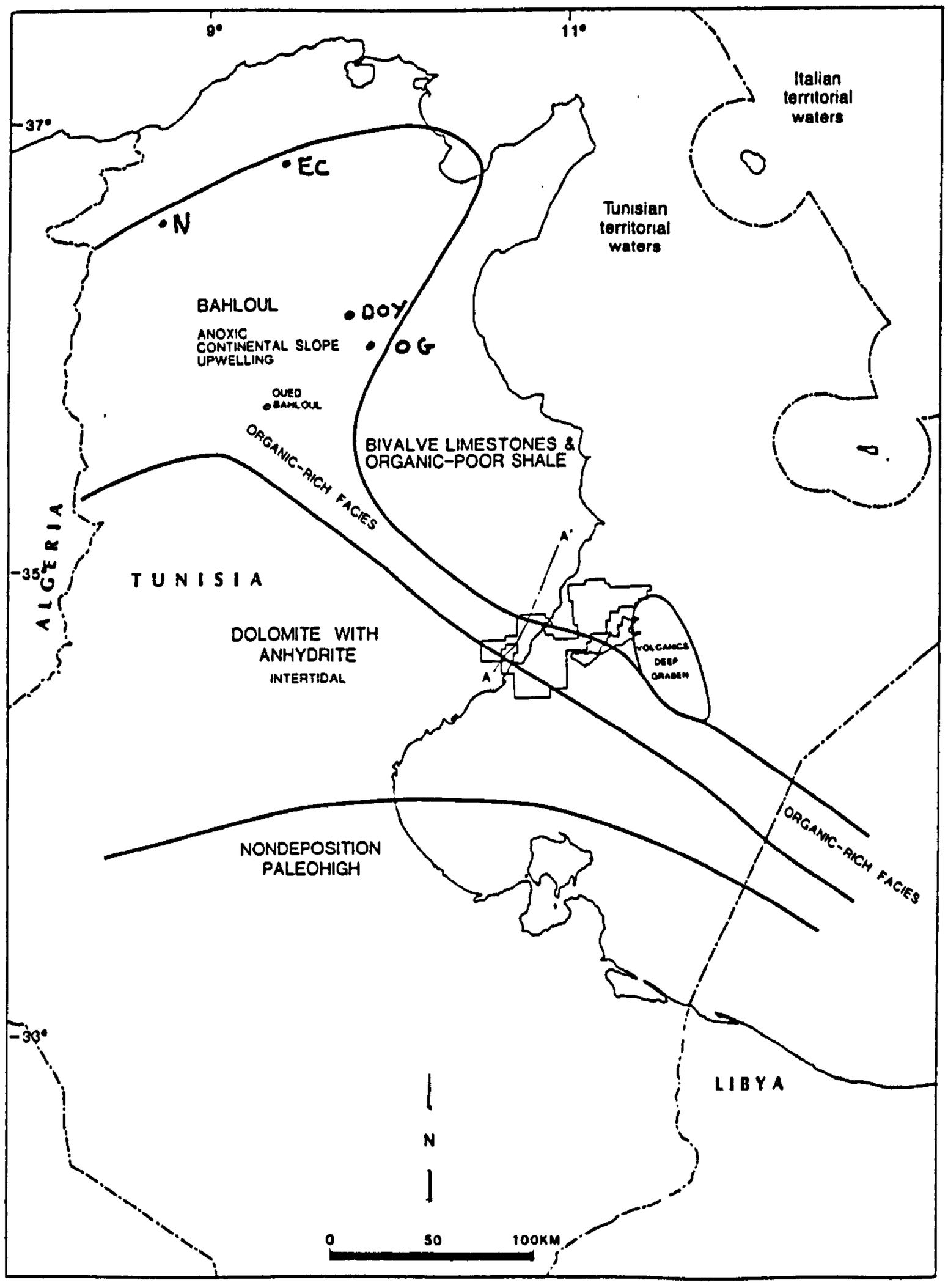

Figure 5.4 Distribution of orgain-rich facies Bahloul Formation (Bishop, 1988).

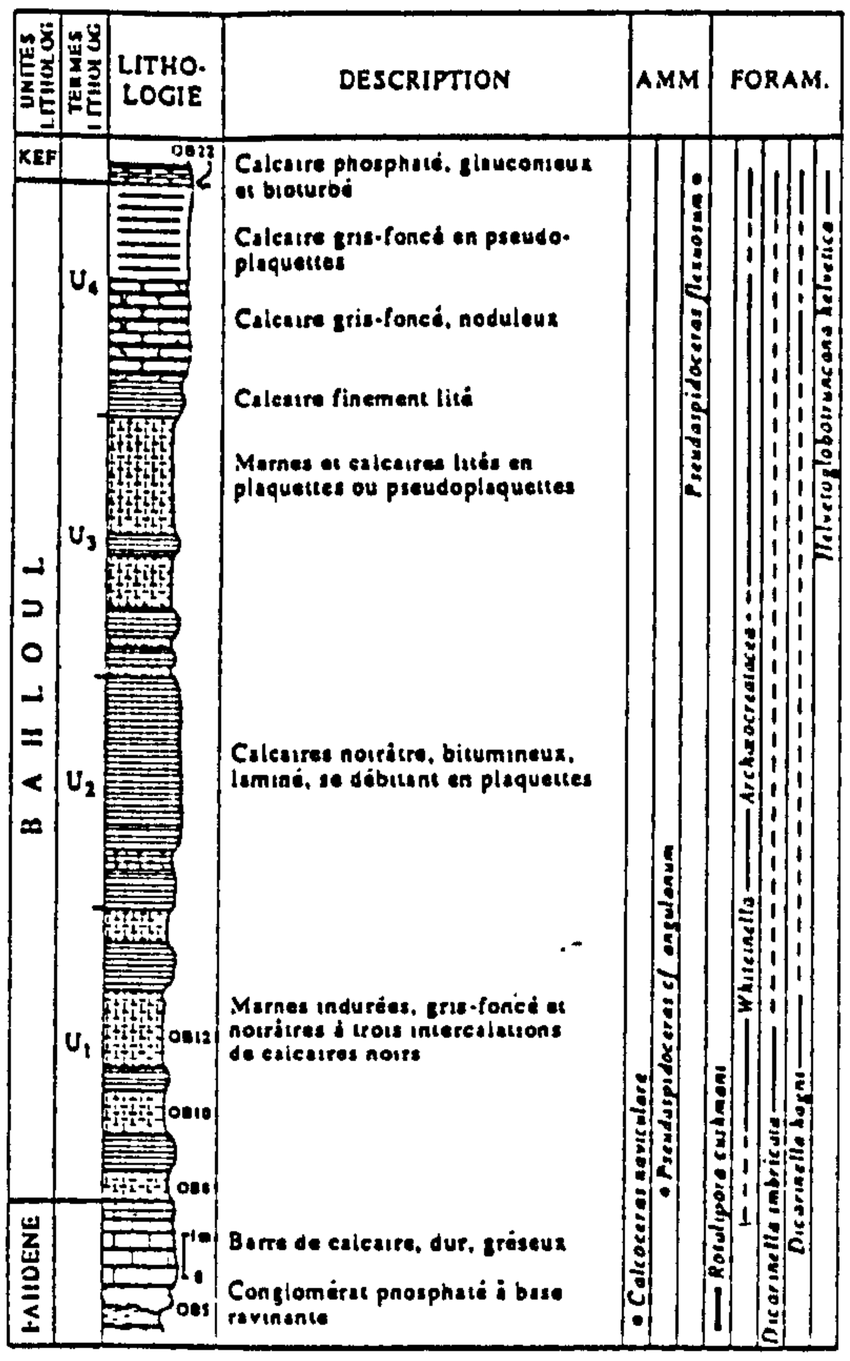

Figure 5.5 Biostratigraphy for the Oued Bahloul section, from Maamouri *et al.* (1994).

Abdallah (1989, 1995) had studied the transgressive phases in the Albian to Turonian sediments in the northern Chotts region of south-central Tunisia (Fig. 5.1). He looked for the effects of eustasy and tectonics on the extensive carbonate platform and how it related to transgression and regression. He concluded that the final Cenomanian transgression phase was controlled by eustasy. He made the first identification of the Bahloul Formation in the northern Chotts area at the Khanguet Besbessa Sghira locality (Fig. 5.1), and confirmed that the Bahloul is situated below the Gattar Formation. The 9.5m outcrop at K. Besbessa Sghira is split into 3 units: the lower unit comprises organic-poor white limestones; the second unit contains organic-poor white limestones with bioturbated upper surfaces; the uppermost unit contains white to grey limestones where the lowermost bed is bioturbated and uppermost bed is relatively rich in organic matter. Abdallah (*ibid.*) correlates the basal limestone (below the Bahloul) and the Gattar Formation from this section through the Chotts and up to the Oued Smara locality (cf. Robaszynski *et al.*, 1993a). He proposes an uppermost Cenomanian age for the first two Bahloul units at K. Besbessa Sghira. However, the uppermost unit contained ammonites that had not then been identified.

Abdallah *et al.* (1995) detail the biostratigraphy of the Chotts area, including data from ammonites, foraminifera, ostracods and echinoids. They use the biostratigraphic data to correlate the Cenomanian-Turonian from the Chotts area with coveal sections in Portugal, Spain, Morocco, Algeria and the Oued Smara locality. Abdallah and Meister (1996) date the lower two thirds of the Bahloul in the Chotts area as Cenomanian and the upper third as Turonian, based on ammonite data. They observe that the anoxia is diachronous at both the base and the top of the Bahloul Formation, with the anoxic event appearing earlier, based on the lithologic framework, in the central west area (Kalaat Senan area). The anoxia is also observed to cover all of the lower Turonian at the Wadi Berda (N. Chotts) locality and some of the west central localities (Robaszynski *et al.*, 1990, 1993a; Maamouri *et al.*, 1994), whereas it limited to the lowermost part of the Turonian further south in the Chotts area.

From further studies of the northern Chotts area (Abdallah & Meister, 1997) conclude that the Cenomanian-Turonian boundary strata in this area are composed of platform sediments, rich in pyritised ammonites, weathered pyrite, foraminifera, coccoliths and with a stunted neritic fauna. From this faunal assemblage they propose a model with an anaerobic sediment-water interface but a generally oxygenated water column. They also suggest that oxygen depletion was less drastic on the platforms, based on the presence of organic-poor white limestones with foraminifera and bivalves.

Farrimond *et al.* (1990) in a molecular geochemical study of 5 samples from the Oued Bahloul outcrop, recorded TOC values in the range of 3 to 7%, carbonate values from 62 to 81% and total sulphur values from 0.13 to 0.32%. Optically the samples were AOM-dominated with a low terrestrial input and of high maturity (C_{31} $\alpha\beta$ hopane 22S/(22S + 22R) = 0.53 to 0.57). Gas chromatography of the extracted aliphatic fraction showed Pr/nC$_{17}$ values of 2.5 to 3.4 and the Pr/Ph ratio was in the range of 0.9 to 1.3. Further analysis of the aliphatic fraction using gas chromatography-mass spectrometry identified abundant hopanes (total hopanoids/total steroids ratio range 1.1 to 3.1), and also relatively high amounts of methylhopanes at the base of the section. They interpreted the relatively high 17α (H), 18α (H), 21β (H)-28, 30-bisnorhopane input as a specific bacterial source possibly associated with a highly reducing sulphur-rich depositional environment or bacterial mats in an upwelling environment. They also made the first record of an A-ring methylated 28, 30-bisnorhopane. The presence of methylsteranes was also noted. Their interpretation of the source of the organic matter was abundant algal material

with significant dinoflagellate input (a chemical not optical interpretation), and abundant bacterial material, including cyanobacteria.

Robaszynski *et al.* (1990, 1993a) and Robaszynski and Gale (1993) have studied the biostratigraphy and sequence stratigraphy of Cenomanian and Turonian sediments in the Kalaat Senan area of west-central Tunisia (Fig. 5.1). They have determined the Bahloul to be entirely of Cenomanian age in this area, based on ammonite data. However, they suggest that the Bahloul sediments may locally persist into the Turonian to the east of this area. Bulk geochemical analysis of 30 samples from the Bahloul Formation at Oued Smara gave TOC values in the range 0.2 to 3.0% and carbonate values of 55 to 85%. The foraminifera *R. cushmani* has its extinction in the basal limestone at this section. From a combination of the biostratigraphic record and changes in the lithofacies these workers have identified the position of depositional sequences in a detailed stratigraphic framework. They noted a transgressive surface just above a basal thick grey limestone bed, with the following "black shales" deposited in a transgressive systems tract. The Cenomanian-Turonian boundary at the end of the Bahloul Fm in the Kalaat Senan region is described as a flooding surface towards the end of the major transgressive episode. Robaszynski *et al.* (1990) noted in their samples (SM124 to 140; the middle to the end of the Bahloul Formation) a low (5%) kaolinite content in the clay mineral assemblages. Chlorite and irregular mixed-layers were the main clay components. They also noted that the Bahloul contains a very low clay content.

Accaire *et al.* (1996) studied the cyclic 21m exposure at Oued Smara, in the Kalaat Senan area. They observed that TOC values (0.5 to 4.0%) were highest at the base of the section with a sudden increase, and a subsequent stable area in the middle of section before a second increase at the top of the section. Carbonate values (65 to 80%) show a general increase through the sequence, followed by a slight drop at the top. They established the first carbonate carbon $\delta^{13}C$ reference profile for the Cenomanian-Turonian in Tunisia. The carbonate carbon isotope curve shows a positive excursion within the lower part of the section, just before the first TOC maximum, followed by a second positive excursion also at the base of the section. The $\delta^{13}C$ carbonate values increase from 2.25‰ in the basal limestone to 3.20‰ at the highest point of the excursion, within the 'black shales', before gradually dropping to 2.00‰ by the top of the Bahloul Formation. The isotope excursion for this section has been correlated with other excursions in the Tethys, Boreal and Atlantic realms (Fig 5.3). Using the available biostratigraphy and the two sub peaks in the isotope curve, correlations have been made with Pueblo (Pratt & Threlkeld, 1984), Dover

(Lamolda *et al.*, 1994) and Menoyo, Spain (Paul *et al.*, 1994). Accaire *et al.* (1996) propose that the Cenomanian-Turonian boundary occurs just above the second $\delta^{13}C$ carbonate maximum.

Unpublished data obtained by Mohsen Layeb (care of British Gas, Tunis, Tunisia), comes from the cyclic, 44m thick L'Agraine outcrop, 50 km north east of Oued Bahloul. The TOC values are highest at the base and top of the section, with 4 maxima above 4% at the base of the sequence. The TOC values are cyclic at the top and base of the sequence, but TOC values are lower and less cyclic in the middle of the sequence. The onset of the anoxic event is very sudden as recorded from the sudden increase in TOC values.

5.4 The samples

The Oued Bahloul (OB) section occurs in the south of the sampled area (35°42'N 9°20'E; Fig. 5.1), 16km south east of Maktar, near the small village of Kesra. The literal translation of Oued Bahloul is "River of the mad man", and refers to a mad hermit who used to live there. The section is a 26.8m thick exposure of alternating shale and marl lithologies, found in a small river valley. A thick sandstone is found at the base of the section and bioturbated limestones at the top. Eighty three samples were collected from this cyclic sequence. All 83 samples were analysed using bulk geochemical techniques; 36 samples were chosen for further aliphatic molecular geochemical and optical study, based on their range of bulk geochemical values. To coincide with the pyrolysis work (Chapter 7) 7 samples were analysed using aromatic molecular geochemical techniques. Forty nine samples were chosen for organic matter isotope analysis; the samples were selected to provide representative cover for the whole section; more samples were taken from the base of the section where the isotope signal was believed to be strongest, based on published data (i.e. Accaire *et al.*, 1996).

The Ech Cheid (EC) section, in the extreme north of the sampled area (36°24'N, 9°20'E; Fig. 5.1), is 9 km north of Gafour; it is a weathered outcrop between two fields, and exposes 16.5m of shales, marls and limestones. The basal limestone and possibly some of the basal organic-rich beds are not exposed and could not be sampled. From this cyclic section 25 samples were collected. All samples were subjected to bulk geochemical analysis. From these samples 12 were picked in the same way as above for further aliphatic molecular geochemical and optical study.

The aromatic hydrocarbon fraction from 4 of the samples was studied to coincide with pyrolysis work. For organic matter isotope analysis, fifteen samples were selected.

The Dir Oulad Yahia (DOY) locality occurs in a small village 6km south of Rabâa Oulad Yahia, situated in the centre of the sampled area (36°06'N 9°40'E; Fig. 5.1). Fifty samples were taken from this 37.2m exposure of cyclic shales and marls. All 50 samples were subjected to bulk geochemical analysis and 16 samples were chosen for organic matter isotope analysis. Due to time constraints, only one sample (DOY25) was chosen for aliphatic and aromatic molecular geochemical and optical studies; this sample was chosen because it exhibited average bulk geochemical characteristics.

Oued El Gsab (OG), 10km north-east of the town Ksar Lemsar, is a 15.3m exposure in a stream bed and adjoining cliff, to the south east of the sampled area (36°06'N, 9°48'E; Fig. 5.1). At this locality 45 samples were taken from the cyclic shales and marls. All samples were subjected to bulk geochemical analysis and 16 were chosen for organic matter isotope analysis. Due to time constraints, only one sample (OG16) was chosen for molecular geochemical (aliphatic and aromatic) and optical studies; this sample was chosen as it exhibited average bulk geochemical characteristics.

The Nebour (N) locality outcrops on a mountain top near the town of Nebour 12km north of El Kef in the north west part of the sampled area (36°12'N, 8°42'E; Fig. 5.1). The 23.9m exposure is an inverted sequence of shales and calcareous shales, from which 47 samples were taken. All samples were analysed using bulk geochemical techniques and 15 samples were chosen for organic matter isotope analysis. Due to time constraints, only one sample (N18) was chosen for molecular geochemical (aliphatic and aromatic) and optical studies; this sample was chosen in the same way as above.

5.5 Results for the Oued Bahloul section

5.5.1 Bulk and isotopic geochemistry

The bulk geochemical and isotopic results for the Oued Bahloul section are recorded in Appendix 2, Table III and Figure 5.6. The stratigraphic plot of the TOC values shows they are highest from the base to the middle of the section (0.7 to 14.2m), where there are 4 TOC peaks above 6.5%. Carbonate values are lowest (ca. 50%) around the base of the sequence but they steadily increase upwards through the

section (to 85%); the constrained clustering data suggests that the values drop first before they increase through the sequence. In the central part of the sequence (OB48 to OB61) the TOC values are lower and more uniform, but then increase and become more variable towards the top of the sequence (OB65 to OB83). Rock-Eval whole rock hydrogen index values range from 50 to 680 mgHC/gTOC (Table 5.1). Kerogen hydrogen index measurements carried out on four samples (OB7, 18, 43 and 65) have up to 70% relatively higher values than their whole rock counterparts (Table 5.1). A summary of the bulk geochemical data for each section is given in Table 5.2 (pg. 102)

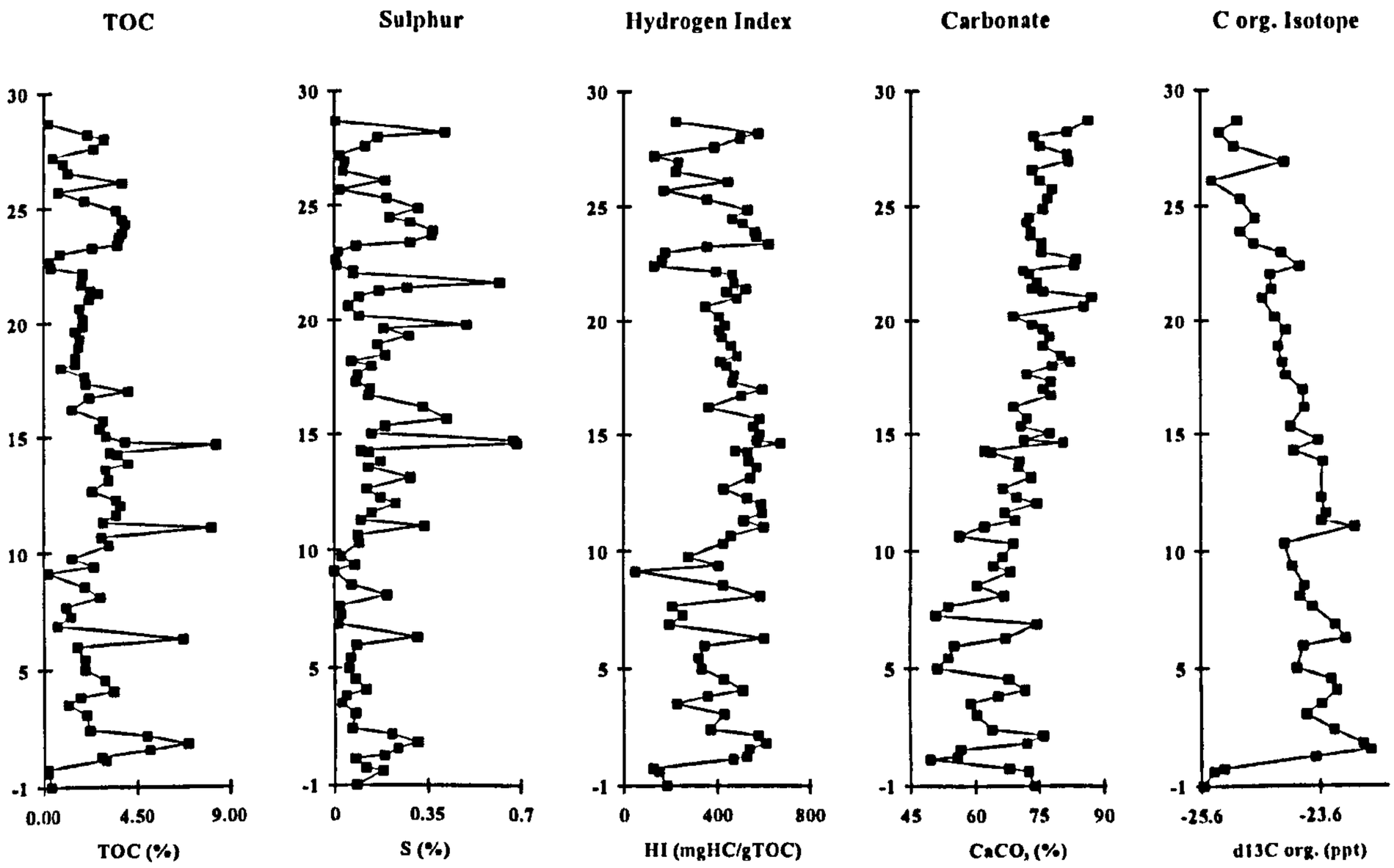

Figure 5.6 Stratigraphical plots of mean bulk and isotope geochemistry for the Oued Bahloul section (data given in Appendix 2, Table III).

Sample	TOC (wr) (%)	HI (wr) (mgHC/gTOC)	HI (ker) (mgHC/gTOC)	Difference in HI	Retained (%)
OB7	5.00	585	593	8	1.4
OB18	0.69	199	549	350	63.7
OB43	2.88	584	661	77	11.7
OB65	0.30	164	531	367	69.1
EC11	0.93	133	235	102	43.4
EC13	0.79	152	258	106	41.1
DOY25	1.46	458	597	139	23.3
OG16	1.66	322	497	175	35.2
N18	1.92	174	198	24	12.2

Table 5.1 Whole rock and kerogen hydrogen index data for the Tunisian sections.
Key: TOC, Total Organic Carbon; HI, Hydrogen Index; wr, whole rock; ker, kerogen; Retained, percentage of hydrocarbons retained by the matrix material, calculated by difference in S2 data between whole rock and kerogen Rock-Eval Pyrolysis.

The $\delta^{13}C_{org}$ plot shows an initial sharp positive isotope excursion at the base of the section from -25.6‰ to an initial maximum of -22.6‰, in about the same position as the first TOC peak; the values then drop slightly before a second smaller maximum is observed. There is then a gradual return to background $\delta^{13}C_{org}$ values over the remaining part of the section (Fig. 5.7). The $\delta^{13}C_{org}$ values show no apparent overall correlation with TOC ($r^2 = 0.26$) or hydrogen index ($r^2 = 0.08$). The total excursion covers 24m of the section. A summary of the isotope geochemical data is given in Table 5.3 (pg. 103).

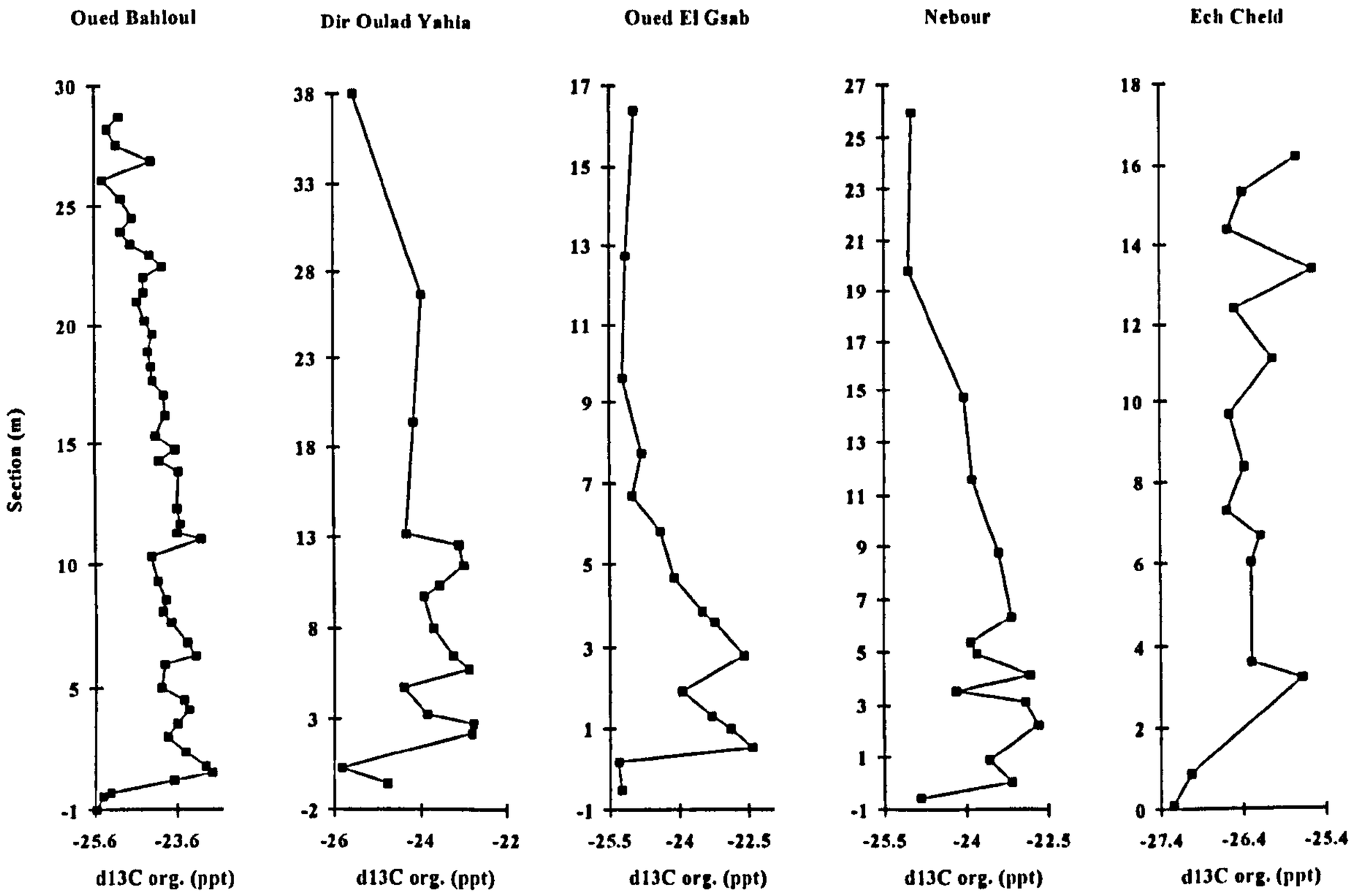

Figure 5.7 Stratigraphic plots of $\delta^{13}C$ (‰) kerogen isotope data for the Tunisian sections. Note the sharp positive excursion near the base in each section.

5.5.2 Microscopy

Reflected light microscopy of polished blocks (OB2 and OB79; Appendix 3, Table I) carried out by Dr J. M. Jones revealed decomposed pyrite, light to moderate bitumen staining, and a dominance (>90%) of inertinite in the very rare phytoclast fraction. Vitrinite reflectance was determined on the sample from 26.75m based on only 3 selected vitrinite particles, and gave a maturity of 0.37%R_o. Vitrinite reflectance values could not be determined on sample OB2 due to the absence of vitrinite.

The kerogen is generally dominated (<99%) by yellow-orange to bright yellow-orange fluorescing marine AOM (Appendix 3, Table VI). Samples OB2, 23

and 79 have a dull yellow-orange fluorescing marine AOM; these samples have a lower TOC (<0.5% TOC) and also have a significant but subordinate terrestrial content (12 to 18%) and some palynomorphs, including dinoflagellate cysts with a dull yellow fluorescence. Tyson (1995, p. 347) proposed a qualitative preservation scale based on unoxidised, immature kerogen, under incident blue light fluorescence. The Oued Bahloul samples would typically register 5 on this scale, as the AOM demonstrates a strong and heterogeneous fluorescence approaching that of the rare palynomorphs. However, samples OB2, 23 and 79 are more characteristic of 4 on the scale, as the AOM shows a moderate fluorescence much less than that of the *in situ* palynomorphs.

5.5.3 Molecular geochemistry

Molecular geochemical data from gas chromatography are presented in Appendix 4, Table III. Gas chromatogram traces typically have an *n*-alkane distribution from $n C_{11}$ to $n C_{36}$, with maxima at $n C_{15}$, $n C_{16}$ or $n C_{17}$ (Fig. 5.8). Pristane is typically the largest peak on the traces and the Pristane/Phytane ratio is greater than 1.0 in all samples (range 1.4 to 2.6). Other isoprenoids are abundant, especially the C_{16} and C_{18} isoprenoids (in samples OB6 and OB7 and also to a lesser extent in samples OB28 and OB40). These four samples also showed strong traces of biomarker compounds in the gas chromatography traces. The Pr/$n C_{17}$ and Ph/$n C_{18}$ ratios gave a wide range of values from 0.9 to 3.7 and 0.5 to 2.5 respectively.

The aliphatic biomarker data from gas chromatography-mass spectrometry analysis show some variation in maturity parameters through the section (Appendix 4, Table IX; cf. Mackenzie, 1984). The aliphatic ratios generally show high isomer R to S conversion and dominance of αβ over βα hopanes. Hop-13(18)-enes are found throughout the Oued Bahloul section. The Ts/Tm ratios for this section are all less than 1.0 (range 0.2-0.7). The relative abundance of methylhopanes was quite high in some samples (especially OB6 and OB7), and they show different carbon number distribution to their non-methylated counterparts, the homohopanes (Fig. 5.9a and b). The 17α (H), 18α (H), 21β (H)-28, 30-bisnorhopane was noted in relatively high abundance, especially in the centre of the section (OB39 and OB40); these samples also showed the presence of the A-ring methylated bisnorhopane. Aromatic biomarker data are given in Appendix 4, Table XII and show that the Methylphenanthrene index (MPI; Radke, 1987) has an average value of 0.37 (range 0.12 to 0.56). The triaromatic to monoaromatic steroid ratio (aromatic steroid ratio 1; cf. Riolo *et al.*, 1986) has an average value of 0.87 (range 0.81 to 0.91). The ratio of

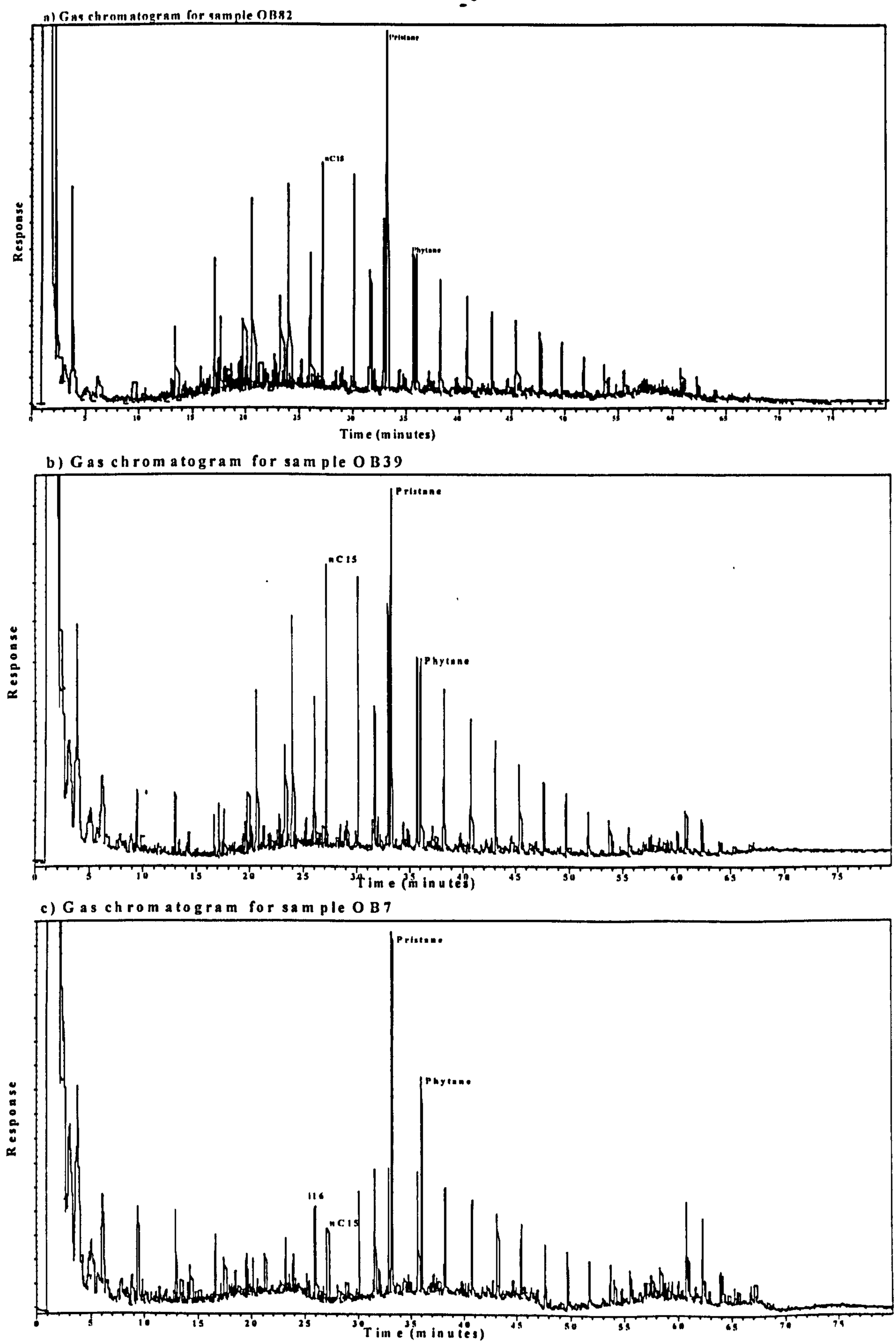

Figure 5.8 Gas Chromatograms for the Oued Bahloul section; *n*C, normal alkane; i, isoprenoid with carbon number; a) sample OB82, 27.7m; b) sample OB39, 14.1m; c) sample OB7, 1.6m, note the dominance of isoprenoids in this sample.

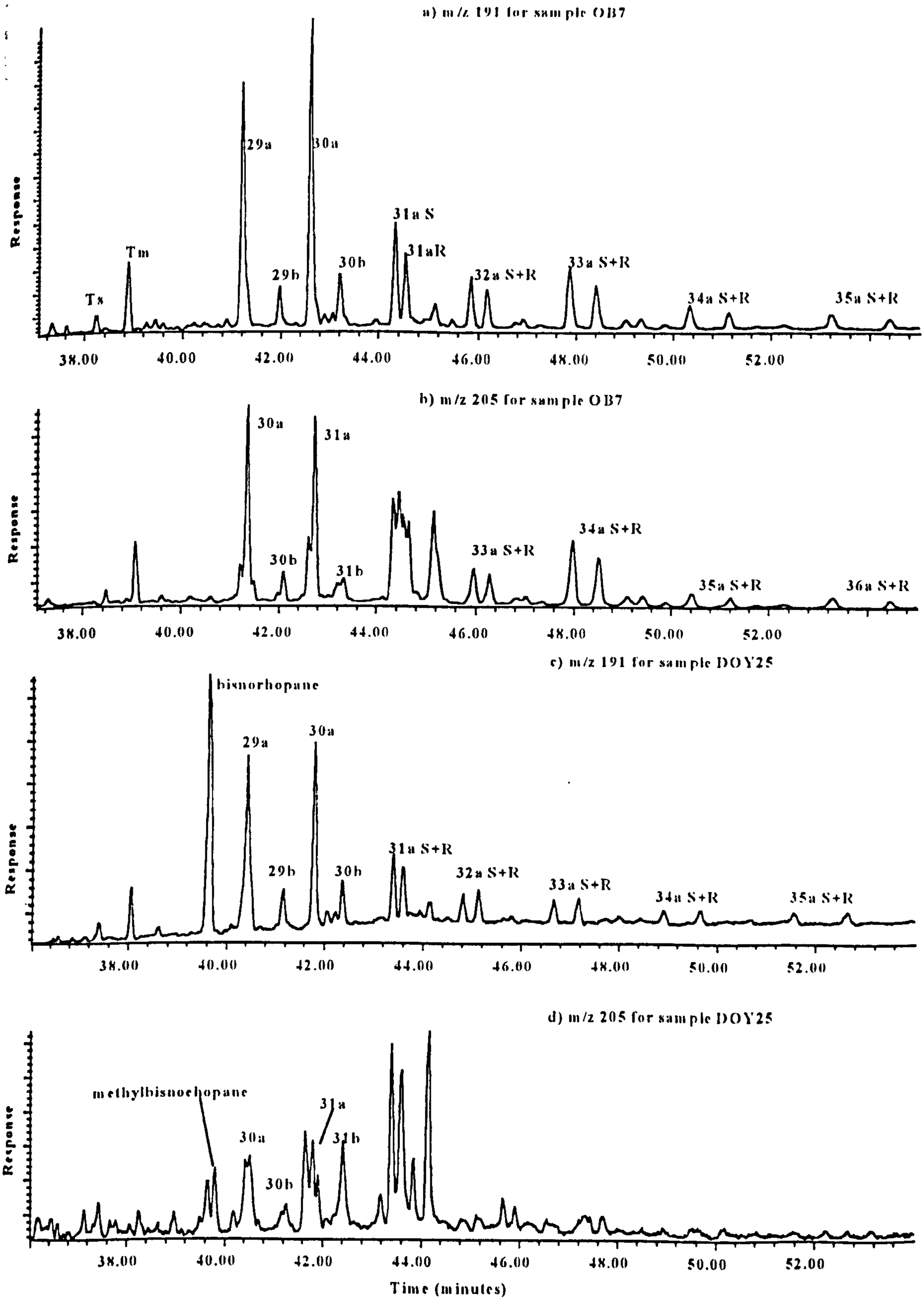

Figure 5.9 Mass fragmentograms for the Oued Bahloul and Dir Oulad Yahia sections. Key: 30, carbon number; a, αβ configuration; b, βα configuration; S+R, S and R configurations; a) m/z 191 fragmentogram for sample OB7, note the carbon number distribution favouring the C_{33} homologue; b) m/z 205 fragmentogram for sample OB7, note the carbon number distribution favouring the C_{34} homologue; c) m/z 191 fragmentogram for sample DOY25, note the large bisnorhopane peak; d) m/z 205 fragmentogram for sample DOY25, note the large, but less pronounced, methylbisnorhopane peak.

the relative increase in short chain triaromatics (21T/21T + 28TR; aromatic steroid ratio 2) all give values less than 0.1 (cf. Riolo *et al.*, 1986).

5.5.4 Constrained cluster analysis

Constrained cluster analysis (Section 2.6.2) of the bulk geochemical data for the Oued Bahloul section identified twelve units. The mean values of TOC, hydrogen index and carbonate data for each unit are plotted stratigraphically in Figure 5.10. The TOC and hydrogen index values show a similar trend with a kick at the base; carbonate values show a drop at the base of the section followed by a steady upward increase.

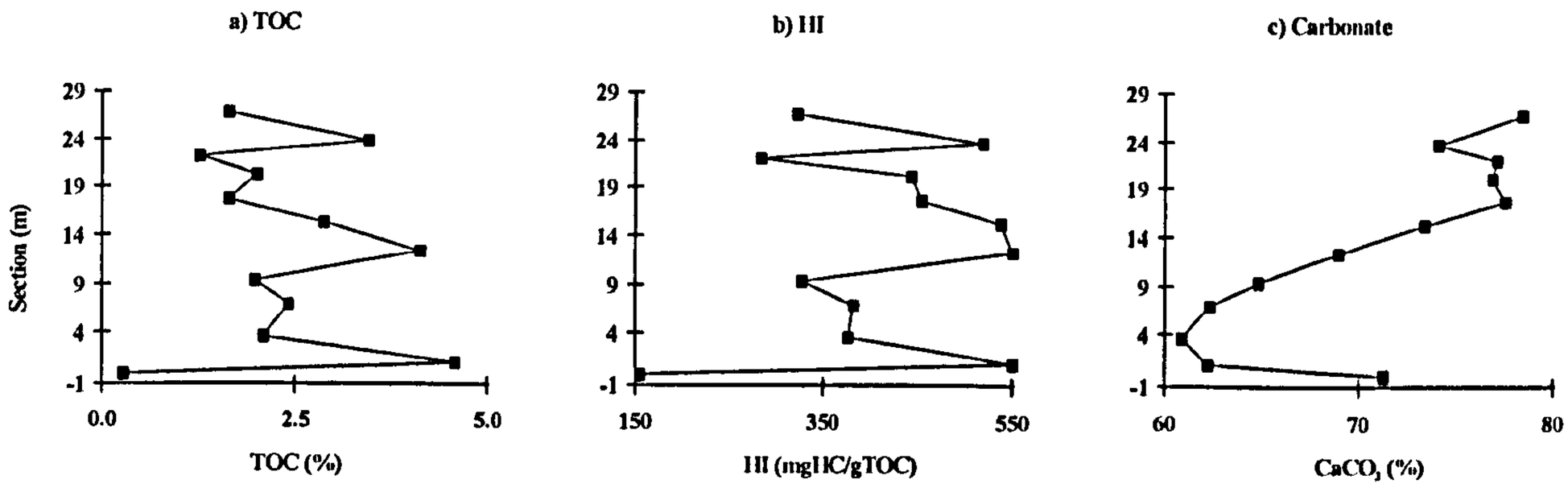

Figure 5.10 Mean bulk geochemical data from constrained clustering unit data of the Oued Bahloul section. TOC, total organic carbon; HI, hydrogen index; $CaCO_3$, carbonate.

5.6 Results for the Ech Cheid section

5.6.1 Bulk and isotope geochemistry

The bulk geochemical and isotopic results for the Ech Cheid section are recorded in Appendix 2, Table IV and Figure 5.11. Compared with the Oued Bahloul section the TOC values are quite low (<1% TOC), but are highest towards the top of the section where they show greater variability. Whole rock hydrogen index values range from 34 to 198 mgHC/gTOC. Total sulphur values are less than 0.1. Kerogen hydrogen indices measured on samples EC11 and EC13 (235 & 258 mgHC/gTOC respectively) are 40% higher (relatively) than those of whole rock samples (133 & 152 mgHC/gTOC).

A slight positive isotopic shift is seen at the base of the Ech Cheid section, with $\delta^{13}C_{org}$ values from -27.5‰ to a maximum of -25.5‰ (Fig.5.7). There is no correlation between $\delta^{13}C_{org}$ and TOC ($r^2 = 0.08$) or $\delta^{13}C_{org}$ and hydrogen index ($r^2 =$

0.03). The excursion is a very different shape to that of Oued Bahloul. The $\delta^{13}C$ maximum is still at the base of the section (EC3) but the values are more negative, and the curve does not appear to return to a background level. There is a second apparent $\delta^{13}C_{org}$ maximum towards the top of the section (EC17, 13.4m).

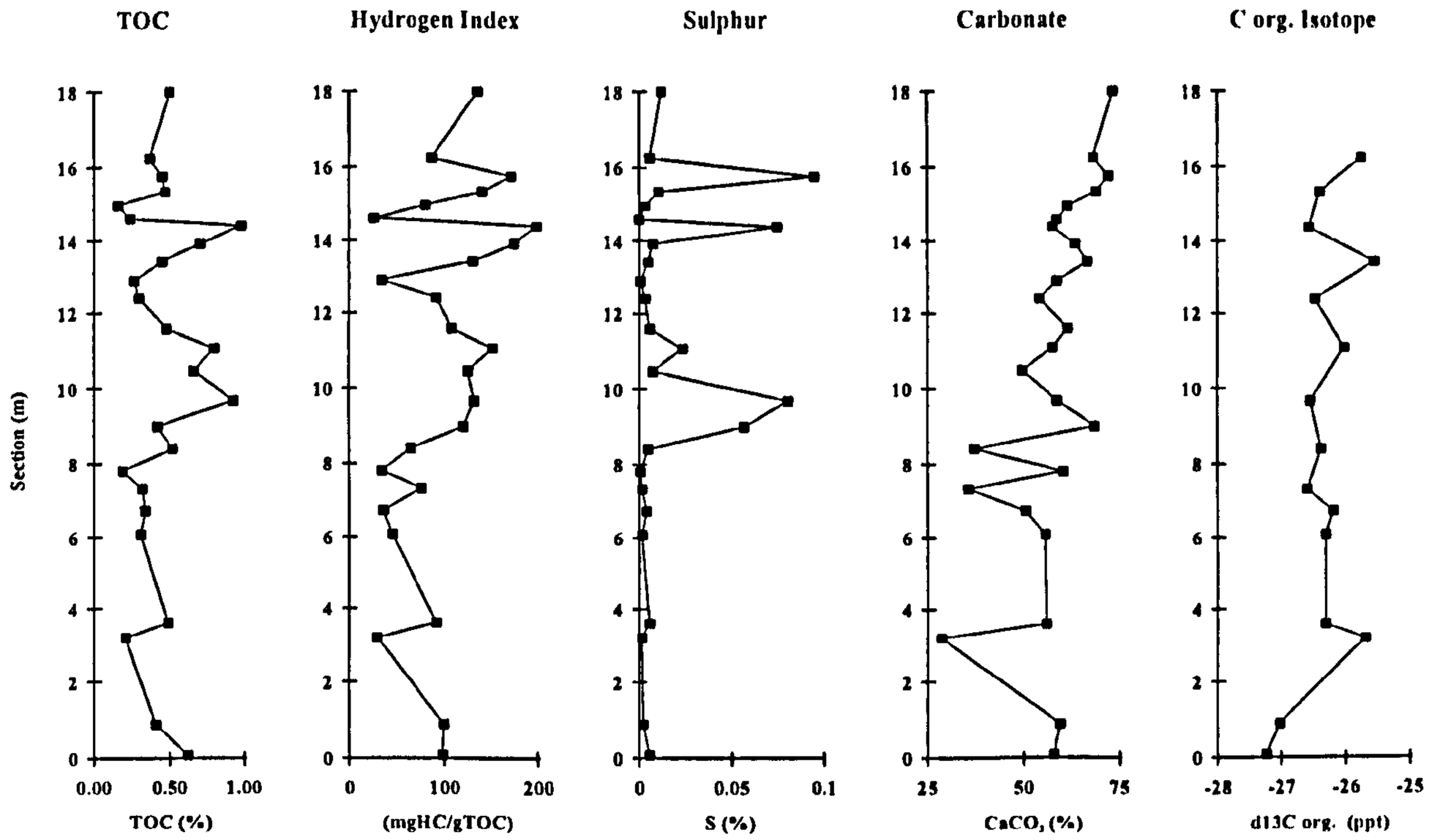

Figure 5.11 Stratigraphical plots of mean bulk and isotope geochemistry data for the Ech Cheid section (data given in Appendix 2, Table IV).

5.6.2 Microscopy

Reflected light microscopy carried out by Dr J. M. Jones on samples EC6 and EC23 revealed decomposed pyrite, light to moderate bitumen staining and only trace amounts of inertinite and vitrinite. The vitrinite reflectance values for samples EC6 and EC23 (Appendix 3, Table I.) are 0.41%R_o and 0.37%R_o respectively, based on only 2 vitrinite particles in each sample.

Marine AOM with a dull fluorescence dominates (<89%) through most of the Ech Cheid section (Appendix 3, Table VIII) and correlates well with TOC ($r^2 = 0.63$) and S2 ($r^2 = 0.65$). There is a significant phytoclast input at the base of the section, and generally a higher phytoclast input in samples where a lower TOC is observed. Dinoflagellate cysts dominate the palynomorph fraction (71 to 97%), the majority of which are proximochorate cyst forms; chorate cyst forms are rare through the section and there is a relative increase in cavate cysts at the base of the section. A fluorescence preservation scale value of 3 occurs throughout this section, as the

palynomorphs fluoresce but the AOM is dull and fluoresces just above the background.

5.6.3 Molecular geochemistry

Molecular geochemical data for the Ech Cheid section is presented in Appendix 4, Table IV. There are typically three types of gas chromatography traces from the Ech Cheid section (Fig. 5.12). Samples EC11, 13, 19, 22 and 25 have a unimodal *n*-alkane distribution with their maxima at nC_{15}. The samples EC 4, 6, 16, and 20 also have a unimodal distributions but with the maximum at nC_{26}. Two of the more central samples EC 8 and 9 show a bimodal *n*-alkane distribution with maximum at both nC_{15} and nC_{26}. The *n*-alkanes dominate over the isoprenoids, which is reflected in the Pr/nC_{17} and Ph/nC_{18} ratios of less than 1.0. However, the Pristane /Phytane ratios are still greater than 1.0. The majority of the samples have a maximum at nC_{31}.

Both aliphatic and aromatic biomarker data from gas chromatography-mass spectrometry show some variation in maturity parameters through the section (Appendix 4, Table X; cf. Mackenzie, 1984; Radke 1987). They generally show very high isomer R to S conversion, and a strong dominance of αβ over βα hopanes. Hop-13(18)-enes are found throughout. The Ts/Tm ratios are all greater than 1.0 (range 1.2 to 2.5). The Methylphenanthrene Index (MPI; Appendix 4, Table X; Radke, 1987) has an average value of 0.38 (range 0.21 to 0.58). The aromatic steroid ratio 1 (cf. Riolo *et al.*, 1986) has an average value of 0.81 (range 0.71 to 0.96), and the aromatic steroid ratio 2 gives a value 0.19 (range 0.12 to 0.23; cf. Riolo *et al.*, 1986).

5.6.4 Constrained clustering

Six units were identified from constrained clustering based on the bulk geochemical data. Stratigraphic plots of the TOC, hydrogen index and carbonate data are given in Figure 5.13. The TOC and hydrogen index follow a similar pattern, and the carbonate values drop at the base of the section before gradually increasing upwards.

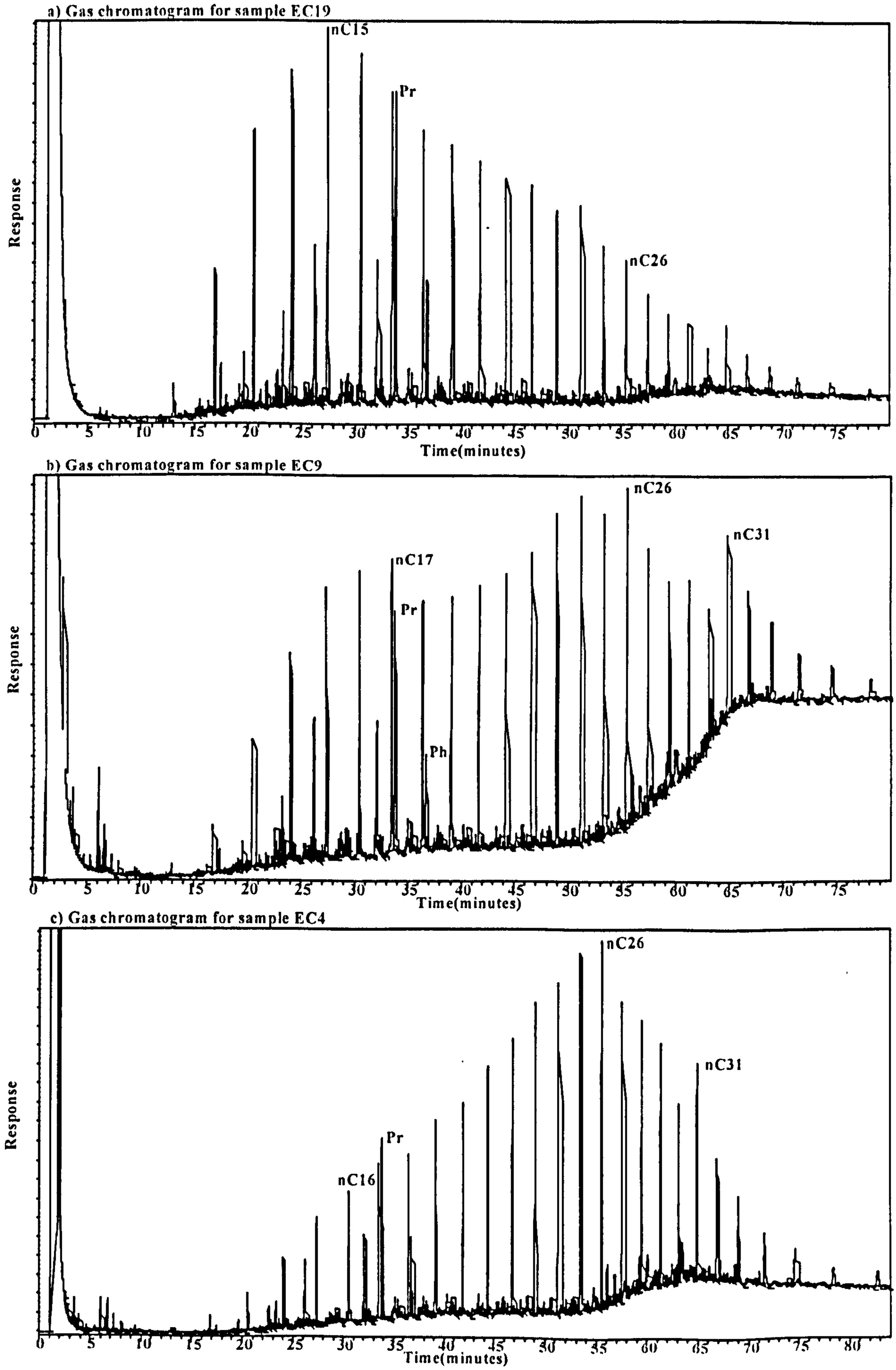

Figure 5.12 Gas Chromatograms for the Ech Cheid section. Pr, Pristane; Ph, Phytane; *n*C, normal alkane; a) sample EC19, 14.4m, maximum at nC_{16}; b) sample EC9, 8.4m, maximum at nC_{17} and nC_{16}; c) sample EC4, 3.6m, maximum at nC_{26}.

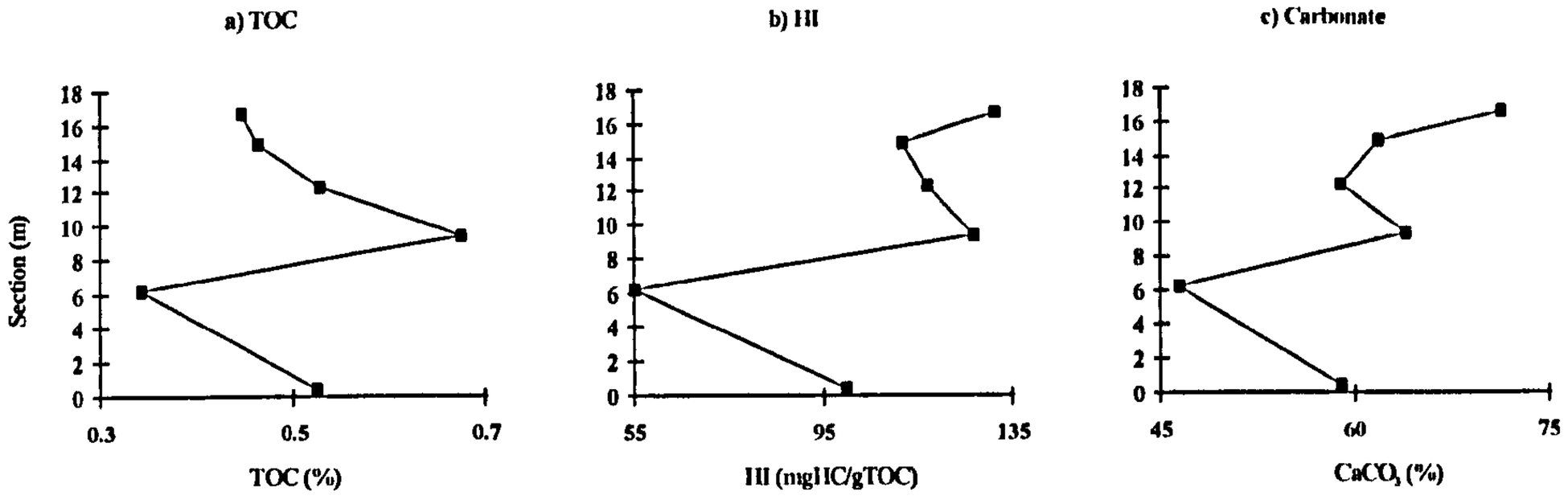

Figure 5.13 Mean bulk geochemical data from constrained clustering unit data of the Ech Cheid section. TOC, total organic carbon; HI, hydrogen index; CO_3, carbonate.

5.7 Results for the Dir Oulad Yahia section

5.7.1 Bulk and isotope geochemistry

The bulk geochemical and isotopic results for the Dir Oulad Yahia section are recorded in Appendix 2, Table V and Figure 5.14. The TOC values are high at the base (3.3 to 11.5m) and top (28.5 to 39.7) of the section, but are generally lower and more uniform in the middle of the section (DOY19 to DOY39). There are two peaks in TOC at the base of the section (above 6%). Total sulphur values range from 0.01 to 0.76% and they are highest in the basal part of the section. The carbonate values increase gradually (13 to 80%) up through the section but this is not reflected in the TOC ($r^2 = 0.10$). Rock-Eval whole rock hydrogen index values range from 100 to 850 mgHC/gTOC. Rock-Eval pyrolysis carried out on the kerogen for sample DOY25 gave a 23% higher hydrogen index value (598 mgHC/gTOC) than the whole rock analysis (458 mgHC/gTOC).

The $\delta^{13}C_{org}$ curve is not well defined due to the lower number of analyses, but does seen somewhat similar to the curve seen at Oued Bahloul. The $\delta^{13}C_{org}$ values range from -25‰ to -22.6‰ at the maximum then gradually return to background values over the remaining part of the section (Fig. 5.7). There is a slight correlation of $\delta^{13}C_{org}$ with TOC ($r^2 = 0.33$) and a poor correlation of $\delta^{13}C_{org}$ with hydrogen index ($r^2 = 0.18$). The heaviest $\delta^{13}C$ values occur within the basal organic-rich part of the section. The excursion covers approximately 30m of the section.

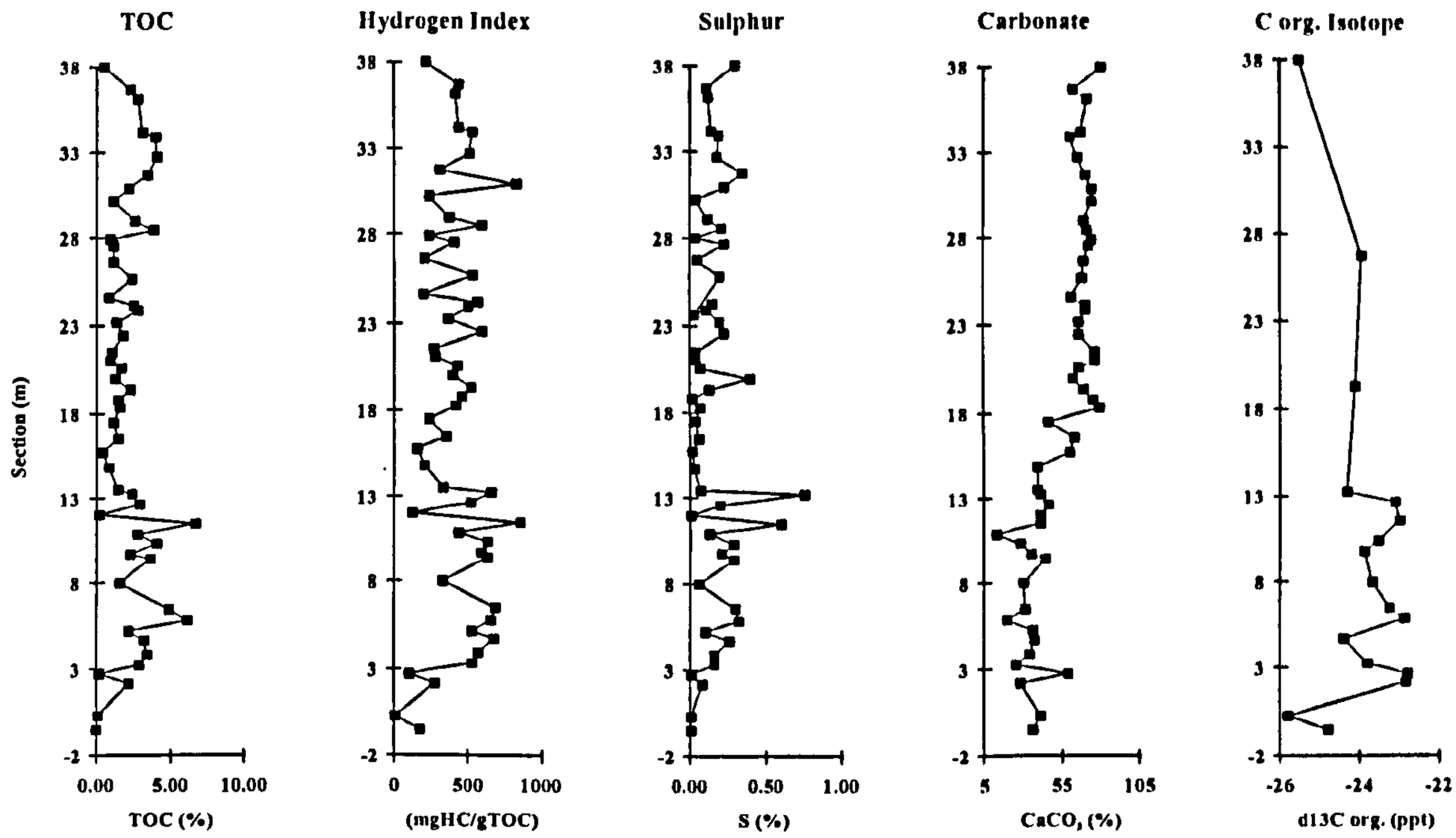

Figure 5.14 Stratigraphical plots of mean bulk and isotope geochemistry data for the Dir Oulad Yahia section (data given in Appendix 2, Table V).

5.7.2 Microscopy

Reflected light microscopy analysis for sample DOY25 (Appendix 3, Table I) performed by Dr J. M. Jones showed the presence of partly-decomposed pyrite, light to moderate bitumen staining, and the dominance (90%) of inertinite in the very rare phytoclast fraction. The mean random vitrinite reflectance values measured on 9 vitrinite particles was 0.33%R_o.

In transmitted and fluorescent light sample DOY25 is seen to be dominated (98%) by highly fluorescing (bright yellow-orange) marine AOM, with rare woody fragments and yellow fluorescing dinoflagellate cysts (Appendix 3, Table VII), similar to the kerogen observed in the Oued Bahloul samples. Palynomorphs and phytoclast material were rare in this sample, but may have been masked by the dominant AOM. This sample has a fluorescence preservation scale value of 5.

5.7.3 Molecular geochemistry

Data from molecular geochemistry for the Dir Oulad Yahia section is presented in Appendix 4, Table V. The Dir Oulad Yahia gas chromatography trace (Fig.5.15a) shows similarities to those from the Oued Bahloul section, with an *n*-alkane distribution from nC_{11} to nC_{36}, and the *n*-alkane maxima at nC_{16}. Pristane is

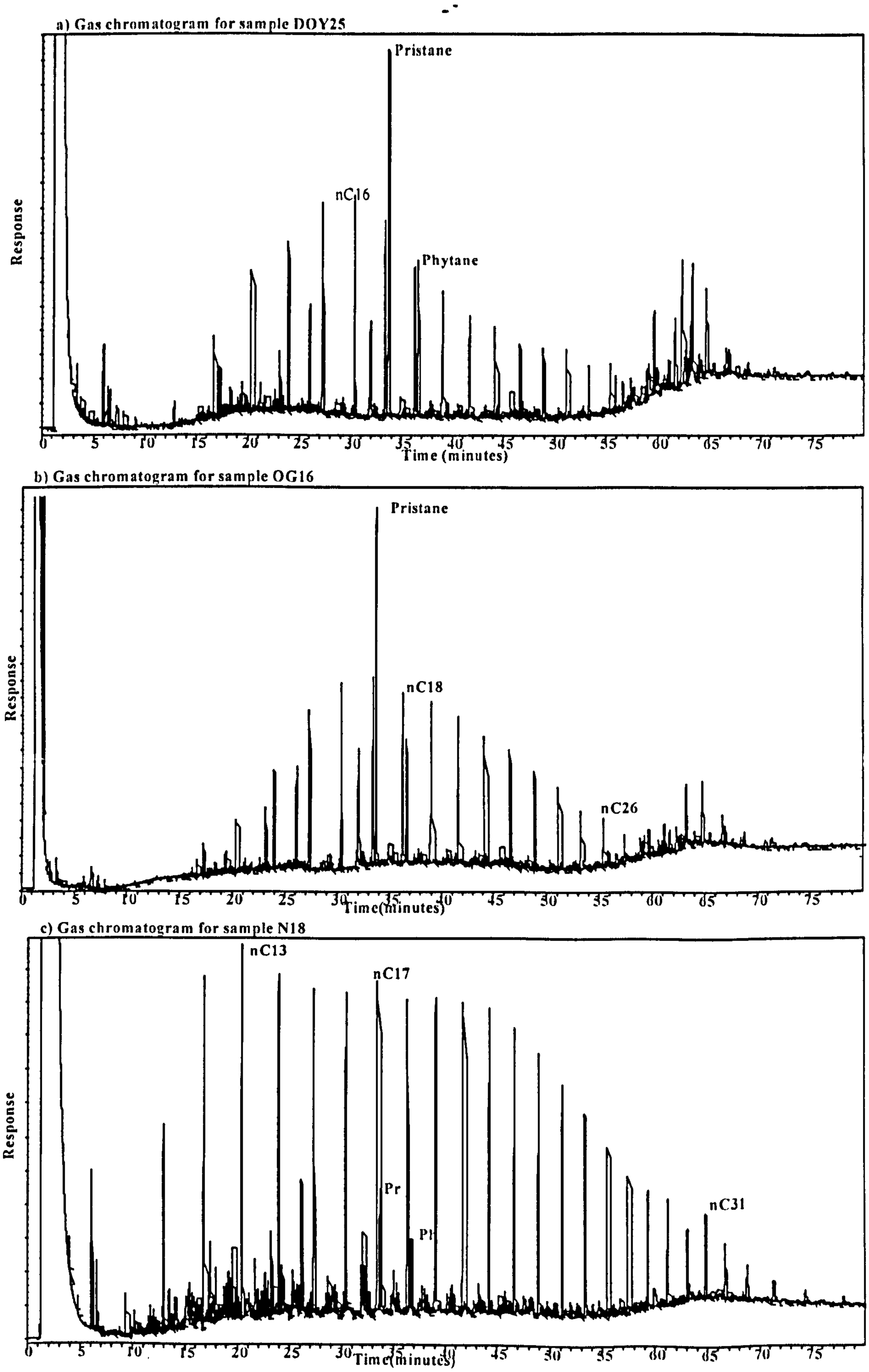

Figure 5.15 Gas chromatograms for the Dir Oulad Yahia, Oued El Gsab and Nebour sections; Pr, Pristane; Ph, Phytane; *n*C, normal alkane; a) sample DOY25, 18.8m; b) sample OG16, 7.4m; c) sample N18, 9.3m.

the dominant peak and the biomarkers show through quite strongly. The Pr/nC$_{17}$ and Ph/nC$_{18}$ ratios are 1.9 and 1.1 respectively, and the Pristane/Phytane ratio is 2.3.

Aliphatic and aromatic biomarker data from gas chromatography-mass spectrometry for sample DOY25 are given in Appendix 4, Table XI. The aliphatic maturity parameters (cf. Mackenzie, 1984) show high hopane isomer R to S conversion, and a dominance of αβ over βα hopanes; the sterane maturity parameters are quite low. Hop-13(18)-enes are abundant in this sample. The Ts/Tm ratio is 0.43. Methylhopanes are abundant in the sample and show a different carbon number distribution to their non-methylated counterparts the homohopanes (Fig 5.9c and d). The 17α (H), 18α (H), 21β (H)-28, 30-bisnorhopane is the most abundant peak in the m/z 191 trace, and the A-ring methylbisnorhopane is also abundant in the m/z 205 trace (Fig 5.9c and d). The steranes appear to be relatively more abundant than the hopanes for this sample, and the relative abundance of methylsteranes is also higher. The value for MPI in sample DOY25 is 0.44 (cf. Radke, 1987; Appendix 4 Table XII), and for aromatic steroid ratio 1 and aromatic steroid ratio 2 (cf. Riolo *et al.*, 1986) the values are 0.62 and 0.01 respectively.

5.7.4 Constrained clustering

Constrained clustering carried out on the bulk geochemistry data from the Dir Oulad Yahia section identified 10 units. Stratigraphic plots of the unit means for TOC, hydrogen index and carbonate data are given in Figure 5.16. The TOC shows a sharp rise (4%) at the base of the section, and the hydrogen index values follow a similar trend. The trend in the carbonate values shows a drop at the base of the section followed by a gradual rise upwards.

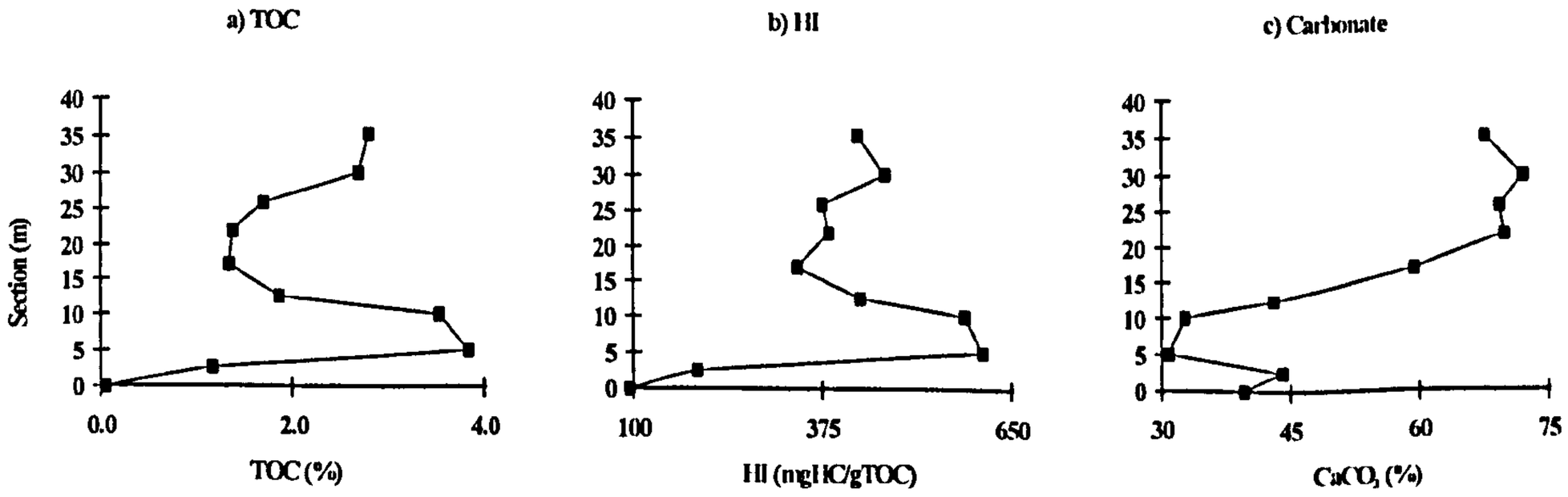

Figure 5.16 Mean bulk geochemical data from constrained clustering unit data of the Dir Oulad Yahia section. TOC, total organic carbon; HI, hydrogen index; CO_3, carbonate.

5.8 Results for the Oued El Gsab section

5.8.1 Bulk and isotope geochemistry

The bulk geochemical and isotopic results for the Oued El Gsab section are recorded in Appendix 2, Table VI and Figure 5.17. The TOC values are highest but more variable at the base of the section; they are also higher and variable at the top of the section (8.4 to 15m). The intermediate samples (1.9 to 7.4m) have lower and more uniform TOC. The base and middle of the section have lower carbonate values than the top and there is a general increase in carbonate up through the section. The variability observed in TOC values show no correlation with the carbonate values ($r^2 = 0.04$). Rock-Eval whole rock hydrogen indices have a range from 159 to 565 mgHC/gTOC. The total sulphur contents range from 0.01 to 0.54%, and show a poor correlation ($r^2 = 0.22$) with TOC, due to a couple of anomalies with very high sulphur values (OG25 and OG32, 0.54% and 0.43% respectively) compared to the rest of the section; when these anomalies are excluded the correlation is quite good ($r^2 = 0.54$). The kerogen hydrogen index value for sample OG16 (497 mgHC/gTOC) is 35% higher than that for whole rock (322 mgHC/gTOC).

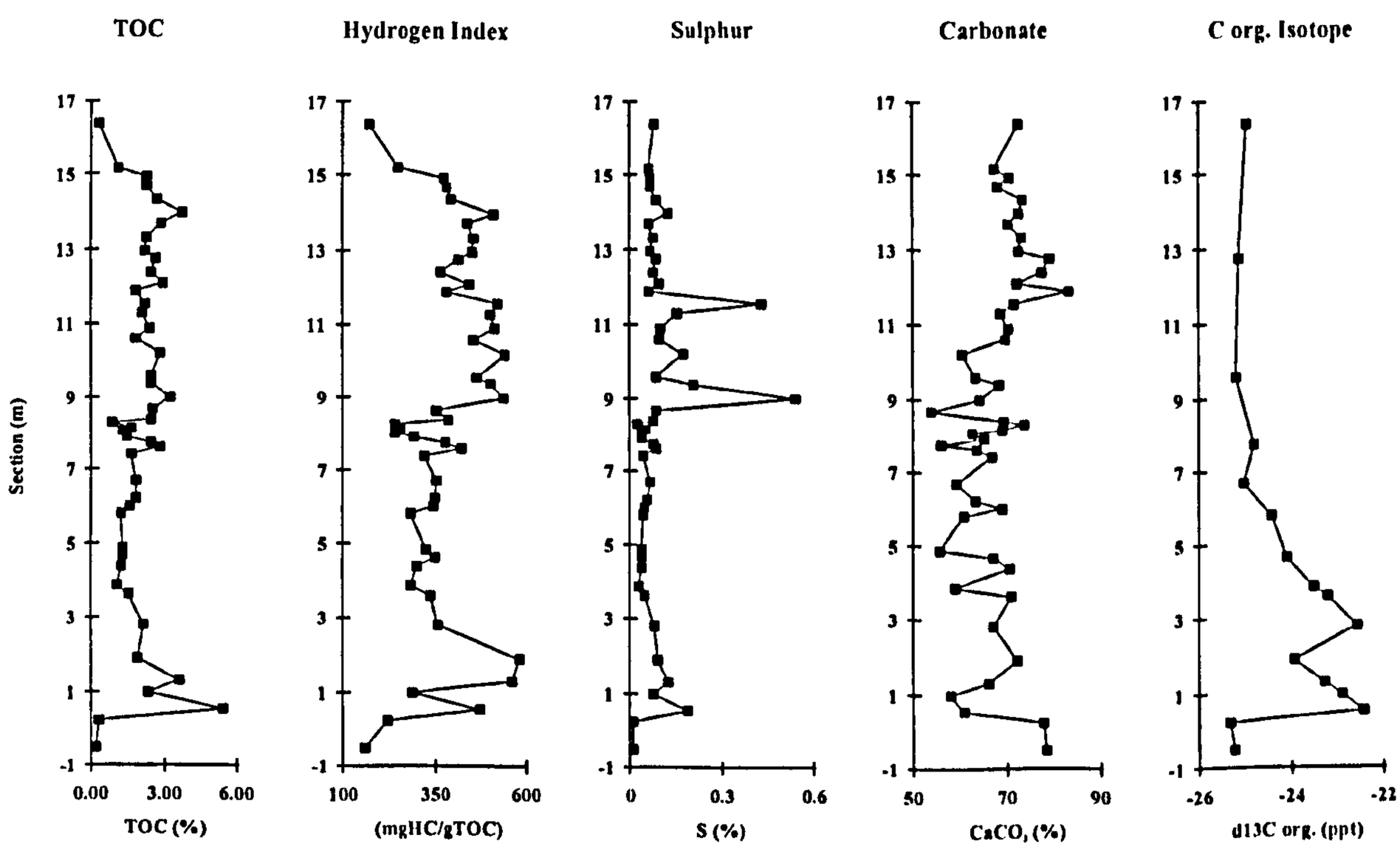

Figure 5.17 Stratigraphical plots of mean bulk and isotope geochemistry data for the Oued El Gsab section (data given in Appendix VI).

The $\delta^{13}C_{org}$ values show a shift from -25.5‰ to -22.5‰ at the base of the section, then gradually return to background values of -25.5‰ before the end of the

section (Fig 5.7). There is a poor correlation of $\delta^{13}C_{org}$ with TOC ($r^2 = 0.30$), and no correlation with hydrogen index is observed ($r^2 = 0.11$). The maximum isotope excursion occurs in the organic-rich basal part. The overall excursion reaches background values by sample OG27 (an excursion thickness of 10m) before the deposition of the black shales is complete.

5.8.2 Microscopy

Sample OG16 analysed by reflected light microscopy (Appendix 3, Table I) performed by Dr J. M. Jones contains decomposed pyrite, light bitumen staining, moderate to rich bitumen wisps, and negligible amounts of both inertinite and vitrinite. Random vitrinite reflectance, measured on 12 wispy vitrinite particles gave a mean value of 0.4%R_o.

The kerogen assemblage of sample DOY25 (Appendix 3, Table VII) is dominated (99%) by yellow-orange fluorescing marine AOM; phytoclast material is virtually absent and the rare dinoflagellate cysts fluoresce bright yellow/orange (stronger than the AOM). This sample has a fluorescence preservation scale of 4 (cf. Tyson, 1995, p. 347).

5.8.3 Molecular geochemistry

Molecular geochemical data for the Oued El Gsab sample OG16 are given in Appendix 4, Table V. The gas chromatography trace (Fig. 5.15b) shows an *n*-alkane distribution ranging from nC_{12} to nC_{36}, with an *n*-alkane maxima at nC_{17}. Pristane is the dominant peak, and the Pristane/Phytane ratio is 2.9. The Pr/nC_{17} and Ph/nC_{18} ratios are 2.9 and 1.9 respectively. Biomarkers are seen in the later part of the trace.

The aliphatic biomarker maturity parameters (Appendix 4, Table XI; cf. Mackenzie, 1984) for sample OG16 show high isomer R to S conversion in the hopanes, and a dominance of αβ over βα hopanes; the sterane maturity parameters are also quite low. Hop-13(18)-enes are present in this sample. The Ts/Tm ratio is 0.31. The steroids and hopanoids occur in a similar relative abundance. Methylsteranes are also present. The value for MPI (Appendix 4, Table XII; Radke, 1987) is 0.23, and for aromatic steroid ratio 1 and aromatic steroid ratio 2 the values are 0.94 and 0.01 respectively (cf. Riolo *et al.*, 1986).

5.8.4 Constrained clustering

Seven units were defined by constrained clustering analysis of the bulk geochemical data. The TOC, hydrogen index and carbonate means for each unit are plotted in Figure 5.18. There is a similar trend between the TOC and hydrogen index values for the units. An initial drop at the base of the section is observed in the carbonate data, followed by a gradual upward increase in values.

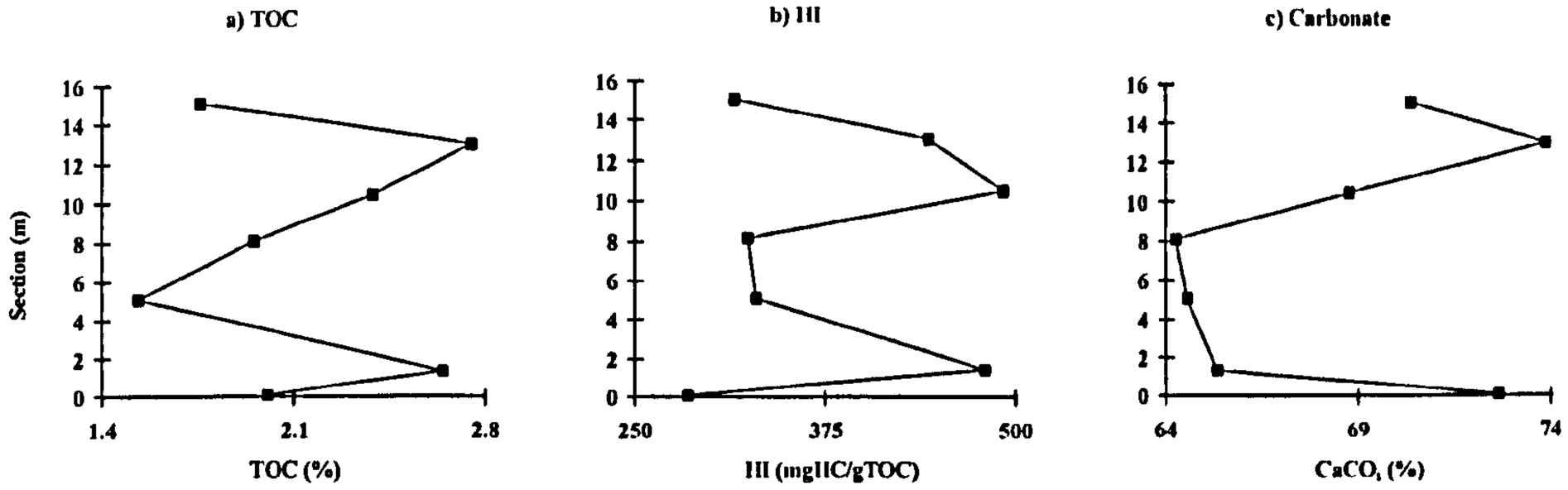

Figure 5.18 Mean bulk geochemical data from constrained clustering unit data of the Oued El Gsab section. TOC, total organic carbon; HI, hydrogen index; CO_3, carbonate.

5.9 Results for the Nebour section

5.9.1 Bulk and isotope geochemistry

The bulk geochemical and isotopic results for the Nebour section are recorded in Appendix 2, Table VII and Figure 5.19. The TOC values are more variable at the base and top of the section but are more stable in the middle; TOC values are also slightly higher at the base (N12) and top (N29-N43). The carbonate values (50-79%) generally increase from the base of the section to the top. The sulphur values range from 0.01 to 0.5%. Whole rock Rock-Eval hydrogen index values range from 36 to 395 mgHC/gTOC. Rock-Eval of the kerogen gives a 12% higher hydrogen index for sample N18 (198 mgHC/gTOC) than that of whole rock hydrogen index (174 mgHC/gTOC).

The $\delta^{13}C_{org}$ curve varies from -25‰ to -22.5‰ at the base of the section, then gradually returns to background values of -25‰ before the top of the section (Fig 5.7). There appears to be no overall correlation between $\delta^{13}C_{org}$ and TOC ($r^2 = 0.03$) or hydrogen index ($r^2 = 0.01$). The overall excursion occurs between samples N0 and N39, and covers 21m of the section.

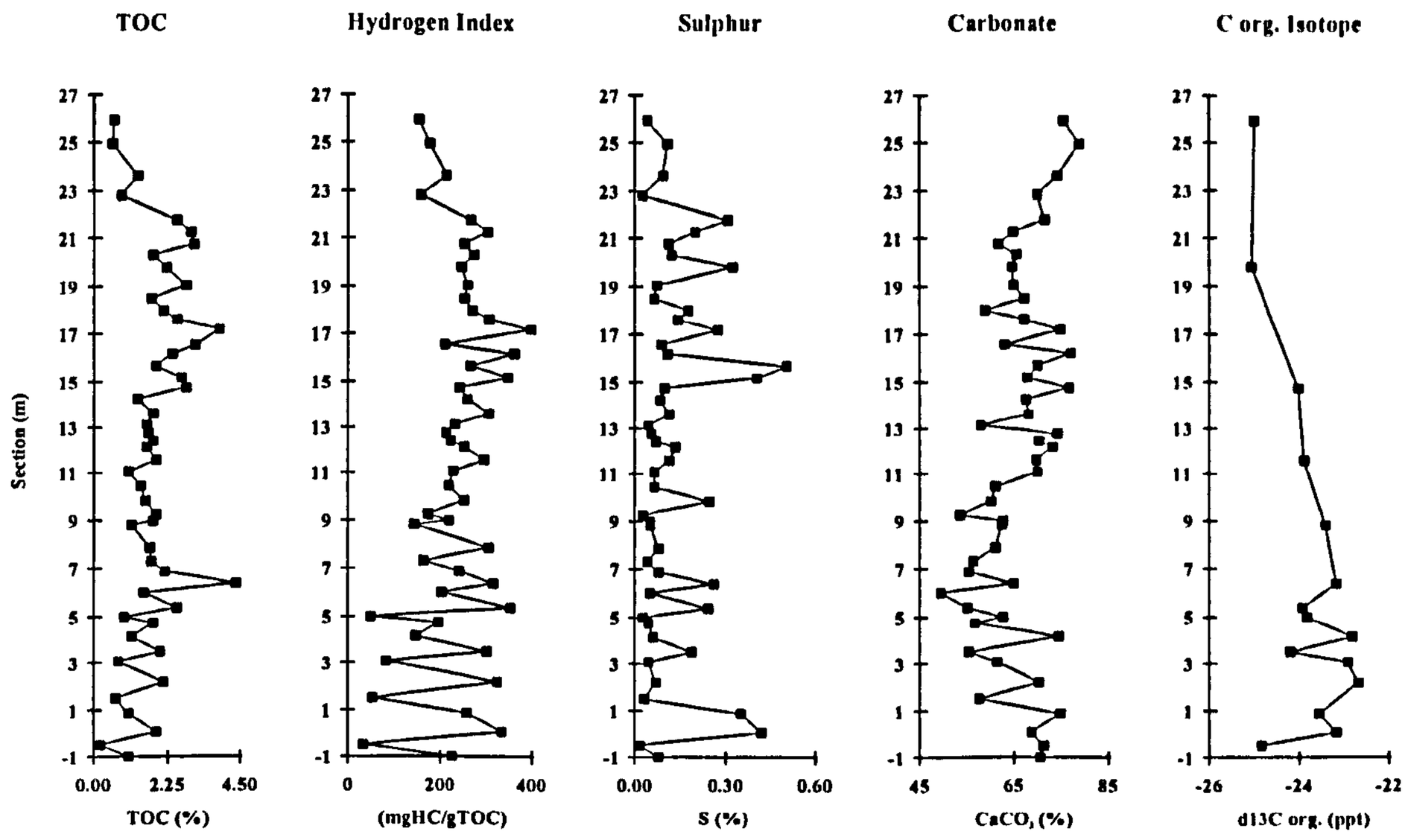

Figure 5.19 Stratigraphical plots of mean bulk and isotope geochemistry for the Nebour section (data given in Appendix 2, Table VII).

Section	Descriptive statistics	TOC (%)	HI	TS (%)	Carbonate (%)	PI (S1/S1+S2)
Oued Bahloul *(83 samples)*	**Mean**	2.51	426	0.17	71	0.06
	Range	0.21-8.15	50-681	0.002-0.70	51-86	0.1-0.31
	Std. Dev.	1.61	144	0.15	8.4	0.04
Ech Cheid *(25 samples)*	**Mean**	0.47	100	0.02	58	0.21
	Range	0.16-0.98	34-198	0.00-0.10	29-74	0.1-0.4
	Std. Dev.	0.22	49	0.03	11	0.13
Dir Oulad Yahia *(50 samples)*	**Mean**	2.22	423	0.16	55	0.07
	Range	0.10-6.77	100-850	0.01-0.76	13-80	0.02-0.25
	Std. Dev.	1.47	187	0.15	18	0.13
Oued El Gsab *(46 samples)*	**Mean**	2.09	383	0.09	68	0.06
	Range	0.21-5.47	159-565	0.01-0.54	54-79	0.02-0.27
	Std. Dev.	0.95	104	0.1	7	0.04
Nebour *(47 samples)*	**Mean**	1.83	237	0.13	66	0.08
	Range	0.2-4.33	36-395	0.05-0.55	50-79	0.02-0.47
	Std. Dev.	0.83	79	0.12	7	0.06

Table 5.2 Summary of bulk geochemistry data for the Tunisian sections. Key: TOC, Total Organic Carbon; HI, hydrogen index (mgHC/gTOC); TS, total sulphur; PI, production index; Std. Dev., standard deviation.

Section	$\delta^{13}C$ min.	$\delta^{13}C$ max.	Size of exc.	Thickness of exc. interval	Distance between base and max.
Oued Bahloul	-25.6‰	-22.8‰	+3.0‰	25m	1.0m
Dir Oulad Yahia	-25.8‰	-22.8‰	+3.0‰	38m	2.2m
Oued El Gsab	-25.3‰	-22.4‰	+3.0‰	10m	0.6m
Nebour	-25.1‰	-22.7‰	+2.0‰	20m	2.2m
Ech Cheid	-27.3‰	-25.6‰	+1.5‰	-	3.2m

Table 5.3 Summary of isotope geochemical data for the Tunisian sections. Key: $\delta^{13}C$ min., $\delta^{13}C_{org}$ minimum, i.e. background values; $\delta^{13}C$ max., $\delta^{13}C_{org}$ maximum, i.e. value at excursion maximum; size of excursion, difference between basal $\delta^{13}C_{org}$ and maximum; Thickness of exc. interval, distance between basal $\delta^{13}C_{org}$ value and point at which the curve returns to back ground value, note the Ech Cheid section does not return to background values; Distance between base and max., distance from the base of the section to the maximum of the excursion.

5.9.2 Microscopy

Reflected light microscopy of sample N18 (Appendix 3, Table I) carried out by Dr J. M. Jones revealed no pyrite, moderate to rich bitumen staining, moderate bitumen wisps, and only trace amounts of inertinite and vitrinite. The mean random vitrinite reflectance was 0.40%R_o, measured on two vitrinite particles.

Palynofacies analysis of the kerogen fraction (Appendix 3, Table VII) revealed a dominance (95%) of dull brown fluorescing marine AOM, with rare phytoclast material present and rare dull yellow-orange fluorescing dinoflagellate cysts. The sample has a fluorescence preservation scale of 3 (cf. Tyson, 1995, p. 347).

5.9.3 Molecular geochemistry

Molecular geochemical data for Nebour sample N18 are given in Appendix 4, Table V. The gas chromatography trace (Fig. 5.15c) shows a bimodal distribution of *n*-alkanes from nC_{11} to nC_{36} with maxima at nC_{13} and nC_{17}; the *n*-alkanes from nC_{12} to nC_{20} form a plateau and are in greater abundance than the isoprenoids. There is a significant nC_{31} peak. The Pristane/Phytane ratio is 1.7; and the Pr/nC_{17} and Ph/nC_{18} ratios are 0.37 and 0.24 respectively.

Maturity parameters (Appendix 4, Table XI; cf. Mackenzie, 1984) from biomarkers identified during gas chromatography-mass spectrometry analysis of the aliphatic hydrocarbon fraction show a high isomer R to S conversion for the hopanes and steranes, and a strong dominance of the αβ over the βα C30 hopane. Hop-13(18)-enes are present in this sample. The Ts/Tm ratio is 1.27. The hopanoid compounds are relatively more abundant than the steroids. The MPI (Radke, 1987) measured from gas chromatography-mass spectrometry analysis of the aromatic hydrocarbon fraction for sample N18 gave an extremely low value of only 0.12 (Appendix 4, Table XII). The values for aromatic steroid ratio 1 and 2 (cf. Riolo *et al.*, 1986) were 0.92 and 0.29 respectively.

5.9.4 Constrained clustering

Constrained clustering carried out on the bulk geochemical data identified ten units. Stratigraphic plots of the TOC, hydrogen indices and carbonate means for each unit are presented in Figure 5.20. The TOC and hydrogen index both show two maxima: one in the basal part of the section and one in the upper part of the section, separated by a plateau. The carbonate values drop from the base of the section, over the first 7m, then gradually increase to the top of the section.

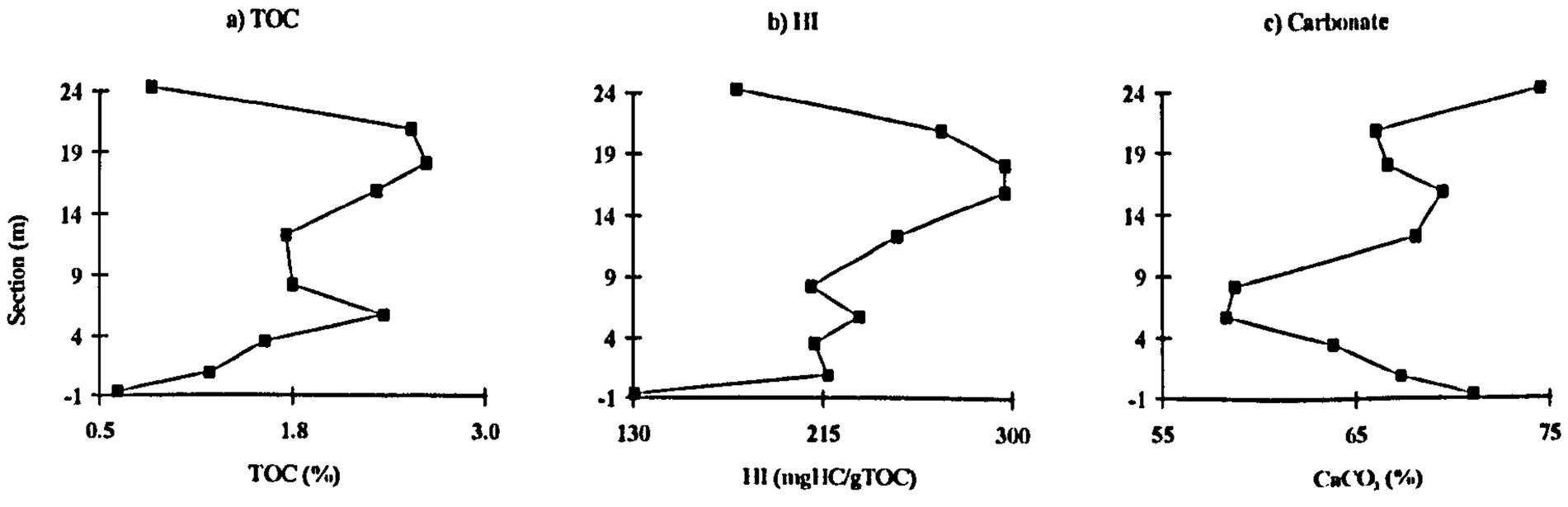

Figure 5.20 Mean bulk geochemical data from constrained clustering unit data of the Nebour section. TOC, total organic carbon; HI, hydrogen index; CO_3, carbonate.

The interpretation of these results will be discussed in the next chapter.

CHAPTER 6

6. The Bahloul Formation in Tunisia: interpretation of the data

6.1 Lithological and bulk geochemical characteristics

The five Tunisian sections generally all show an abrupt change in bulk geochemical characteristics at the base and throughout the outcrop, suggesting abrupt changes in water column anoxicity. This is highlighted at the base of the sections by initial high TOC values, which also show strong variability. Towards the central part of the sections the TOC values tends to stabilise and become uniform. The TOC values then tend to increase and become variable again at the top of the section, before an abrupt end in deposition of the organic-rich beds and the appearance of a limestone unit at the top of the sections. In all five sections the carbonate values show a general increase up through the succession. This is particularly highlighted by the constrained clustering data (Figs. 5.10, 5.13, 5.16, 5.18 and 5.20), where an initial drop in the mean carbonate values is followed by an increase in the mean values towards the top of the formation. This may be an indication of increased deposition of inoceramid debris toward the top of the Bahloul Formation, similar to that observed at Misberg (Hilbrecht & Dahmer, 1994), although the upper units are not macroscopically shelly. The variations in the carbonate curve observed from the constrained clustering data cannot be correlated between the five sections as the minimum in the values occurs at different levels relative to the kerogen isotope curve. The bulk geochemical data for the five Tunisian sections show no overall correlation of TOC (or carbonate free TOC) values with carbonate values (Fig. 6.1; range $r^2 = 0.01$ to 0.10), suggesting that the fluctuations in TOC are not controlled by carbonate dilution (although there are no data to assess the influence of changes in siliclastic flux). This is also observed in cross plots of the unit means from constrained clustering (not shown); such plots exclude noise, and make identification of general trends easier.

The mean TOC and hydrogen index values are generally higher in samples with a darker colour and shale lithology (Appendix 6, and Fig.6.2); however, the Ech Cheid section does contain some organic-rich limestones (0.75% TOC). The mean sulphur values are also higher in the darker-coloured samples; however, there is no clear correlation with lithology, although the values tend to be highest in the shales and marls. A parameter based on the combination of degrees of lamination and bioturbation (the "biolam" parameter; Appendix 1.) indicates that the most laminated part of the section is in the organic-rich unit at the base. There is also some correlation with bulk geochemistry in that the mean TOC and hydrogen index values generally increase with increasing lamination and a reduction in bioturbation. The

total sulphur values appear to be highest in samples with no lamination or bioturbation.

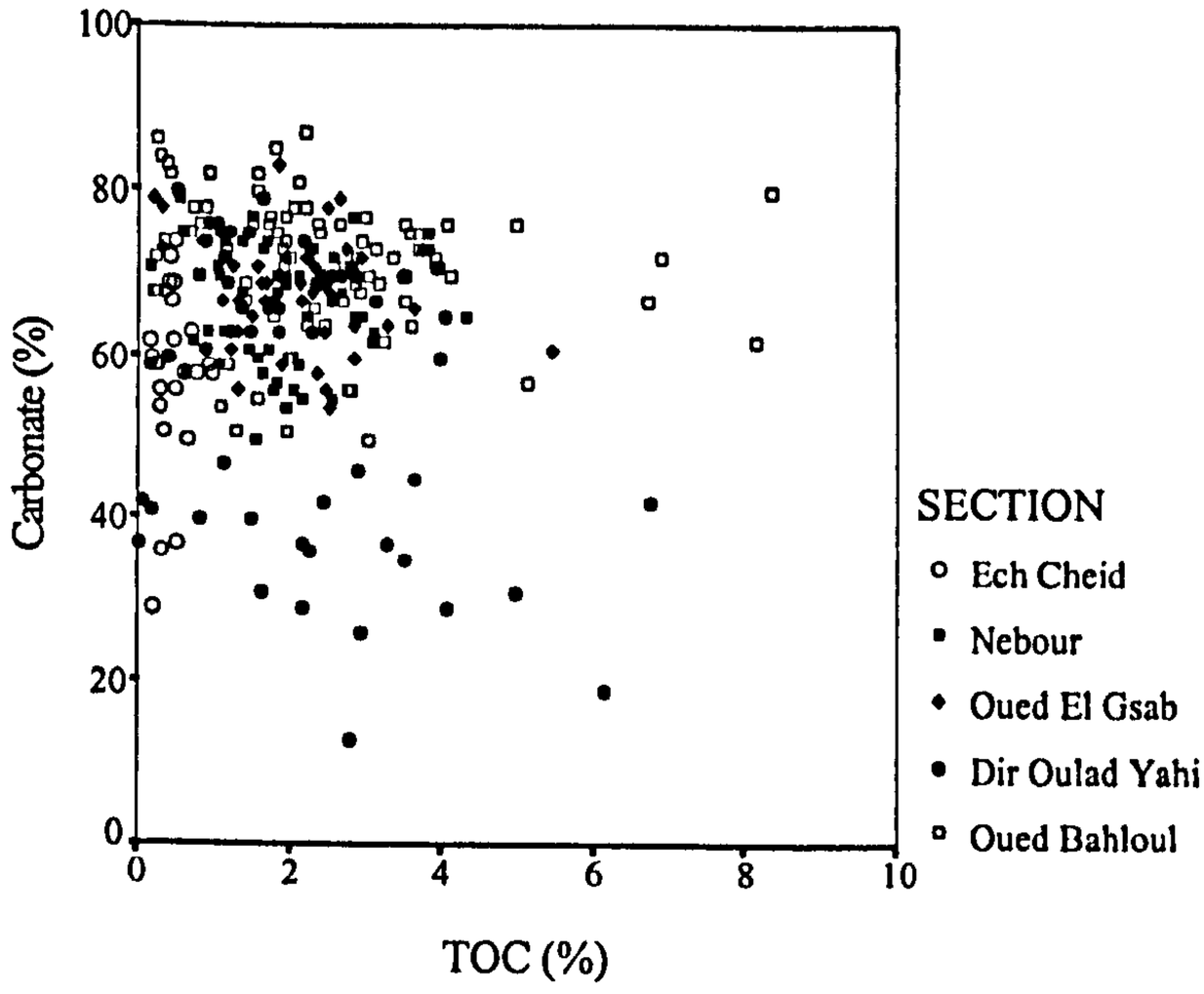

Figure 6.1 Cross plot of TOC versus carbonate data (all Tunisian samples). Note the poor correlation between the parameters: Oued Bahloul, $r^2 = 0.02$; Dir Oulad Yahia, $r^2 = 0.10$; Oued El Gsab, $r^2 = 0.04$; Nebour, $r^2 = 0.01$; Ech Cheid, $r^2 = 0.02$.

The whole rock hydrogen index values for the Oued Bahloul, Oued El Gsab and Dir Oulad Yahia sections (Appendix 2, Table III, V and VI) indicate a Type II kerogen through the majority of each section with some Type III-II and IV kerogens found at the extreme base and top of the sections. The hydrogen indices are lower toward the north of the sample area, in the Nebour and Ech Cheid sections. The Nebour samples typically exhibit a Type III-II kerogen and the Ech Cheid samples a Type III-II to Type III kerogen. This suggests north-south differences in either organic matter source, preservation or maturity, or a combination of these.

Kerogen hydrogen index values for all the sections indicate that a degree of matrix adsorption affects all samples (Table 5.1); however it is especially apparent in those samples with a TOC lower than 1%. These values suggest that (in Oued Bahloul and Ech Cheid samples) only 40% of the hydrocarbons will be released from the rock on maturation, the remainder will be trapped by the matrix material. The adsorption effect of the matrix was much lower in the Nebour sample; this may reflect the more calcareous nature of the section (Appendix 1, Table VII).

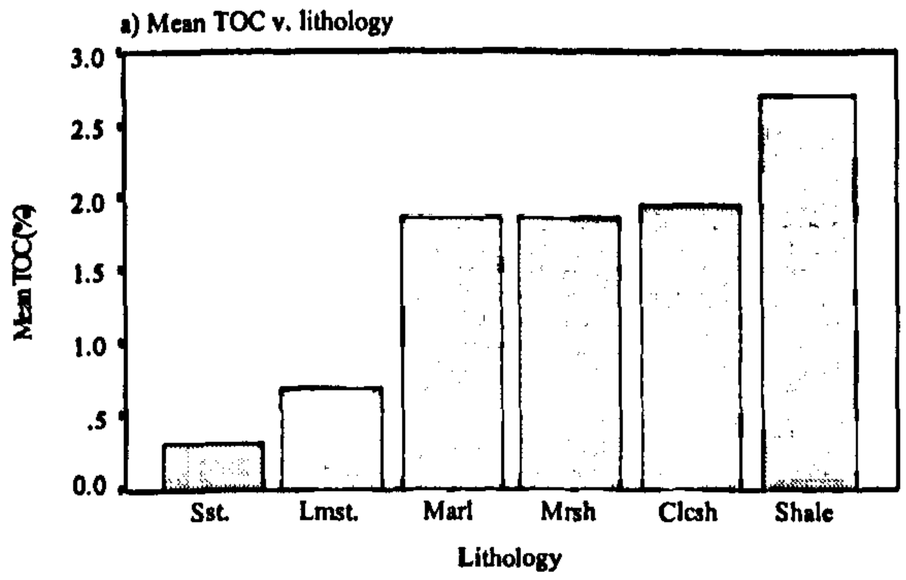

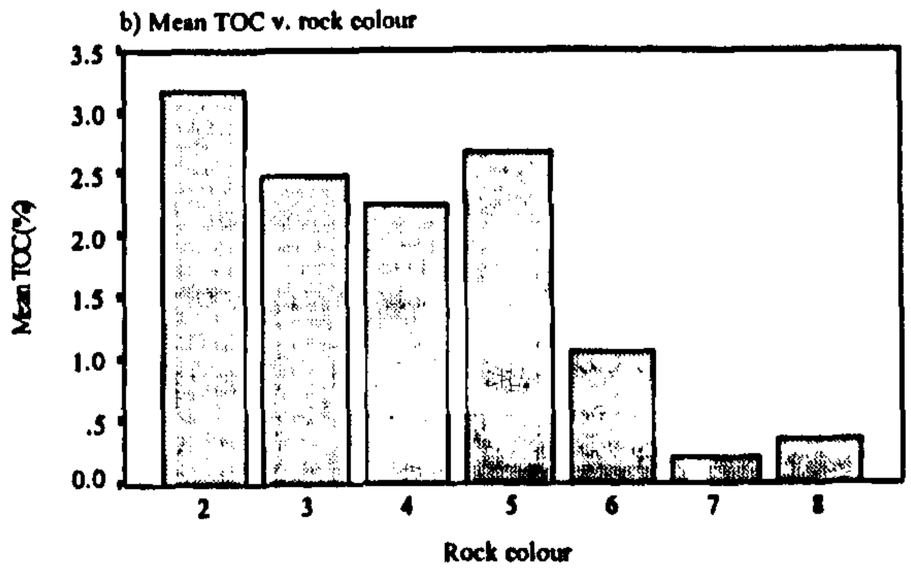

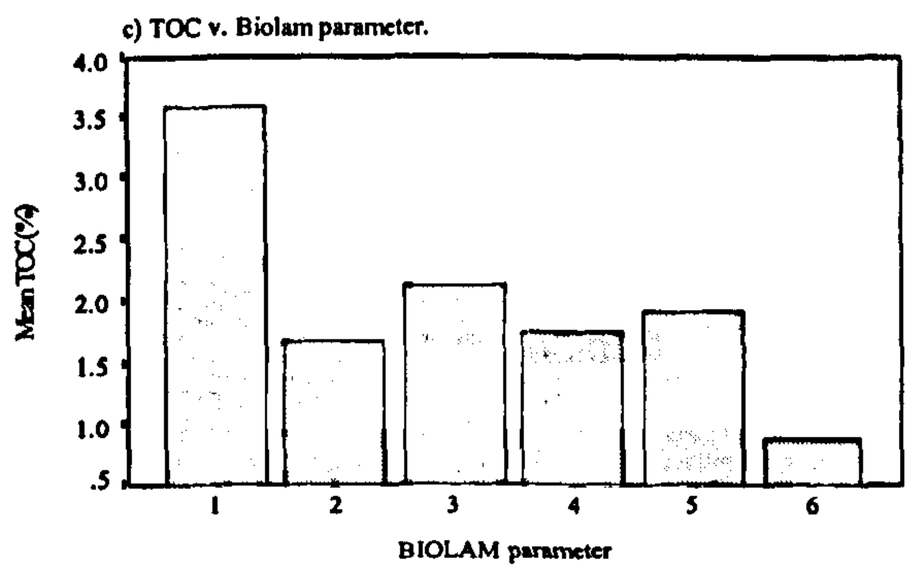

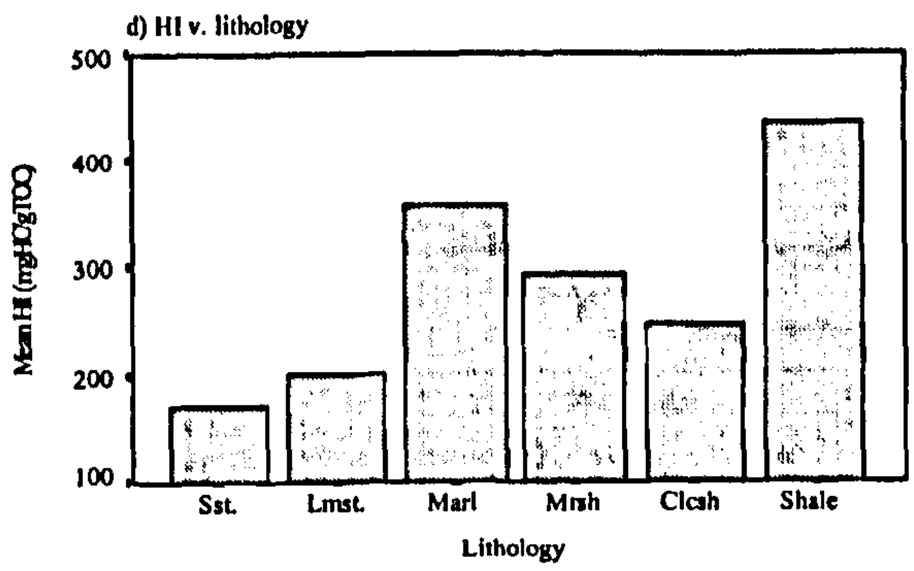

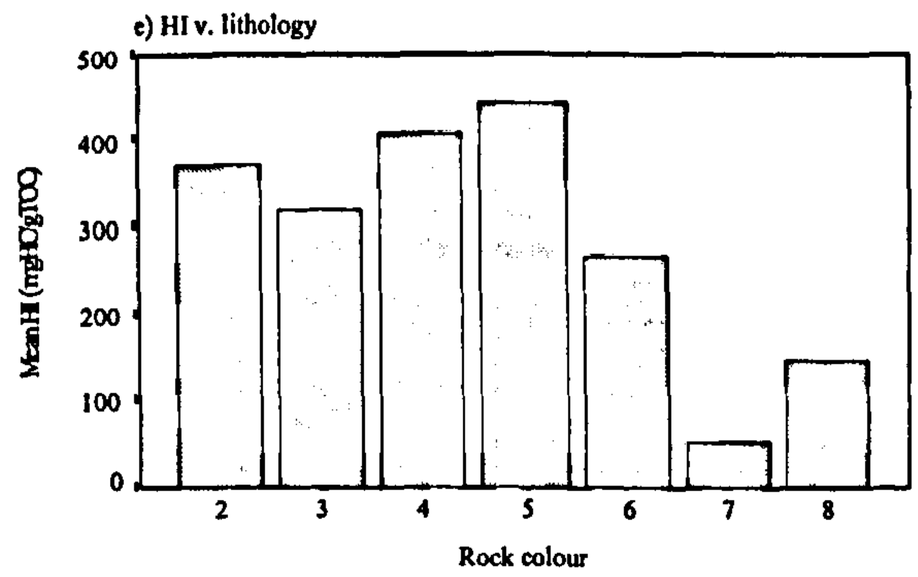

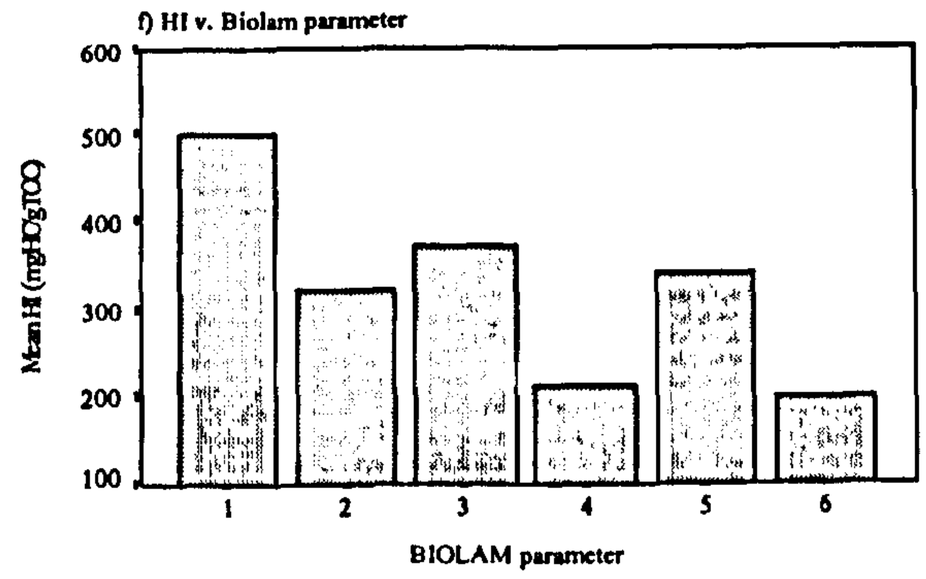

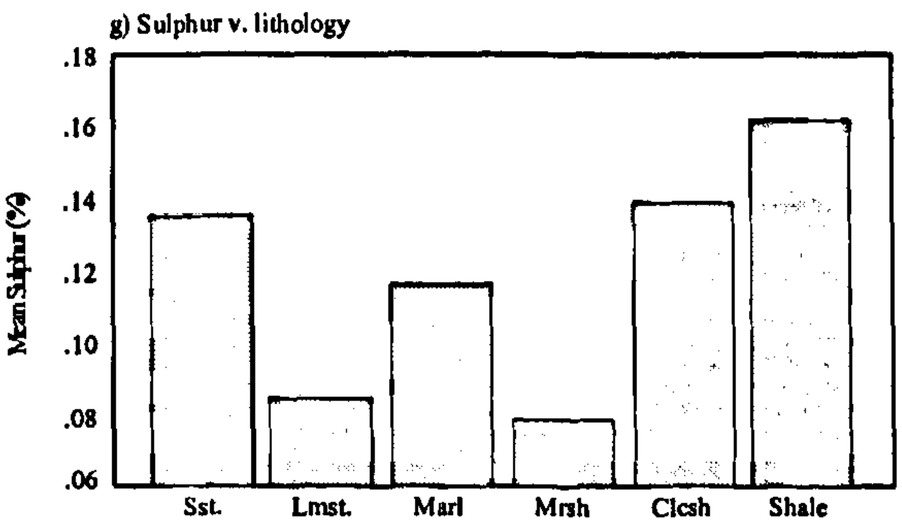

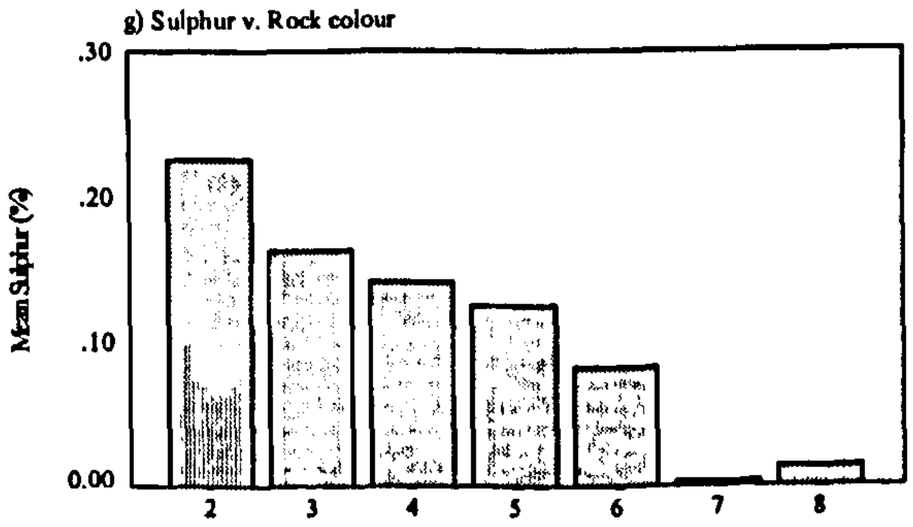

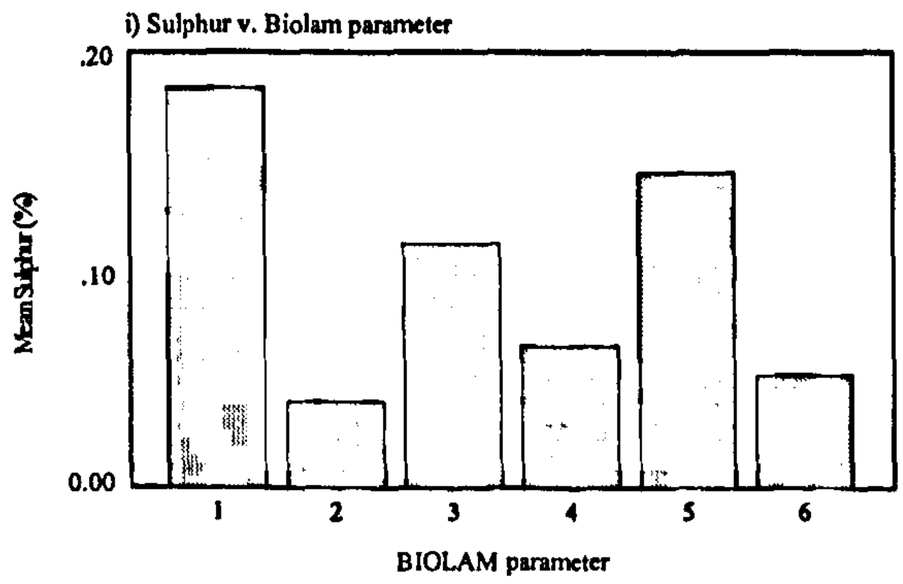

Figure 6.2 Cross plot of bulk geochemical and lithological data for the Tunisian sections. Rock colour, 2 = darkest, 8 = lightest; Biolam parameter (Appendix 1.) relates to the amount of bioturbation and lamination, 1 = most lamination, 6 = most bioturbation.

Katz (1983) observed that in rocks with low concentrations of organic matter the amount of generated hydrocarbons may be insufficient to overcome the effects of adsorption and surface tension. Espitalié and Bordenave (1993, p. 244) reported that adsorption-retention effects are pronounced in illite-rich clays. The dominant clay material in the Bahloul Formation is kaolinite and illite (Robaszynski *et al.*, 1990). The presence of these clays appears to be having an effect on the expulsion of hydrocarbons from the matrix. The minimum initial organic matter concentration necessary for effective expulsion of hydrocarbons has been suggested to be 0.3% in carbonates and 0.5% TOC in shales (Tissot & Welte, 1984, p.497). Although many of the sediments from the five sections have TOC values greater than this, the adsorption effect is still seen in samples with TOC values >4%, whereas they are normally considered to be minimal above 1-2% TOC (Cooper, 1990).

Langford and Blanc-Valleron (1990), used plots of TOC v. S2 to calculate true average hydrogen index for samples where matrix effects of clays may be affecting the value. Individual plots of TOC v. S2 for each section were constructed using Excel (Table 6.1).

Section	Regression equation	Average HI
Oued Bahloul	Y = 5.51x - 3.83	551
Dir Oulad Yahia	Y = 7.11x - 4.31	711
Oued El Gsab	Y = 5.44x - 2.64	544
Nebour	Y = 3.52x - 1.66	352
Ech Cheid	Y = 2.00x - 0.39	200

Table 6.1 Regression equations and hydrogen index data calculated from TOC versus S2 data (cf. Langford & Blanc-Valleron, 1990).

The values for the mean hydrogen index, calculated from the S2 v. TOC regression equation, generally compare quite well with the values determined from Rock-Eval pyrolysis of the kerogen isolates for the samples to the south of the sample area (within 16%); however, they are not as accurate for the samples to the north (within 43 and 29% for Nebour and Ech Cheid respectively). The values for hydrogen indices indicate that the sections to the south of the study area (OB, DOY and OG) have a dominant Type II to I/II kerogen input whereas the two sections to the north of the study area (EC and N) have a dominant Type III to II kerogen. The difference in

kerogen Type can be affected by the source and maturity of the organic matter, which will be dealt with later (Section 6.3).

A plot of TOC versus S2 (after Langford & Blanc-Valleron, 1990) for the combined Tunisian sections (Fig 6.3), shows that the organic-lean (<1% TOC), and especially the Ech Cheid and Nebour samples, fall close to the kerogen Type II/III boundary, and the majority of the organic-rich (>1% TOC) samples lie in the central Type II zone. The trends observed between the sections are clarified when the data are plotted in two groups which relate to the northern (Nebour and Ech Cheid) and the southern sections (Oued Bahloul, Dir Oulad Yahia, and Oued El Gsab; Fig 6.4). This plot suggests that the northern and southern groups have average hydrogen indices of 308 and 662 respectively.

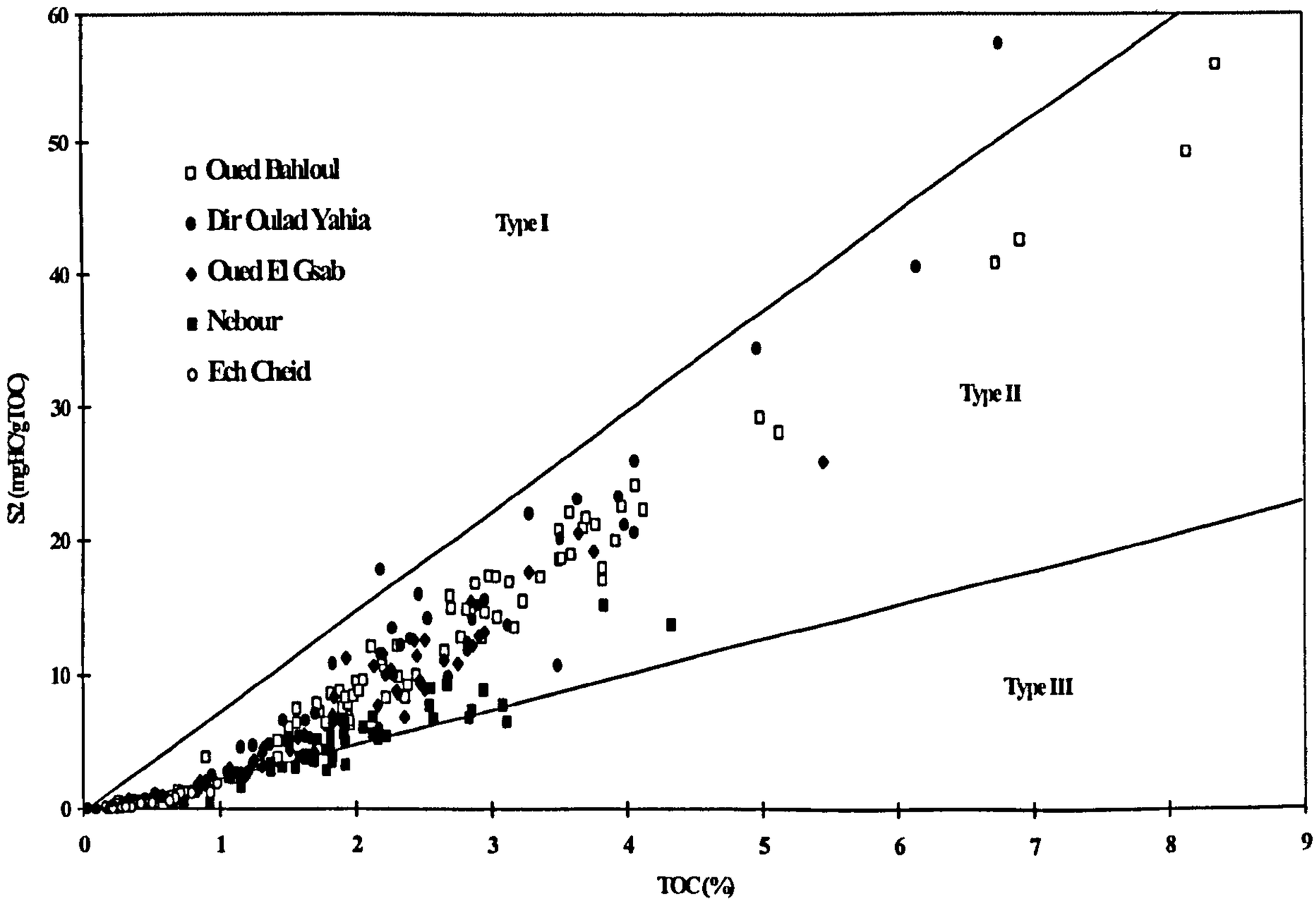

Figure 6.3 Cross plot of TOC versus S2 data for the Tunisian sections (based on Langford & Blanc-Valleron, 1990). The majority of the data plots in the Type II zone; however, samples with a low TOC (<1.5%) plot on the Type II/III border.

The relationship between TOC and S2 suggests that the more organic-lean samples also had less well-preserved marine organic matter or a greater terrestrial contribution. Mineral matrix effects may not be the only controlling factor for the quadratic relationship between TOC and S2. A similar relationship was noticed between the AOM and S2 data from the Ech Cheid section (Fig. 6.5; Linear $r^2 = 0.65$, Quadratic $r^2 = 0.66$). The type of organic matter input changes as well as the TOC, so

the change in S2 is not just derived from the increased TOC but also from changes in organic matter type.

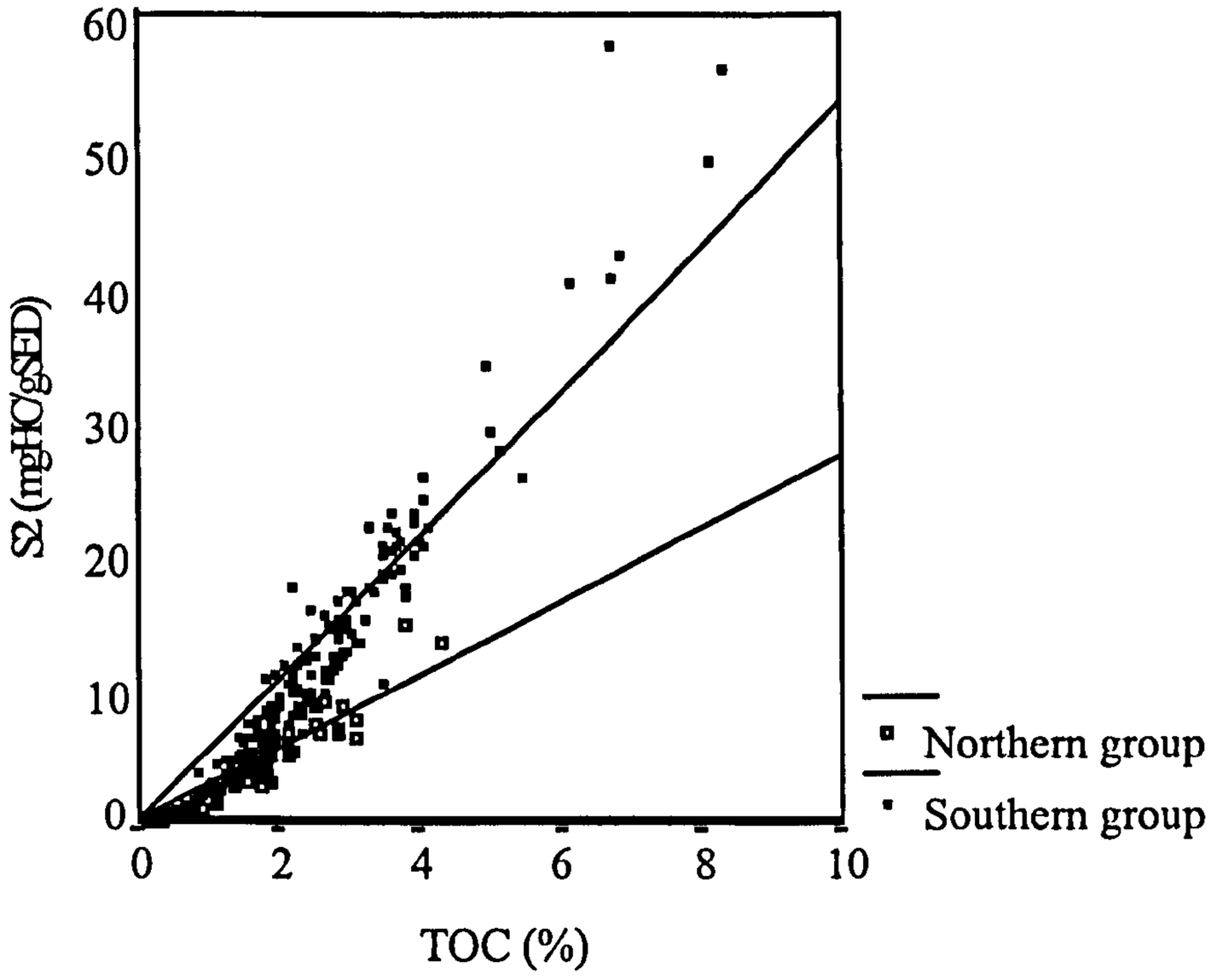

Figure 6.4 Cross-plot of TOC versus S2 data for the northern and southern groups; note they plot with different trends, this is possibly a result of differing matrix materials.

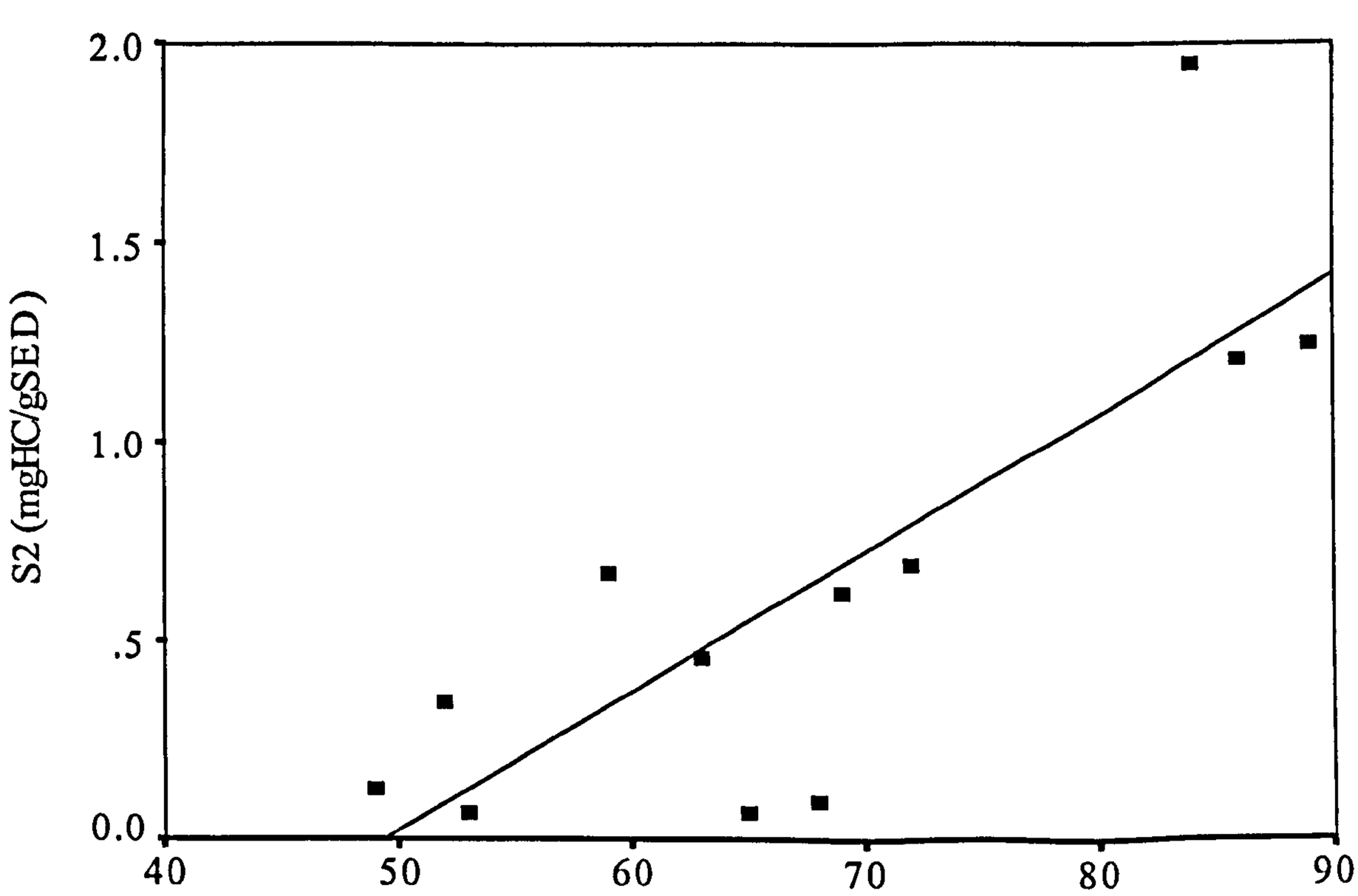

Figure 6.5 Cross plot of AOM versus S2 for the Ech Cheid section. The good correlation (r^2 = 0.65) between the parameters suggests that petroleum potential is controlled by increased preservation and/or productivity of AOM.

The Ech Cheid samples show a good correlation of AOM with TOC (r^2 = 0.63; not shown) and S2 (r^2 = 0.65; Fig 6.5). The data fit is significant enough to show that increased TOC (%) within the samples is controlled by higher preservation and/or productivity of AOM within the depositional area. The relationship with S2 suggests that the petroleum potential of these samples is also controlled by higher preservation and/or productivity of AOM for this section. As the majority of samples for the other Tunisian sections are dominated by AOM (≥99%) no trend was observed with S2 data.

6.2 Isotope geochemistry

This study gives five new organic matter carbon isotope profiles for the Cenomanian-Turonian sequence in Tunisia and demonstrates that they exhibit similar profiles to the $\delta^{13}C$ carbonate curve obtained by Accaire *et al.* (1996) and it is proposed that they can be used for correlation between localities within Tunisia and elsewhere.

All the Tunisian sections with the exception of Ech Cheid, have organic matter $\delta^{13}C$ values that fall in the range of -25‰ to -22‰ (Appendix 2, Table IV), these values appear to be typical for Cenomanian-Turonian marine organic matter in other parts of the world (e.g. Pratt & Threlkeld, 1984; Thurow *et al.*, 1988; Kuhnt *et al.*, 1990). The organic matter curves show an equal or slightly greater excursion compared to reported carbonate $\delta^{13}C$ curves (e.g. Accaire *et al.*, 1996). The Ech Cheid section has lighter $\delta^{13}C$ values (-27‰ to -25‰) compared to the other four sections. This variation may be controlled by the difference in the composition of the organic matter seen in this section (Section 6.4).

There are similarities between the shapes of the isotope excursions for all the localities with the exception of Ech Cheid (Fig 5.7). Each of these sections exhibits an isotope curve with a rapid shift at the base of the section, with either 2 or 3 sub-peaks, before the excursion gradually returns to background values over the remaining part of the section (Table 5.2). The Ech Cheid section does show some increase at the base of the section followed by uniform values with little variability and no apparent return to background values. It is unclear whether the basal excursion seen at the Ech Cheid section is equivalent to that of the other sections, as the maximum shift is significantly lower than at the other sections (Table 5.2). The shape of the Ech Cheid curve may indicate that the first and most prominent part of the excursion was not

sampled at this locality, and occurred in the lowermost part of the section that was not exposed, or that the shift is partly masked by terrestrial input.

The basal positive shift in the isotope excursion occurs after the extinction of *R. cushmani* in all the fully sampled Tunisian sections, i.e. after the basal sandstone or limestone unit (also observed by Accaire *et al.*, 1996; cf. Pratt & Threlkeld, 1984). The highest $\delta^{13}C$ values are always observed in the *W. archeocretacea* zone and then return to background values before the start of the *H. helvetica* zone.

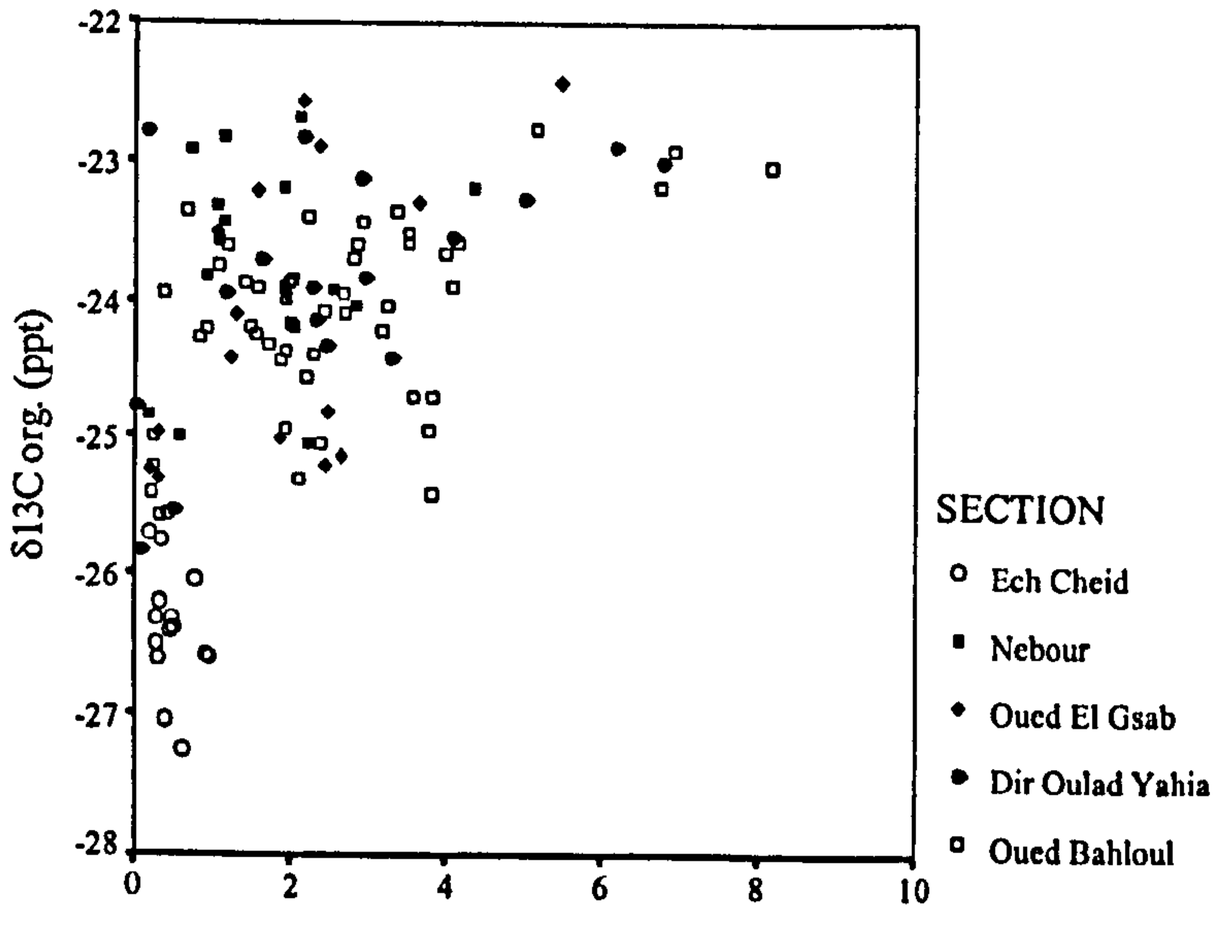

Figure 6.6 Cross plot of TOC versus $\delta^{13}C$ (‰) organic matter isotope data (all Tunisian samples). The parameters show a poor correlation: Oued Bahloul, $r^2 = 0.26$; Dir Oulad Yahia, $r^2 = 0.32$; Oued El Gsab, $r^2 = 0.30$; Nebour, $r^2 = 0.03$; Ech Cheid, $r^2 = 0.10$.

The $\delta^{13}C$ sub-peaks occur at about the same time as the TOC maxima, but are not necessarily correlated with the TOC values. The correlation of $\delta^{13}C$ values with TOC values for the Tunisian sections (Fig. 6.6; range $r^2 = 0.03$ to 0.30) suggests that the isotope excursion is not controlled by the amount of organic matter being deposited. There is no correlation of $\delta^{13}C$ values with carbonate data either (Fig 6.7). Accaire *et al.* (1996) noted that the carbonate carbon isotope values for the Oued Smara locality varied independently of lithology (i.e. TOC and carbonate values). A similarly poor correlation between $\delta^{13}C$ values and hydrogen index is also observed (Fig 6.8; range $r^2 = 0.01$ to 0.18); this suggests that the type or preservation state of the organic matter is not a controlling factor on the variations in the isotope excursions. This makes the organic matter isotope excursion an excellent tool for correlation as it does not appear to be affected by local conditions or facies, and reflects changes that are more likely to be regional, or even global. The form of the curve will also be influenced by differences in sediment accumulation rate and

sampling density. Robaszynski *et al.* (1993) observed a flooding surface which may be linked with lower sedimentation rates just above the basal limestone unit at the Oued Smara locality. It is likely that flooding surfaces occur in the other Cenomanian -Turonian sections just above the basal limestone and a lower sedimentation rate at this point will effectively enhance the variation in the isotope curve. The organic matter isotope excursion is also not affected by diagenetic reactions which can alter the isotopic signature of the carbonate data. The organic matter isotope data for this study suggest that the organic carbon results give a better defined curve (depending on sampling density) than the carbonate isotope values as the $\delta^{13}C_{org}$ shift is generally more pronounced than that of the $\delta^{13}C_{carb}$ data and may be more useful for correlation purposes as variations in the curve are easier to detect.

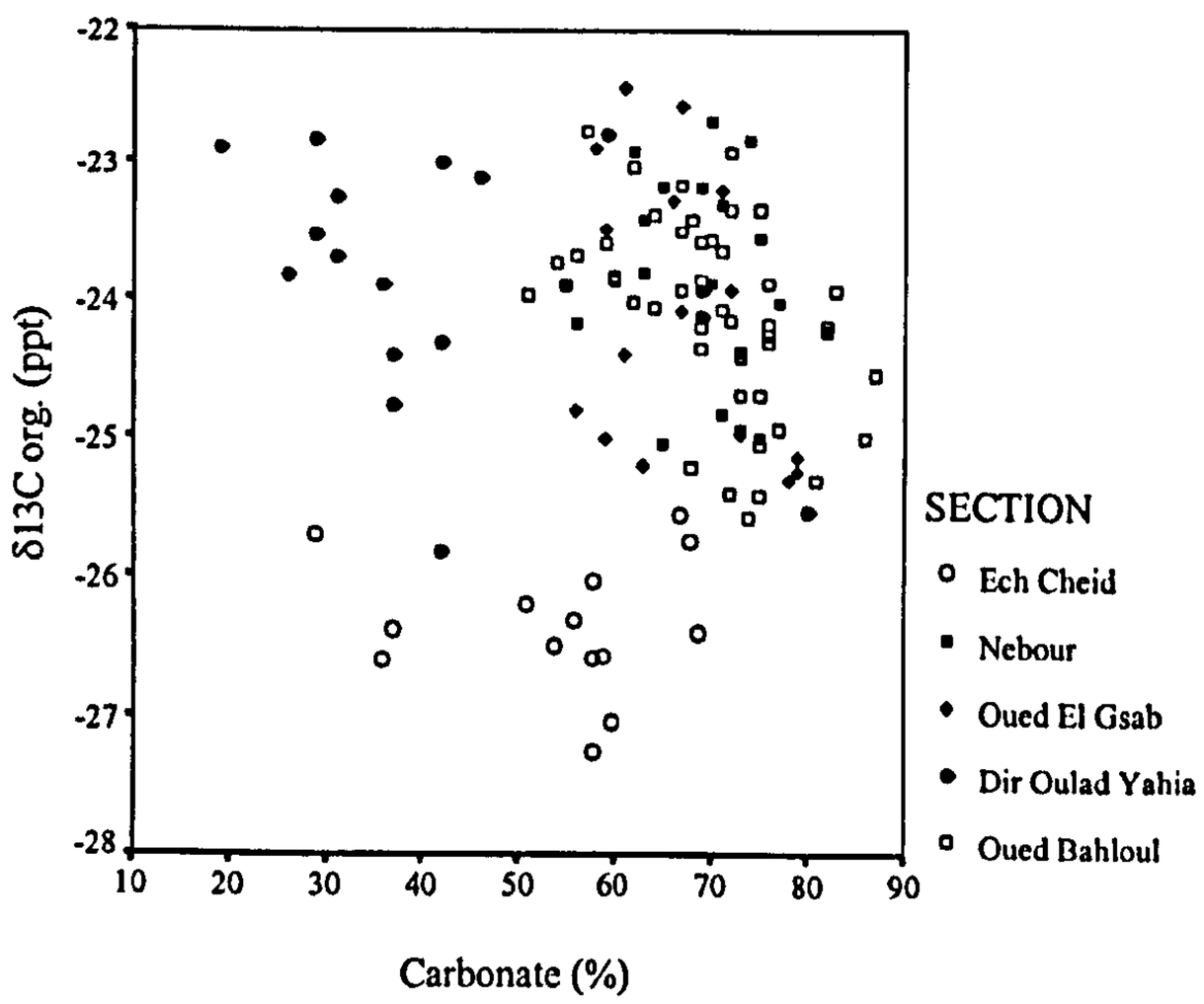

Figure 6.7 Cross plot of Carbonate versus $\delta^{13}C$ (‰) organic matter isotope data for the Tunisian sections. The parameters show a poor correlation: Oued Bahloul, $r^2 = 0.22$; Dir Oulad Yahia, $r^2 = 0.14$; Oued El Gsab, $r^2 = 0.15$; Nebour, $r^2 = 0.00$; Ech Cheid, $r^2 = 0.00$.

The correspondence between the TOC curve and the $\delta^{13}C$ isotopic excursion, for this data set and that of Accaire *et al.* (1996), suggest that the onset of the "anoxic event" and of the black shale facies occurred more or less synchronously throughout most of central Tunisia. In the Oued Bahloul, and to some extent in the Dir Oulad Yahia, sections the organic matter $\delta^{13}C$ values return to background levels at approximately the same time as the deposition of "black shale" comes to an end; however, in the Oued El Gsab and Nebour sections the $\delta^{13}C$ values reach background levels before the end of black shale deposition. This suggests that termination of black shale deposition is not synchronous with the end of the isotope excursion, and that the Oued El Gsab and Nebour have extended black shale deposits, after the deposition at the other localities had ceased. The diachronous nature of the Bahloul

was also documented biostratigraphically by Abdallah *et al.* (1995) and Abdallah and Meister (1997). They noted that anoxia extended beyond the end of the isotope excursion in the Northern Chotts area of Tunisia.

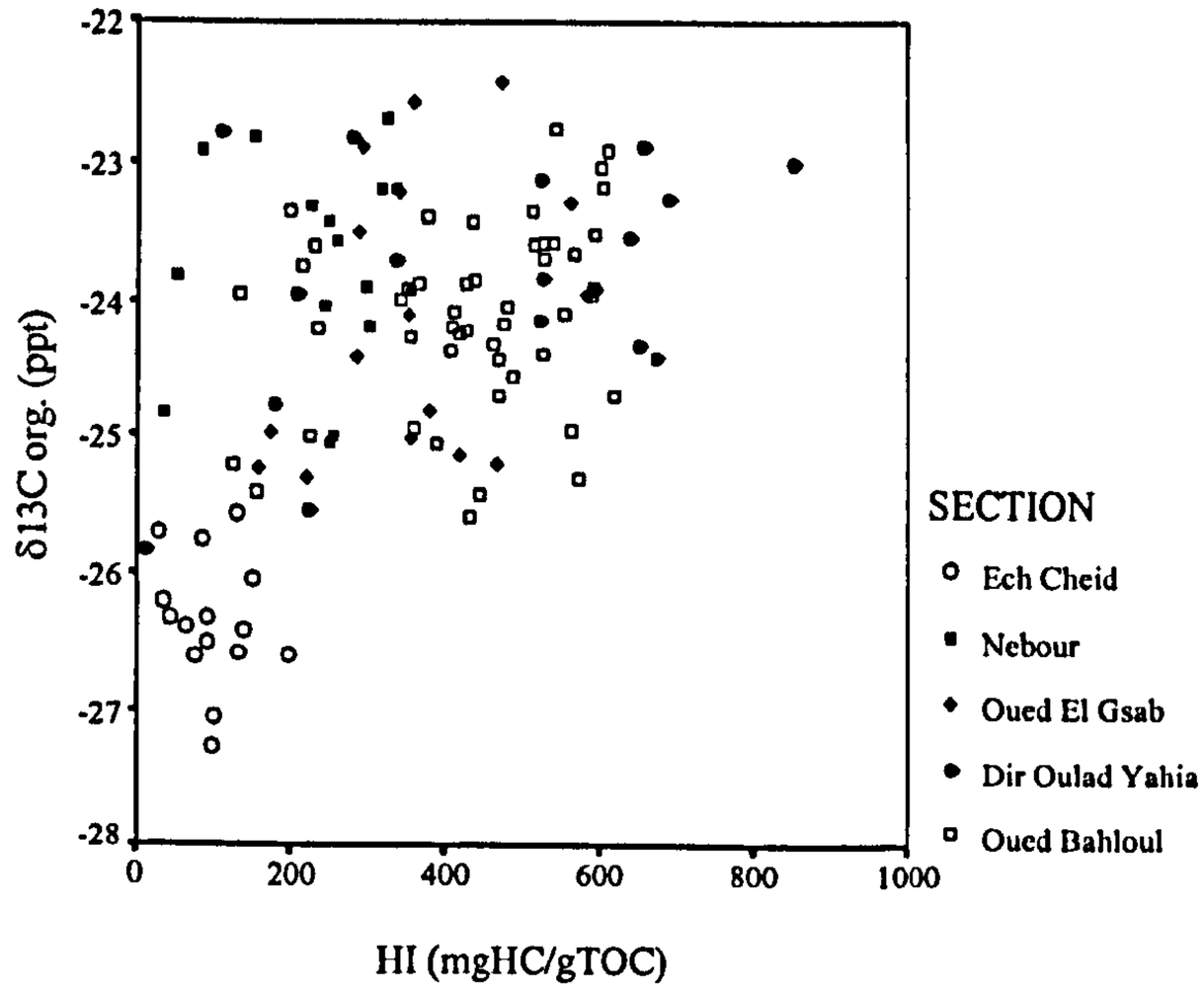

Figure 6.8 Cross plot of Hydrogen Index versus $\delta^{13}C$ (‰) organic matter isotope data (all Tunisian samples). The parameters show a poor correlation: Oued Bahloul, $r^2 = 0.08$; Dir Oulad Yahia, $r^2 = 0.18$; Oued El Gsab, $r^2 = 0.11$; Nebour, $r^2 = 0.12$; Ech Cheid, $r^2 = 0.03$.

The $\delta^{13}C$ values for the Ech Cheid section are heavier with a fairly stable mean of -26‰, compared to the other Tunisian sections where the values are between -23 to -24‰. The difference observed between the Ech Cheid $\delta^{13}C$ curve and those of the other four sections may be caused by one of several factors. The optical data suggest that the Ech Cheid section has a significantly higher terrestrial content; however this organic matter was generally isotopically heavier than marine organic matter during the Cretaceous (Dean *et al.*, 1986), so it is unlikely that the mixing of the terrestrial $\delta^{13}C$ signal with the marine $\delta^{13}C$ signal is the cause for the lighter $\delta^{13}C$ values observed at this section. It is possible that the differences in maturity between the sections may have caused the shift, but this should also be observed at the Nebour section which has an even higher maturity. Another possibility is the effect of marine plankton productivity. It has been demonstrated that isotopic fractionation by phytoplankton decreases as primary productivity increases, resulting in heavier (less negative) $\delta^{13}C$ values (e.g. Nakatsuka *et al.*, 1992). The low increase in TOC (6-fold) compared to background values suggests that this locality was not influenced by increased primary productivity, whereas the other sections may have been (their TOC increases were 22-fold to 68-fold).

6.3 Organic matter maturity

The data from vitrinite reflectance analysis suggests that all the sections are immature as they have VRo ≤0.4% (Bostick, 1979). However, these vitrinite reflectance values do not correspond well with the VR equivalent values suggested from aliphatic and aromatic biomarkers (cf. Killops & Killops, 1993, p. 204) or from bulk geochemistry. The directly determined VR values appear to underestimate the maturity suggested by the other data. The VRo data may not be reliable due to the very sparse nature of the vitrinite upon which the determinations were made, often on only 2 or 3 particles. Suppression of VRo is generally common in all AOM-rich source rocks, especially where hydrogen index is high (R. Tyson, 1998, pers. comm.).

The Production Indices and Tmax data for all five Tunisian locations (Appendix 2, Tables III to VII) show a range of values but generally indicate that the Oued Bahloul, Dir Oulad Yahia and Oued El Gsab section have similar maturities and would be classed as early mature (Espitalié *et a*l., 1977; Orr, 1983; Peters, 1986). By contrast, the Ech Cheid section has a slightly higher maturity and the Nebour section slightly higher still. Even so the Nebour section would still only be classed as early mature to mature. The indication of low maturities for these five sections generally agrees with the bulk geochemistry results of other Tunisian Cenomanian-Turonian studies (e.g. Farrimond *et al.*,1990b; Pervaz & Püttmann, 1995).

The Pr/nC$_{17}$ ratios calculated from gas chromatograms for all the Tunisian sections are given in Appendix 4, Tables III to V. The Oued Bahloul, Dir Oulad Yahia and Oued El Gsab sections have ratios greater than 0.5 and the majority of the ratios are between 1.0 and 4.2. These values strongly agree with those presented by Farrimond *et al.* (1990b). Values in this range are typical of moderately biodegraded oils or low maturity source rocks (Leythaeuser & Schwarzkopf, 1986). As there is no other evidence of biodegradation in these samples, it is assumed that the Pr/nC$_{17}$ values reflect their low maturity. The Ech Cheid section has values for this parameter below 0.5, but the majority are between 0.5 and 1.0; again this suggest a slightly higher maturity than observed in the previously mentioned sections. The value for the Pr/nC$_{17}$ ratio at Nebour is one of the lowest observed for these sections, and agrees with the assumptions made from the PI and Tmax data, that the Nebour outcrop is the most mature section out of the five studied in Tunisia. Although this observation is based on only one sample for the Nebour section it is confirmed by the production index (PI) data (Appendix 2, Table VII). The PI value for sample N18 is below

average for the section and may suggest that the mean Pr/nC$_{17}$ for this section will be higher.

The absence of 17β (H), 21β (H) hopanes (e.g. Ourisson *et al.*, 1987) and hop-17(21)-enes in the Tunisian samples suggests that these sections are not extremely immature. Hop-13(18)-enes are present in all the sections, although these hopenes are normally absent in mature samples, they have been found at greater depths than the hop-17(21)-enes (Farrimond *et al.*, 1986). Generally, the conversion of the R isomer to the S isomer in the C_{31} and C_{32} 17α (H) 21β (H) hopanes is quite high, reaching equilibrium values in all the sections (range 0.55 to 0.65); this 100% conversion is associated with source rocks that are early mature, approaching the oil window (cf. Mackenzie, 1984).

The C_{30} hopane αβ/αβ+βα maturity parameter for the Oued Bahloul section has a mean value of approximately 0.8, indicating the immaturity of this section (cf. Mackenzie, 1984). The C_{30} hopane αβ/αβ+βα values for the other localities suggest that the Dir Oulad Yahia section is the most immature, followed closely by the Oued El Gsab and Oued Bahloul sections, then the Ech Cheid section and finally the Nebour section appears to be the most mature, as was also noted from bulk geochemical observations.

The Trisnorneohopane/Trisnorhopane (Ts/Tm) ratio shows some variation within the Oued Bahloul and the Ech Cheid sections which may suggest some variations in maturity. However, comparative plots with other biomarker maturity parameters (e.g. C_{30} hopane αβ/αβ+βα) show a poor correlation, this may reflect the low maturity of these samples as the Ts/Tm ratio operates best near or within the oil window. The Oued Bahloul, Dir Oulad Yahia and Oued El Gsab sections all have Ts/Tm ratios <1.0 whereas the Ech Cheid and Nebour sections both have values >1.0. Little is known of the source of Ts; it is a rearranged hopane and it may be a result of diagenesis reactions. The Ts/Tm ratio appears to be affected by many differing conditions, and is known to be strongly facies dependant (Moldowan *et al.*, 1986). It appears from these results that the Ech Cheid and Nebour sections, both in the north west of the study area, are of differing facies or have undergone differing diagenetic reactions, possibly related to the maturity differences, to the Oued Bahloul, Dir Oulad Yahia and Oued El Gsab sections to the south east of the study area.

The C_{29} sterane 20S/20S+20R ratio for the Tunisian sections shows some variability between and within the sections, but values generally indicate a low

maturity. It is unlikely that the variations in maturity parameters within the Oued Bahloul and Ech Cheid sections are due to heating; they are more probably due to organic matter input and/or mineral interactions catalysing or impeding the thermal alterations of the compounds. Pervaz & Püttmann (1995) also observed variations in this sterane ratio at the Bou Grine locality; they suggest that the ratio was affected by biodegradation, preferentially removing the R isomer (Chossen *et al.*, 1991) and increasing the ratio value. However, this would be more likely in oils rather than source rocks, and to have been biodegraded to the extent that the steranes were being removed would mean that the *n*-alkanes should be totally degraded, but, they are clearly observed in the gas chromatogram traces of all samples analysed for this study, including those with high C_{29} sterane 20S/20S+20R values.

Gas chromatography-mass spectrometry was carried out on the aromatic hydrocarbon fractions for only a few of the Tunisian samples (Appendix 4, Table XII). The MPI ratio shows a range of values within the Oued Bahloul and Ech Cheid sections, and would indicate that the Dir Oulad Yahia section is the most mature, and the Nebour section is the least mature, contrary to all the other maturity observations. The anomalous variations in the MPI values may be due to poor peak resolution within the aromatic gas chromatography-mass spectrometry traces. The ratio of long chain to short chain triaromatics indicate the same maturity relationship between the sections as the aliphatic data, with Dir Oulad Yahia being the least mature and Nebour the most mature section. Generally the aliphatic and aromatic maturity parameters correlate well with each other and with the bulk geochemical data (cf. Killops & Killops, 1993, p. 204).

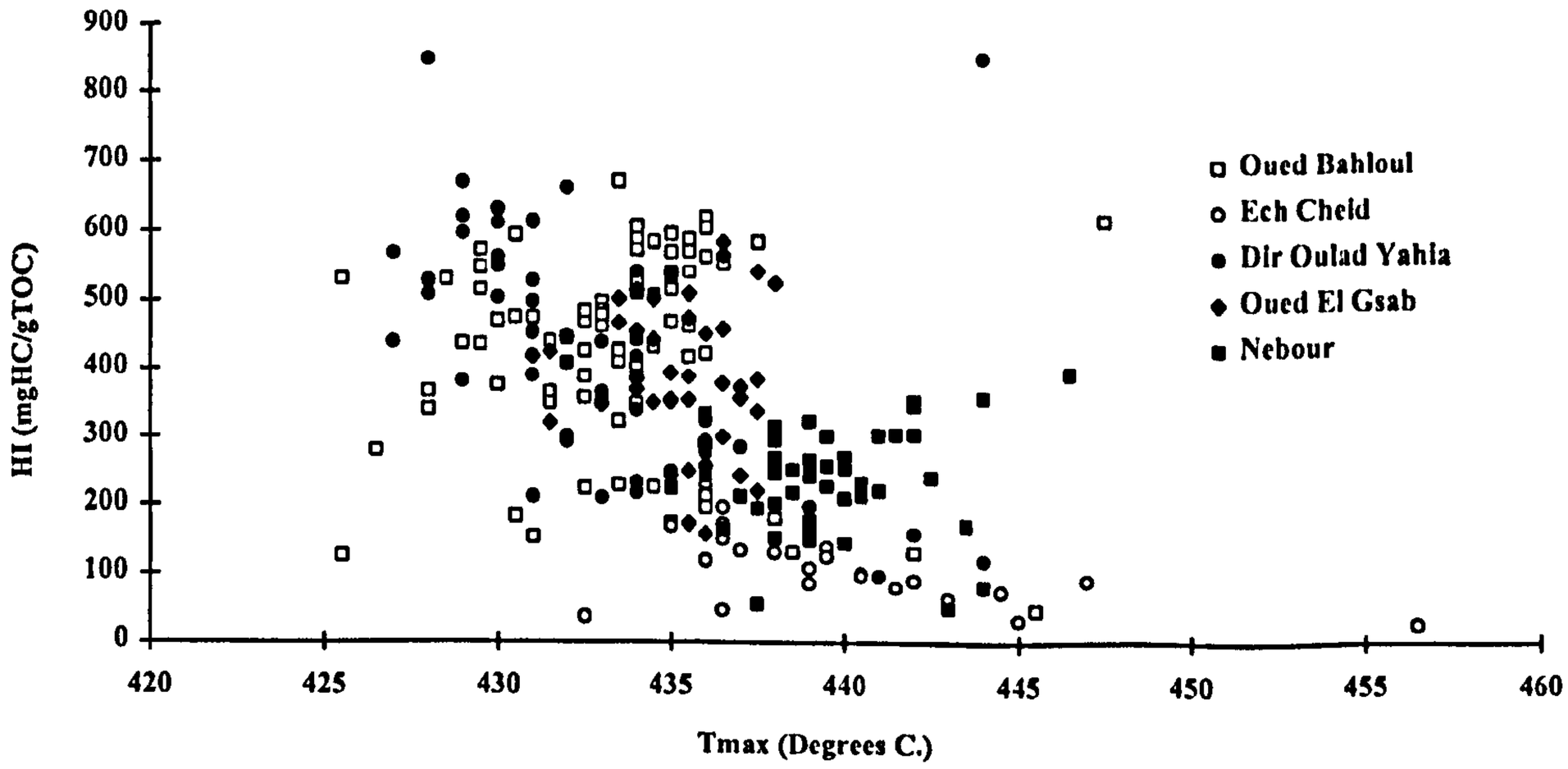

Figure 6.9 Cross plot of hydrogen index versus Tmax data (all Tunisian samples), note that the Nebour section with the higher maturity also has lower hydrogen indices, this is because higher maturity may be affecting the chemical composition of the organic matter.

A Plot of the Tmax maturity parameter versus hydrogen indices (Fig. 6.9) indicate that the Nebour section with the slightly higher maturity also has the lower hydrogen indices. The lower hydrogen indices in the Ech Cheid section may be explained by the mixing of organic matter types in the kerogen, as this section has a higher terrestrial content. However, the Nebour section has a similar AOM-dominated organic matter type to the other three sections, and so the lower hydrogen indices are very probably an effect of changes in chemical composition of the organic matter due to the higher maturity.

6.4 Organic matter sources

Optical kerogen analysis of the Oued Bahloul section using transmitted light microscopy clearly shows that these samples are dominated by marine AOM. This dominance may have caused the masking or simple dilution of the palynomorph fraction, making it impossible to determine their true abundance and composition. Attempts were made to concentrate the palynomorph fraction by oxidising the AOM material with a combination of oxidants (Section 2.4.4), but they were largely unsuccessful. The optical appearance of the kerogen from the Dir Oulad Yahia and Oued El Gsab samples (DOY25 and OG16) is very similar to that of the Oued Bahloul section. The sample N18 from the Nebour section also shows a dominance of AOM material, but, with a higher palynomorph content (ca. 4%) and a rare phytoclast content.

The Ech Cheid section also shows a dominance of marine AOM in the kerogen, but includes a significant phytoclast contribution, suggesting that this section was situated closer to a terrestrial source than the Oued Bahloul section. However, the palaeogeographic map (Fig. 1.4) suggests that the Ech Cheid section was deposited in a more distal environment compared to Oued Bahloul. An alternative explanation for the higher phytoclast content may be that poorer preservation has decreased the AOM dilution of the phytoclasts. The dominance of dinoflagellate cysts in the palynomorph fraction is not surprising considering that they are the most common form of fossilising phytoplankton in most Mesozoic marine sediments, and can form a high percentage of the fossilised organic-walled microplankton (Tyson, 1995). There is a significant input of acritarchs to the palynomorph fraction; although

common in near-shore facies they have also been found within the AOM of deep water "oceanic" sediments (Tyson, 1984, p. 8) and cannot be used as truly diagnostic of shallow water, especially as the Ech Cheid section appears to be deposited in a deeper offshore environment.

The gas chromatograms of the aliphatic hydrocarbon fraction from the Oued Bahloul section (Fig. 5.8) typically show an *n*-alkane maximum around nC_{16}, which indicates a dominant algal phytoplankton and/or bacterial input for this section (cf. Gelpi *et al.*, 1970). The relative increase of isoprenoids and biomarkers in the gas chromatogram traces of samples OB6, 7, 28, 40 appears to coincide with the relative methylhopane abundance of the total hopanoids, but it is a common observation to see strong isoprenoids and biomarkers in the gas chromatogram traces of good Type II immature source rocks (*pers. comm.* P. Farrimond,1988). The relative increase of methylhopanes is more likely to be related to the general increase in hopanoids in these samples, which is a likely result of increased bacterial productivity and will be discussed later in this section.

The five Ech Cheid samples which have the nC_{15} maximum in the *n*-alkane envelope (Fig. 5.12a) indicate the dominant phytoplankton algal/bacterial input of these samples (cf. Gelpi *et al.*, 1970). The other five Ech Cheid samples with the *n*-alkane maximum at nC_{26} and abundant long chain *n*-alkanes up to nC_{37} (Fig. 5.12c), suggest a stronger terrestrial input (cf. Eglinton *et al.*, 1962). This appears to correlate with the optical observations, in that the samples with the nC_{26} maximum have >10% phytoclast input. Samples EC 8 and EC9 (Fig. 5.12b) show a bimodal *n*-alkane distribution with maximum at both nC_{15} and nC_{26} which may suggest a mixed palynofacies. The *n*-alkane distribution also appears to reflect the hydrogen index of the samples, the algal-dominated samples having higher hydrogen indices (>100 mgHC/gTOC) and the samples with the stronger terrestrial signal having lower hydrogen indices (37 to 90 mgHC/gTOC). The dominance of nC_{31} alkane over the adjacent nC_{30} peak through much of the section also suggests a strong contribution from a plant wax source, indicating land plant input and generally a more proximal setting compared with the Oued Bahloul locality. However, a ratio of nC_{31} to nC_{17} does not show a strong correlation with the percentages of phytoclasts, although it does show a good correlation ($r^2 = 0.63$) with hydrogen index. This indicates that the chemical interpretation of the biomarkers favours a higher terrestrial content than the interpretation from optical kerogen analysis. It must be noted that chemical studies may more accurately reflect the mass of terrestrial material whereas palynofacies studies are based on relative counts of fragments and not their volume or mass.

The gas chromatogram traces for samples DOY25 and OG16 (Fig. 5.15a and b) show strong similarities to the gas chromatogram traces from the Oued Bahloul section, leading to a similar interpretation that the *n*-alkanes are dominantly algal/bacterial sourced (cf. Gelpi *et al.*, 1970). At the Nebour section the dominance of *n*-alkanes from nC_{13} to nC_{20} in sample N18 (Fig 5.15c) is again a good indication of a dominant algal/bacterial source. However, the *n*-alkane maximum at nC_{31} suggests some input from a land plant wax source that is not observed optically.

The sterane $C_{27}\alpha\alpha\alpha R/C_{29}\alpha\alpha\alpha R$ ratio (Huang & Meinschein, 1979), which can be used to determine the type of organic matter that sourced the steranes, gives an average value of 0.75 (range 0.54 to 0.94; Appendix 4, Table IX) for the Oued Bahloul section. These values agree strongly with those recorded by Farrimond *et al.* (1990b). A value in this range should indicate a substantial terrestrial input for these samples, although optical analysis suggests this is not the case. The rationale that C_{27} steranes are marine source and C_{29} steranes are terrestrially sourced is very simplistic, as some C_{29} steranes are found in marine algae (Volkman, 1986). The Oued Bahloul locality must have a high proportion of C_{29}-rich marine algae. The values for the sterane $C_{27}\alpha\alpha\alpha R/C_{29}\alpha\alpha\alpha R$ ratio from Dir Oulad Yahia and Oued El Gsab suggest similar algal contributions.

The sterane $C_{27}\alpha\alpha\alpha R/C_{29}\alpha\alpha\alpha R$ (Huang & Meinschein, 1979) ratio gives an average value for the Ech Cheid section of 0.49 (range 0.30 to 0.62), this shows that the C_{29} sterane is relatively more abundant compared to the Oued Bahloul section. This would suggest a relatively higher terrestrial input at this section, which is consistent with the optical and molecular geochemical results. However, the constraints mentioned earlier have to be taken into consideration when using this ratio. The value for the sterane $C_{27}\alpha\alpha\alpha R/C_{29}\alpha\alpha\alpha R$ ratio from the Nebour sample is more comparable with the Ech Cheid section than the Oued Bahloul section, which may be an effect of maturity or steroid source.

A ternary plot of the C_{27}:C_{28}:C_{29} $\alpha\alpha\alpha R$ steranes (after Huang & Meinschein, 1979) shows that the Oued Bahloul samples cluster in a central position (Fig. 6.10) with only one outlier (sample OB15), having an anomalously high C_{29} sterane values. These samples plot in an identical area to the Oued Bahloul samples from Farrimond *et al.* (1990b). A plot of the C_{27}:C_{28}:C_{29} $\alpha\alpha\alpha R$ steranes for the Ech Cheid samples (Fig. 6.10) shows that the data points plot in-between the Oued Bahloul data and the C_{29} pole, reflecting the higher terrestrial input for the Ech Cheid samples. The Ech Cheid samples with lower TOC values and high proportions of phytoclast material

generally plot closest to the C_{29} pole. The similarity between the Dir Oulad Yahia and Oued El Gsab samples with the Oued Bahloul section is also seen from the C_{27}:C_{28}:C_{29} ααα*R* steranes plot, where the two samples plot within the Oued Bahloul data cluster. This suggests that the algal sources at these two sections are similar to the Oued Bahloul section, indicating similar algal contributions for the south east part of the study area containing these three localities. The sterane C_{27}:C_{28}:C_{29} ααα*R* relationship for sample N18 plots within the organic-rich samples from the Ech Cheid data. This suggests that the N18 sample has a similar algal input to the organic-rich samples of the Ech Cheid section, and that the algal material is different in the north west part of the study area compared to the south east. However, the higher maturity of the Nebour section needs to be taken into account. Davies (1997) demonstrated that maturity tended to increase the C_{27} homologue relative to the C_{28} and C_{29} homologues. It is apparent from the ternary diagram that the samples from the northern area plot with relatively higher C_{29} homologue and that the slight maturity differences suggested for the Nebour section do not appear to be affecting this plot to any great extent.

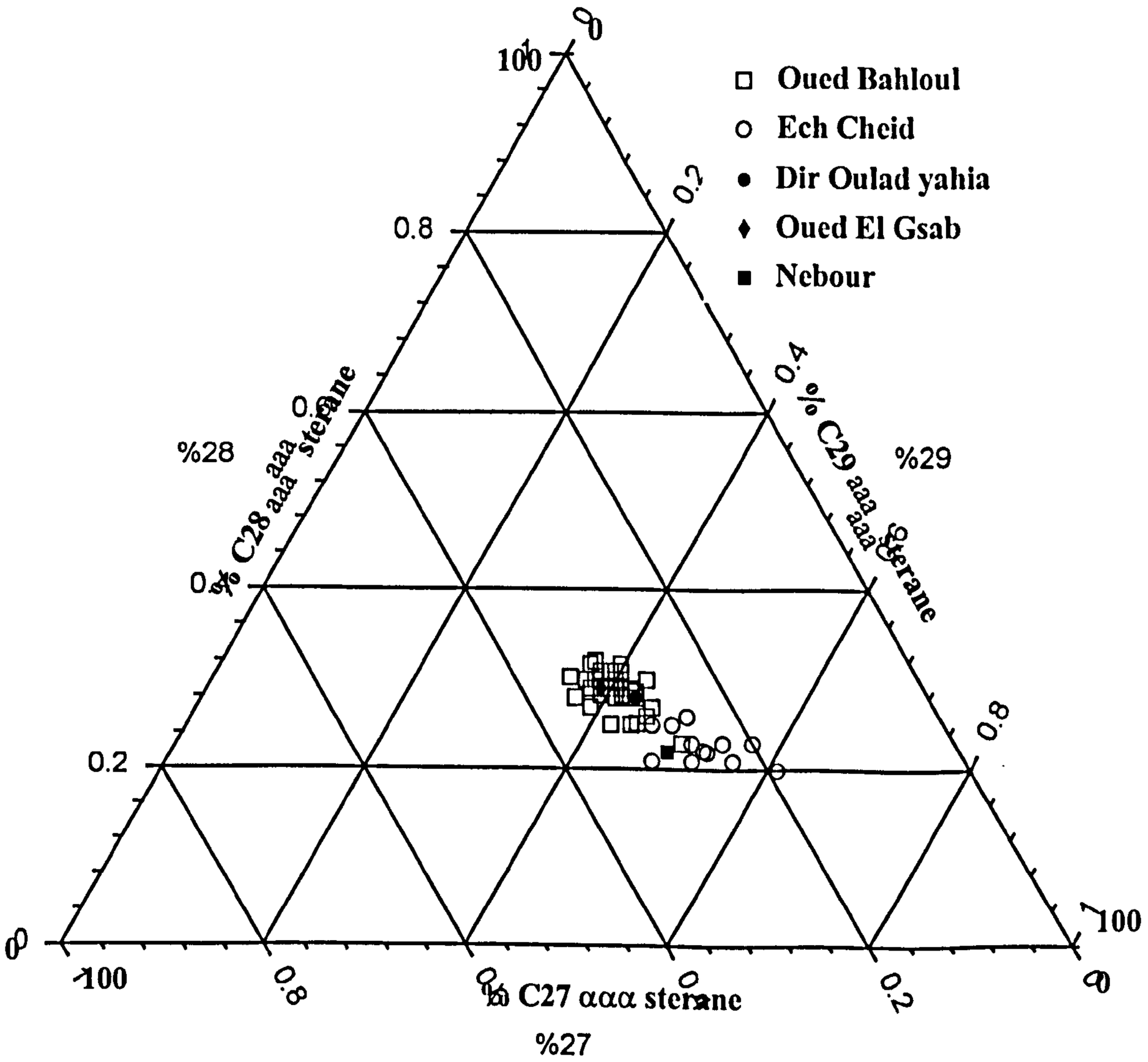

Figure 6.10 Ternary C_{27}-C_{28}-C_{29} ααα*R* sterane plot (after Huang & Meinschein, 1979) for the Tunisian sections, based on relative amounts (%) data from Appendix 4,

Tables IX, X and XI. The Dir Oulad Yahia and Oued El Gsab points plot within the Oued Bahloul cluster, and the Nebour point plots within the Ech Cheid cluster.

Methylsteranes comprise between 4 and 9% of the total steranes recorded in the Oued Bahloul section (Appendix 4, Table IX). The occurrence of methylsteranes has been linked with dinoflagellate input (Wolff *et al.*, 1986), although dinoflagellate cysts are not evident from optical analysis. However, due to the dominance of AOM and the fact that many dinoflagellates are non-cyst forming (Tyson, 1995), chemical analysis may be the only way of detecting their presence in these samples.

At Ech Cheid methylsteranes are present in a similar abundance to those at Oued Bahloul (4 to 7% of the total steranes recorded; Appendix 4, Table X), although here dinoflagellates are observed optically as the dominant palynomorphs. The presence of methylsterane input from non-cyst forming dinoflagellates, as suggested in the Oued Bahloul section, may be reflected in the poor correlation between the relative methylsterane abundance and the relative abundance of dinoflagellates seen optically. Methylsteranes are also noted in the other three Tunisian sections.

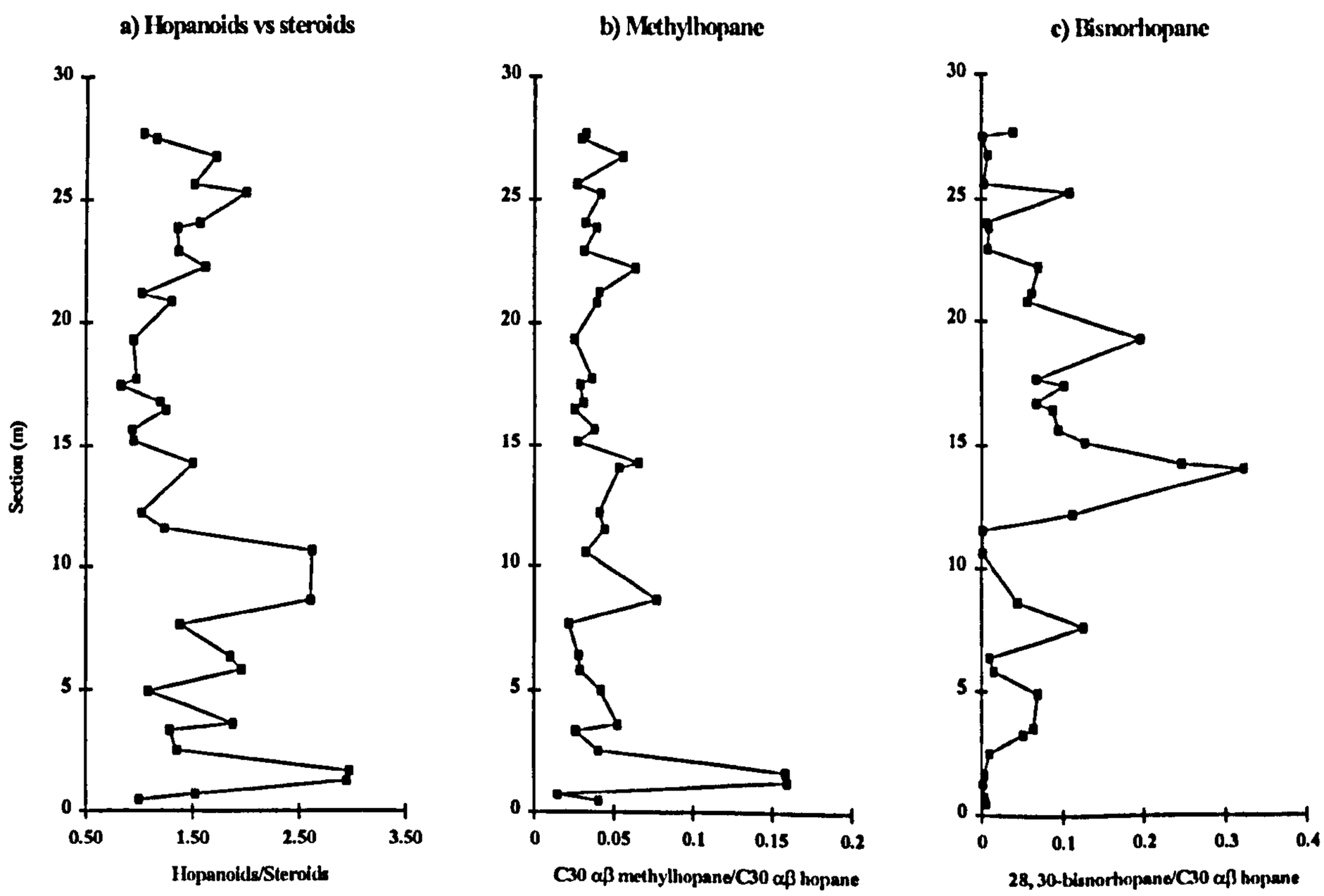

Figure 6.11 Stratigraphic hopanoid plots for the Oued Bahloul section. a) Total hopanoids versus total steroids identified from GCMS; note that hopanoids are more abundant at the base of the section at 1.4m, 8.6 and 10.6m; b) C_{30} αβ Methylhopane content relative to the C_{30} αβ hopane content; note the high concentrations of methlyhopanes at 1.4m; c) C_{28}, C_{30}-bisnorhopane content relative to the C_{30} αβ hopane content.

The bacterial contribution to the Oued Bahloul sediments is noted from the high input of hopanoids (cf. Ourisson *et al.*, 1979) relative to the steroids, especially at the base (OB6 and OB7) and top of the section (Fig. 6.11). In the central part of the section the relative increase in steroids suggests increased algal preservation and perhaps higher productivity. The relative dominance of hopanoids in Bahloul sediments is also seen from sections in the Bou Grine area (Pervaz & Püttmann, 1995) and in a previous Oued Bahloul study (Farrimond *et al.*, 1990b). The predominance of these hopanoids in basal samples from the Oued Bahloul section is probably due to a lower sedimentation rate allowing greater bacterial reworking of the sediments. The basal Oued Bahloul samples coincide with a flooding surface (Robaszynski *et al.*, 1993b) which would have a lower sedimentation rate. The dominance of hopanoids over steroids was also noted in the Ech Cheid, Oued El Gsab and Nebour sections, indicating their substantial bacterial input. The ratio of hopanoids to steroids at Ech Cheid is similar to that of the Oued Bahloul section. The variability of the hopanoid to steroid ratio at Ech Cheid reflects the amount of TOC in the samples ($r^2 = 0.66$), where samples with higher TOC values are dominated by steroidal compounds; this is also seen in a plot of TOC versus AOM for the Ech Cheid section ($r^2 = 0.63$) and suggests that increased TOC values are controlled by increased algal amorphous preservation and perhaps higher productivity for these samples. The Dir Oulad Yahia sample (DOY 25) also contains abundant hopanoids; however, the hopanoid to steroid ratio suggest that the steroids are relatively twice as abundant as the hopanoids in this sample, whereas it is apparent in the other sections that hopanoids are generally present in larger quantities.

Methylhopanes are observed in abundance through the Oued Bahloul section, especially in samples OB6 and OB7 (1.3 to 1.6m; Fig 6.11), where there was also the higher relative abundance of hopanoids to steroids. The presence of the 2α-methylhopanes in the Oued Bahloul section was also noted by Farrimond *et al.* (1990b), and may be an indication of a relative increase in a specific bacterial input such as cyanobacteria or methyltrophs (Zundel & Rohmer, 1985). However, of the thousands of bacteria in the geosphere, only a few have been analysed for hopanoids, and from these only a couple contained methylhopanoids. It is tentatively suggested that methylhopanes have a specific bacterial source such as cyanobacteria or methyltrophs and more work needs to be done in this area.

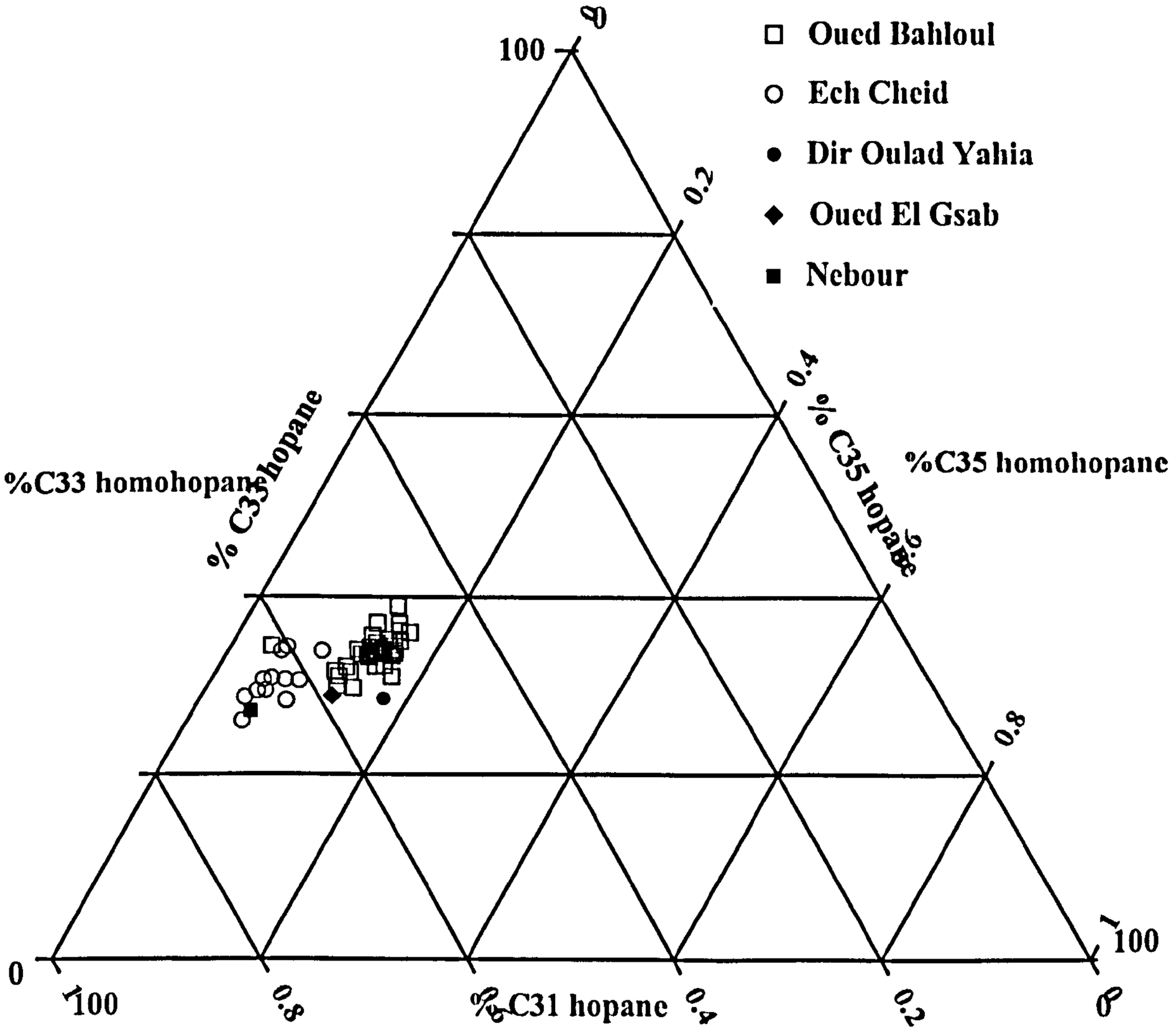

Figure 6.12 Ternary C_{31}-C_{33}-C_{35} 17α (22S + R) hopane plot (after Bishop & Farrimond, 1995), for the Tunisian sections, based on relative amounts (%). Note how the data from the South of the study area plot together generally with higher C_{33} and C_{35} homologues and the data from the north of the study area cluster together with higher C_{31} homologue.

Differences in carbon number distribution between the methylhopane compounds and their non-methylated counterparts, the homohopanes, are interesting. If these compounds had the same carbon number distribution it could suggest that they had the same bacterial source. A ternary hopanoid plot (Bishop & Farrimond, 1995) can be used to show variations in extended hopane distributions. The plot of the C_{31}:C_{33}:C_{35} 17α (22S + R) hopanes for the Oued Bahloul section (Fig. 6.12) shows that these samples plot in a tight cluster and have relatively high amounts of the C_{33} homologue. A similar ternary plot for the C_{32}:C_{34}:C_{36} 2α-methylhopanes (22S + R) from the Oued Bahloul section (Fig. 6.13), show a wider plot range of the C_{34} homologue, and that it is even more predominant in the samples than the comparative C_{33} homohopane. This would suggest that there are at least two separate bacterial

sources contributing to the hopanoid data set. Both bacterial sources contribute to the hopanes distribution but the second bacterial source contributes specifically to the methylhopanes with the more pronounced carbon number distribution. Similar inferences can also be made from ternary plots for the C_{32}:C_{33}:C_{34} 17α (22S + R) hopanes and the C_{33}:C_{34}:C_{35} 2α-methylhopanes (22S + R). The hopanoid data suggests that the carbon number distribution for the homohopanes observed in the m/z 191 trace is a mixture of hopanoids from at least two bacterial sources, whereas the distribution in the methylhopanes (m/z 205) reflects the specific bacterial input only.

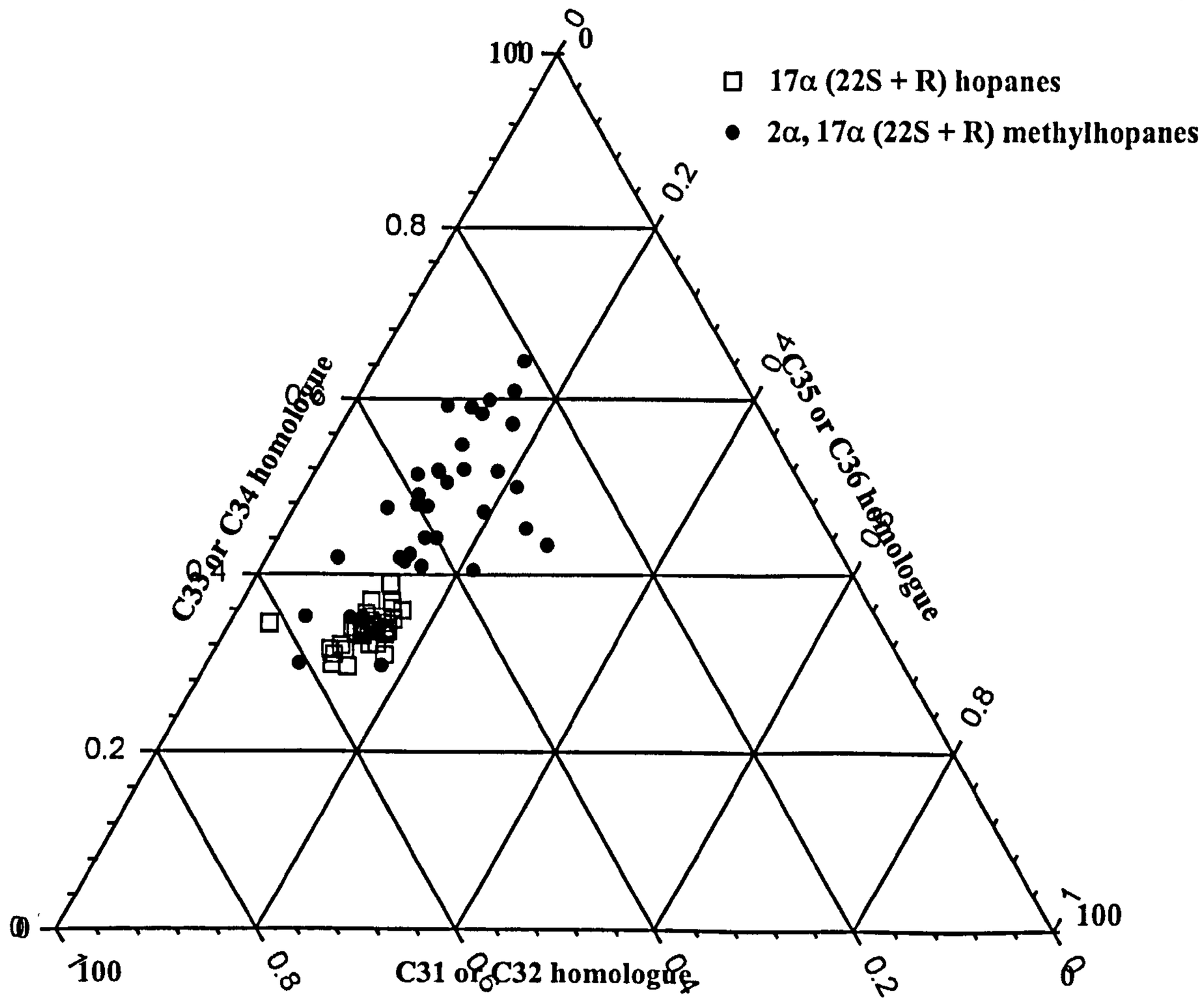

Figure 6.13 Combined ternary C_{31}-C_{33}-C_{35} 17α (22S + R) hopane and C_{32}-C_{34}-C_{36} 2α, 17α, (22S + R) methylhopane plot (based on Bishop & Farrimond, 1995) for the Oued Bahloul section. Note that the samples with the strong methylhopane content plot higher on the C_{33} or C_{34} homologue axis, demonstrating the strong difference in carbon number distribution between the hopanes and methylhopanes.

Elevated levels of C_{33} hopanes (and C_{34} methylated analogues) have been observed previously in oils and source rocks (Farrimond *et al.*, 1990a; McEvoy & Giger, 1986). There is currently no explanation for their elevated abundance. However, two suggestions were made by Peters and Moldowan (1993). The first was an origin from biological precursors with $<C_{35}$ carbon atoms. Biohopanoids are thought to be either C_{30} or C_{35} structures (or C_{31} and C_{36} methylated analogues; e.g.

Rohmer *et al.*, 1972). This suggestion is unlikely. Some C_{33} hopanoids (unsaturated hopandiols) have been detected in certain acetic acid bacteria (Peiseler & Rohmer, 1991) although the authors suggested that these were degradation products rather than natural biohopanoids, again suggesting that the occurrence of elevated C_{33} hopanes from a C_{33} precursor is unlikely. Peters and Moldowan (1993) further suggested that elevated C_{33} hopanes occurred as a result of changes in redox conditions during early diagenesis. However, geohopanoid distribution in Recent sediments tend to be dominated by the C_{32} homologues, and the contribution of C_{33} components is generally minor (Helen Innes, pers comm. 1998).

It is possible that the bond between the C_{33} and C_{34} carbons in C_{35} precursor compounds is weak and is therefore easier to cleave during maturation (Helen Innes, pers comm. 1998). However, there is no conclusive data to support this, and there is therefore a need to do molecular modelling to see if this bond between the two diol groups is weaker. Innes (1998) observed lower levels of isomerisation (22R to 22S and $\beta\beta$ to $\alpha\beta$ and $\beta\alpha$) for both the C_{35} and C_{33} in relation to other carbon numbers in hyrdrouspyrolysates from modern sediments, this suggests that they were being released from the "kerogen" (insoluble organic matter) at lower temperature during the procedure, thus suggesting weaker bonds.

The ternary C_{31}:C_{33}:C_{35} 17α (22S + R) hopane plot (Fig. 6.12) for the other four Tunisian sections shows that the Dir Oulad Yahia and the Oued El Gsab samples (DOY25 & OG16) cluster with the Oued Bahloul samples and that the Nebour sample (N18) clusters with the Ech Cheid samples. It would appear that this hopanoid plot is distinguishing bacterial differences between the north and south of the sampled area. However, it is likely that increased maturity would move the data points towards the C_{31} pole (Paul Farrimond pers. comm.) and the two localities from the northern part of the study area plot with relatively higher abundances of the C_{31} homologue. The Oued Bahloul section has a higher relative abundance of the C_{33} homologue compared to the other sections, suggesting a preference in the carbon number distribution for this homologue, which is discussed above. However, further molecular geochemical work should be carried out on the Dir Oulad Yahia, Oued El Gsab and Nebour sections before this can be confirmed.

The hopane odd-over-even predominance (HOEP; Bishop & Farrimond, 1995) for the 17α (22S + R) hopanes gives a mean value of 1.4 (range = 1.1 to 1.9) for the Oued Bahloul section (Fig. 6. 14). A similar ratio applied to the C_{32}, C_{34} and C_{36} 2α (22S + R) methylhopanes gives a higher value of 1.7 (range = 0.8 to 2.6) showing the

dominance of the C_{34} homologue (equivalent of the C_{33} homohopane) in the methylhopane input. A plot of the C_{34} methylhopane predominance versus the relative increase in methylhopane input suggests that this predominance is partly controlled by the relative input of methylhopanes to some extent ($r^2 = 0.37$). The HOEP for the Ech Cheid section gives a mean value of 1.1, lower than that for the Oued Bahloul section, suggesting that the effect from specific bacterial input on the hopane distribution is not as apparent in this section. This is confirmed by the lower relative methylhopane input for the Ech Cheid section.

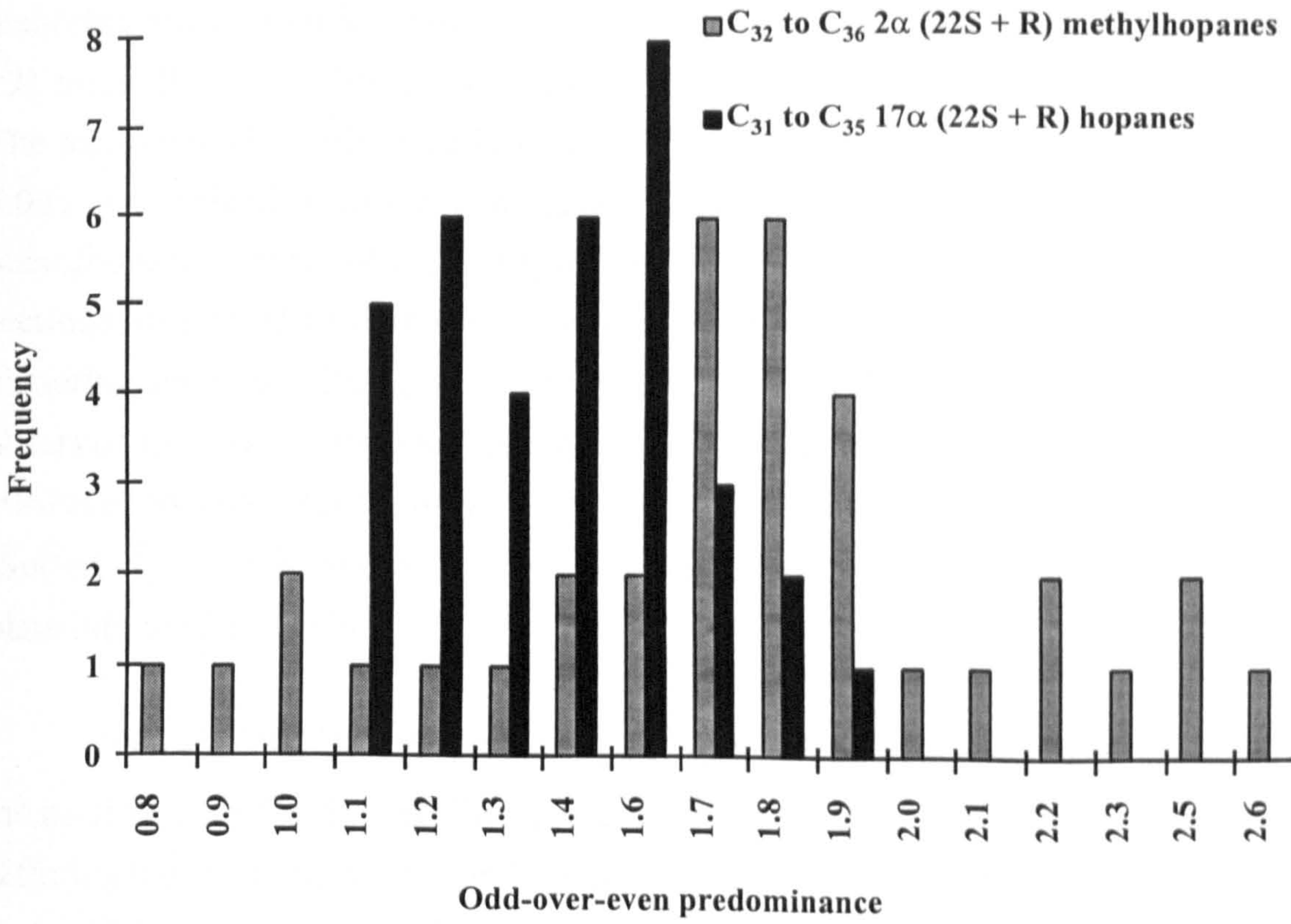

Figure 6.14 Bar chart of hopanoid odd-over-even predominance (after Bishop & Farrimond, 1995) for the Oued Bahloul data.

The 17α (H), 18α (H), 21β (H)-28, 30-bisnorhopane is abundant in the Oued Bahloul section, especially in the central samples (OB21, 39, 40, and 55; Fig. 6.11). This compound is not common in geological samples, and the biological origin and environmental significance is as yet undetermined, although it has been related to upwelling environments (Seifert *et al.*, 1978; Grantham *et al.*, 1980). The relative increase in bisnorhopane occurs in the same part of the section that the sulphur values show the largest increase, and there are also high TOC and hydrogen indices in this part of the section. The predominance of the C_{35} hopane is also highest, suggesting that the bisnorhopane has some correlation with anoxicity. The correlation of bisnorhopane with sulphur is poor towards the top of the section; this may be a result of the increase in bioturbation observed in this part of the section. Farrimond *et al.*

(1990b) suggested that its presence in the Oued Bahloul section may represent a specific bacterial source possibly associated with a highly reducing sulphur-rich depositional environment and/or bacterial mats in an upwelling environment. The A-ring methylated 28, 30-bisnorhopane is also present in the samples where bisnorhopane is relatively more abundant, and was first identified in the Oued Bahloul section by Farrimond *et al.* (1990b) who suggested a specific bacterial input for this compound, but noted that it did not covary with the abundance of methylhopanes.

At the Dir Oulad Yahia section the17α (H), 18α (H), 21β (H)-28, 30-bisnorhopane is significant in sample DOY25, as it is the dominant peak in the m/z 191 trace (Fig. 5.9c), being 1.4 times more abundant relative to the C_{30} αβ hopane. The methylated bisnorhopane is also present in abundance in the m/z 205 trace (Fig. 5.9d). The specific bacterial and diagenetic conditions at this section must favour the bisnorhopane compound compared to the normal hopanoid input observed at the other sections; this could explain the lower hopanoid to steroid ratio and the large bisnorhopane peak. Dominant bisnorhopane peaks in the m/z 191 trace have been observed in work by other authors (Huc *et al.*, 1985); although it has not been attributed to a specific environment or source, it has been linked with marine anoxia (Seifert *et al.*, 1978) and upwelling zones (Grantham *et al.*, 1980) both of which are plausible for this section.

The 17α (H), 18α (H), 21β (H)-28, 30-bisnorhopane compound is absent in the m/z191 trace for the Ech Cheid, Oued El Gsab and Nebour sections, suggesting differing bacterial inputs and/or diagenetic conditions to the Oued Bahloul and Dir Oulad Yahia sections, or at least the absence of those conditions and/or specific bacteria related to the bisnorhopane input.

6.5 Environment of deposition

Chondrites bioturbation is seen at all the localities (especially at the base) and generally quite heavy bioturbation is observed at the top of the sections marking the end of the Cenomanian-Turonian "black shales" and the start of the Annaba Formation. *Chondrites* bioturbation is also seen in some samples through the sections (e.g. OB64 to OB66 and EC7 to EC9); these sample are generally organic-poor. This suggests that these samples were deposited at a sediment/water interface where O_2 concentrations exceeded 0.2ml/L, the level needed to support burrowing life (Tyson & Pearson, 1991). Laminated sediments are seen in some of the Oued Bahloul, Dir Oulad Yahia and the Oued El Gsab sections, indicating the periodic absence of

burrowing organisms. The organic-rich samples at the base of the sections appear to be the most laminated (samples OB4 to OB40, DOY5 to DOY35 and OG2 to OG20) indicating that bottom water oxygen levels dropped below those that support active burrowing marine life, with possible periods of temporary dysoxia-anoxia for at least part of the section.

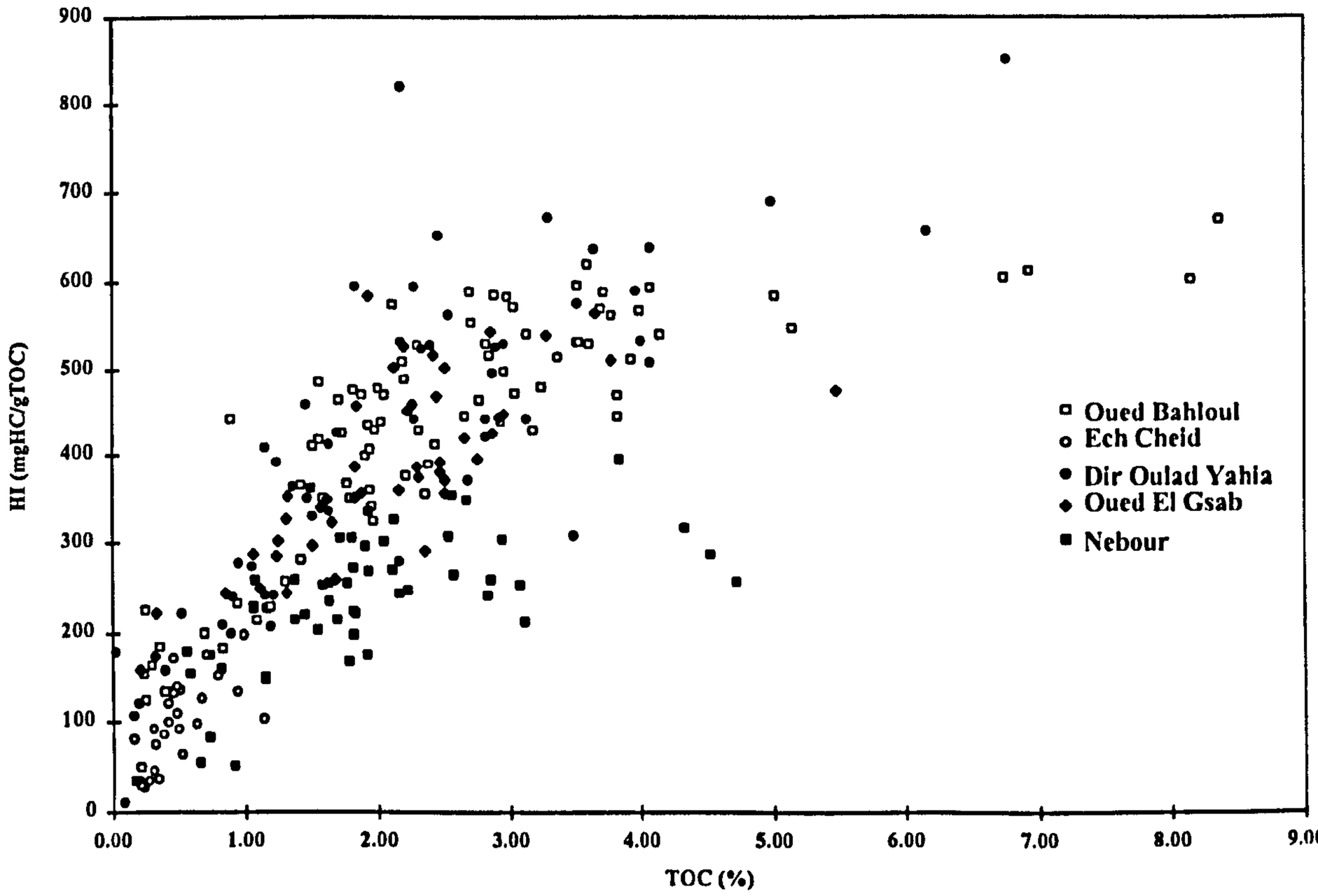

Figure 6.15 Cross plot of TOC versus Hydrogen Index data (all Tunisian samples). Note how hydrogen index values start to level off at about 3% TOC, 500-600 mgHC/gTOC for the sections from the southern part of the study area and 2% TOC and 200 mgHC/gTOC in the north.

A plot of TOC versus hydrogen index for the Oued Bahloul, Dir Oulad Yahia and Oued El Gsab sections (Fig. 6.15) shows some degree of stabilisation of hydrogen index values with increasing TOC. Values begin to stabilise at about 2.5 to 3.0% TOC with hydrogen index values of approximately 500 to 600 mgHC/gTOC; these values are typical of marine derived Type II kerogen at optimum preservation. The Nebour section also shows the levelling off at about 2.5% TOC; however, it is not as apparent as the other sections and the hydrogen index at the point of levelling off is lower (300 mgHC/gTOC), possibly due to the higher maturity or differences in organic matter of this section. The Ech Cheid section shows a slight levelling off of TOC values with increasing hydrogen index at about 0.60% TOC. The levelling off of hydrogen indices indicates that optimum preservation was achieved at these locations. However, the differences in hydrogen indices between the sections,

suggests that the organic matter being preserved differs; this is most apparent from the lower hydrogen indices observed to the north of the study area. This could suggest differing organic matter type between the north and south parts of the study area as was noted by the steroid and hopanoid data.

Figure 6.16 shows the relationship between TOC and sulphur (wt. % values) for the Tunisian sections. The majority of the samples plot in the "non-marine freshwater" field defined by Raiswell and Berner (1985), and only a few of the samples plot in the "normal marine" field, although all the samples are known to be marine. Even the most organic-rich samples have low sulphur contents (≤0.76%). This is presumably due to iron limitation of pyrite formation; iron limitation can be particularly strong when carbonate content is greater than 65% (Raiswell *et al.*, 1988) which is the case for the majority of the Tunisian sections; this is perhaps related to sedimentation rate in the environment of deposition.

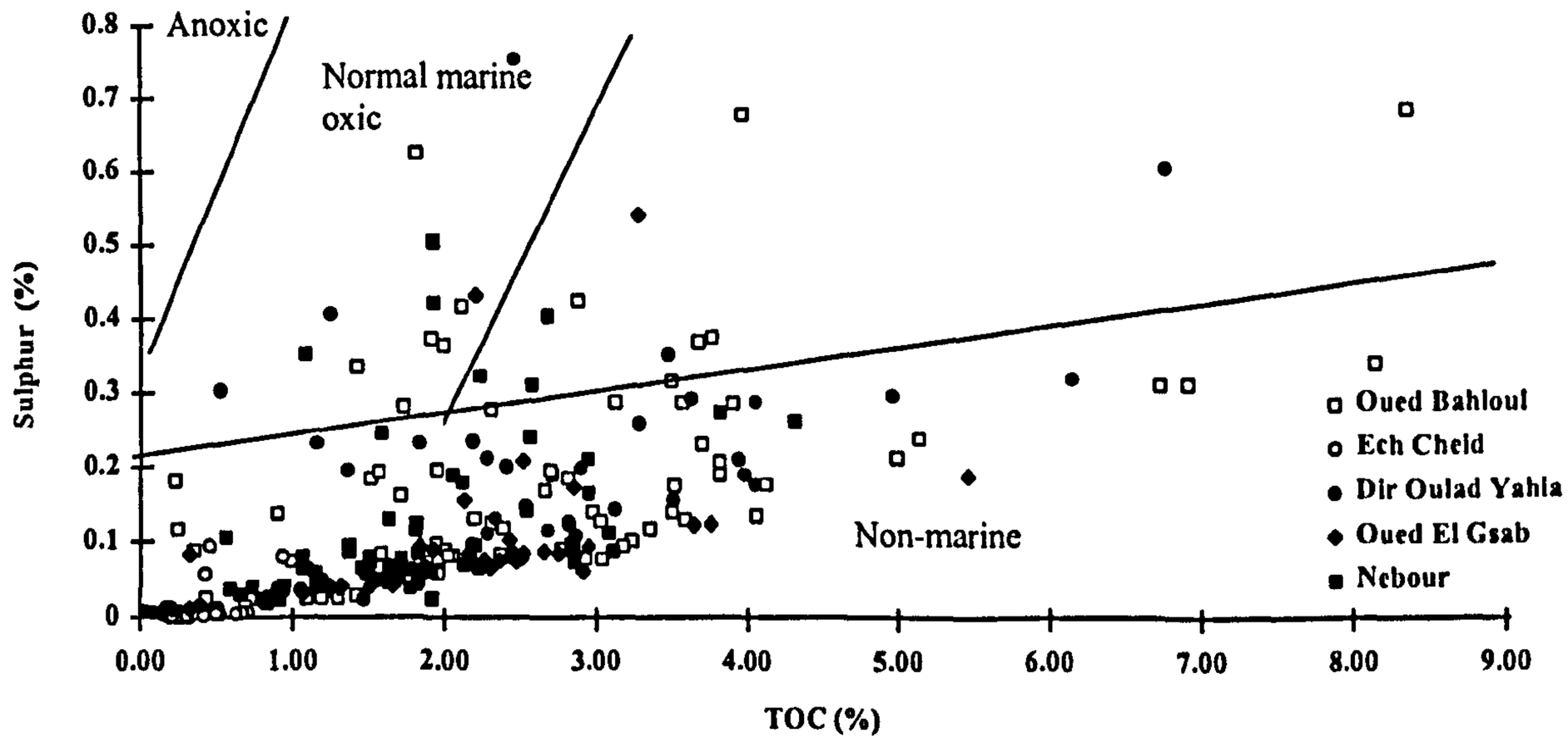

Figure 6.16 Cross plot of TOC versus Sulphur data (after Raiswell & Berner, 1985) for the Tunisian sections. Only a few samples plot in the "normal marine field" defined by Raisewell and Berner (1985); the majority of samples plot in the "non-marine freshwater field" even though they are known to be from a marine environment.

The relative increase in TOC levels from background values to those in the organic-rich samples for all the sections (except Ech Cheid) is greater than 6-fold (range 22 to 68-fold). The normal increase accounted for by preservation in anoxic conditions is generally no more than 6-fold (Tyson, 1995). This suggests that either an increase in productivity and organic matter flux or a reduction in sedimentation rate (dilution) has also occurred during the deposition of these sections. The basal organic-rich part of the section, above the basal limestone unit, is a slowly deposited flooding surface (Robaszynski *et al.*, 1993b) and may explain some of the increase in

TOC values. The Ech Cheid section shows only a 6-fold increase in TOC values, but the most organic-rich interval may be absent here.

The Pr/Ph ratio is greater than 1.0 in all the sections (Appendix 4, Tables III to V) indicating an oxic environment of deposition (Didyk *et al.*, 1978); however, the palynofacies data suggests at least periodic dysoxic-anoxic conditions (cf. Tyson, 1995). This suggest that an alternative source of isoprenoids, such as tocopherols (Goosens *et al.*, 1984) may be affecting the ratio. Although absolute values are not a good indication of the redox conditions at these sections, lower values of Pr/Ph are generally consistent with the low O_2 samples (org-rich samples) in the Oued Bahloul section. The Pr/Ph values are also lower at the Oued Bahloul section (1.3 to 2.7) than at the Ech Cheid section (1.4 to 3.4), indicating that the Oued Bahloul Section was deposited in a less oxic environment.

A ternary plot of the relative percentages of AOM, Palynomorphs and Phytoclasts (Fig. 6.17) for the Tunisian sections can be used to indicate depositional environments (cf. Tyson, 1995). The majority of the Oued Bahloul samples cluster around the AOM pole, as do the three samples from the Dir Oulad Yahia, Oued Gsab and Nebour sections (DOY25, OG16 and N18). This indicates deposition in a distal suboxic-anoxic basin for these samples, where AOM-dominated assemblages, and low abundances of palynomorphs, partly due to masking, are common. An environment removed from terrestrial source area is not surprising considering the carbonate-dominated regime. A deep basin or stratified shelf sea environment is likely. The three organic-poor Oued Bahloul samples (OB2, 23 and 79) plot away from the AOM pole suggesting local differences due to *in situ* O_2 changes. The Ech Cheid locality shows a greater variation in depositional environments through the section. The data follow a line from the AOM pole towards the middle of the opposite axis, which is typical of many Mesozoic marine sediments (Tyson, 1993). The data suggest that the organic-poor samples were deposited in a distal dysoxic-anoxic shelf, and that the organic-rich samples were deposited in a distal dysoxic-oxic shelf (Tyson, 1995). The most organic-rich samples for this section (EC11, 13 and 19) appear to be deposited in an environment approaching that of the Oued Bahloul section.

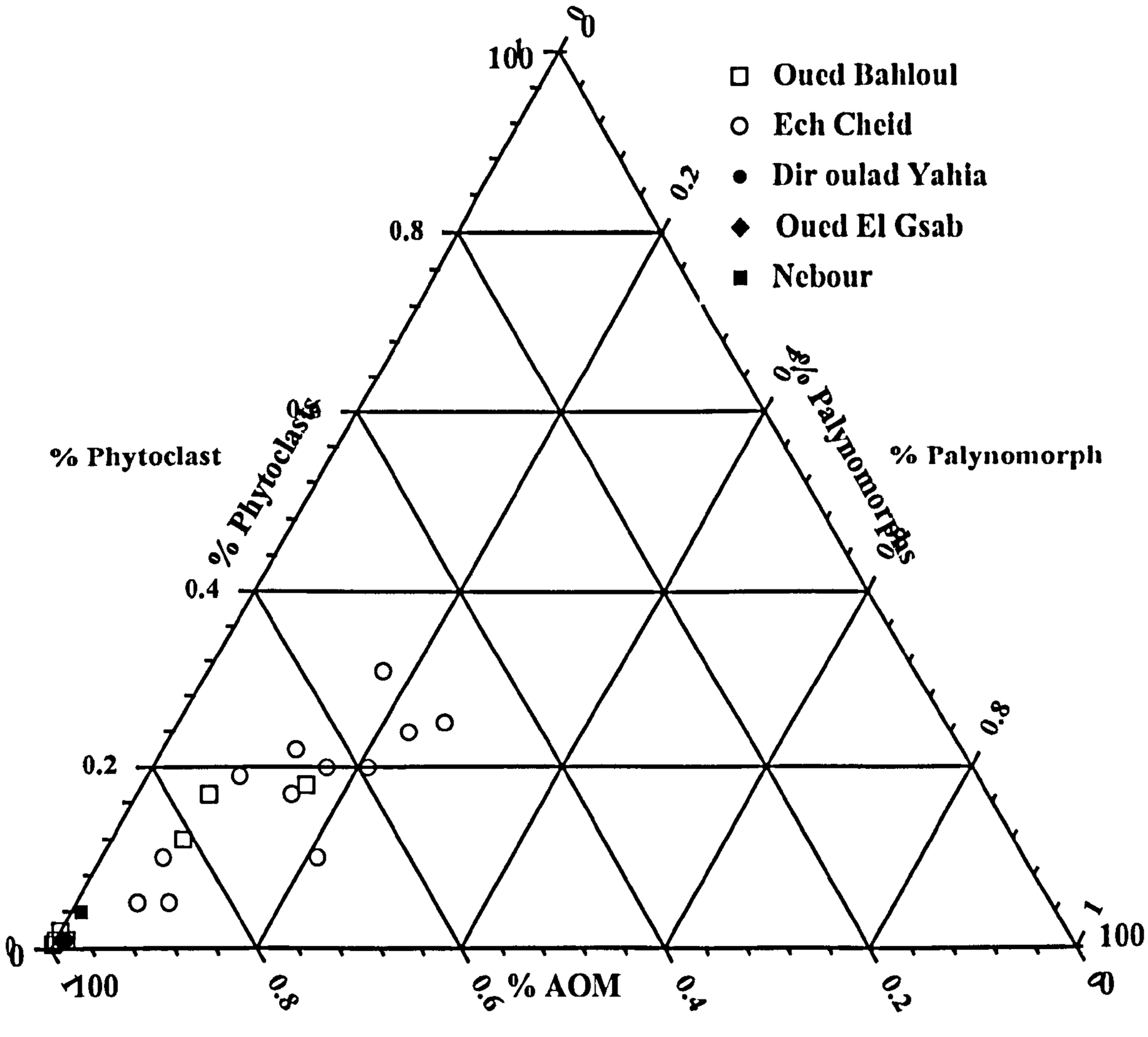

Figure 6.17 Ternary 'AOM'-phytoclast-palynomorph kerogen plot (after Tyson, 1995) for the Tunisian sections, based on relative numeric frequency (%RNF) data from Appendix 3, Tables VI, VII and VIII. Note that the majority of the Oued Bahloul samples cluster at the 'AOM' pole, and that the Dir Oulad Yahia and Oued El Gsab points plot within this cluster.

Kuhnt *et al.* (1990) proposed a model for the distribution of organic-rich Cenomanian-Turonian facies based on palaeobathymetry and depositional environment. According to this model all the sections, with the exception of Ech Cheid, were deposited in shallow (200m) high productivity waters with enhanced nutrient input and upwelling in a deep shelf environment, which fits well with the position of the sections with relation to the anoxic zone defined by Bishop (1988; Fig 5.4). The Ech Cheid may have been deposited in a deeper environment explaining the poorer preservation and lower hydrogen indices.

Optical fluorescence data for the Tunisian sections (Appendix 3, Tables VI to VIII) shows that kerogen fluorescence is stronger in the Oued Bahloul, Dir Oulad Yahia and Oued El Gsab sections compared to the Ech Cheid and Nebour sections. A

plot of hydrogen index versus kerogen fluorescence (Fig. 6.18) shows a general correlation between the parameters, in that samples with greater kerogen fluorescence generally have higher hydrogen indices. This suggests that the variation in hydrogen index between the samples and the sections is largely controlled by preservation. The higher fluorescence in the samples from the south of the sample area compared to those from the northern part suggest better preservation and a less oxic environment during deposition of organic matter in the south of the area, also maturity difference have been noted for the Ech Cheid and Nebour sections.

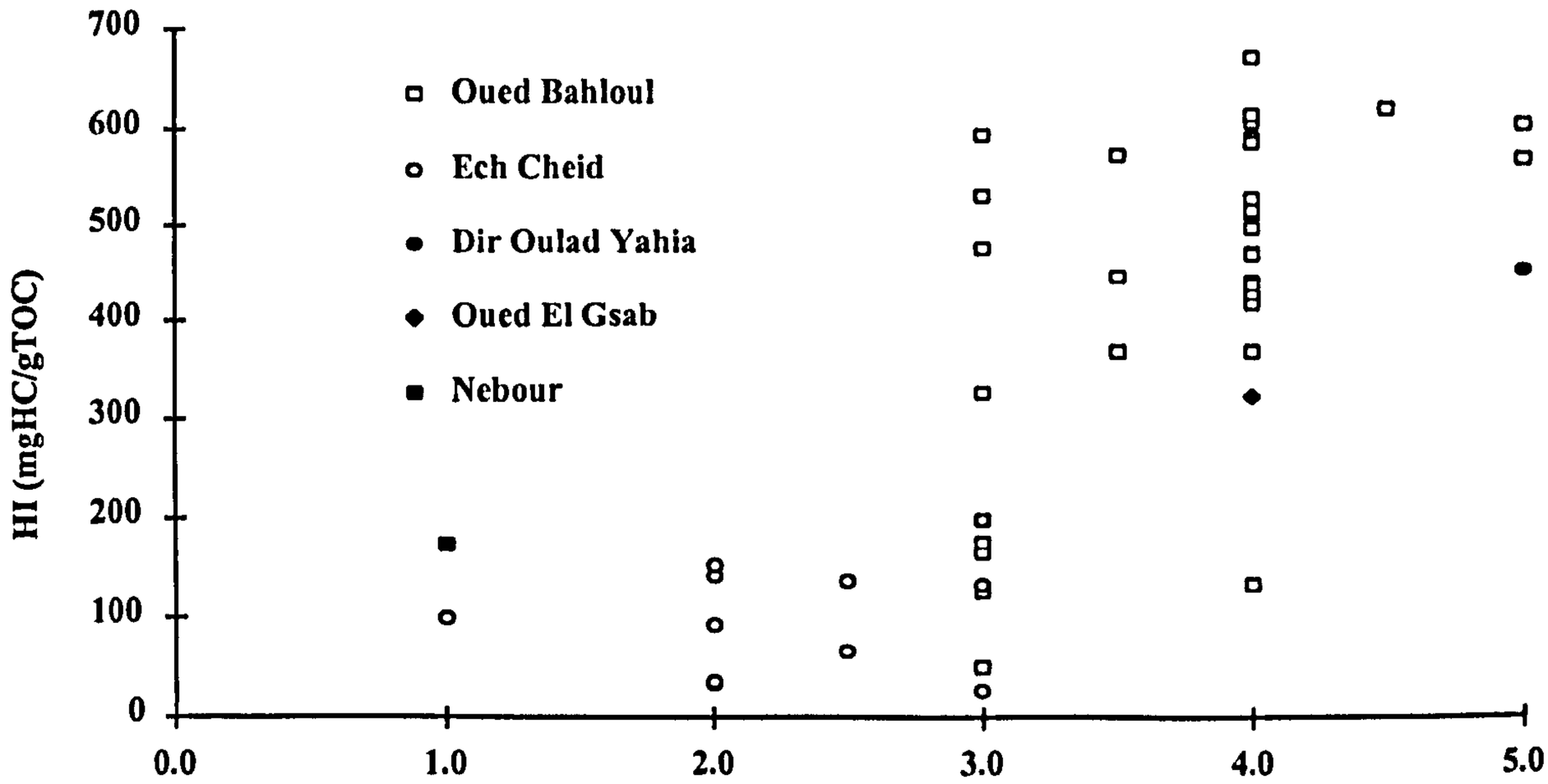

Figure 6.18 Cross plot of hydrogen index and kerogen fluorescence data for all Tunisian sections.

The optical data for the Oued Bahloul and Ech Cheid localities suggest that the variability in hydrogen indices through each section largely reflects preservation rather than changing marine:terrestrial ratios. Based on work by Tyson (1995) this can be confirmed by comparison of the intensity (brightness) of the kerogen fluorescence with hydrogen indices for the Oued Bahloul section (Table 6.2). Samples which showed similar palynomorph fluorescence colours under blue light exhibited variations in the intensity of the fluorescence. This was controlled by differences in the hydrogen index. Samples with higher hydrogen indices had the greatest intensity of fluorescence.

The relative predominance of the C_{35} 17α (22S + R) hopanes over the sum of the C_{31} to C_{35} 17α (22S + R) hopanes (Peters & Moldowan, 1993), has been used to express the anoxicity of a depositional area, in which the C_{35} homologue is preferentially preserved. Figure 6.19 shows the stratigraphical plot of this ratio for the

Oued Bahloul section. It suggests that anoxic conditions occurred rapidly from the base of the section (samples OB2 to OB11), but were at their greatest towards the

Sample	HI (mgHC/gTOC)	Fluor. colour	Fluor intensity	Relative scale
OB23	50	dk-or	dull	1
OB2	126	dk-or	dull	1
OB79	134	or/br	dullish	2
OB18	199	or	dullish	2
OB15	324	or	brightish	3
OB11	368	or	brightish	3
OB49	441	or/y	bright	4
OB6	448	or/y	bright	4
OB12	515	or/y	bright	4
OB82	573	y/or	v. bright	5
OB68	620	y	v. bright	5
OB39	671	y	v. bright	5

Table 6.2 Relative fluorescence intensity of amorphous organic matter; HI, hydrogen index; Fluor, fluorescence, under a blue light source; dk, dark; or, orange; y, yellow.

central part of the section (samples OB28 to OB44) where relative bisnorhopane abundance was also greatest. This fits with fluorescence and preservation scale observations from this section, the optical data indicating that preservation was greatest at the same point that bisnorhopane was at its highest relative abundance. The data suggest that at the top of the section the levels of oxicity did not return to those before the "black shale" event. The profile of this ratio through the Ech Cheid section, indicates fluctuations in the anoxicity of the environment, it appears to be highest at the base of the section (EC1 and EC4) and then again at the top of the section (EC19). The absolute values for the C_{35} 17α (22S + R) hopane predominance are lower than those at Oued Bahloul suggesting that the Ech Cheid section was deposited in a less anoxic environment compared to the Oued Bahloul section. The ternary C_{31}:C_{33}:C_{35} 17α (22S + R) hopane plot (Fig. 6.12) shows that the sections from the southern part of the sample area have relatively higher abundances of the C_{35} homologue compared to the samples from northern part of the area sampled area. This suggests that the anoxicity of the sediment-water interface was greater in the southern part of the sample area, preferentially preserving the C_{35} homologue (Peters & Moldowan, 1993). However, Paul Farrimond (pers comm., 1998) suggests that the data points would move towards the C_{31} pole with increasing maturity; this would fit with the maturity observations noted earlier as the Ech Cheid and Nebour samples

plot closer to this pole. It is thus difficult to assess the relative effects that anoxicity and organic matter maturity are having on the data set.

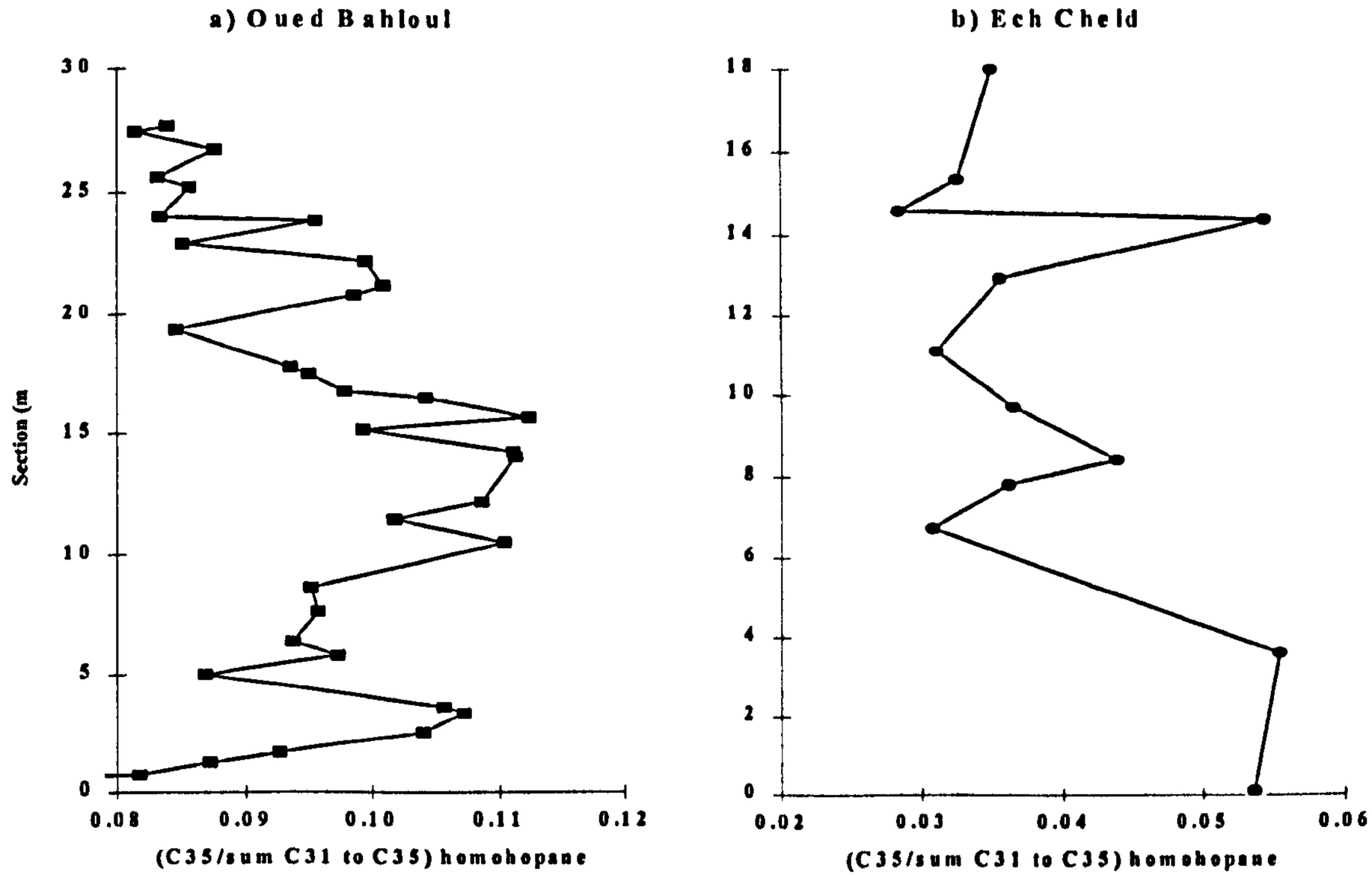

Figure 6.19 Stratigraphical plot of C_{35} hopane predominance (after Peters & Moldowan, 1991); a) Oued Bahloul, note that the lowermost point is off the scale and plots at 0.02, indicating the sudden change from oxic to anoxic conditions; b) Ech Cheid, note that the values are lower than that of Oued Bahloul, and the sharp excursion is not observed at the base of the section, this suggests differences in anoxicity between the two sections.

Changes in dinoflagellate cyst type were associated with a suitable environment for the bloom forming proximochorate cyst types at the Misberg section (Section 4.7.5). The Ech Cheid section also shows a higher relative abundance (≤ 97%) of proximochorate cysts compared to chorate cysts which are believed to be dominant in offshore facies, due to hydrodynamic sorting (Vozzhennikova, 1965), although this is often not the case (Tyson, pers comm. 1998). It has already been mentioned that *Cyclonephelium* (a proximochorate cyst form) is dominant in the organic-rich lithologies of Cenomanian-Turonian age (Marshall & Batten, 1988). This is because *Cyclonephelium* is a bloom-forming genus which typically occurs in high density low diversity assemblages in probable eutrophic settings, and its dominance is thus mainly a function of ecology rather that hydrodynamics. The proximochorate dinoflagellates were probably suited to the particular environment during deposition of the organic-rich lithologies and thus either inhibited the growth of other species or simply diluted them.

6.6 Principal Component Analysis of biomarker data

6.6.1 Introduction

Principal Component Analysis was run on several different groups of Tunisian data (Appendix 5), to allow for a greater spread of information to be gathered. The first PCA looked at 80 aliphatic compounds in each of the 36 samples run on gas chromatography-mass spectrometry from the Oued Bahloul section (Appendix 5, Table III). These compounds included C_{29} hopanes (m/z 177), tricyclic terpenoids and hopanes (m/z 191), methylated hopanes (m/z 205), steranes (m/z 217 & 218), 4-methylsteranes (m/z 231), diasterenes (m/z 257) and C_{29} hop-13(18)-ene (m/z 204). These compounds were selected as they could be easily identified and integrated between samples and suffered no co-elution problems. The second PCA was run on just the hopanoid and tricyclic terpane data for the Oued Bahloul section (Appendix 5, Table III) in order to identify the important source and environmental changes seen in these compounds. The third PCA used 71 compounds (Appendix 5, Table IV) for each of the 12 Ech Cheid samples run on gas chromatography-mass spectrometry. The fourth PCA group looked at 66 compounds from the 36 Oued Bahloul samples and the 12 Ech Cheid samples as well as the DOY25, OG16 and N18 biomarker data, a total of 53 samples (Appendix 5, Table V). The compounds used were similar to the set that was previously used, although compounds that were not common to all sections were discarded. The final PCA group used just the hopanoid and tricyclic terpane compounds common to each section (34 in total) for each of the 53 samples from the sections (Appendix 5, Table V).

6.6.2 PCA of Oued Bahloul biomarker data

The first three Principal Components account for approximately 70% of the total variance. The first Principal component (PC1) records 45% of the total variance in the data set; the loadings plot for PC1 is controlled by the majority of the hopanoids on the positive axis and all the of the steroids on the negative axis. A cross-plot of the scores data for PC1 shows an excellent correlation ($r^2 = 0.96$; Fig 6.20) with the ratio of hopanoids to steroids from the biomarker data (Appendix 4, Table IX). As observed in the biomarker, data the hopanoids dominate in the lower part of the section, especially samples OB6, 7, 28 and 39 (Fig 6.11). This PC represents the relative input from algal and bacterial sources through the section; this suggests that bacterial input was relatively dominant in the basal (0 to 11m) and upper parts (22 to 26m) of the section, whereas algal input was relatively dominant in the central parts of

the section (believed to be the most anoxic from the C_{35} predominance plot (Fig 6.19). Higher relative concentrations of hopanoids in the basal part of the section suggest higher bacterial reworking which indicates a lower sedimentation rate for this part of this section; this corresponds with the proposed flooding surface above the basal limestone unit (Robaszynski *et al.*, 1993b). It is important to note that the relative abundance of hopanoids and steroids is the dominant variability in these biomarker data set and that this relates to the controls on the primary organic matter sources.

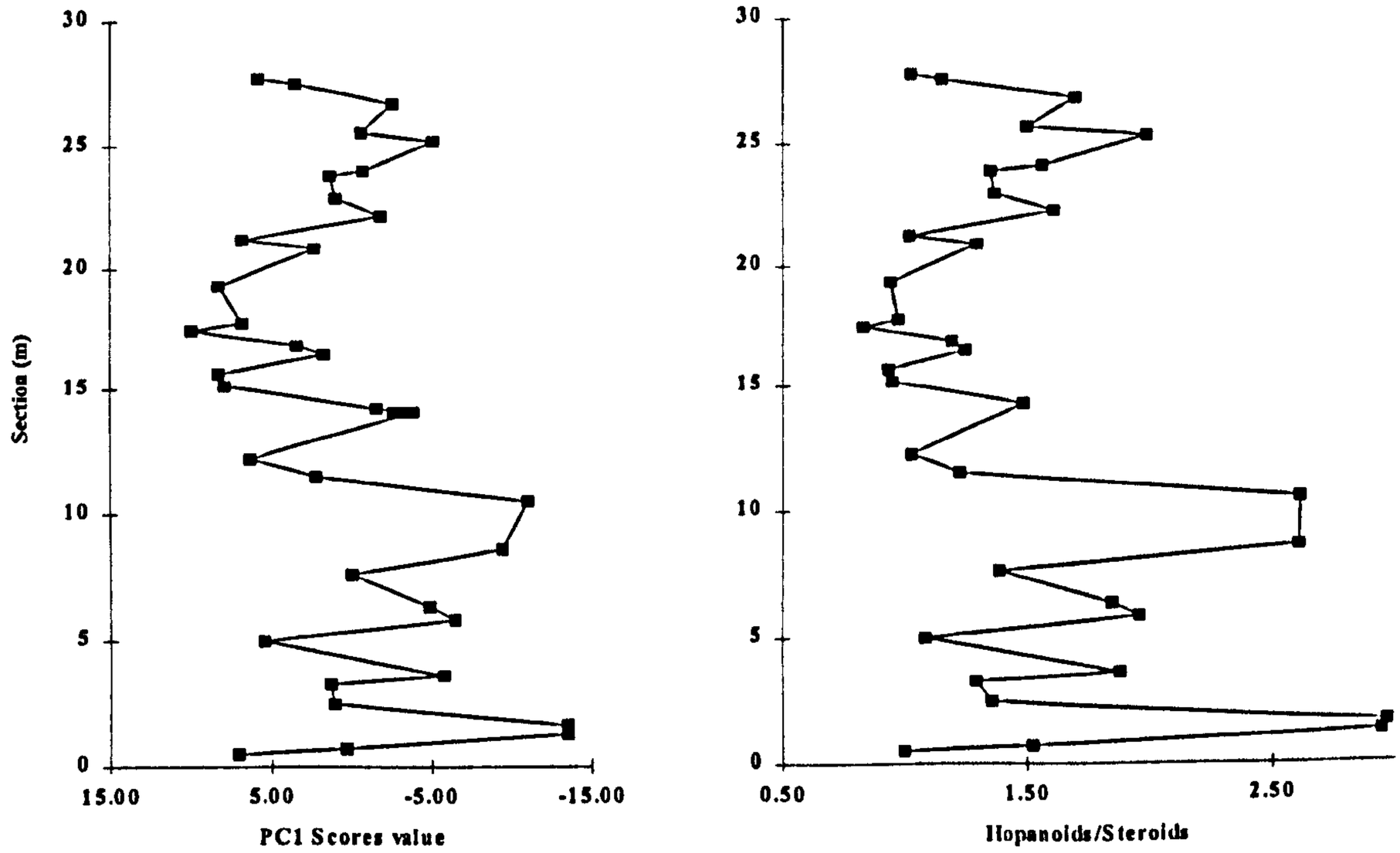

Figure 6.20 Stratigraphical plots of Oued Bahloul biomarker data PC1 scores and Oued Bahloul hopanoid versus steroid data. The two parameters show excellent correlation ($r^2 = 0.96$).

Principal Component 2 accounts for 15% of the variance in the total data set. The loadings are controlled by dominant tricyclic terpanes on the negative axis and dominant homohopanes (C_{31} to C_{35}) and methylhopanes on the positive axis. A cross-plot of PC2 versus the ratio of tricyclic terpanes to the homohopanes and methylhopanes shows a good correlation ($r^2 = 0.87$; not shown). This principal component may be controlled, to some extent, by the differing sources of the hopanoid and tricyclic terpane compounds through the section, and appears to show a general shift of increasing relative contents of tricyclic terpanes towards the top of the section.

Principal Component 3 records 9% of the variance in the total data set. Loadings data shows that the methylhopanes and the bisnorhopane plot dominantly on

the negative axis and the hopanes plot dominantly on the positive axis. This Principal Component, may reflect relative increases in hopanoid content from specific bacteria as was noted earlier in the biomarker data. The source and environmental significance of these compounds is not fully understood. The cores data also indicate that the samples at the base of the section (OB6 and OB7) contain significant amounts of methylhopanes.

6.6.3 PCA of Oued Bahloul hopanoid and tricyclic terpenoid data

The first three Principal Components account for over 60% of the total variance for this analysis. The first PC accounts for 28% of the variance in the total data set, and shows the homohopanes and methylhopanes plot on the negative axis, and the tricyclic terpanes and remaining hopanoids plot on the positive axis. The scores for PC1 show a good correlation ($r^2 = 0.62$) with the relative methylhopane input and an even better correlation ($r^2 = 0.95$) with the ratio of homohopanes + methylhopanes to the remaining hopanoids and tricyclic terpanes used (Fig. 6.21). This relationship was also noted in PC2 for the PCA analysis of the total biomarker data for the Oued Bahloul section (section 6.6.2). The relative amounts and distribution of the methylhopanes clearly affect the hopanes distribution. It is interesting to note that the bisnorhopane and the methylated bisnorhopane also plot on the negative axis with the methyl hopanes in this PCA analysis, although no strong correlation was directly observed in the biomarker data.

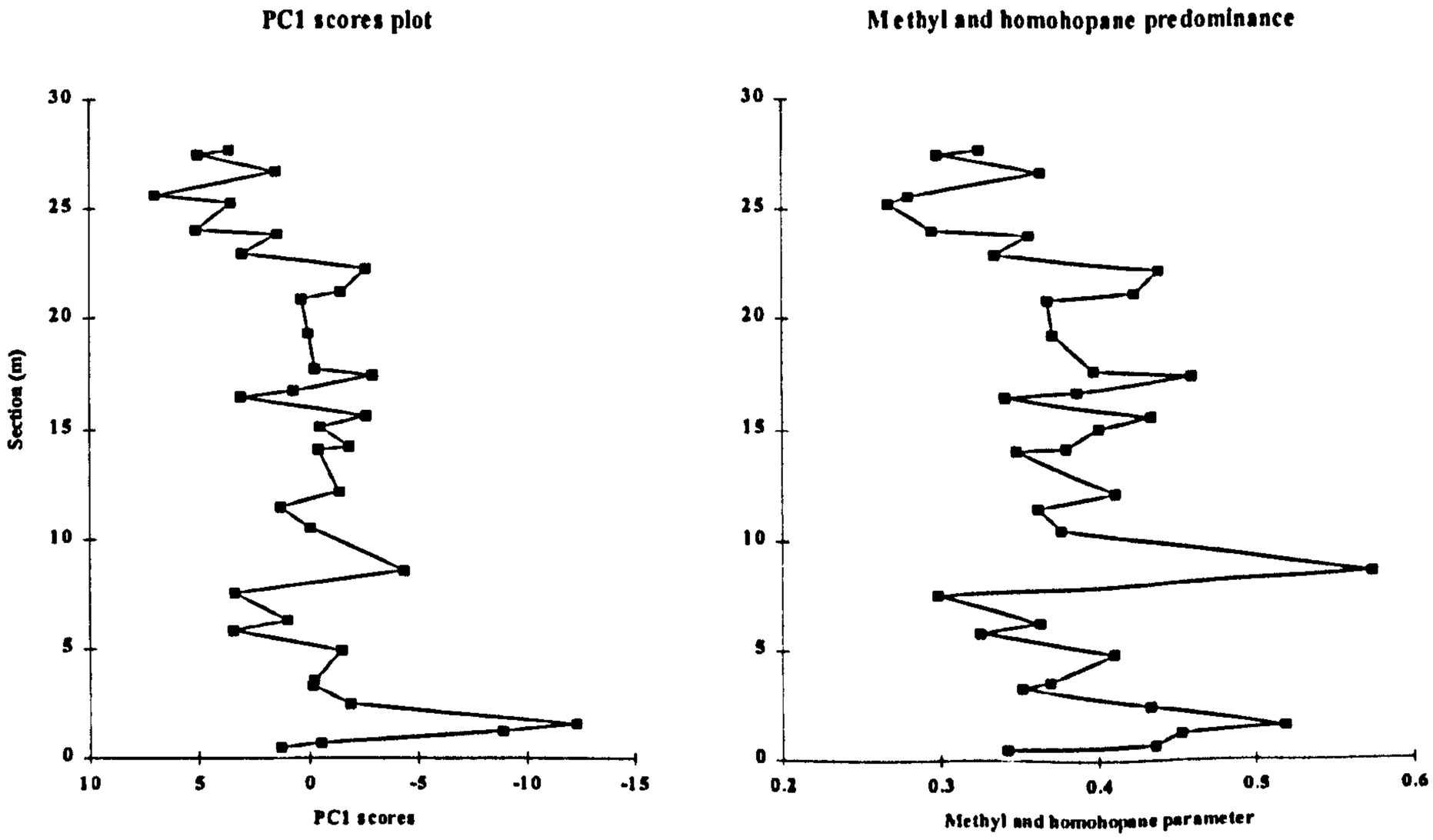

Figure 6.21 Stratigraphical plots of Oued Bahloul biomarker data PC2 scores and Oued Bahloul methylhopane and homohopane predominance over the sum of all other

hopanoid and tricyclic terpanoid compounds identified. The two parameters show excellent correlation ($r^2 = 0.96$).

Principal Component 2 controls 21% of the total variance. The loadings show that the homohopanes plot strongly on the negative axis and the methylhopanes and tricyclic terpanes plot on the positive axis. There appears to be some control on the carbon number distribution as well. The odd number homohopanes plot slightly more positively that the even number hopanes. A similar distribution is seen in the methylhopanes: here the even number homologue (equivalent to the odd carbon number homohopanes) plot more positively than the odd number homologues. However, a poor correlation ($r^2 = 0.27$) is seen in a cross plot of the PC2 scores and the Hopane odd-over-even parameter. It is possible that this PC reflects hopanoid input from differing bacterial sources, i.e. those that show a strong methylhopane content and those that do not. This would suggest that the PCA is identifying samples with two bacterial sources as described earlier (Section 6.4).

The third PC accounts for 12% of the total variance in the data set. The loadings show that the C_{35} (22S + R) homohopane plots strongly on the positive axis and the C_{31} hopanes plot on the negative axis. A good correlation ($r^2 = 0.79$; not shown) of the PC3 scores data is seen with the $C_{35}/\Sigma\ C_{31}$ to C_{35} hopane ratio (cf. Peters & Moldowan, 1993), this is believed to be an anoxicity parameter. The bisnorhopane compound also plots quite significantly on the positive axis; this compound has been linked with anoxic environments (Seifert *et al.*, 1978).

6.6.4 PCA of Ech Cheid biomarker data

Over 70% of the total variance is accounted for by the first three Principal Components for the Ech Cheid data set. The first Principal Component accounts for over 42% of the total variance, and describes the relationship of hopanoids and tricyclic terpanes (positive axis) to steroids (negative axis). This is confirmed by a cross-plot with a good correlation ($r^2 = 0.93$; Fig. 6.22) between the PC1 scores and the total hopanoids and tricyclic terpanes/total steroids ratio from the biomarker data. As was observed from the Oued Bahloul biomarker data set the dominant control on the biomarker data is the variation in hopanoids and steroids which relates to variability in the primary organic matter sources.

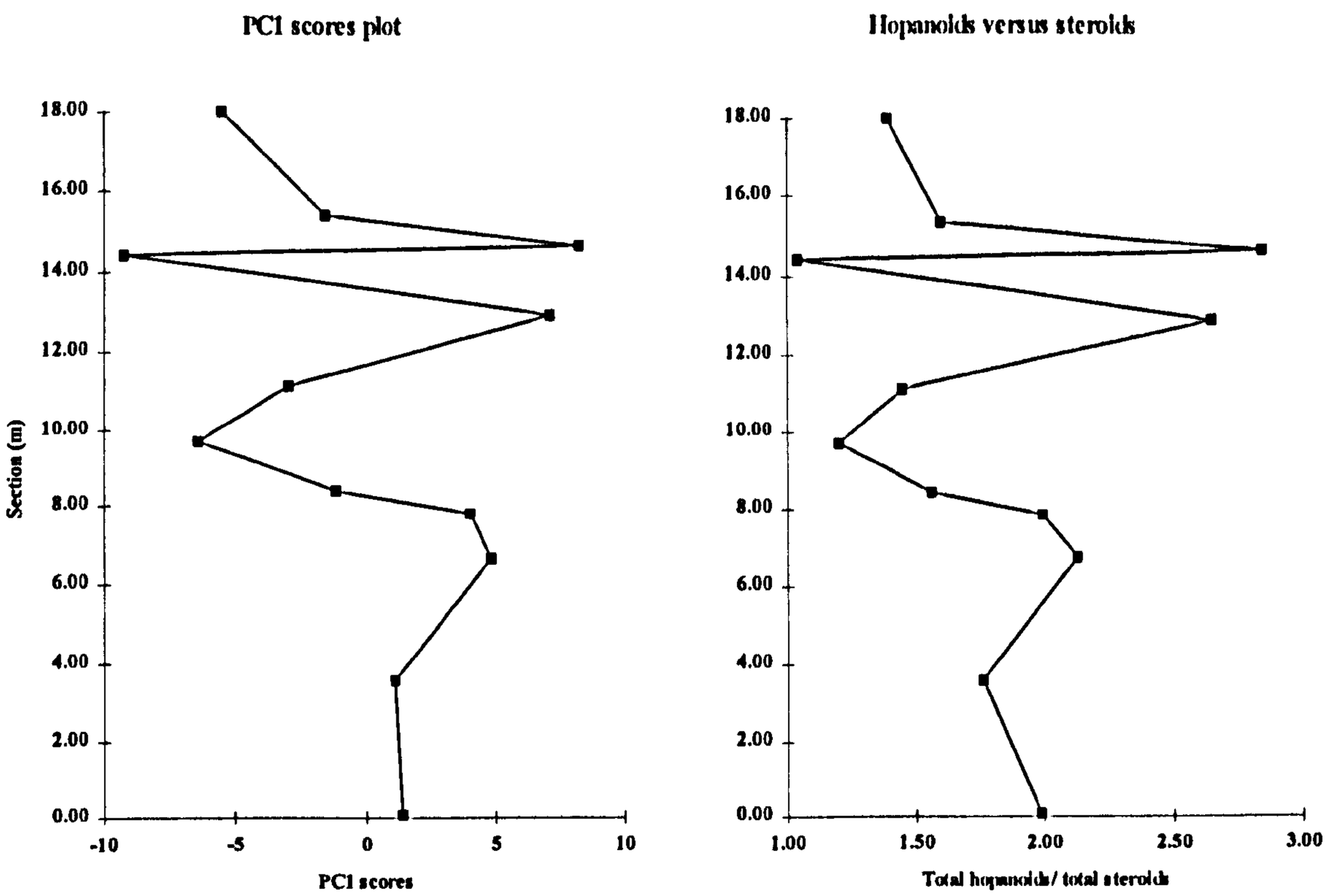

Figure 6.22 Stratigraphical plots of PC1 scores data and hopanoid/steroid data for the Ech Cheid section. The two parameters show an excellent correlation ($r^2 = 0.93$).

The second Principal Component controls 15% of the total variance of the data set. The positive axis shows dominant demethylated hopanes, trisnorneohopane, diasterenes and the R configuration for the homohopanes, while the negative axis shows a dominant trisnorhopane, C_{29} and C_{30} $\alpha\beta$ hopanes, C_{31} 2α-methyl $\beta\alpha$ hopane and methylsteranes. Some correlation ($r^2 = 0.46$; not shown) is seen in a cross-plot of PC2 scores and the Ts/Tm ratio. The position of the homohopane R isomers (and other hopanoids controlled by higher maturities) on the positive axis suggests that this PC is controlled by the maturity of the samples; however, cross-plots of the PC2 scores with hopanoid and steroid maturity parameters show poor correlation. The inference from the relationship with the Ts/Tm ratio, could be that this PC is to some extent controlled by the slight variability in maturity of the samples. However, as the Ts/Tm ratio is affected by other factors such as facies, this conclusion is far too simplistic.

Principal Component 3 controls 13% of the variance in the data. The tricyclic terpanes plot dominantly on the positive axis in the loadings data, but the other compounds show no obvious trend. This PC may be controlled by the relative content of tricyclic terpanes through the section. However, a direct plot of tricyclic terpanes versus the other compounds shows little correlation; this is because compounds other

than the tricyclic terpanes are affecting this PC, although the trend of these other compounds is unclear from the loadings.

6.6.5 PCA of all Tunisian biomarker data

For this Principal Component Analysis group the first three Principal Components account for over 70% of the total variance. Principal Component 1 records over 31% of the total variance in this data set. The loadings plot for this PC are controlled by those compounds associated with mature source rocks (e.g. Ts, homohopane S isomers, αβ hopanes, and αββ steranes) on the positive axis, and the compounds associated with immature source rocks (e.g. Tm, homohopane R isomers, βα hopanes and ααα steranes) plot on the negative axis. A cross-plot of the scores data for PC1 with maturity data for the Tunisian sections shows a good correlation with the C_{29} αββ/αββ+ααα sterane ($r^2 = 0.79$; not shown) and the C_{30} αβ/αβ+βα ($r^2 = 0.70$ not shown) ratios. A plot of PC1 versus PC2 (Fig. 6.23) scores data indicates that the Tunisian sections plot in order of maturity from the Dir Oulad Yahia section to the Oued Bahloul and Oued El Gsab sections of approximately the same maturity, through to the slightly more mature Ech Cheid and Nebour sections. This variation in maturity data agrees well with the bulk and molecular geochemical interpretations.

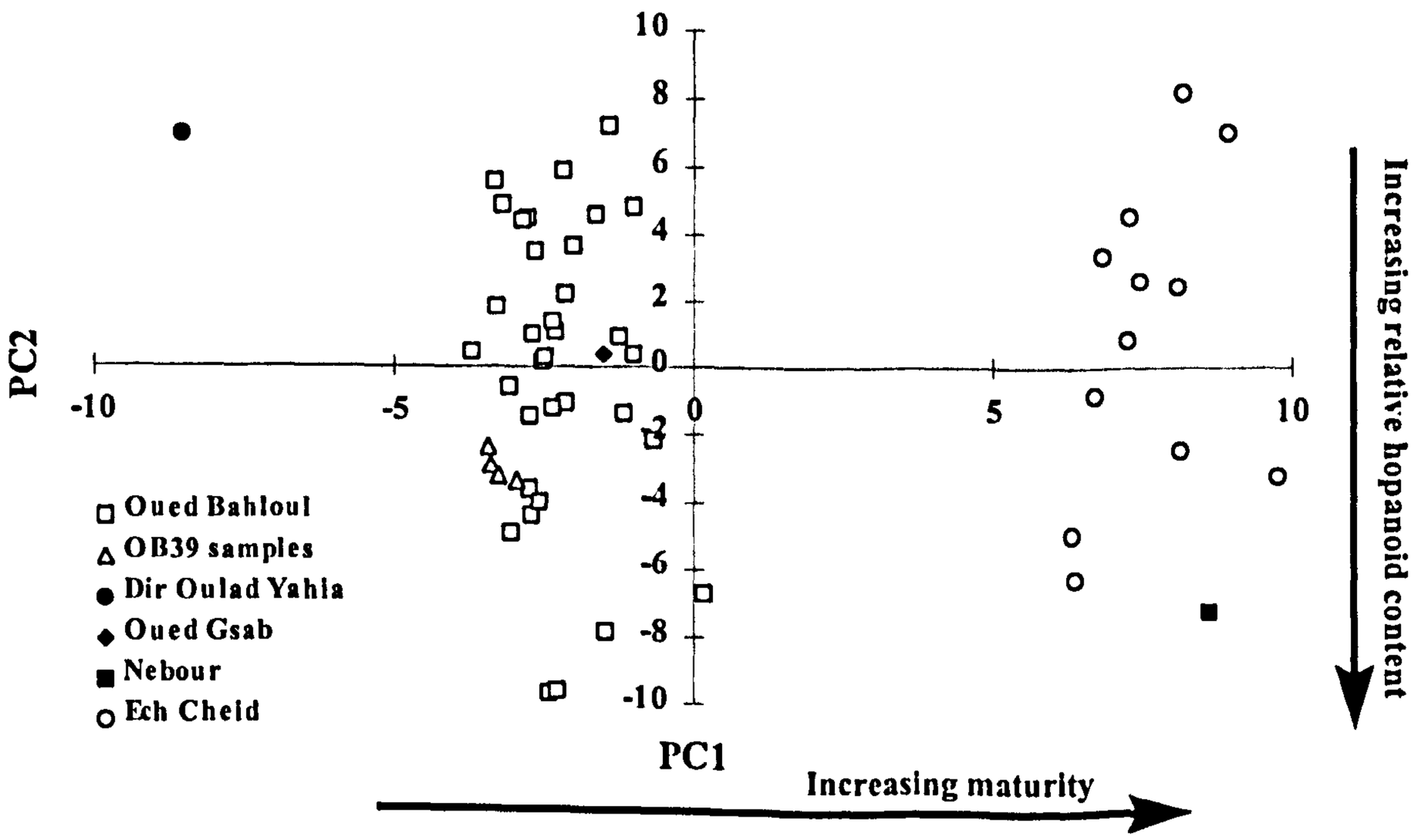

Figure 6.23 Cross plot of PC1 and PC2 scores data for the Tunisian PCA data. The plot demonstrates the relationship in maturity and relative hopanoid content between the sections.

The second principal component accounts for 30% of the variance in the data set. The loadings plot clearly shows that the steroid compounds plot on the positive axis and the hopanoid compounds plot on the negative axis. A cross-plot of the PC2 scores and the hopanoid:steroid ratio for the Tunisian sections shows a good correlation ($r^2 = 0.78$; not shown). A cross-plot of PC1 versus PC2 (Fig. 6.23) shows the relationship in relative amounts of hopanoids and steroids between the sections. The plot indicates that the Dir Oulad Yahia and the Nebour sections, which have relatively high amounts of steroids and hopanoids respectively, are not outside the ranges observed in the Oued Bahloul and Ech Cheid sections. There is some possibility that this is controlled by maturity as the hopane/sterane ratio increases with maturity, but this normally only occurs in the oil window. Multiple gas chromatography-mass spectrometry analyses were made on sample OB39; their clustering in Figure 6.23 indicates the reproducibility of the data.

Principal Component 3 accounts for 10% of the variance in the data set. The loadings data indicate that the tricyclic terpanes plot dominantly on the positive axis, and the majority of the hopanoids plot on the negative axis. A cross-plot of the PC3 scores against the ratio of demethylated hopanes, hopanes, homohopanes and methylhopanes to the tricyclic terpanes, shows a good correlation ($r^2 = 0.62$; not shown). The PC3 scores also indicate that there is a relative change in this ratio up through the Oued Bahloul and Ech Cheid sections, showing an increase in the relative abundance of the tricyclic terpanes toward the top of both sections. This was also observed in PC2 of the Oued Bahloul data set (Section 6.6.2). Why this occurs is unclear, as the source and environmental significance of tricyclic terpanes is not fully understood.

6.6.6 PCA of all Tunisian hopanoid and tricyclic terpane data

Conducting Principal Component Analysis on just the hopanoid data allows us to get more information out of the data set without the hopanoid/steroid ratio controlling the majority of the variance. The first three Principal components account for 55% of the total variance. The first Principal Component records 34% of the total variance, and as observed in the PCA of the Tunisian total biomarker data set (Section 6.6.5), it reflects the maturity of the samples. Those hopanoids associated with mature source rocks (e.g. C_{30} αβ and 17α (H), 21β (H) hopane S isomers) plot on the positive axis of the loadings chart and those hopanoid compounds associated with immature source rocks (e.g. C_{30} βα and 17α (H), 21β (H) hopane R isomers) plot on

the negative axis. The tricyclics plot dominantly on the positive axis suggesting that these compounds have some correlation with maturity.

Principal Component 2 accounts for 21% of the variance in the data set. The loadings data show that the tricyclic terpanes plot dominantly on the positive axis, and that the methylhopanes and homohopanes plot dominantly on the negative axis. It is clear from the loadings and the scores data that this is the same control on the biomarker data that was seen in PC3 for the Tunisian hopanoid and steroid data set (Section 6.6.5). Figure 6.24 shows a cross plot of PC1 versus PC2 scores data. As was discussed in Section 4.8.1 the source of tricyclic terpenoids is not fully understood although by their ubiquitous nature they could be bacterially derived, in which case they may represent a bacterial source signal in these sediments; however, as they show no relationship with other hopanoid data, they may be derived from a different bacterial source.

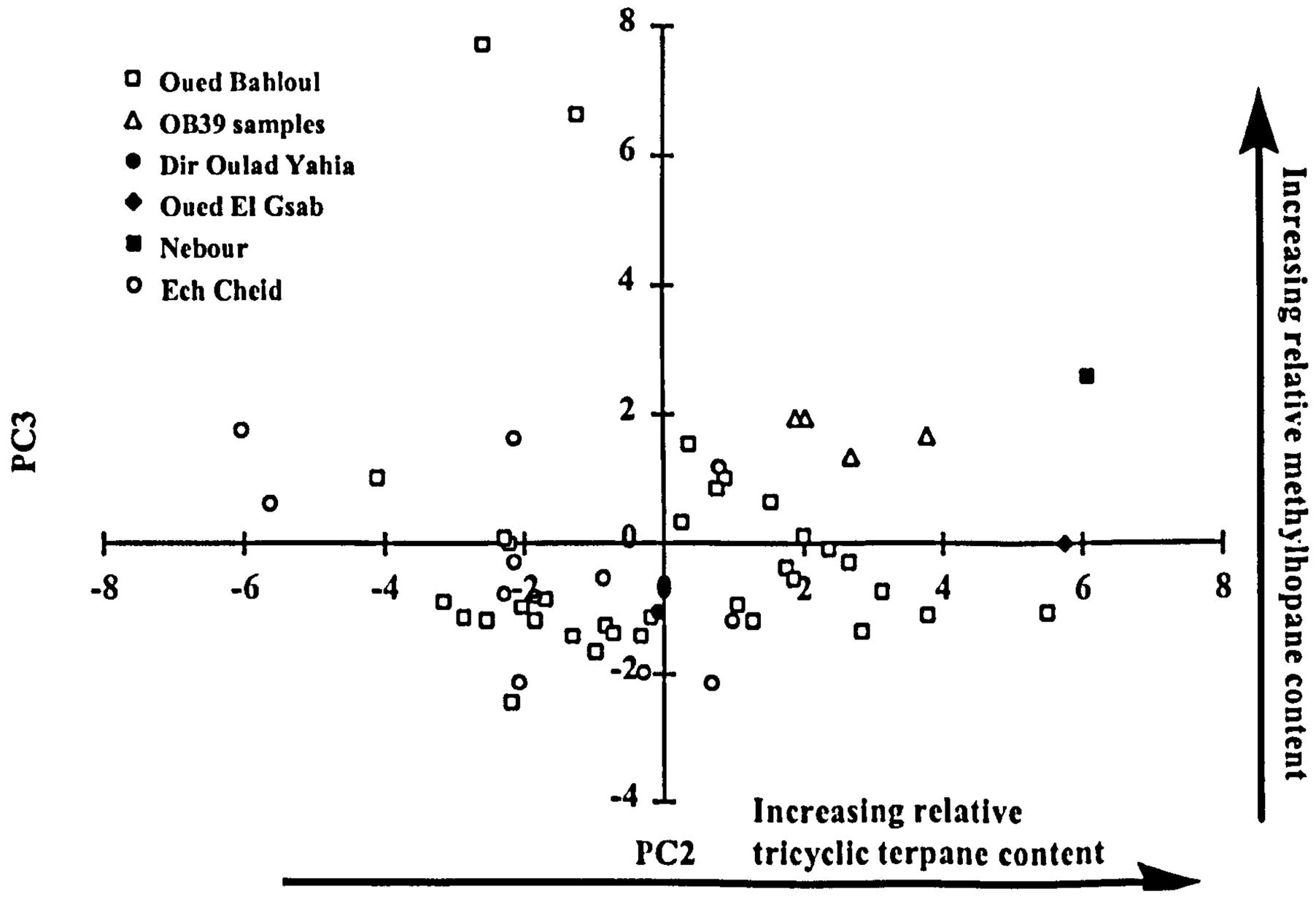

Figure 6.4 Cross plot of PC2 and PC3 scores data for the Tunisian hopanoid PCA data. This plot shows the relationship of increasing relative methylhopane and tricyclic terpane content for the Tunisian sections. Note that the two points that plot at +8 on the PC3 axis are samples OB6 and OB7.

The third Principal Component, which records only 10% of the variance, shows more interesting information (but less relative) than PC1 and PC2. The loadings plot is controlled by dominant methylhopanes on the positive axis, and hopanes and homohopanes on the negative axis. The scores data show that samples

OB6 and OB7 plot strongly on the positive side of the axis; these two samples have a high relative methylhopane content that was observed in the biomarker data (Section 6.4). A plot of PC2 versus PC3 (Fig. 6.23) for the Tunisian hopanoid PCA data shows that the majority of the samples plot with similar relative amounts of methylhopanes. However, samples OB6 and OB7 (and to a lesser extent samples OB39, OB40, N18, EC8 and EC16) indicate relatively higher methylhopane contents, suggesting that they have a relatively higher hopanoid input from a specific bacterial source. This was also noted from the methylhopane ratio calculated from the molecular geochemistry data (Appendix 4, Table IX).

Principal component analysis of the different data sets appear to indicate that variations in relative algal/bacterial input and (in cases of combined data sets) maturity, are the dominant controls on the distribution of biomarkers through the Tunisian sections. To a lesser extent, the variations in hopanoid compounds are also important. The relative dominance of tricyclic terpanes towards the top of the Oued Bahloul and Ech Cheid sections may relate to either changes in algal/bacterial input or diagenetic reactions for these sections, although not enough information is known about these compounds to make any specific conclusions. The relative changes in methylhopane content are likely to be a result of changes in bacterial communities, possibly reflecting changes in environmental conditions or bacterial diversity in an area of reduced sedimentation rate (a flooding surface). Another possible cause for variations in methylhopane content are changes in the diagenetic pathway of the precursor compounds, favouring the methylation of hopanes under differing environmental conditions. The problems encountered in understanding the source and/or environmental importance of methylhopanes in these sections is hindered by the lack of research in the literature on these compounds.

6.7 Conclusions

The organic facies of the Bahloul Formation are dominated by variably preserved, predominantly marine-derived Type III-II to II kerogen. The high TOC values and thickness of the formation combined with the kerogen Type and low maturity of the Bahloul Formation suggest that it is likely to be an excellent source rock for oil and gas if buried to a suitable depth.

Suboxic-anoxic conditions are apparent from the lack of bioturbation and presence of laminations in parts of the formation. The onset of anoxia was apparently abrupt as observed from the rapid increase in TOC values, the change in lithologies

from massive organic-poor limestones to "black shales" and rapid increase in predominance of C_{35} 17α hopanes from the base of the Oued Bahloul section; although the apparent abruptness may reflect slow sedimentation rate at a flooding surface. Culmination of the organic-rich deposits and the $\delta^{13}C$ peak occur in the *W. archaeocretacea* Zone (90mya).

The fluctuations in TOC values are not affected by carbonate dilution. Although the trend in carbonate data is similar in all sections, it cannot be correlated between them, because the minimum in the carbonate values, as observed from the constrained clustering data, occurs at different places relative to the $\delta^{13}C$ kerogen curve.

Several new kerogen $\delta^{13}C$ curves for the Bahloul Formation have been reported in this study and appear to be a useful tool for identifying and correlating the CTBE, within Tunisia and with other palaeogeographic settings. The curve is especially useful for correlating the base of the formation, where most fluctuation in $\delta^{13}C$ values is observed. Comparison with geochemical and optical data enables anomalous curves to be identified and possibly corrected, making them potentially superior in "black shale" facies where carbonate curves may be diagenetically altered.

Onset of the organic-rich facies and isotopic excursion is broadly synchronous between the sections studied and that of Accaire *et al.* (1996). There is evidence of slight diachroneity of the Bahloul Formation, especially its top, suggesting that the deposition of black shale continued beyond the isotope event in some sections. There is also some evidence of diachroneity between the north and south of the sample area. The basal TOC maximum occurs after the isotope excursion in the Nebour section, whereas the two events occur at approximately the same time to the south of the sample area.

The enhanced TOC levels for the Bahloul Formation are probably due to a combination of increased preservation due to suboxic-anoxic conditions, increased primary productivity and lower sediment dilution levels. Preservation does not appear to be as good to the north of study area, but this may be a partial effect of maturity.

Higher maturity to the north of the study area, suggests higher post-Turonian burial rates or higher heat flows in this area. The higher maturity appears to have an effect on the hydrogen index of the Nebour section, where some chemical alteration may have occurred. The difference in hydrogen indices for the Ech Cheid section is

more likely due to a combination of kerogen mixing and poorer preservation. This is demonstrated in the correlation ($r^2 = 0.51$) between hydrogen index and AOM:phytoclast ratio.

Ternary steroid plots suggest that algal inputs are different between north and south of study area. The two sections to the north have a relatively higher C29 ααα R sterane input, which is a possible indication of a terrestrial source; this is noted optically in the Ech Cheid section, but not in the Nebour section. The relative abundance of methylsteranes in all the sections may be an indication of dinoflagellate input which is not apparent from optical examination of some of the sections. In AOM-dominated kerogen assemblages, where oxidation techniques to reduce the AOM content do not work, determination by chemical analysis may be the only way of identifying input from such phytoplankton.

Ternary hopanoid plots are a good way of visually expressing the differences in diagenetic pathways of these compounds and/or bacterial input within and between the Tunisian sections. These plots identified hopanoid inputs from differing bacterial sources for the Bahloul Formation. Specifically, differences in methylhopane content within the Oued Bahloul section and between the sections to the north of the sampled area and those to the south. These differences can only be detected chemically and are not apparent from any optical examination. Differences in the carbon number distribution suggest that the diagenetic pathway for these hopanoids favours the C_{33} hopane and the C_{34} methylhopane homologues.

This study confirms the presence of the A-ring methylated bisnorhopane at the Oued Bahloul locality and notes its relatively higher abundance at the Dir Oulad Yahia locality, and also that of bisnorhopane. The presence of bisnorhopane may reflect the anoxicity of the depositional area as it co-varies with the predominance of the C_{35} 17α (22S + R) hopane in Principal Component loadings plots for the Oued Bahloul data.

The use of Principal Component Analysis confirms the slight maturity differences between the sections that was proposed from the bulk geochemical and biomarker data. Principal Component Analysis indicates that the greatest control on biomarker data for individual sections is the relative input from algal or bacterial sources. The PCA also identified the variations in methylhopanes between the sections, which itself indicates variability in bacterial sources at the Oued Bahloul section and also the importance of tricyclic terpanes in all the sections.

It is important to note that only a multidisciplinary approach (optical, bulk, molecular and isotopic geochemical) in a source rock investigation can give the whole picture; some techniques fail to recognise all the characteristics of the samples under investigation, and only the combined approach gives sufficient data for meaningful conclusions.

CHAPTER 7

7. Pyrolysis (Py-GC and Py-MS) investigation of Cenomanian-Turonian kerogens

7.1 Introduction

Kerogen comprises the bulk of the organic carbon in the Earth's crust (Tissot & Welte, 1984). It has been defined as the organic material in sedimentary rocks that is insoluble in common organic solvents, alkalis and non-oxidising acids (Durand, 1980; Tissot & Welte, 1984). It is the major organic Component in sediments that is responsible for oil and gas formation. The composition of the kerogen is controlled by a combination of the maceral type, environment of deposition and thermal maturity and it is this composition that determines the type of hydrocarbons that will be produced on maturation (Tissot & Welte, 1984; Larter & Horsfield, 1993).

Van Krevelen (1961) used a H/C v. O/C diagram to distinguish kerogen types. This work was further refined by Forsman (1963) and Tissot *et al.*, (1979) who used atomic H/C and O/C ratios to sub-divide kerogen into four types. These types reflect the origin of the organic matter, the hydrocarbon generation potential, the type of hydrocarbons typically generated and to some extent the sulphur content (Tissot & Welte, 1984). Type I kerogens are typically hydrogen-rich, mainly composed of aliphatic structures and are the equivalent of the alginite maceral group (e.g. as found in the Green River Shale, Messel Oil Shale and the Guttenberg Oil Shale). Type II kerogens are similar to the liptinite or exinite maceral group; they have a lower H/C ratio than Type I kerogens and tend to generate cyclic and acyclic hydrocarbons and higher amounts of aromatic hydrocarbons than Type II kerogens. Immature marine Type II kerogens generally contain the highest abundance of organic sulphur compounds, explained by the reaction of organic matter with H_2S produced by sulphate reducing bacteria (Tissot & Welte, 1984; Sinninghe Damsté *et al.*, 1989b). Typical source rocks with Type II kerogens include the Jet Rock and the Kimmeridge Clay Formation. Classic Type III kerogens are derived from terrestrial plant material; they have a higher aromatic content including abundant phenols, and correspond to the vitrinite maceral group. Type IV kerogens correspond to the inertinite maceral group; they generate mainly polyaromatic hydrocarbon groups, and are generally inert.

Pyrolysis techniques are a widely used method of analysing kerogen to determine its type and chemical composition. Horsfield (1984) defines pyrolysis as the process where solid, liquid and gaseous materials are thermally degraded into

smaller fragments in the absence of oxygen. Bulk flow pyrolysis techniques such as Rock-Eval (e.g. Espitalié *et al.*, 1977) are used for geochemical screening and provide information on kerogen type and hydrocarbon producing potential only. To obtain information about the molecular composition of kerogen pyrolysate, analytical pyrolysis devices are connected to chromatographic systems and detectors such as a flame ionisation detector (FID). Such techniques include pyrolysis-gas chromatography (Py-GC) and pyrolysis-mass spectrometry (Py-MS). A description of the range of commonly used analytical pyrolysis techniques is given in Irwin (1982) and Larter and Douglas (1982).

The pyrolysis techniques described here (Py-GC and Py-MS) are both flash pyrolysis techniques. The Py-GC uses an electrically heated CDS-Platinum coil probe, and the Py-MS uses an inductively heated Curie-point pyrolyser, to heat the samples. These techniques are described in section 2.3.5 and 2.3.7 respectively.

Both Py-GC and the Py-GCMS are commonly used in the characterisation of kerogens (Larter *et al.*, 1977; Larter and Douglas, 1980a; Eglinton *et al.*, 1991). A review of the determination of structural components of kerogen by the use of analytical pyrolysis is given by Larter and Horsfield (1993). This review notes that the dominant species in kerogen pyrolysates are the normal hydrocarbons (alk-1-enes and *n*-alkanes). Other common compounds identified from pyrolysates include alkylbenznes, alkylnapthalenes, phenols, indane and indene (Larter & Horsfield, 1993). Toluene, xylene and higher alkylbenzenes are also commonly found in pyrolysates. Larter (1988) demonstrated that the although these compounds all provide some indication of a samples aromaticity, it is the relative abundance of the xylenes that are considered to provide the most accurate estimate of this parameter.

Eglinton *et al.* (1990) use a ternary diagram based on relative abundances of 1,2 dimethylbenzene, *n*-non-1-ene and 2,3-methylthiophene from pyrolysis-gas chromatography analyses to identify kerogen types. Their work was based on several well defined kerogens from well known deposits and included the Kimmeridge Clay Formation, Marakham Delta and the Green River Formation. They distinguished four categories for kerogen typing: Type I, Type II, Type IIS (representing a sulphur-rich kerogen) and Type III.

Sinninghe Damsté *et al.* (1988, and 1989b) have extensively characterised organic sulphur compounds in pyrolysates. They noted that the organic sulphur content of kerogens varies with kerogen type and is determined by depositional

environment, precursor organisms and thermal evolution. They observed that immature marine Type II kerogens tend to have higher sulphur contents than other kerogen types.

7.1.1 Aim of pyrolysis work

This multidisciplinary study of the Cenomanian-Turonian is an excellent opportunity to observe the effects of differing depositional palaeoenvironments on kerogen pyrolysates and also the different plankton sources and (certain) variations in preservation and maturity. Pyrolysis-gas chromatography and pyrolysis-mass spectrometry are used to investigate the correlation between changes in kerogen pyrolysates with changes observed from other analytical techniques (bulk, molecular and isotope geochemistry and also optical analysis). A set of Cenomanian-Turonian samples was selected from each of the areas studied in this thesis. Seven samples from Oued Bahloul (OB), four samples from Ech Cheid (EC) and the three samples (DOY25, OG16, N18) from the other Tunisian sections made up the set from the Tethyan realm. From the Boreal realm, four samples from Misberg (MQ) and two samples from South Ferriby (SF) were chosen. These samples were selected based on their differing bulk and molecular geochemical properties (Table 7.1), and availability of kerogen for analysis. The Tunisian samples with the exception of Ech Cheid were all AOM dominated, the Ech Cheid section has some phytoclast content. The Ech Cheid and Nebour samples are both poorly preserved and contain degraded marine AOM. The German and UK samples both contain degraded marine-AOM and some phytoclast material.

In order to calibrate the data, and provide comparative end members several well defined kerogens from varying depositional environments were also selected for analysis. These include kerogens from the Jet Rock (Type II), Kimmeridge Clay Formation (Type II), Guttenberg oil shale (Type I), Green River oil shale (fresh-water, Type I), Messel oil shale (freshwater, Type I), and the Pumpherston shale, (Type III; 60% phytoclast material; R. Tyson, 1998, pers. comm.) (Table 7.2). These kerogens had been isolated in several previous NRG studies (not by this author) and so it was necessary to test the several chemical kerogen isolation methods used in order to assess differences in pyrolysates which may have arisen as a result of the different isolation methods. This would also enable chemical composition of pyrolysates of kerogens from this work and those from other studies to be compared.

Kerogen was isolated from samples of Jet Rock following three different procedures outlined in Section 2.4.2. The kerogens from each isolation method were analysed in a group, and several groups were analysed over a few months to observe

Sample No.	S	TOC	Tmax	HI	PI	Carbonate	Pres. scale	C30hop	Ster
OB2	0.12	0.25	426	126	0.18	68	4	0.81	0.36
OB7	0.21	5.00	435	585	0.04	76	5	0.83	0.37
OB18	0.02	0.69	436	199	0.06	75	5	0.83	0.38
OB33	0.13	2.31	434	429	0.04	66	5	0.83	0.37
OB65	0.01	0.30	439	164	0.13	84	5	0.84	0.37
OB72	0.21	3.82	433	470	0.04	73	5	0.83	0.38
OB81	0.17	2.95	433	497	0.05	74	5	0.83	0.38
DOY25	0.02	1.46	431	453	0.04	75	5	0.79	0.19
OG16	0.04	1.66	432	322	0.05	67	4	0.81	0.42
N18	1.92	0.03	444	174	0.05	54	3	0.92	0.44
EC11	0.08	0.93	438	133	0.12	59	3	0.91	0.50
EC13	0.02	0.79	437	152	0.15	58	2	0.86	0.49
EC19	0.08	0.98	437	198	0.14	58	3	0.90	0.49
EC25	0.01	0.51	437	136	0.11	74	3	0.97	0.45
MQ14	1.01	1.79	430	100	0.07	62	4	0.85	0.42
MQ16	0.56	1.07	431	75	0.10	62	4	0.79	0.38
MQ18	0.06	0.23	545	6	0.75	62	3	0.85	0.49
MQ27	0.34	1.13	433	56	0.16	31	3	0.84	0.34
SF6a	-	3.99	-	142	0.03	71	3	-	-
SF6b	-	2.08	-	67	0.05	62	3	-	-

Table 7.1 Comparison table of bulk, molecular and optical characteristics of Cenomanian-Turonian samples used for pyrolysis work. Key: S, total sulphur (%); TOC, Total Organi Carbon (%); Tmax, Rock-Eval pyroysis temperature of maximum hydrocarbon genesis (C°); HI, hydrogen index (mgHC/gTOC), PI, production index (Rock-Eval S1/S1+S2); Carbonate, total carbonate (%); Pres Scale, kerogen preservation scale (Tyson, 1995) C30hop, C30 αβ/αβ+βα hopane; Ster, C29 ααα 20S/20S + R sterane.

Sample	Sample no.	Kerogen Type	Worker	Reference
Jet Rock (Jet)	none	II	P. Barrett	none
Kimmeridge Clay (Kim)	Blackstone Band	II	A. Home	Home, 1992
Messel Oil Shale (Me)	none	I	NRG sample	none
Green River Shale (Gr)	none	I	NRG sample	none
Guttenberg Oil Shale (Gu)	none	I	M. Fowler	Fowler, 1984
Pumpherston Shale (Ps)	SQ36	III/IV	B. Follows	none

Table 7.2 List of other kerogens used in this study and the reference for this work where applicable. All sample are stored at the Department of Fossil Fuels and Environmental Geochemistry, University of Newcastle.

the effect of differences in analytical conditions on pyrolysates as well. The samples were analysed by pyrolysis-gas chromatography (Section 2.3.5) and pyrolysis-gas chromatography-mass spectrometry (for compound identification; Section 2.3.6). Compounds were identified based on their relative retention times (from Py-GC) and mass spectral data (from Py-GC-MS), and peak area and height data were obtained.

The two analytical techniques used (Py-GC and Py-MS) have been shown to be applicable for kerogen typing (e.g. Larter & Senftle, 1985; Eglinton *et al.*, 1990). The pyrolysis-gas chromatography method takes a relatively long time (ca. 1.5 hours) per sample and and requires more data interpretation time compared to pyrolysis-mass spectrometry (Section 2.4.7) which is rapid (ca. 2 minutes per sample). Information can be difficult to extract from the Py-GC traces especially if *n*-alkane and *n*-alkene doublets dominate the pyrolysates, but the Py-MS method gives abundances for each fragment from m/z 51 to m/z 200 almost instantly, which only need to be transferred to a spread-sheet before they can be interpreted. Fragment ions were identified from the literature (Irwin, 1982).

Peak area data from Py-GC (Section 2.3.5) were collected for a range of compounds from all the samples. Compounds identified from Py-GC (given in Appendix 5, Table VI) include: *n*-alkanes, *n*-alkenes, alkylated benzenes, thiophenes, toluene, styrene , xylene, indane, indene, phenols and naphthalenes. Mass fragment data (m/z 51 to 200) was collected for all the samples using Py-MS.

Earlier in this thesis (Sections 4.7.3 and 6.3) aromatic compound and biomarker data were shown from the solvent extractable organic matter (EOM) from the Cenomanian-Turonian samples. These data have been used in this chapter to calculate aromatic maturity parameters (Appendix 4, Table XII). The aromatic compound data were also used to calculate sulphur to non-sulphur compound ratios. Two of these ratios (dibenzothiophene:phenanthrene and methyldibenzothiophene: methylphenanthrene) were used in comparison with the Py-MS data, in order to determine differences in the ratio of sulphur to non-sulphur compounds between the bound and free hydrocarbon fractions.

7. 2 Results

Py-GC peak area data from the samples isolated using three kerogen isolation techniques (Section 2.4.2) were tested using Principal Component Analysis. One hundred and fifty compounds were identified including: *n*-alkanes, *n*-alkenes,

alkylated benzenes, thiophenes, xylenes, phenols, naphthalenes, phenanthrenes and anthracenes. Visual interpretation of the gas chromatograms suggested that there was little effect on the chemical character of pyrolysates from the differing isolation methods. This was confirmed by Principal Component Analysis of the data set. The first Principal Component records 45% of the variance in the data set. Cross plots of the PC1 v. PC2 scores show that the samples from different isolation methods group together but that the groups analysed over a period of approximately two months apart plot separately. This suggested that GC column deterioration was the major control on the data variance and that the effect of differing chemical kerogen isolation techniques on the pyrolysates was minimal. Based on these results it was decided to use the most simple kerogen isolation method (Section 2.4.2, Method 1) for preparation of the Cenomanian-Turonian kerogens to be used in this study.

7.2.1 Results from pyrolysis-gas chromatography (Py-GC)

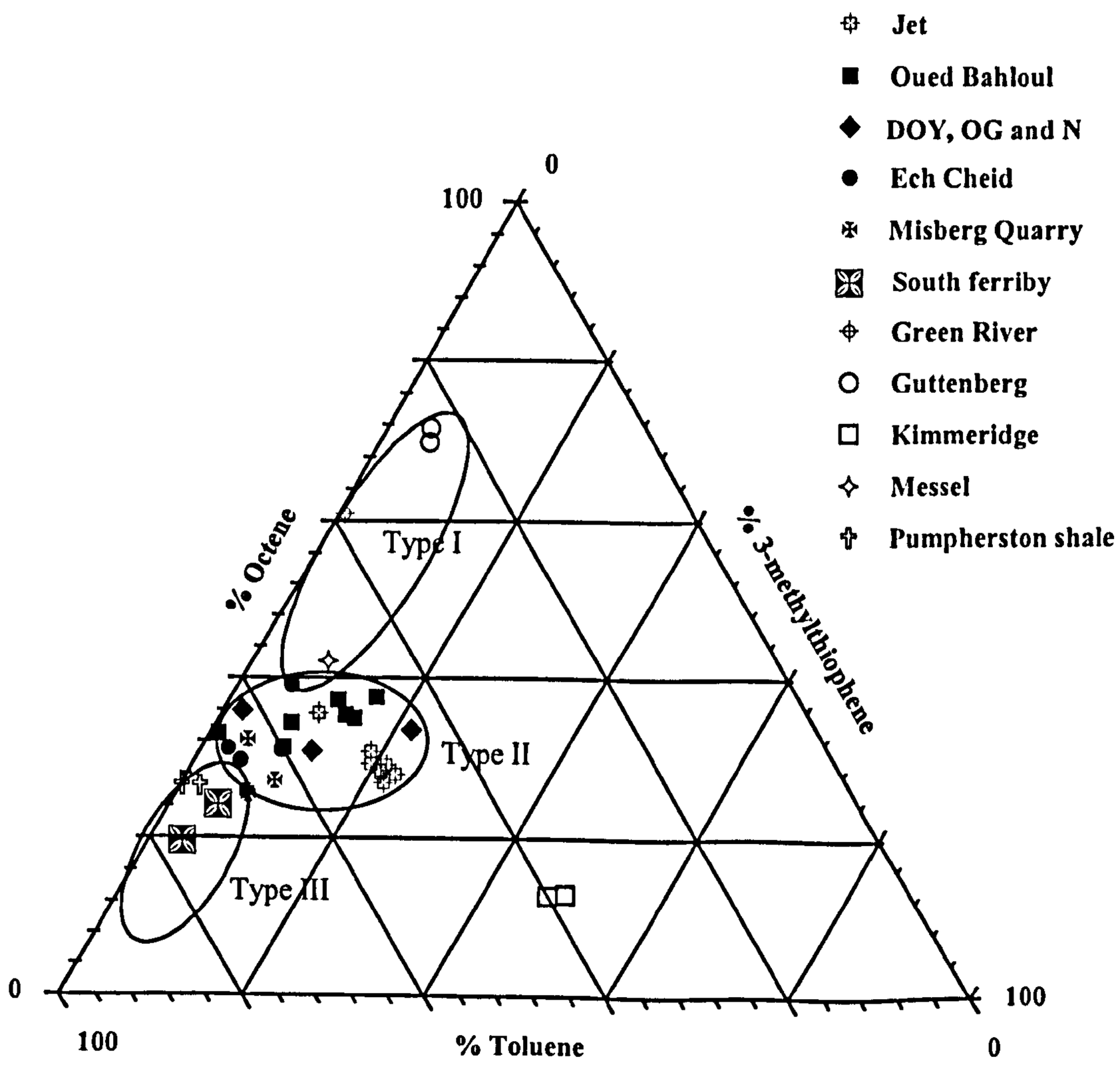

Figure 7.1 Ternary octene-3-methylthiophene-toluene plot (after Eglinton *et al.*, 1990) from Py-GC data for Cenomanian-Turonian samples and for reference samples: Jet, Type II; Green River, Type I (freshwater); Guttenberg Oil Shale, Type I; Kimmeridge Shale, Type II; Messel Oil Shale, Type I (freshwater); Pumpherston, Type III.

A pyrolysate octene:3-methylthiophene:toluene ternary plot for the Cenomanian-Turonian samples and the characterised kerogens based on Eglinton *et al.* (1990) is given in Figure 7.1. The set of well characterised kerogens plot in their appropriate kerogen type zones defined by Eglinton *et al.* (1990) partly because the same kerogens were used. The Type I kerogens plot with relatively higher abundance of *n*-alkenes, and the Type III kerogens with relatively higher abundance of non-sulphur aromatics. The Misberg and South Ferriby samples from the Boreal realm plot with relatively higher amounts of non-sulphur aromatics, in the same area as the Type III Pumpherston Shale. The ternary plot indicates that these two sections have a Type II/III kerogen as was also indicated from bulk geochemical and optical data (Appendix 2). The samples from the Tethyan realm plot with a relatively higher aliphatic component, compared to the Boreal realm samples. The plot indicates that these samples have a Type II kerogen, although three of the four Ech Cheid samples plot closer to the Type III kerogen zone; this was also observed in the bulk geochemical and optical analysis. The organic-rich Oued Bahloul samples (OB33, 7, 81 and 72) and sample DOY25 (Appendix 2) plot with relatively higher amounts of sulphur aromatic compounds, compared to the other Tethyan realm samples. The amount of total sulphur in the Oued Bahloul samples (Appendix 2) corresponds with the plotting order on the ternary diagram (i.e. the samples with highest amounts of total sulphur plot closer to the 3-methylthiophene pole). However, the Dir Oulad Yahia sample has a lower total sulphur content than the other Tunisian samples, but it still plots closest to the 3-methylthiophene pole. This suggests that the environment of deposition for the Dir Oulad Yahia sample may have favoured sulphur incorporation but not pyrite formation.

7.2.2 Results from Pyrolysis-Mass Spectrometry (Py-MS)

Mass chromatograms for each sample are given in Appendix 6. The sulphur to non-sulphur compound ratios from the source rock EOM compound data (from GC-MS analysis) were compared with ratios calculated from Py-MS spectra. The ions m/z 178, 184, 192 and 198 were used as they represent molecular ions for phenanthrene, dibenzothiophene, methylphenanthrenes and methyldibenzothiophenes respectively. Cross plots of the source rock EOM aromatic ratios with the equivalent ratio measured from the pyrolysis-mass spectral data showed a poor correlation (r^2 = 0. 17; Fig. 7. 2). However, when the two anomalous samples (EC11 and SF6a) are removed from the plot the data shows a slightly better correlation ($r^2 = 0.49$). The data between bound and free sulphur and non-sulphur compounds do not compare well. This could be because the nC$_{14}$ alkane shares the same molecular ion (m/z 184)

as dibenzothiophene and the nC_{15} alkane share the same molecular ion (m/z 198) as the methyldibenzothiophenes. Data for the dibenzothiophene and methyldibenzothiophene compounds was not available from Py-GC, as these compounds were lost in background noise of the traces.

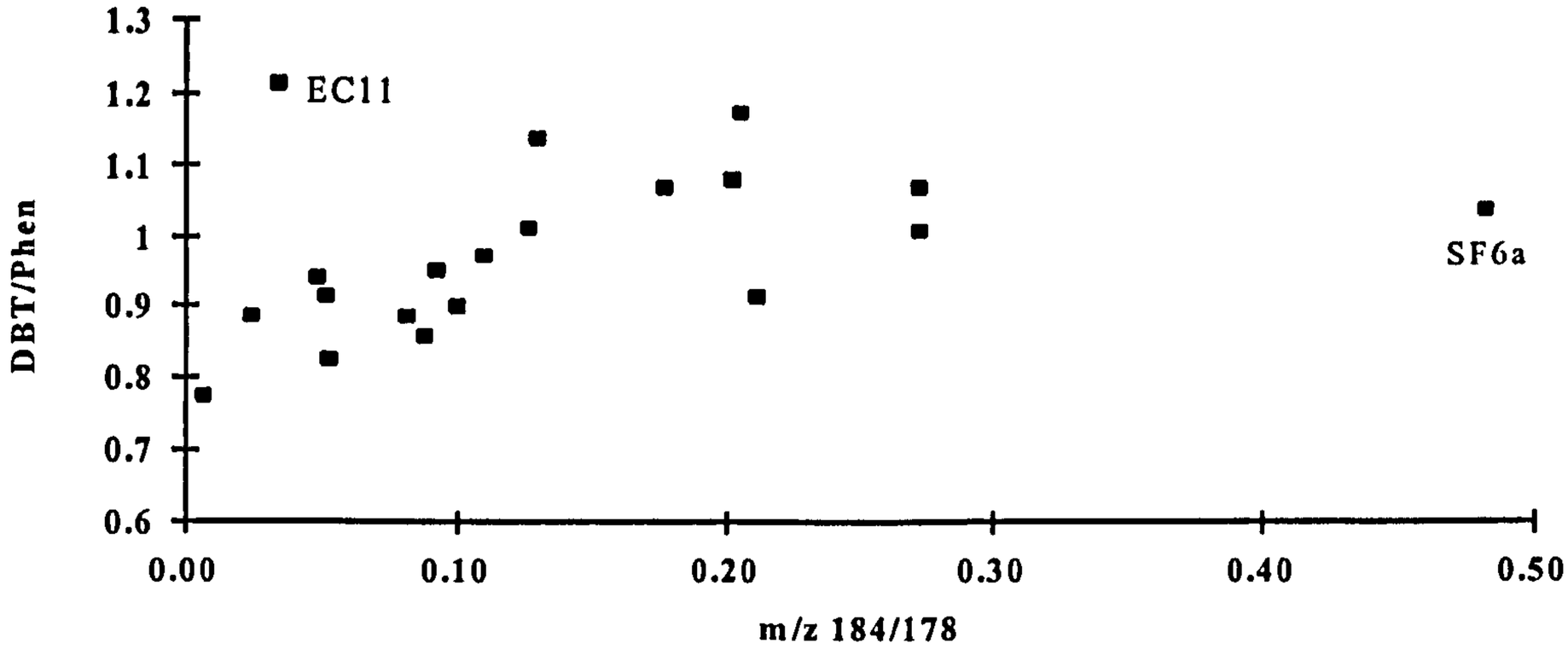

Figure 7.2 Cross-plot of dibenzothiophene/phenanthrene versus m/z 184/178. The data shows some correlation ($r^2 = 0.49$) after the two anomalous points (EC11 and SF6a) are removed. The poor correlation may be caused by interference from *n*-alkanes.

7.3. Principal Component Analysis

Principal Component Analysis was carried out on the Py-GC and Py-MS results, in order to identify trends and relationships within the data. The Py-GC data included all 61 compounds identified for all the samples analysed (Appendix 5, Table VI). Mass fragment data (m/z 51 to 200) for each of the samples analysed was used in the Principal Component Analysis. The data from these analyses were split into six groups for Principal Component Analysis:

Group 1: PCA of Cenomanian-Turonian data from Py-GC analyses.

Group 2: PCA of Cenomanian-Turonian and comparison kerogen data from Py-GC analyses.

Group 3: PCA of Cenomanian-Turonian data from Py-MS analyses.

Group 4: PCA of Cenomanian-Turonian and comparison kerogen data from Py-MS analyses.

Group 5: PCA of Cenomanian-Turonian data from combined Py-GC and Py-MS analyses.

Group 6: PCA of Cenomanian-Turonian and comparison kerogen data from combined Py-GC and Py-MS analyses.

The loadings and scores from each PCA group are given in Tables 7.3 and 7.4 respectively.

PCA group	%	Loadings (positive axis)	Loadings (negative axis)
1. C-T Py-GC data	**51**		
PC1	**26**	**alkanes, alkenes, thophenes**	**benzenes, + *other aromatic compounds***
PC2	**15**	**nC14+ alkanes, napthalenes**	**nC6 to nC13 alkenes, alkylpheonl, some thiophenes**
PC3	**10**	**alkylthiophenes, Indan+**	**alkenes, thiophene, napthalenes**
2. C-T + ker Py-GC data	**55**		
PC1	**23**	**alkenes, alkanes,**	**benzenes, thiophenes, aromatics**
PC2	**18**	**nC12+ alkanes,**	**alkenes, nC6 to nC11 alkanes, thiophenes**
PC3	**13**	**nC11+ alkenes, thiophenes, napthalene**	**nC9 to nC14 alkanes, benzenes, Toluene**
3. C-T Py-MS data	**86**		
PC1	**49**	**majority of fragment ions**	**m/z 55, 60, 61, 64, 65, 76, 149, 150**
PC2	**32**	**m/z 78, 92, 106, 120, 94, 108, 132, 146**	**m/z 84, 86, 98, 100, 112, 114, 126**
PC3	**6**	**m/z 55, 56, 67, 76, 160, 186, 198**	**m/z 103, 104, 105, 87, 73, 75**
4. C-T + ker Py-MS data	**80**		
PC1	**47**	**majority of fragment ions**	**m/z 55 to 58, 64, 69 to 71, *73, 83, 84, 149, 150***
PC2	**19**	**m/z 78, 92, 106, 120**	**m/z 84, 86, 98, 100, 112, 114, 126**
PC3	**14**	**m/z 60 to 62, 74, 75, 85 to 90, 102, 160, 186**	**m/z 67, 80, 94, 108, 122, 136, *164***
5. C-T Py-GC + Py-MS data	**74**		
PC1	**38**	**alkanes, thiophenes, majority of fragment ions**	**nC6 to nC9 alkenes, napthalene, m/z 55, 60 to 66, 73 to 76**
PC2	**28**	**benzenes, aromatics, m/z 78, 92, 106, 120, 62**	**alkanes, alkenes, thiophenes, m/z 84, 86, 98, 100, 112, 114, 126**
PC3	**7**	**indan, toluene, m/z 87, 103, 104, 105**	**alkenes, alkanes, m/z 67, 55, 160**
6. C-T + ker Py-GC + Py-MS data	**67**		
PC1	**37**	**aromatics, majority of fragment ions**	**alkanes, alkenes, m/z 55 to 58, 64, 68 to 73, 83, 84**
PC2	**17**	**alkanes, alkenes, m/z 57, 71, 84, 98, 112, 126**	**benzenes, *aromatics*, 63 to 66, 92, 106, 120, 118**
PC3	**13**	**alkenes, m/z 53, 54, 80, 94, 108, 122, 136, 147**	**nC11+ alkanes, m/z 57 to 62, 74, 75, 85, 87, 102, 114, 160, 186**

Table 7. 3 Loadings data for Principal Component Analysis of pyrolysis data. Key: C-T, Cenomanian-Turonian; Py-GC, pyrolysis gas chromatography; PC, Principal Component; ker, well defined kerogens; Py-MS, pyrolysis-mass spectrometry; %, cumulative percentage of first three principal Components (in bold font), percentage of total variance for individual Principal Components (in plain font). Loadings data: 75-100% of greatest data point (bold font); 25 to 75% of greatest data point (plain font); <25% of greatest data point (italic font).

PCA group	%	Scores (positive axis)	Scores (negative axis)
1. C-T Py-GC data	**51**		
PC1	26	OB, DOY, OG, EC (11 & 19)	MQ, SF, N, EC (13 &25)
PC2	15	OB2, EC, OG, MQ (14, 16, 18)	OB, DOY, N, SF
PC3	10	DOY, OG, EC, SF	OB2, OB18, MQ27
2. C-T + ker Py-GC data	**55**		
PC1	23	OB, OB2, DOY, OG, EC, MQ27, GR, Gu, Me	Jet, MQ (14, 16, 18), SF, Kim, Ps
PC2	18	EC, OB, DOY, OG, MQ, SF, Ps	Jet, OB (18, 65), N, Gu, Kim
PC3	13	DOY, Kim, OB, OG, EC, Me	Ps, Jet, N, EC13, MQ, SF, Gr, Gu
3. C-T Py-MS data	**86**		
PC1	49	DOY, OB, OG, SF	OB (2, 8), N, EC, MQ
PC2	32	MQ, SF, OB65, EC13	OB, DOY, OG, N, EC
PC3	6	OB, DOY, OG, MQ, SF	EC13, EC 19 and 25
4. C-T + ker Py-MS data	**80**		
PC1	47	Kim, OB (7, 33, 65, 81), DOY, OG, SF	Jet, OB (2, 18, 72), N, EC, MQ, Gr, Gu, Me, Ps
PC2	19	Jet, OB65, EC13, MQ, SF, Kim, Me	OB, DOY, OG, N, EC, GR, Gu, Ps
PC3	14	Ps (dom), Kim, Me, MQ	Jet, OB, OG, N, EC, SF, GR, Gu
5. C-T Py-GC + Py-MS data	**74**		
PC1	38	DOY, OB, SF	OB (2, 18), MQ, EC
PC2	28	MQ, SF, EC13, OB65	OB, OG, N, EC
PC3	7	EC13, EC25	OB, DOY, EC (11, 19), MQ, SF
6. C-T + ker Py-GC + Py-MS data	**67**		
PC1	37	Kim, SF, DOY, OG, OB (7, 33, 65, 81) EC13	Gu, Me, OB (2, 18, 72), EC, MQ, Ps
PC2	17	OB, DOY, OG, N, EC, Gr, Gu	MQ, SF, Jet, Kim, Ps
PC3	13	Jet, OB, DOY, OG, N, SF, GR, Gu	Ps (dom), Kim, EC (11, 19), Me

Table 7.4 Scores data for Principal Component Analysis of pyrolysis data. Key: C-T, Cenomanian-Turonian; Py-GC, pyrolysis gas chromatography; PC, Principal Component; ker, well defined kerogens; Py-MS, pyrolysis-mass spectrometry; %, cumulative percentage of first three principal Components (in bold font), percentage of total variance for individual Principal Components (plain font).

7.3.1 Group 1. Cenomanian-Turonian Py-GC data

The first Principal Component (PC1) is controlled by the relative amounts of aliphatic hydrocarbons and sulphur aromatic (thiophene) compounds compared to other aromatic compounds. A cross plot of the scores against hydrogen indices for the samples shows a good degree of correlation (Fig. 7.3; $r^2 = 0.64$). This suggests that this Principal Component is controlled by organic matter Type. The samples with a distinct Type II kerogen (Oued Bahloul, Dir Oulad Yahia, Oued Gsab and some of the Ech Cheid) plot on the positive axis, whereas the samples with a Type II/III kerogen (Nebour some Ech Cheid, but especially the Misberg and South Ferriby samples) plot on the negative axis (Fig. 7.4). The scores showed a poor correlation with maturity parameters, the strongest correlation was with Aromatic Steroid Ratio 1 (Appendix 4, Table XII; Fig. 7.5; $r^2 = 0.49$). This shows that the slight maturity differences between the sections is not overprinting the data set or strongly affecting this Principal Component. This Principal Component separates the southern Tunisian sections from the northern Tunisian sections as was seen in the previous chapters. The difference in kerogen type is also noted between the Boreal and Tethyan realms. It is interesting to note that the thiophenes plot on the same axis as the alkanes and alkenes for this PC and may reflect the carbonate nature of the environments (cf. Waldo *et al.*, 1991); this will be discussed in further detail later (Section 7.3.5)

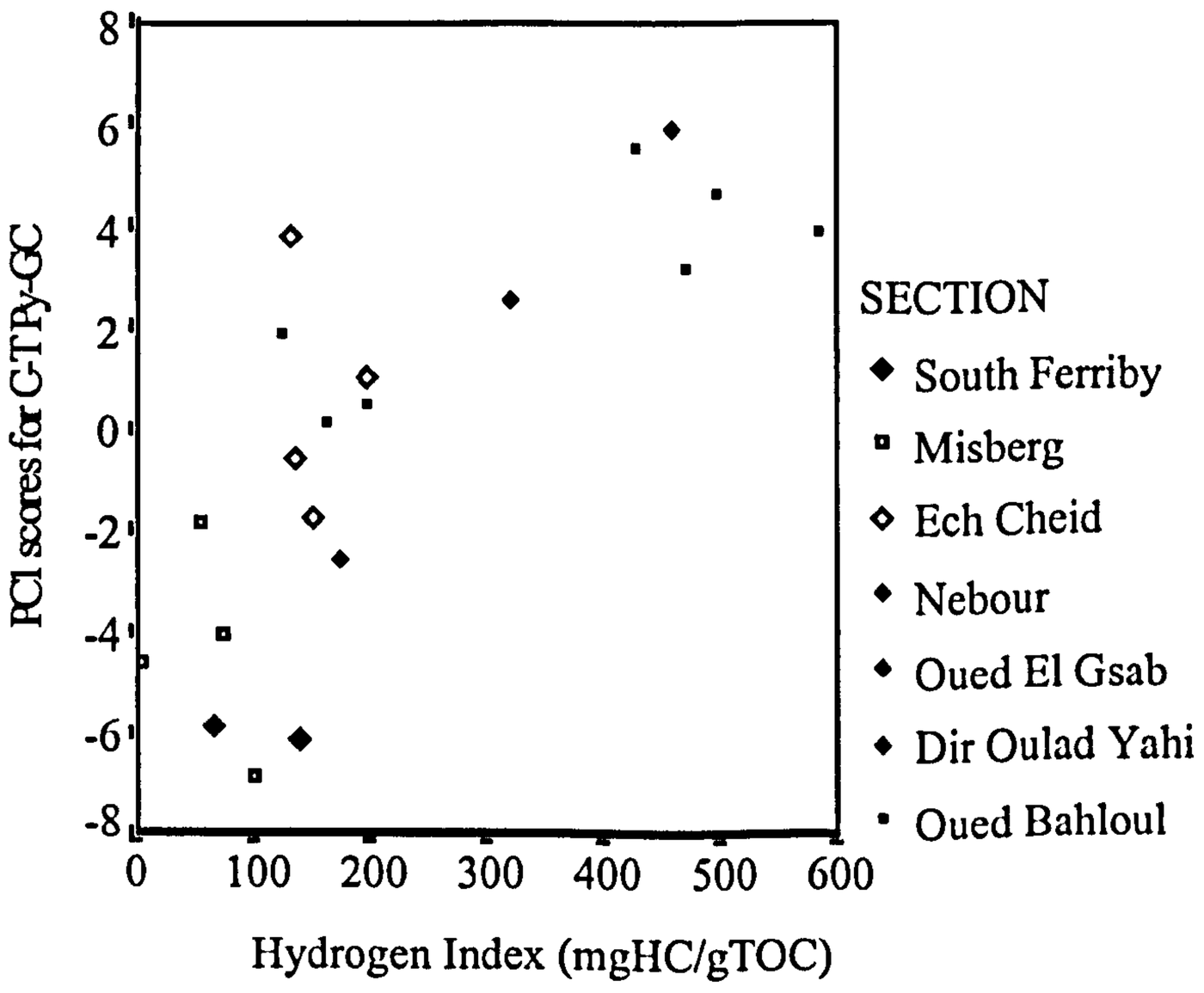

Figure 7.3 Cross plot of PC1 scores data from the Cenomanian-Turonian Py-GC samples versus hydrogen index. The parameters show a good correlation ($r^2 = 0.64$).

Principal Component 2 reflects the ratio of short chain alkanes versus long chain alkanes. The scores suggest that this is partly correlated with the organic richness (TOC) of the samples; however the correlation coefficient with TOC is poor ($r^2 = 0.33$). It is unclear what controls this Principal Component, as the scores show little correlation with any optical, bulk or molecular geochemical parameter.

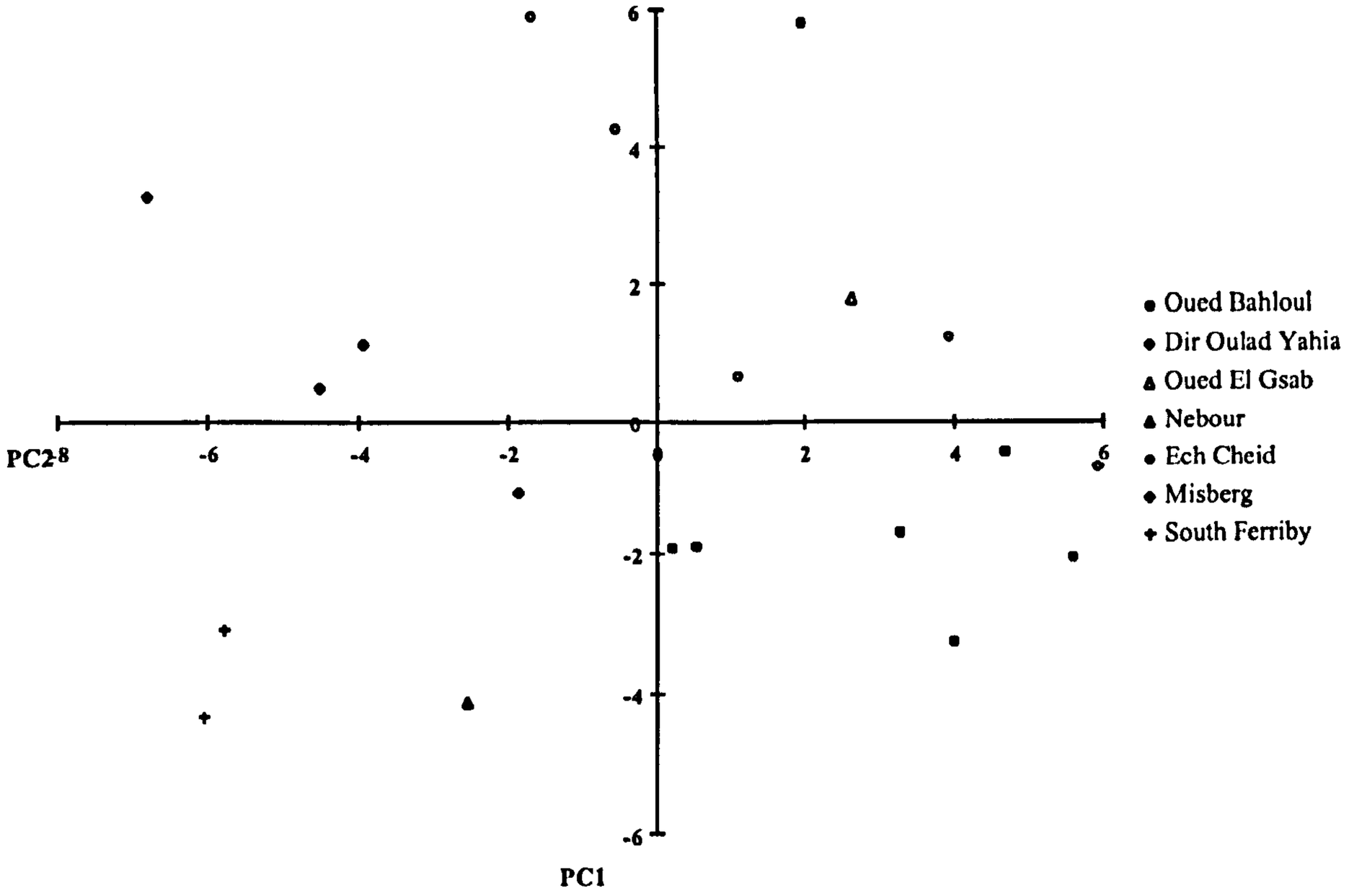

Figure 7.4 Cross plot of PC1 versus PC2 scores data for the Group1 Py-GC data.

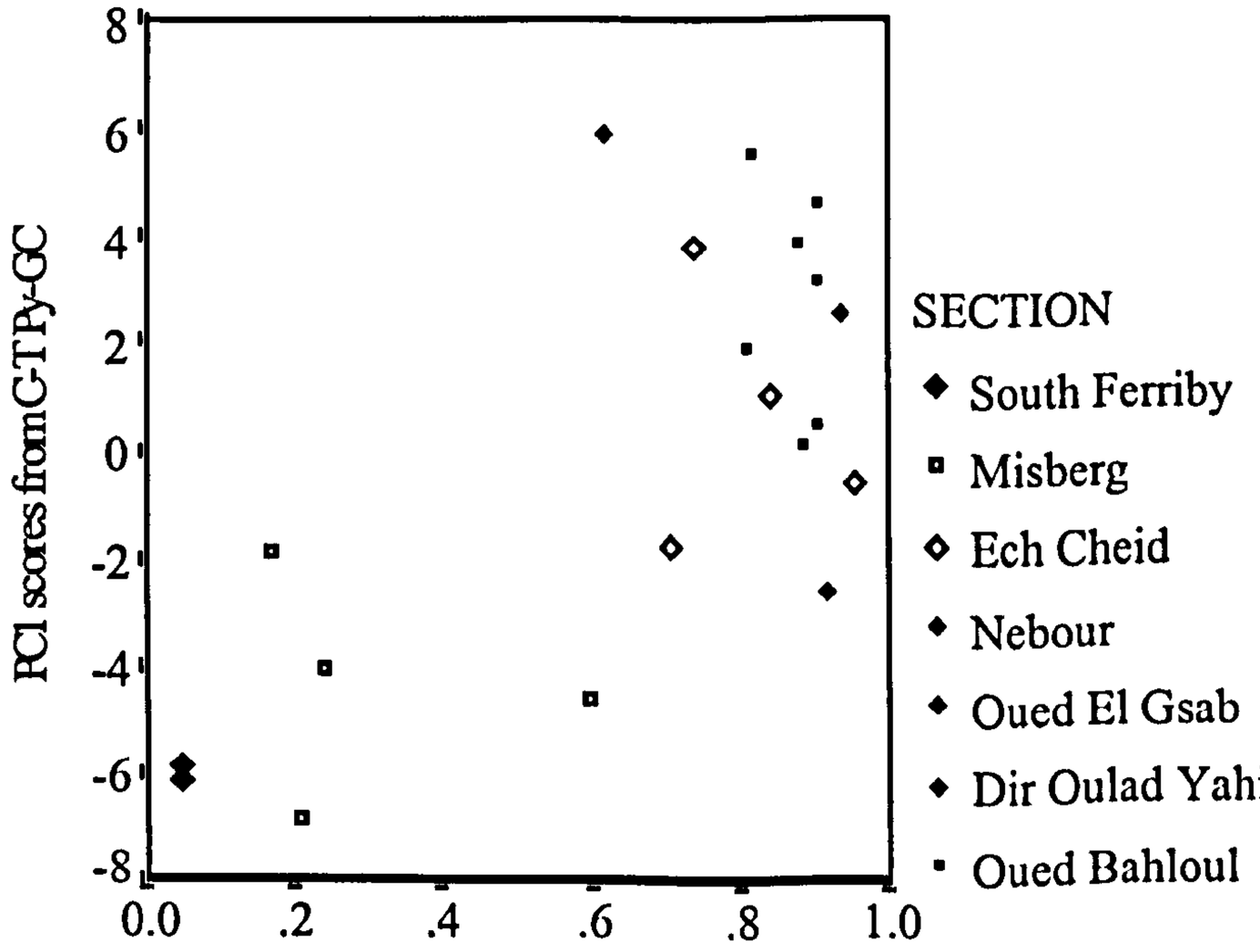

Figure 7.5 Cross plot of PC1 scores data from the Cenomanian-Turonian Py-GC samples versus Aromatic Steroid Ratio 1. The parameters show some correlation ($r^2 = 0.49$).

The third Principal Component may be partly controlled by the aliphatic:aromatic signature of the kerogens, as the majority of the aliphatic hydrocarbons plot on the negative axis and the majority of the aromatic compounds plot on the positive axis. The negative axis of the scores is dominated by OB2, whereas the DOY25, OG18, Ech Cheid and the South Ferriby samples plot on the positive axis. Although the samples may be controlled by the aliphatic:aromatic nature of their kerogens there is no correlation of the scores with hydrogen index.

7.3.2 Group 2. Cenomanian-Turonian and comparison kerogen Py-GC data

The first Principal Component reflects the aliphatic:aromatic signature of the kerogens as was noted in Group1 PC1 (Section 7.3.1); however, the thiophenes plot with the other aromatic compounds for this PC. In the first PC from Group 1 the thiophene compounds plotted with the aliphatic hydrocarbons; however, for Group 2 PC1 they plot on the same axis as the aromatic compounds. This is likely to be due to larger variances in sulphur contents in the end member kerogens (e.g. Kimmeridge Clay Formation) as was seen in Figure 7.1, which is likely to overprint any control by the carbonate environment for the Cenomanian-Turonian samples that was suggested from the previous PCA data set.

The scores for PC1 indicate that the Kimmeridge Clay and the Pumpherston shale samples are the richest in aromatic compounds and the Green River, Guttenberg, and Messel Oil Shale are richer in aliphatic compounds (Fig. 7.6). In relation to this, the Tunisian samples plot with the relatively aliphatic-rich kerogens while the Misberg and South Ferriby samples plot with relatively aromatic richer kerogens. The scores show a poor correlation with hydrogen index, even after the apparently anomalous sample OB2 is removed ($r^2 = 0.32$). The reason why this occurs is unclear, but it suggests that hydrogen index is controlled by more than the aliphatic:aromatic ratio of the kerogen for this data set. The scores show a slightly better correlation with Aromatic Steroid Ratio 1 ($r^2 = 0.43$), which suggests that an overprint of maturity differences could be the reason for the poor correlation with hydrogen index.

Principal Component 2 appears to reflect changes in the ratio of short chain length to long chain length aliphatic hydrocarbon compounds. The scores show that the Pumpherston shale (SQ36; Table 7.2) plots strongly on the postive axis, whereas the Kimmeridge clay samples plot on the negative axis (Fig. 7.6); the Tethyan samples plot on the positive axis and the Boreal samples on the negative. The scores

show no correlation with any bulk geochemical parameters, and the interpretation of this PC is unclear. However, as the Pumpherton shale dominates the positive axis it is clear that the dominant Type III nature of the kerogen of this sample is controlling the data set. As noted earlier, the grouping of the Boreal kerogens on the negative suggests that these sample exhibit some Type III characteristics.

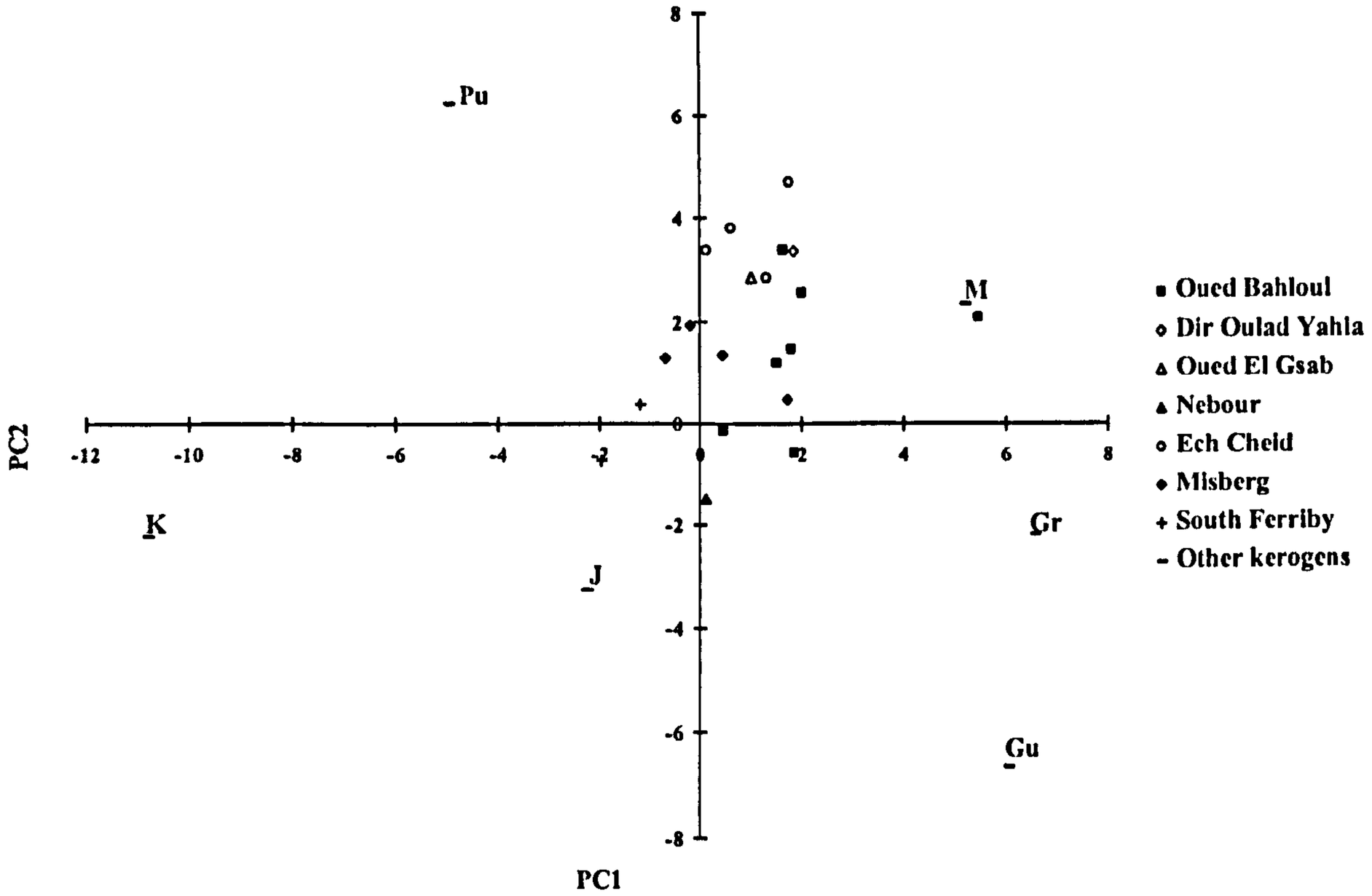

Figure 7.6 Cross plot of PC1 versus PC2 scores data for the Group 2 Py-GC data. Key: J, Jet Rock; K, Kimmeridge Clay, Gu, Guttenberg; Gr, Green River, M, Messel; Pu, Pumpherston.

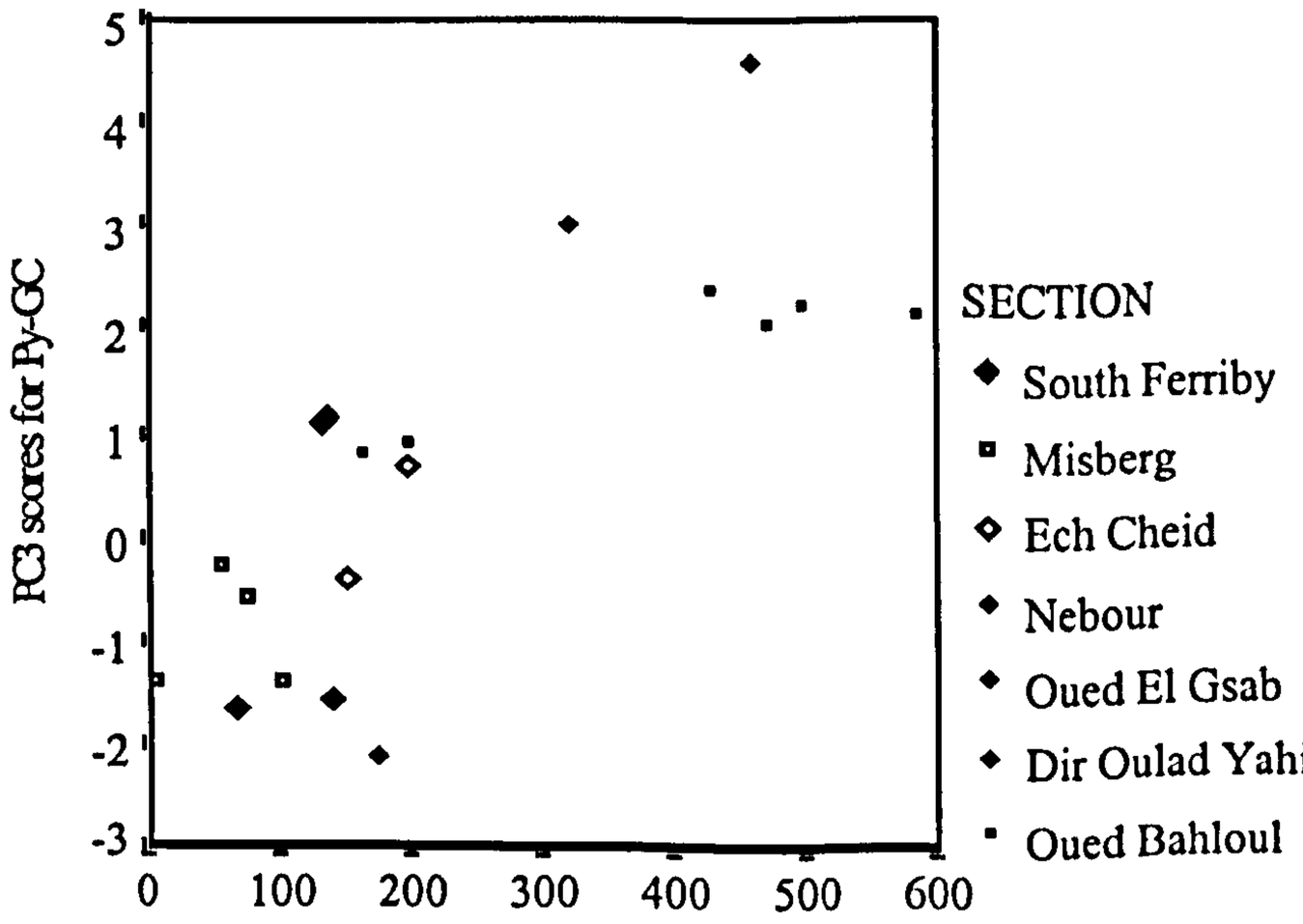

Figure 7.7 A cross plot showing PC3 scores from combined Py-GC versus hydrogen index. The parameters show a good correlation ($r^2 = 0.62$).

The third Principal Component identifies the relationship of sulphur compounds and long chain alkenes with alkanes, alkylbenzenes and toluene. The scores shows that DOY25 and Kimmeridge plot strongly on the positive axis and that the Pumpherston shale plots strongly on the negative axis. The scores shows a good correlation with hydrogen index (Fig. 7.7; $r^2 = 0.62$) and a poor correlation with the Aromatic Steroid Ratio 2 maturity parameter ($r^2 = 0.38$). The scores also show a good correlation with Group 1, PC1 scores (Fig. 7.8; $r^2 = 0.83$). It was observed from the ternary diagram (Fig. 7.1) that Kimmeridge and DOY25 samples plotted with relatively high thiophene contents, and that the Pumpherston shale contained a very low thiophene content. The loadings suggest that the thiophenes compounds are important in this Principal Component (Section 7.3.5).

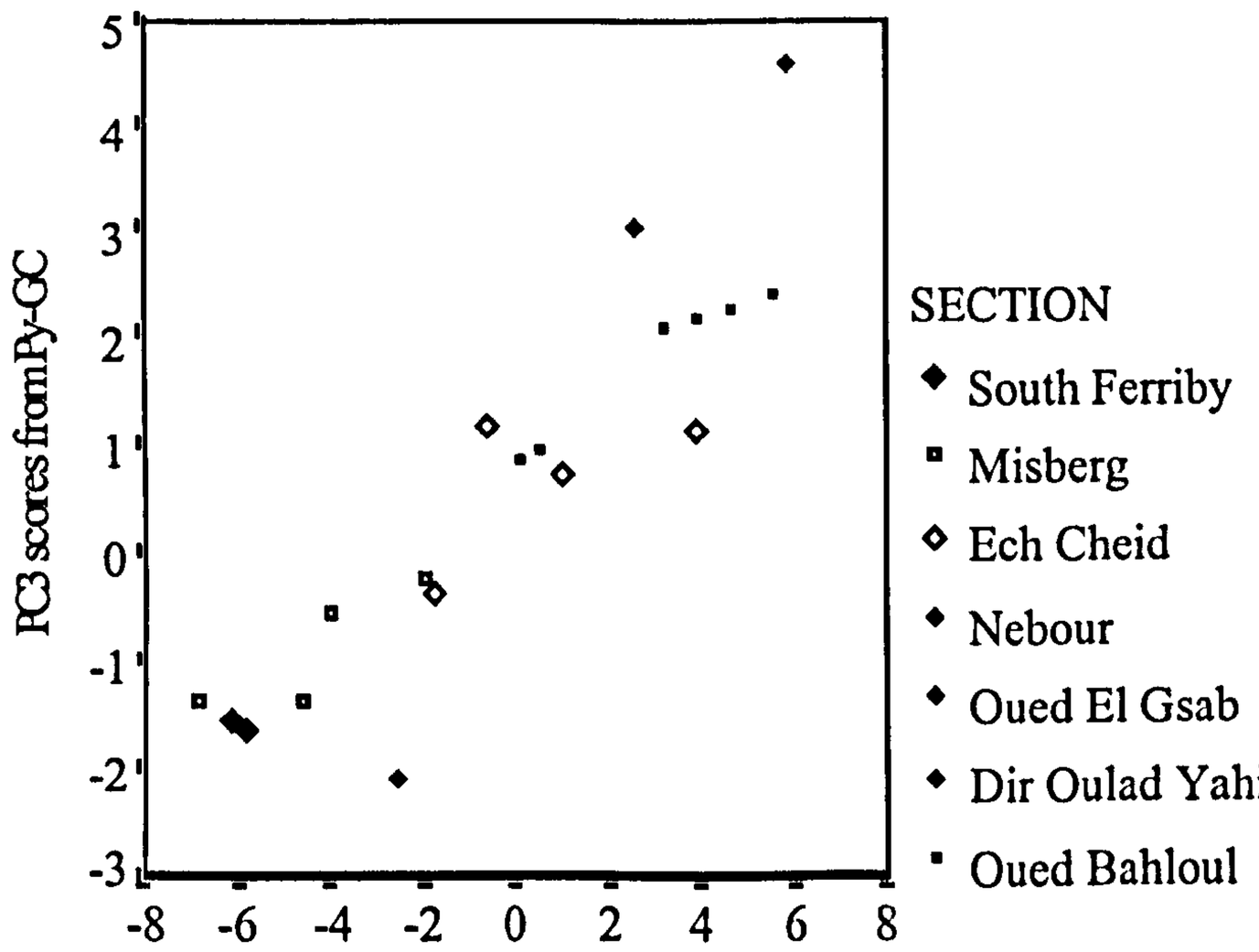

Figure 7.8 A cross plot of PC3 scores from combined Py-GC versus PC1 scores from C-T Py-GC. The parameters show a good correlation ($r^2 = 0.83$) suggesting that they are controlled by the same factors.

7.3.3 Group 3. Cenomanian-Turonian Py-MS data

The first Principal Component controls the majority of the variance in the Cenomanian-Turonian Py-MS Group 3 data set (49%). It is possible that this Principal Component is controlled by the relative amounts of the most common fragment ions of the alkenes, alkanes and other common low fragments (e.g. m/z 60, COS; m/z 64, SO_2; m/z 76, CS_2); m/z 149 and 150 are observed on the same axis as the low m/z value fragments and indicates contamination from phthalates. The changes in relative abundance in low m/z value fragment ions between the samples

can be seen from the Py-MS fragmentograms (Appendix 6). The scores show that the samples with higher relative amounts of low m/z value fragments are samples OB2, OB18, N18 the Ech Cheid and the Misberg sections (Fig. 7.9). These samples generally have the lowest TOC and hydrogen index values of the sample set, although a poor correlation was seen between the scores and hydrogen index ($r^2 = 0.37$). Metcalf *et al.* (1987) and Meuzelaar *et al.* (1984) noted that inertinite macerals tend to produce more SO_2 on pyrolysis. It is unlikely that the samples which show a higher relative abundance of SO_2 are dominated by inertinite, but these samples contain relatively more phytoclast and degraded marine AOM material than the other samples (Appendix 3). The abundance of SO_2 in coal pyrolysates has been demonstrated to correlate with pyrite content (Meuzelaar *et al.*, 1984); however, as the Misberg samples contain no pyrite (Appendix 3, Table 1), it is unlikely that this is the source of the SO_2 in these samples. The relative abundance of these low value fragment ions does not appear to be conclusively source or environment specific, an observation also noted by Skjevrak (1997). It is possible that this PC reflects the hydrocarbon yield of the samples and the loadings data differentiates between the hydrocarbons on the positive axis and the non-hydrocarbons on the negative axis.

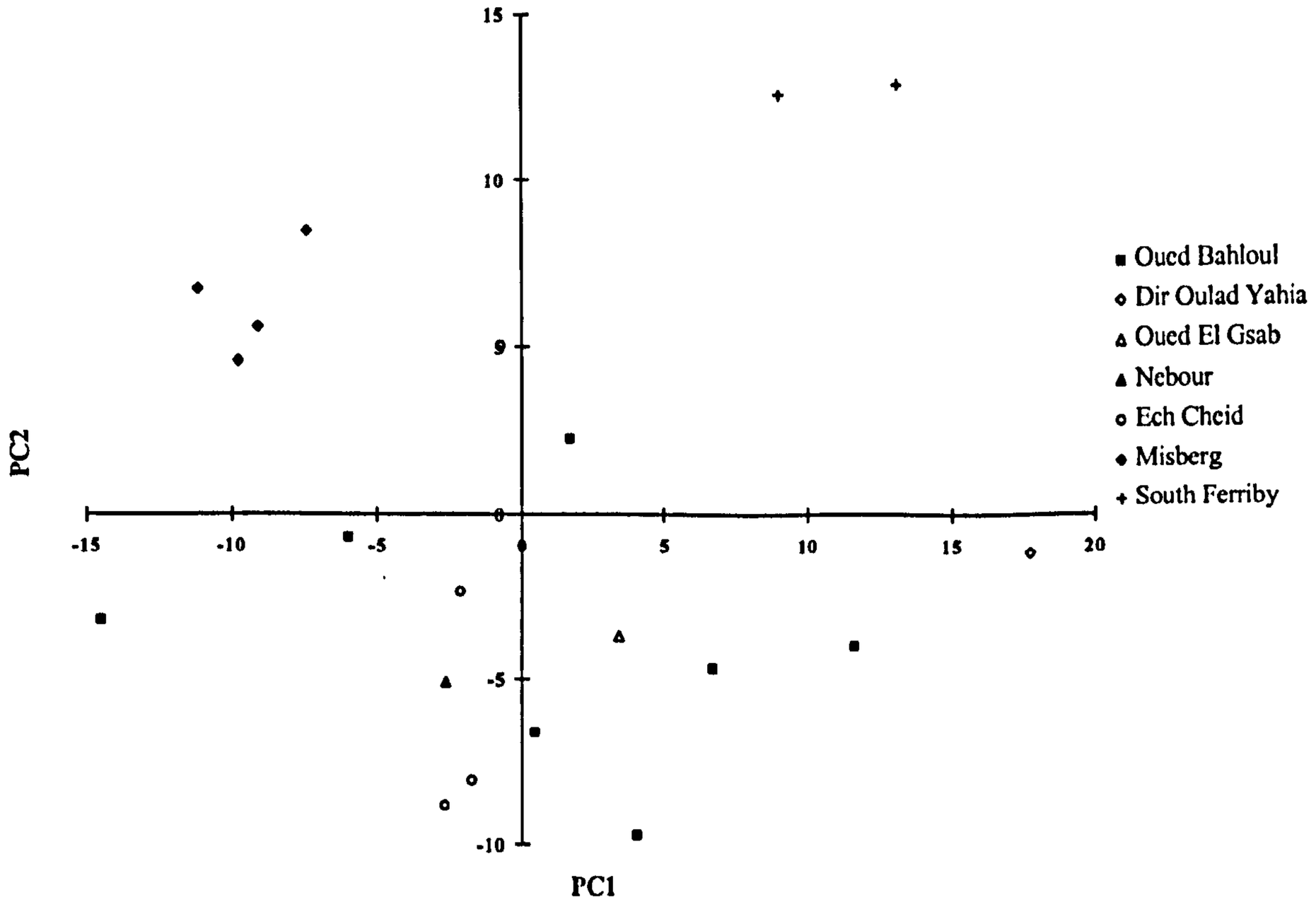

Figure 7.9 Cross plot of PC1 versus PC2 scores data for the Group3 Py-MS data.

The second Principal Component is controlled by the relative amounts of aliphatic (alkanes and alkenes) and aromatic (alkylbenzenes) compounds in the kerogen of these samples. The scores suggest that these samples from the Boreal realm are relatively richer in aromatic compounds (Fig. 7.9), a finding that was also

noted from the Py-GC analyses (Group 1, PC1; Section 7.3.1) and the scores from these two Principal Components show a good correlation (Fig. 7.10; $r^2 = 0.67$). There is an excellent correlation (Fig. 7.11; $r^2 = 0.96$) of the scores with a ratio of the sum of the alkylbenzene fragment series over the sum of alkene fragment series (Σm/z 78, 92, 106, 120, 133, 147/Σm/z 70, 84, 98, 112, 126, 140); the sub-groups for the individual sections also show a good correlation. Although this Principal Component characterises the aliphatic versus aromatic nature of the kerogens, there is only a poor correlation of the scores with hydrogen index (Fig. 7.12; $r^2 = 0.34$).

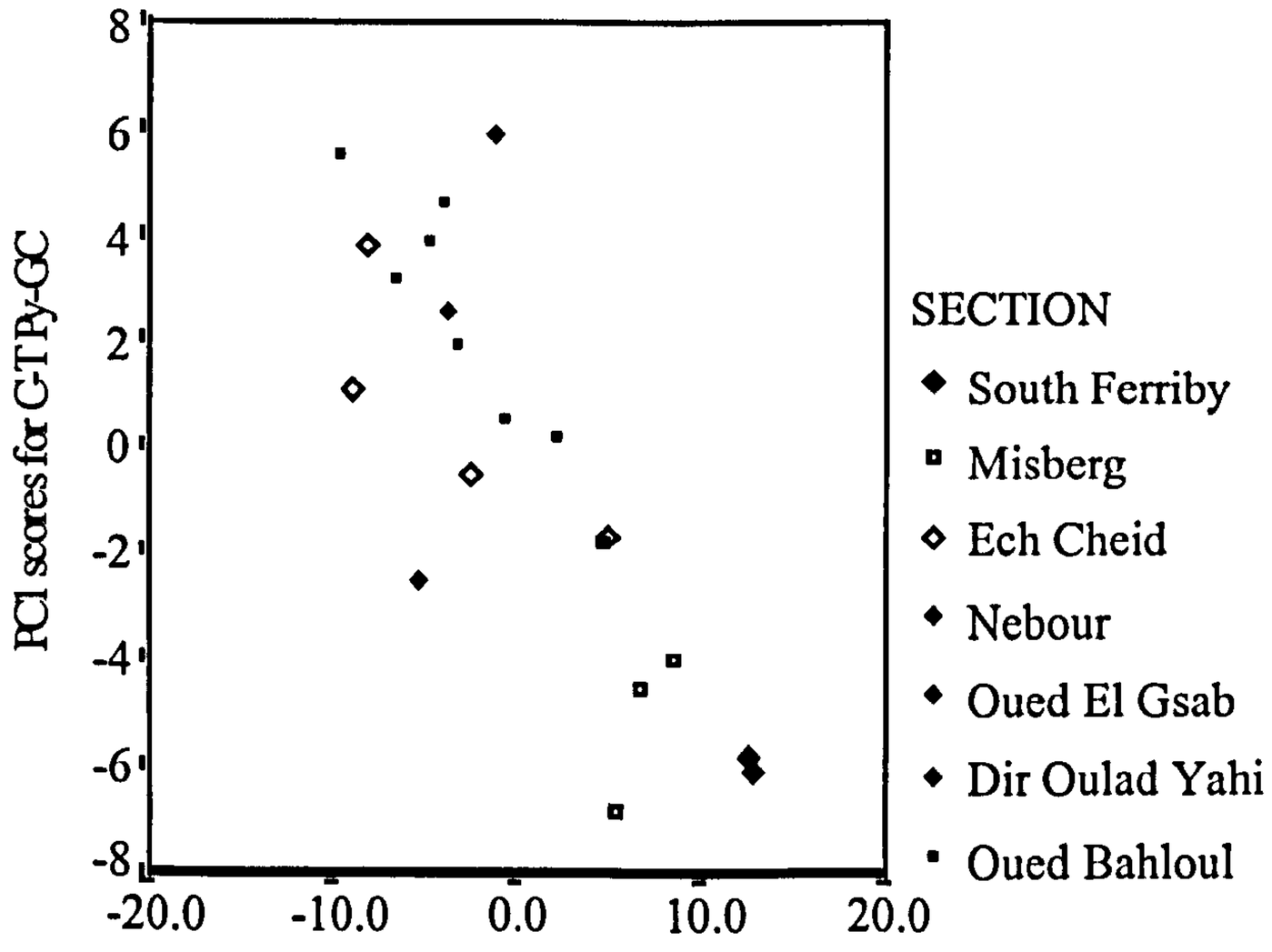

Figure 7.10 Cross plot of PC1 scores from Cenomanian-Turonian Py-GC versus PC2 scores from Cenomanian-Turonian Py-MS. The parameters show a good correlation ($r^2 = 0.67$).

It is unclear from the loadings what controls the third Principal Component, but styrene fragment ions (m/z 103, 104, 105) dominate the negative axis. The scores show that the Ech Cheid samples EC13, 19 and 25 plot dominantly on the negative axis. Styrene is a compound found in natural rubber, and its presence in the Ech Cheid samples may suggest a specific plant source, but this is unlikely. The possibility that these compounds came from the O-ring seal (Section 2.3.7) was dismissed after consultation with the manufacturers. Further consultation with Mr C Hetherington of the Biomedical Mass-Spectrometry unit, University of Newcastle, ruled out the possibility of contamination from disposable plastic inoculating needles used by other workers on the instrument, or as a result of the cleaning process on the glass pyrolysis tubes. It is unclear why these fragment ions were found to dominate in

three of the Ech Cheid samples, but the above suggests that this result is genuine and not a result of other factors introduced during the analysis.

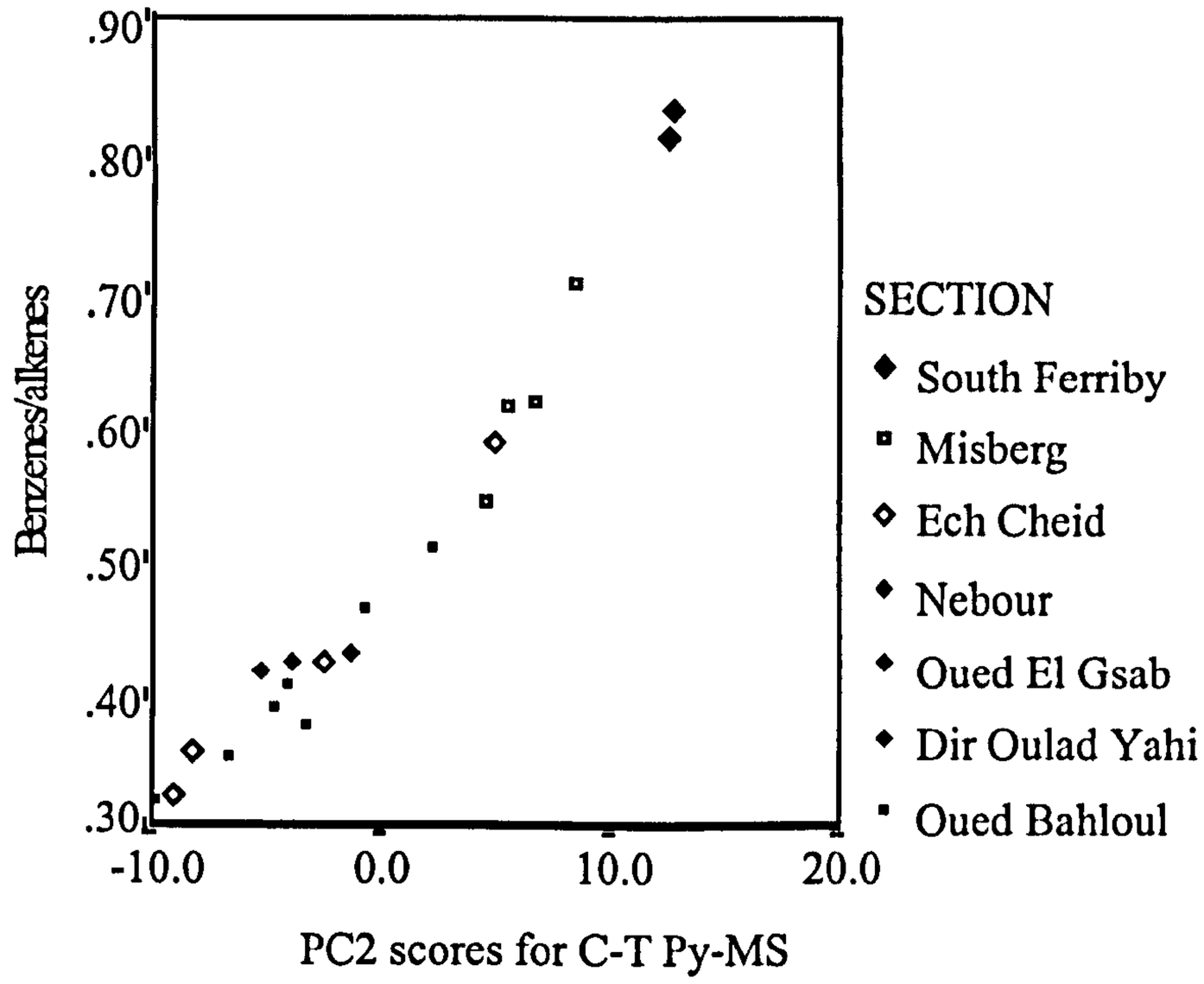

Figure 7.11 A cross plot of PC2 score from Cenomanian-Turonian Py-MS versus a benzene/alkene ratio calculated from the m/z fragment series for these compounds. There is an excellent correlation ($r^2 = 0.96$) between the parameters.

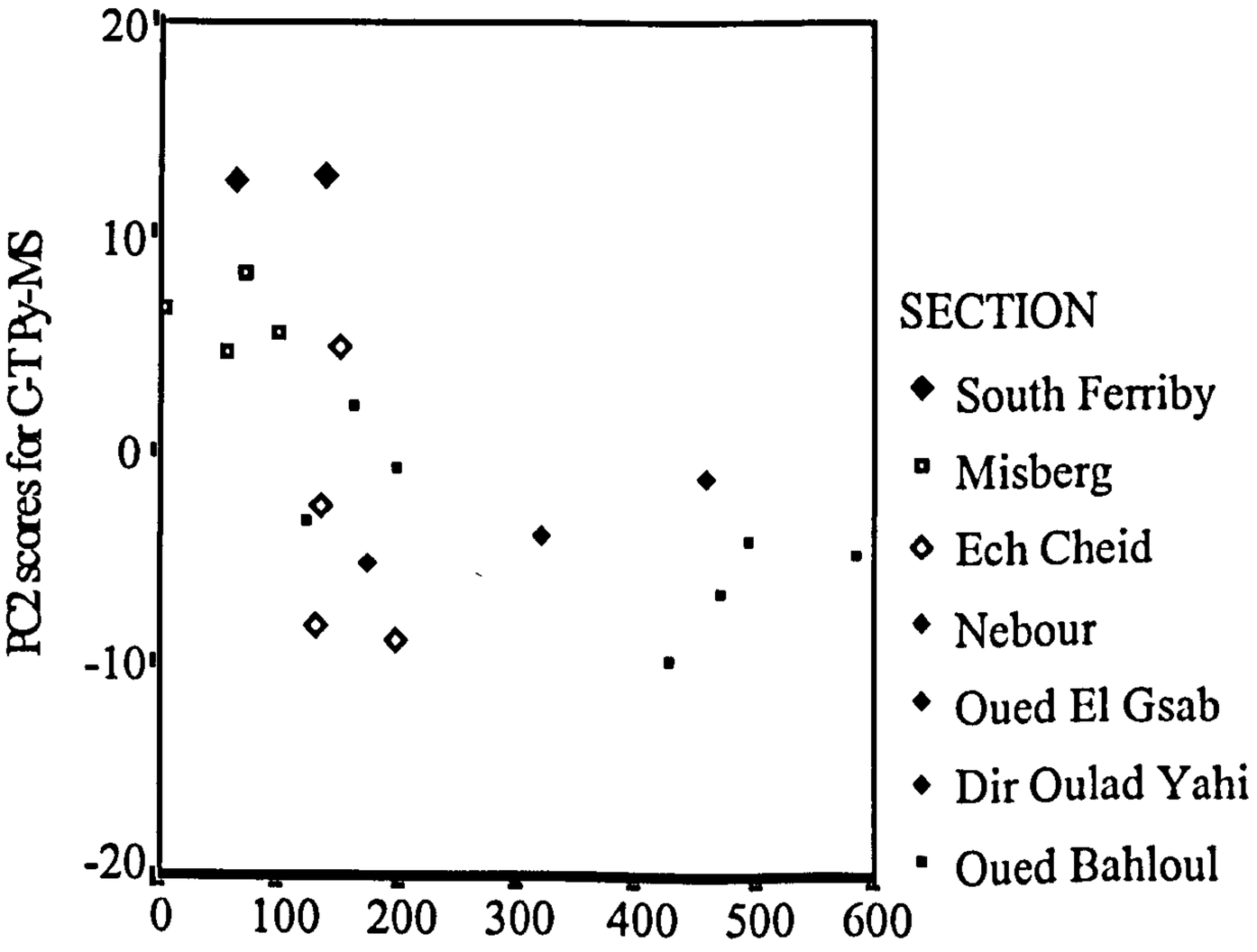

Figure 7.12 Cross plot of PC2 scores data from the Cenomanian-Turonian Py-MS samples versus hydrogen index. The parameters show a poor correlation ($r^2 = 0.34$)

7.3.4 Group 4. Cenomanian-Turonian and characterised kerogen Py-MS data

The first Principal Component again records the majority of the variance (47%) in the data set, and it identifies a similar trend as that seen in PC1 Group 3 (7.3.3); i.e. it reflects the relative changes in abundance of short chain *n*-alkane and *n*-alkene fragments between the samples (Fig. 7.13). The influence of the m/z 64 (SO_2) fragment is not as apparent in this PC. The scores show a very good correlation (r^2 = 0. 97) with the scores from PC1 Group 3, but it is still unclear what controls this relative abundance of *n*-alkene and *n*-alkane fragments between the samples.

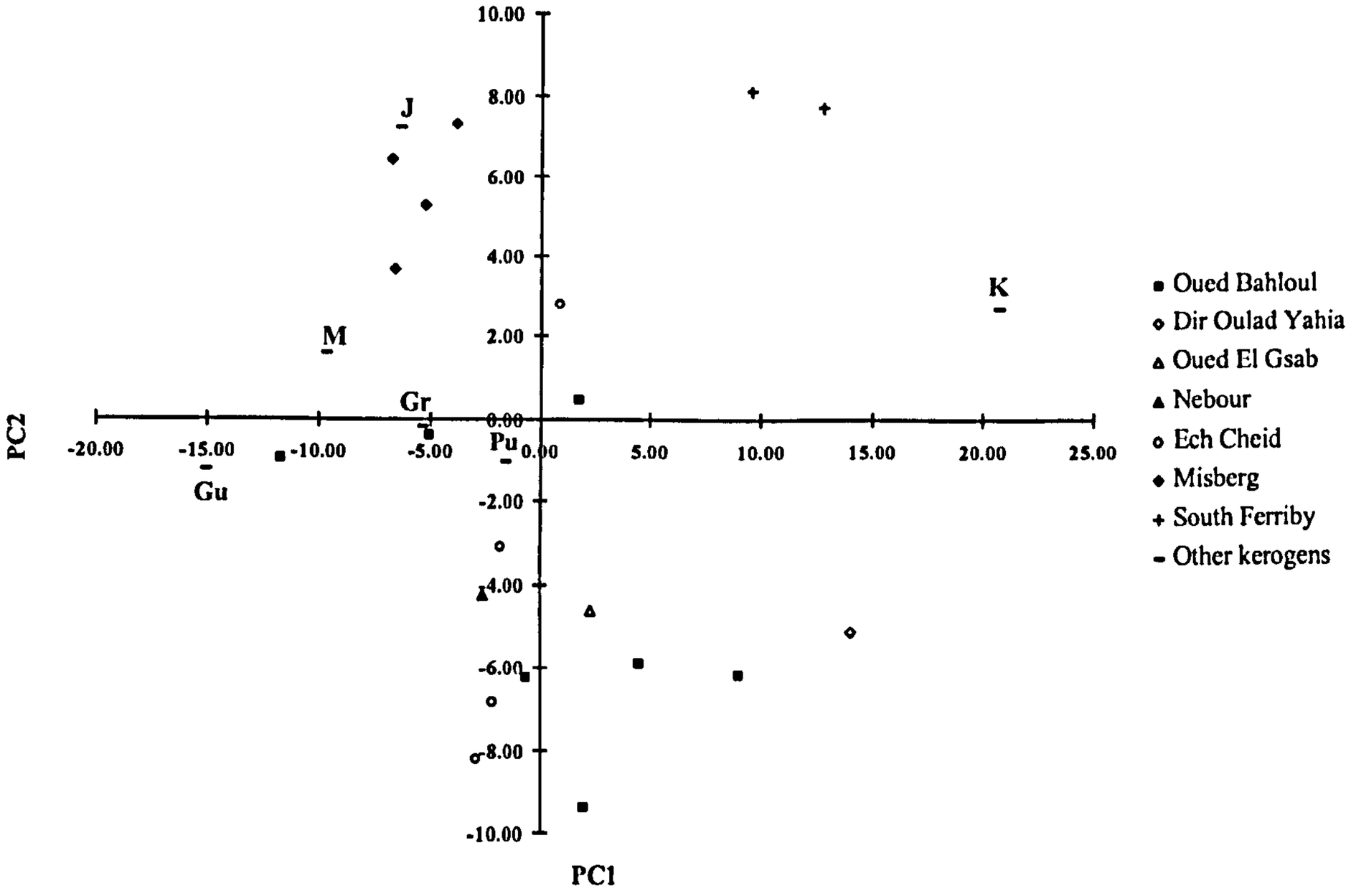

Figure 7.13 Cross plot of PC1 versus PC2 scores data for the Group 4 Py-MS data. Key: J, Jet Rock; K, Kimmeridge Clay, Gu, Guttenberg; Gr, Green River, M, Messel; Pu, Pumpherston.

Principal Component 2 appears to be controlled by the relative variation between aliphatic (alkane and alkene) and alkylbenzene compounds, as was also seen in PC2 Group 3 (7.3.3). The scores show that the Jet Rock, Kimmeridge Clay and Boreal samples plot on the positive axis (indicating that they have relatively higher amounts of alkylbenzenes in their kerogen pyrolysates) compared to the Tethyan samples (which plot on the negative axis, indicating their relative higher aliphatic content). The ratio of the alkene to alkylbenzene fragment ions shows a good correlation (Fig. 7.14; $r^2 = 0.75$) with the scores. Excluding the end member kerogens from this plot shows that the Cenomanian-Turonian samples correlate even better (r^2 = 0.88), and the correlation is also good for the data from the individual sections. The

scores from the Cenomanian-Turonian samples from the Group 4 data set show a good correlation ($r^2 = 0.78$) when plotted against PC1 Group 1 scores (if the anomalous sample OB2 is omitted). This shows that both pyrolysis techniques record the same trend in kerogen typing between the samples. The plot of PC2 against hydrogen index shows some relationship (Fig. 7.15; $r^2 = 0.50$), but the data show a better correlation with Aromatic Steroid Ratio 1 (Fig. 7.16; $r^2 = 0.63$) suggesting some overprint of maturity for this Principal Component.

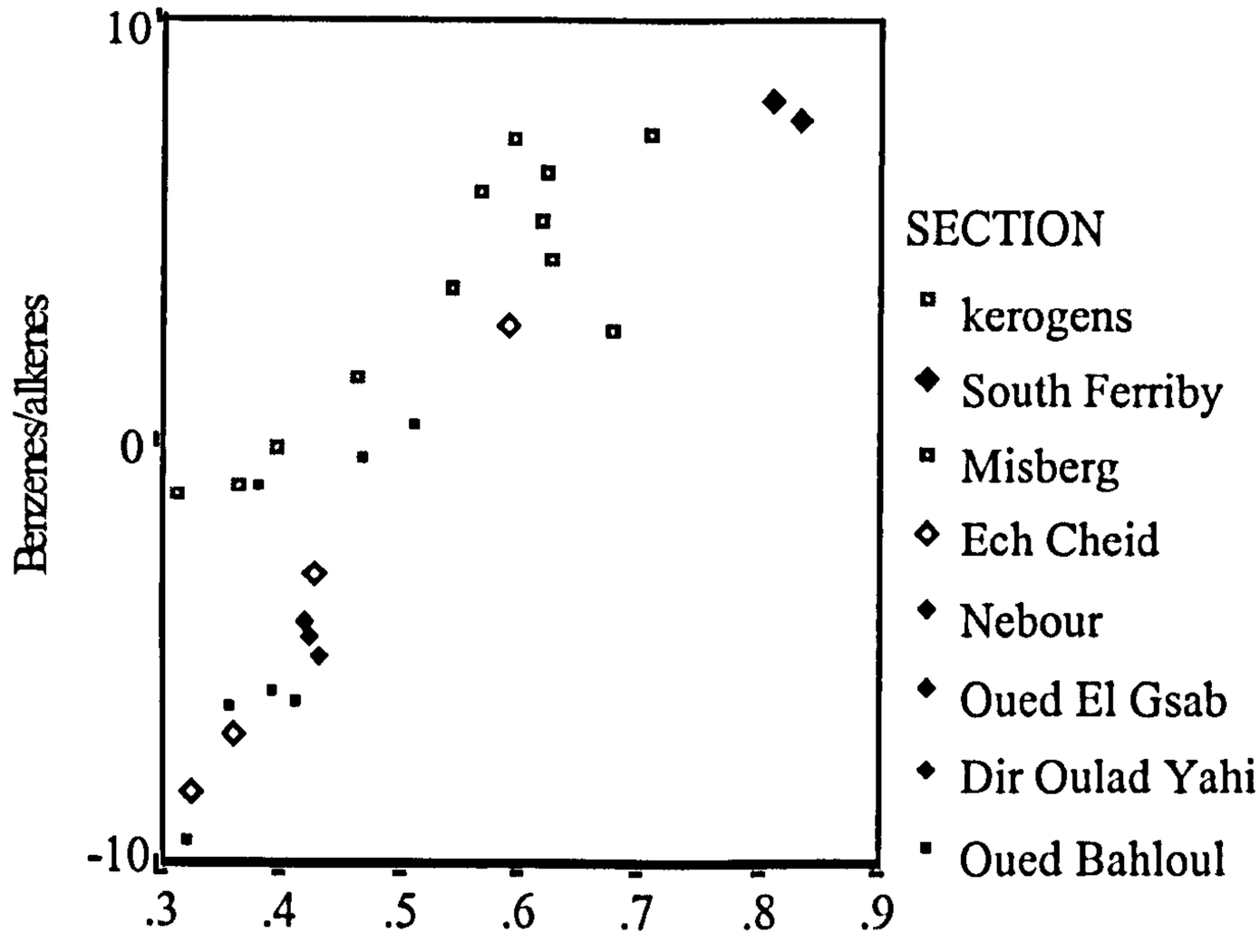

Figure 7.14 A cross plot of PC2 score from combined Py-MS versus a benzene/alkene ratio calculated from the m/z fragment series for these compounds. There is an excellent correlation (r2 = 0.75) between the parameters. The correlation is better (r^2 = 0.88) if just the Cenomanian-Turonian data is used. Kerogens under the section key refers to the comparison kerogens used in this study.

The negative axis on the loadings plot for the third Principal Component relates to lignin-derived compounds (i.e. phenols, methoxyphenols, dimethoxyphenols and diterpenoid resins), whereas the positive axis shows a dominance of acidic compounds (e.g. m/z 60 acetic acid; m/z 74 propanoic acid; m/z 88 butanoic acid; and m/z 102 pentanoic acid). The significance of the acid compounds on the positive axis is unclear. The scores shows that sample SQ36 (the Pumpherston Shale, Type III) strongly dominates the positive axis; the majority of the other samples plot close to zero on this axis. This Principal Component is controlled by the dominance of the acidic compounds in the Pumpherston shale, and probably reflects the Type III nature of the kerogen.

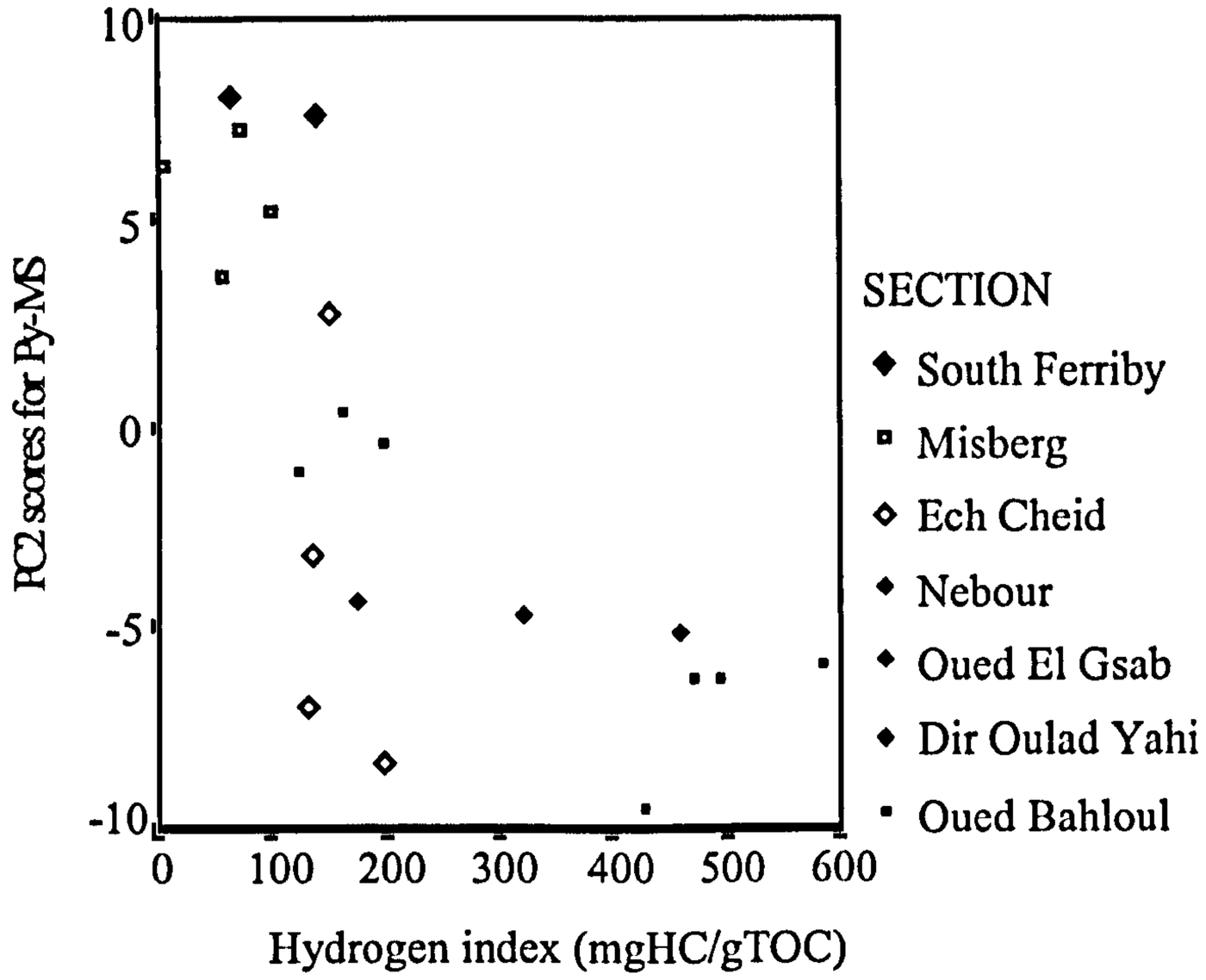

Figure 7.15 Cross plot of PC2 scores data from the combined Py-MS samples versus hydrogen index. The parameters show some correlation ($r^2 = 0.50$).

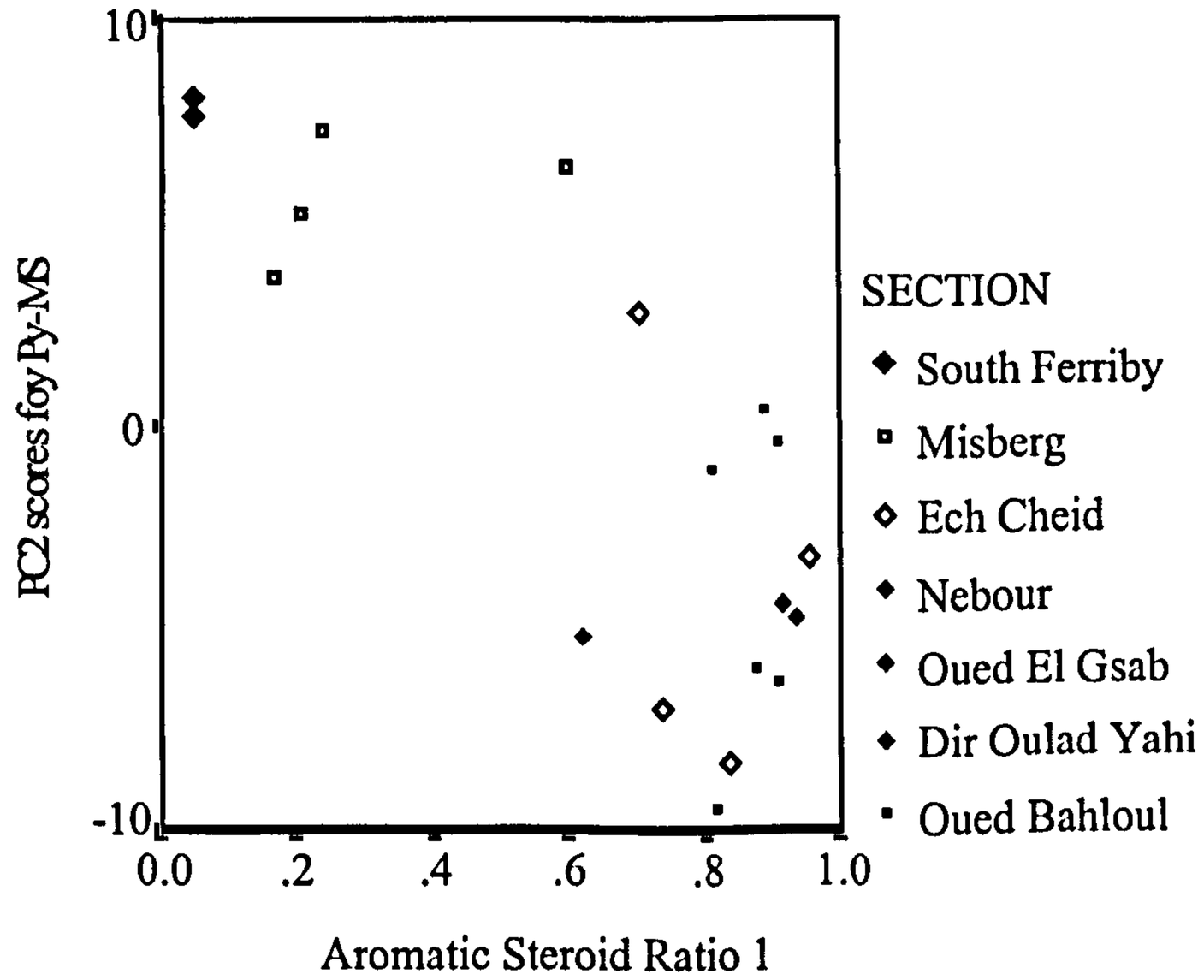

Figure 7.16 Cross plot of PC2 scores data from the combined Py-MS samples versus Aromatic Steroid Ratio 1. The parameters show a good correlation ($r^2 = 0.63$).
The negative axis on the loadings plot for the third Principal Component

7.3.5 Group 5. Cenomanian-Turonian Py-GC and Py-MS data

The dominance of the short chain alkenes and low m/z fragment ions suggests that Principal Component 1 for this group is controlled by similar factors to those

deduced for PC1 of the Group 3 data (Section 7.3.3). The data appear to be controlled by the relative abundance of low fragment ions (Fig. 7.17). There is a good correlation ($r^2 = 0.97$) of these scores with the scores from Group 3 PC1. In the loadings of this PC the nC_6 to nC_{10} alkenes plot on the same axis as the fragment ions m/z 55, 64 (SO_2) and 76 (CS_2). This confirms the influence of the *n*-alkenes in this Principal Component, and again highlights the influence of SO_2 and CS_2.

Principal Component 2 demonstrates the relationship between the alkenes, alkanes and thiophenes versus the other aromatic compounds (alkylbenzenes and indanes), as was also observed from PC1 Group 1. Although the loadings and scores suggest this PC is controlled by kerogen type there is a poor correlation with hydrogen index ($r^2 = 0.33$). It is interesting to note that the thiophenes plot on the opposite axis to the other aromatic compounds. This was observed earlier in Group 1 PC1 and Group 3 PC3. Waldo *et al.* (1991) report that higher thiophene contents in high-sulphur petroleums reflect the diagenetic conditions in a carbonate environment, compared to relatively higher sulphide compounds associated with clastic environments. Although these Cenomanian-Turonian samples have relatively low sulphur contents, the Tethyan realm samples have relatively higher thiophene contents than the Boreal realm samples, and also higher mean carbonate contents. The dimethylsulphide ion (m/z 62) is noted to plot on the same axis as the Boreal realm samples in this Principal Component. This Principal Component appears to be controlled by the kerogen type and the carbonate lithofacies for the samples (Fig. 7.17).

The scores for the third Principal Component data shows that sample EC13 is the only sample that plots strongly on the positive axis; all other samples (with the exception of EC25) plot on the negative axis. The dominant fragment ions (m/z 103, 104, 105) are the same as were seen in PC3 Group 3 (7.3.3). The loadings show that indane also plots strongly on this axis as do the nC_{13}+ alkanes. No correlation of the scores was observed with the optical, bulk or molecular geochemical data. As was noted in Group 3 PC3 that it is difficult to determine what controls this Principal Component; it appears to reflect some control specific to the Ech Cheid section.

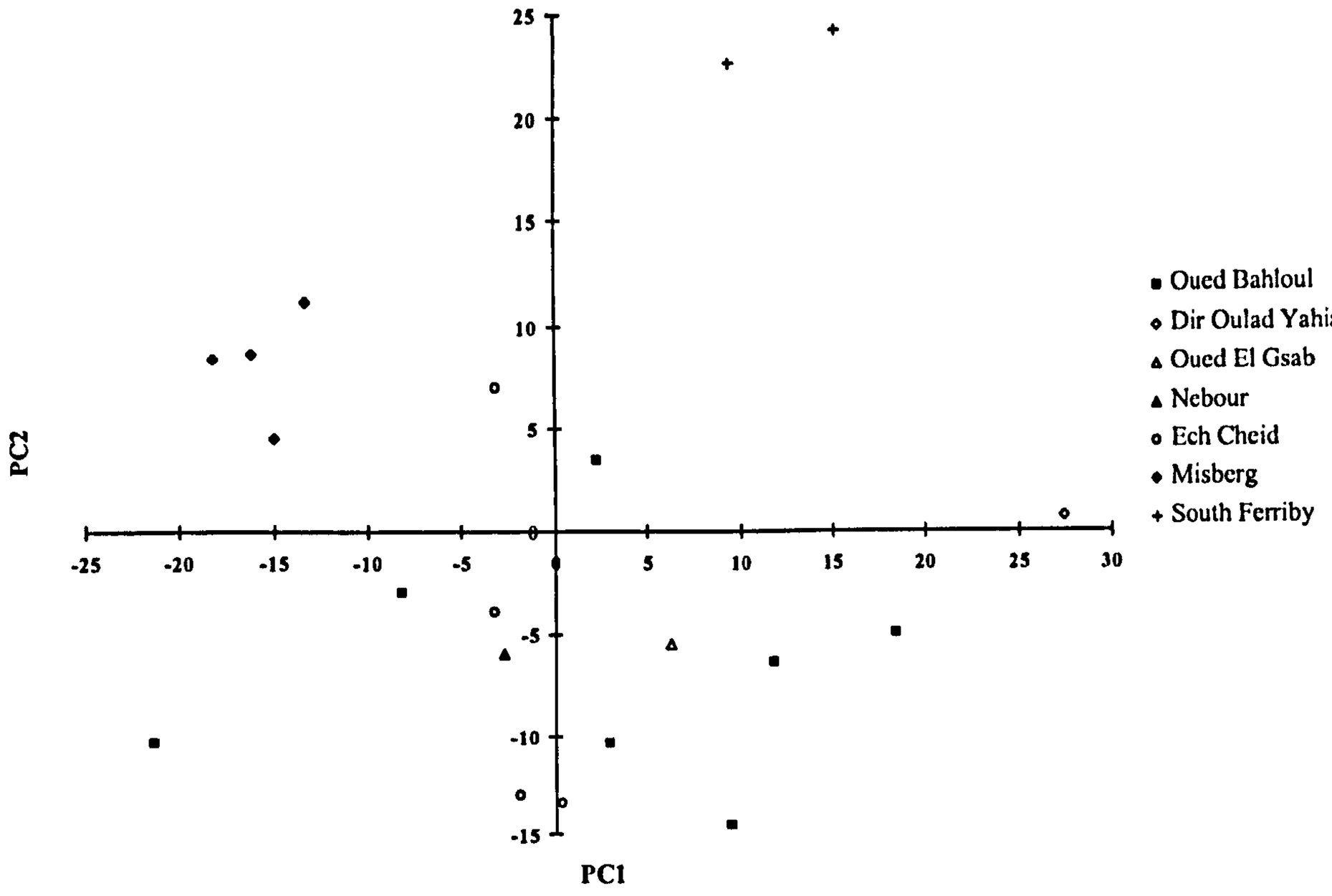

Figure 7.17 Cross plot of PC1 versus PC2 scores data for the Group 5 Py-GC and Py-MS data.

7.3.6 Group 6. Cenomanian-Turonian and characterised kerogen Py-GC and Py-MS data

The combination of Py-GC and Py-MS in Principal Component Analysis of all the samples, clearly shows that the dominant control (PC1) on the variation in pyrolysates is the relative abundance of *n*-alkane, *n*-alkenes and their low fragment ion series (m/z 55 to 58, 69 to 72, 83 to 86) compared to all other compounds. This was also observed in Group 4, PC1 ($r^2 = 0.99$). The samples which show this dominance of low m/z alkene and alkane fragments are samples OB2, OB18, Misberg, Green River, Guttenberg Jet Rock and Messel (Fig. 7.18). No direct correlation is observed between the scores and the optical, bulk and molecular geochemical data.

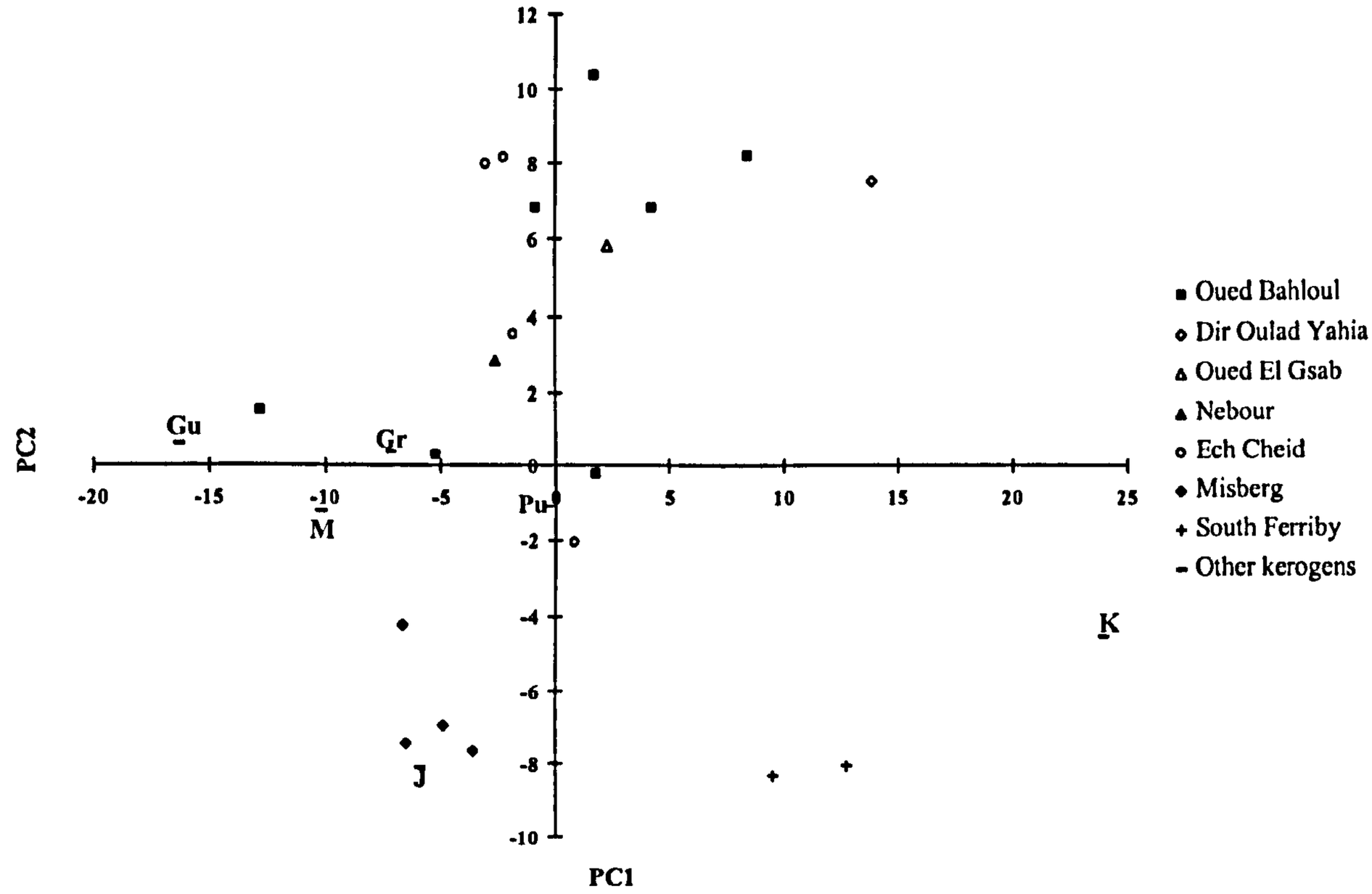

Figure 7.18 Cross plot of PC1 versus PC2 scores data for the Group 5 Py-GC and Py-MS data. Key: J, Jet Rock; K, Kimmeridge Clay, Gu, Guttenberg; Gr, Green River, M, Messel; Pu, Pumpherston.

Principal Component 2 is controlled by the relative amounts of aliphatic and aromatic (especially the alkylbenzenes) compounds. This was also seen in the analyses mentioned above The scores show that the Tethyan samples plot dominantly on the positive axis and the Boreal realm samples plot on the negative axis (Fig. 7.18), confirming that the Boreal kerogen pyrolysates have a stronger aromatic signature than the Tethyan realm. This is probably controlled by a combination of the higher phytoclast content in the Boreal realm sections (Appendix 3) and their poorer preservation.

The third Principal Component controls shows the same control exhibited by Group 5 PC3 (Section 7.7.5), i.e. lignin-derived compounds versus acidic compounds. This Principal Component may reflect differences in the source of phytoclast material in the samples. The phenolic compounds reflect a lignin source and the compounds on the negative axis represent a woody source strongly typical of the Pumpherston shale, since it plots dominantly on the negative axis. The scores are strongly influenced by the Pumpherston shale and the other samples plot relatively close to zero which suggests that they are largely unaffected by these factors. Because the scores are dominated by the Pumpherston shale they can give us very little information on palaeoenvironmental differences between the other sections.

7.4 PCA for quantified and TOC-normalised Py-GC data

The use of the internal standard poly-tertiary-butyl-styrene allows the data from Py-GC to be quantified, giving absolute compound abundances. These data were also analysed using Principal Component Analysis. The first three Principal Components account for 87% of the variance in the data set. The first Principal Component records 80% (the majority) of the variance in the data set. The loadings plot show that this Principal Component is controlled by all the compounds, as they all plot on the positive axis, as do all the samples in the scores. This suggests that the majority of the variance in the data set is controlled by bound hydrocarbon concentration differences between the samples, as would be expected in samples with varying TOC and hydrogen index values.

The quantified data was further normalised to TOC values, in order to reduce the effect of concentration differences between the samples. However, when Principal Component Analysis was done on this data set, the first Principal Component (68%) was still controlled by concentration differences between the samples. These data were further normalised to sum all variables for each sample to unity. Principal Component Analysis on this data set gave identical loadings and scores values to the non quantified data sets. This demonstrates the validity of using the non-quantified data for Principal Component Analysis.

The same observations were made for the Py-MS data. When quantified and TOC-normalised data were used the majority of the variance (PC1; >70%) was controlled by the differences in compound concentration between the samples. These concentration differences between samples were cancelled out when the data was further normalised to unity.

7.5 Discussion of PCA data

Principal Component Analysis was used to provide a concise summary of Py-GC and Py-MS data from kerogen pyrolysates in order to establish the significant controls on the data sets from samples used in this thesis. It is clear from the Principal Component Analysis of the pyrolysis-gas chromatography data that the major control on the data set is the relative abundance of aliphatic versus aromatic compounds. Horsfield (1984) noted that the aromaticity of kerogens was a function of source type and maturity level, which changed systematically depending on the proportions of differing compounds in the pyrolysates. Highly aromatic kerogens (vitrinite and

inertinite) produced relatively more aromatic compounds such as phenols and alkyaromatic hydrocarbons, whereas pyrolysates dominated by aliphatic hydrocarbons are typical of aliphatic carbon and hydrogen-rich kerogens (such as liptinites). The data in this thesis demonstrate that kerogens from the Boreal realm typically have a more significant aromatic signature than kerogens from the Tethyan realm. This agrees with the observations from the other analytical techniques described earlier in this thesis, that the Boreal kerogens contain some Type III kerogen and the Tethyan realm kerogens contain mainly Type II kerogens (Appendix 3).

The Cenomanian-Turonian samples used in this study are of similar maturity so it is likely that the differences in relative aliphatic to aromatic content is a result of differences in organic matter type (which reflects preservational conditions). This is confirmed by comparison of the scores data with optical and molecular geochemical data described earlier which identify differences in organic matter sources and preservation between the European Shelf and Tunisian samples. Stout (1991) used PCA to differentiate between kerogen from dissimilar depositional settings (marine, lacustrine and terrestrial), and he noted that the Principal Component distribution of aliphatic and aromatic compounds in pyrolysates reflected organic matter type. He also observed that PC1 separated the lacustrine samples from the marine and terrigenous samples and that this was due to the relatively higher abundances of aliphatic compounds in the lacustrine samples. The PCA data from the Group 2 data set shows that the aliphatic compounds plot dominantly on the positive axis as do the Green River and Messel Oil Shale samples, which were both deposited in lacustrine environments. Stout (1991) also noticed that PC2 separated marine (positive scores) and terrigenous (negative scores) samples due to thiophene compounds plotting on the positive axis of the loadings. This separation is not observed in the Group 2 data but is found in PC1 of the Group 1 data. The thiophenes plot dominantly on the positive axis as do the kerogens with dominant Type II marine kerogen (Oued Bahloul, Dir Oulad Yahia and Oued El Gsab). The relative abundance of aliphatic and aromatic compounds was also noted in the pyrolysis-mass spectrometry data; however, this was a secondary (PC2) control in this data set.

The abundance of thiophenes relative to other aromatic compounds in the Group 1 data may be an indication of the separation of marine organic matter from that with a more significant terriginous source. This is similar to the findings of Stout (1991) who noted that PC2 separated marine and terrigenous samples according to the relative abundance of thiophenes. The scores plots separate the German, UK and Ech Cheid sections, which have a higher terrestrial fraction observed optically, from the

other Tunisian sections which were typically marine AOM-dominated. This is consistent with the observations of Tissot and Welte (1984) and Sinninghe Damsté *et al.* (1989b) who noted that immature marine Type II kerogens typically had the highest contents of organic sulphur compounds.

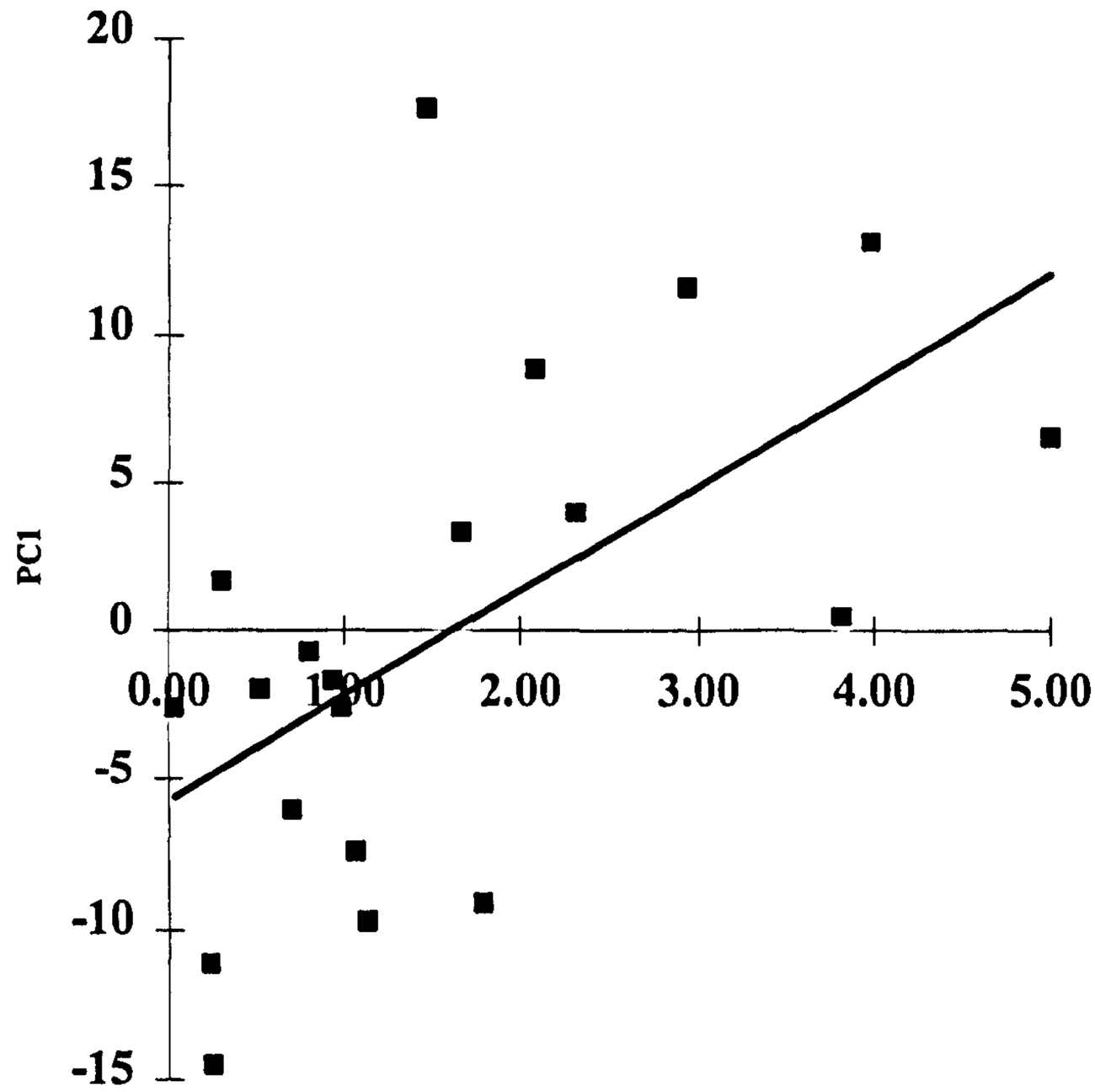

Figure 7.19 Cross plot of Cenomanian-Turonian Py-MS PC1 scores data (Group 3) versus Rock-Eval S2 (mgHC/gSED) parameter. Generally the samples with higher hydrocarbon yields plot on the positive axis.

Principal Component Analysis of the pyrolysis-mass spectrometry data (Groups 3 and 4) indicates that the main Principal Component (PC1) reflects the majority of the hydrocarbons, which plot on the positive axis, whereas non-hydrocarbons (e.g. m/z 64, SO_2 and m/z 76, CS_2) and some *n*-alkanes and alkenes plot on the negative axis. This suggests that the total yield of aliphatic and aromatic hydrocarbons from the kerogens controls the majority of the variance in these samples. This is confirmed to some extent from cross plots of the PC1 scores data with the Rock-Eval S2 parameter (Fig. 7.19). A very general relationship is seen between these two parameters indicating that samples on the positive scores axis tend to have higher Rock-Eval S2 values than those on the negative axis. This reflects the relative abundance of the lower m/z fragments (m/z 51 to 84) to the higher m/z

fragments (m/z 85+). Skjevrak (1997) also noted that PC1 of the Py-MS data in her thesis was dominated by high pyrolysis yields of aliphatic and aromatic hydrocarbons. Larter and Horsfield (1993) noted that the absolute yields of kerogen pyrolysis products of all types was simply a function of the overall aliphatic carbon and hydrogen content of the kerogen, and that Type I and II kerogens produced higher absolute yields of both aliphatic and aromatic hydrocarbons than Type III kerogens. This is also consistent with the observation made from the scores data for Groups 3 and 4. The Dir Oulad Yahia, South Ferriby and some Oued Bahloul samples have relatively higher hydrocarbon yields than the Misberg Ech Cheid and OB2 samples (Appendix 2), suggesting that they have a more Type II kerogen, which is also confirmed by other observations (Appendix 3).

The compound SO_2 (m/z 64) is noted in several of the Py-MS PCA groups. Skjevrak (1997) observed that this compound was not suitable for differentiating between kerogens as its abundance can be caused by factors other than differences in organic matter input and maturity. These include release of SO_2 from sulphonic acids, inertinite groups (Metcalf *et al.*, 1987) and pyrite (Meuzelaar *et al.*, 1984). The presence of SO_2 in pyrolysates is also thought to arise from the weathering process of sulphides in the sedimentary organic matter from outcrop samples (Schouten *et al.*, 1995). As the Cenomanian-Turonian samples are all from outcrop and contain pyrite to variable degrees, it is difficult to ascertain the reason for SO_2 being highlighted in PCA.

7.6 Stratigraphic variations in pyrolysis data

The relative abundance of individual compounds and fragment ions in the pyrolysates of the seven Oued Bahloul samples, analysed using Py-GC and PY-MS, were plotted stratigraphically in order to attempt to correlate their general trends with those observed from optical, bulk and molecular geochemistry.

The *n*-alkenes and *n*-alkanes are generally more abundant in the samples which have relatively higher C_{35} hopane predominance, which in turn suggests a more anoxic environment (e.g. C_{35} hopane predominance v. nC_8, $nC_{9,}$, nC_{10}, nC_{11} alkanes and nC_{17} alkene; e.g. Fig. 7.20). This suggests better preservation of algal amorphous kerogen in samples with relative higher *n*-alkane and *n*-alkene contents, which is consistent with the hydrogen index and and fluorescence data (Appendix 2 and 3).

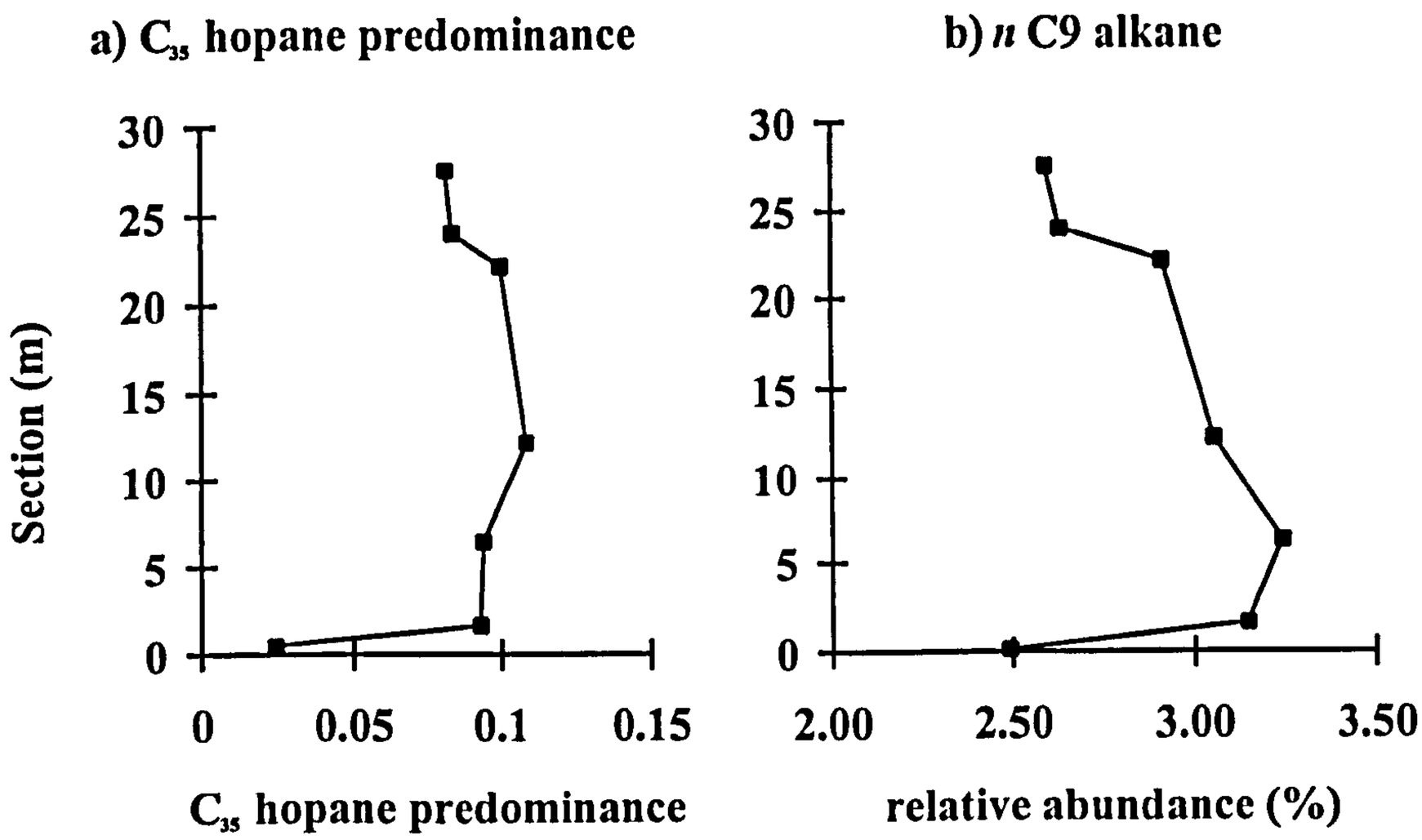

Figure 7.20 Stratigraphical plots for: a) C35 hopane predominance for the Oued Bahloul section (after Bishop and Farrimond, 1995); b) Relative abundance of nC_9 alkane, calculated from Py-GC traces.

The aromatic compounds benzene and toluene are relatively more abundant in organic-poor Oued Bahloul samples (OB2, OB18 and OB65); this is possibly a result of the higher relative phytoclast content for OB2 as these compounds are abundant in phytoclast material (Larter & Horsfield, 1993), and poorer preservation of aliphatic components in the these three samples as indicated from the lower hydrogen index and kerogen fluorescence for these samples

It was observed from the Principal Component Analysis loadings (Group 1, PC1 and Group 5, PC2) that the thiophene compounds differ between the Tunisian and Boreal samples. This difference is believed to reflect the diagenetic incorporation of sulphur into the organic matter in varying clastic to carbonate environments. Waldo *et al.* (1991) demonstrated that sulphur-rich oils have characteristic thiophene versus sulphide relationships controlled by diagenetic incorporation of sulphur under either a carbonate or clastic environment respectively. As most reactive iron is supplied in detrital clastic form then in carbonate regimes its supply is limited, the iron limitation means that less S from H_2S produced by sulphate reducing bacteria goes into pyrite formation and more can be potentially incorporated into organic matter (Tyson, 1995 p.63; Berner, 1985; Sinninghe Damsté *et al.*, 1989a). Mean carbonate values are higher for the Tethyan realm than the Boreal, and this could be one explanation for the relatively higher thiophene content in the Tethyan samples, and for the sulphide fragment (m/z 62) plotting on the same axis as the Boreal realm

samples. However, stratigraphic plots of thiophene show a poor correlation with carbonate plots. This may be because the thiophene content to some extent reflects the general differences in carbonate environment between the sections and not the actual differences in carbonate values within the sections.

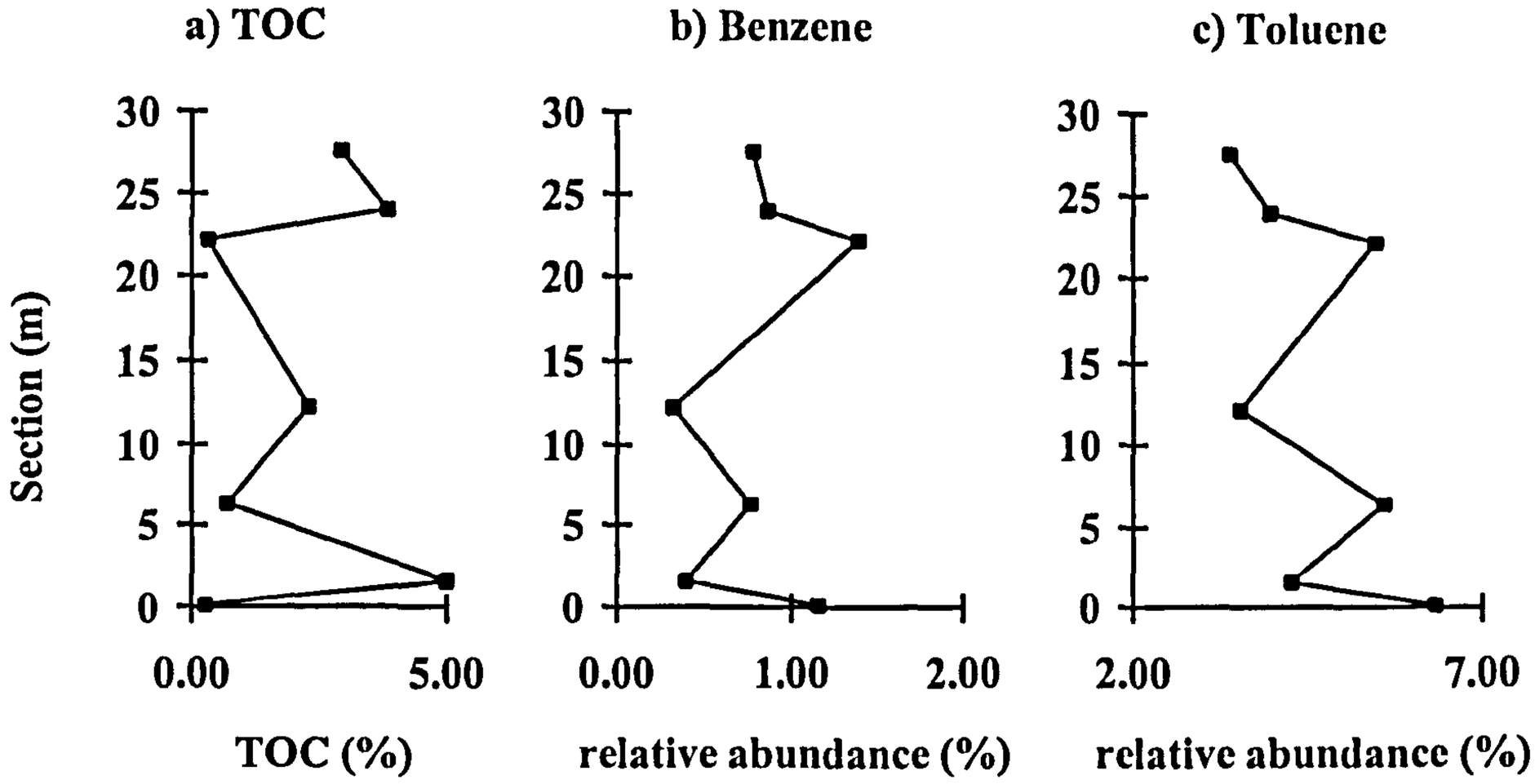

Figure 7.21 Stratigraphical plots of: a) TOC for the Oued Bahloul section; b) Relative abundance of benzene, calculated from Py-GC traces; c) Relative abundance of toluene, calculated from Py-GC traces. Note that these aromatic compounds are at their gratest abundance in samples with low TOC values.

7.7 Conclusions

Statistical multivariate analysis was carried out on Py-GC and Py-MS data from 20 Cenomanian-Turonian kerogens and a further seven well characterised kerogens from differing palaeoenvironments for comparison. The main conclusions drawn from this work are:

Principal Component Analysis suggests that the differing methods of chemical isolation of kerogen material do not appear to greatly affect the chemical characteristics of kerogen pyrolysates.

The main control on the relative distribution of pyrolysate compounds as determined by Principal Component Analysis of the Py-GC data is the relative abundances of aliphatic and aromatic hydrocarbons, which itself is a reflection of the kerogen type. This highlights the difference in kerogen type between the European

Shelf (Type III/II) and the Tunisian (Type II) sections, which is probably due to a combination of differing organic matter sources and degrees of preservation. This was confirmed by the optical examination of the samples (Appendix 3). The European samples, and to some extent the northern Tunisian samples, have slightly greater terrestrial input and poorer preservation, reflected chemically by the relatively more aromatic nature of the kerogens.

The main Principal Component (PC1) for Py-MS data is controlled by the relative abundance of hydrocarbons (aliphatic and aromatic) versus non-hydrocarbons. This observation was also consistent with that in published work by other authors on different samples. The second Principal Component for this data set is controlled by the relative amount of aliphatic and aromatic hydrocarbons, which again is a reflection of kerogen type.

Overall, the Principal Component Analysis data suggests that kerogen type (aliphatic versus aromatic compounds) dominates the pyrolysate compositions of the samples analysed by Py-GC and Py-MS. However, these data show a poor correlation with hydrogen index, suggesting that some other control is affecting the data; this could be due to the slight maturity differences between the sections which has been shown to have an impact on the biomarker data (Appendix 4).

Principal Component Analysis of combined Py-GC and Py-MS data sets shows that the main controls of the distribution on hydrocarbons in these kerogen are hydrocarbon yield and kerogen type. The influence of these factors on the data sets reduces the chance of multivariate analysis identifying significant palaeoenvironmental information.

CHAPTER 8

8. Discussion and future work

This thesis presents a study of Cenomanian-Turonian organic-rich basinal shelf sediments from the south Tethyan margin in Tunisia and the European Boreal epeiric shelf in Germany and the UK. In order to test the Oxygen Minimum Zone model proposed for the south Tethyan margin (Jenkyns, 1985; Arthur *et al.*, 1987), comparisons have been made between the sections on the basis of their bulk, molecular, stable carbon isotope, kerogen pyrolysis geochemistry, and kerogen microscopy.

8.1 Regional Contrasts

Table 8.1 shows a summary of some of the main findings of this thesis. The samples from the UK sections contain immature, poorly preserved organic matter, mainly degraded marine AOM and some phytoclast material. Bulk geochemical values for TOC and hydrogen index are generally low, but TOC does exceed 2% in some samples. The samples from the Misberg section contain relatively mature, poorly preserved, degraded marine AOM and some terrestrial material. The TOC and hydrogen index values are generally low, but total sulphur values do reach 1% in some samples. Bioturbation is quite common in these sections and only the organic-rich samples (>1%TOC) show evidence of lamination.

Samples from the southernmost Tunisian sections (Oued Bahloul, Dir Oulad Yahia and Oued El Gsab) contain early mature, well preserved, marine AOM, with high TOC and hydrogen index values (but low sulphur values). The samples are commonly laminated and strong bioturbation is only observed at the very base and top of the sections. The northernmost sections (Ech Cheid and Nebour) are strikingly different. The Nebour samples are non-laminated, contain poorly preserved marine AOM, and exhibit a marginally higher maturity than the other Tunisian sections; hydrogen index and TOC values are high, but not as high as those from the southern localities. The sediments from the Ech Cheid section are commonly bioturbated and contain poorly preserved marine AOM with some plant debris. These samples have a similar maturity to those from the south of the study area, but the TOC, hydrogen index and total sulphur values are much lower.

Microscopic observation of the kerogens have shown that the fluorescence and thus preservation of the AOM are greater in the Tunisian samples compared to those from the European shelf. Combined with the observation of higher bioturbation in the

Section	Group	TOC (%)	HI	S (%)	Carbonate (%)	$\delta^{13}C$ (‰)	Opt. pres.	Maturity	Palynofacies	% Woody	Pres. scale	TOC fold inc.
Oued Bahloul	Tunisia	2.51	426	0.167	71	3	yes	Early mature	AOM (dom)	-	3.8	38
(83 samples)	south	0.21-8.15	50-681	0.002-0.7	51-86					-	3-5	
Dir Oulad Yahia	Tunisia	2.22	423	0.16	55	3	yes	Early mature	AOM (dom)	-	5	68
(50 samples)	south	0.1-6.77	100-850	0.01-0.76	13-80					-	*	
Oued El Gsab	Tunisia	2.09	383	0.09	68	3	yes	Early mature	AOM (dom)	-	4	26
(46 samples)	south	0.21-5.47	159-565	0.01-0.54	54-79					-	*	
Ech Cheid	Tunisia	0.47	100	0.017	58	1.5	yes	Early mature	AOM (dom)	6-26	2.25	6
(25 samples)	north	0.16-0.98	34-198	0.0003-0.1	29-74				(some woody)	-	1-3	
Nebour	Tunisia north	1.83	237	0.13	66	2	yes	Mature	AOM (dom)	-	1	22
(47 samples)		0.2-4.33	36-395	0.05-0.55	50-79					-	*	
Misberg Quarry	European	0.5	27	0.18	55	1.5	no	Mature	AOM/woody/	9-70	2.2	9
(28 samples)		0.02-1.81	56-124	0.021-1.05	39-82					-	1-3	
South Ferriby	European	0.75	55	n/d	55	1	no	Immature	AOM/woody/	20-60	n/d	40
(20 samples)		0.1-4.0	20-120	n/d	50-75				dino	-	n/d	
Buckton Cliff	European	1.4	43	n/d	31	1	no	Immature	AOM/woody/	18-55	2.4	10
(5 samples)		0.5-2.4	20-100	n/d	13-69				dino	-	2-3	

Table 8.1 Summary of the Cenomanian-Turonian data determined in this work. Key: TOC, Total Organic Carbon (%); HI, hydrogen index (mgHC/gTOC); S, sulphur (%); Carbonate, % of Calcium Carbonate; $\delta^{13}C$ (‰), magnitude of $\delta^{13}C$ excursion; Opt Pres, optimum preservation based on levelling off of HI with increasing TOC; Maturity, organic matter maturity based on bulk and molecular geochemical data; Palynofacies, based on transmitted light microscopy; % Woody, percentage of phytoclasts; Pres scale, kerogen preservation scale; TOC fold inc., fold increase in TOC from background values. For bulk geochemical parameters the first value refers to the mean for the section the second line refers to the range. * = no range (based on a single sample).

European samples (Appendix 1), this strongly suggests that the Tunisian samples were deposited in an environment with lower mean dissolved oxygen concentrations.

Although the observed HI-TOC relationship suggests optimal preservation conditions were periodically achieved in the Tunisian sections (Fig. 6.15), it is probable that they were never achieved at either Misberg (Fig. 4.19) or the two Humberside sections (Fig. 3.12). However, the presence of laminations in some of the black shales at Misberg indicates that at least suboxic conditions periodically developed there (<0.2 ml/l O_2). Enhanced preservation attributed to suboxia-anoxia is not normally associated with more than a 6-fold increase in TOC above background levels (Tyson, 1995), and as the relative difference in TOC between adjacent oxic and anoxic facies ranges from 6-40 fold (Table 8.1), it is likely that increased primary productivity or condensation are also partly responsible for the enhanced TOC. The increase in the relative concentrations of steroids to hopanoids (Fig. 6.20 and 6.22) suggests increased algal preservation and perhaps also higher productivity.

Tunisian Cenomanian-Turonian sediments are generally thicker compared to their counterparts from the European shelf. The exception to this are some of the German sequences which reach up to 30m thick The latter is likely to be a result of local palaeobathymetric differences reflecting stronger subsidence (Hilbrecht & Dahmer, 1994; Kocker, 1994).

8.2 Variations within Tunisia

Bulk, molecular and optical differences were noted between the sections from the northern and the southern parts of Tunisia (Table 8.1). The differences in hydrogen index between these two areas can largely be attributed to differences in preservation, as observed from variations in kerogen fluorescence. The Ech Cheid section also has a slightly greater terrestrial input and the mixing of kerogen types may also contribute to lower hydrogen indices there. It is possible that local currents were responsible for introducing more terrestrial material in this area, perhaps via submarine valleys (cf. Gross *et al.*, 1972) The sediments from the Nebour section (which are dominated by marine AOM) have marginally higher maturity than the other Tunisian sections; this may have lowered the hydrogen index slightly, but it is likely that much of the difference reflects lower original preservation.

Bisnorhopane and methylbisnorhopane were noted in high abundances in both the Oued Bahloul samples and the Dir Oulad Yahia section (sample DOY25), but not in the sections from the northern part of the study area. These compounds have been associated with marine anoxic conditions (Seifert *et al.*, 1978) and upwelling environments (Grantham *et al.*, 1980) although their source and environmental significance are still unclear.

8.3 Depositional model.

Coastal upwelling has been proposed as the main control on the development of Cenomanian-Turonian organic-rich sediments off north and north west Africa (Einsele & Wiedmann, 1982; Thurow *et al.*, 1982). The high productivity may have intensified the Tethyan OMZ, with the latter impinging on the Tunisian margin, extending southward across the slope and outer shelf during the peak transgression (Jenkyns, 1985; Arthur *et al.*, 1987). Further to the south (Abdallah 1989, Abdallah & Meister, 1996 and 1997; Abdallah *et al.*, 1995) the organic-rich Bahloul gives way to a shallow water carbonate platform facies that were apparently deposited above the OMZ depth (Fig. 5.4).

Modern day continental margins where the sediment-water interface lies within the oxygen minimum zone and the overlying water contains <1-2 ml/l O_2 typically have TOC values >2% (Gross *et al.*, 1972; Pedersen *et al.*, 1992; Calvert *et al.*, 1992). Generally higher hydrogen indices and better organic matter preservation have also been observed in modern day sediments found in association with OMZ's (e.g. Demaison, 1991; Dean *et al.*, 1994; Paropkari *et al.*, 1993). Oxygen Minimum Zone sediments are also typically dominated by marine AOM (Tyson, 1995; Lückge *et al.*, 1996) due to the high productivity and onshore aridity which leads to a low phytoclast input. Palynofacies observations on the Tunisian samples show that the four organic-rich sections do contain a dominance of marine-AOM (Fig. 6. 17). Although the kerogen from the Ech Cheid section is AOM-dominated it also contains a significant proportion of terrestrial material (Fig. 6.17), which might suggest that this section was deposited in an area not as strongly affected by upwelling (Lückge *et al.*, 1996).

For samples with similar TOC's the highest hydrogen indices should indicate the best preservation. Emeis *et al.* (1991) show TOC v. hydrogen index plots for samples from different parts of the Peruvian OMZ. The samples with the highest hydrogen indices correlate to depths where dissolved oxygen concentrations were at

their minimum and low enough to prevent bioturbation (i.e. suboxic). According to palaeogeographic reconstructions (Fig 1.4), the sections from the northern part of Tunisia would have been deposited in deeper water. By analogy with the Peruvian OMZ, the poorer preservation in northern Tunisia may thus reflect greater intra water column degradation, and deposition below the suboxic core, at the lower margin of the OMZ, in waters that were only dysoxic. This deeper and more offshore area may also have had a lower surface water productivity (perhaps explaining the lower TOC contents and reduced shift in isotope values for the Ech Cheid section?). The most oxygen depleted conditions are suggested for the Dir Oulad Yahia and Oued Bahloul sections, based on the TOC-HI relationship; this may be reflected in the greater abundances of bisnorhopane and methylbisnorhopane observed in these two sections (cf. Seifert *et al.*, 1978; Grantham, 1980).

The greater rarity of lamination and lower quality of the preserved organic matter, suggest deposition of organic-rich sediments on the European Shelf occurred under more oxic conditions than those of the south Tethyan margin. The swell and basin pattern of organic-rich (black shale) and organic-poor (red/brown or pale mudstones) observed for both Germany and the UK (e.g. Hilbrecht, 1986; Jeans *et al.*, 1991; Paul *et al.*, 1994) suggests that low oxygen conditions only occurred in areas that had deeper water by virtue of more rapid subsidence. The latter facies may have been associated with higher productivity, as suggested by dinocyst blooms (cf. Marshall & Batten, 1988), but if this is the case, it clearly only resulted in organic-rich shale deposition at sites that were deep enough for dysoxic conditions to be periodically established. The sections studied would suggest that conditions were mostly dysoxic rather than suboxic or anoxic.

8.4 Isotope data and correlation

As carbonate $\delta^{13}C$ value can be severely affected by diagenetic alteration of the carbonate material, organic matter $\delta^{13}C$ values offer a potentially more reliable alternative. The four organic-rich sections for Tunisia all contain AOM-dominated kerogens, and therefore the isotopic signal is unlikely to have been affected by variations in organic matter source. Although hydrogen index varies with TOC, there is no correlation between the carbon isotope and hydrogen index curves for the Tunisian and European samples. The optical data suggests that the variability in hydrogen index reflects preservation rather than changing marine: terrestrial ratios. This independence of the $\delta^{13}C$ organic matter values suggests that the isotope curves have excellent correlation potential, although the form of the curves will also be

influenced by differences in sediment accumulation rates and sampling density. The shape and prominence of the isotope spike for the Tunisian sections (cf. Bechtel *et al.*, 1998) may be partly a reflection of condensed sedimentation, as the spike occurs at a flooding surface (cf. Robaszynski *et al.*, 1993b).

The amplitude of the organic matter isotopic excursion compares well with published data; however, the organic matter curves show an equal or slightly greater excursion compared to reported carbonate curves. This may be a reflection of diagenetic alteration of carbonate material or an influence of increased productivity on the $\delta^{13}C$ organic matter values, which can be responsible for up to a 2‰ increase in upwelling facies (Müller *et al.*, 1985).

The correspondence between the TOC curve and the $\delta^{13}C$ isotopic excursion suggests that onset of the "anoxic event" and of the black shale facies occurred more or less synchronously throughout most of Tunisia and on the north west European shelf. However, the organic-rich shale lithologies and isotope excursion start within the end of the *R. cushmani* zone at Misberg (Hilbrecht & Dahmer 1994), while in Tunisia they start at the base of the following *W. archaeocreatacea* zone (Robaszynski *et al.*, 1993b; Maamouri *et al.*, 1994). Slight diachroneity of the basal Bahloul Formation is also reported between different palaeogeographic regimes within south central Tunisia (Abdallah & Meister, 1997). There is no precise correlation between the isotopic excursion and the local occurrence of the "black shale" facies; organic-rich beds are present in several sections even after the isotope curve has returned to background values. The thickness of the post-excursion organic-rich interval varies between the Tunisian sections, in agreement with the diachroneity also documented biostratigraphically by Abdallah and Meister (1997).

8.5 Conclusions

- The CTBE organic facies are dominated by variably preserved, predominantly marine-derived amorphous Type III/II to II kerogen in Tunisia, Humberside (UK) and Lower Saxony (Germany). The organic matter is frequently better preserved and more oil-prone in Tunisia.

- Organic matter $\delta^{13}C$ curves appear to be a useful tool for identifying and correlating the Cenomanian-Turonian boundary event, especially its base. Comparison with geochemical and optical data enables anomalous curves to be identified, and possibly corrected, making them potentially superior in black shale facies where carbonate

isotope curves may be diagenetically altered. The apparently abrupt $\delta^{13}C$ excursion at the base of the studied successions may relate to slow sedimentation rates at the transgressive surface (Robaszynski *et al.*, 1993b).

• The enhanced TOC levels are probably due to a combination of increased preservation due to suboxic-anoxic conditions, increased primary productivity, and lower sediment dilution levels. The south Tethyan margin sediments experienced a lower oxygenation than those from the European shelf. Local differences in anoxicity are observed between the north and south of the Tunisian sample area, suggesting that the Nebour and Ech Cheid samples were deposited in deeper more oxygenated water.

• Bacterial derived hopanoids are relatively more abundant at the base of the Oued Bahloul section; this may reflect the lower sedimentation rates associated with a major flooding surface, which allows greater time for bacterial reworking to occur. The greater relative abundance of methylhopanes and bisnorhopane in the Dir Oulad Yahia sample suggests that these compounds are in even greater abundance in this section, and that bacterial activity may have been greater at this section.

• Variations in carbon number distribution between the hopanes and methylhopanes of the Oued Bahloul section suggest that there are two specific bacterial sources for these compounds at this section. A carbon number preference is observed in samples from this section for the C_{33} hopane and the C_{34} methylhopane; it has been suggested that this may be linked with weaker bonding between the relevant carbon atoms associated in the formation of these homologues, and that these bonds are preferentially broken at lower levels of maturation during diagenesis (Helen Innes, 1998, pers. comm.).

• The relationship of bisnorhopane with anoxicity indicators (i.e. C_{35} predominance; Bishop & Farrimond 1995) suggests that this compound is controlled by oxygen deficient conditions, in strong support of the previously reported empirical association with anoxic environments. The reasons for its abundance, and its source have not been precisely identified, despite the unusual abundance of bisnorhopane and methylbisnorhopane in the Oued Bahloul and Dir Oulad Yahia samples.

• Principal Component Analysis of Py-GC and Py-MS kerogen pyrolysates shows that the main variation in the kerogens between the Tunisian and European sections and the northern and southern Tunisian sections is the relevant abundance of aliphatic and aromatic hydrocarbons. This is primarily controlled by kerogen type and hence

preservation. These observations are supported by the results from optical analyses of the samples.

• The information presented in this thesis, along with that from other workers on Tunisian Cenomanian-Turonian sediments, supports the model that an Oxygen Minimum Zone impinged upon the southern Tethyan margin. The Oued Bahloul and Dir Oulad Yahia sections were apparently deposited near the suboxic core of the OMZ, while the Ech Cheid and Nebour sections were deposited in the deeper and only dysoxic waters at the lower margin of the OMZ. Cenomanian-Turonian sections from the northern Chotts area of Tunisia (cf. Abdallah & Meister, 1997) are less organic-rich and were apparently deposited in carbonate platform waters shallower than the OMZ.

8.6 Future work

The results of this work have raised several questions and points which warrant further study:

• The north-south extent of an Oxygen Minimum Zone has been potentially identified on the southern Tethyan margin for the Tunisian area. Comparison of this data set with others collected in the Tunisia and those from surrounding countries may allow the OMZ to be mapped more accurately to assess its lateral extent on the north and north west African shelf.

• The Oued Bahloul and Dir Oulad Yahia sections contain abundant methylhopanes, bisnorhopane and methylbisnorhopane. The source of these compounds is unclear. As the samples from these sections contain abundant hopanoids, useful information could be gained from the application of techniques which measure the carbon isotopic composition of individual hopanoids (i.e. GCC/IRMS; Gas Chromatography Combustion/Isotope Ratio Mass Spectrometry). The use of this technique may allow us to be more specific about the source of these hopanoids and then relate this to their environmental significance. This technique would be extremely useful in the Oued Bahloul and Dir Oulad Yahia sections, especially at the base of the sections for the methylhopanes and also the central samples where bisnorhopane and methylbisnorhopane are relatively more abundant.

• The distribution of hopanoid carbon numbers (especially the predominance of C_{33} hopane and C_{34} methylhopane) was observed to vary between the Oued Bahloul

samples. It has been proposed (Helen Innes, 1998, pers. comm.) that variations in the bond strengths of those bonds need to be broken in the formation of the C_{31} to C_{35} hopanoid compounds may preferentially favour the formation of the C_{33} hopane and C_{34} methylhopane homologues at lower levels of thermal maturation. In order to fully resolve this, molecular modelling (using hydrous pyrolysis techniques) could be carried out to determine the relative bond strengths involved in the release of these homologues and the controls for their preferential generation during diagenesis.

• This thesis attempts to demonstrate the fluctuation of individual compounds and mass fragment ions released during Py-GC and Py-MS respectively. Further and potentially more useful information could be gleaned if a fuller analysis of one section using these techniques was carried out. This would then permit the trends in pyrolysates through a section to be compared with those of bulk, molecular, isotope geochemical and optical data in greater detail. The use of high resolution mass spectrometry would help compound verification and permit a differentiation between compounds with similar mass fragments, which otherwise would not be separated. Alternatively a data set with more varied and better constrained characteristics, especially one where the variation in organic matter sources can be better quantified by microscopy - i.e. samples with a significant range of phytoclast contents, may provide more useful information.

• The use of Principal Component Analysis on Py-GC and Py-MS kerogen pyrolysate data has not identified any significant palaeoenvironmental trends in the kerogen pyrolysis data used in this thesis. This is largely due to the major influences of hydrocarbon yield and kerogen type on the pyrolysate data. It may be possible to identify further trends in kerogen pyrolysate data if PCA is run separately for aromatic and aliphatic compounds, thus removing the aliphatic:aromatic control on the data sets. This could be achieved easily if high resolution mass spectrometry was used to differentiate between compounds which co-elute in chromatographic analyses.

• The use of porphyrins, aryl isoprenoids, and isorenieretane biomarkers to assess water column anoxia during the deposition of these samples. As most OMZs are predominantly dysoxic-suboxic, rather than anoxic (as upwelling also supplies oxygen; Tyson & Pearson, 1991) would allow a better determination of the variance in dissolved oxygen concentrations between the sections.

REFERENCES

9. References

ABDALLAH, H., 1989, Les transgressions du Crétacé moyen entre les tectoniques et les eustatiques (Sud Tunisien). In COTILLON, P., *Colloque: Les, évenements de la partie moyenne du Crétacé (Aptien à Turonien)*, Lyon, 1987, *Geobios, Mémoire Spécial,* **11**, 83-94.

ABDALLAH, H., 1995, Découverte du Bahloul au-dessous du Gattar dans la chaîne nord des Chotts (Centre-sud de la Tunisie: conséquences de la trangression-anoxie du Cénomanian supérieur., *Compte Rendu de l'Academie des Sciences Paris,* **320**, 463-468.

ABDALLAH, H., MEMMI, L., DAMOTTE, R., RAT, P. & MAGNIEZ-JANNIN, F., 1995, La Crétacé de la chaîne nord des Chotts (Tunisie du centre-sud): biostratigraphie et comparaison ave les regions voisines., *Cretaceous Research,* **16**, 487-538.

ABDALLAH, H., MEISTER, C.,1996, La limite Cénomanien-Turonien en Tunisie du Centre-Sud. Extension du facies Bahloul (Cénomanien supérieur-Turonien inférieur):biostratigraphie, palaéoenvironnements., *Compte Rendu de l'Academie des Sciences Paris,* **322**, 39-46.

ABDALLAH, H. & MEISTER, C.,1997, The Cenomanian-Turonian boundary in the Gasfa-Chott area (southern part of central Tunisia): biostratigraphy, palaeoenvironments., *Cretaceous Research,* **18**, 197-236.

ACCARRIE, H., EMMANUEL, L., ROBASZYNSKI, F., BAUDIN, F., AMEDRO, F., CARON, M. & DECONINCK, J-F., 1996, La géochimie isotopique du carbone ($\delta^{13}C$) comme outil stratigraphique. Application à la limite Cénomanien-Turonien en Tunisie centrale *Compte Rendu de l'Academie des Sciences Paris,* **322**, 579-586.

ALEXANDER, R., KAGI, R. I., WOODHOUSE, G. W. & VOLKMAN, J. K., 1983, The geochemistry of some biodegraded Australian oils., *Australian Petroleum Exploration Association Journal*, **23**, 53-63.

ANDERSON, D. M., LEVELY, J. J., REARDON, E. M. & PRICE, C. A., 1985, Sinking charateristics of dinoflagellate cysts, *Limnology and Oceanography.*, **30**, 1000-1009.

ARTHUR, M. A., SCHLANGER, S. O. & JENKYNS H. C., 1987, The Cenomanian-Turonian anoxic event, II. Palaeoceanographic controls on organic matter production and preservation., *In:* BROOKS, J., & FLEET, A. J. (eds) *Marine Petroleum Source rocks, Geological Society of London Special Publication,* **26**, 401-420.

ARTHUR, M. A., & PREMOLI-SILVA, I., 1982, Development of widespread organic carbon-rich strata in the Mediterranean Tethys., *In:* SCHLANGER, S. O. & CITA, M. B., (eds) *Nature and Origin of Cretaceous Carbon-Rich Facies.*, Academic Press, London, pp. 7-54.

ARTHUR, M. A., DEAN, W. E. & PRATT, L. M., 1988, Geochemical and climatic effects of increased marine organic carbon burial at the Cenomanian/Turonian boundary., *Nature*, **335**, 714-717.

ARTHUR, M. A., SCHLANGER, S. O. & JENKYNS H. C. & BRUMSACK, H. J., 1990 Stratigraphy, geochemistry and paleoceanography of organic carbon-rich Cretaceous sequences., *In:* GINDBERG, R. N. & BEAUDOIN, B., *Cretaceous Resources, Events and Rhythms*, Kluwer Academic, Netherlands, 75-119.

BARNES, C., HALLAM, A., KALJO, D., KAUFFMAN, E. G., & WALLISER, O. H., 1996, Global event stratigraphy, *In:* WALLISER, O. H., (ed.), Global Events and Event Stratigraphy in the Phanerozoic, Springer-Verlag, Berlin, Heidelberg, pp333.

BARRETT, P., 1994, *A geochemical and optical study of the Cenomanian-Turonian (Late Cretaceous) "Black Band" of Humberside*, MSc. disertation, University of Newcastle upon Tyne, 58pp.

BARRETT, P., TYSON, R. V., FARRIMOND, P., JONES, D. M., 1995, Organic facies and kerogen isotopic signature of the Cenomanian-Turonian Boundary Event in Tunisia and NW Europe, Abstract of the European Association of Organic Geochemists, St Sebastian, pp569.

BARRS, M. S., & WILLIAMS, G. L., 1973, Palynology and nannofossil techniques., *Geological Survey of Canada, Department of Energy, Mines and Resources, Paper,* **73-26**, 1-25pp.

BATTEN, D. J., 1974, Wealden palaeoecology from the distribution of plant fossils., *Proceedings of the Geologists' Association*, **85**, 433-458

BAUDIN, F., 1995, Depositional Controls on Mesozoic Source Rocks in the Tethys., *In:* HUC, A., *Paleogeography, Paleoclimate, and Source Rocks, American Association of Petroleum Geologists, Studies in Geology,* **40**, Oklahoma, 191-212.

BAYLISS, P., BERRY, L. G., MROSE, M. E., SMITH, D. K., 1980, Mineral powder diffraction file: search manuel., *Joint Committee on Powder Diffraction Standards*, USA.

BECHTEL, A., PERVAZ, M., PUTTMANN, W., 1997, Role of organic matter and sulphate-reducing bacteria for metal sulphate precipitation in the Bahloul Formation at the Bou Grine Zn/Pb deposit (Tunisia), *Chemical Geology*, **144**, 1-21.

BERGER, W. H., 1979, Impact of deep sea drilling on palaeoceanography., *In:* TALWANI, M., HAY, W. & RYAN, W. B. F., (eds), *Deep Drilling Results in the Atlantic Ocean: Continental margins and paleoenvironments, American Geophysical Union, Maurice Ewing Series*, **3**, 297-314.

BERNER, R. A., 1985, Sulphate reduction, organic matter decomposition and pyrity formation., *Philosophical Transactions of the Royal Society of London*, **A315**, 25-38

BERNER, R. A., 1994, GEOCARB II: A revised model for atmospheric CO_2 over Phanerozoic time., *American Journal of Science*, **294**, 56-91.

BERRY, W. B. N. & WILDE, P., 1978, Progressive ventilation of the oceans - an explanation for the distribution of Lower Paleozoic black shales., *American Journal of Science*, **278**, 257-275

BIRD, C. W., LYNCH, J. M., PIRT, E. J. & REID, W. W., 1973, Steroids and squalene in *Methylococcus capsulatus* grown on methane., *Nature*, **230**, 473-474.

BISHOP, A. N. & FARRIMOND, P., 1995, A new method for comparing hopane distributions., *Organic Geochemistry*, **10**, 987-990.

BISHOP, W. F., 1988, Petroleum geology of east-central Tunisia., *American Association of Petroleum Geologists Bulletin*, **72**, 1033-1058.

BOSTICK, N. H., 1979, Microscopic measurements of catagenesis of solid organic matter in sedimentary rocks to aid exploration for petroleum to detremine former burial temperatures - a review., *Soc. Econ. Pal. Min., Special Publication*, **26**, 17-43.

BRASSELL, S. C., WARDROPER, A. M. K., THOMPSON, I. D., MAXWELL, J. R. & EGLINTON, G., 1981, Specific isoprenoids as markers of methanogenic bacteria in marine sediments., *Nature*, **290**, 693-696.

BROSSE, E., 1982, Les formation d'âge crétacé de L'Atlantique Nord et leur matiére organique: paléogéographie et milieux de dépôt., *Revue de L'Insitut Françis du Petrole*, **37**, 275-336.

BURNHILL, T. J. & RAMSAY, W. V., 1981, Mid-Cretaceous palaeontology and stratigraphy, central North Sea., *In:* ILLING, L. V. & HOBSON, G. D., *Petroleum geology of the Continental Shelf of North West Europe.*, Hayden, London, pp245-254.

BUROLLET, P. F., 1956, Contribution à l' étude stratigraphique de la Tunisie Centrale., *Annalesdes Mines et de la Géologie.*, Tunis, **18**, 345pp

BUROLLET, P. F., DUMSTRE, A., KEPPEL, D. & SALVADOR, A., 1954, Unités stratigraphiques en Tunisie centrale., *19e Congress geoloie internationale.* Algeriers, **21**, 243-254.

BUROLLET, P. F., MUGNIOT, J. M. & SWEENEY, P., 1978, The geology of the Pelagian Block: the margins and basins off Southern Tunisia and Tripolitania., *In:* NAIRN, A., KANES, W. H., & STEHLI, F. G., *The Oceans Basins and Margins, **4B** The western Mediterranean*, Plenum Press, New York, 331-359.

CALVERT, S. E., BUSTIN, R. M. & PEDERSEN, T. F., 1992, Lack of evidence for enhanced organic matter preservation of sedimentary organic matter in the oxygen minimum zone of the gulf of California, *Geology*, **20**, 757-760.

CHOSSEN, P., LANAU, C., CONNAN, J. & DESSORT, D., 1991, Biodegradation of refractory hydrocarbon biomarkers from petroleum under laboratory conditions., *Nature*, **351**, 640-642.

COOPER, B. S., 1990, *Practical Petroleum Geochemistry.*, Robertson Scientific Publication, London, 174pp.

DAVIES, C. P. N., 1997, Unusual biomarker maturation changes through the oil window, a consequence of varied thermal history., *Organic Geochemistry*, **27**, 537-560.

DAVIES, J. C., 1986, *Statistics and Data Analysis in Geology.* Wiley, New York, N. Y., 2nd ed., 646pp.

DAVIES, H. R., BYERS, C. W. & DEAN, W. E., 1988, Pyrite formation in the Lower Cretaceous Mowry Shale: effect of organic matter type and reactive iron content, *American Journal of Science*, **288**, 873-890.

DEAN, W. E., ARTHUR, M. A. & CLAYPOOL, G. E., 1986, Depletion of 13C in Cretaceous marine organic matter: source, diagenetic or environmental signal?, *Marine Geology*, **70**, 119-57.

DEAN, W. E., GARDNER, J. V. & ANDERSON., 1994, Geochemical evidence for enhanced preservation of organic matter in the oxygenminimum zone of the continental margin of northern Califonia during the late Pliestocene., *Paleoceaonagraphy*, **9**, 47-61.

DEEGAN, C. E., & SCULL, B. J., 1977, A standard lithostratographic nomenclature for the central and northern North Sea., *Institute of Geological Sciences, London, Report*, **77/25**.

DEMAISON, G., 1991, Anoxia vs. Preservation: What controls the formation of organic sediments and sedimentary rocks?., *American Association of Petroleum Geologists Bulletin*, 75, 499.

DIDYK, B. M., SIMONEIT, B. R. T., BRASSELL, S. C. & EGLINTON, G., 1978., Organic geochemical indicators of palaeoenvironmental conditions of sedimentation., *Nature*, **272**, 216-222.

DODSWORTH, P.,1996, Stratigraphy, microfossils and depositional environments of the lowermost part of the Welton Chalk Formation (late Cenomanian to early Turonian, Cretaceous) in Eastern England., *Proceedings of the Yorkshire Geological Society,* **51**, p45-64.

DOWNIE, C., HUSSAIN, M. & WILLIAMS, G. L., 1971, Dinoflagellate cysts and acritarch associations in the Palaeogene of southeast England., *Geoscience and Man*, **3**, 29-35.

DURAND, B., 1980, *Kerogen, Insoluble Organic Matter From Sedimentary Rocks.*, Editions Technip, Paris, 519pp.

EGLINTON, G., HAMILTON, R. J., RAPHAEL, R. A. & GONZALEZ, A. G., 1962, Hydrocarbon constituents of wax coatings of plant leaves: a taxonomic survey., *Nature,* **193**, 739-742.

EGLINTON, T. I., LARTER, S. R. & BOON, J. J., 1991, Characterisation of kerogens coals and asphaltenes by quantitative pyrolysis-mass spectrometry., *Journal of Analytical and Applied Pyrolysis*, **20**, 25-45.

EGLINTON, T. I., SINNINGHE DAMSTE, J. S., KOHNEN, M. E. L., DE LEEUW, J. W., LARTER, S. R. & PATIENCE, R. L., 1990, Analysis of the organic sulphur composition of kerogens by flash pyrolysis-gas chromatography., *In:* ORR, W. L. & WHITE, C. M., (eds.) *Geochemistry of Sulphur in Fossil Fuels., American Chemical Society Symposium Series,* **429**. 529-567.

EINSELE, G. & WIEDMANN, J., 1982, Turonian Black Shale in the moroccan Coastal Basins: First Upwelling in the Atlantic?., *In:* VON RAD *et al.*, (eds*). Geology of the Northwest African Continental Margin.*, Springer, New York 396-414.

EMIES, K. -C., WHELAN, J. K. & TARAFA, M., 1991, Sedimentary and geochemical expressions of oxic and anoxic conditions on the Peru Shelf., *In:* TYSON, R. V. & PEARSON, T. H., *Modern and Ancient Continental Shelf Anoxia.*, Geological Society of London Special Publication, **58**, 155-170.

ERNST, G., 1975, Stratigraphie, fauna, und sedimentologie der Oberkreide von Misberg und Höver bei Hamburg., *Mitteilungen. Geologische.-Paläeontologische. Institut. Universitat. Hamburg*, **44**, 69-94.

ERNST, G., SCHMID, F., SEIBERTZ, E. & WOOD, C. J., 1983, Event stratigraphie im Cenoman und Turon NW-Deutschlands., *Zitteliana*, **10**, 531-554.

ERNST, G., HILBRECHT, H. & WOOD, C. J., 1984, The Cenomanian-Turonian boundary problem in NW-Germany, with comments on the north-south correlation in the Regensburg area., *Bulletin of the Geological Socity of Denmark*, **33**, 103-113.

ERNST, G., SCHIMID, F. & KLISCHIES, 1979, Multistratigraphische Untersuchungen in der Oberkeride des Raumes Braunschweig- Hanover., In: Wiedmann, J., *Aspekte der Kreide Europas*, 1st symposium German Cretaceous, Int. Union. Geol. Sci. Ser. Schweizerbert, Stuttgart, **6**, 11-46.

ESPITALIÉ, J., DEROO, G., & MARQUIS, F., 1985a, La pyrolyse Rock-Eval et ses applications., *Review de l'Institute Français du Pétrole*, **40**, 563-579.

ESPITALIÉ, J., DEROO, G., & MARQUIS, F., 1985b, La pyrolyse Rock-Eval et ses applications., *Review de l'Institute Français du Pétrole*, **40**,755-784.

ESPITALIÉ, J., DEROO, G., and MARQUIS, F., 1986, La pyrolyse Rock-Eval et ses applications: Troisiéme partie., *Review de l'Institute Français du Pétrole*, **41**, 73-89.

ESPITALIÉ, J., LAPORTE, J. L., MADEC, M., MARQUIS, F., LEPLAT, P., PAULET, J. & BOUTEFEU, A., 1977, Methode rapide de caracterisation des roches meres, de leur potential petrolier et de leur degre d'evolution *Review de l'Institute Français du Pétrole*, **32**, 23-42.

ESPITALIÉ, J., & BORDENAVE, M. L., 1993, Rock-Eval pyrolysis, *In: Applied Petroleum Geochemistry,* BORDENAVE, M. L., (ed.), Editions Technip, Paris, pp.237-261.

FARRIMOND, P., EGLINTON, G. & BRASSELL, S. C., 1986, Alkenones in Cretaceous Black Shales. **In:** LEYTHAUESER, D. & RULKOTTER, J., *Advances in Organic Geochemistry, 1985, Organic Geochemistry*, **10**, 897-903.

FARRIMOND, P., EGLINTON, G., BRASSELL, S. C. & JENKYNS, H. C., 1990a, Toarcian Anoxic Event in Europe: an Organic Geochemical Study., *Marine and Petroleum Geology*, **6**, 136-147.

FARRIMOND, P., EGLINTON, G., BRASSELL, S. C. & JENKYNS, H. C., 1988, The Toarcian black shale event in northern Italy *In:* MATAVELLI, L. & NOVELLI, L. (eds), *Advances in Organic Geochemistry 1987, Organic geochemistry,* **13**, 823-832.

FARRIMOND, P., EGLINTON, G., BRASSELL, C. & JENKYNS, H. C.,1990b, The Cenomanian/Turonian anoxic event in Europe: an organic geochemical study., *Marine and Petroleum Geology*, **7**, 75-89.

FARRIMOND, P., STODDART, D.P. & JENKYNS, H. C., 1994, An organic geochemical profile of the Toarcian anoxic event in northern Italy, *Chemical Geology,* **111**, 17-33.

FISCHER, A. G. & ARTHUR, M. A., 1977. Secular variations in the pelagic realm, *In: Deep-water Carbonate Environments,* COOK, H. E., & ENOS, P., (eds.), *Special Publication of Economic and Palaeotological Mineralurgy*, **25**, 19-50.

FORSMAN, J. P., 1963 Geochemistry of kerogen, *In:* BERGER, I. A., (ed*), Organic Geochemistry*, Pergamon, 148-182.

FOURNIÉ, D., 1978, Nomenclature lithostratigraphique des séries du Crétacé Supérieur au Tertaire de Tunisie., *Bulletin Des Centres Rechersches Exploration -Production, Elf-Aquitaine*, **2**, 97-148.

FOWLER, M. G., 1984, *Organic Geochemistry of Pre-Carboniferous Sedimentary Organic Matter*, PhD Thesis, University of Newcastle.

FUNNELL, B. M., 1978, Productivity control of chalk sedimentation., *In:* FRIEDMAN, G. M., (ed.) *Abstracts of the 10th International Congress of Sedimentology, Jerusalem*, **1**, 228.

GALE, A. S., JENKYNS, H. C., KENNEDY, W. J. & CORFIELD, R. M., 1993, Chemostratigraphy versus Biostratigraphy: data from around the Cenomanian-Turonian boundary., *Journal of the Geological Society of London*, **150**, 29-32.

GELPI, E., SCHNIEDER, H., MANN, J. & ORO, T., 1970, Hydrocarbons of geochemical significance in microscopic algae., *Phytochemistry*, **9**, 603-612.

GOOSENS, H., DE LEEUW, J. W., SCHENCK, P. A. & BRASSELL, S. C., 1984, Tocopherols as likely precursors of pristane in ancient sediments and crude oils., *Nature*, **312**, 440-442.

GRAAS, G. V., VIETS, T. C., DE LEEUW, J. W. & SCHENCK, P. A., 1983, A study of the soluable and insoluble organic matter from the Livello Bonarelli, a Cretaceous black shale deposit in Central Apennines Italy., *Geochimica et Cosmochimica Acta*, **47**, 1051-1059.

De GRACIANSKY, P. C. & DEROO, G., 1984, A stagnation event of ocean wide extent in the Upper Cretaceous, *Nature*, **308**, 346-349.

GRANTHAM, P. J., POSTHUMA, J. & DEGROOT, K., 1980, Variation and significance of the C27 and C28 triterpane content of a North Sea core and various North Sea crude oil., *In:* DOUGLAS, A. G. & AND MAXWELL, J. R., (eds*). Advances in Organic Geochemistry*, Pergamon, New York, 29-38.

GROSS, M. G., CAREY, A.G. FOWLER, Jr. G. A. & KULUM, L. D., 1972, Distribution of organic carbon in surface sediment, northeast Pacific Ocean, *In*: PRUTER, A. T. & ALVERSON, D., *The Columbia River Estuary and Adjacent Ocean Waters - Bioenvironmental Studies*., University of Washington Press, 254-264.

HABIB, D., 1982, Sedimentary supply origin of Cretaceous of Cretaceous black shales., *In:* SCHLANGER, S. O., & CITA, M. B., *Nature and Origin of Cretaceous Carbon-Rich Facies*, Acadmic Press, London, 113-127.

HÅKANSSON, E., BROMLEY, R. G., & PERCH-NIELSEN, K., 1974, Maastrichtian chalk of north-west Europe - a pelagic shelf sediment. *In:* HSÜ, K. J., &JENKYNS, H.C., (eds.), *Pelagic Sediments: on Land and Under the Sea, Special Publication of the International Association of Sedimentologists*, **1**, 211-233.

HALLAM, A. & SELLWOOD, B. W., 1968, Origin of Fullers Earth in the Mesozoic of southern England, *Nature*, **220**, 1193-1195.

HANCOCK, J, M., 1993, Sea-level changes around the Cenomanian-Turonian Boundary., *Cretaceous Research*, **14**, 553-562.

HANCOCK, J, M., & KAUFFMAN, E, G., 1979, The great transgressions of the late Cretaceous, *Journal of the Geological Society of London.*, **136**, 175-186.

HASEGAWA, T., 1997, Cenomanian-Turonian carbon Isotope events recorded in terrestrial organic matter from northern Japan., *Palaeogeography Palaeoclimatology Palaeoecology*, **130**, 251-273.

HAQ, B. U., HARDENBOL, J. & VAIL, P. R., 1987, Chronology of fluctuating sealevels since the Triassic., *Science*, **235**, 1156-1167.

HARDENBOL, J., CARON, M., AMEDRO, F., DUPIS, C. & ROBASZYNSKI, F., 1993, The Cenomanian-Turonian boundary in central Tunisia in the context of a sequence-stratigraphic interpretation., *Cretaceous Research*, **14**, 449-454.

HARLAND, W. B., COX, A. U., LLEWELLYN, P. G., PICKTON, C. A. G., SMITH, A. G. & WALTERS, R., 1982, *A Geological Time Scale*, Cambridge University Press, Cambridge, 131pp.

HART, M. B.& BIGG, P. J., 1981, Anoxic events in the late Cretaceous chalk seas of North-West Europe., *In:* NEALE, J. W. & BRASIER, M. D. (eds) *Microfossils of Recent and Fossil Shelf Seas*, Halsted Press, New York, 177-185.

HEIM, D., 1957, Über die mineralischen nichtkarbonatischen Bestandteile des Cenoman und Turon der mitteldeutschen Kreidemulden und ihre Verteilung., *Heidelberger Beitrage zur Mineralogie und Petrographie.*, **5**, 302-330, Berlin, Göttingen, Heidelberg.

HERBERT, T. D. & FISCHER, A. G., 1986, Milankovitch climatic origin of mid-Cretaceous black shale rhythms in central Italy., *Nature*, **321**, 739-743.

HERBIN, J. P., & DEROO, G., 1979, Etude sedimentologique de la matière organique dans la argilites noirs crètacèes de l'Atlantique Sud., *Documents des Laboratories de Gèologie de la Faculte des sciences de Lyon,* **75**, 71-87.

HERBIN, J. P., & DEROO, G., 1982, Sedimentologique de la matière organique dans la formations du Mèsozoic de l'atlantique Nord., *Buletin de la Societe Gèologique de France,* **24**, 497-510.

HERBIN, J. P., MONTADERT, L., MÜLLER, C., GOMEZ, THUROW, J., & WEIDMAN, J., 1986, Organic rich sedimentation at the Cenomanian-Turonian boundary in oceanic and coastal basins in the North Atlantic and Tethys., *In:* SUMMERHAYES, C. P., SHACKLETON, N. J., (eds.), *North Atlantic Palaeoceanography, Geological Society of London, Special Publication*, **21**, 389-422.

HILBRECHT, H.,1986, On the correlation of the Upper Cenomanian and Lower Turonian of England and Germany (Boreal and N-Tethys)., *Newsletters in Stratigraphy*, **15**, 115-138.

HILBRECHT, H., 1989, Redeposition of late Cretaceous pelagic sediments controlled by sea-level fluctuations., *Geology,* **17**, 1072-1075.

HILBRECHT, H. & DAHMER, D., 1994, Sediment dynamics during the Cenomanian-Turonian (Cretaceous) oceanic anoxic event in Northwestern Germany., *Facies,* **30**, 63-84.

HILBRECHT, H. & HOEFS, J., 1986, Geochemical and palaeontological studies of the $\delta^{13}C$ anomaly in boreal and North Tethyan Cenomanian-Turonian sediments in Germany and adjacent areas., *Palaeogeography, Palaeoclimatology, Palaeoecology,* **53**, 169-189.

HILBRECHT, H., ARTHUR, M. A. & SCHLANGER, S. O., 1986, The Cenomanian-Turonian boundary event: sedimentary, faunal, and geochemical criteria developed from stratigraphic studies in NW-Germany., *In:* WALLISER, O, *Global Bio-Events*, *Lectures In Earth Sciences,* **8**, 345-350.

HILBRECHT, H., HUBBERTEN, H. W. & OBERHËANSLI, H., 1992, Biogeography of plankton foraminifera and regional isotope variations: productivity and water masses in the Late Cretaceous Europe., *Palaeogeography, Palaeoclimatology, Palaeoecology*, **92**, 407-421.

HILBRECHT, H., FRIEG, C., TRÖGER, K. A., VOIGHT, S. & VOIGHT, T., 1996, Shallow water facies during the Cenomanian Turonian anoxic event: bioevents, isotopes and sealevel rise in southern Germany., *Cretaceous Research*, **17**, 229-253.

HOME, A. K., 1992, *A Quantitative Study of Sedimentary Organic Matter Evolution During Hydrous Pyrolysis*., PhD Thesis, University of Newcastle.

HORSFIELD, B., 1984, Pyrolysis studies and petroleum exploration, *In:* BROOKS, J., & WELTE, D. H., *Advances in Petroleum Geochemistry*, Academic Press, London pp. 247-292.

HUANG, W. Y. & MEINSCHEIN, W. G., 1979, Sterols as ecological indicators., *Geochimica et Cosmochimica Acta*, **47**, 739-745.

HUC, A. Y., IRWIN, H., SCHOELL, M., 1985, Organic matter Quality changes in an Upper Jurassic shale sequence from the Viking Graben, *In:* THOMAS, B. M., *et al.*, (eds), *Petroleum Geochemistry in Exploration of the Norwegian shelf.*, Norwegian Petroleum Society, Graham and Trotman, 179-183.

INNES H, 1998, Hopanoid distributions and diagenesis in recent sediments, PhD Thesis, University of Newcastle, pp256.

IRWIN, W. J., 1982, *Analytical Pyrolysis: A Comprehensive Guide*., Chromatographic Science Series, 22, Marcel Dekker, Inc. New York, 578pp.

IRVING, E., NORTH, F. K. & COVILLARD, R., 1974, Oil and climate tectonics., *Canadian Journal of Earth Sciences*, **11**, 1-25.

JEANS, C. V., LONG, D., HALL, M. A., BLAND, D. J. & CORNFORD, C., 1991, The geochemistry of the Plenus Marls at Dover, England; evidence of fluctuating oceanographic conditions and of glacial control during the development of the Cenomanian-Turonian $\delta^{13}C$ anomaly., *Geolological Magazine*. **128**, (6), 603-632.

JEFFERIES, R. P. S., 1963, The stratigraphy of the *Actinocamax plenus* subzone (Turonian) in the Anglo-Paris Basin,, *Proceeding of the Geologists Association*, **74**, 1-33.

JENKYNS, H. C., 1980, Cretaceous anoxic events: from continents to oceans., *Journal of the Geological Society London*, **137**, 171-188.

JENKYNS, H. C., 1985, The early Toarcian and Cenomanian-Turonian anoxic events in Europe: comparisons and contrasts., *Geologische Rundschau,* **74**, 505-518.

JENKYNS, H. C., GALE, H. C., & CORFIELD, R. M., 1994, Carbon and oxygen-isotope stratigraphy of the English Chalk and the Italian Scaglia and its palaeoclimate significance, *Geological Magagazine,* **131**, 1-34

JONES, D. M., 1980, *Hydrocarbons, fatty acids and kerogen from the Kimmeridge Clay*, MSc. dissertation, University of Newcastle upon Tyne.

JUDD, J. W., 1867, On the strata for thye base of the Lincolnshire Wolds, *Quarterly Journal of the Geological Society London,* **23**, 227-251.

KATZ, B. J., 1983, Limitations of 'Rock-Eval' pyrolysis for typing organic matter, *Organic Geochemistry*, **4**, 195-199.

KAUFFMAN, E. G., 1977, Geological and biological overview: Western Interior Cretaceous Basin., *The Mountain Geologist*, **14**, 75-99.

KAUFFMAN, E. G., & HART, M. B., 1996, Cretaceous Bio-Events., *In:* WALLISER, O. H., (ed.), Global Events and Event Stratigraphy in the Phanerozoic, Springer-verlag, Berlin, Heidelberg, 285-312.

KEIL, R. G., TSMASKIS, E., FUH, C. B., GIDDINGS, J. C. & HEDGES, J. I., 1994, Mineralogical and textural controls on the organic composition of coastal marine sediments: hydrodynamic separation using SPLITT-fractionation., *Geochimica et Cosmochimica Acta*, **58**, No.2 p879-893.

KENNEDY, W, J., WRIGHT, C. W. & HANCOCK, J. M., 1981, Ammonite zonation and correlation of the uppermost Cenomanian and Turonian of southern England, Sarthe and Touraine., *In: Groupe Francais de Cretace. Colleque sur le Turonien, Memoires du Museum National d'Histoire Naturelle*, Paris, 175-183.

KILLOPS, S. D., KILLOPS, V. J., 1993, *An Introduction to Organic Geochemistry.*, Longman, Harlow, 265pp.

KOCKER, F., WEHNER, H. & GERLING, P., 1994, Petroleum systems of the Lower Saxony Basin, *In:* MAGOON, L. B., & DOW, W. G., (eds), *The Petroleum System- From Source to Trap: American Association of Petroleum Geologist Bulletin*, Memoir **60**, 573-591.

KOVACH, W. L., 1989, Comparisons of multivariate analytical techniques for use in pre-Quaternary plant palaeoecology., *Review of Palaeobotany and Palynology*, **60**, 255-282.

KOVACH, W. L., 1993, MVSP - A Multivariate Statistical Package for IBM-PC's, Version 2.1, Kovach Computing Services, Pentraeth, Wales, UK.

KOVACH, W. L. & BATTEN, D. J., 1994, Association of palynomorphs and palynodebris with depositional environments: quantitative approaches., *In:* TRAVERSE, A. (ed.) *Sedimentation of Organic Particles*, Cambridge University Press.

KRUGE, M. A., HUBERT, J. F. & KAGI, R. I., 1990, Biological markers in the Lower Jurassic synrift lacustrine black shales, Hartford Basin, Connecticut., *Organic Geochemistry*, **15**, 281-289.

KUHNT, W, HERBIN, J. P., THUROW, J. & WIEDMAN, J., 1990, Distribution of Cenomanian-Turonian organic facies in the Western Mediterranean and along the adjacent Atlantic margin., *In:* HUC, A. H., (ed.), Deposition of Organic Facies, *American Association of Petroleum Geologist Bulletin, Studies in geology,* No. **30**, 133-160.

LANGFORD, F. F. & BLANC-VALLERON, M. M., 1990, Interpreting Rock-Eval pyrolysis data using graphs of pyrolizable hydrocarbons vs. total organic carbon., *American Association of Petroleum Geologist Bulletin*, **74**, 799-804.

LARTER, S., 1988, Some pragmatic perspectives in source rock geochemistry., *Marine and Petroleum Geology*, **5**, 194-204.

LARTER, S. R. & HORSFIELD, B., 1993, Determination of structural components of kerogens by the use of analytical pyrolysis methods., *In:* ENGLE, M. H., & MACKO, A., (eds) *Organic Geochemistry*., Plenum Press, New York. 271-287.

LARTER, S., DOUGLAS, A. G., 1980a, A pyrolysis-gas chromatographic method for kerogen typing., *In:* DOUGLAS, A. G., & MAXWELL, J. R., (eds), *Advances in Organic Geochemistry*, *Organic Geochemistry*, 579-584.

LARTER, S. & DOUGLAS, A. G., 1980b, Melanoidins - kerogen precursors and geochemical lipid sinks: a study using pyrolysis-gas chromatography(P-GC)., *Geochimica et Cosmochimica Acta*, **44**, 2087-2095.

LARTER, S. & DOUGLAS, A. G., 1982, Pyrolysis methods in organic geochemistry: an overview., *Journal of Analyical and Applied Pyrolysis*, **4**, 1-19.

LARTER, S., HORSFIELD, B. & DOUGLAS, A. G., 1977, Pyrolysis as a possible means of determining the petroleum generating potential of sedimentary organic matter., *Analytical Pyrolysis*, 189-202.

LARTER, S., & SENTFLE, J., 1985, Improved kerogen typing for petroleum source rock analysis, *Nature*, **318**, 277-280.

LAMBOLDA, M., GOROSTIDI, A. & PAUL,C. R. C., 1994, Quantitative estimates of calcaerous nannofossil changes across the Plenus Marls (latest Cenomanian), Dover, England: implications for the generation of the Cenomanian-Turonian boundary event., *Cretaceous Research*, **15**, 143-163.

LEVENTHAL, J. S., 1983, An interpretation of carbon and sulfur relationships in the Black Sea sediments as indicators of environment of deposition, *Geochimica et Cosmochimica Acta*, **47**, 133-137.

LEYTHAEUSER, D. & SCHWARZKOPF, T., 1986, The pristane/*n*-heptadecane ratio as an indicator for recognition of hydrocarbon migration effects., *Organic Geochemistry*, **10**, 191-197.

LÜCKGE, A., BOUSSAFIR, M., LALLIER-VERGES, E. & LITTKE, R., 1996, Comparative study of organic matter preservation in immature sediments along the continental margins of Peru and Oman. Part 1: Results of petrographical and bulk geochemical data., *Organic Geochemistry*, **24**, 437-451.

MAAMMOURI, A. L., ZAGHIBB-TURKI, M. F., CHICKAOUI, M. & SALAJ, J., 1994, La Formation Bahloul en Tunisie centro-septentrionale: variations laterales, nouvelle interpretation en terme de stratigraphie sequentielle., *Journal of African Earth Sciences*, **18**, 37-50.

MACKENZIE, A. S., PATIENCE, R. L., MAXWELL, J. R., VANDENBROUCKE, M. & DURAND, B., 1980, Molecular parameters of maturation in the Toarcianshales, paris Basin, France-III. Changes in the configuration of acyclic isoprenoid alkanes, steranes, and triterpanes., *Geochimica et Cosmochimica Acta*, **44**, 1709-1721.

MACKENZIE, A. S., 1984, Application of biological markers in petroleum geochemistry, *In:* BROOKS, J., & WELTE, *D., Advances in Petroleum Geochemistry*, **1**, 115-214, Academic Press, New York.

MARSHALL, K. L. & BATTEN, D. J., 1988, Dinoflagellate cyst associations in Cenomanian/Turonian "black shale" sequences of northern Europe., *Review of Palaeonbotany and Palynology*, **54**, 85-103.

MASSE, J. P., PHILIP, J., CAMOIN, G., 1995, The Cretaceous Tethys, *In*: NAIRN, A. E. M., RICOU, L. M., VRIELYNCK, B., and DERCOURT, J., *(eds*), The Ocean Basins and Margins, Volume 8 The Tethys Ocean, Plenum Press.

MAYER, L. M., 1994, Adsorptive control of organic matter accumulation in continental shelf sediments., *Geochimica et Cosmochimica Acta*, 4, 1271-1284.

McEVOY, J. & GEIGER, W., 1986, Origin of hydrocarbons in Triassic Serpiano oil shales: hopanoids, *Organic Geochemistry*, **10**, 943-949.

MEGLAN, R. R., 1992, Examining large databases: a chemometric approach using principal component analysis., *Marine Chemistry*, **39**, 217-237.

MENARD, H. W. & SMITH, S. M., 1966, Hypsometry of ocean basin provinces, *Journal of Geophysical Research*, **71**, 4305-4325.

METCALF, S. G., WINDIG, W., HILL, G. R. & MEUZELAAR, H. L. C., 1987, Characterisation of US lignites by pyrolysis mass spectrometry and multivariate analysis., *International Journal of Coal Geology*, **7**, 245-268.

MEUZELAAR, H. L. C., HARPER, A. M., PUGMIRE, R. J. & KARAS, J., 1984, Characterisation of coal maceral concentrates by curie point pyrolysis mass spectrometry., *International Journal of Coal Geology*, **4**, 143-171.

MOBERLY, R. & LARSON R. L., 1975, Mesozoic magnetic anomalies, ocean plateaus, and seamount chains in the northwestern Pacific Ocean, *In:* LARSON R. L., & MOBERLY, R., et al., *Initial Reports of the Deep Sea Drilling Project*, **32**, (U. S. Government Printing Office, Washington), 945-957.

MOLDOWAN, J. M., SUNDARARAMAN, P. & SCHOELL, M., 1986, Sensitivity of biomarker properties to depositional environment and/or source input in the Lower Toarcian of SW Germany,, *Organic Geochemistry*, **10**, 915-926.

MONTACER, M., DISNAR, J. R., ORGEVAL, J. J. & TRICHET, J., 1988, Relationship between Zn-Pb ore and oil accumulation processes: examples of the Bou Grine deposit (Tunisia), *Advances in Organic Geochemistry*, 1987, *Organic Geochemistry,* **13**, 423-431.

MÜLLER, P. J., ERLENKEUSER, H. &VON GRAFENSTEIN, R., 1985, Glacial-interglacial cycles in oceanic productivity inferred from organic carbon contents in eastern North atlantic sediments cores., *In:* THIEDE, J. & SUESS, E., (eds*), Coastal Upwelling: Its Sediment Record. Part B: Sedimentary Records of Ancient Upwelling.*, NATO Conference Series IV, **10b**, Plenum Press, New York, 365-398.

NAKATSUKA, T., HANDA, N., WADA, E., AND WONG, C. S., 1992, The dynamic changes of stable isotopic ratios of carbon and nitrogen in suspended and sedimented particulate organic matter during a phytoplankton bloom., *Journal of Marine Research,* **50**, 267-96.

ORR, W. L., 1983, Comments on pyrolytic hydrocarbon yields in source rock evaluation., *In:* M. BJORØY *et al.*, (eds) *Advances in Organic Geochemistry, 1981, Organic Geochemistry,* 775-787.

OURISSON, G., ALBRECHT, P. & ROHMER, M., 1979, The hopanoids: palaeochemistry of a group of natural products., *Pure and Applied Chemistry*, **51**, 709-729.

OURISSON, G., ROHMER, M. & PAROLLA, K., 1987, Prokayotic hopanoids and other polyterpanoid steroid surrogates., *Annual Review of Microbiology*, **41**, 301-333.

PAROPKARI, A. L., PRAKASH BABU, C. & MASCARENHAS., 1993, New evidence for enhanced preservation of organic carbon in contact with oxygen minimum zone on the western continental slope of India., *Marine Geology*, **111**, 7-13.

PAUL, C. R. C., MITCHELL, S. F., MARSHALL, J. D., LEARY, P. N., GALE, A. S., DUANE, A. M. & DITCHFIELD, P. W., 1994, Palaeoceangraphic events in the middle Cenomanian of North West Europe., *Cretaceous Research*, **15**, 707-738.

PEDERSEN, T. F., SHIMMIELD, G. B. & PRICE, N. B., 1992, Lack of enhanced preservationof organic matter in sediments under the oxygen minimum zone on the Oman margin., *Geochimica et Cosmochimica Acta*, **56**, 545-551

PEISELER, B. & ROHMER, M., 1991, Prokaryotic triterpenoids (22R, 32R)-34,35-dinorbacteriohopane-33,32-diols from *Acetobacte acetii* ssp. *xylinum*: new bacteriohopane derivatives with shortend side chain., *Journal of the Chemical Society, Perkin Transactions 1*, 2449-2453.

PERVAZ, M. & PÜTTMANN, W., 1995, Biodegradation of hydrocarbons by sulphate reducing bacteria in the Cretaceous Bahloul Formation (Tunisia)., *In:* SNAPE, C., (ed.) *Composition, Geochemistry and Conversion of Oil Shales,* Kluwer Academic, Dordrecht, p407-418.

PERYT, D. & WRYWICKA, K., 1991, The Cenomanian-Turonian anoxic event in SE Poland., *Cretaceous Research*, **12**, 65-80.

PETERS, K. E. & MOLDOWAN, J. M., 1993, *The Biomarker Guide. Interpreting Molecular Fossils in Petroleum and Ancient Sediments*., Prentice Hall, Inc, New Jersey, 363pp.

PETERS, K. E., 1986, Guidelines for evaluating petroleum source rock using programmed pyrolysis, *American Association of Petroleum Geologists Bulletin,* **70**, 318-329.

PHILIP, J., & AIRAUD-CRUMIERE, C., 1991, The demise of rudist-bearing carbonate platforms at the Cenomanian-Turonian: a global control., *Coral Reefs*, **10**, 115-125.

PHILIP, J. BABINOT, J. F., TROCHETTI, G., FOURCADE, E., GURIARD, R., BELLION, Y., HERBIN, J. P., COMBES, P. J., CORNEE, J. J., DERCOURT, J., RICOU, L. E., 1993, Late Cenomanian (94-92 MA) in: *Atlas Tethys Palaeoenvironmental Maps, Explanatory notes*, 153-178 (DERCOURT, J., RICOU, L. E., & VRIELYCK,. EDs) Gauther-Villas, Paris.

PHILIP, J., MASSIE, J. P. & BESSIAS, H., 1989, Organisation et évolution sédimentaires d'une marge de plate-forme carbonatée: l'Albian-Cénomanien de Tunisie centrale., *Géologie Méditerranéenne*, **16**, 155-169.

POMEROL, B., 1983, Geochemistry of late Cenomanian-early Turonian chalks of the Paris Basin: manganesse and carbon isotopesin carbonates as palaeoceanographic indicators., *Cretaceous Research*, **4**, 85-93.

POMEROL, B. & MORTIMORE, R. N., 1993, Lithostratigraphy and correlation of the Cenomanian-Turonian boundary sequence., *News Letters on Stratigraphy,* **28**, 59-78.

PRATT, L. M., 1984, Influence of palaeoenvironmental factors on preservation of organic matter in middle cretaceous greenhorn formation, pueblo, Colorado., *American Association of Petroleum Geologists Bulletin*, **68**, 9, 1146-1159.

PRATT, L. M., FORCE, E. R. & POMEROL, B., 1991, Coupled manganese and carbon-isotopic events in marine carbonates at the Cenomanain-Turonian boundary., *Journal of Sedimentary Pertology*, **61**, 370-383.

PRATT, L. M., CLAYPOOL, G. E. & KING, D., 1986, Geochemical imprint of depositional conditions on organic matter in laminated-bioturbated interbedded fine grained marine sequences., *Marine Geology,* **70**, 67-84.

PRATT, L. M. & THRELKELD, C. N., 1984, Stratigraphic significance of the 13C/12C ratios in mid-Cretaceous rocks of the Western Interior, U.S.A., *Memoir of the Canadian Society of Petroleum Geologists*, **9**, 305-312.

PRICE, P. L., O'SULLIVAN, T. O. & ALEXANDER, R., 1987, The nature and occurence of oil in Seram, Indonesia., *In: Proceedings of the 16th Annual Convension Of the Indonesian Petroleum Association, Jakarta,* 141-173.

RADKE, M., 1987, Organic geochemistry of aromatic hydrocarbons., *In: BROOKS, J. & WELTE, D., Advances in Petroleum Geochemistry*, **2**, 141-207, Academic Press, New York.

RADKE, M., WELTE, D. H. & WILLS, H., 1985, Maturity parameters based on aromatic hydrocarbons: influence of the organic matter type., *Organic Geochemistry*, **10**, 51-63.

RAISWELL, R., & BERNER, R. A., 1985, Pyrite formation in euxinic and semi-euxinic sediments., *American Journal of Science*, **285**, 710-724.

RAISWELL, R., BUCKLEY, F., BERNER, R. A., & ANDERSON, T. F., 1988, Degree of pyritisation of iron as a paleoenvironmental indicator of bottom water oxygenation., *Journal of Sedimentary Petrology*, **58**, 812-819.

RAZGALLAH, S., PHILIP, J., THOMEL, G., ZAGHBIB-TURKI, D., CHAABANI, F., BEN HAJ ALI, N. & M'RABET, A., 1994, La Limite Cénomanien-Turonien en Tunisie centrale et méridionale: biostratigraphie et paléoenvironnements., *Cretaceous Research*, **15**, 507-533.

REYMENT, R. A., & DINGLE, R. V., 1987, Palaeoecology of Africa during the Cretaceous period, *Palaeogeography, Palaeoclimatology, Palaeoecology*, **59**, 93-116.

RICKEN, W., 1996, Bedding rhythms and cyclic sequences as documented in organic carbon-carbonate patterns, Upper Cretaceous Western Interior., *Sedimentary Geology,* **102,** 131-154.

RICOU, L. E., 1995, Plate tectonic history of the Tethys Ocean, *In*: NAIRN, A. E. M., RICOU, L. M., VRIELYNCK, B., and DERCOURT, *J.*, (eds*), The Ocean Basins and Margins, Volume 8 The Tethys Ocean*, Plenum Press.

RIOLO, J., HUSSLER, G., ALBRECHT, P. & CONNAN, J., 1986, Distribution of aromatic steroids in geological samples: their evaluation as geochemical parameters., *Organic Geochemistry*, **10**, 981-90.

ROBASZYNSKI, F. & GALE, A. S., 1993, The Cenomanian-Turonian boundary: a discussion held at the final session of the colloquium on Cenomanian-Turonian events, Grenoble, 26th May 1991 (France)., *Cretaceous Research*, **14**, 607-611.

ROBASZYNSKI, F., AMEDRO, F. & CARON, M., 1993a, The Cenomanian-Turonian boundary formation in some central Tunisian locations., *Cretaceous Research,* **14**, 4-5, 477-486.

ROBASZYNSKI, F., CARON, M., DUPIS,C., AMEDRO, F., GONZALEZ DONOSO, J. M., LINARES, D., HARDENBOL, J., GARTNER, S., CALANDRA, F. & DELOFFE, R., 1990, A tentative integrated stratigraphy in the Turonian of Central Tunisia: formations, zones, and sequential stratigraphy in the Kalaat Senan area., *Bulletin des Centres de Recherches Exploration Producttion, Elf Aquitaine,* **14,** 213-384.

ROBASZYNSKI, F., HARDENBOL, J., CARON, M., AMEDRO, F., DUPUIS, C., GONZALEZ DONOSO, J. M., LINARES, D. & GARTNER, S., 1993b, Sequence stratigraphy in a distal environment: the Cenomanian of the Kalaat Senan Region (Central Tunisia)., *Bulletin des Centres de Recherches Exploration Producttion, Elf Aquitaine,* **17**, 395-433.

ROHMER, M., BISSERT, P. & NEUNLIST, S., 1992 The hopanoids, prokaryotic triterpenoids and precursors of ubiquitous molecular fossils., *In:* MOLDOWAN, J. M., *et al.* (eds), *Biological Markers in Sediments and Petroleum*., Prentice Hall, Englewood Cliffs, New Jersey, 1-17.

ROWE, A. W., 1904, The zones of white chalks of the English Coast, IV- Yorkshire., *Proceeding of the Geologists Association*, **18**, 193-296.

SARJEANT, W. A. S. & LACALLI, T, GAINES, G., 1987, The cysts and skeletal elements of dinoflagellates: speculations on the ecological causes for their morphology and development., *Micropaleontology*, **33**, 1-36.

SAUNDERS, J. B., EDGAR, N. T., DONELLY, T. W. & HAY, D. W., 1973, Cruise synthesis, *In:* EDGAR, N. T. & SAUNDERS, J. B., *Initial Reports of the Deep Sea Drilling Project*, **15**, (U. S. Government Printing Office, Washington), 1077-1111.

SCHLANGER, S. O., & JENKYNS, H. C., 1976, Cretaceous oceanic anoxic events: causes and consequences., *Geologie en Mijnbouw*, **55**, 179-184.

SCHLANGER, S. O. & JACKSON, E. D., 1976, Initial Reports of the Deep Sea Drilling Project, 33, (U. S. Government Printing Office, Washington), 973pp.

SCHLANGER, S. O., ARTHUR, M. A., JENKYNS, H. C. & SCHOLLE, P. A., 1987, The Cenomanian-Turonian Oceanic Anoxic Event, I. Stratigraphy and distribution of organic carbon rich beds and the marine $\delta^{13}C$ excursion., *In:* BROOKS, S. J., & FLEET, A. J. (eds) *Marine Petroleum Source rocks, Geological Society of London Special Publication,* **26**, 401-420.

SCHOLLE, P. A. & ARTHUR, M. A., 1980, Carbon isotope fluctuations in Cretaceous pelagic limestones: potential stratigraphic and petroleum exploration tool, *American Association of Petroleum Geologists Bulletin*, **64**, 67-87.

SCHOUTEN, S., SINNINGHE DAMSTÉ, J. S. & DE LEEUW, J. W., 1995, The occurence and distribution of low molecular weight sulphoxides in polar fractions of sediments, extracts and petroleum., *Organic Geochemistry*, **23**, 129-138.

SEIFERT, W. K., MOLDOWAN, J. M., SMITH, G. W. & WHITEHEAD, E. N., 1978, First proof of a C28 pentacyclic triterpane in petroleum., *Nature*, **271**, 436-437.

SENFTLE, J. F., LARTER, S. R.& BROWN, J. H., 1987, Refinement of organic petrographic methods for kerogen characterisation., *International Journal of Coal Geology*, **7**, 105-117.

SHI JIYANG, WANG BENSHAN, ZHANG LIJIE & HONG ZHIQING, 1988, Study on diagenesis of organic matter in immature rocks., *In:* MATAVELLI, L. & NOVELLI, L. (eds), *Advances in Organic Geochemistry 1987, Organic geochemistry,* **13**, 869-874.

SINNINGHE DAMSTÉ, J. S., KOCK-VAN DALEN, A. C., DE LEEUW, J. W. & SCHENCK, P. A., 1988, Identification of homologous series of alkylated thiophenes, thiolanes and benzothiophenes present in pyrolysates of sulphur-rich kerogens., *Journal of Chromatography,* **435**, 435-452.

SINNINGHE DAMSTÉ, J. S., EGLINTON, T. I., DE LEEUW J. W. & SCHENCK, P. A., 1989a, Organic sulphur in macromolecula sedimentary organic matter: I Structure and origin of sulphur-containing moieties in kerogens, asphaltenes and coals as revealed by flash pyrolysis., *Geochimica et Cosmochimica Acta*, **53**, 873-889.

SINNINGHE DAMSTÉ, J. S., IRENE, C., RIJPSTRA, C. A. C., DE LEEUW J. W. & SCHENCK, P. A., 1989b, The occurence and identification of a series of organic sulphur compounds in oils and sediment extracts: II. Their presence in samples from hypersaline and non-hypersaline palaeoenvironments and possible application as source, palaeoenvironmental and maturity indicators., *Geochimica et Cosmochimica Acta*, **53**, 1323-1341.

SKJEVRAK, I., 1997, *Quantitative Group Type Analysis of Kerogens Using Pyrolysis-Mass Spectrometry.*, PhD. Thesis, University of Newcastle upon Tyne.

SOLI, H., LARTER, S. & DOUGLAS, A. G., 1981, Analysis of kerogens by Pyrolysis-Gas Chromatography-Mass Spectrometry using selective ion monitoring. III. Long-Chain Alkylbenzenes., *Journal of Analytical and Applied Pyrolysis,* 591-597.

SOLI, H., LARTER, S. & DOUGLAS, A. G., 1980, The Analysis of kerogens by Pyrolysis-Gas Chromatography-Mass Spectrometry using selective ion monitoring., *Journal of Analytical and Applied Pyrolysis*, 1, 231-241.

STOUT, S. A., 1991, Principal component analysis of quantatative pyrolysis gas chromatography and organic petrographic data of kerogens., *Journal of Analytical and Applied Pyrolysis*, **18**, 277-292.

SUMMERHAYES, C. P., 1981, Organic facies of Middle Cretaceous black shales in deep North Atlantic., *American Association of Petroleum Geologists Bulletin*, **65**, 2364-2380.

SUMMERHAYES, C. P., 1987, Organic rich Cretaceous sediments from the North Atlantic., *In:* BROOKS, S. J., & FLEET, A. J. (eds) *Marine Petroleum Source rocks, Geological Society of London Special Publication,* **26**, 301-316.

TEN HAVEN, H. L., DE LEEUW, J. W., RULLKOTTER, J. & SINNINGHE DAMSTÉ, J. S., 1987, Restricted use of pristane/phytane ratio as palaeoenvironmental indicator., *Nature*, **330**, 641-643.

THUROW, J., KUHNT, W. & WIEDMANN, J., 1982, Phthanitic and black shale sedimentationin the moroccan Upper Cretaceous - Correlation and palaeogeographic implications., *Neues Jahrbuch fur Geologie und palaontologie. Abhandlungen*, **165**, 147-176.

THUROW, J., MOULLADE, M., BRUMSACK, H. -J., MASURE, E., TAUGOURDEAU-LANTZ, J. & DUNHAM, K., 1988, The Cenomanian/Turonian boundary event (CTBE) at hole 641A, ODP Let 103 (compared with the CTBE interval at Site 398)., *In:* BOILLOT, G., WINTERER, E. L., *Proceedings of the Ocean Drilling Program Scientific Results*, **103**, 587-599.

TISSOT, B., DEROO, G., & HERBIN, J. P., 1979, Organic matter in Cretaceous sediments of the North Atlantic: contribution to sedimentology and palaeogeography., *In:* TALWANI, M., HAY, W. & RYAN, W. B. F., (*eds*), *Deep Drilling Results in the Atlantic Ocean: Continental Margins and Paleoenvironments, American Geophysical Union, Maurice Ewing Series*, **3**, 362-374.

TISSOT, B. P. & WELTE, D, H., 1984, Petroleum Formation and Occurrence., Springer-Verlag, Berlin, 699pp.

TRAVERSE, A., 1988, Paleopalynology, Unwin, Boston 600pp.

TUCHOLKE, B. E. & VOGT, P. R., 1979, Western North Atlantic sedimentary evolution and aspects of tectonic history., *Initial Reports of the Deep Sea Drilling Project*, **43**, 791-826.

TUWENI, A. O. & TYSON, R. V., 1994, Organic facies variation in Westbury Formation (Rhaetic, Bristol Channel, S.W. England)., *Organic Geochemistry*, **200**, 1001-1014.

TYSON, R.V. 1984, Palynofacies investigation of Callovian black shales (Middle Jurassic) sediments from DSDP Site 534, Blake-Bahama Basin, western Central Atlantic., *Marine and Petroleum Geology*, **1**, 3-13.

TYSON, R. V., 1993, Palynofacies analysis., *In:* JENKINS, D. G. (eds) *Applied Micropalaeontology*., Dordrecht, pp 153-191.

TYSON, R.V. 1995, *Sedimentary Organic Matter: Organic Facies and Palynofacies.* Chapman & Hall, London, 615pp.

TYSON, R. V. & FUNNELL, B. M., 1987, European Cretaceous shorelines, stage by stage., *Palaeogeography, Palaeoclimatology, Palaeoecology*, **59**, 69-91.

TYSON, R. V. & PEARSON, T. H., 1991, Modern and ancient continental shelf anoxia: an overview., *In:* TYSON, R. V. & PEARSON, T. H., (eds.), *Modern and Ancient Continental Shelf Anoxia*, *Geological Society Special Publication*, **58**, 1-24.

VAN KREVELEN, D. W., 1961, *Coal.*, Elsevevier, New York, 519pp.

VOLKMAN, J. K., 1986, A review of sterol markers for marine and terrigenous organic matter., *Organic Geochemistry*, 9, 83-99.

VOZZHENNIKOVA, T. F., 1965, Vvedenie v izuchenie iskopaemykh Peridineevykh vodoroslei, Akademiya Nauk SSSR, Sibirskae Otedlenie Instituta Geologii I Geofiziki, Izdatel,stvo, Moscow, 156pp. (Introduction to the Study of Fossil *Peridinien Algae*. Sayers, K., (transl,) and Sarjeant, W. A. S., (eds), National Lending Library for Science and Technology, Boston Spa, UK, (now British Library Document Supply Centre, Boston Spa, 233pp.).

WALDO, G. S., CARLSON, R. M. K., MOLDOWAN, J. M., PETRES, K. E. & PENNER-HAHN, J. E., 1991, Sulfur speciation in heavy petroleums: Information from X-ray adsorption near-edge structure., *Geochimica et Cosmochimica*, **55**, 801-814.

WOLFF, G. A., LAMB, N. A. & MAXWELL, J. R., 1986, The origin and fate of 4-methylsteroid hydrocarbons I. 4-methylsteranes., *Geochimica et Cosmochimica Acta.*, **50**, 335-342.

ZUNDEL, M., & ROHMER, M., 1985, Prokaryotic triterpenoids. 3. The biosynthesis of 2β-methylhopanoids and 3β-methylhopanoids of *Methylobacterium organophilum* and *Acetobacter pasteurianus spp. pasteurianus*, *Eurpean Journal Biochemistry,* **150**, 35-39.

APPENDICES

Appendix 1. Lithological data.

Section depth is recorded from the base upwards; sample OB2 at 0.48m, DOY2 at 2.20m, OG1 at 0.20m and N1 at 0.10m represent the start of the Cenomanian-Turonian sequence. The very base of the Ech Cheid section could not be sampled as it was unexposed. Lithology was determined from observations in the field. Rock colour was determined by comparison to the Rock Colour Chart. Laminations refer to fine laminae observed in the rock samples during laboratory description. Bioturbation refers to observations of C*hondrites* within the samples. The "Biolam" parameter is based on the relative amounts of bioturbation and lamination within a sample:

"Biolam" value	Lamination	Bioturbation
1	yes	no
2	yes	yes
3	some	no
4	some	yes
5	none	no
5	none	yes

Table I. Comparison of samples studied with Hilbrecht & Dahmer (1994)

Published bed no.	Bed thicknes	Depth (m)	Misberg Hilbrechts sample No.	Misberg Sample No. in Thesis
95	5	36.06	bed 58	1
100 (Base)	68	34.54	51	2
105 (Top)	150	31.66	211	3
105 (Base)			214	4
106 (Top)	10	30.16	206	5
106 (Base)			204	6
107 (Top)	53	30.06	201	7
107 (Base)			202	8
108	25	29.53	200	9
110 A	75	27.28	189	10
118	65	25.05	178	11
120	45	23.7	175	12
122	46	22.8	171	13
124	30	21.59	166a	14
126	250	20.99	160	15
128	165	18.49	144	16
128			143	17
130	104	16.84	142	18
132 B	192	11.74	127	19
133			121	20
137 II	82	9.45	114	21
137 IV	30	7.93	97	22
137 VI	10	6.88	89	23
137 (base)	40	2.38	5	24
138 (top)	100	1.98	88	25
138 (base)			84	26
140	43	0.98	80	27
141	55	0.55	71	28

Table II. Lithological descriptions for Misberg Quarry Samples

Sample No.	Section depth (m)	Lithology	Colour
MQ1	36.04	Marly limestone	N8
MQ2	34.20	Limestone	N7
MQ3	31.50	Marly limestone	N8
MQ4	30.50	Marly limestone	N8
MQ5	30.16	Marl	N8
MQ6	30.07	Marl	N6
MQ7	30.00	Marly limestone	5Y 8/1
MQ8	29.60	Marly limestone	5GY 8/1
MQ9	29.41	Marly shale	N8
MQ10	26.91	Marly shale	N8
MQ11	24.73	Marl	N8
MQ12	23.48	Marl	N7
MQ13	22.57	Marl	N6
MQ14	21.44	Marl	N6
MQ15	19.74	Marl	5Y 8/1
MQ16	18.00	Marl	N6
MQ17	17.00	Marl	N6
MQ18	16.32	Marl	N6
MQ19	11.00	Shale	N5
MQ20	10.00	Shale	N5
MQ21	9.04	Marl	N7
MQ22	7.78	Marl	N5
MQ23	6.83	Shale	N7
MQ24	2.18	Limestone	N7
MQ25	1.80	Marl	5Y 8/1
MQ26	1.10	Shale	5Y 8/1
MQ27	0.77	Shale	N6
MQ28	0.28	Marl	5Y 8/1

Tablel III. Lithological descriptions for Oued Bahloul Samples

Sample No.	Section depth (m)	Lithology	Colour	Laminations	Bioturbation
OB83	28.20	Limestone	5Y 6/1	no	Yes
OB82	27.70	Limestone	5Y 4/1	no	no
OB81	27.50	Limestone	5Y 4/1	no	no
OB80	27.10	Shale	N4	some	no
OB79	26.75	Marl	5Y 6/1	no	no
OB78	26.45	Marl	5Y 6/1	no	no
OB77	26.10	Marl	5Y 6/1	no	no
OB76	25.60	Shale	N4	some	no
OB75	25.25	Shale	5Y 6/1	some	no
OB74	24.85	Marl	N4	no	yes
OB73	24.40	Marl	N4	no	no
OB72	24.00	Shale	N4	some	no
OB71	23.80	Marl	N4	no	no
OB70	23.45	Marl	N4	no	no
OB69	23.20	Shale	N4	some	no
OB68	22.90	Shale	N4	some	no
OB67	22.75	Shale	N4	some	no
OB66	22.50	Marl	5Y 8/1	no	yes
OB65	22.20	Marl	5Y 8/1	no	yes
OB64	21.95	Marl	5Y 6/1	no	yes
OB63	21.70	Marl	5Y 4/1	no	yes
OB62	21.55	Marl	5Y 4/1	no	yes
OB61	21.15	Marl	5Y 4/1	no	no
OB60	20.90	Marl	5Y 4/1	no	no
OB59	20.80	Marl	5Y 4/1	no	no
OB58	20.50	Marl	5Y 4/1	no	no
OB57	20.10	Shale	5Y 4/1	some	no
OB56	19.70	Marl	5Y 4/1	no	no
OB55	19.30	Marl	5Y 4/1	no	no
OB54	19.10	Marl	5Y 6/1	no	no
OB53	18.75	Marl	5Y 6/1	no	no
OB52	18.35	Marl	5Y 6/1	no	no
OB51	17.95	Marl	5Y 4/1	no	no
OB50	17.70	Shale	5Y 4/1	some	no
OB49	17.45	Marl	5Y 6/1	no	no
OB48	17.10	Marl	5Y 4/1	no	no
OB47	16.75	Marl	5Y 4/1	no	no
OB46	16.45	Shale	5Y 4/1	yes	no
OB45	16.15	Shale	5Y 4/1	some	no
OB44	15.65	Marl	5Y 4/1	no	no
OB43	15.15	Marl	N4	no	no
OB42	14.80	Marl	5Y 4/1	no	no
OB41	14.50	Shale	5Y 4/1	some	no
OB40	14.25	Shale	N3	yes	no
OB39	14.10	Shale	N3	yes	no
OB38	13.80	Marl	5Y 4/1	no	no
OB37	13.70	Marl	5Y 4/1	no	no
OB36	13.35	Shale	N5	some	no
OB35	13.05	Shale	N4	some	no

Sample No.	Section depth (m)	Lithology	Colour	Laminations	Bioturbation
OB34	12.65	Shale	5Y 4/1	some	no
OB33	12.20	Marl	5Y 4/1	no	no
OB32	11.80	Shale	N4	some	no
OB31	11.50	Shale	5Y 4/1	yes	no
OB30	11.15	Shale	N4	yes	no
OB29	10.80	Shale	N4	yes	no
OB28	10.55	Shale	N3	yes	no
OB27	10.15	Shale	N4	yes	no
OB26	9.85	Shale	N4	yes	no
OB25	9.25	Shale	5Y 6/1	some	no
OB24	8.85	Shale	N4	some	no
OB23	8.60	Marl	5Y 7/2	no	no
OB22	8.05	Shale	N4	yes	no
OB21	7.60	Shale	N4	yes	no
OB20	7.15	Marl	5Y 6/1	no	no
OB19	6.75	Marl	5Y 6/1	no	no
OB18	6.35	Marl	5Y 6/1	some	no
OB17	5.80	Shale	N3	yes	no
OB16	5.45	Marl	5Y 4/1	no	no
OB15	4.95	Marl	5Y 4/1	no	no
OB14	4.45	Marl	5Y 4/1	no	no
OB13	4.00	Shale	5Y 4/1	yes	no
OB12	3.60	Shale	5Y 4/1	yes	no
OB11	3.30	Marl	5Y 6/1	some	no
OB10	3.00	Marl	5Y 6/1	no	yes
OB9	2.51	Marl	5Y 4/1	irr	no
OB8	1.88	Marl	5Y 4/1	no	no
OB7	1.63	Shale	N3	yes	no
OB6	1.28	Shale	N3	yes	no
OB5	1.03	Marl	N4	irr	yes
OB4	0.70	Shale	N5	yes	no
OB3	0.58	Marl	N4	no	no
OB2	0.48	Marl	5Y 6/1	no	no
OB1	0.50	Sandstone	5Y 6/1	no	no
OB0	-0.50	Sandstone	5Y 6/1	no	no

Table IV. Lithological descriptions for Ech Cheid Samples

Sample No.	Section depth (m)	Lithology	Colour	Laminations	Bioturbation
EC25	18.00	Limestone	N4	no	Yes
EC24	16.25	Limestone	N4	no	no
EC23	15.75	Marly shale	N4	no	no
EC22	15.35	limestone	N4	no	no
EC21	14.95	Marl	N4	no	no
EC20	14.60	Marl	N4	some	no
EC19	14.40	Shale	N4	no	no
EC18	13.90	Shale	N4	no	no
EC17	13.40	Marl	N4	no	yes
EC16	12.90	Marly shale	N4	no	no
EC15	12.40	Shale	N4	some	no
EC14	11.60	Shale	N4	irr	no
EC13	11.10	Shale	N4	irr	no
EC12	10.50	Marl	N4	no	no
EC11	9.70	Marl	N4	no	no
EC10	9.00	Marl	N3	no	yes
EC9	8.40	Shale	5Y 4/1	some	no
EC8	7.80	Shale	5Y 4/1	some	yes
EC7	7.30	Shale	5Y 4/1	irr	yes
EC6	6.70	Marl	5Y 4/1	no	no
EC5	6.05	Marl	5Y 4/1	no	yes
EC4	3.60	Shale	5Y 4/1	some	no
EC3	3.20	Shale	5Y 6/1	no	no
EC2	0.90	Shale	5Y 6/1	irr	no
EC1	0.10	Shale	N3	some	yes

Table V. Lithological descriptions for Oued El Gsab Samples

Sample No.	Section depth (m)	Lithology	Colour	Laminations	Bioturbation
OG45	16.40	Limestone	5Y 6/1	None	yes
OG44	15.20	Marl	5Y 4/1	None	no
OG43	14.95	Marl	5Y 4/1	None	no
OG42	14.70	Marl	5Y 2/1	None	no
OG41	14.35	Marl	5Y 2/1	None	no
OG40	13.95	Marly shale	N3	None	no
OG39	13.70	Marl	N4	None	no
OG38	13.30	Marl	N3	None	no
OG37	12.95	Marl	5Y 4/1	None	no
OG36	12.75	Marl	N4	None	Yes
OG35	12.40	Marl	5Y 4/1	None	no
OG34	12.10	Marly shale	N3	Some	no
OG33	11.90	Marl	5Y 4/1	None	no
OG32	11.55	Marl	5Y 4/1	None	no
OG31	11.30	Marl	5Y 4/1	None	no
OG30	10.90	Marl	5Y 4/1	None	no
OG29	10.60	Marl	5Y 4/1	None	no
OG28	10.20	Marl	5Y 4/1	None	no
OG27	9.60	Marl	5Y 4/1	None	no
OG26	9.40	Marl	N3	None	no
OG25	9.00	Marl	N3	None	no
OG24	8.65	Marl	N3	None	no
OG23	8.40	Marl	N4	None	yes
OG22	8.30	Shale	N4	Some	no
OG21	8.15	Marl	5Y 4/1	None	Yes
OG20	8.05	Marl	5Y 6/1	None	no
OG19	7.90	Marl	5Y 6/1	None	no
OG18	7.75	Marl	N4	None	no
OG17	7.60	Marl	N4	None	no
OG16	7.40	Shale	N4	yes	yes
OG15	6.70	Marl	5Y 4/1	None	no
OG14	6.20	Shale	N4	Some	no
OG13	6.00	Shale	N4	Some	no
OG12	5.80	Shale	N4	Some	no
OG11	4.85	Marl	5Y 4/1	None	no
OG10	4.65	Marl	5Y 4/1	None	yes
OG9	4.40	Marl	5Y 4/1	Some	no
OG8	3.85	Shale	N4	Yes	no
OG7	3.60	Shale	N5	Some	no
OG6	2.80	Shale	N5N	Yes	no
OG5	1.90	Shale	N4	Yes	no
OG4	1.30	Shale	N3	Yes	no
OG3	1.00	Shale	N4	Some	yes
OG2	0.55	Marl	N4	Some	no
OG1	0.20	Marl	5Y 6/1	None	no
OG0	-0.50	Limestone	5Y 8/1	None	no

Table VI. Lithological descriptions for Dir Ouled Yahia Samples

Sample No.	Section depth (m)	Lithology	Colour	Laminations	Bioturbation
DOY50	38.00	Limestone	5Y 6/1	None	yes
DOY49	36.70	Shale	N3	None	no
DOY48	36.10	Shale	N3	Yes	no
DOY47	34.20	Shale	N3	Yes	no
DOY46	33.90	Shale	N3	Yes	no
DOY45	32.70	Shale	N3	Yes	no
DOY44	31.70	Shale	5Y 4/1	Some	no
DOY43	30.90	Shale	5Y 4/1	None	no
DOY42	30.20	Marl	5Y 4/1	None	no
DOY41	29.00	Marl	5YR 4/1	None	no
DOY40	28.50	Marl	5YR 4/1	Some	no
DOY39	27.95	Marl	10YR 4/2	None	no
DOY38	27.60	Marl	10 YR 6/2	None	no
DOY37	26.70	Marl	10 YR 6/2	None	no
DOY36	25.70	Shale	10YR 4/2	None	no
DOY35	23.60	Marl	10 YR 6/2	Some	no
DOY34	24.20	Marl	10YR 4/2	Some	no
DOY33	23.90	Marl	10 YR 6/2	Some	no
DOY32	23.20	Marl	10YR 4/2	None	no
DOY31	22.50	Shale	5Y 4/1	None	no
DOY30	21.50	Marl	10 YR 6/2	Some	no
DOY29	21.10	Marl	10 YR 6/2	Some	no
DOY28	20.60	Marl	10YR 4/2	Some	no
DOY27	20.00	Shale	5Y 6/1	Some	no
DOY26	19.35	Shale	5Y 6/1	Some	no
DOY25	18.80	Shale	5Y 6/1	Yes	no
DOY24	18.30	Marl	10 YR 6/2	Some	no
DOY23	17.45	Marl	10 YR 6/2	None	no
DOY22	16.50	Marl	10 YR 6/2	Some	no
DOY21	15.75	Marl	10YR 8/2	Some	no
DOY20	14.80	Marl	10YR 8/2	None	no
DOY19	13.50	Shale	5Y 4/1	Some	no
DOY18	13.20	Shale	5Y 4/1	None	no
DOY17	12.60	Marl	10YR 4/2	Yes	no
DOY16	12.00	Marl	10YR 8/2	None	no
DOY15	11.45	Shale	5YR 4/1	None	no
DOY14	10.85	Shale	5YR 4/1	Some	no
DOY13	10.30	Shale	5YR 4/1	Some	no
DOY12	9.70	Shale	5YR 4/1	Some	no
DOY11	9.40	Marl	5YR 4/1	Some	no
DOY10	8.00	Marl	10 YR 6/2	Some	no
DOY9	6.50	Shale	5YR 4/1	None	no
DOY8	5.80	Shale	5YR 4/1	None	no
DOY7	5.20	Shale	5YR 4/1	None	no
DOY6	4.70	Shale	N4	Some	no
DOY5	3.90	Marl	5YR 4/1	Some	no
DOY4	3.30	Marl	5YR 4/1	None	no
DOY3	2.70	Marl	10YR 8/2	None	no
DOY2	2.20	Marl	10 YR 6/2	None	no

Sample No.	Section depth (m)	Lithology	Colour	Laminations	Bioturbation
DOY1	0.30	Limestone	10YR 8/2	None	no
DOY0	-0.50	Limestone	10YR 8/2	None	yes

Table VII. Lithological descriptions for Nebour Samples

Sample No.	Section depth (m)	Lithology	Colour	Laminations	Bioturbation
N47	25.90	Limestone	5Y 6/1	None	Yes
N46	24.90	Limestone	5Y 6/1	None	no
N45	23.60	Calcareous shale	N3	None	no
N44	22.80	Calcareous shale	N3	None	no
N43	21.80	Calcareous shale	N3	None	no
N42	21.30	Calcareous shale	N3	None	no
N41	20.80	Calcareous shale	N3	Some	no
N40	20.30	Calcareous shale	N3	None	no
N39	19.80	Calcareous shale	N3	None	no
N38	19.10	Calcareous shale	N3	None	no
N37	18.50	Calcareous shale	N3	None	no
N36	18.00	Calcareous shale	N3	None	no
N35	17.60	Calcareous shale	N3	None	no
N34	17.20	Calcareous shale	N2	None	no
N33	16.55	Calcareous shale	N3	None	no
N32	16.20	Calcareous shale	N3	None	no
N31	15.70	Calcareous shale	N3	None	no
N30	15.20	Calcareous shale	N2	None	no
N29	14.75	Calcareous shale	N3	None	no
N28	14.20	Calcareous shale	N3	None	no
N27	13.60	Calcareous shale	N3	None	no
N26	13.10	Calcareous shale	N3	None	no
N25	12.70	Calcareous shale	N3	None	no
N24	12.40	Calcareous shale	N3	None	no
N23	12.15	Calcareous shale	N3	None	no
N22	11.60	Calcareous shale	N3	None	no
N21	11.05	Calcareous shale	N3	None	no
N20	10.45	Calcareous shale	N3	None	no
N19	9.85	Calcareous shale	N3	None	no
N18	9.25	Calcareous shale	N3	Some	no
N17	9.00	Calcareous shale	N3	None	no
N16	8.80	Calcareous shale	N3	None	no
N15	7.90	Calcareous shale	N3	None	no
N14	7.30	Calcareous shale	N4	None	no
N13	6.85	Calcareous shale	N3	Some	no
N12	6.35	Calcareous shale	N2	None	no
N11	6.00	Calcareous shale	N4	None	no
N10	5.35	Calcareous shale	N3	None	no
N9	4.95	Calcareous shale	N3	None	yes
N8	4.70	Calcareous shale	N3	None	yes
N7	4.15	Calcareous shale	N3	Yes	no
N6	3.50	Calcareous shale	N3	None	no
N5	3.10	Calcareous shale	N3	Yes	no
N4	2.20	Calcareous shale	N3	Yes	no
N3	1.50	Calcareous shale	N3	None	yes
N2	0.90	Calcareous shale	N3	None	no
N1	0.10	Calcareous shale	N3	None	no
N0	-0.50	Limestone	5Y 6/1	None	no
N00	-1.00	Limestone	N3	None	no

VIII) Lithological descriptions for Buckton Cliff samples (BC).

Sample No.	Section depth (cm)	Lithology	Colour
BC1	6.50	Marl	N7
BC2	4.50	Marl	N7
BC3	3.25	Marly shale	N3
BC4	2.00	Marly shale	N3
BC5	0.50	Marl	N5

Appendix 2. Bulk geochemical and isotopic data.

Bulk geochemical results are the mean value of triplicate analyses.

Key to tables:

TS (%), wt percentage total sulphur;

TOC (%), wt percentage Total Organic Carbon;

S1, Rock-Eval pyrolysis S1 peak measured in mgHC/gSED;

S2, Rock-Eval S2 peak measured in mgHC/gSED;

Tmax, Rock-Eval pyrolysis temperature of maximum hydrocarbon generation measured in °C;

HI, hydrogen index measured in mgHC/gTOC;

PI, production index calculated from S1/S1 + S2;

Carbonate (%), wt percentage carbonate in the sample;

Isotope, $\delta^{13}C$ organic carbon value.

I) Bulk geochemical data for Buckton Cliff section (BC).

Sample No.	Section depth (cm)	TOC	S1	S2	Tmax	HI	PI	Carbonate	Isotope
BC1	6.50	0.56	0.02	0.11	424	20	0.18	12	-24.0
BC2	4.50	0.67	0.02	0.15	433	22	0.12	11	-23.1
BC3	3.25	2.39	0.33	1.34	433	56	0.20	34	-24.5
BC4	2.00	2.42	0.06	2.41	429	99	0.03	71	-24.3
BC5	0.50	0.96	0.04	0.18	439	19	0.17	29	-24.3

II) Bulk geochemical data for Misburg Quarry section (MQ).

Sample No.	Section depth (m)	S	TOC	S1	S2	Tmax	HI	PI	Carbonate
MQ1	36.04	0.05	0.17	0.14	0.01	545	3	0.96	46
MQ2	34.20	0.01	0.11	0.04	0.02	545	18	0.67	57
MQ3	31.50	0.00	0.03	0.21	0.06	545	175 (na)	0.78	69
MQ4	30.50	0.01	0.05	0.22	0.04	545	72 (na)	0.86	67
MQ5	30.16	0.00	0.02	0.07	0.07	545	436 (na)	0.48	73
MQ6	30.07	0.01	0.62	0.06	0.09	545	15	0.39	42
MQ7	30.00	0.01	0.08	0.23	0.01	545	12	0.96	62
MQ8	29.60	0.03	0.20	0.12	0.03	545	15	0.79	59
MQ9	29.41	0.04	0.32	0.07	0.05	544	16	0.58	53
MQ10	26.91	0.01	0.09	0.10	0.06	545	64 (na)	0.65	58
MQ11	24.73	0.02	0.12	0.08	0.02	545	12	0.84	62
MQ12	23.48	0.05	0.13	0.18	0.02	546	11	0.92	51
MQ13	22.57	0.09	0.55	0.10	0.33	436	59	0.23	58
MQ14	21.44	1.01	1.79	0.14	1.79	430	100	0.07	62
MQ15	19.74	0.03	0.08	0.06	0.01	544	6	0.92	54
MQ16	18.00	0.56	1.07	0.09	0.81	431	75	0.10	62
MQ17	17.00	0.33	0.85	0.06	0.53	434	62	0.10	51
MQ18	16.32	0.06	0.23	0.05	0.02	545	6	0.75	62
MQ19	11.00	0.99	1.60	0.12	0.92	432	58	0.12	38
MQ20	10.00	1.05	1.81	0.24	2.24	429	124	0.09	56
MQ21	9.04	0.12	0.17	0.08	0.02	545	9	0.84	46
MQ22	7.78	0.11	0.36	0.09	0.02	545	4	0.85	54
MQ23	6.83	0.10	0.19	0.08	0.02	544	8	0.84	43
MQ24	2.18	0.05	0.31	0.09	0.06	544	18	0.62	56
MQ25	1.80	0.02	0.03	0.17	0.05	545	147 (na)	0.77	56
MQ26	1.10	0.04	0.11	0.12	0.02	545	18	0.85	49
MQ27	0.77	0.34	1.13	0.12	0.63	433	56	0.16	31
MQ28	0.28	0.02	0.05	0.58	0.01	545	19	0.98	67

III) Bulk geochemical data for Oued Bahloul samples.

Sample No.	Section depth (m)	S	TOC	S1	S2	Tmax	III	PI	Carbonate	Isotope
OB83	28.20	0.01	0.25	0.09	0.57	433	225	0.13	86	-25.0
OB82	27.70	0.42	2.11	0.65	12.07	434	573	0.05	81	-25.3
OB81	27.50	0.17	2.95	0.82	14.65	433	497	0.05	74	nd.
OB80	27.10	0.12	2.38	0.27	9.28	433	390	0.03	75	-25.0
OB79	26.75	0.02	0.43	0.07	0.58	439	134	0.11	82	nd.
OB78	26.45	0.04	0.94	0.10	2.20	436	234	0.04	82	-24.2
OB77	26.10	0.04	1.17	0.12	2.65	435	227	0.04	73	nd.
OB76	25.60	0.19	3.82	0.65	17.05	432	446	0.04	75	-25.4
OB75	25.25	0.03	0.73	0.09	1.29	435	175	0.06	78	nd.
OB74	24.85	0.20	1.94	0.27	6.96	433	359	0.04	77	-24.9
OB73	24.40	0.32	3.50	0.82	18.62	434	532	0.04	76	nd.
OB72	24.00	0.21	3.82	0.73	17.96	433	470	0.04	73	-24.7
OB71	23.80	0.29	3.92	0.98	20.03	434	511	0.05	72	nd.
OB70	23.45	0.38	3.77	1.06	21.23	436	563	0.05	73	-24.9
OB69	23.20	0.37	3.68	1.23	20.98	436	570	0.06	73	nd.
OB68	22.90	0.29	3.58	1.29	22.15	436	620	0.05	75	-24.7
OB67	22.75	0.08	2.36	0.32	8.39	433	355	0.04	76	nd.
OB66	22.50	0.02	0.83	0.10	1.51	438	182	0.06	76	-24.2
OB65	22.20	0.01	0.30	0.08	0.50	439	164	0.13	84	nd.
OB64	21.95	0.01	0.39	0.08	0.53	442	133	0.13	83	-23.9
OB63	21.70	0.07	1.90	0.38	7.59	434	399	0.05	71	nd.
OB62	21.55	0.07	1.88	0.39	8.82	433	469	0.04	73	-24.4
OB61	21.15	0.63	1.81	0.41	8.61	431	476	0.04	75	nd.
OB60	20.90	0.28	2.30	0.58	12.14	434	528	0.05	73	-24.4
OB59	20.80	0.17	2.65	0.62	11.78	434	445	0.05	76	nd.
OB58	20.50	0.10	2.20	0.53	10.70	433	487	0.05	87	-24.5
OB57	20.10	0.06	1.79	0.27	6.28	434	351	0.04	85	nd.
OB56	19.70	0.10	1.94	0.36	7.87	434	407	0.04	69	-24.4
OB55	19.30	0.50	1.92	0.46	8.33	435	434	0.05	74	nd.

Sample No.	Section depth (m)	S	TOC	S1	S2	Tmax	HI	PI	Carbonate	Isotope
OB54	19.10	0.19	1.50	0.34	6.15	432	410	0.05	76	-24.2
OB53	18.75	0.28	1.73	0.41	7.33	436	425	0.05	77	nd.
OB52	18.35	0.16	1.71	0.36	7.90	433	463	0.04	76	-24.3
OB51	17.95	0.19	1.56	0.42	7.55	433	485	0.05	80	nd.
OB50	17.70	0.07	1.56	0.38	6.52	436	418	0.05	82	-24.2
OB49	17.45	0.14	0.89	0.25	3.95	432	441	0.06	78	nd.
OB48	17.10	0.09	2.00	0.57	9.53	431	476	0.06	72	-24.2
OB47	16.75	0.08	2.05	0.45	9.63	435	470	0.04	78	nd.
OB46	16.45	0.14	4.07	1.24	24.17	431	594	0.05	76	-23.9
OB45	16.15	0.13	2.19	0.50	11.13	435	508	0.04	78	nd.
OB44	15.65	0.34	1.42	0.30	5.18	432	366	0.05	69	-23.9
OB43	15.15	0.43	2.88	0.92	16.80	435	584	0.05	72	nd.
OB42	14.80	0.19	2.70	0.76	14.97	437	554	0.05	71	-24.1
OB41	14.50	0.14	2.98	0.93	17.38	438	584	0.05	77	nd.
OB40	14.25	0.68	3.97	1.06	22.59	435	569	0.04	71	-23.6
OB39	14.10	0.69	8.36	3.86	56.07	434	671	0.06	80	nd.
OB38	13.80	0.10	3.23	0.68	15.49	433	480	0.04	62	-24.0
OB37	13.70	0.13	3.59	0.80	18.97	435	528	0.04	64	nd.
OB36	13.35	0.18	4.13	1.00	22.34	436	541	0.04	70	-23.6
OB35	13.05	0.13	3.03	0.90	17.32	430	573	0.05	70	nd.
OB34	12.65	0.29	3.13	0.69	16.91	435	541	0.04	73	nd.
OB33	12.20	0.13	2.31	0.45	9.89	434	429	0.04	66	nd.
OB32	11.80	0.18	3.52	0.82	18.69	426	531	0.04	70	-23.6
OB31	11.50	0.23	3.70	1.20	21.77	436	588	0.05	75	nd.
OB30	11.15	0.14	3.50	0.99	20.86	435	596	0.05	67	-23.5
OB29	10.80	0.10	2.85	0.59	14.69	435	516	0.04	69	-23.6
OB28	10.55	0.34	8.15	2.09	49.17	436	604	0.04	62	-23.0
OB27	10.15	0.09	2.77	0.63	12.81	436	463	0.05	56	nd.
OB26	9.85	0.10	3.17	0.39	13.56	434	428	0.03	69	-24.2
OB25	9.25	0.03	1.42	0.18	3.97	427	281	0.04	67	nd.
OB24	8.85	0.08	2.44	0.47	10.01	434	411	0.04	64	-24.1
OB23	8.60	0.00	0.21	0.05	0.11	446	50	0.30	68	nd.

Sample No.	Section depth (m)	S	TOC	S1	S2	Tmax	HI	PI	Carbonate	Isotope
OB22	8.05	0.07	1.98	0.40	8.47	433	428	0.04	60	-23.9
OB21	7.60	0.20	2.69	0.94	15.86	434	590	0.06	67	-23.9
OB20	7.15	0.03	1.09	0.15	2.34	436	214	0.06	54	-23.7
OB19	6.75	0.03	1.30	0.21	3.33	436	257	0.06	51	nd.
OB18	6.35	0.02	0.69	0.08	1.37	436	199	0.06	75	-23.3
OB17	5.80	0.31	6.74	2.63	40.80	434	606	0.06	67	-23.2
OB16	5.45	0.08	1.58	0.32	5.52	432	350	0.05	55	-23.9
OB15	4.95	0.06	1.96	0.34	6.35	434	324	0.05	54	nd.
OB14	4.45	0.06	1.95	0.35	6.66	428	342	0.05	51	-24.0
OB13	4.00	0.08	2.93	0.38	12.79	430	437	0.03	68	-23.4
OB12	3.60	0.12	3.36	0.70	17.29	430	515	0.04	72	-23.3
OB11	3.30	0.05	1.77	0.23	6.51	428	368	0.03	65	nd.
OB10	3.00	0.03	1.19	0.11	2.72	434	229	0.04	59	-23.6
OB9	2.51	0.08	2.02	0.31	8.85	429	438	0.03	60	-23.8
OB8	1.88	0.07	2.22	0.22	8.34	430	377	0.03	64	-23.4
OB7	1.63	0.21	5.00	1.30	29.24	435	585	0.04	76	nd.
OB6	1.28	0.32	6.92	2.27	42.48	448	614	0.05	72	-22.9
OB5	1.03	0.24	5.14	1.01	28.13	430	547	0.03	57	-22.7
OB4	0.70	0.19	2.81	0.41	14.89	429	530	0.03	56	-23.7
OB3	0.58	0.08	3.04	0.43	14.30	430	471	0.03	50	nd.
OB2	0.18	0.12	0.25	0.07	0.31	426	126	0.18	68	-25.2
OB1	0.05	0.18	0.23	0.07	0.36	431	155	0.16	72	-25.4
OB0	-0.50	0.09	0.35	0.07	0.66	431	185	0.10	74	-25.6

IV) Bulk geochemical data for Ech Cheid section.

Sample No.	Section depth (m)	S	TOC	S1	S2	Tmax	HI	PI	Carbonate	Isotope
EC25	18.00	0.01	0.51	0.09	0.69	437	136	0.11	74	nd.
EC24	16.25	0.01	0.38	0.07	0.33	439	87	0.18	68	-25.8
EC23	15.75	0.09	0.45	0.17	0.77	435	171	0.18	72	nd.
EC22	15.35	0.01	0.48	0.08	0.67	440	141	0.11	69	-26.4
EC21	14.95	0.00	0.16	0.05	0.13	442	82	0.26	62	nd.
EC20	14.60	0.00	0.24	0.04	0.07	457	27	0.38	59	nd.
EC19	14.40	0.08	0.98	0.31	1.95	437	198	0.14	58	-26.6
EC18	13.90	0.01	0.71	0.14	1.24	437	174	0.10	63	nd.
EC17	13.40	0.01	0.46	0.06	0.61	438	132	0.08	67	-25.6
EC16	12.90	0.00	0.28	0.06	0.10	445	34	0.39	59	nd.
EC15	12.40	0.00	0.31	0.06	0.29	447	93	0.17	54	-26.5
EC14	11.60	0.01	0.48	0.07	0.53	439	109	0.12	62	nd.
EC13	11.10	0.02	0.79	0.21	1.21	437	152	0.15	58	-26.0
EC12	10.50	0.01	0.67	0.08	0.85	440	127	0.08	50	nd.
EC11	9.70	0.08	0.93	0.17	1.25	438	133	0.12	59	-26.6
EC10	9.00	0.06	0.42	0.14	0.51	436	121	0.21	69	nd.
EC9	8.40	0.00	0.52	0.06	0.35	443	66	0.15	37	-26.4
EC8	7.80	0.00	0.19	0.07	0.07	539	36	0.48	60	nd.
EC7	7.30	0.00	0.32	0.07	0.25	445	77	0.22	36	-26.6
EC6	6.70	0.00	0.35	0.09	0.13	433	37	0.40	51	-26.2
EC5	6.05	0.00	0.31	0.05	0.15	437	47	0.26	56	-26.3
EC4	3.60	0.01	0.50	0.09	0.46	442	92	0.16	56	-26.3
EC3	3.20	0.00	0.21	0.10	0.07	540	30	0.59	29	-25.7
EC2	0.90	0.00	0.42	0.07	0.42	441	101	0.13	60	-27.0
EC1	0.10	0.01	0.63	0.11	0.62	441	99	0.15	58	-27.2

V) Bulk geochemical data for Dir Oulad Yahia section

Sample No.	Section depth (m)	S	TOC	S1	S2	Tmax	HI	PI	Carbonate	Isotope
DOY50	38.00	0.30	0.52	0.08	1.14	434	219	0.07	80	-25.5
DOY49	36.70	0.11	2.28	0.48	10.36	431	455	0.04	63	nd.
DOY48	36.10	0.12	2.82	0.49	11.84	431	420	0.04	71	nd.
DOY47	34.20	0.15	3.12	0.31	13.83	434	443	0.02	67	nd.
DOY46	33.90	0.19	3.99	0.68	21.08	431	528	0.03	60	nd.
DOY45	32.70	0.18	4.06	0.66	20.60	428	507	0.03	65	nd.
DOY44	31.70	0.36	3.49	0.34	10.53	432	302	0.03	70	nd.
DOY43	30.90	0.24	2.18	0.64	18.43	428	847	0.03	74	nd.
DOY42	30.20	0.04	1.21	0.12	3.02	435	251	0.04	75	nd.
DOY41	29.00	0.12	2.68	0.29	10.45	431	391	0.03	70	nd.
DOY40	28.50	0.21	3.95	0.70	24.10	430	611	0.03	71	nd.
DOY39	27.95	0.04	0.90	0.11	2.09	434	233	0.05	74	nd.
DOY38	27.60	0.23	1.15	0.14	4.70	432	409	0.03	72	nd.
DOY37	26.70	0.05	1.18	0.12	2.50	433	212	0.05	69	-23.9
DOY36	25.70	0.20	2.40	0.37	12.98	434	541	0.03	69	nd.
DOY35	24.60	0.03	0.89	0.10	1.78	439	200	0.05	61	nd.
DOY34	24.20	0.15	2.53	0.47	14.21	430	562	0.03	70	nd.
DOY33	23.90	0.11	2.86	0.89	14.25	431	498	0.06	70	nd.
DOY32	23.20	0.20	1.36	0.17	4.98	433	368	0.03	66	nd.
DOY31	22.50	0.23	1.83	0.29	10.92	429	597	0.03	66	nd.
DOY30	21.50	0.04	1.05	0.13	3.01	437	287	0.04	76	nd.
DOY29	21.10	0.04	0.94	0.14	2.63	436	278	0.05	76	nd.
DOY28	20.60	0.07	1.70	0.47	7.46	433	440	0.06	66	nd.
DOY27	20.00	0.41	1.24	0.19	4.73	429	381	0.04	63	nd.
DOY26	19.35	0.13	2.33	0.46	12.80	430	549	0.03	69	-24.1
DOY25	18.80	0.02	1.46	0.26	6.61	431	453	0.04	75	nd.
DOY24	18.30	0.07	1.63	0.49	6.82	434	420	0.07	79	nd.
DOY23	17.45	0.04	1.15	0.16	2.78	436	243	0.05	47	nd.
DOY22	16.50	0.06	1.48	0.38	5.22	433	354	0.07	63	nd.

Sample No.	Section depth (m)	S	TOC	S1	S2	Tmax	HI	PI	Carbonate	Isotope
DOY21	15.75	0.02	0.39	0.06	0.63	442	160	0.09	60	nd.
DOY20	14.80	0.03	0.83	0.10	1.77	431	213	0.05	40	nd.
DOY19	13.50	0.07	1.51	0.23	5.11	434	340	0.04	40	nd.
DOY18	13.20	0.76	2.46	0.56	16.23	432	661	0.03	42	-24.3
DOY17	12.60	0.20	2.90	0.48	15.31	428	529	0.03	46	-23.1
DOY16	12.00	0.01	0.20	0.05	0.25	444	123	0.17	41	nd.
DOY15	11.45	0.61	6.77	3.14	57.66	444	852	0.05	42	-23.0
DOY14	10.85	0.13	2.82	0.47	12.40	427	440	0.04	13	nd.
DOY13	10.30	0.29	4.07	1.04	25.20	429	620	0.04	29	-23.5
DOY12	9.70	0.21	2.27	0.44	12.88	427	567	0.03	36	-23.9
DOY11	9.40	0.29	3.64	0.75	22.26	431	612	0.03	45	nd.
DOY10	8.00	0.07	1.63	0.19	5.28	436	325	0.03	31	-23.7
DOY9	6.50	0.30	4.98	0.96	33.25	429	668	0.03	31	-23.3
DOY8	5.80	0.32	6.16	1.19	38.84	430	631	0.03	19	-22.9
DOY7	5.20	0.10	2.18	0.94	11.46	428	527	0.08	37	nd.
DOY6	4.70	0.26	3.28	1.26	20.14	431	614	0.06	37	-24.4
DOY5	3.90	0.16	3.51	0.46	19.32	430	550	0.02	35	nd.
DOY4	3.30	0.17	2.95	0.45	14.84	430	504	0.03	26	-23.8
DOY3	2.70	0.01	0.16	0.05	0.16	441	98	0.24	59	-22.8
DOY2	2.20	0.08	2.17	0.23	6.37	432	294	0.03	29	-22.8
DOY1	0.30	0.01	0.09	0.04	0.00	526	0	1.00	42	-25.8
DOY0	-0.50	0.01	0.03	0.02	0.06	542	195	0.25	37	-24.8

VI) Bulk geochemical data for Oued El Gsab section.

Sample No.	Section depth (m)	S	TOC	S1	S2	Tmax	HI	PI	Carbonate	Isotope
OG45	16.40	0.08	0.33	0.16	0.57	436	174	0.22	73	-25.0
OG44	15.20	0.06	1.12	0.25	2.79	436	250	0.08	67	nd.
OG43	14.95	0.07	2.31	0.41	8.64	437	375	0.04	71	nd.
OG42	14.70	0.07	2.30	0.43	8.85	438	385	0.05	68	nd.
OG41	14.35	0.09	2.75	0.64	10.86	435	395	0.06	73	nd.
OG40	13.95	0.13	3.76	1.04	19.18	436	510	0.05	73	nd.
OG39	13.70	0.06	2.91	0.66	12.90	435	443	0.05	70	nd.
OG38	13.30	0.08	2.26	0.74	10.38	437	459	0.07	73	nd.
OG37	12.95	0.07	2.22	0.74	10.03	436	452	0.07	72	nd.
OG36	12.75	0.09	2.65	0.41	11.09	431	418	0.04	79	-25.1
OG35	12.40	0.08	2.50	0.51	9.25	434	370	0.05	78	nd.
OG34	12.10	0.09	2.95	0.59	13.17	432	447	0.04	72	nd.
OG33	11.90	0.06	1.83	0.37	7.05	434	386	0.05	83	nd.
OG32	11.55	0.43	2.20	0.64	11.55	438	525	0.05	72	nd.
OG31	11.30	0.16	2.13	0.59	10.66	434	501	0.05	69	nd.
OG30	10.90	0.10	2.43	0.66	12.51	434	516	0.05	70	nd.
OG29	10.60	0.10	1.84	0.44	8.37	434	456	0.05	70	nd.
OG28	10.20	0.17	2.85	0.81	15.44	438	542	0.05	60	nd.
OG27	9.60	0.09	2.45	0.62	11.42	434	467	0.05	63	-25.2
OG26	9.40	0.21	2.51	0.78	12.56	435	501	0.06	68	nd.
OG25	9.00	0.54	3.28	1.08	17.66	435	539	0.06	64	nd.
OG24	8.65	0.09	2.51	0.34	8.93	436	356	0.04	54	nd.
OG23	8.40	0.08	2.47	0.48	9.63	436	390	0.05	69	nd.
OG22	8.30	0.02	0.85	0.16	2.08	437	244	0.07	74	nd.
OG21	8.15	0.05	1.69	0.25	4.36	436	258	0.05	69	nd.
OG20	8.05	0.04	1.31	0.16	3.19	435	244	0.05	65	nd.
OG19	7.90	0.04	1.51	0.24	4.46	436	296	0.05	65	nd.
OG18	7.75	0.08	2.47	0.35	9.37	437	380	0.04	56	-24.8
OG17	7.60	0.09	2.86	0.49	12.17	432	425	0.04	64	nd.

Sample No.	Section depth (m)	S	TOC	S1	S2	Tmax	III	PI	Carbonate	Isotope
OG16	7.40	0.04	1.66	0.29	5.34	432	322	0.05	67	nd.
OG15	6.70	0.07	1.88	0.37	6.67	435	355	0.05	59	-25.0
OG14	6.20	0.06	1.83	0.33	6.43	435	351	0.05	63	nd.
OG13	6.00	0.05	1.62	0.27	5.63	433	349	0.05	69	nd.
OG12	5.80	0.04	1.24	0.27	3.53	436	286	0.07	61	-24.4
OG11	4.85	0.04	1.31	0.23	4.26	436	326	0.05	56	nd.
OG10	4.65	0.04	1.32	0.31	4.65	435	353	0.06	67	-24.1
OG9	4.40	0.04	1.25	0.18	3.76	437	302	0.05	71	nd.
OG8	3.85	0.03	1.07	0.18	3.07	436	288	0.06	59	-23.5
OG7	3.60	0.05	1.57	0.23	5.33	438	339	0.04	71	-23.2
OG6	2.80	0.08	2.16	0.49	7.74	437	359	0.06	67	-22.6
OG5	1.90	0.09	1.93	0.94	11.22	437	583	0.08	72	-23.9
OG4	1.30	0.12	3.65	0.92	20.59	437	565	0.04	66	-23.3
OG3	1.00	0.08	2.36	0.25	6.88	436	292	0.03	58	-22.9
OG2	0.55	0.19	5.47	0.53	25.95	436	474	0.02	61	-22.4
OG1	0.20	0.01	0.33	0.11	0.73	438	221	0.13	78	-25.3
OG0	-0.50	0.01	0.21	0.13	0.34	436	159	0.27	79	-25.2

VII) Bulk geochemical data for Nebour section.

Sample No.	Section depth (m)	TOC	S	S1	S2	Tmax	HI	PI	Carbonate	Isotope
N47	25.90	0.59	0.04	0.17	0.91	438	155	0.15	75	-25.0
N46	24.90	0.56	0.11	0.19	1.00	439	180	0.16	79	nd.
N45	23.60	1.37	0.10	0.39	2.92	437	214	0.12	74	nd.
N44	22.80	0.81	0.02	0.15	1.30	439	159	0.10	70	nd.
N43	21.80	2.57	0.31	0.34	6.81	440	265	0.05	72	nd.
N42	21.30	2.94	0.21	0.40	8.91	440	303	0.04	65	nd.
N41	20.80	3.08	0.11	0.33	7.82	438	254	0.04	62	nd.
N40	20.30	1.81	0.13	0.37	4.93	440	272	0.07	66	nd.
N39	19.80	2.22	0.33	0.35	5.52	438	249	0.06	65	-25.1
N38	19.10	2.85	0.08	0.33	7.39	440	259	0.04	65	nd.
N37	18.50	1.77	0.06	0.27	4.51	440	255	0.06	67	nd.
N36	18.00	2.12	0.18	0.36	5.73	438	271	0.06	59	nd.
N35	17.60	2.54	0.14	0.41	7.78	442	307	0.05	67	nd.
N34	17.20	3.83	0.28	0.92	15.15	447	395	0.06	75	nd.
N33	16.55	3.11	0.09	0.20	6.59	440	212	0.03	63	nd.
N32	16.20	1.50	0.08	0.13	5.42	444	361	0.02	77	nd.
N31	15.70	1.92	0.51	0.29	5.15	439	268	0.05	70	nd.
N30	15.20	2.67	0.41	0.34	9.30	442	348	0.04	68	nd.
N29	14.75	2.83	0.10	0.25	6.88	443	243	0.04	77	-24.0
N28	14.20	1.37	0.09	0.25	3.54	440	259	0.06	68	nd.
N27	13.60	1.81	0.12	0.46	5.50	441	305	0.08	68	nd.
N26	13.10	1.63	0.05	0.24	3.82	441	234	0.06	58	nd.
N25	12.70	1.69	0.05	0.31	3.64	441	215	0.08	74	nd.
N24	12.40	1.82	0.09	0.32	4.06	441	223	0.07	70	nd.
N23	12.15	1.63	0.13	0.44	4.16	439	255	0.10	73	nd.
N22	11.60	1.91	0.06	0.38	5.66	438	297	0.06	70	-23.9
N21	11.05	1.07	0.07	0.33	2.45	440	230	0.12	70	nd.
N20	10.45	1.45	0.07	0.35	3.20	439	220	0.10	61	nd.
N19	9.85	1.58	0.25	0.45	4.00	439	254	0.10	60	nd.

Sample No.	Section depth (m)	TOC	S	S1	S2	Tmax	HI	PI	Carbonate	Isotope
N18	9.25	1.92	0.03	0.19	3.34	444	174	0.05	54	nd.
N17	9.00	1.83	0.05	0.21	4.03	441	221	0.05	63	nd.
N16	8.80	1.15	0.05	0.21	1.69	440	147	0.11	63	-23.4
N15	7.90	1.71	0.08	0.36	5.23	442	306	0.06	61	nd.
N14	7.30	1.78	0.04	0.16	2.97	437	167	0.05	56	nd.
N13	6.85	2.16	0.08	0.15	5.27	439	244	0.03	55	nd.
N12	6.35	4.33	0.27	0.25	13.71	438	317	0.02	65	-23.2
N11	6.00	1.55	0.05	0.25	3.15	438	204	0.07	50	nd.
N10	5.35	2.55	0.24	0.45	9.04	442	355	0.05	55	-23.9
N9	4.95	0.92	0.02	0.12	0.48	443	52	0.19	63	-23.8
N8	4.70	1.82	0.04	0.18	3.58	438	197	0.05	57	nd.
N7	4.15	1.15	0.06	0.08	1.73	439	151	0.04	74	-22.8
N6	3.50	2.05	0.19	0.26	6.17	438	301	0.04	56	-24.2
N5	3.10	0.73	0.04	0.07	0.61	444	83	0.10	62	-22.9
N4	2.20	2.12	0.07	0.23	6.90	439	325	0.03	70	-22.7
N3	1.50	0.65	0.03	0.07	0.37	438	57	0.16	58	nd.
N2	0.90	1.08	0.35	0.28	2.79	439	259	0.09	75	-23.6
N1	0.10	1.92	0.42	0.31	6.45	436	336	0.05	69	-23.2
N0	-0.50	0.18	0.01	0.05	0.07	538	36	0.41	71	-24.8
N00	-1.00	1.06	0.08	0.19	2.40	435	226	0.07	71	nd.

Appendix 3. Microscopy data.

Key to Tables:

Table I:

nd., no data available

Carb, carbonate

y, yellow

y/o, yellow/orange

m.o, mid orange.

Tables II, IV, VI, VII and VIII:

Data is based on 300 counts per slide.

AOM (%), percentage amorphous organic matter

Palynomorphs (%), percentage palynomorphs

Phytoclasts (%), percentage phytoclasts

Black phytoclasts, percentage of black phytoclasts that make up the phytoclast fraction

Brown phytoclasts, percentage of brown phytoclasts that make up the phytoclasts fraction

Black/Brown, the ratio of black phytoclasts to brown phytoclasts

PhyTOC, the PhyTOC parameter (Tyson, 1995)

Preservation Scale, fluorescence preservation scale (Tyson, 1995).

Tables III, V and IX:

Data is based on 100 counts per slide.

Chorate (%), percentage chorate dinocysts

Proximochorate (%), percentage proximochorate dinocysts

Cavate (%), percentage cavate dinocysts

Bisaccate pollen (%), percentage bisaccate pollen

Other pollen (%), percentage other pollen

Spores (%), percentage spores

Prasinophyte (%), percentage prasinophytes

Acritarchs (%), percentage acritarchs.

I) Vitrinite Reflectance data for Cenomanian-Turonian samples (performed by Dr. M. Jones)

Sample	Lithology	Pyrite mineralogy	Bitumen	Phytoclasts	Fluorescence	Mean VRo. (%)	No. of vitrinite particles measured
OB2	Marl	Pyrite-decomposed	staining-light wisps-trace	Inertinite-100%	Carb-y-y/o	nd	0
OB79	Marly Shale	Pyrite-decomposed	staining-light/mod wisps-light/mod	Inertinite-90% Vitrinite-10%	Carb-y/o spores-y/o	0.37	3
DOY25	Marly Shale	Pyrite- part-decomposed	staining-light/mod wisps-light/mod	Inertinite-90% Vitrinite-10%	Carb-y/o spores-y-y/o	0.33	9
OG16	Shaly Marl	Pyrite-decomposed	staining-light wisps-mod/rich	Inertinite-trace Vitrinite-trace	Spores-y-y/o	0.4	12
N18	Calcareous Shale	none observed	staining-mod/rich wisps-mod	Inertinite-trace Vitrinite-wispy-trace	Carb- m.o	0.4	2
EC6	Marly Shale	Pyrite-decomposed	staining-light/mod wisps-low	Inertinite-trace Vitrinite-trace	Spores-y-y/o	0.41	2
EC23	Marly Shale	Pyrite-decomposed	staining-mod wisps-low/mod	Inertinite-trace Vitrinite-trace	Spores-y-y/o	0.37	2
MQ5	Marl	none observed	staining-trace	none	Carb-y/o	nd	0
MQ10	Marly Shale	none observed	staining-v-light wisps-v.low	Inertinite-100% Vitrinite-trace	Spores-y	0.27	3
MQ20	Shale	none observed	staining-light wisps-mod/rich	Inertinite-80% Vitrinite-20%	Spores-y-y/o	0.34	20
SF6c	Shale	Pyrite-decomposed	staining-light wisps-mod	Inertinite-90% Vitrinite-10%	Carb-y/o Spores-y-y/o	0.28	20
BC4	Shale	Pyrite-decomposed	staining-light wisps-mod/rich	Inertinite-90% Vitrinite-10%	Spores-y-y/o	0.37	20

II) Palynofacies kerogen data for the Buckton Cliff section.

Sample No.	Section depth (cm)	AOM (%)	Palynomorphs (%)	Phytoclasts (%)	Black Phytoclasts	Brown Phytoclasts	Black/ Brown	Fluor scale
BC1	6.50	30.7	14.7	54.6	39.0	15.6	0.40	2
BC2	4.50	31.0	11.9	57.1	36.1	20.0	0.55	2
BC3	3.25	66.6	18.9	14.5	4.0	8.0	2.00	3
BC4	2.00	61.0	21.5	17.5	5.6	9.4	1.68	3
BC5	0.50	14.7	36.7	48.6	24.3	24.3	1.00	2

III) Palynomorph data for the Buckton Cliff section.

Sample No.	Section depth (cm)	Dino cysts			Bisaccate Pollen (%)	Other Pollen (%)	Spores (%)	Prasinophytes (%)	Acritarchs (%)
		Chorate (%)	Proximochorate (%)	Cavate (%)					
BC1	6.50	3	65	19	4	5	1	0	3
BC2	4.50	8	74	11	0	1	2	0	4
BC3	3.25	0	62	4	2	6	6	1	19
BC4	2.00	0	72	2	2	9	2	0	13
BC5	0.50	25	63	4	1	1	0	0	6

IV) Palynofacies kerogen data for the Misberg Quarry section.

Sample No.	Section depth (cm)	AOM (%)	Palynomorphs (%)	Phytoclasts (%)	Black Phytoclasts (%)	Brown Phytoclasts (%)	Black/ Brown	Preservation scale	Fluor scale
MQ5	30.16	24.5	5	70.5	31.2	39.3	0.79	1	1
MQ6	30.07	26.2	49.3	24.5	16.6	7.9	2.10	3	2
MQ9	29.41	26.9	47.6	25.5	17.6	7.9	2.23	3	2
MQ 10	26.91	27.5	42.3	30.2	20.9	9.3	2.25	3	2
MQ 12	23.48	32.6	34.6	32.8	24.6	8.2	3.00	4	3
MQ 14	21.44	69.8	21.3	8.9	5.6	3.3	1.70	4	3
MQ 16	18.00	71.5	15.3	13.2	9.6	3.6	2.67	4	3
MQ 18	16.32	52.7	28.6	18.7	9.9	8.8	1.13	3	2 to 3
MQ 20	10.00	21.2	46.6	32.2	28.9	3.3	8.76	3	2
MQ23	6.83	17.3	54	28.7	21.6	7.1	3.04	3	2
MQ 24	2.18	31.8	43.3	24.9	15.3	9.6	1.59	3	2
MQ 27	0.77	39.2	39.6	21.2	7.6	13.6	0.56	3	2

V) Palynomorph data for the Misberg Quarry section.

Sample	Section depth (m)	Dino cysts			Bisaccate Pollen	Other Pollen (%)	Spores (%)	Prasinophytes (%)	Acritarchs (%)
		Chorate (%)	Proximochorate (%)	Cavate (%)					
MQ6	30.07	23	36	26	4	7	2	0	2
MQ9	29.41	12	39	32	6	2	4	0	3
MQ 10	26.91	15	41	23	7	3	2	1	8
MQ 12	23.48	11	41	19	9	5	5	4	5
MQ 14	21.44	2	42	12	10	6	10	3	15
MQ 16	18.00	5	58	6	4	15	3	3	6
MQ 18	16.32	5	51	10	4	5	9	1	15
MQ 20	10.00	27	50	10	3	2	0	0	8
MQ23	6.83	34	41	18	4	1	0	0	2
MQ 24	2.18	22	51	10	3	1	6	1	6
MQ 27	0.77	20	47	16	2	1	10	0	4

VI) Palynofacies kerogen data for the Oued Bahloul section.

Sample No.	Section depth (m)	AOM (%)	Palynomorphs (%)	Phytoclasts (%)	Preservation Scale	Fluor Scale
OB82	27.70	99.5	0.5	0	5	3 to 4
OB81	27.50	99.5	0.5	0	5	4
OB79	26.75	76	17	7	4	4
OB76	25.60	99.5	0.5	0	5	3 to 4
OB75	25.25	98	1	1	5	3
OB72	24.00	99	1	0	5	4
OB71	23.80	99	1	0	5	4
OB68	22.90	99	1	0	5	5 to 4
OB65	22.20	98.5	1	0.5	5	3
OB61	21.15	98.5	1	0.5	5	3
OB59	20.80	98.5	1	0.5	5	4
OB55	19.30	98.5	1	0.5	5	4
OB50	17.70	98.5	1	0.5	5	4
OB49	17.45	98.5	1	0.5	5	4
OB47	16.75	99	1	0	5	4
OB46	16.45	99	1	0	5	3
OB44	15.65	98.5	1	0.5	5	3 to 4
OB43	15.15	99	1	0	5	4
OB40	14.25	99	1	0	5	5
OB39a	14.10	99	1	0	5	4
OB33	12.20	99	1	0	5	4
OB31	11.50	99	1	0	5	4
OB28	10.55	98	1	1	5	5
OB23	8.60	66	18	16	4	3
OB21	7.60	99	1	0	5	4
OB18	6.35	99	1	0	5	3
OB17	5.80	99	1	0	5	4
OB15	4.95	99	1	0	5	3
OB12	3.60	99	1	0	5	4
OB11	3.30	99	1	0	5	4
OB9	2.51	99	1	0	5	4
OB7	1.63	99	1	0	5	4
OB6	1.28	99	1	0	5	4
OB4	0.70	98	2	0	5	3
OB2	0.48	81	12	7	4	3

VII) Palynofacies kerogen data for the Dir Oulad Yahia, Oued El Gsab and Nebour sections.

Sample	Section depth (m)	AOM (%)	Palynomorphs (%)	Phytoclasts (%)	Preservation Scale	Fluor Scale
DOY25	-	98	1.5	0.5	5	5
OG16	-	99	0.5	0.5	4	4
N18	-	95	4	1	3	1

VIII) Palynofacies kerogen data for the Ech Cheid section.

Sample No.	Section depth (m)	AOM (%)	Palynomorphs (%)	Phytoclasts (%)	Black Phytoclasts (%)	Brown Pyhtoclasts (%)	Black/ Brown	PhytOC	Prerservation Scale	Fluor Scale
EC25	18.00	72	19	9	8	1	8.00	0.18	3	2 to 3
EC22	15.35	59	20	21	17	4	4.25	0.44	3	2
EC20	14.60	65	22	13	10	3	3.33	0.54	3	3
EC19	14.40	84	10	6	4	2	2.00	0.06	3	3
EC16	12.90	68	17	15	14	1	14.00	0.54	3	2
EC13	11.10	86	5	9	7	2	3.50	0.11	2	2
EC11	9.70	89	5	6	5	1	5.00	0.06	3	3
EC9	8.40	52	31	17	15	2	7.50	0.33	3	2 to 3
EC8	7.80	53	24	23	22	1	22.00	1.21	3	2
EC7	6.70	49	25	26	18	8	2.25	0.74	3	2
EC4	3.60	63	20	17	10	7	1.43	0.34	3	2
EC1	0.10	69	10	21	15	6	2.50	0.33	1b	1

IX) Palynomorph data for the Ech Cheid section.

Sample No.	Section depth (m)	Dino cysts			Bisaccate Pollen (%)	Other Pollen (%)	Spores (%)	Prasinophytes (%)	Acritarchs (%)
		Chorate (%)	Proximate (%)	Cavate (%)					
EC25	18.00	0	95	0	0	0	0	0	5
EC22	15.35	0	93	0	0	0	0	0	7
EC20	14.60	0	97	0	0	1	0	0	2
EC19	14.40	0	89	0	0	0	0	0	11
EC16	12.90	2	95	0	0	0	0	0	3
EC13	11.10	0	95	1	2	0	0	0	2
EC11	9.70	0	90	0	0	0	0	0	10
EC9	8.40	1	65	5	7	5	0	4	13
EC8	7.80	3	65	3	3	6	0	3	16
EC7	6.70	0	62	21	4	7	1	0	5
EC4	3.60	4	72	10	6	6	0	0	2
EC1	0.10	2	88	0	0	0	0	0	10

Appendix 4. Molecular geochemistry data.

Key to tables:

Tables I to IV:
EOM, Extractable Organic matter measured in mgHC/gSED
Pr/Ph, Pristane/Phytane ratio
Pr/nC$_{17}$, Pristane/normal alkane C$_{17}$
Ph/nC$_{18}$, Phytane/normal alkane C$_{18}$
n-alk max, normal alkane carbon number maximum in envelope
n-alk range, range of normal alkanes identified from GC trace;
UCM, unresolved complex material.

Tables VII to XI: Ts/Tm, Trisnorneohopane/Trisnorhopane
C31 homo, 22S/22S + 22R C31 homohopane
C32 homo, 22S/22S + 22R C32 homohopane
C30 hopane, C30 αβ/αβ+βα hopane
Mehop, C30 αβ methylhopane/C30 αβ hopane
C29 sterane C29 ααα 20S/20S + R sterane
C29 sterane (2), C29 αββ/αββ+ααα sterane
Me ster, percentage methylsteranes of sum identified steroids
Hop/ster, sum of identified hopaanoids/sum of identified steroids
Hop/ster (2), C29 + C30 αβ hopane/C29 + C30 ααα R sterane
% C27 to C29 ster, relative amounts of C27 ααα R sterane, C28 ααα R sterane and C29 ααα R sterane.

Table XII:
2MP/1MP, 2-methylphenantherne/3-methylphenanthrene
1MP/9MP, 1-methylphenanthrene/9-methylphenanthrene
MPI, Methylphenanthrene Index
Aromatic steroid ratio 1, C28ββ triaromatic /(C29αα monoaromatic + C28ββ triaormatic)
Aromatic steroid ratio 2, C28 triaromatic R/(C28 triaromatic R + C29αR + C29βR monoaromatic)
DBT/P, Dibenzothiophene/phenanthrene
SumMDBT/sumMP, Sum 1, 2, 3 and 4-methyldibenzothiophene/sum of 1 and 9 methylphenanthrene.

I) Molecular geochemical data for Buckton Cliff section.

Sample No.	Section depth (cm)	EOM	Pr/Ph	Pr/nC17	Ph/nC18	n-alk max	n-alk range	Comments
BC1	6.50	0.13	2.5	1.2	0.6	16, 17	13 to ?	Large UCM from nC21 onwards
BC2	4.50	0.16	2.5	1.6	0.8	16, 17	13 to ?	Large UCM from nC21 onwards
BC3	3.25	0.34	2.8	3.2	1.1	19	13 to ?	Large UCM from nC21 onwards
BC4	2.00	0.48	1.6	9.7	3.5	21	13 to 35	Large UCM, abundant isoprenoids inc. Lycopane, huge Pristane
BC5	0.50	0.16	2.0	1.7	0.9	17, 19	13 to ?	Large UCM from nC21 onwards

II) Molecular geochemical data for Misberg Quarry section.

Sample No.	Section depth (m)	EOM	Pr/Ph	Pr/nC17	Ph/nC18	n-alk range
MQ5	30.16	0.10	1.6	0.4	0.4	11 to 33
MQ6	30.07	0.24	1.4	0.4	0.3	11 to 32
MQ9	29.41	0.39	1.5	0.6	0.5	11 to30
MQ10	26.91	0.30	1.4	0.5	0.4	11 to 32
MQ12	23.48	0.46	1.1	0.4	0.4	11 to 32
MQ14	21.44	0.91	1.3	0.4	0.4	11 to 31
MQ16	18.00	0.65	1.3	0.4	0.4	11 to 31
MQ18	16.32	0.43	1.3	0.4	0.4	11 to 30
MQ20	10.00	1.04	1.2	0.3	0.3	11 to 31
MQ23	6.83	0.44	1.1	0.2	0.2	11 to 31
MQ24	2.18	0.39	1.5	0.4	0.4	11 to 33
MQ27	0.77	0.65	1.3	0.4	0.4	11 to 33

The *n*-alkane max is at nC_{17} for all Misberg samples, and all the gas chromatograms show a rapid tailing off after nC_{20}

III) Molecular geochemical data for the Oued Bahloul section.

Location	Section depth (m)	EOM	Pr/Ph	Pr/nC17	Ph/nC18	n-alk max	n-alk range	Comments
OB82	27.70	3.50	2.6	2.1	1.0	15	11 to 36	Rise to nC15 then drops off to nC36, some biomarkers
OB81	27.50	4.20	2.4	2.3	1.2	15, 16	11 to 36	Rise to nC15, 16 then drops off to nC36, some biomarkers
OB79	26.75	0.20	1.9	3.0	2.5	17	12 to 35	Weak, biomarkers present
OB76	25.60	4.27	2.1	2.6	1.3	17	12 to 36	Rises to nC17 then drops off to nC36, biomarkers present
OB75	25.25	0.30	1.9	4.2	2.4	16, 17	12 to 36	Weak, biomarkers present
OB72	24.00	5.11	2.3	2.4	1.3	16, 17	12 to 36	Rises to nC17 then drops off to nC36, biomarkers present
OB71	23.80	5.50	2.2	2.2	1.3	15	11 to 36	Rise to nC15 then drops off to nC36, some biomarkers
OB68	22.90	6.00	2.3	1.8	1.0	15	12 to 36	Rise to nC15 then drops off to nC36, some biomarkers
OB65	22.20	0.24	1.7	2.4	1.7	16	12 to 36	Weak, biomarkers present
OB61	21.15	3.00	2.4	1.6	0.8	15, 16	11 to 36	Rise to nC15, 16 then drops off to nC36, some biomarkers
OB59	20.80	4.40	2.4	1.7	0.9	16	12 to 36	Rise to nC16 then drops off to nC36, biomarkers present
OB55	19.30	3.40	2.4	1.3	0.7	15, 16	11 to 36	Rise to nC15, 16 then drops off to nC36, some biomarkers
OB50	17.70	2.81	1.9	1.3	0.9	16	12 to 36	Rise to nC16 then drops off to nC36, biomarkers present
OB49	17.45	1.84	2.5	1.2	0.6	15, 16	11 to 36	Rise to nC15, 16 then drops off to nC36, some biomarkers
OB47	16.75	3.42	1.9	1.5	0.9	16	12 to 36	Rise to nC16 then drops off to nC36, some biomarkers
OB46	16.45	7.53	1.5	1.9	1.5	17	12 to 36	Rises to nC17 then drops off to nC36, biomarkers present
OB44	15.65	2.38	2.5	1.2	0.6	15, 16	12 to 35	Rise to nC15, 16 then drops off to nC36, some biomarkers
OB43	15.15	5.21	2.1	1.4	0.9	15, 16	11 to 35	Rise to nC15, 16 then drops off to nC36, some biomarkers
OB40	14.25	7.46	1.7	3.5	2.2	19, 20	12 to 36	Large isoprenoids, biomarkers present
OB39	14.10	14.50	1.9	1.5	1.0	15	12 to 36	Rises to nC15 then drops off to nC36, biomarkers present
OB33	12.20	3.75	2.4	1.4	0.7	16	12 to 36	Rises to nC17 then drops off to nC36, biomarkers present
OB31	11.50	6.75	1.8	1.7	1.1	17	12 to 36	Rises to nC17 then drops off to nC36, biomarkers present
OB28	10.55	14.90	1.8	2.4	1.4	17	12 to 36	Large isoprenoids, biomarkers present
OB26	9.85	3.81	1.4	0.9	0.8	17	13 to 32	Very weak, some biomarkers present
OB23	8.60	0.12	1.9	0.9	0.6	16	12 to 36	Weak, biomarkers present
OB21	7.60	4.77	1.8	1.4	1.0	15, 16	11 to 36	Rise to nC15, 16 then drops off to nC36, some biomarkers
OB18	6.35	0.54	1.7	2.3	1.3	18	12 to 36	Weak, biomarkers present
OB17	5.80	9.70	1.7	1.7	1.1	16	11 to 36	Rise to nC16 then drops off to nC36, some biomarkers
OB15	4.95	3.06	2.5	1.0	0.5	15, 16	11 to 36	Rise to nC15, 16 then drops off to nC36, some biomarkers

Sample No.	Section depth (m)	EOM	Pr/Ph	Pr/nC17	Ph/nC18	n-alk max	n-alk range	Comments
OB12	3.60	4.98	1.8	3.5	1.6	18	12 to 36	Large isoprenoids, biomarkers present
OB11	3.30	3.80	2.0	1.7	1.0	17	12 to 36	Rises to nC17 then drops off to nC36, biomarkers present
OB9	2.51	4.19	1.9	1.1	0.7	17	12 to 36	Rises to nC17 then drops off to nC36, biomarkers present
OB7	1.63	12.30	1.7	2.9	1.8	17	12 to 36	Large isoprenoids, biomarkers present
OB6	1.28	15.50	1.7	3.7	1.7	17	12 to 36	Large isoprenoids, biomarkers present
OB4	0.70	5.50	2.2	1.2	0.7	17	12 to 35	Biomarkers present
OB2	0.18	0.32	2.4	1.7	0.7	19	12 to 32	Weak, Biomarker present

IV) Molecular geochemical data for the Ech Cheid section

Sample No.	Section depth (m)	EOM	Pr/Ph	Pr/nC17	Ph/nC18	n-alk max	range	comments
EC25	18.00	0.49	3.3	0.5	0.3	16	13 to 22	Weak chromatogram rises to nC16 then drops to nC21
EC22	15.35	0.37	2.4	0.5	0.2	17, 31	11 to 36	Rises to nC17 then drops off to nC36
EC20	14.60	0.13	1.7	0.3	0.2	15, 26, 31	12 to 37	Bimodal around nC15 and 26 however nC26 three time as large.
EC19	14.40	0.88	2.5	1.0	0.5	15, 31	10 to 36	Rises to nC15 then gradually drops off to nC37
EC16	12.90	0.13	1.6	0.5	0.4	17, 26, 31	13 to 37	Rises gradually to nC26 then drops off
EC13	11.10	0.44	2.7	0.7	0.3	15, 31	11 to 36	Rises to nC15 then gradually drops off to nC37
EC11	9.70	0.58	2.7	0.7	0.3	15, 31	10 to 37	Rises to nC15 then gradually drops off to nC37
EC9	8.40	0.14	2.5	0.8	0.4	7, 24, 26, 3	11 to 37	Bimodal around nC17 and 26, abundant long chain alkanes eg. nC37
EC8	7.80	0.10	2.5	0.8	0.4	7, 26, 29, 3	12 to 37	Bimodal around nC17 and 26, abundant long chain alkanes eg. nC37
EC7	6.70	0.09	1.5	1.1	0.6	26, 31	12 10 37	Rises gradually to nC26 then drops off
EC4	3.60	0.18	2.2	1.1	0.5	26, 31	12 to 37	Rises gradually to nC26 then drops off
EC1	0.10	0.27	2.7	0.6	0.3	15, 21, 31	11 to 37	Bimodal at 15 and 21

V) Molecular geochemical data for the Dir Oulad Yahia, Oued El Gsab and Nebour samples.

Sample No.	Section depth (m)	EOM	Pr/Ph	Pr/nC17	Ph/nC18	n-alk max	range	comments
DOY25	na.	1.89	2.3	1.9	1.1	16	11 to 36	Biomarkers present,
OG16	na.	1.78	2.9	1.9	0.7	17	12 to 36	Biomarkers present,
N18	na.	0.80	1.7	0.4	0.2	13, 17, 31	10 to 36	High nC12 to 20 before dropping off to 36, bimodal

VII) Biomarker parameters for the Buckton Cliff section.

Sample	Depth (cm)	C31 homo	C30 hopane	C29 sterane	C29 sterane (2)	% Mester	Hop/Ster	Hop/Ster (2)	%C27ster	%C28ster	%C29ster	27/29
BC1	6.50	0.54	0.91	0.40	0.35	8.22	1.93	3.11	32	22	46	0.71
BC2	4.50	0.53	0.87	0.37	0.36	6.99	1.98	3.25	33	23	44	0.75
BC3	3.25	0.51	0.79	0.25	0.32	6.33	1.75	2.33	34	28	38	0.89
BC4	2.00	0.41	0.63	0.08	0.29	4.81	1.53	1.55	33	36	30	1.09
BC5	0.50	0.54	0.85	0.32	0.33	3.85	2.11	2.82	34	25	41	0.83

VIII) Biomarker parameters for the Misberg Quarry section.

Sample	Depth	Ts/Tm	C31homo	C32 homo	C30 hopane	Me Hop	C29 steranes	C29 sterane (2)	% Mester	Hop/Ster	Hop/Ster (2)	%C27ster	%C28ster	%C29ster	27/29
MQ5	30.16	0.60	0.59	0.59	0.91	0.16	0.41	0.31	9.33	3.51	8.53	31	19	50	0.62
MQ6	30.07	0.64	0.48	0.47	0.80	0.14	0.47	0.25	5.27	8.29	10.71	27	16	57	0.48
MQ9	29.41	0.49	0.58	0.57	0.91	0.14	0.51	0.46	7.16	4.22	9.61	32	19	49	0.66
MQ 10	26.91	0.72	0.54	0.54	0.85	0.20	0.43	0.30	8.74	3.68	8.32	33	21	46	0.71
MQ 12	23.48	0.99	0.61	0.59	0.90	0.43	0.44	0.26	2.61	5.66	10.30	38	31	32	1.19
MQ 14	21.44	0.79	nd.	0.53	0.85	nd.	0.42	0.40	6.15	5.58	0.91	37	34	29	1.26
MQ 16	18.00	0.83	0.42	0.59	0.79	0.08	0.38	0.37	6.45	4.96	5.52	39	28	33	1.17
MQ 18	16.32	0.84	0.60	0.45	0.85	0.13	0.49	0.25	4.17	6.96	10.76	39	33	28	1.38
MQ 20	10.00	0.90	0.56	0.56	0.82	0.15	0.46	0.28	2.37	5.86	11.21	34	34	33	1.03
MQ23	6.83	0.70	0.52	0.66	0.90	0.13	0.32	0.42	8.55	7.11	4.99	40	14	46	0.86
MQ 24	2.18	0.41	0.51	0.59	0.86	0.11	0.34	0.29	6.99	7.07	6.83	31	17	52	0.60
MQ 27	0.77	0.44	0.44	0.45	0.84	nd.	0.34	0.39	13.78	5.77	5.51	36	21	43	0.85

IX) Biomarker parameters for the Oued Bahloul section.

Sample	Depth	Ts/Tm	C31homo	C32homo	C30 hopane	Me Hop	C29 ster	C29 ster (2)	% Me ster	Hop/Ster	Hop/Ster (2)	%C27ster	%C28ster	%C29ster
OB82	27.70	0.45	0.58	0.54	0.83	0.033	0.36	0.28	7.17	1.04	3.02	32	30	38
OB81	27.50	0.45	0.58	0.55	0.83	0.030	0.38	0.30	6.87	1.16	3.46	31	31	38
OB79	26.75	0.47	0.58	0.56	0.84	0.057	0.36	0.29	6.50	1.70	4.52	27	30	43
OB76	25.60	0.32	0.60	0.55	0.84	0.027	0.38	0.28	9.35	1.51	4.61	30	31	39
OB75	25.25	0.41	0.58	0.55	0.84	0.042	0.38	0.31	9.03	2.00	6.07	30	30	40
OB72	24.00	0.40	0.59	0.56	0.83	0.032	0.38	0.28	8.49	1.57	4.74	32	29	39
OB71	23.80	0.36	0.59	0.55	0.83	0.040	0.37	0.28	8.35	1.36	3.80	32	28	39
OB68	22.90	0.36	0.58	0.54	0.83	0.032	0.37	0.29	8.16	1.37	4.06	34	27	39
OB65	22.20	0.34	0.57	0.56	0.84	0.064	0.37	0.31	8.13	1.62	4.37	30	28	42
OB61	21.15	0.55	0.57	0.54	0.82	0.041	0.36	0.28	6.88	1.02	2.73	31	29	40
OB59	20.80	0.51	0.57	0.56	0.83	0.039	0.35	0.28	7.25	1.31	3.31	29	29	43
OB55	19.30	0.67	0.61	0.53	0.83	0.026	0.35	0.28	7.28	0.94	2.34	29	29	42
OB50	17.70	0.54	0.57	0.54	0.84	0.036	0.37	0.30	6.12	0.98	2.62	30	30	40
OB49	17.45	0.63	0.60	0.52	0.83	0.029	0.36	0.29	5.41	0.83	2.26	29	28	43
OB47	16.75	0.51	0.58	0.53	0.83	0.031	0.36	0.29	7.31	1.20	3.10	29	29	42
OB46	16.45	0.31	0.60	0.55	0.84	0.026	0.36	0.28	7.99	1.25	3.21	31	31	38
OB44	15.65	0.54	0.60	0.55	0.83	0.038	0.36	0.29	6.65	0.94	2.31	28	27	45
OB43	15.15	0.51	0.58	0.53	0.84	0.028	0.35	0.28	7.11	0.95	2.31	30	29	41
OB40	14.25	0.25	0.58	0.55	0.83	0.066	0.35	0.29	6.89	1.50	3.66	33	30	37
OB39	14.10	0.30	0.62	0.54	0.83	0.054	0.34	0.26	7.84	1.79	4.45	31	32	37
OB33	12.20	0.62	0.58	0.54	0.83	0.042	0.37	0.29	6.37	1.03	2.72	30	28	41
OB31	11.50	0.36	0.59	0.55	0.84	0.045	0.36	0.28	7.63	1.23	3.12	29	32	40
OB28	10.55	0.28	0.59	0.56	0.83	0.032	0.39	0.28	8.07	2.62	6.84	30	31	39
OB23	8.60	0.42	0.57	0.58	0.88	0.077	0.38	0.27	7.58	2.61	7.19	31	25	44
OB21	7.60	0.38	0.58	0.55	0.84	0.022	0.36	0.29	7.29	1.39	3.83	35	28	37
OB18	6.35	0.53	0.58	0.55	0.83	0.029	0.38	0.29	8.18	1.85	5.05	31	28	41
OB17	5.80	0.31	0.58	0.55	0.84	0.029	0.35	0.28	8.31	1.96	5.02	33	29	38
OB15	4.95	0.54	0.58	0.54	0.82	0.042	0.32	0.28	6.97	1.09	2.48	27	23	50
OB12	3.60	0.39	0.60	0.55	0.83	0.053	0.37	0.30	7.59	1.88	4.61	31	29	40
OB11	3.30	0.69	0.58	0.55	0.83	0.027	0.38	0.31	5.86	1.29	3.53	29	26	45
OB9	2.51	0.69	0.61	0.54	0.83	0.040	0.36	0.30	6.60	1.36	3.57	29	26	45

OB7	1.63	0.25	0.62	0.55	0.83	0.159	0.37	0.28	7.88	2.97	7.53	29	31	40
Sample	**Depth**	**Ts/Tm**	**C31homo**	**C32homo**	**C30 hopane**	**Me Hop**	**29 sterane**	**C29 sterane (2**	**% Me ster**	**Hop/Ster**	**Hop/Ster (2)**	**%C27ster**	**%C28ster**	**%C29ster**
OB6	1.28	0.28	0.62	0.56	0.83	0.159	0.37	0.29	8.52	2.95	7.86	30	30	40
OB4	0.70	0.66	0.62	0.55	0.83	0.015	0.35	0.30	8.40	1.53	4.54	30	25	44
OB2	0.48	0.57	0.59	0.52	0.81	0.041	0.36	0.29	4.21	1.00	3.30	33	25	42

X) Biomarker parameters for the Ech Cheid section

Sample	Depth	Ts/Tm	C31 homo	C32 homo	C30 hopane	Me Hop	C29 ster	C29 ster (2)	%mester	Hop/Ster	Hop/Ster (2)	%C27ster	%C28ster	%C29ster
EC 25	18.00	2.25	0.63	0.59	0.97	0.021	0.45	0.31	4.85	1.39	12.12	23	23	54
EC 22	15.35	1.88	0.64	0.59	0.88	0.042	0.51	0.32	4.95	1.60	12.51	29	25	46
EC 20	14.60	2.48	0.67	0.54	0.89	0.054	0.46	0.26	6.84	2.84	17.09	25	22	52
EC 19	14.40	2.36	0.63	0.61	0.90	0.025	0.49	0.36	3.81	1.04	9.39	27	25	48
EC 16	12.90	2.28	0.66	0.58	0.91	0.050	0.47	0.31	7.29	2.64	15.09	25	22	53
EC 13	11.10	2.11	0.63	0.56	0.86	0.030	0.49	0.32	4.52	1.45	11.40	26	23	51
EC 11	9.70	2.44	0.64	0.55	0.91	0.024	0.50	0.34	4.62	1.20	10.29	25	26	49
EC 9	8.40	2.26	0.65	0.62	0.90	0.041	0.47	0.32	3.97	1.56	12.59	27	21	52
EC 8	7.80	1.65	0.65	0.51	0.88	0.058	0.49	0.33	6.59	1.99	10.28	20	23	57
EC 6	6.70	1.20	0.68	0.54	0.89	0.059	0.42	0.25	3.96	2.13	10.01	19	20	61
EC4	3.60	2.52	0.64	0.60	0.90	0.042	0.47	0.29	4.45	1.76	13.99	23	21	56
EC 1	0.10	2.08	0.64	0.64	0.90	0.023	0.46	0.28	4.62	1.99	16.32	31	21	48

XI) Biomarker parameters for the Dir Oulad Yahia, Oued El Gsab and Nebour sections.

Sample	Depth	Ts/Tm	C31 homo	C32 homo	C30 hopane	Me Hop	29 sterane	C29 sterane (2	%mester	Hop/Ster	Hop/Ster (2)	%C27ster	%C28ster	%C29ster
DOY 25	na.	0.43	0.58	0.41	0.79	0.059	0.19	0.10	11.68	0.57	1.09	29	28	43
OG 16	na.	0.31	0.64	0.55	0.81	0.035	0.42	0.18	8.12	1.19	3.97	32	29	39
N 18	na.	1.27	0.67	0.53	0.92	0.047	0.44	0.32	7.12	2.49	12.63	29	22	49

XII) Aromatic biomarker maturity parameters for Cenomanian-Turonian samples.

Sample No.	2MP/ 1MP	1MP/ 9MP	MPI	ASR1	ASR2	DBT/P	Sum MDBT/ sum MP
OB2	1.12	0.49	0.43	0.81	0.07	0.21	0.28
OB7	0.79	0.78	0.42	0.88	0.01	0.05	0.09
OB18	0.92	0.87	0.12	0.91	0.01	0.05	0.35
OB33	0.77	0.62	0.47	0.82	0.06	0.20	0.24
OB65	0.90	0.77	0.20	0.89	0.01	0.08	0.34
OB72	0.85	0.60	0.42	0.91	0.01	0.27	0.29
OB81	0.94	0.58	0.56	0.91	0.07	0.21	0.18
DOY25	0.80	0.75	0.44	0.62	0.01	0.27	0.39
OG18	1.07	0.67	0.23	0.94	0.01	0.10	0.29
N18	0.90	1.47	0.12	0.92	0.29	0.01	0.06
EC11	0.92	0.83	0.35	0.74	0.23	0.03	0.13
EC13	1.10	1.28	0.21	0.71	0.12	0.02	0.11
EC19	1.18	0.66	0.58	0.84	0.17	0.05	0.09
EC25	1.15	1.06	0.39	0.96	0.23	0.09	0.20
MQ14	1.29	0.63	0.53	0.21	0.73	0.18	0.32
MQ16	1.32	0.70	0.43	0.24	0.67	0.13	0.32
MQ18	1.42	0.70	0.40	0.60	0.52	0.09	0.29
MQ27	1.37	0.56	0.34	0.17	0.42	0.11	0.35
SF6a	0.92	0.91	0.55	0.05	0.14	0.48	0.31
SF6b	0.84	0.96	0.22	0.05	0.13	0.13	0.23

Appendix 5. List of compounds used in Principal Component Analysis in this Thesis.

Table I. Compounds used in Buckton Cliff and South Ferriby Principal Component Analysis.

m/z 191

1. C27 17α Trisnorhopane (Tm)
2. C27 β(H) hopane
3. C29 hop-13(18)-ene
4. C29 αβ hopane
5. C29 βα hopane
6. C30 αβ hopane
7. C30 hop-13(18)-ene
8. C29 ββ hopane
9. C31 αβ homohopane S
10. C31 αβ homohopane R
11. C30 ββ hopane
12. C31 ββ hopane
13. C32 ββ hopane

m/z 205

14. C29 hop-13(18)-ene

m/z 217

15. C27 βαα sterane R
16. C27 ααα sterane R
17. C28 βαα sterane R
18. C28 ααα sterane R
19. C29 ααα sterane S
20. C29 βαα sterane R
21. C29 ααα sterane R
22. C30 ααα sterane R
23. C27 aββ sterane S
24. C28 aββ sterane S

m/z 231

25. C28 4α aββ R methylsterane
26. C29 4α aββ R methylsterane
27. C30 4α aββ S methylsterane
28. C30 4α ααα R methylsterane

m/z 257

29. C27 10α diasterene S
30. C27 10α diasterene R
31. C28 10α diasterene S
32. C28 10α diasterene R

m/z 271

33. C28 4 methyldiasterene S
34. C28 4 methyldiasterene R

m/z 367

35. C30 hop-17(21)-ene
36. C31 hop-17(21)-ene S
37. C31 hop-17(21)-ene R
38. C32 hop-17(21)-ene S
39. C32 hop-17(21)-ene R

Table II. Compounds used in Misberg Principal Component Analysis

m/z 177

1. C29 αβ hopane
2. C29 βα hopane
3. C30 αβ hopane S
4. C31 αβ hopane S
5. C31 αβ hopane R

m/z 191

6. C27 18α Trisnorneohopane (Ts)
7. C27 17α Trisnorhopane (Tm)
8. C28 bisnorhopane
9. C29 αβ hopane
10. C29 βα hopane
11. C30 αβ hopane
12. C30 βα hopane
13. C31 αβ homohopane S
14. C31 αβ homohopane R
15. C32 αβ homohopane S
16. C32 αβ homohopane R
17. C33 αβ homohopane S

m/z 205

18. C31 2α αβ methylhopane
19. C31 αβ homohopane S
20. C31 αβ homohopane R
21. C31 βα hopane

m/z 259

22. C27 βα diasterene S
23. C27 βα diasterene R
24. C27 αβ diasterene S
25. C28 βα diasterene S (24 S)
26. C28 βα diasterene S (24 R)
27. C28 βα diasterene R (24S+R)
28. C29 βα diasterene S
29. C29 βα diasterene R
30. C30 βα diasterene S
31. Unknown compound A

m/z 217

32. C27 ααα sterane S
33. C27 αββ sterane R + C29 βα diasterene S
34. C27 αββ sterane S
35. C27 ααα sterane R
36. C28 ααα sterane S
37. C28 αββ sterane R
38. C28 αββ sterane S
39. C28 ααα sterane R
40. C29 ααα sterane S
41. C29 αββ sterane R + S
42. C29 ααα sterane R

m/z 218

43. C27 αββ sterane R
44. C27 αββ sterane S
45. C28 αββ sterane R
46. C28 αββ sterane S
47. C29 αββ sterane R + S
48. C29 αββ sterane R + S
49. C30 hop-13(18)-ene

m/z 231

50. C28 4α ααα R methylsterane
51. C29 4α ααα R methylsterane
52. C30 4α ααα S methylsterane
53. C30 4α αββ R + S methylsterane
54. C30 4α αββ R + S methylsterane
55. C30 4α ααα R methylsterane

m/z 204

56. C29 hop-13(18)-ene

m/z 191

57. C20 βα tricyclicterpane
58. C21 tricyclicterpane
59. C23 βα tricyclicterpane
60. C24 βα tricyclicterpane
61. C25 βα tricyclicterpane S + R
62. C24 tetracyclicterpane
63. C26 βα tricyclicterpane S
64. C26 βα tricyclicterpane R

Table III. Compounds used in Oued Bahloul Principal Component Analysis

m/z 177

1. C29 αβ hopane
2. C29 βα hopane
3. C30 αβ hopane S
4. C31 αβ hopane S
5. C31 αβ hopane R

m/z 191

6. C27 18α Trisnorneohopane (Ts)
7. C27 17α Trisnorhopane (Tm)
8. C28 bisnorhopane
9. C29 αβ hopane
10. C29 βα hopane
11. C30 αβ hopane
12. C30 βα hopane
13. C31 αβ homohopane S
14. C31 αβ homohopane R
15. C32 αβ homohopane S
16. C32 αβ homohopane R
17. C33 αβ homohopane S
18. C33 αβ homohopane R
19. C34 αβ homohopane S
20. C34 αβ homohopane R
21. C35 αβ homohopane S
22. C35 αβ homohopane R

m/z 205

23. C29 2α 28,30 bisnorhopane
24. C30 2α αβ methylhopane
25. C31 2α αβ methylhopane
26. C31 2α βα methylhopane
27. C31 αβ homohopane S
28. C31 αβ homohopane R
29. C32 2α αβ methylhopane R
30. C31 βα hopane
31. C33 2α αβ methylhopane S
32.. C33 2α αβ methylhopane R

m/z 259

33. C27 βα diasterene S
34. C27 βα diasterene R
35. C27 αβ diasterene S
36. C28 βα diasterene S (24 S)
37. C28 βα diasterene S (24 R)
38. C28 βα diasterene R (24S+R)
39. C29 βα diasterene S
40. C29 βα diasterene R
41. C30 βα diasterene S
42. Unknown compound A

m/z 217

43. C27 ααα sterane S
44. C27 αββ sterane R + C29 βα diasterene S
45. C27 αββ sterane S
46. C27 ααα sterane R
47. C28 ααα sterane S
48. C28 αββ sterane R
49. C28 αββ sterane S
50. C28 ααα sterane R
51. C29 ααα sterane S
52. C29 αββ sterane R + S
53. C29 ααα sterane R
54. C30 ααα sterane R

m/z 218

55. C27 αββ sterane R
56. C27 αββ sterane S
57. C28 αββ sterane R
58. C28 αββ sterane S
59. C29 αββ sterane R + S
60. C29 αββ sterane R + S

m/z 231

61. C28 4α ααα R methylsterane
62. C29 4α ααα R methylsterane
63. C30 4α ααα S methylsterane
64. C30 4α αββ R + S methylsterane
65. C30 4α ααα R + S methylsterane

m/z 191

66. C20 βα tricyclicterpane
67. C21 tricyclicterpane
68. C23 βα tricyclicterpane
69. C24 βα tricyclicterpane
70. C25 βα tricyclicterpane S + R
71. C24 tetracyclicterpane
72. C26 βα tricyclicterpane S
73. C26 βα tricyclicterpane R

Table IV. Compounds used for Ech Cheid Principal Component Analysis

m/z 177

1. C29 βα hopane
2. C30 αβ hopane S
3. C30 αβ hopane R
4. C31 αβ hopane S
5. C31 αβ hopane R

m/z 191

6. C27 18α Trisnorneohopane (Ts)
7. C27 17α Trisnorhopane (Tm)
8. C29 αβ hopane
9. C29 βα hopane
10. C30 αβ hopane
11. C30 βα hopane
12. C31 αβ homohopane S
13. C31 αβ homohopane R
14. C32 αβ homohopane S
15. C32 αβ homohopane R
16. C33 αβ homohopane S
17. C33 αβ homohopane R
18. C34 αβ homohopane S
19. C34 αβ homohopane R

m/z 205

20. C29 2α 28,30 bisnorhopane
21. C30 2α αβ methylhopane
22. C31 2α αβ methylhopane
23. C31 2α βα methylhopane
24. C31 αβ homohopane S
25. C31 αβ homohopane R
26. C31 βα hopane
27. C33 2α αβ methylhopane S
28. C33 2α αβ methylhopane R

m/z 231

29. C28 4α ααα R methylsterane
30. C29 4α ααα R methylsterane
31. C30 4α ααα S methylsterane
32. C30 4α αββ R methylsterane
33. C30 4α αββ S methylsterane
34. C30 4α αββ R + S methylsterane

m/z 259

35. C27 βα diasterene S
36. C27 βα diasterene R
37. C27 αβ diasterene S
38. C28 βα diasterene S (24 S)
39. C28 βα diasterene S (24 R)
40. C28 βα diasterene R (24S+R)
41. C29 βα diasterene S
42. C29 βα diasterene R
43. C30 βα diasterene S
44. Unknown compound A

m/z 217

45. C27 ααα sterane S
46 C27 αββ sterane R + C29 βα diasterene S
47. C27 αββ sterane S
48. C27 ααα sterane R
49. C28 ααα sterane S
50. C28 αββ sterane R
51. C28 αββ sterane S
52. C28 ααα sterane R
53. C29 ααα sterane S
54. C29 αββ sterane R + S
55. C29 αββ sterane R + S
56. C29 ααα sterane R
57. C30 ααα sterane R

m/z 218

58. C27 αββ sterane R
59. C27 αββ sterane S
60. C28 αββ sterane R
61. C28 αββ sterane S
62. C29 αββ sterane R + S
63. C29 αββ sterane R + S

m/z 191

64. C20 βα tricyclicterpane
65. C21 tricyclicterpane
66. C23 βα tricyclicterpane
67. C24 βα tricyclicterpane
68. C25 βα tricyclicterpane S + R
69. C24 tetracyclicterpane
70. C26 βα tricyclicterpane S
71. C26 βα tricyclicterpane R

Table V. Compounds used in Tunisian Principal Component Analysis.

m/z 177

1. C29 βα hopane
2. C30 αβ hopane S
3. C31 αβ hopane S
4. C31 αβ hopane R

m/z 191

5. C27 18α Trisnorneohopane (Ts)
6. C27 17α Trisnorhopane (Tm)
7. C29 αβ hopane
8. C29 βα hopane
9. C30 αβ hopane
10. C30 βα hopane
11. C31 αβ homohopane S
12. C31 αβ homohopane R
13. C32 αβ homohopane S
14. C32 αβ homohopane R
15. C33 αβ homohopane S
16. C33 αβ homohopane R

m/z 205

17. C30 2α αβ methylhopane
18. C31 2α αβ methylhopane
19. C31 2α βα methylhopane
20. C31 αβ homohopane S
21. C31 αβ homohopane R
22. C32 2α αβ methylhopane R
23. C31 βα hopane
24. C33 2α αβ methylhopane S
25. C33 2α αβ methylhopane R

m/z 259

26. C27 βα diasterene S
27. C27 βα diasterene R
28. C27 αβ diasterene S
29. C28 βα diasterene S (24 S)
30. C28 βα diasterene S (24 R)
31. C28 βα diasterene R (24S+R)
32. C29 βα diasterene S
33. C29 βα diasterene R
34. C30 βα diasterene S
35. Unknown compound A

m/z 217

36. C27 ααα sterane S
37. C27 αββ sterane R
    + C29 βα diasterene S
38. C27 αββ sterane S
39. C27 ααα sterane R
40. C28 ααα sterane S
41. C28 αββ sterane R
42. C28 αββ sterane S
43. C28 ααα sterane R
44. C29 ααα sterane S
45. C29 αββ sterane R + S
46. C29 ααα sterane R
47. C30 ααα sterane R

m/z 218

48. C27 αββ sterane R
49. C27 αββ sterane S
50. C28 αββ sterane
51. C28 αββ sterane S
52. C29 αββ sterane R
53. C29 αββ sterane S
54. C28 4α ααα R methylsterane
55. C29 4α ααα R methylsterane
56. C30 4α ααα S methylsterane
57. C30 4α αββ R + S methylsterane
58. C30 4α ααα R + S methylsterane

m/z 191

59. C20 βα tricyclicterpane
60. C21 tricyclicterpane
61. C23 βα tricyclicterpane
62. C24 βα tricyclicterpane
63. C25 βα tricyclicterpane S + R
64. C24 tetracyclicterpane
65. C26 βα tricyclicterpane S
66. C26 βα tricyclicterpane R

Table VI. Compounds used in Pyrolysis-gas chromatography Principal Component Analysis.

1. *n*C6 alkene
2. *n*C7 alkene
3. *n*C8 alkene
4. *n*C10 alkene
5. *n*C11 alkene
6. *n*C12 alkene
7. *n*C13 alkene + 2-methylnapthaline
8. *n*C14 alkene
9. *n*C15 alkene
10. *n*C16 alkene
11. *n*C17 alkene
12. *n*C18 alkene
13. *n*C19 alkene
14. *n*C6 alkane
15. *n*C7 alkane
16. *n*C8 alkane
17. *n*C9 alkane
18. *n*C10 alkane
19. *n*C11 alkane
20. *n*C12 alkane
21. *n*C13 alkane
22. *n*C14 alkane
23. *n*C15 alkane
24. *n*C16 alkane
25. *n*C17 alkane
26. *n*C18 alkane
27. *n*C19 alkane
28. Benzene
29. Ethylbenzene
30. 2,3,4-trimethylbenzene
31. Alkylbenzene
32. Thiophene
33. 2-methylthiophene
34. 3-methylthiophene
35. Ethylthiophene + coel
36. 2,4-dimethylthiophene
37. 2,3-dimethylthiophene +2-vinylthiophene
38. 2-ethyl-5-methylthiophene + Methylethylbenzene
39. Alkylthiophene
40. Benzothiophene + coel
41. Alkylphenol
42. Napthaline
43. 1-methylnapthaline
44. Toluene
45. M-xylene +2,5-dimethylthiophene
46. *n*C9 alkene+ Stryene + O +P Xylene
47. methylstyrene
48. Indan
49. Indene
50. Methylindene
51. Methylindene
52. methylyclohexane
53. Unidentified
54. Unidentified
55. Unidentified
56. Unidentified
57. Unidentified
58. Unidentified
59. Unidentified
60. Unidentified
61. Unidentified

Appendix 6. Mass fragmentograms from Pyrolysis-Mass Spectrometry.

Numbers on the x axis refer to the m/z number (m/z 51 to 200).

a) Pyrolysis Mass Spectrogram for OB2

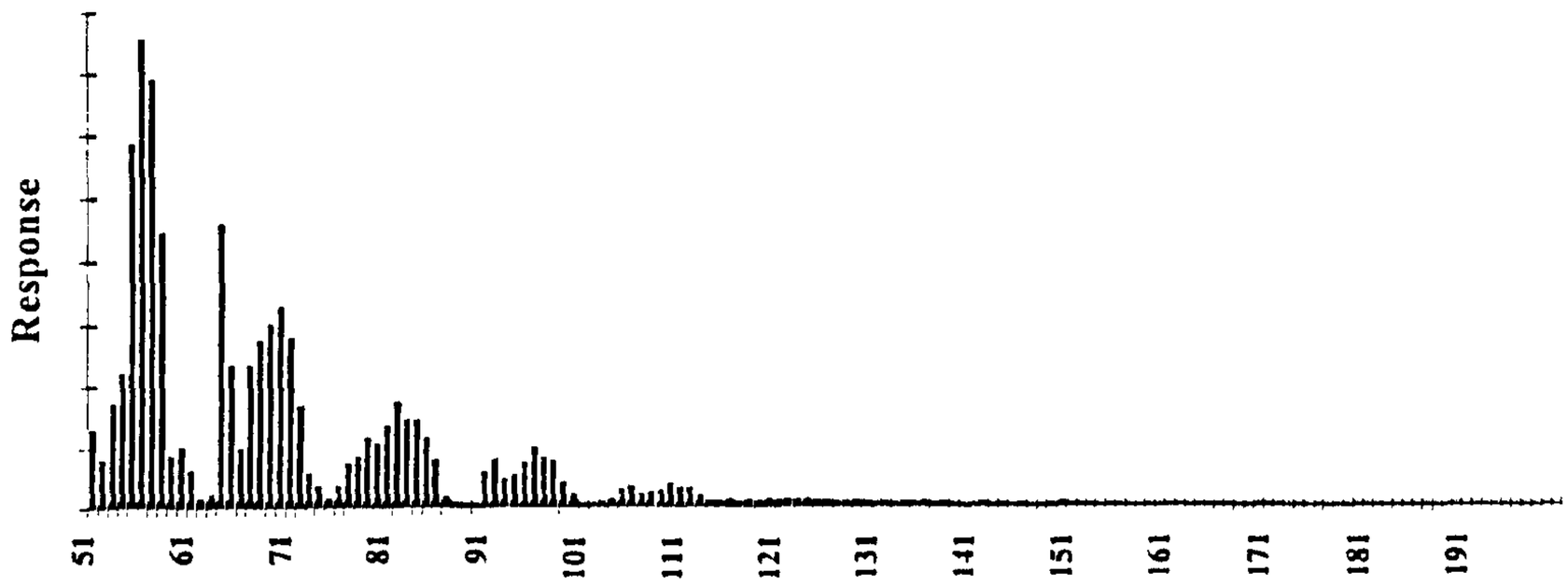

b) Pyrolysis Mass Spectrogram for OB7

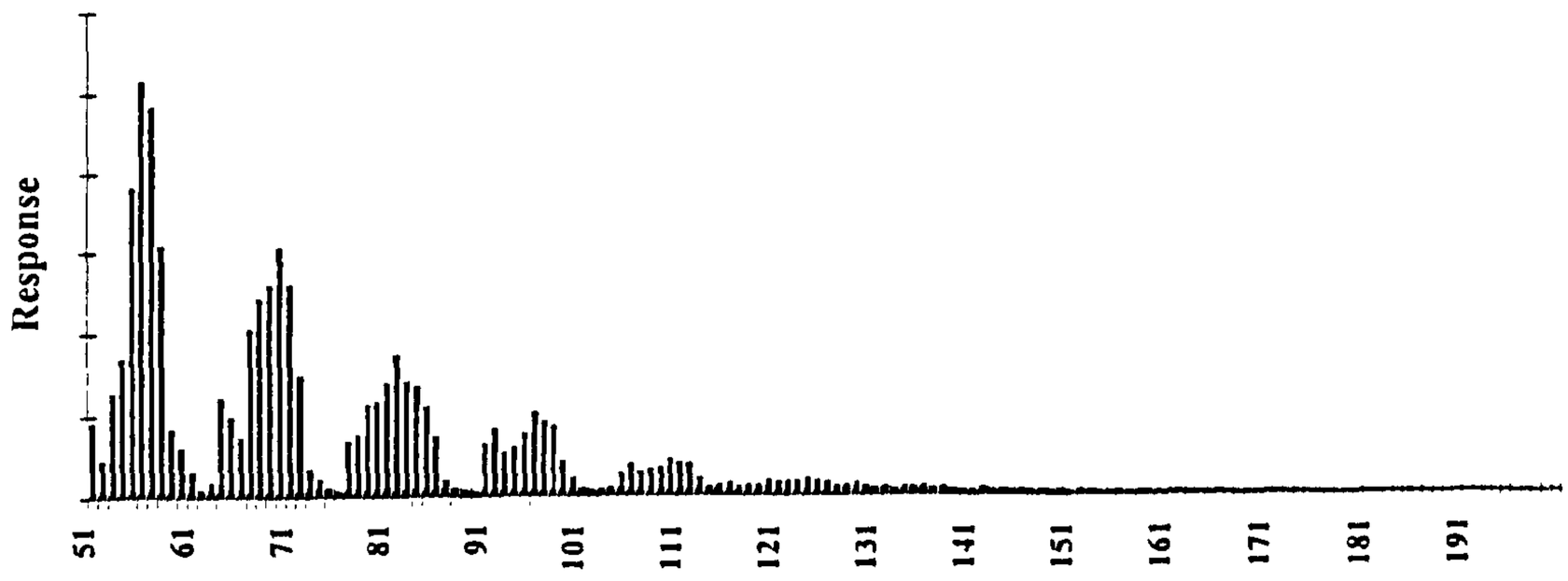

c) Pyrolysis Mass Spectrogram for OB18

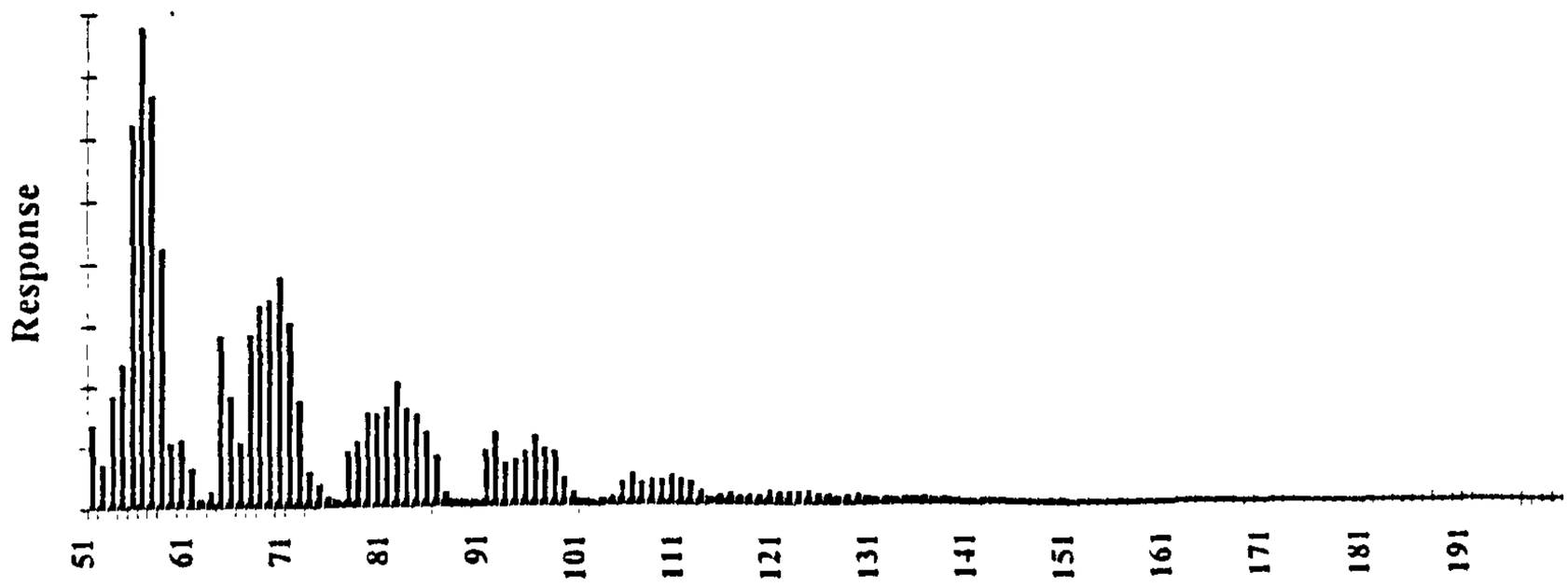

d) Pyrolysis Mass Spectrogram for OB33

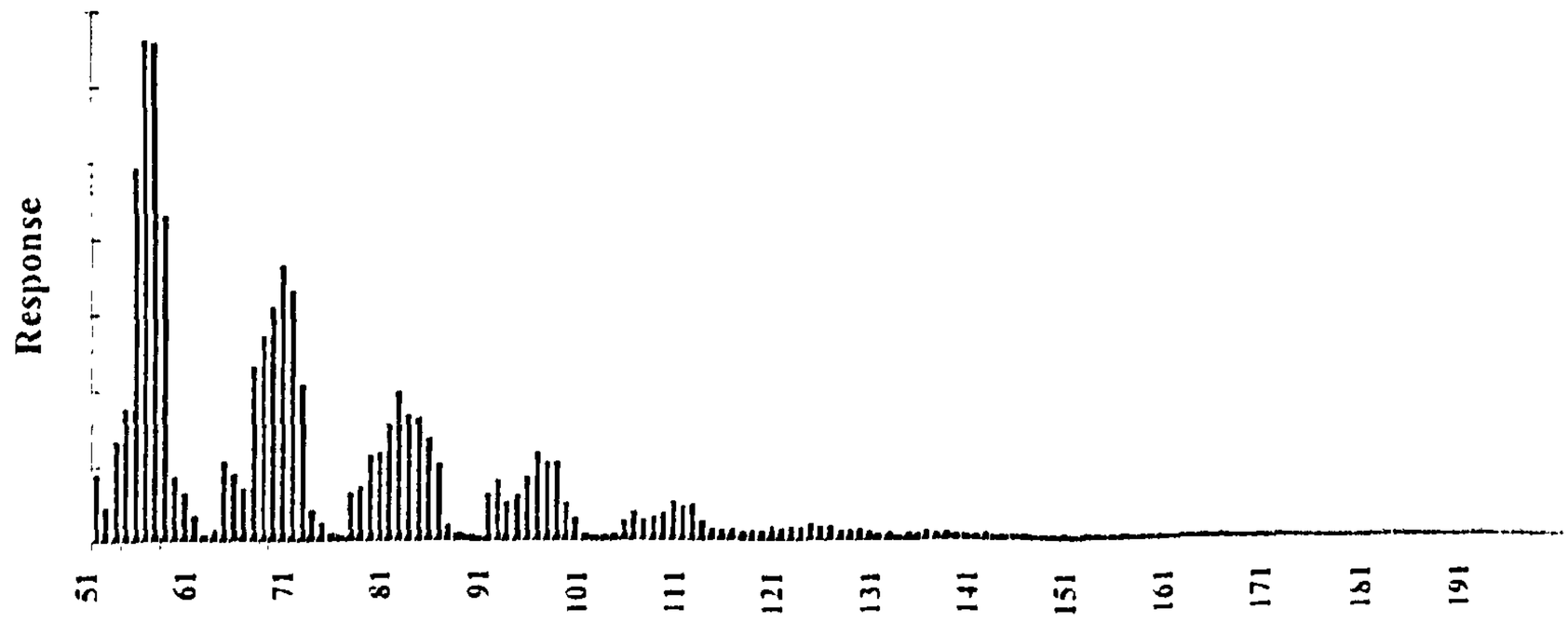

e) Pyrolysis Mass Spectrogram for OB65

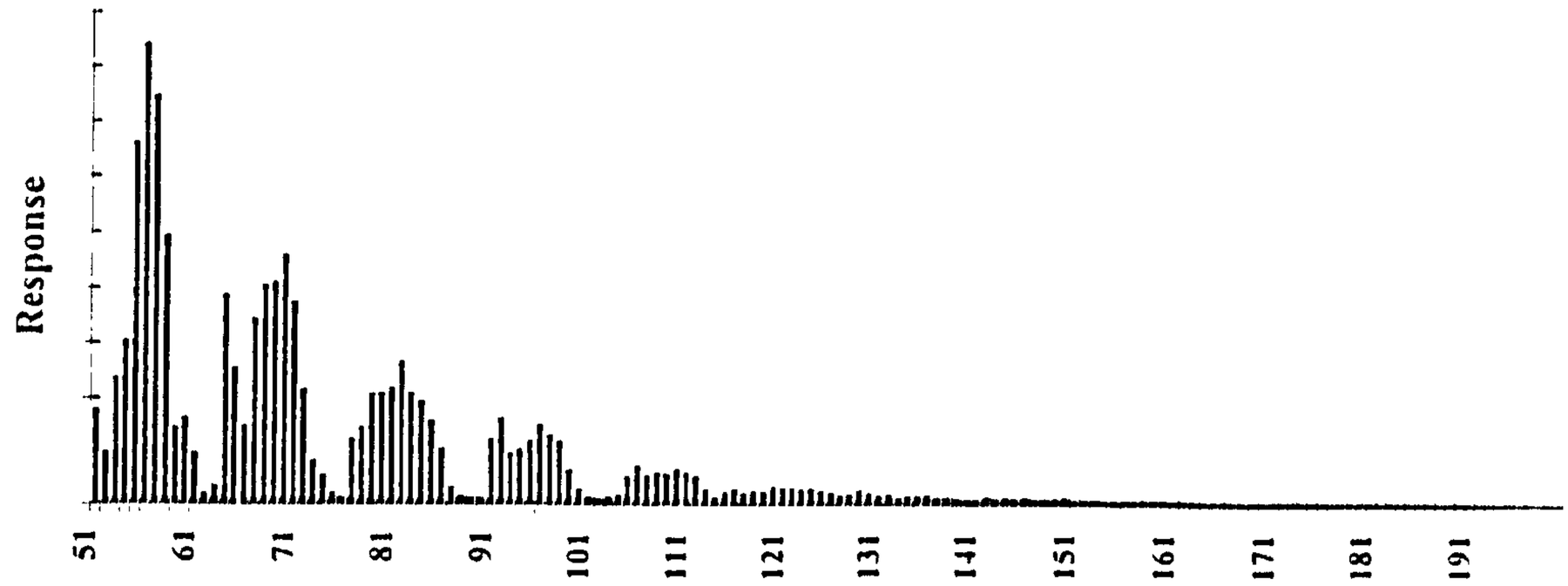

f) Pyrolysis Mass Spectrogram for OB72

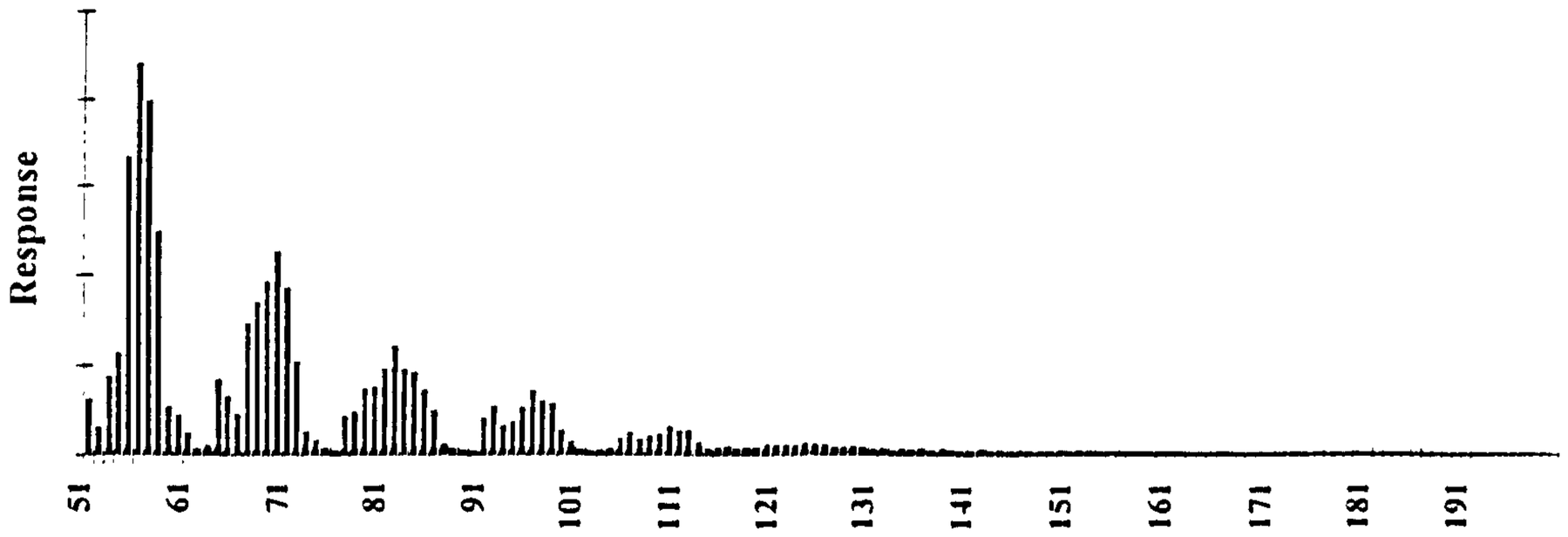

g) Pyrolysis Mass Spectrogram for OB81

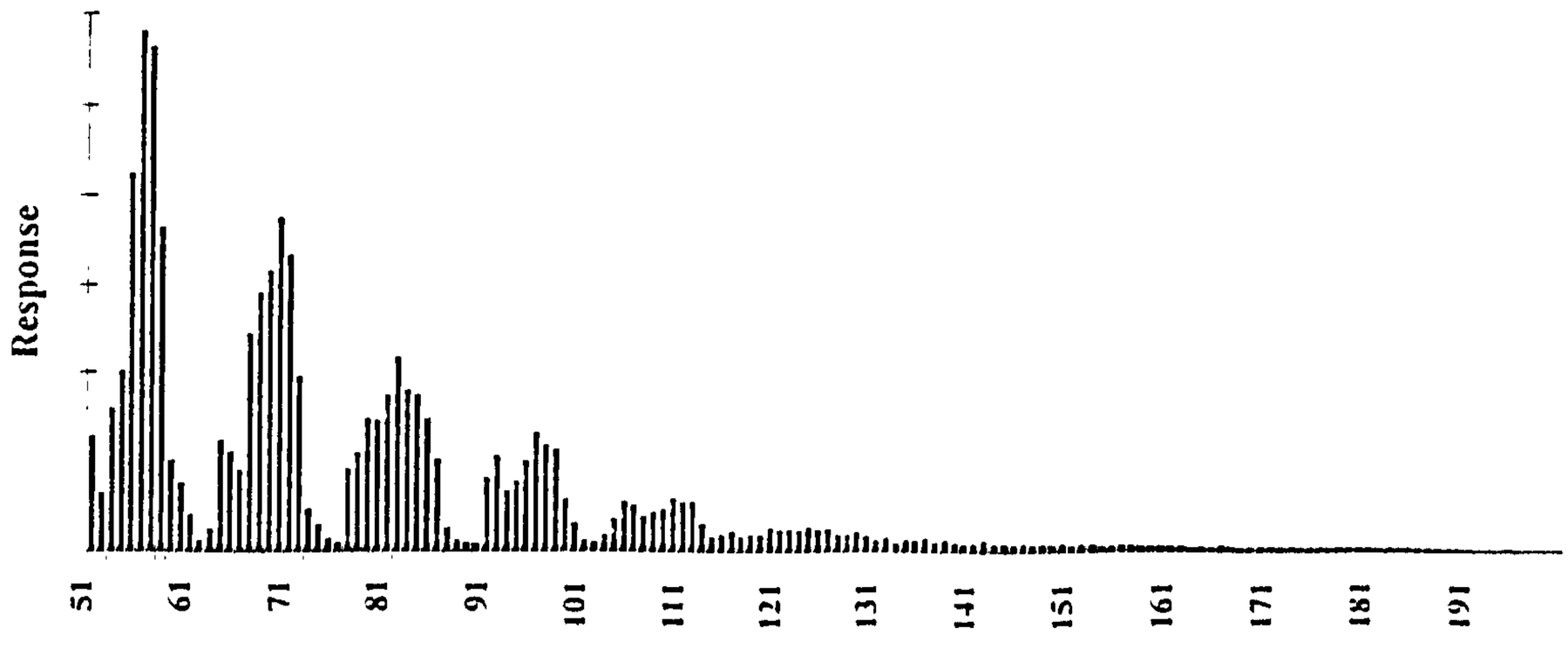

Figure 1. Pyrolysis mass spectrograms for the Oued Bahloul section. The numbers of the x axis refer to the m/z fragment ion.

a) Pyrolysis Mass Spectrogram for DOY25

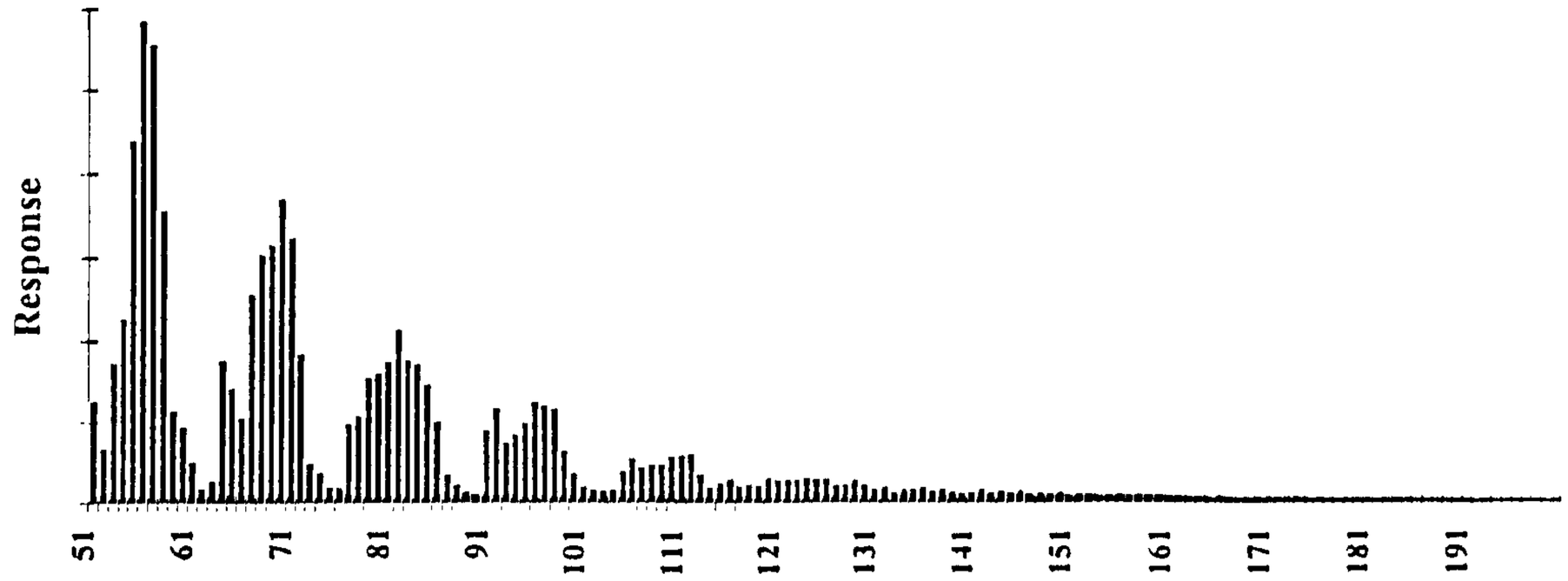

b) Pyrolysis Mass Spectrogram for OG16

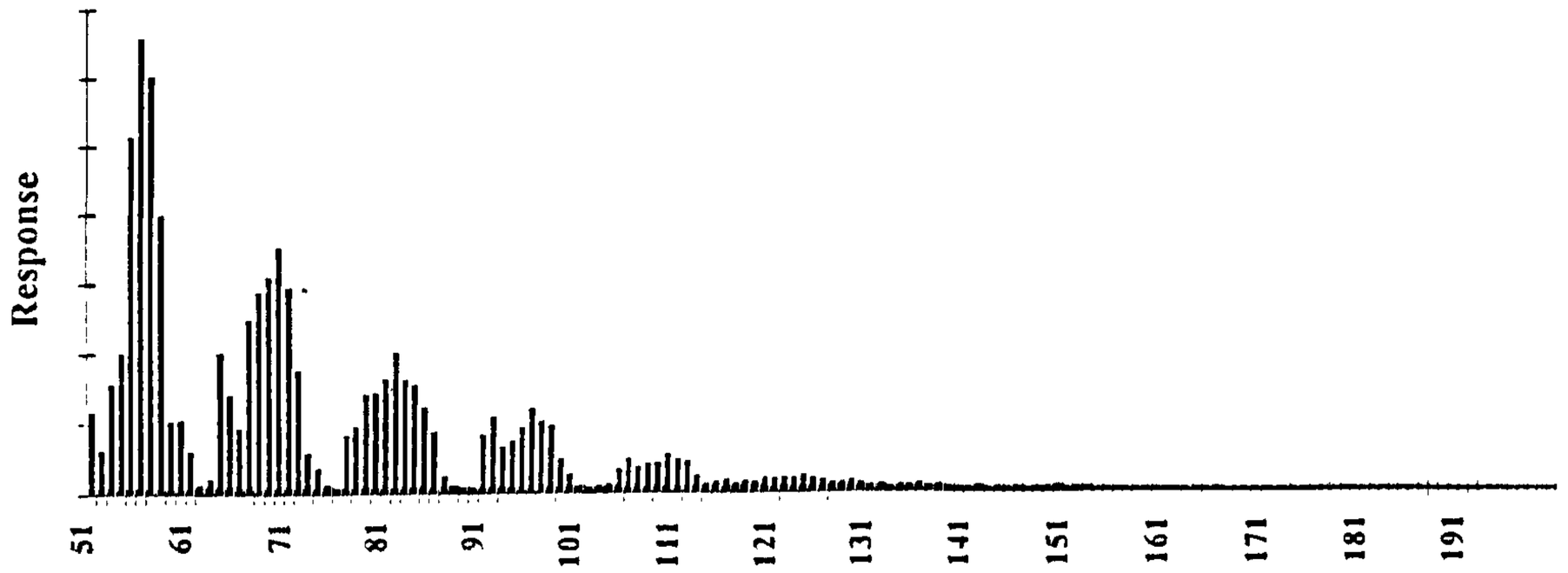

c) Pyrolysis Mass Spectrogram for N18

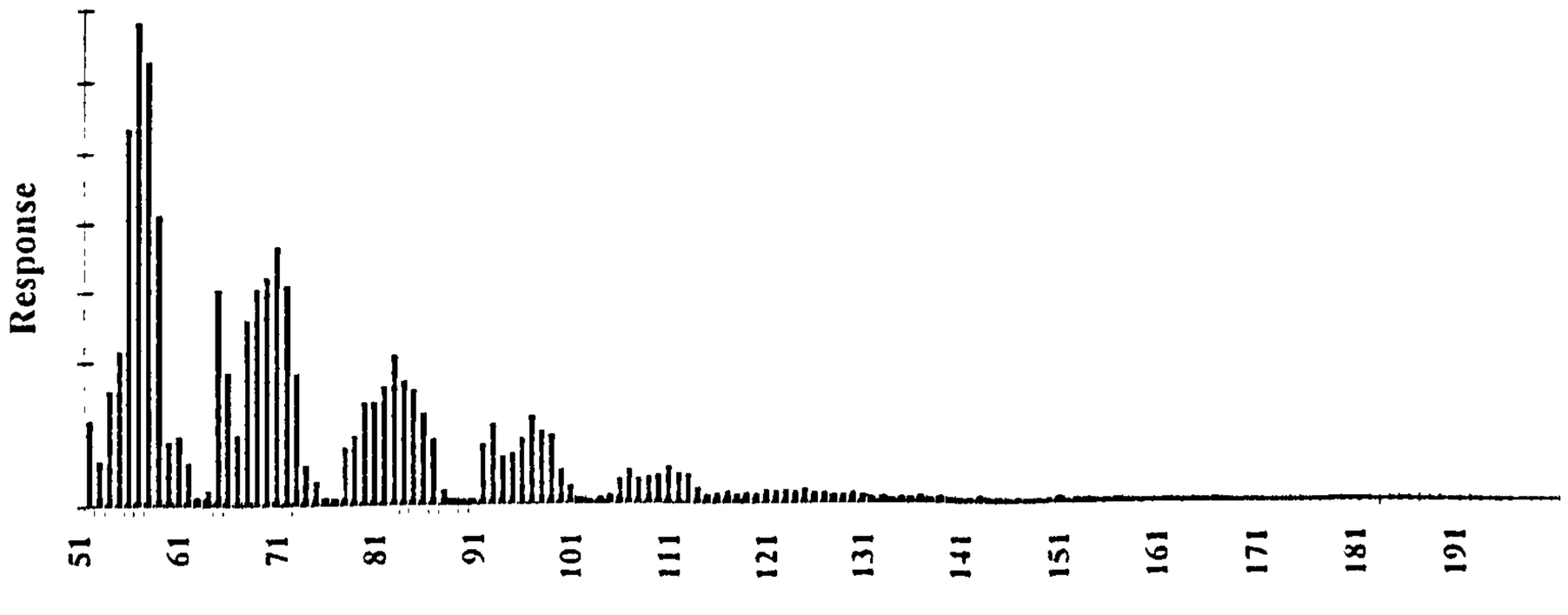

Figure 2. Pyrolysis mass spectrograms for the a) Dir Oulad Yahia; b) Oued El Gsab; c) Nebour sections. The numbers of the x axis refer to the m/z fragment ion.

a) Pyrolysis Mass Spectrogram for EC11

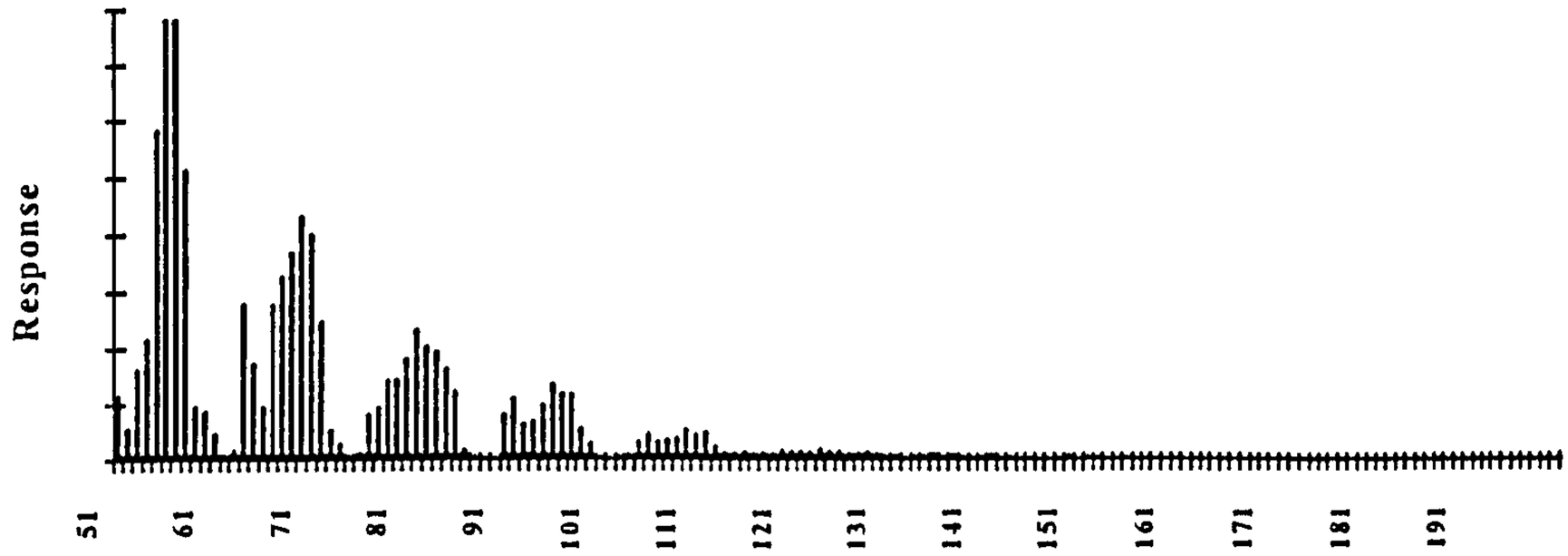

b) Pyrolysis Mass Spectrogram for EC13

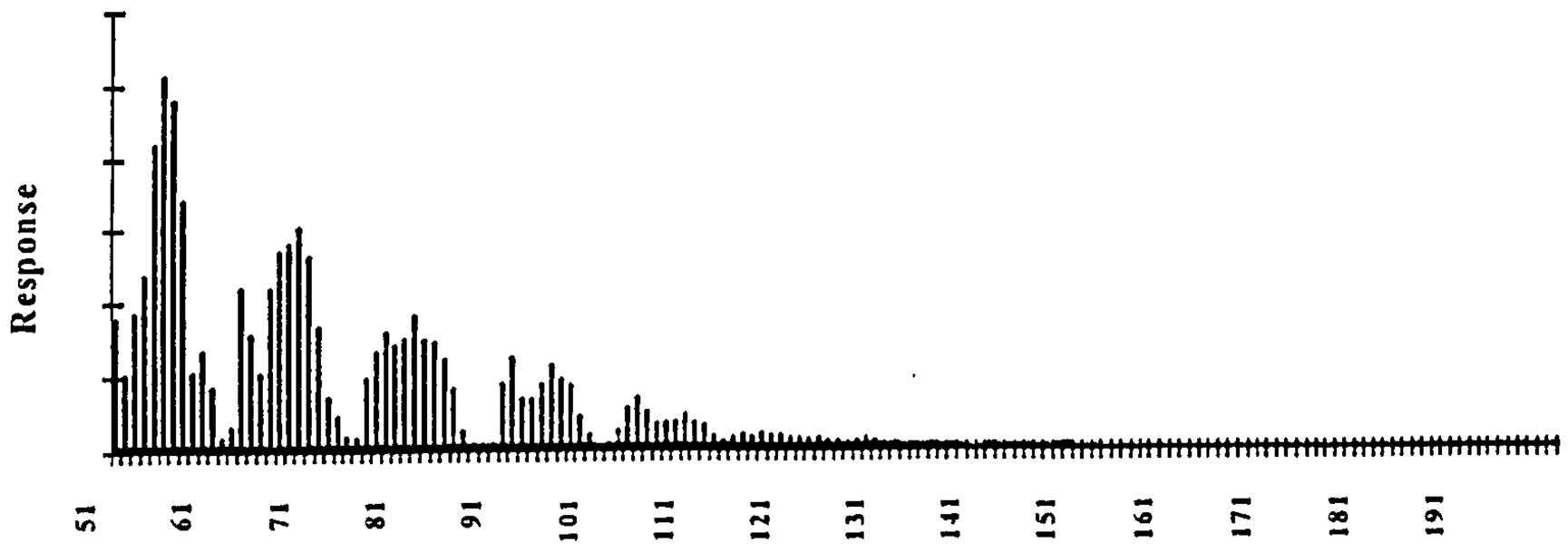

c) Pyrolysis Mass Spectrogram for EC19

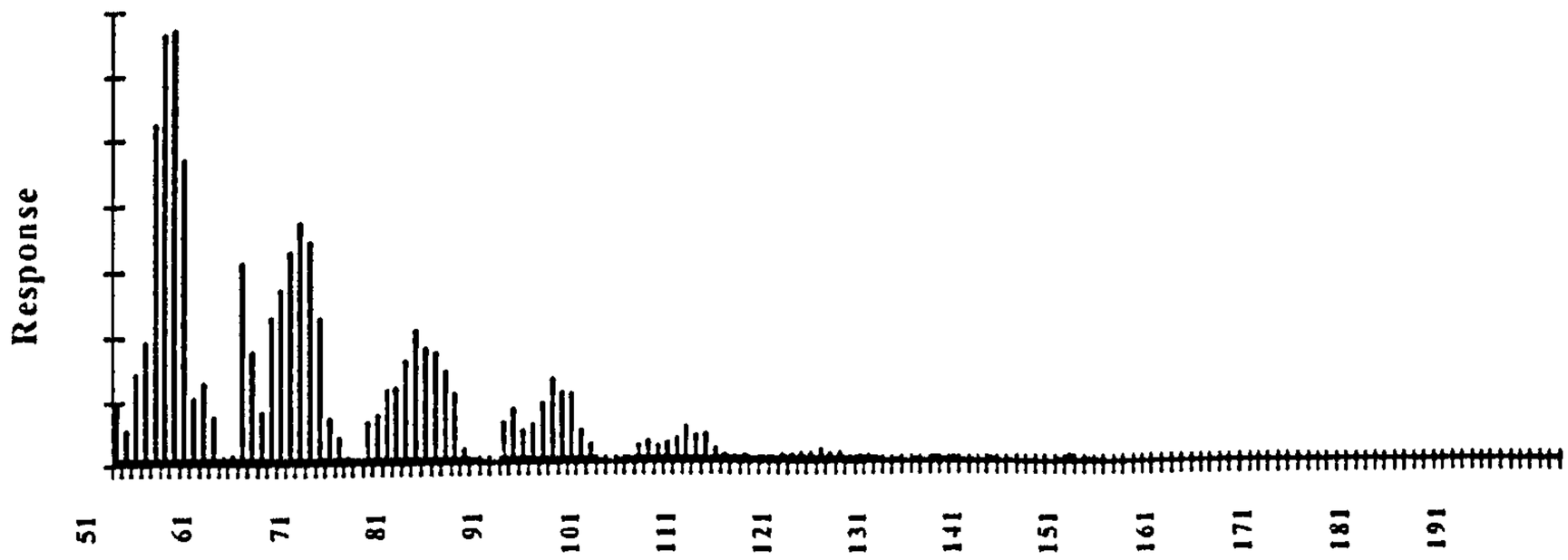

d) Pyrolysis Mass Spectrogram for EC25

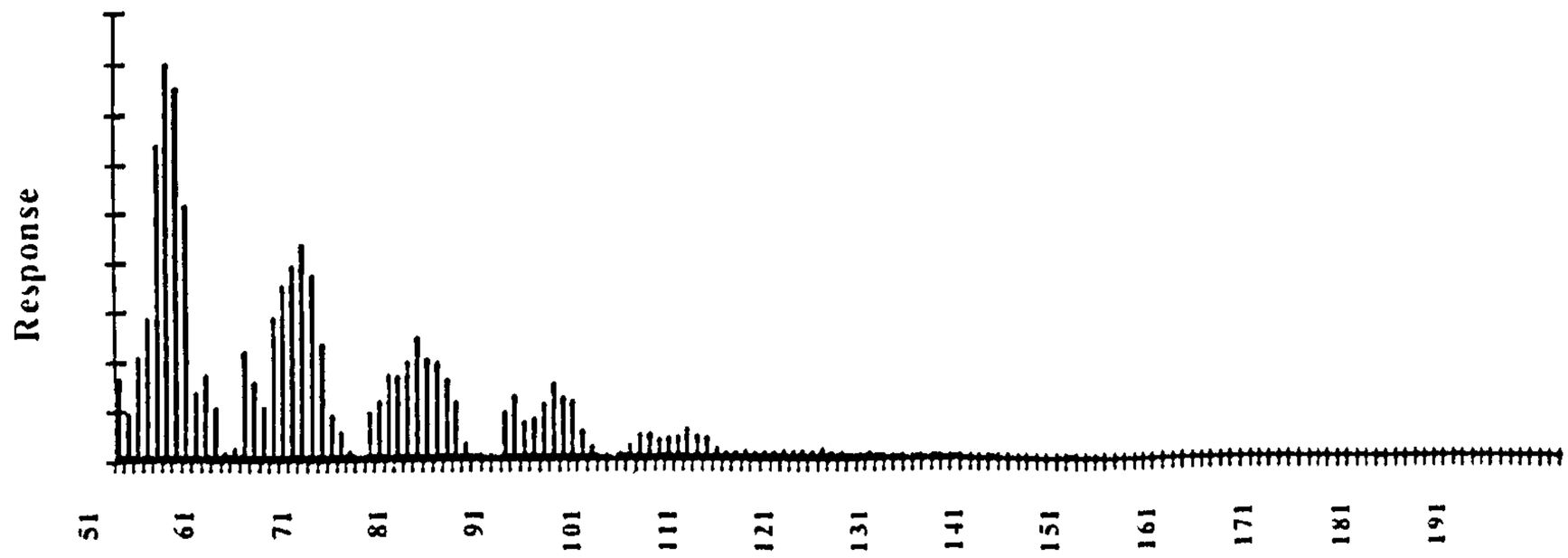

Figure 3. Pyrolysis mass spectrograms for the Ech Cheid section. The numbers of the x axis refer to the m/z fragment ion.

a) Pyrolysis Mass Spectrogram for MQ14

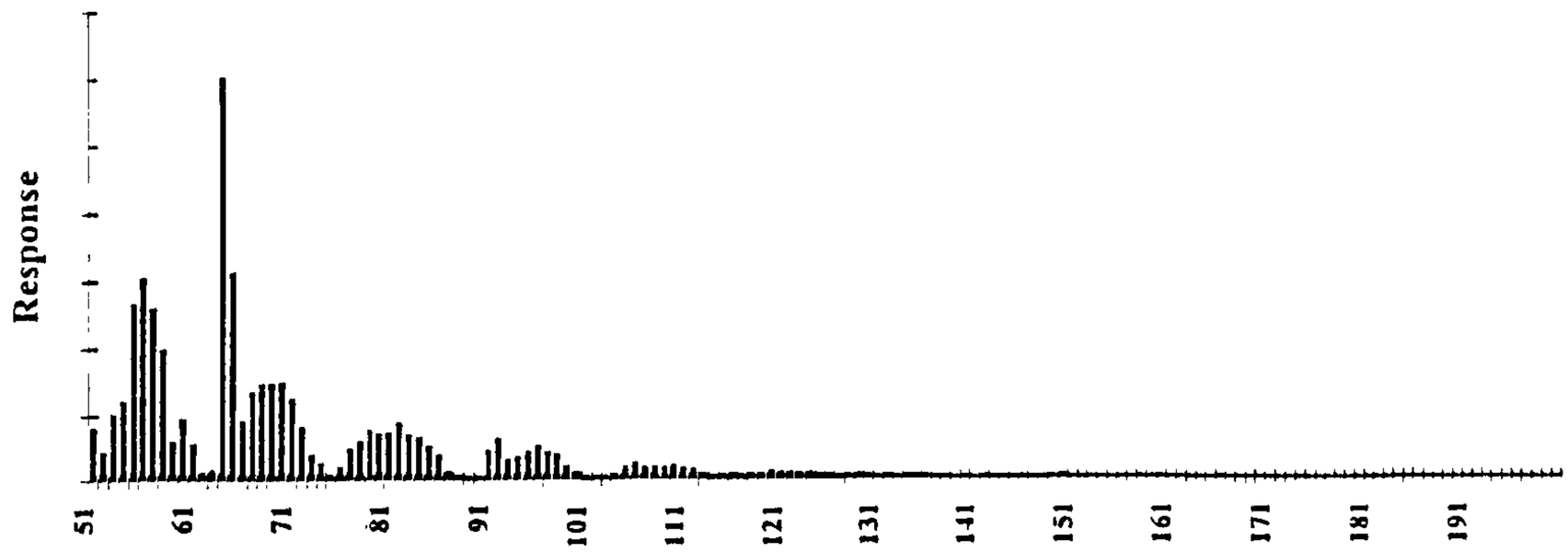

b) Pyrolysis Mass Spectrogram for MQ16

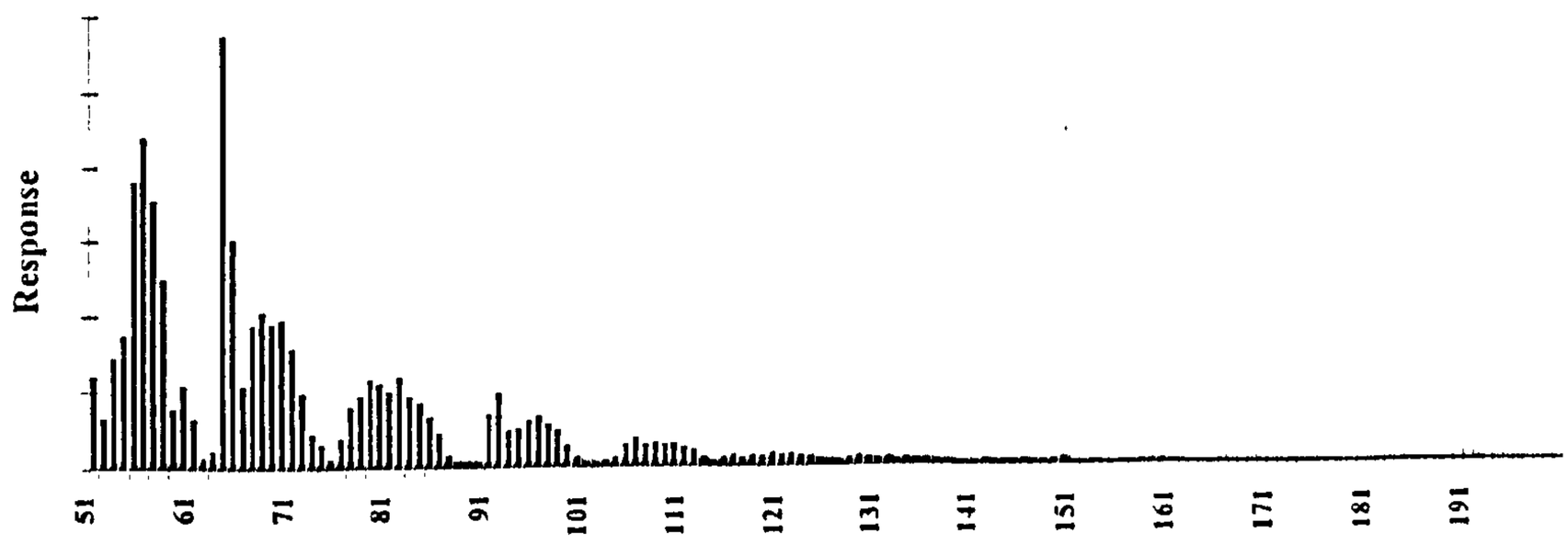

c) Pyrolysis Mass Spectrogram for MQ18

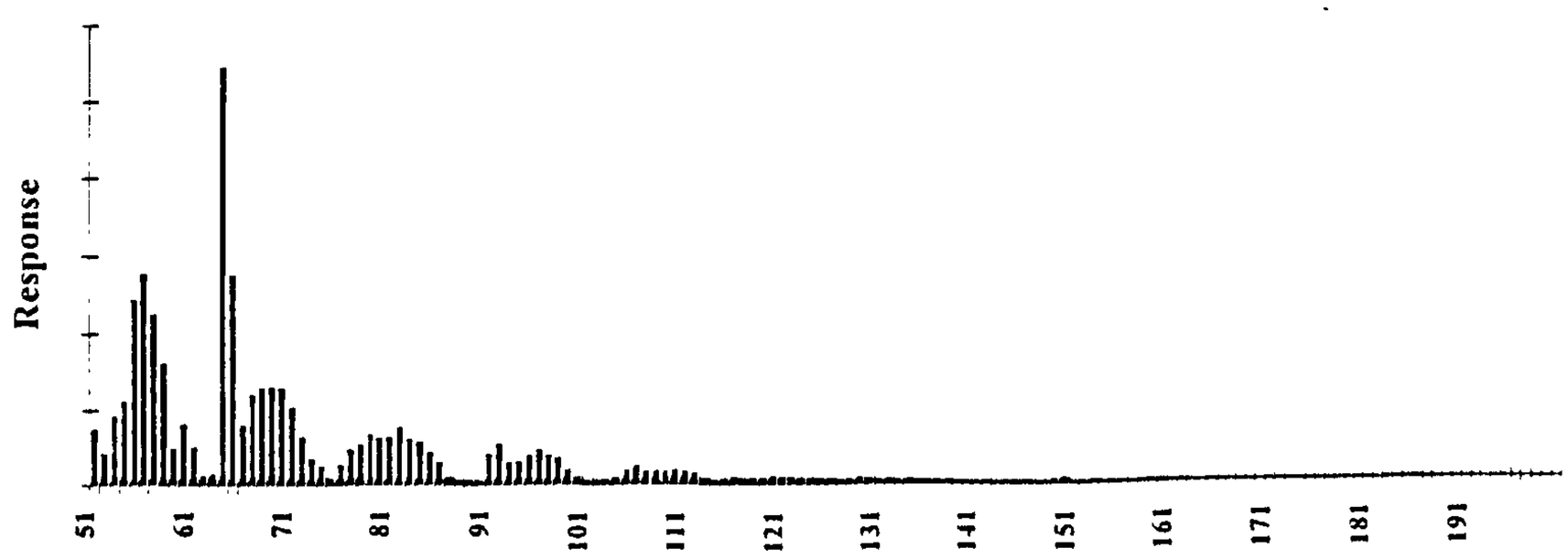

d) Pyrolysis Mass Spectrogram for MQ27

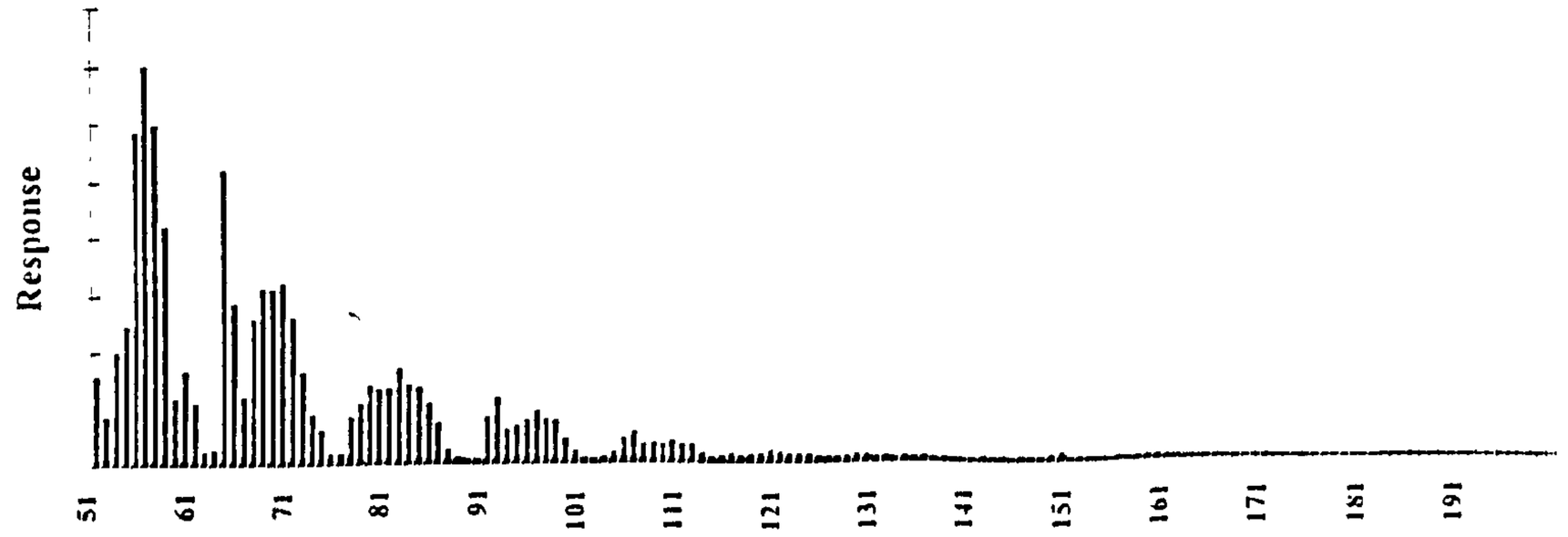

Figure 4. Pyrolysis mass spectrograms for the Misberg section. The numbers of the x axis refer to the m/z fragment ion.

a) Pyrolysis Mass Spectrogram for SF6a

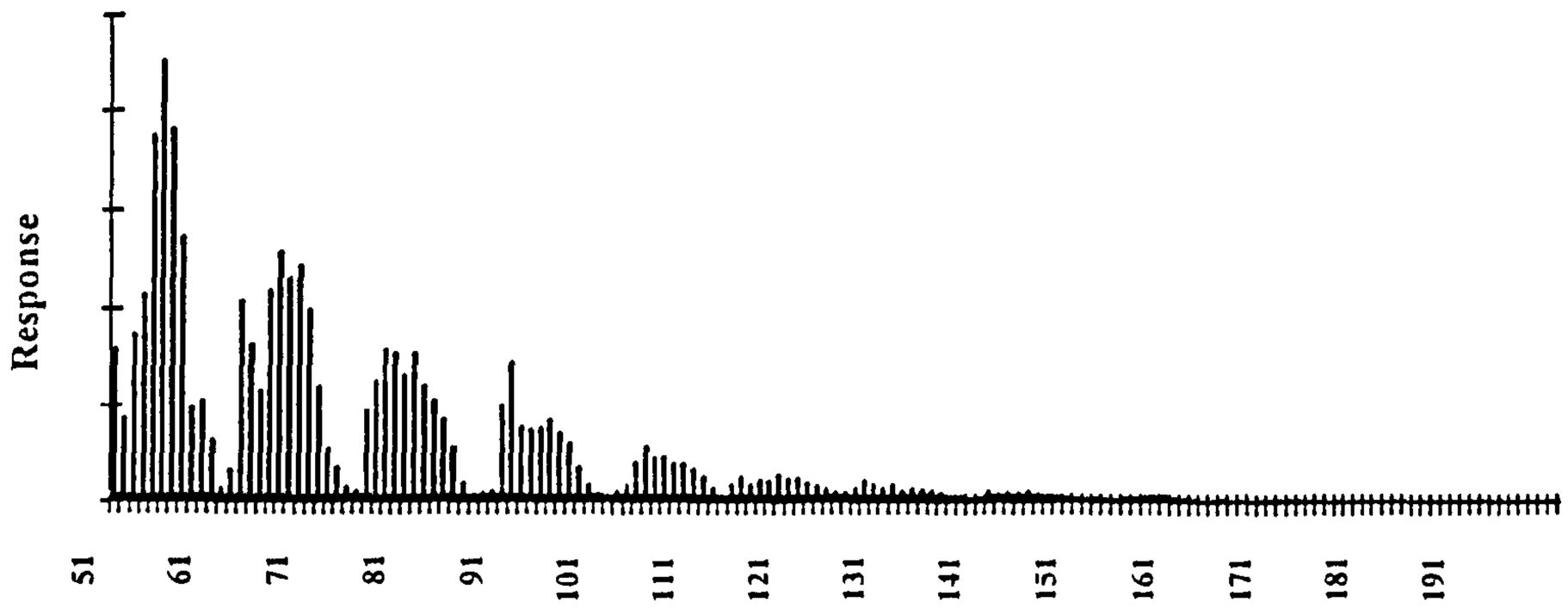

b) Pyrolysis Mass Spectrogram for SF6b

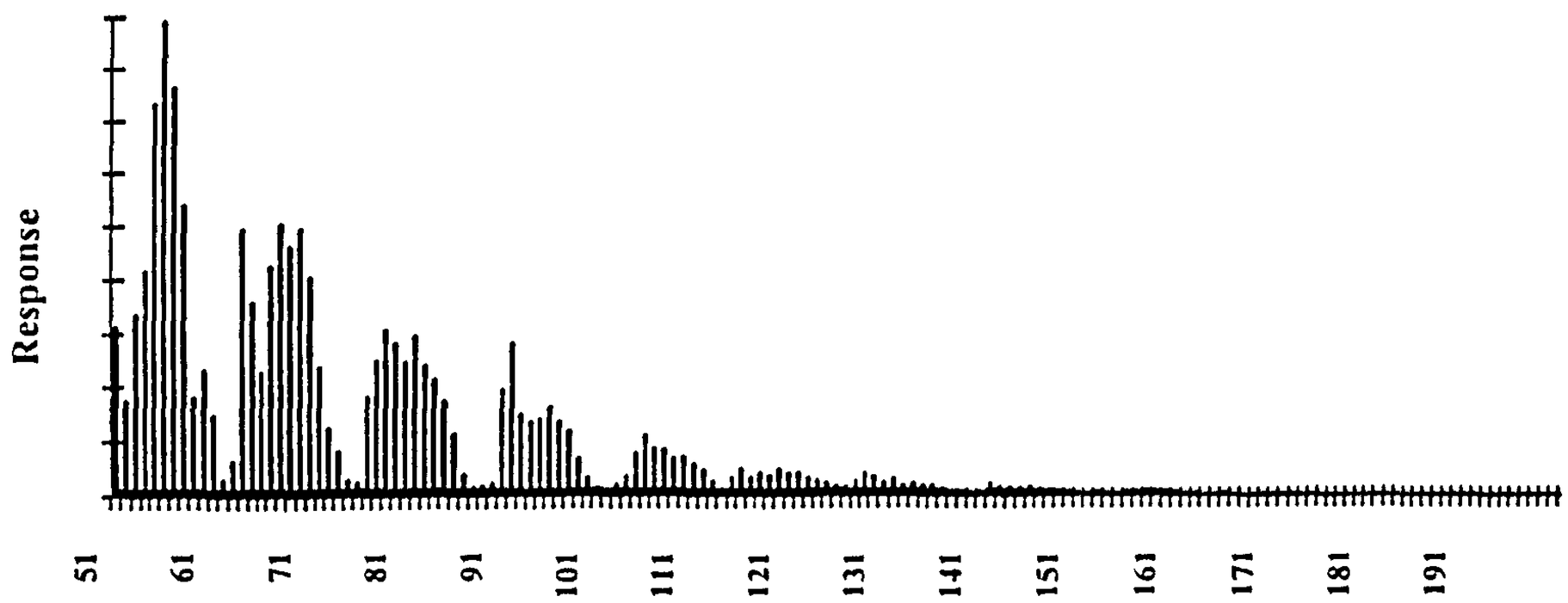

Figure 5. Pyrolysis mass spectrograms for the South Ferriby section. The numbers of the x axis refer to the m/z fragment ion.

a) Pyrolysis Mass Spectrogram for Guttenberg kerogen

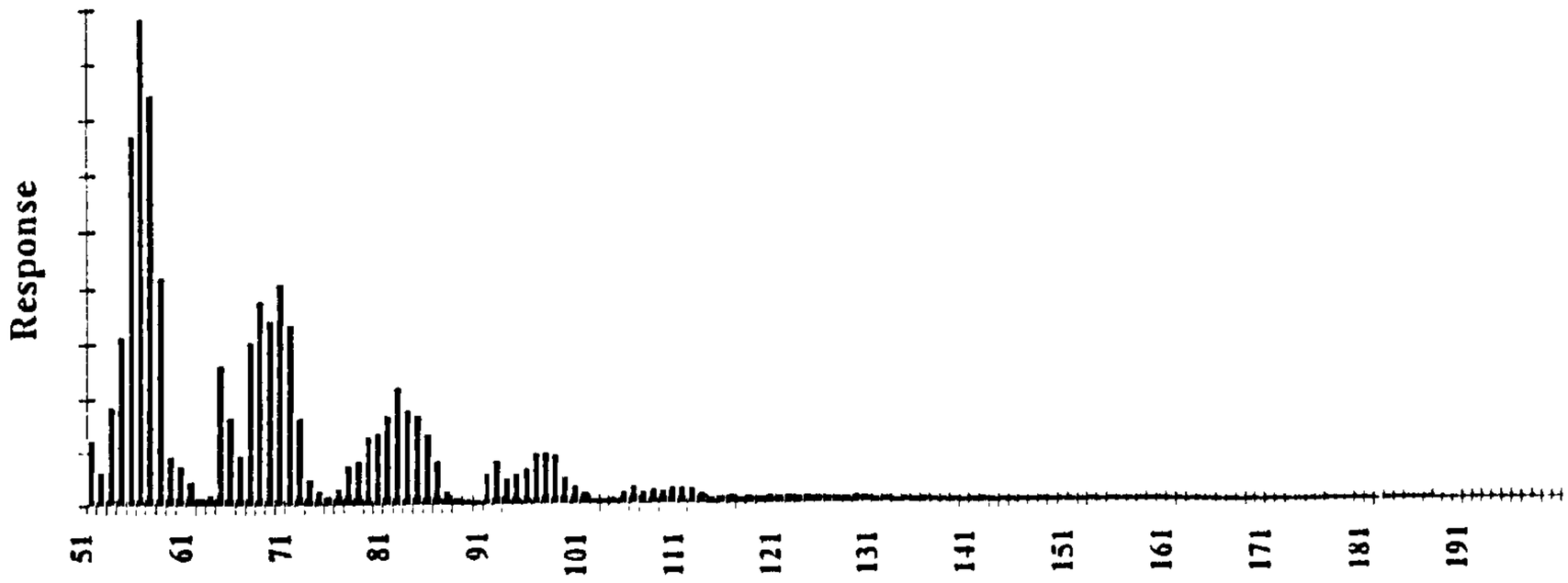

b) Pyrolysis Mass Spectrogram for Green River shale kerogen

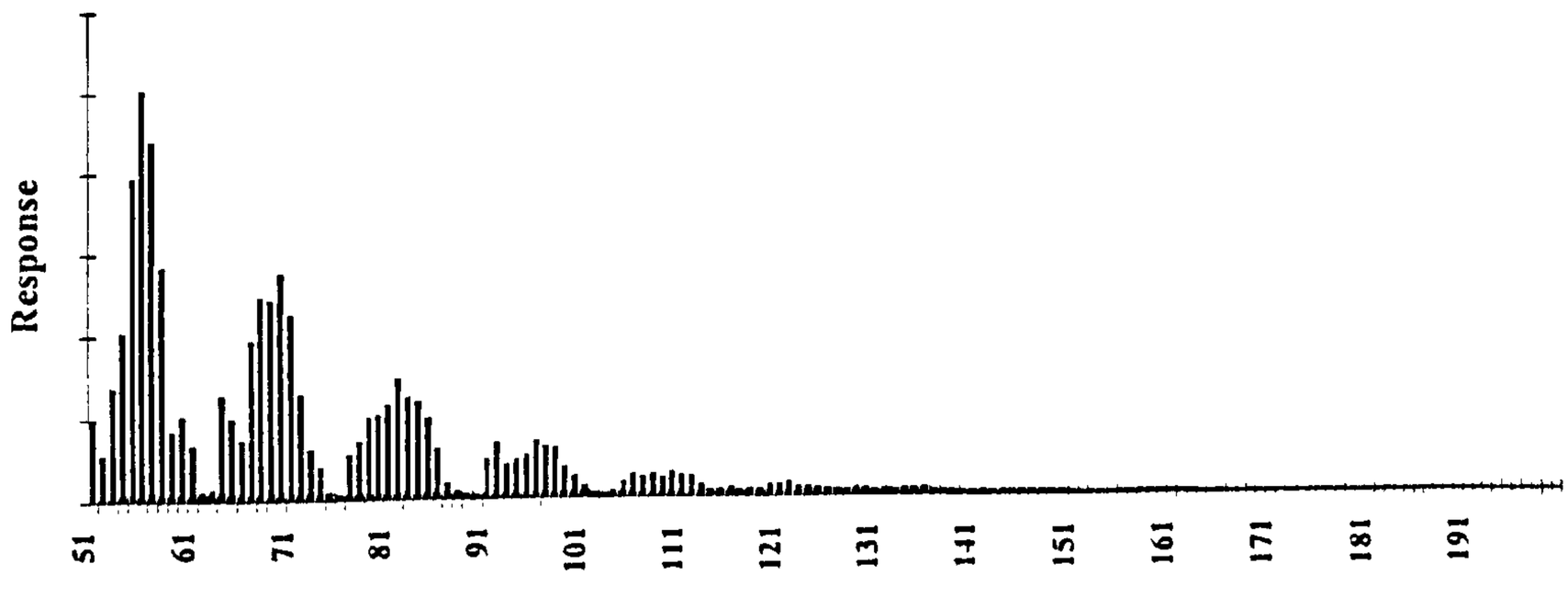

c) Pyrolysis Mass Spectrogram for Messel Oil Shale kerogen

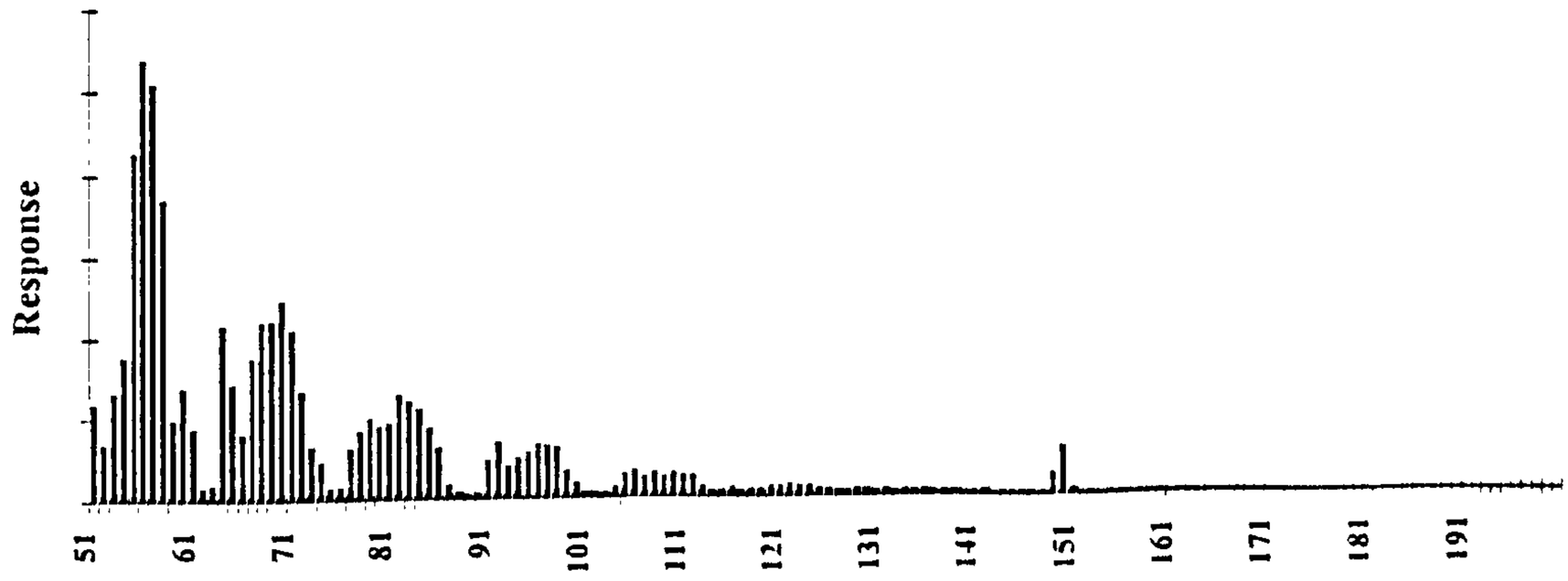

d) Pyrolysis Mass Spectrogram for Kimmeridge

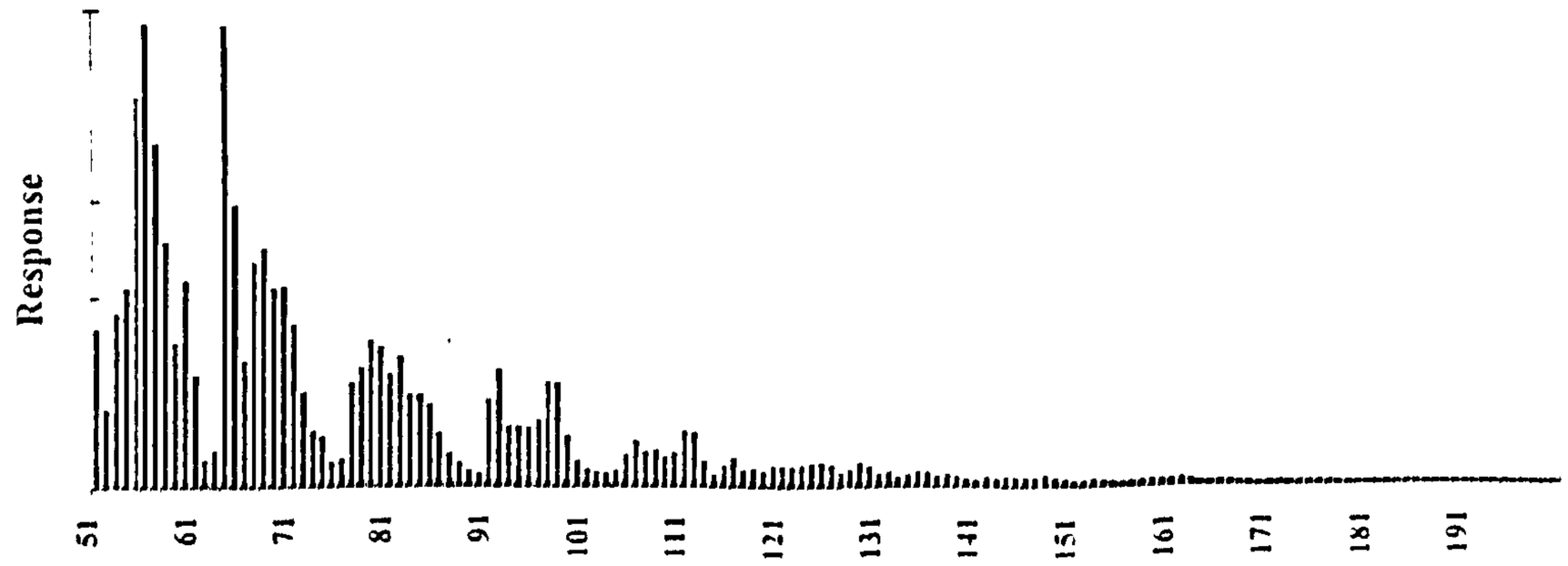

e) Pyrolysis Mass Spectrogram for Jet kerogen

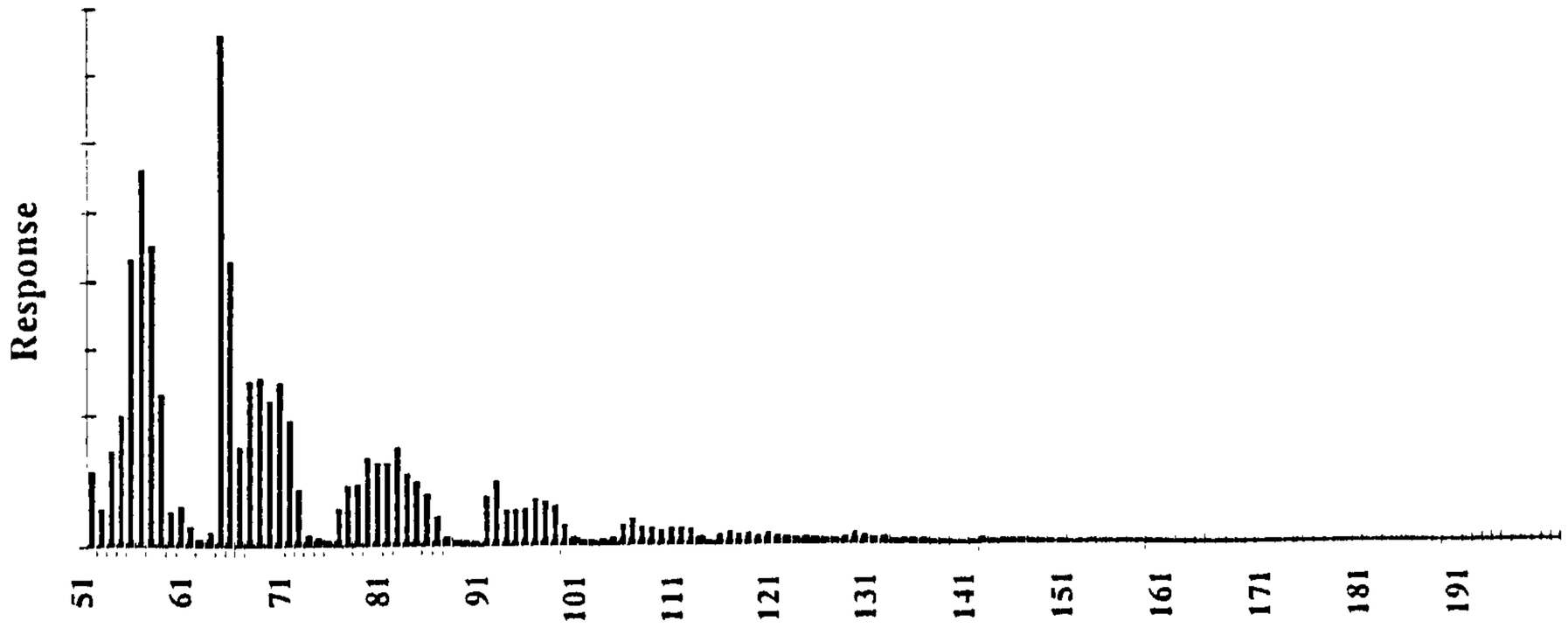

f) Pyrolysis Mass Spectrogram for SQ36

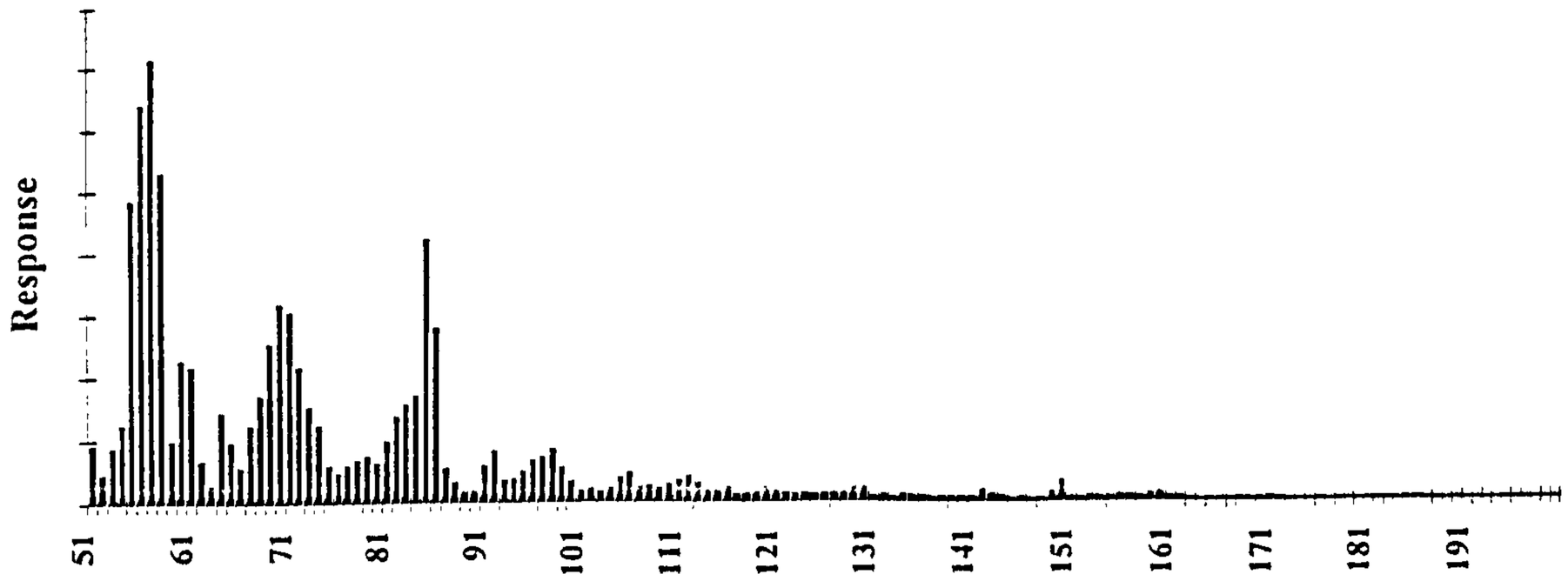

Figure 6. Pyrolysis mass spectrograms for the well characterised kerogens. The numbers of the x axis refer to the m/z fragment ion.